Society of Engineering Science
49th Annual Technical Meeting

Oct. 10-12, 2012 • Atlanta, GA

ABSTRACTS

Georgia Institute of Technology

www.ses2012.gatech.edu

Welcome!

We are delighted that you are joining us for the Society of Engineering Science 49th Annual Technical Meeting.

Over the next three days, several hundred leading researchers in the engineering sciences from around the world will exchange ideas and progress in research.

We are honored to host this important meeting, which addresses the SES vision to:
- Focus on the interfaces between engineering, sciences and mathematics
- Strike a balance between emerging and established fields
- Engage the next generation through undergraduate student paper competitions

Your involvement helps ensure that this event brings together diverse, interdisciplinary groups of researchers to discuss advances in the context of highly engaging and focused symposia.

While you're here, we invite you to enjoy Atlanta's attractions, such as the World of Coca-Cola, the Georgia Aquarium and, of course, Georgia Tech.

Many thanks to our presenters and our local organizing committee, as well as you, for making the SES 49th Annual Technical Meeting a priority. Your support makes this meeting possible!

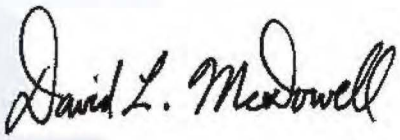

David L. McDowell
Conference Chair
Georgia Institute of Technology, Regents' Professor,
Mechanical Engineering/Materials Science and Engineering

Georgia Tech Welcomes SES Members to the 49th Annual Technical Meeting

Georgia Tech and its George W. Woodruff School of Mechanical Engineering are the hosts of the SES 49th Annual Technical Meeting.

Founded in 1885, Georgia Tech is one of the nation's top research universities, distinguished by its commitment to improving the human condition through advanced science and technology. Georgia Tech's campus occupies 400 acres in the heart of the city of Atlanta, where 20,000 undergraduate and graduate students receive a focused, technologically based education.

Accredited by the Southern Association of Colleges and Schools, Georgia Tech offers many nationally recognized programs. Undergraduate and graduate degrees are offered in the Colleges of Architecture, Computing, Engineering, Management, Sciences and the Ivan Allen College of Liberal Arts.

Georgia Tech is consistently the only technological university ranked in U.S. News & World Report's listing of America's top 10 public universities. In addition, Georgia Tech's College of Engineering is regularly ranked in the nation's top five by U.S. News. Mechanics of solids and fluids also has deep roots across Georgia Tech's College of Engineering.

Over the past decade, overall research expenditures at Georgia Tech have nearly doubled, increasing 99 percent to $525 million in 2008, while federal research expenditures increased 150 percent. Georgia Tech now ranks among the top 10 in research expenditures among universities without a medical school.

About the Technical Program

The three-day technical meeting consists of more than 500 presentations, three symposia in honor of medal recipients, and graduate and undergraduate student paper competitions.

Standard presentations last 20 minutes, including discussion time, and the keynote lectures are 40 minutes, including discussion time.

The technical program schedule is presented in a quick-reference matrix format on pages 12-29. An abstract along with author affiliations for each can be seen at **www.ses2012.gatech.edu/abstracts** or by using the QR code found on page 3.

Acknowledgements and Sponsors

Thank you to our sponsors for their involvement and support of the Society of Engineering Science 49th Annual Technical Meeting:

National Science Foundation (NSF)
Dr. Martin L. Dunn, Program Manager

U.S. Army Research Office
Dr. David M. Stepp, Program Officer

Georgia Tech College of Engineering

Georgia Tech The George W. Woodruff School of Mechanical Engineering

We also acknowledge the support of the College of Engineering, the Woodruff School of Mechanical Engineering and the Carter N. Paden Distinguished Chair in Metals Processing at Georgia Tech.

We thank senior administrative professional Cecelia Jones, faculty of the Local Organizing Committee and participating Georgia Tech graduate students for their diligent efforts in supporting this meeting.

Technical Meeting Organization

Conference Chair

Dr. David McDowell, Regents' Professor, SES Fellow and Past President of SES (2002), Mechanical Engineering/Materials Science and Engineering

Local Organizing Executive Committee

Dr. Antonia Antoniou, Assistant Professor, Mechanical Engineering

Dr. Ken Gall, Professor, Materials Science and Engineering/Mechanical Engineering

Dr. Richard Neu, Professor, Mechanical Engineering/Materials Science and Engineering

Dr. Olivier Pierron, Assistant Professor, Mechanical Engineering

Dr. Min Zhou, Professor, Mechanical Engineering/Materials Science and Engineering

Dr. Ting Zhu, Associate Professor, Mechanical Engineering

Additional Members of the Local Organizing Committee

Dr. Gang Bao, Professor, Biomedical Engineering/Mechanical Engineering

Dr. Rudy Gleason, Associate Professor, Biomedical Engineering/Mechanical Engineering

Dr. Ari Glezer, Professor, Mechanical Engineering

Dr. Dewey Hodges, Professor, Aerospace Engineering

Dr. Karl Jacob, Professor, Materials Science and Engineering/Mechanical Engineering

Dr. Laurence Jacobs, Professor, Civil and Environmental Engineering/Mechanical Engineering

Dr. W. Steven Johnson, Professor, Materials Science and Engineering/Mechanical Engineering

Dr. George Kardomateas, Professor, Aerospace Engineering

Dr. Kimberly Kurtis, Professor, Civil and Environmental Engineering

Dr. Michael Leamy, Associate Professor, Mechanical Engineering

Dr. Suresh Menon, Professor, Aerospace Engineering

Dr. Massimo Ruzzene, Professor, Aerospace Engineering/Mechanical Engineering

Dr. Naresh Thadhani, Professor, Materials Science and Engineering/Mechanical Engineering

Dr. Arash Yavari, Associate Professor, Civil and Environmental Engineering

Awards and Honors

Plenary Speakers and Medalists

David Barnett
2012 Eringen Medalist

David Barnett received his BA and MS degrees in Mechanical Engineering from Rice University in 1961 and 1963 and his PhD in Materials Science and Engineering from Stanford University in 1967. He was a NATO post-doctoral fellow at the Technical University Clausthal in (then) West Germany, spent a year as a staff scientist in the metallurgy division of the Ford Motor Company Scientific Laboratory in Dearborn, Mich., before joining the faculty of Stanford University with a joint appointment in Materials Science and Engineering and Mechanical Engineering in 1969. He was a visiting professor at the Physics Institute at the University of Oslo in 1974, and has devoted much of his career to pursuing research in the theory of dislocations and elastic waves in anisotropic elastic and piezoelectric media.

Zhigang Suo
2012 Prager Medalist

Zhigang Suo is Allen E. and Marilyn M. Puckett Professor of Mechanics and Materials at Harvard University. He earned a bachelor degree from Xi'an Jiaotong University in 1985, majoring in Engineering Mechanics. Upon earning a PhD degree in Engineering Science from Harvard University, in 1989, Suo joined the faculty of the University of California at Santa Barbara, and established a group studying the mechanics of materials and structures. The group moved to Princeton University in 1997, and to Harvard University in 2003. Suo teaches courses in solid mechanics and applied mathematics. His research centers on the mechanical behavior of materials and structures.

Kyung-Suk Kim
2012 SES Medalist

Kyung-Suk Kim is currently a Professor of Engineering and a member of Solids and Structures Group at Brown University, directing the Nano and Micromechanics Laboratory. Dr. Kim has played a central role in understanding and utilizing mechanical behavior of nanostructures by developing creative theories and conducting precision experiments. In particular, he leads his respective field of research by providing fundamental theories for the motion and deformation as well as for the formation and assembly of nanostructures.

Awards and Honors

Joe D. Goddard
2012 Taylor Medalist

J.D. Goddard received his PhD in chemical engineering from the University of California, Berkeley in 1962. He joined the chemical engineering faculty of the University of Michigan in 1963, and in 1976 he accepted the position of Fluor Professor and Chair in the Department of Chemical Engineering at the University of Southern California. He has been Professor of Applied Mechanics and Engineering Science at the University of California, San Diego, since 1991. He has published research in a wide range of fields, including the mechanics of complex fluids and solids, and the thermodynamics and transport properties of physical and biological systems.

Markus Buehler
2012 SES Young Investigator Medalist

Markus J. Buehler is an Associate Professor in the Department of Civil and Environmental Engineering at the Massachusetts Institute of Technology (MIT), where he directs the Laboratory for Atomistic and Molecular Mechanics (LAMM). He is the Co-Director of the MIT Computation for Design and Optimization Program, Director of the MIT-Germany Program, and leads the Mechanics and Materials Group in the Department of Civil and Environmental Engineering. Buehler has published more than 200 articles on computational materials science, nanotechnology and nanoscience, authored several monographs, and given several hundred invited, keynote and plenary talks.

Student Presentations

Organizer: Olivier Pierron, Georgia Tech

Two student presentation competitions, at the graduate and undergraduate level, will take place during the first day of the meeting. The competitions are sponsored by the National Science Foundation. The three best presentations in each category will be announced at the conference banquet on Thursday night.

Symposium IX.1: Graduate students

Zachary Aitken (Cal Tech): Mechanical Properties of Bi-crystalline, Aluminum Nano-Pillars containing Σ-3 and Σ-5 boundaries

Lisa Chen (U Penn): Size-Dependent Nonlinear Elasticity in Pd Nanowhiskers

Huanyu Cheng (Northwestern): Elastomer surfaces with directionally dependent adhesion strength and their use in transfer printing with continuous roll-to-roll applications

Yan Li (GT): A multiscale computational model for predicting fracture toughness from microstructure

Jia Liu (Harvard): Exploiting buckling Buckling to design structures with negative Thermal Expansion

Chang-Tsan Lu (CMU): Kinetic Relations Associated with Phase Transformation in A One-Dimensional Atomic Chain

Xia Ma (Iowa State): Dynamic Force Spectroscopy of Specific Binding between Protein and DNA Aptamer

Hassan Masoud (GT): Harnessing responsive gels to design synthetic microswimmers

Alice Nasto (MIT): Localization (s-cones) in thin shells under indentation

Parisa Pour Shahid Saeed Abadi (GT): Nanoindentation of Conformally-coated Carbon Nanotube Forests

Marcos Reyes-Martinez (U Mass): Wrinkled organic crystals: Determining the elastic constants of highly ordered rubrene

Andrew Richards (Cal Tech): Modelling of martensitic phase transformation and plastic slip in polycrystalline materials

Symposium IX.2: Undergraduate students

Chandana Ramitha Edirisinghe (Georgia Tech): Water Hammer Suppression using Voided PDMS Liners

Arvind Kalidindi (Drexel): Effects of Interfacial Morphology on Polymer Electrolyte Fuel Cell Performance

Yean Lee (Rice): Control and maneuver of nanodevice by inducing piezoelectric effect on nanowires using electromagnetic waves

Robert Mannino (Georgia Tech): Mechanics of Sickle Cell Disease: A Purely Physical Cause of Endothelial Cell Dysfunction

Mohamad Ali Najia (Georgia Tech): Influencing encapsulated stem cell factor secretion through hypoxic conditioning

Emmanuel Jose Ochoa (University of Texas at El Paso / Purdue University): Cyber-enabled modeling of adhesion-based deformation in low-dimensional nanostructures

Matthew Perrella (Auburn): Optimization of Micro-encapsulated Phase Change Material in Gypsum Wall Boards

Caleb Piercy (Georgia Tech): FerroFluid Heat Exchanger Pump

Anita Rajamani (Georgia Tech): Side specific responses of shear stress on AV calcification

Brian Ramirez (Cal Tech): Mechanics of Deformation and Fracture of Soft Fiber Reinforced Composites

Radu Reit (Georgia Tech): Growth Time Performance Dependence of Vertically Aligned Carbon Nanotube Supercapacitors Grown on Aluminum Substrates

Stefan Troen Stephenson-Moe (Georgia Tech): Automated procedure for functionalization of non-magnetic micro particles

Schedule at a Glance

Tuesday, Oct. 9

5:00 - 7:00 p.m. Registration
5:00 - 7:00 p.m. Reception

Wednesday, Oct. 10

7:00 - 8:30 a.m.	Continental Breakfast
8:00 - 5:00 p.m.	Registration
8:30 - 9:15 a.m.	Prager Medal Lecture Zhigang Suo
9:15 - 9:30 a.m.	Break
9:30 - 11:30 a.m.	Session W1 - 13 Parallels
11:30 a.m. - 12:30 p.m.	Lunch
12:30 - 2:30 p.m.	Session W2 - 13 Parallels
2:30 - 2:45 p.m.	Break
2:45 - 4:45 p.m.	Session W3 - 13 Parallels
5:00 - 5:45 p.m.	Eringen Medal Lecture David Barnett
6:00 - 7:00 p.m.	SES Members Meeting
7:00 - 9:00 p.m.	SES Board Meeting

Thursday, Oct. 11

7:00 - 8:30 a.m.	Continental Breakfast
8:00 - 5:00 p.m.	Registration
8:30 - 9:15 a.m.	Taylor Medal Lecture Joe D. Goddard
9:15 - 9:30 a.m.	Break
9:30 - 11:30 a.m.	Session T1 - 13 Parallels
11:30 a.m. - 12:30 p.m.	Lunch
12:30 - 2:30 p.m.	Session T2 - 13 Parallels
2:30 - 2:45 p.m.	Break
2:45 - 4:45 p.m.	Session T3 - 13 Parallels
5:00 - 5:45 p.m.	SES Medal Lecture Kyung-Suk Kim
7:00 - 9:00 p.m.	Conference Banquet

Friday, Oct. 12

7:00 - 8:30 a.m.	Continental Breakfast
8:00 - 5:00 p.m.	Registration
8:30 - 9:15 a.m.	Young Investigator Medal Lecture Markus Buehler
9:15 - 9:30 a.m.	Break
9:30 - 11:30 a.m.	Session F1 - 13 Parallels
11:30 a.m. - 12:30 p.m.	Lunch
12:30 - 2:30 p.m.	Session F2 - 13 Parallels
2:30 - 2:45 p.m.	Break
2:45 - 4:45 p.m.	Session F3 - 13 Parallels

Parallel Schedule

Wednesday, Oct. 10					
Room	8:30-9:15a.m. (Medal Lecture)	9:30-11:30a.m. (Session W1)	12:30-2:30p.m. (Session W2)	2:45-4:45p.m. (Session W3)	5:00-5:45p.m. (Medal Lecture)
Ballroom	Prager (Suo)				Eringen (Barnett)
Salon 3		I.1 (Suo)	I.1 (Suo)	I.1 (Suo)	
Salon 4		IV.7(1/3)	IV.7(2/3)	IV.7(3/3)	
Conference A		III.3(1/2)	III.3(2/2)	III.4(1/4)	
Conference B		IV.5(1/3)	IV.5(2/3)	IV.5(3/3)	
Conference C		V.4(1/1)	IX.2(1/2)	IX.2(2/2)	
Conference D		V.2(1/1)	IX.1(1/2)	IX.1(2/2)	
Conference E		III.1(1/9)	III.1(2/9)	III.1(3/9)	
Conference 6		IV.1(1/4)	IV.1(2/4)	IV.1(3/4)	
Conference 7		IV.8(1/3)	IV.8(2/3)	IV.8(3/3)	
Conference 8		II.1(1/2)	II.1(2/2)	IV.12(1/1)	
Salons 1 & 2		II.4(1/2)	II.4(2/2)	II.3(1/1)	
Salon 5		IV.15(1/2)	IV.15(2/2)	IV.16(1/1)	
Salon 6		IV.2(1/6)	IV.2(2/6)	IV.2(3/6)	

Parallel Schedule

Thursday, Oct. 11					
Room	8:30-9:15a.m. (Medal Lecture)	9:30-11:30a.m. (Session W1)	12:30-2:30p.m. (Session W2)	2:45-4:45p.m. (Session W3)	5:00-5:45p.m. (Medal Lecture)
Ballroom	Taylor (Goddard)				SES (Kim)
Salon 3		I.3 (Barnett)	I.3 (Barnett)	I.3 (Barnett)	
Salon 4		I.2 (Kim)	I.2 (Kim)	I.2 (Kim)	
Conference A		III.4(2/4)	III.4(3/4)	III.4(4/4)	
Conference B		II.2(1/4)	II.2(2/4)	II.2(3/4)	
Conference C		IV.11 (1/3)	IV.11 (2/3)	IV.11 (3/3)	
Conference D		IV.6 (1/4)	IV.6 (2/4)	IV.6 (3/4)	
Conference E		III.1 (4/9)	III.1 (5/9)	III.1 (6/9)	
Conference 6		IV.1 (4/4)	IV.3 (1/2)	IV.3 (2/2)	
Conference 7		VI.5 (1/5)	VI.5 (2/5)	VI.5 (3/5)	
Conference 8		IV.10 (1/4)	IV.10 (2/4)	IV.10 (3/4)	
Salons 1 & 2		IV.9 (1/4)	IV.9 (2/4)	IV.9 (3/4)	
Salon 5		IV.14 (1/4)	IV.14 (2/4)	IV.14 (3/4)	
Salon 6		IV.2(4/6)	IV.2(5/6)	IV.2(6/6)	

Friday, Oct. 12					
Room	8:30-9:15a.m. (Medal Lecture)	9:30-11:30a.m. (Session W1)	12:30-2:30p.m. (Session W2)	2:45-4:45p.m. (Session W3)	
Ballroom	Young Investigator (Buehler)				
Salon 3		I.3 (Barnett)	VIII.2 (1/2)	VIII.2 (2/2)	
Salon 4		I.2 (Kim)	I.2 (Kim)		
Conference A		IV.4 (1/3)	IV.4 (2/3)	IV.4 (3/3)	
Conference B		II.2(4/4)	VI.4 (1/2)	VI.4 (2/2)	
Conference C		VI.2 (1/2)	VI.2 (2/2)		
Conference D		IV.6 (4/4)	VII.3 (1/2)	VII.3 (2/2)	
Conference E		III.1 (7/9)	III.1 (8/9)	III.1 (9/9)	
Conference 6		VIII.1 (1/2)	VIII.1 (2/2)		
Conference 7		VI.5 (4/5)	VI.5 (5/5)		
Conference 8		IV.10 (4/4)	VII.1 (1/1)	VII.2 (1/1)	
Salons 1 & 2		IV.9 (4/4)	IV.13 (1/2)	IV.13 (2/2)	
Salon 5		IV.14 (4/4)	VIII.3 (1/1)	V.1 (1/1)	
Salon 6		VI.3 (1/1)	VI.6 (1/1)		

PLENARY PRESENTATIONS

Prager Medal Lecture

Zhigang Suo
Harvard University

Lithium-ion batteries—when mechanics meets chemistry

ID: 352

Lithium-ion Batteries – When Mechanics Meets Chemistry

Zhigang Suo
Harvard University
USA

Abstract:
Lithium-ion batteries are the batteries of choice for applications sensitive to size and weight, such as portable electronics and electric cars. Intense efforts are being made to develop lithium-ion batteries to achieve safe operation, high capacity, fast charging, and long life. At the heart of a lithium-ion battery is a process that couples mechanics and chemistry. The electrodes in a lithium-ion battery are hosts of lithium. When the battery is charged and discharged, the electrodes absorb and desorb lithium, inducing inelastic flow and possibly fracture. Lithiation-induced fracture not only occurs in commercial lithium-ion batteries, but is also a bottleneck in developing future lithium-ion batteries. This talk describes a theory of concurrent diffusion, reaction, and flow, and relates the theory to recent experimental observations of high-capacity electrodes. The theory places driving forces for flow and reaction on the same footing, giving chemomechanical yield condition and chemomechanical flow rule. This combination of mechanics and chemistry generalizes the theory of plasticity of von Mises, Drucker, and Prager, and describes a large family of phenomena: reactive flow in solids. In addition to lithiation of electrodes, examples include oxidation of metals, hydration of gels, and growth of biological tissues.

Eringen Medal Lecture

David Barnett
Stanford University

Free surface (Rayleigh) waves and interfacial (Stoneley) waves in anisotropic linear elastic half-spaces: the surface impedance method

ID: 98

Free Surface (Rayleigh) Waves and Interfacial (Stoneley) Waves in Anisotropic Linear Elastic Half-Spaces: The Surface Impedance Method

David M. Barnett
Stanford University
USA

Abstract:
Using the Stroh formalism and Ingebrigtsen and Tonning's surface impedance tensor, the questions of existence and uniqueness of free surface (Rayleigh) waves in linear elastic half-spaces of general anisotropy are easily settled. The same framework allows one to simply and thoroughly study the existence of interfacial (Stoneley) waves in bonded elastic half-spaces of general anisotropy. Numerical studies to find Rayleigh wave speeds and to determine if Stoneley waves exist and their speeds based on this framework are easily executed.

This work represents the results of many years of collaboration with, primarily, Jens Lothe (Oslo) and Peter Chadwick (East Anglia), and I am extremely proud to have enjoyed the pleasure of their insight, guidance, and friendship for almost 40 years.

Taylor Medal Lecture

Joe D. Goddard
University of California - San Diego

Playing in sand, for science, engineering and fun

ID: 750

Playing in Sand for Science, Engineering and Fun

2012 G.I. Taylor Medalist Lecture
Society of Engineering Science

Joe Goddard
Department of Mechanical and Aerospace Engineering
University of California, San Diego

Abstract

"[Granular media] are omnipresent: from the rings of Saturn to the snow of our mountains. [They] represent a major object of human activities: as measured in tons, the first material manipulated on earth is water; the second is granular matter."
P.-G. de Gennes "From Rice to Snow", *2008 Nishina Foundation Nobelist Lectures*, In *Lect. Notes Phys.* **746**, 297-318 (2008).

The past forty years or so have witnessed a resurgence and continuous growth of interest in the mechanics of granular materials, whose scientific origins go back at least to the 18th Century. The subject is relevant to a number of geotechnical and technological processes, such as stability of slopes and natural avalanches, mechanics of desert sands, and vibratory conveying and compaction. The challenge of understanding and mathematically modeling these materials and processes has attracted researchers from a wide array of disciplines, ranging from soil mechanics to theoretical physics, who bring complementary but sometimes opposing philosophies and methodologies to the table.

This lecture provides a broad overview of the field, including the distinguished flow régimes of elastoplastic solid, viscoplastic fluid and viscous gas. The focus here is on the first two, which involve several fascinating phenomena such as Reynolds dilatancy, seismic liquefaction, mesoscopic force chains, shear bands and Faraday patterns on vibrated layers. An effort is made to relate these qualitatively to the geotechnical and technological processes mentioned above.

As a second aspect of the lecture, a discussion is given of the challenges and puzzles associated with the mathematical modeling of granular media. In contrast to molecular solids and fluids, whose relatively small particles are governed by reversible ("frictionless") intermolecular forces and strong thermal motion ("kT"), the typical granular material consists of particles ranging in size from microns to meters, whose individual and collective motion is dominated by frictional contacts and external forces such as gravity. This severely limits the traditional approaches of molecular-kinetic theory and statistical mechanics, yet the typical number of particles in such systems renders a brute-force numerical description by the so-called "distinct element method" (DEM) impracticable for many purposes. Hence, one important challenge is the development of continuum models of the kind that have proved indispensable for traditional solid and fluid mechanics.

A brief summary is given of some of the more promising phenomenological continuum models for the elastoplasticity and viscoplasticity of non-cohesive granular media. One conclusion is that multiscale or "multipolar" continuum models involving additional kinematic degrees of freedom and conjugate "hyperstresses", may be essential to the rheology of granular media, particularly the elastoplatic behavior. Because of the typical particle sizes, this becomes much more compelling for granular media than for other complex solids and fluids.

SES Medal Lecture

Kyung-Suk Kim
Brown University

Mechanics of nanostructures: hybrid-analysis of experiment and computation

ID: 778

Mechanics of Nanostructures: Hybrid-Analysis of Experiment and Computation

Kyung-Suk Kim
Brown University
USA

Young Investigator Medal Lecture

Markus Buehler
Massachusetts Institute of Technology

From atoms to structures - how spiders turn weakness into strength

ID: 096

From atoms to structures – how spiders turn weakness into strength

Markus J. Buehler
Laboratory for Atomistic and Molecular Mechanics (LAMM), Department of Civil and Environmental Engineering, Massachusetts Institute of Technology
United States

Abstract:
This talk will explain how materials in biology are synthesized, controlled and used for a variety of purposes—structural support, force generation, catalysis, or energy conversion—despite severe limitations in available energy, quality and quantity of building blocks. We demonstrated that the chemical composition of biology's materials plays a minor role in achieving functional properties. Rather, the way components are connected at different length-scales defines what material properties can be achieved, how they can be altered to meet functional requirements, and how they fail in disease states. We have achieved this by using the world's fastest supercomputers to predict properties of complex materials from first principles, in a multiscale approach that spans orders of magnitude in scale. This method, combined with experimental studies, allows us to build virtual "*in silico*" material models that provide unseen insight into the workings of natural and synthetic materials from the bottom up.

We demonstrate this approach in a case study of spider silk, one of the strongest yet most flexible materials in Nature, despite being made out of some the simplest, most abundant and intrinsically weak proteins, including weak hydrogen bonding. We discovered that the great strength and flexibility of spider silk—exceeding that of steel and other engineered materials—can be explained by the material's unique structural makeup that involves multiple hierarchical levels. These hierarchical levels span from the genetic information that defines the protein sequence to the structural scale of an entire spider web. Thereby, each level contributes to the overall properties, but the remarkable properties emerge because of the synergistic interaction across the scales where the sum is more than its parts. We showed that the nonlinear material behavior of silk fibers, softening at the yield point to dramatically stiffen during large deformations until point of failure, is what allows for localization of deformation upon loading, and is precisely what makes spider webs robust and extremely resistant to defects, as compared to other linear-elastic or elastic-plastic materials. Through *in situ* experiments on webs of a European garden spider, we confirm the prediction that locally applied loading results in minimal damage. We further show that under global loads such as wind, the material behavior of silk under small-deformation is crucial to maintaining the web. By translating this insight gained from the study of natural materials such as spider silk to engineered materials such as carbon nanotube fibers, graphene composites or metal-polymer films, our research has resulted in an engineering paradigm that facilitates the design of sustainable materials starting from the molecular level, leading to the formation of hierarchical structures that span all scales from nano to macro.

[1] T. Knowles, M.J. Buehler , "Nanomechanics of functional and pathological amyloid materials," *Nature Nanotechnology*, Vol. 6(7), 2011

[2] M.J. Buehler, “Tu(r)ning weakness to strength,” *Nano Today*, Vol. 5 , pp. 379-383, 2010
[3] S. Keten, Z. Xu, B. Ihle, M.J. Buehler, “Nanoconfinement controls stiffness, strength and mechanical toughness of beta-sheet crystals in silk,” *Nature Materials*, Vol. 9, pp. 359-367, 2010
[4] S. Cranford, A. Tarakanova, N. Pugno, M.J. Buehler, “Nonlinear material behaviour of spider silk yields robust webs,” *Nature*, doi:10.1038/nature10739, 2012

I.1

Awards Symposium – Prager Medal (Zhigang Suo)

ID: 121

A Locking-Free Finite Element Formulation for Dielectric Elastomers

Harold Park
Boston University

Abstract:
We present a three-dimensional nonlinear finite element formulation for dielectric elastomers based upon the recently developed nonlinear field theory of Suo and co-workers (Z. Suo et al., Journal of the Mechanics and Physics of Solids 2008; 56:467-486). The approach is based upon the Q1P0 formulation of Simo et al (Computer Methods in Applied Mechanics and Engineering 1985; 51:177-208) to remove volumetric locking effects in both the mechanical and coupled electromechanical response of the elastomers. We present numerical examples to demonstrate the performance of the new formulation.

ID: 134

Fracture and Fragmentation of Layered Soft Materials

Xuanhe Zhao
Soft Active Materials Laboratory
Duke University
USA

Abstract:
Many modern materials and material systems are layered. Current studies on fractures of layered materials have been focused on relatively rigid and brittle materials under small deformations. On the other hand, many layered materials in biological systems and biomedical devices are compliant and capable of large deformation prior to fracture. Here, we present a combined experimental and theoretical study on the fracture and fragmentation of a layered soft-material system. We bonded a thin layer of a polymer with relatively low stretchability to a thick substrate with relatively high stretchability. The laminate was subjected to tensile strain up to 1000%, with the fracture and fragmentation process of the layer with low stretchability observed. A theory was further developed to relate the energy release rate in the layered structure and the fracture toughness of the polymer. We found the moduli, stiffening properties, and dimensions of the layers all have significant effect on the energy release rate. The new theory can predict the experimental observations without fitting parameters. The current study is closely related to Prof. Zhigang Suo's fundamental contribution to fracture mechanics of layered materials.

ID: 137

Postbuckling Analysis and its Application to Stretchable Electronics

Yonggang Huang
Northwestern University
USA

Abstract:
A versatile strategy for fabricating stretchable electronics involves controlled buckling of bridge structures in circuits that are configured into open, mesh layouts (i.e. islands connected by bridges) and bonded to elastomeric substrates. Quantitative analytical mechanics treatments of the responses of these bridges can be challenging, due to the range and diversity of possible motions. Koiter (1945) pointed out that the postbuckling analysis needs to account for all terms up to the 4th power of displacements in the potential energy. Existing postbuckling analyses, however, are accurate only to the 2nd power of displacements in the potential energy since they assume a linear displacement curvature relation. Here, a systematic method is established for accurate postbuckling analysis of beams. This framework enables straightforward study of the complex buckling modes under arbitrary loading, such as lateral buckling of the island-bridge, mesh structure subject to shear (or twist) or diagonal stretching observed in experiments. Simple, analytical expressions are obtained for the critical load at the onset of buckling, and for the maximum bending, torsion (shear) and principal strains in the structure during postbuckling.

ID: 151

Modeling Fracture and Failure in Si thin film Nanoelectrodes on Substrates

Huajian Gao
Brown University

Hamed Haftbaradaran

Abstract:
Silicon is one of the most interesting materials with the highest known charge capacity for application as negative electrodes in lithium-ion batteries. However, due to huge volume changes during cycling, Si anodes can lose a substantial part of their storage capacity due to mechanical failure, fracture and degradation. Recent experiments suggest that patterned Si thin film patches with nanoscale thickness can be designed to remain elastic and well-adhered to substrate during cycling, if the patch size falls below a critical length scale. In this paper, we investigate fracture spacing in continuous Si thin films as well as the mechanics of interfacial cracking and delamination of patterned Si islands. We describe in situ experimental measurements and theoretical investigations that show evidence of substantial interfacial sliding and improved cycling stability in patterned Si electrodes on substrates. Our theoretical analysis takes into account interfacial sliding due to a finite interfacial shear strength and reveals the existence of a class of critical length scales, such that if the island size falls below these critical sizes, interfacial cracking and delamination and plastic deformation become unfavorable. Our theoretical predictions of these critical sizes appear to be in good agreement with the experimental observations.

ID: 272

Convoluted Thermal/Spatial Statistics of Nanoindentation Pop-in Tests as Plasticity Initiation in Small Stressed Volumes

Yanfei Gao
University of Tennessee
USA

Tianlei Li

Abstract:
Sudden discontinuities, or called pop-ins, are often found on nanoindentation load-displacement curves for single crystals. For defect-free crystals under nano-contacts, the pop-in is a result of homogeneous dislocation nucleation because the maximum shear stress approaches the theoretical strength as shown by Mo and NiAl experimental results presented in this talk using spherical indenters with very small radius (around 100-300 nanometers). The observed fluctuations in the pop-in load result purely from the thermally activated process of homogeneous dislocation nucleation. On the other hand, at intermediate contact sizes, such fluctuations can arise from the spatial statistics of pre-existing defects. One example of such defect-assisted processes is a sudden and unstable change of existing dislocation network as in the Frank-Read model. It is found that the convolution of the above thermal and spatial effects exhibits a distinct dependence on the stressed volume size, dislocation density, and geometric factors that describe crystallography and slip anisotropy. The latter can be quantified by the indentation Schmid factor, namely, the ratio of maximum resolved shear stress to the maximum contact pressure. These essential features are captured in a unified model that includes both homogeneous dislocation nucleation and heterogeneous activation of pre-existing dislocations. The model here predicts how the fluctuations of pop-in loads vary with respect to the change of indenter radius (as compared to our Mo indentation tests), the change of pre-existing dislocation density (as compared to our pre-strain experiments), and the change of crystallographic orientation (as compared to our NiAl indentation tests). Implications for other small-scale mechanical tests such as micro-pillar compression are discussed.

ID: 291

Surface Instability of Swollen Gels

Rui Huang
University of Texas at Austin
USA

Abstract:
Consider a layer of a gel attached to a rigid substrate, immersed in a solvent, and swelling in the thickness direction. The flat surface of the gel remains stable if the swelling ratio is small, but becomes unstable if the swelling ratio is large. While surface creases have been commonly observed, surface wrinkles have also been observed in some cases. We compare the critical conditions for the onset of creases and wrinkles based on a nonlinear theory of polymer gels. The critical swelling ratio for the onset of creases is calculated by using a finite element method, and that for wrinkles is calculated by using a linear perturbation method. We find that the critical swelling ratio for the onset of creases is significantly lower than that for wrinkles. Next we consider a gel layer with thickness-graded properties (e.g., crosslink density). In particular, for a bilayer model, we show that the surface instability depends on the stiffness ratio of the two layers. When the upper layer is softer, surface creases occur before wrinkles. When the upper layer is stiffer, surface wrinkles occur before creases. These theoretical findings are compared with experimental observations of various gel systems.

ID: 374

Phase Field Approach for Stress- and Surface-Induced Solid-Solid Phase Transformations and Melting

Valery Levitas
Iowa State University
USA

Abstract:
Thermodynamically consistent phase field theory for solid-solid and solid-liquid phase transformations is developed for large strains and lattice rotations [1]. This theory represents a generalization of our small strain theory [2,3] for a general geometrically nonlinear case and it satisfies all the same conditions necessary for a conceptually correct description of the effects of stress tensors and temperature on martensitic phase transformations. Then this theory, including energy contribution related to the gradient of the order parameters, is further generalized to incorporate description of the surface effects [4-7]. Fully geometrically nonlinear formulation is crucial for this generalization, even if the strains are small. The generalizations include introducing the surface tension at the internal interfaces and external surfaces, correct description of the variant-variant interface energy, description of phenomena related to the finite width and variation of the energy of the external surface during phase transformations, as well as tensorial transformation strain for melting. Boundary conditions take into account variation of surface energy during transformation and lead to surface-induced pre-transformation and transformations. Computational algorithms based on FEM for coupled phase field and mechanics problems are developed. Various surface-induced phenomena and morphological transitions for solid-solid and solid-liquid phase transformations are presented. Martensitic phase transformations are focused on NiAl. Size-dependence of the melting temperature of Al nanoparticles and temperature-dependence of the width of the molten layer for Al are quantitatively reproduced.

[1] Levitas V. I., Levin V. A., Zingerman K. M., and Freiman E. I., Physical Review Letters, 2009, 103, 025702. [2] Levitas V.I., Preston D.L. Part I&II. Physical Review B, 2002, 66, 134206&134207. [3] Levitas V.I., Preston D.L. and Lee D.-W. Physical Review B, 2003, 68, 134201. [4] Levitas V.I. and Javanbakht M. Physical Review Letters, 2010, 105, 165701. [5] Levitas V.I. and Samani K. Nature Communications, 2011, 2, 284. [6] Levitas V.I. and Javanbakht M. Physical Review Letters, 2011, 107, 175701. [7] Levitas V.I. and Samani K. Physical Review B, Rapid Communication, 2011, 84, 140103(R).

ID: 389

ID: 389

INTERFACIAL EXCESS ENERGY, EXCESS STRESS AND EXCESS STRAIN IN CRYSTALLINE SOLIDS

JIANMIN QU
Northwestern University

Remi Dingreville
USA

Abstract:
In this talk, interfacial excess energy and interfacial excess stress for coherent interfaces in an elastic solid are reformulated within the framework of continuum mechanics. It is shown that the well-known Shuttleworth relationship between the interfacial excess energy and interfacial excess stress is valid only when the interface is free of transverse stresses. To account for the transverse stress, a new relationship is derived between the interfacial excess energy and interfacial excess stress. Dually, the concept of transverse interfacial excess strain is also introduced, and the complementary Shuttleworth equation is derived that relates the interfacial excess energy to the newly introduced transverse interfacial excess strain. This new formulation of interfacial excess stress and excess strain naturally leads to the definition of an in-plane interfacial stiffness tensor, a transverse interfacial compliance tensor, and a coupling tensor that accounts for the Poisson's effect of the interface. These tensors fully describe the elastic behavior of a coherent interface upon deformation. A semi-analytical method to evaluate these tensors based on given inter-atomic potentials is also presented. Size dependent elastic properties of nano-structure elements (particles, wires, films) will be used as examples to illustrate the importance of surface/interface stresses.

ID: 404

Buckliballs: Buckling-Induced Pattern Transformation of Structured Elastic Shells

Katia Bertoldi

Jongmin Shim

Abstract:
We present a class of continuum shell structures, the buckliball, which, undergo a structural transformation induced by buckling under pressure loading. The geometry of the buckliball comprises a spherical shell patterned with a regular array of circular voids. Moreover, we show that the buckling-induced pattern transformation is possible only with five specific hole arrangements. These voids are covered with a thin membrane, thereby making the ball air tight. Beyond a critical internal pressure, the thin ligaments between the voids buckle leading to a cooperative buckling cascade of the skeleton of the ball. Both precision desktop-scale experiments and finite element simulations are used to explore the underlying mechanics in detail and proof of concept of the proposed structures. We find excellent qualitative and quantitative agreement between experiments and simulations. This pattern transformation induced by a mechanical instability opens the possibility for reversible encapsulation, over a wide range of length scales.

ID: 418

In Situ Chemo-mechanics of Electrode Degradation in Lithium Ion Batteries

Ting Zhu
Georgia Tech
USA

Abstract:
Lithium ion batteries (LIBs) are critically important for a wide range of applications, from portable electronics to electric vehicles. However, they cannot meet requirements for demanding applications due to limitations in capacity, rate and cyclability. One leading cause of such limitations is the lithiation/delithiation-induced mechanical degradation of electrodes that results in capacity fading of LIBs. We made in situ observations of deformation and fracture in individual nanowire/nanoparticle electrodes using a nanobattery cell inside a transmission electron microscope. Novel phenomena were discovered, including the size dependent fracture in silicon nanoparticles, anisotropic swelling and self-splitting in silicon nanowires, reversible nanoporosity formation in germanium nanowires during cycling, and cracking in the coatings of tin oxide nanowires. We developed the chemo-mechanics models to reveal the mechanistic origin of failures. The results provide insights into the electrochemically induced microstructural evolution and mechanical degradation in nanomaterial electrodes, with implications for designing the durable electrodes in high-capacity LIBs. This work is a collaboration with Dr. Jianyu Huang at Sandia National Lab.

ID: 426

Forming 3D Nanoscale Filament Assemblies by Elastocapillary Forces

Wei Lu
University of Michigan, Ann Arbor
USA

Zhouzhou Zhao
USA

Abstract:
We report a mechanism by which nanoscale filaments, such as nanotubes, self-assemble into asymmetric aggregates by elastocapillary forces. Specifically, capillary rise of liquid into an asymmetric pattern of vertically aligned filaments causes the filaments to deflect laterally during elastocapillary densification. We quantitatively show that the lateral deflection can be controlled precisely by the pattern shape and the coupling strength among the filaments. We exploit this mechanism to fabricate asymmetric micropillars and multi-directional bridges of densely packed carbon nanotubes. Analogous behavior occurs as biological filaments interact with liquids, and these findings enable scalable fabrication of anisotropic filament assemblies for manipulating surface interactions between solids and liquids.

ID: 451

Mechanics of Serpentine

Nanshu Lu
Department of Aerospace Engineering and Engineering Mechanics
University of Texas at Austin
United States

Thomas Widlund
Arts et Métiers Paristech
51006 Châlons-en-Champagne
France

Abstract
High-performance flexible electronics integrate high-quality inorganic electronic materials such as metal, semiconductor and oxide with polymer substrates. To minimize strains in inorganic materials under large deformation, metals and ceramics can both be patterned into serpentine structures. When the polymer substrate is stretched, the serpentines can rotate and twist to accommodate the applied deformation, resulting in minimized system-level stiffness and greatly reduced strain in the inorganic materials. The choice of the shape of the serpentine depends on systematic study of the geometric variables. This study reveals the effect of serpentine shape on their mechanical behaviors. Different horseshoe and V-shaped serpentines with various ribbon width, arc opening angle and radius, and arm length are investigated. The maximum strain and effective stiffness can be determined through curved beam theories as well as finite element modeling (FEM). Our results conclude that the narrower ribbon, the bigger arc radius and opening angle, and the longer arm length will yield lower strain and effective stiffness. With more specific spacial constraints such as finite breadth or non-overlapped two dimensional mesh, an optimal serpentine shape can be determined from this study.

References

[1] D. S. Gray, J. Tien, C. S. Chen, 2004, *Advanced Materials* 16, 393.
[2] T. Li, Z. Suo, S. P. Lacour, S. Wagner, 2005, *Journal of Materials Research* 20, 3274.
[3] M. Gonzalez, F. Axisa, M. V. Bulcke, D. Brosteaux, B. Vandevelde, J. Vanfleteren, 2008, *Microelectronics Reliability* 48, 825
[4] D.-H. Kim, *et al*, 2008, *Proceedings of the National Academy of Sciences USA* 105, 18675.
[5] D.-H. Kim†, N. Lu†, R. Ghaffari†, *et al*, 2011, *Nature Materials* 10, 316.
[6] D.-H. Kim†, N. Lu†, R. Ma†, *et al*, 2011, *Science* 333, 838.
[7] R. Verplancke, F. Bossuyt, D. Cuypers and J. Vanfleteren, 2011, *J. Micromech. Microeng.* 22, 015002.
[8] J. H. Ahn, J. H. Je, 2012, *J. Phys. D: Appl. Phys.* 45, 103001.
[9] Timoshenko, Theory of elasticity, New York, McGraw-Hill, 1969.

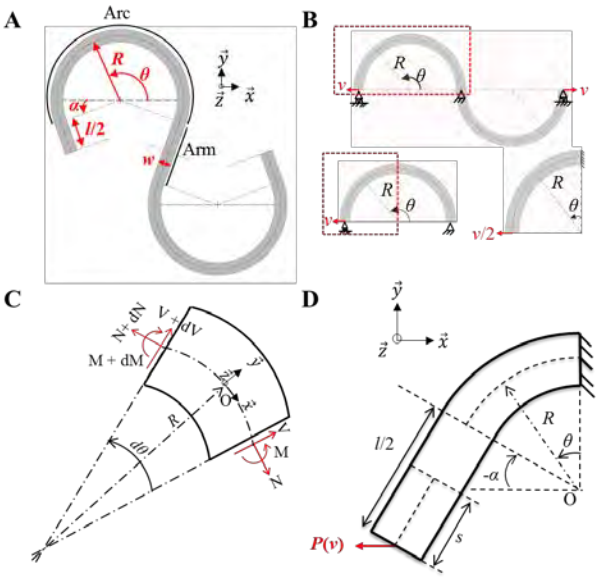

Figure 1 Schematic illustrations of analytical modeling of 2D serpentines. (A) A unit cell of serpentine with an arc of radius R and an arm with a length l. The width of the serpentine ribbon is w. (B) Simplification of the boundary condition of a unit cell taking advantage of the symmetry. (C) Free body diagram of an infinitesimally small segment of a curved beam. N is the normal force, M is the moment and V is the shear force. (D) Schematics of the simplified serpentine cell for the load-displacement relation.

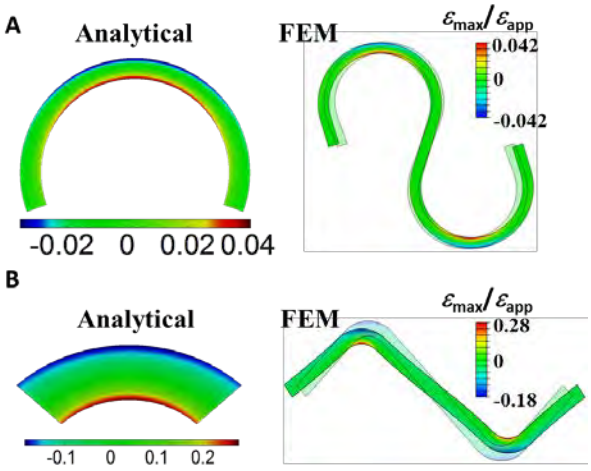

Figure 2 Contour plots of analytical and FEM results of the strain distribution in serpentine. (A) A horseshoe-shaped serpentine with α = 20°, w/R = 1/5 and l/R = 1. (B) A V-shaped serpentine with α = -45°, w/R = 1/2 and l/R = 5. In both shapes, the maximum strain occurs at the center of the inner edge of the arc.

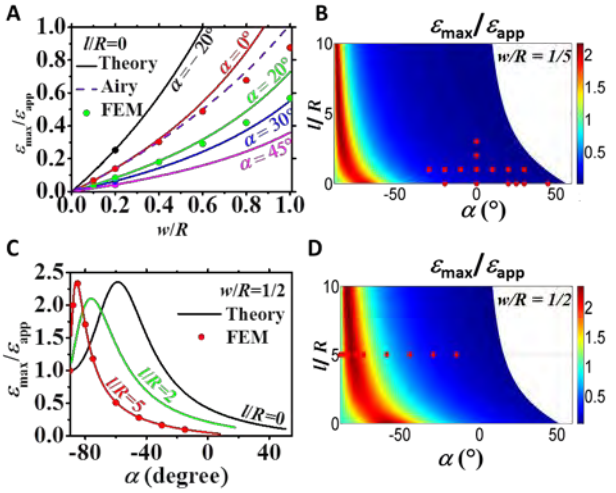

Figure 3 Comparison of analytical and FEM results. (A) Normalized maximum strain as a function of normalized ribbon width for horseshoe-shaped serpentine with different values of α (-20°, 0°, 20°, 30°, 45°) and fixed l/R = 0. (B) At fixed w/R = 1/5, a contour plot of normalized maximum strain value for various α and l/R combinations. (C) Normalized maximum strain as a function of arc angle α for V-shaped serpentine with different values of l/R (5, 2, 0) and fixed w/R = 1/2. (D) At fixed w/R = 1/5, a contour plot of normalized maximum strain value for various α and l/R combinations.

ID: 505

A Combinatorial Nano-Calorimetry Technique to Probe Phase Transformations in Complex Materials Systems

Joost Vlassak
Harvard University
USA

Abstract:
Calorimetric studies of bulk metallic glasses are typically performed at heating or cooling rates smaller than about 102 K/s, because of experimental limitations associated with bulk calorimeters. While faster cooling rates can be attained in uncontrolled quench procedures, the systematic study of glass formation and crystallization kinetics is limited by these experimental capabilities. By employing the thin-film architecture of the parallel nano-scanning calorimeter (PnSC), we perform calorimetric characterization of glass formation, crystallization, and melting with 102 and 104 K/s heating and cooling rates. These experiments are performed over an array of compositions in the glass-forming system Au-Si-Cu. X-ray diffraction (XRD) experiments provide characterization of the crystalline and amorphous components of as a function of quench rate and composition. Combining these XRD results with PnSC enables to decode in an effective manner the complex crystallization of these alloys. More generally, the power of combining these experimental techniques will be discussed not only in the context of materials characterization, but also with regard to the high-throughput probing of glass physics.

ID: 620

Fluctuation Pressure on a Bio-membrane Confined Within a Parabolic Potential Well

L B Freund
University of Illinois
USA

Abstract:
The physical system considered is a homogenous bio-membrane immersed in water. The membrane experiences thermal fluctuation driven by the Brownian motion of water molecules. If motion of the membrane is constrained by a parallel plane or other geometrical feature tending to confine the motion to a region smaller than the range of nature motion, the total free energy of the system increases as the admissible range decreases. This influence, in turn, implies the action of a confining pressure on the membrane. The phenomenon is inherently nonlinear and the dependence of this pressure on degree of confinement has been of interest for some time. Here, we discuss results for the particular case when membrane motion is confined within a resisting parabolic potential, a configuration for which the analysis can be carried through to a conclusion with little ambiguity. The model is described and the influence of various system parameters on the results is discussed.

ID: 654

Strain Engineering of Graphene

Teng Li

Abstract:

The corrugating physics of graphene are closely tied to its electronic, magnetic, optical and phonon properties. The symmetries of the grapheme honeycomb lattice, the atomic origin of many of graphene exceptional properties, are mitigated by corrugation. A local curvature in graphene changes the interatomic distances and angles between chemical bonds, and thus leads to changes in the graphene band structure. Graphene is mechanically durable and amenably flexible, suggesting fertile opportunities to control graphene properties via strain engineering. In this talk, I will discuss our recent work on deformation-induced quantum dot formation and resulting pseudomagetic field in freestanding and substrate-supported graphene.

ID: 727

Thermal Weakening in Seismic Shear of Fluid-Infiltrated Fault Gouge

James Rice
Harvard University
USA

Abstract:

Field observations of maturely slipped faults show that despite a generally broad zone of damage by cracking and granulation, large shear deformation, and therefore heat generation, in individual earthquakes takes place with extreme localization to a zone which may be of order 1 mm or less width within a finely granulated fault core. The presentation outlines recent understanding of such strain localization and associated dynamic weakening in fault gouge undergoing seismic shear, with focus on mechanisms involving thermal pressurization of pore fluid. The fluid may be native groundwater, or may be the result of endothermic decomposition reactions releasing a CO2 or H2O fluid phase under conditions that the fluid and solid products would, at the same p and T, occupy more volume than the parent rock, so that the pore fluid is forced to undergo severe pressure increase. The endothermic nature of the reactions buffers against melting of the solid phase because frictional work is absorbed into enthalpy increase of the reactants. The results, applied to modeling of spontaneous slip ruptures, contribute to showing how major faults can be statically strong yet dynamically weak, and operate under low overall driving stress, in a manner that generates negligible heat and meets major seismic constraints on slip, stress drop, and self-healing rupture mode. Some of the studies reviewed have been done collaboratively with N. Brantut (Univ. Col. London), E. M. Dunham (Stanford), H. Noda (JAMSTEC), J. D. Platt (Harvard), and J. W. Rudnicki (Northwestern).

ID: 783

Strong Dependency of Lithium Diffusion on Mechanical Constraints in High-Capacity Li-ion Battery Electrodes

Y. F. Gao
Georgia Institute of Technology
United States

M. Zhou
Georgia Institute of Technology
United States

Abstract:
Negative electrodes based on amorphous lithium alloys have attracted significant interest because they offer capacities much higher than those of graphite electrodes [1]. However, when guest atoms are inserted into or extracted from these electrodes, the material expands or shrinks by up to ~300% [2], inducing stresses that can cause material cracking [3]. One way to mitigate the problem is to reduce the size of the electrodes. In particular, electrodes made of nano-sized structures such as nanowires (NWs), nanotubes and nanoscale core-shell structures have been shown to be particularly effective in avoiding fracture [4-8].

Besides higher capacity and better cyclability, faster operational charging rate is another important desideratum in battery design. In order to shorten the charging time, it is essential to enhance transport kinetics by optimizing material properties and electrode geometries. Recent experiments by Soni et al. suggest that the overall charging speed of Li/Si is more likely to be limited by diffusion inside the electrode rather than by surface transport, at least for thin films with thickness above 250 nm [9]. However, it is not well understood how mechanical constraints affect the diffusion in alloy-based electrodes, especially when both two-way coupling and large deformation are present.

In this study, we investigate the effect of external constraints on Li diffusion using a fully coupled, finite deformation framework. It is found that thin-film electrodes on rigid substrates suffer from much slower diffusion rates compared with free-standing films (or nano-flakes in some applications) with the same material properties and geometric dimensions. Of particular interest is the surprising finding that mechanical driving forces tend to retard diffusion in thin-film electrodes when lithiation-induced softening is considered. This is in sharp contrast to the fact that mechanical stresses always enhance diffusion when the deformation is in the elastic regime.

The finding that lithium diffusion is very sensitive to external constraint can have profound practical implications. The design of battery electrodes involves tradeoffs among capacity, cyclability and operational charging rate. The main advantage of alloy-based electrodes, especially Li/Si, is their much higher capacity compared with carbon-based electrodes. In terms of cyclability, it has been suggested that plastic flow can be beneficial for Li/Si electrodes

because it relaxes stresses and thus reduces the chance of electrode failure. Our results here, however, indicate that there is another mechanism at work. On one hand, plasticity may help avoid electrode fracture – a mechanism that can be utilized by adopting measures that promote inelastic flow through the tailoring of material properties and changing charging regimen. On the other hand, plasticity may inhibit Li transport, especially under tight mechanical constraint. Under any scenario, designs with less mechanical constraint on the electrodes are desirable because mechanical constraints diminishes stress-enhanced diffusion (SED) and magnifies the deleterious effect of plasticity and concentration-induced softening on Li transport. Because of these reasons, even in terms of operational charging rate alone, Li/Si nano-particles (e.g. nanospheres, nanoflakes, nanowires and nanotubes) are superior to Li/Si thin films or bulk materials. The results in this paper provide further support for nano-particles as building blocks for next-generation alloy-based electrodes.

1. Zhang, W.J., *A review of the electrochemical performance of alloy anodes for lithium-ion batteries.* Journal of Power Sources, 2011. **196**(1): p. 13-24.
2. Beaulieu, L.Y., et al., *Colossal reversible volume changes in lithium alloys.* Electrochemical and Solid State Letters, 2001. **4**(9): p. A137-A140.
3. Christensen, J. and J. Newman, *Stress generation and fracture in lithium insertion materials.* Journal of Solid State Electrochemistry, 2006. **10**(5): p. 293-319.
4. Chan, C.K., et al., *High-performance lithium battery anodes using silicon nanowires.* Nature Nanotechnology, 2008. **3**(1): p. 31-35.
5. Cui, L.F., et al., *Crystalline-Amorphous Core-Shell Silicon Nanowires for High Capacity and High Current Battery Electrodes.* Nano Letters, 2009. **9**(1): p. 491-495.
6. Song, T., et al., *Arrays of Sealed Silicon Nanotubes As Anodes for Lithium Ion Batteries.* Nano Letters, 2010. **10**(5): p. 1710-1716.
7. Magasinski, A., et al., *High-performance lithium-ion anodes using a hierarchical bottom-up approach.* Nature Materials, 2010. **9**(4): p. 353-358.
8. Hu, L., et al., *Silicon-Carbon Nanotube Coaxial Sponge as Li-Ion Anodes with High Areal Capacity.* Advanced Energy Materials, 2011: p. 523-527.
9. Soni, S., et al., *Thickness effects on the lithiation of amorphous silicon thin films.* Scripta Materialia, 2011. **64**(4): p. 307-310.

I.2

Awards Symposium - SES Medal (K.-S. Kim)

ID: 135

Multifunctional Crumpling and Unfolding of Large-Area Graphene

ZANG, Jianfeng
Soft Active Materials Laboratory, Department of Mechanical Engineering and Materials Science, Duke University, USA

WANG, Qiming
Soft Active Materials Laboratory, Department of Mechanical Engineering and Materials Science, Duke University, USA

TU, Qing
Soft Active Materials Laboratory, Department of Mechanical Engineering and Materials Science, Duke University, USA

RYU, Seunghwa
Laboratory for Atomistic and Molecular Mechanics, Department of Civil and Environmental Engineering, Massachusetts Institute of Technology, USA

BUEHLER, Markus J.
Laboratory for Atomistic and Molecular Mechanics, Department of Civil and Environmental Engineering, Massachusetts Institute of Technology, USA

PUGNO, Nicola
Laboratory of Bio-Inspired Nanomechanics, Department of Structural, Geotechnical and Building Engineering, Politecnico di Torino, Italy

ZHAO, Xuanhe
Laboratory of Bio-Inspired Nanomechanics, Department of Structural, Geotechnical and Building Engineering, Politecnico di Torino, Italy

Abstract:
Crumpled graphene films of atomic thickness are used in diverse applications including electronics, energy storage, composites, and biomedicine. While it is known that the degree of crumpling strongly affects the properties of graphene and the performance of graphene-based devices and materials, in existing technology it is not possible to fold and unfold crumpled graphene films in a controlled manner. Here we present a new approach, investigated by joint experiment, atomistic simulation and theory, to control reversible crumpling and unfolding of

large-area graphene, achieved by harnessing mechanical instabilities of graphene adhered on highly pre-strained polymer substrate. By relaxing the pre-strain in the substrate in a particular order, we crumple graphene films into tailored self-organized hierarchical structures that mimic super-hydrophobic leaves. The degree of crumpling in graphene is controlled by stretching/relaxing the substrate. The reversible crumpling and unfolding of graphene films enables us to fabricate large-area conductive coatings and electrodes capable of giant stretchability (over 450%), high transparency (up to 80%), super-hydrophobicity, and tunable wettability. We further demonstrate the use of novel graphene-polymer laminates as artificial muscles.

ID: 138

Mechanics of Reversible Adhesion

Yonggang Huang
Northwestern University
USA

Abstract:
By pressure-controlled surface contact area, reversible adhesion can be achieved with strengths tunable by 3 orders of magnitude. This capability facilitates robust transfer printing of active materials and devices onto any surface for the development of stretchable and/or curvilinear electronics. The most important parameter in designing the surfaces of stamps for this process is the height of the microtips relief: tall microtips may fail to pick up electronics from their growth substrate, while short ones may fail to print electronics on the receiver substrate. Mechanics models are developed to determine the range of the microtip height for successful transfer printing. Analytical expressions for the minimum and maximum heights are obtained, which are very useful for stamp design.

ID: 202

Damage Amplification Due to Interacting Microcracks

Xanthippi Markenscoff
University of California
USA

Cristian Dascalu

Abstract:
The singular stress amplification in the ligament between holes and nearby cracks is obtained as a function of the ligament thickness , either by asymptotic analysis of the full solution or by matched inner and outer expansions, with the inner region behaving as a beam. This asymptotic solution allows the study of the effect of micro-defect interaction on the homogenized coefficients of a two-scale damage model of periodic microstructure, with cells containing pairs of interacting microcrack separated by a thin ligament. The damage model that results from energy-release rate based microcrack propagation laws exhibits damage acceleration due to the singular interaction of the microcracks. The local macroscopic response expresses the collective coalescence of a periodic microstructure with interacting microcracks. For infinitely small ligaments, the macroscopic damage energy-release rate becomes infinite as 1 over the square root of the distance between the near-by tips of the microcracks. This leads to damage amplification as the result of the interaction of microcracks

ID: 271

A Peierls Perspective on Mechanisms of Atomic Friction and Stick-Slip Behavior

Yanfei Gao
University of Tennessee
USA

Abstract:
For well-defined contacts with sizes less than hundreds of nanometers, the friction force-displacement curves are characterized by the stick-slip behavior, which are very sensitive to surface atomic structure, lattice mismatch or incommensurability, sliding velocity, surrounding temperature, to name a few. While the stick-slip behavior can be modeled by the one-degree-of-freedom Tomlinson model, it cannot explain the role of lattice structure and interface defects. Molecular simulations, on the other hand, suffer the temporal limitations and thus have difficulties in modeling the dependence on velocity and temperature. Motivated by the Hurtado-Kim model, a Peierls-type model is developed in this work which views the sliding process as the initiation and gliding passage of interface dislocations with diffused cores. The dependence of the friction behavior on the contact size is naturally due to the introduction of the dislocation core size. The spatially inhomogeneous nature of rate-limiting processes is successfully determined, from which a quantitative comparison to the thermally activated friction behavior can be made. While the model predicts the structural lubricity for nearly commensurate surfaces, it fails to model interfaces that cannot be modeled by regular dislocation networks, or that are amorphous. Predictions here are compared to the Hurtdo-Kim work which used the Volterra dislocation model.

ID: 382

Fracture Behaviors of Metal Nanowires: Ductile or Brittle?

Jun Lou
Rice University
USA

Abstract:
This talk presents some of our recent efforts to study the fracture behaviors of metallic nanowires. In the first example, in situ uni-axial tensile tests of single crystalline copper nanowires were performed using a micro mechanical device inside a SEM chamber. Interestingly, both ductile and brittle-like fracture modes were found in the same batch of fabricated nanowires and the fracture modes appeared to be dependent on diameters of tested nanowires. From the analysis of fracture surfaces, sample morphologies and corresponding stress-strain curves, the competition between deformation and fracture mechanisms controlled by initial defects density and by the probability of dislocation interactions was attributed to this intriguing size dependent fracture modes transition. In the second example, we showed that, under uni-axial tensile loading, single crystalline ultrathin gold nanowires might also fracture in two modes, displaying distinctively different fracture morphologies and ductility. In situ HRTEM study suggested that the unexpected brittle-like fracture was closely related to the observed twin structures, which is very different from surface dislocation nucleation/propagation mediated mechanism in ductile fracture mode. Molecular dynamics (MD) simulations further revealed the processes of shear-induced twin formation and damage initiation at the twin structure/free surface interface, confirming the experimentally observed differences in fracture morphology and ductility.

ID: 433

Scale Bridging of Ageing Effect in Rate-and-State Friction

Qunyang Li
Tsinghua University

Terry Tullis

Abstract:
When most rock materials are held in stationary contact, the static friction grows with time. Known as frictional ageing, this behavior is critical for understanding earthquake phenomenon, specifically the evolution effect long discussed in the phenomenological (but highly successful) model of rate-and-state friction. Recently, our experiments reveal that at relatively low contact stresses in a well-defined single-asperity contact, a chemical mechanism is indeed at play in the ageing phenomenon. However, the ageing we observe at the nanoscale has a much larger magnitude than the macroscopic case. We demonstrate with a discrete asperity mechanics model that the large magnitude is in fact required to reconcile single-asperity behavior with ageing in macroscopic, multi-asperity interfaces. Understanding the mechanism and the scale effect underlying the evolution effect would allow formulation of more physically-based frictional constitutive laws, and more confident extrapolation to natural faults for understanding earthquakes and other time-dependent friction phenomena in general.

ID: 527

Stability of Peeling for Adhesive Tapes

Guruswami Ravichandran
California Institute of Technology

Christopher Kovalchick

Abstract:
A new experimental configuration has been developed to investigate the stability of peeling for adhesive tapes. The experimental method allows for independently varying the applied loading and the stiffness of the system. The role of various parameters including the compliance of the loading system and geometry of the film on the stability of peeling is investigated. The stiffness of the system is varied by altering the magnitude and direction of the applied load during an experiment. This change in stiffness can be tuned to trigger or delay the onset of instability. Theoretical stability criteria are also presented to develop insights into the role of various parameters investigated experimentally.

ID: 560

CANTILEVER DEFLECTION ASSOCIATED WITH HYBRIDIZATION OF MONOMOLECULAR DNA FILM

Pranav Shrotriya
Iowa State University
USA

Yue Zhao
USA

Abstract:

Recent experiments show that specific binding between a ligand and surface immobilized receptor such as hybridization of single stranded DNA immobilized on a microcantilever surface leads to cantilever deflection. To understand the mechanism underlying the cantilever deflections, a theoretical model that incorporates the influence of ligand/receptor complex surface distribution and empirical interchain potential is developed to predict the binding induced deflections. The cantilever bending induced due to hybridization of DNA strands is predicted for different receptor immobilization densities, hybridization efficiencies and spatial arrangements. Predicted deflections are compared with experimental reports to validate the modeling assumptions and identify the influence of various components on mechanical deformation. Comparison of numerical predictions and experimental results suggest that at high immobilization densities, hybridization induced mechanical deformation is determined primarily by immobilization density and hybridization efficiency whereas at lower immobilization densities, spatial arrangement of hybridized chains need to be considered in determining the cantilever deflection.

ID: 569

Size Dependent Mechanical Behavior at Nanoscale

Junlan Wang
University of Washington
USA

Abstract:
With the rapid advances in microelectronics and semiconductor industry, structures and devices are becoming smaller and smaller. When metals are scaled down from tens of micron to a fraction of a micron, their mechanical properties display a strong size-dependence when deformed into the plastic range. This phenomenon has motivated a large effort in the mechanics and materials communities to develop both experiments and simulation to investigate the size-dependent material behavior at small scales. In this talk, I will discuss several size dependent behaviors of materials we studied in various metallic systems, including the contact compression of nano and microscale pyramid structures on single crystal gold surfaces and the mechanical properties of multilayer thin films. We show that when the characteristic size of the pyramids or thickness of the individual film layer is in the nanometer scale, significant size dependence can be observed in the strength of the materials.

ID: 615

Modeling of Ductile Fracture Roughness

Alan Needleman
University of North Texas

Abstract:
Experimental observations have shown that the roughness of fracture surfaces exhibits certain characteristic scaling properties. Here, ductile crack growth under mode I plane strain, small scale yielding conditions is analyzed. Although overall plane strain loading conditions are prescribed, full 3D analyses are carried out to permit modeling of a three dimensional material microstructure and of the resulting three dimensional stress and deformation states that develop in the fracture process region. An elastic-viscoplastic constitutive relation for a progressively cavitating plastic solid is used to model the material. Two populations of void nucleating second phase particles are represented, large inclusions with low strength, which result in large voids near the crack tip at an early stage, and small second phase particles, which require large strains before cavities nucleate. The larger inclusions are represented discretely. One question of interest concerns the extent, if any, to which the scaling properties of ductile fracture surfaces depend on material properties such as flow strength, strain hardening and strain rate hardening. Predictions for the fracture surface roughness will be presented with a particular focus on the dependence on material propertt values. The computational results are discussed in light of experimental observations. This is joint work with V. Tvergaard of the Technical University of Denmark, E. Bouchaud of ESPCI Paris Tech, and Y. Cao and L. Ponson of Université Pierre et Marie Curie.

ID: 619

The Forces Driving Self-assembly of Three-Dimensional Micro-Tissues

L B Freund
University of Illinois
USA

Jacquelyn Youssef
USA

Abstract:
In a nonadhesive environment, cells will self-assemble into micro-tissues, a process relevant to tissue engineering. Although this has been recognized for some time, there is no basis for quantitative characterization of this complex process. Here we describe a recently developed assay designed to quantify aspects of the process and discuss its application in comparing behaviors between cell types. Cells were seeded in wells of nonadhesive material, each well with a circular trough at its base formed by the cylindrical sidewalls and by a central peg in the form of a right circular cone. Cells settled into the trough and coalesced into a toroid, which was then driven up the conical peg by the forces of self-assembly. Whereas the driving force for self-assembly has often been viewed as the binding of surface proteins, these data show that cellular contraction is important for cell adhesion.

Missing Abstract

ID: 629

ID: 728

Rate Effects in Frictional Slip , Ill-Posedness, its Resolution, and Consequences for Slip-Rupture Dynamics

James Rice
Harvard University
USA

Abstract:
Friction between solids in contact often weakens with increasing slip rate and such is widely understood, in studies of the sliding of solids that are treated as rigid blocks, to lead to stick-slip instabilities. However, real solids are elastically deformable. When we consider that in formulating mathematical models of the sliding process, and we try to impose interfacial conditions for which the shear traction, at a fixed compressive normal traction, is a function of only the slip rate, and weakens with increasing rate, we find that such models are either ill-posed (short wavelength divergence) or acausal (disturbances move along the interface faster than the fastest body wave speed). In the case of elastically dissimilar solids in sliding contact, we find that problems of sliding contact are often ill-posed even if the friction coefficient has no variation whatever with slip rate. The presentation reviews how these deficiencies are removed when we adopt "rate and state" friction concepts, and why the underlying concepts are consistent with realistic descriptions of processes at microscopic asperity contacts. Working in that framework, it examines the connection between assumed frictional slip laws and modes of rupture propagation, focused on models of earth faulting, especially on conditions for formation of self-healing slip pulses, and on the rich faulting phenomena which result along dissimilar material interfaces due to coupling between slippage and normal stress alteration.

ID: 740

Role of Surface Roughness in Hysteresis During Adhesive Elastic Contact

Haneesh Kesari
Brown University

Joseph Doll

Abstract:
In experiments that involve contact with adhesion between two surfaces, as found in atomic force microscopy or nanoindentation, two distinct contact force (P) vs. indentation-depth (h) curves are often measured depending on whether the indenter moves towards or away from the sample. The origin of this hysteresis is not well understood and is often attributed to moisture, plasticity or viscoelasticity. We present experiments [1] and continuum mechanics models [2] that will show that hysteresis can exist without these effects, and that its magnitude depends on surface roughness. We explain the observed hysteresis as the smeared out effect of a large series of surface instabilities that are induced by the surface roughness and adhesion. These instabilities cause the size of the nominal contact region to be significantly different during the loading and the unloading phases of the contact experiment. We also demonstrate that when this is the case material properties can be estimated uniquely from contact experiments even when the measured P-h curves are not unique. The hysteresis energy loss during contact is also a measure of the adhesive toughness of the contact interface. We show experimentally that roughness can both increase and decrease the adhesive toughness of the contact interface. We show through numerical simulation of continuum adhesive contact models that the contact interface is optimally tough at conditions at which the contact region is at the cusp of the transition at which it turns from being mostly simply connected to being predominantly multiply connected. This insight is useful in increasing an interface toughness by modifying its small scale structure through microfabrication techniques.

References [1] H. Kesari, J. Doll, W. Cai, B. Pruitt, and A. Lew. Role of surface roughness in hysteresis during adhesive elastic contact. Philosophical Magazine Letters, 90(12):891–902, 2010. [2] H. Kesari and A. J. Lew. Effective macroscopic adhesive contact behavior induced by small surface roughness. Journal of the Mechanics and Physics of Solids, 59:2488-2510, 2011.

ID: 749

Dynamic Stress Measurements and Friction Investigations within the Slip Zone of a Supershear Rupture

Michael Mello
Georgia Institute of Technology
United States

Ares J. Rosakis
California Institute of Technology
United States

Harsha S. Bhat
Institut de Physique du globe de Paris (IPG)
France

Abstract:
The compressive and shear stress distributions arising from the passage of a supershear rupture are inferred from the continuous fault-normal (FN) and fault-parallel (FP) particle velocity records obtained at the frictional fault in a dynamic rupture experiment. The experimental arrangement features two interferometer probe beams focused within 100 − 200μm of the H-100 frictional interface as depicted in Figure 1. Stress-velocity relationships gleaned from the general 2D steady-state supershear solution (Dunham and Archuleta, 2005) relate the near-fault particle velocity records to the evolution of the dynamic stress components σ_{xx} and σ_{xy} at the specimen interface. Dynamic stress measurements also require knowledge of the elastic wave speeds (C_s, C_p), density (ρ), and shear modulus (μ) of the test specimen, along with an accurate estimate of the supershear rupture speed (V_r). Each of these physical variables (apart from the

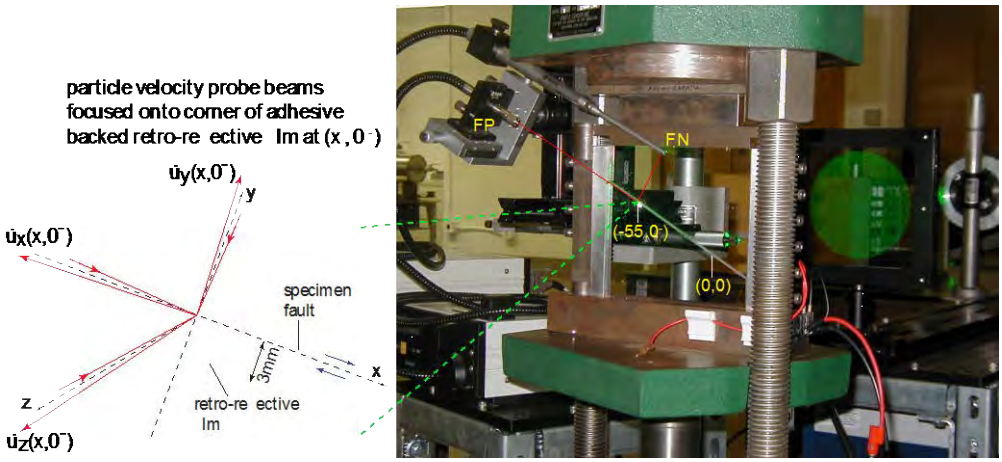

Figure 1. Experimental configuration used for simultaneous measurement of fault-normal and fault-parallel particle velocity measurements at a near-fault measurement station.

density of H-100) is accurately estimated in each experiment through the analysis of synchronized, high-speed photoelastic images.

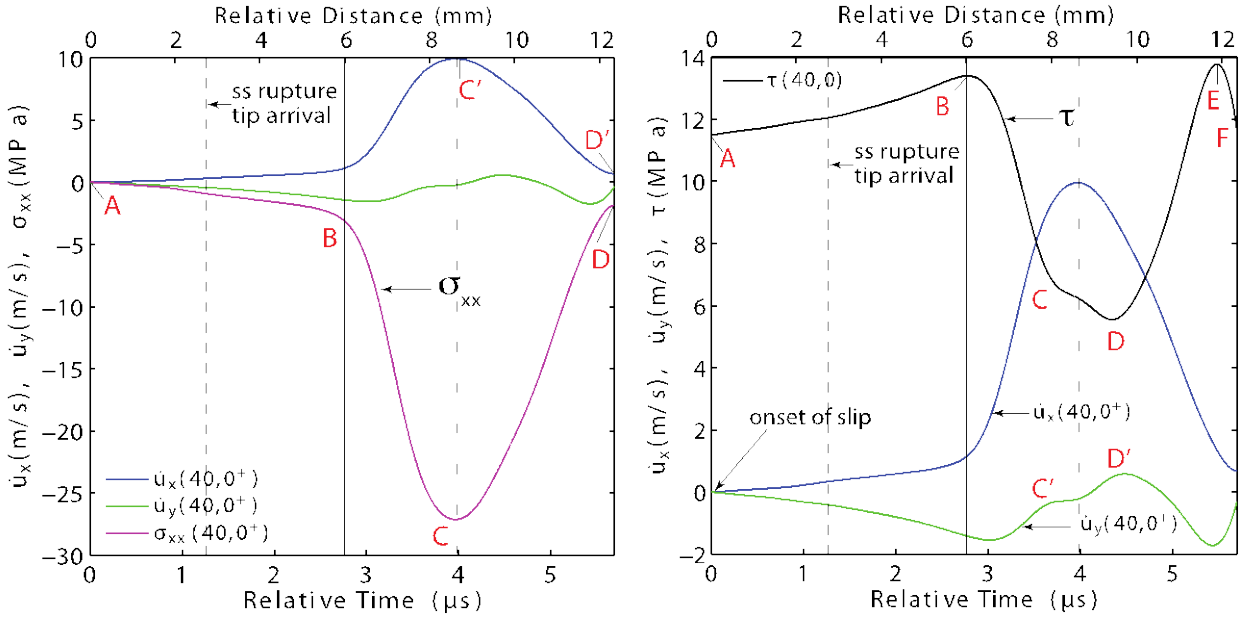

Figure 2. Particle velocity records from a superhsear slip-pulse accompanied by the inferred stress-pulse components σ_{xx} and τ.

Dynamic stress relationships were applied to a subset of near-fault particle velocity measurements obtained using the (FN,FP) laser interferometer configuration depicted in figure 1. Dynamic stress measurements obtained from representative supershear experiments are presented and discussed. Figure 2 depicts the near-fault particle velocity records corresponding to a supershear slip-pulse obtained from a laboratory earthquake experiment. Dynamic stress components inferred from these records are also plotted in the same figure.

The measurement of the shear stress distribution $\tau(x)$ within the supershear slip zone, coupled with an independent measurement of the resolved (static) normal and shear tractions imposed upon the fault, also enables the characterization of the dynamic coefficient f_d. Frictional faulting relationships such as the variation of $\tau(x)$ (or f_d) with the accumulated slip, or its dependency upon the rate of slip, are therefore also directly inferred from the near-fault particle velocity measurements using the proposed stress-velocity relationships.

REFERENCES

A.J. Rosakis, K. W. Xia, G. Lykotrafitis, and H. Kanamori. Treatise in Geophysics, volume 4, Dynamic shear rupture in frictional interfaces: speeds, directionality and modes, pages 153–192. Elsevier, 2007.

E. M. Dunham and R. J. Archuleta. Near-source ground motion from steady state dynamic rupture pulses. Geophys. Res. Lett., 32, Feb 2005.

ID: 767

Study of Ultra-thin Films Mechanical Integrity by Combined Nano-Indentation and Nano-Acoustic Emission

Ashraf Bastawros
Iowa State University

Wei Hong

Abstract:
NO ABSTRACT

ID: 813

Diffraction Assisted Image Correlation (DAIC) for Three-Dimensional Deformation and Profile Measurement

Shuman Xia
Georgia Institute of Technology
USA

Alexandra Gdoutou
USA

Abstract:
Digital Image Correlation (DIC) has emerged as a popular optical technique for full-field mechanical characterization. A classical three-dimensional (3D) DIC arrangement requires stereo imaging with two cameras, which is difficult to implement for dynamic or small-scale measurement. In this talk, we will present the recently developed Diffraction Assisted Image Correlation (DAIC) method for 3D surface displacement and profile measurement. By utilizing a transmission grating to obtain multiple-angle views of a test specimen, the DAIC method provides a simple and yet effective solution to 3D displacement and profile characterization with only a single camera and 2D-DIC algorithm. The validity and accuracy of the DAIC method will be demonstrated through a set of case studies.

ID: 142

Atomistic Mechanical Testing of Nanostructures – Seeing the Invisible and Bridging Theory and Experiments

Horacio Espinosa
Department of Mechanical Engineering
Northwestern University
USA

Abstract:
Recently there has been a major thrust to develop novel nanomaterials exhibiting unique electro-mechanical properties. These nanostructures are envisioned as building blocks for the next generation of electronic and energy harvesting systems. In this context, identification of size dependent properties is essential. Here, a MEMS-based device for in-situ electron microscopy testing of one dimensional nanostructures will be introduced and used to identify mechanical property size effects in ZnO and GaN nanowires. The validity of force fields commonly used to model these semiconducting materials will be discussed by comparison to experimental findings and quantum mechanical simulations. It will be shown that force fields are accurate enough to capture elasticity but that higher order theories are needed to interpret nanowire failure. Furthermore, while both ZnO and GaN possess the same crystal structure, they exhibit quite different elastic and piezoelectric size dependences. Opportunities arising from such size effects in energy harvesting applications will be given as conclusion.

ID: 799

Towards Molecularly Informed Traction-Separation Relations

S. R. Na
Aerospace Engineering and Engineering Mechanics, UT Austin, Austin, TX 78712

K. M. Liechti
Engineering and Engineering Mechanics, UT Austin, Austin, TX

T. Peixoto
Materials Science & Engineering, UT Dallas, Dallas, TX 75080

O. Seitz
Materials Science & Engineering, UT Dallas, Dallas, TX 75080

Y.J. Chabal
Materials Science & Engineering, UT Dallas, Dallas, TX 75080

ABSTRACT:

The paper describes the development of an experiment with associated analysis to determine the adhesive interactions between Si (111) surfaces which were coated with amine and carboxy-terminated self-assembled monolayers (SAMs). The silicon beams were pressed together to form miniature laminated beam specimens which were then separated using a specially developed high vacuum fracture tester. The deposition of the SAMs and associated spectroscopic, scanning probe and ellipsometric diagnostics are described. The delaminations between the silicon strips and the associated normal crack opening displacements (NCOD) were measured via infra-red crack opening interferometry. This, coupled with fracture analyses allowed the traction-separation relation associated with amine/carboxyl interactions to be determined. There were notable differences in the traction-separation relations under mode 1 and mixed-mode conditions. This suggests that the intrinsic toughness at the molecular level depends on the fracture mode thereby motivating some molecular level analyses.

ID: 803

The Secret Lives of Twins

K.T. Ramesh
Department of Mechanical Engineering,
The Johns Hopkins University
USA

Abstract:
We examine the dynamics of deformation twins in metallic materials using a combination of fundamental experiments, theoretical modeling and focused molecular dynamics and crystal plasticity simulations. Three basic crystal structures are considered: face-centered-cubic (aluminum, copper and nickel), body-centered-cubic (tantalum) and hexagonal-close-packed (magnesium). The experimental methods used include high-strain-rate and wave propagation experiments in Kolsky bars and plate impact, coupled with microscale characterization of recovered samples using EBSD and TEM. These methods are used to obtain estimates of twin boundary velocities and twin growth rates as a function of the applied stress under multiaxial stress states. Computational estimates of twin boundary kinetics are then derived from molecular dynamics simulations, and these estimates are compared to the experimental measures and to theoretical limits based on assumed twin growth mechanisms. Finally, the implications of the measured boundary velocities are considered for some extreme dynamic loading conditions.

I.3

Awards Symposium - Eringen Medal (David Barnett)

ID: 128

Efficient Methods to Take into Account the Fluid Lag in Hydraulic Fracturing Simulations through a Variational Inequality Formulation

Yongxing Shen
Universitat Politecnica de Catalunya

Abstract:
We study the fluid-structure interaction encountered in hydraulic fracturing. Simulating this process needs to take into account the interaction between a fracturing solid and the fluid flow in the crack. In particular, with the possible presence of a fluid lag, the evolving fluid front inside the crack and the crack front (crack tip if in 2D) are constrained by a Kuhn-Tucker complementarity condition, similar to the case of contact mechanics. Brute-force methods to keep track of both fronts usually require the use of a costly prediction-correction scheme.

In this presentation, we formulate this coupled problem in which the Kuhn-Tucker condition is accommodated through a variational inequality with respect to the liquid pressure. The resulted numerical methods (finite element method or displacement discontinuity method for the solid): (a) allow modeling the evolution of both fronts with a resolution consistent with the mesh size, and (b) eliminate the need of explicitly tracking the fluid front which leads to substantial saving in computational cost.

Numerical examples with a fixed fracture and a propagating fracture are used to verify the proposed methods

ID: 153

Atomistic Simulations and Modeling of Plastic Deformation and Fracture in Nanotwinned Metals

Huajian Gao
Brown University
USA

Xiaoyan Li

Abstract:
The rapid development of synthesis and characterization of nanostructured materials as well as unprecedented computational power have brought forth a new era of materials research in which experiments, simulation and modeling are performed side by side to probe the mechanical properties of nanostructured materials [1,2]. This talk will present some recent studies on plastic deformation and fracture mechanisms in hierarchical nanotwinned metals. In contrast to conventional metals where there is plenty of space for dislocations to multiply so that the strength of material is often controlled by dislocations interaction with grain boundaries (Hall-Petch strengthening) and other obstacles, in nanotwinned metals there are plenty of dislocation nucleation sites while dislocation motion is not confined, and the twin boundaries can be significantly toughened by interaction with dislocations. Atomistic simulations reveal a number of interesting features of plastic deformation and fracture mechanisms in such materials

ID: 203

The effective mass of moving dislocations and strip inclusions

Xanthippi Markenscoff
University of California
USA

Luqun Ni
USA

Abstract:
Dislocations moving in accelerating motion have "effective mass", or self-force", associated with the acceleration multiplying a logarithmic singularity of the near field. (It may be noted that the acceleration involves a second drivative with respect to time, while, in static loops, the logarithmic singularity is associated with the curvature -- involving a second derivative with respect to a space variable--, Gavazza and Barnett, 1976). Self-forces on expanding inclusions are also analyzed, and it is found that, while the moving plane phase boundary with transformation strain (eigenstrain) does not have an effective mass in accelerating motion (since the self-force depends only on the velocity), the accelerating strip inclusion boundary does.

ID: 229

Dislocation Mechanisms of the Ultrasonic Nonlinearity Parameter in Crystalline Solids

Wei Cai
Stanford University

William Cash
USA

Abstract:
Fatigue is a prevalent failure mechanism of metals caused by progressive damage resulting from repeated stressing. Traditional detection techniques require costly inspections for the presence of macrocracks. Advances in the field of nonlinear ultrasonics are enabling researchers to monitor in-situ the fatigue damage associated with evolution of microstructures. The acoustic nonlinearity parameter beta is known to progressively grow in magnitude from the earliest cycles of fatigue. Unfortunately, the dislocation mechanisms giving rise to this increase are not well understood. An orientation-dependent line energy model of beta arising from a pinned dislocation monopole bowing out in its glide plane is developed using a quasi-static loading assumption. A strong dependence on Poisson's ratio and the orientation of the Burger's vector relative to the initial line direction is found to be missing in the currently accepted model. Discrete dislocation dynamics (DD) simulations are then used for the first time to predict beta and compared with the model. The results are shown to agree over a range of material properties and local stresses. The techniques are then extended to the long-range interactions between straight dislocations to better understand fatigue microstructures. An analytic model of an isolated dislocation dipole is derived and beta is predicted to be primarily dependent on the residual glide stress acting on the dipole, which has not been predicted before. Beta of mutlipolar interactions in an infinite dipole train and an infinite Taylor lattice is shown arise only under the presence of a residual glide stress and not a simple aggregation of dipoles as previously predicted. Agreement with two-dimensional DD simulations is shown for glide stresses well below the critical stress that causes dissolution of the dipole structure. Finally, several finite sections of the Taylor lattice are modeled with DD and are found to have anomalous scaling behaviors.

ID: 236

Mechanics of Failure of Nanostructured Silicon Electrodes for Lithium Ion Batteries

William Nix
Stanford University

Seok Woo Lee

Abstract:
From surface hardening of steels to doping of semiconductors, atomic insertion in solids plays an important role in modifying the chemical and mechanical properties of materials. The insertion of lithium into silicon electrodes for high capacity lithium-ion batteries provides an extreme example of atomic insertion, with a volume expansion of more than 400%, which can result in crumbling of the electrodes. Silicon nanostructures have proven to be attractive candidates for electrodes because they provide less constraint on the volume changes that occur and more resistance to fracture during lithium insertion. Here, we consider the fracture of Si nanopillars during lithiation and find surprising results. We find that fracture is initiated at the surfaces of the nanopillars and not in the interior, as had been predicted by analyses based on diffusion-induced stresses. We also show that the expansion of the nanopillars is highly anisotropic and that the fracture locations are also anisotropic. We find a critical fracture diameter of about 300nm that appears to depend on the electrochemical reaction rate. Some attempts to model and understand these results will be described.

ID: 243

Discussion of Crack-tip Conditions in Linear Elasticity with First-Order Surface Effects

Peter Schiavone

Abstract:
We examine the role of crack-tip conditions in the reduction of stress at a crack-tip in a theory of linear elasticity with surface effects. in both plane and anti-plane elasticity. In particular, we show that the necessary and sufficient conditions for bounded stresses at a crack tip cannot be satisfied with a first-order (curvature-independent) theory of surface effects which leads, at most, to the reduction of the classical strong square root singularity to a weaker logarithmic singularity.

ID: 259

Eshelby Twist: Lots of Dislocations and Short Wires

Christopher Weinberger
Sandia National Laboratories

Wei Cai

Abstract:
Eshelby noted in 1953 that a screw dislocation lying along the axis of a rod is a metastable state in a crystal and provides a plastic twist. In this talk, his original development is extended to an arbitrary number of dislocations. The organization of these dislocations is similar in some respects to point charges on a disk. The energy of distributions of these dislocations is computed as well as the plastic twist, providing an energy-twist relationship similar to grain boundaries. The torque-twist curves of wires whose plasticity is dominated by these dislocations is also simulated using discrete dislocation dynamics and compared to similar results obtained from molecular dynamics simulations. Finally, we revisit the problem of the twist in a wire that is not infinitely long and examine the limits of the twist per unit length as a function of its length. These results are also compared to molecular statics calculations.

ID: 268

Dislocation Entrapment and Plasticity in Nano-sized Cu pillars Coated with Atomic Layer Deposited (ALD) TiO2.

Julia Greer
Caltech
USA

Andrew Jennings
USA

Abstract:

Investigations into the size-dependent strength of single-crystalline nano-pillars suggest that free surfaces play an important role by serving as dislocation annihilation sites and by enabling nucleation of new dislocations. Here we study the effect of ~5-15 nm-thick, ALD-deposited conformal Al2O3/TiO2 coatings on the mechanical response of single crystalline Cu nano-pillars and the related, fundamental problem of dislocation confinement at the nano-scale. We observe that passivated pillars show an increased failure strength, smoother stress-strain curves, and Bauschinger effect-like hysteresis upon unloading/reloading as compared with the uncoated samples. In contrast to as-fabricated pillars, TEM images of post-mortem coated pillars reveal distinct dislocation patterns confirming the coatings role in confining dislocations and causing them to pile-up at the interface. We present a fundamental model, based on classical dislocation theory that suggests a possible mechanism whereby these dislocation pileups account for the observed increased strength.

ID: 469

Multiscale Mechanics of High-Performance Carbon Nanotube Fibers

Horacio D. Espinosa
Northwestern University
United States

Abstract:
Investigation of the mechanics of natural materials such as spider silk, abalone shells, and bone, provide great insight into the design of materials that can simultaneously achieve high specific strength and toughness. Research has shown that their emergent mechanical properties are owed in part to their specific self-organization in hierarchical molecular structures, from nanoscale to macroscale, as well as their mixing and bonding. Following this inspiration, we have addressed the design of carbon nanotube (CNT) based fibers and yarns by applying lessons learned from mulitscale experiments and simulations across multiple length scales. Carbon nanotubes (CNTs) are envisioned to be ideal building blocks in hierarchical macroscopic composite fibers due to their extraordinary strength and stiffness. Macroscopic materials based on CNTs, however, have been limited by weak shear interfaces between adjacent CNT shells and matrix elements [1]. Initial studies have demonstrated that double-walled CNTs (DWNT) are very attractive building blocks for macroscopic high CNT density fibers [2]. Here we present experimental and computational studies at different length scales of hierarchical DWNT yarns that have furthered the understanding of numerous key mechanical mechanisms that contribute to the ultimate behavior of CNT yarns.

At the individual bundle level, we have studied the shear behavior within DWNT bundles through in-situ SEM/TEM mechanical testing coupled with Molecular Mechanics (MM) and Density Functional Theory (DFT) modeling. In-situ SEM pullout experiments conducted on DWNT bundles revealed the typical sword-in-sheath failure mechanism and allowed quantification of the force required to shear a small inner bundle of DWNTs out of an outer sheath of DWNTs [3]. In this study, a normalized pullout force of 1.7 +/- 1.0 nN per CNT-CNT interaction was measured for the sliding of a smaller inner bundle of DWNTs out of a larger outer shell of DWNTs. Through comparison with MM and DFT simulations of sliding between adjacent CNTs in bundles, it was identified that factors contributing to the pullout force include the creation of new CNT surfaces, carbonyl functional groups terminating the free ends, corrugation of the CNT-CNT interaction, and polygonilization of the CNTs in the bundle. In addition, a top-down analysis of the experimental results revealed that greater than one half of the pullout force was due to dissipative forces. This finding of the behavior at the CNT-bundle level significantly differed from the behavior of pullout in individual MWNTs, for which dissipation is found to be negligible. To overcome the weak shear interfaces that lead to sword-in-sheath failure, we have demonstrated that load can be effectively transferred to inner DWNTs and shells within the bundles by applying a controlled dose (9-11 x 1020e/cm2) of electron

irradiation (200 keV) to induce covalent crosslinks at the interfaces of adjacent DWNTs and shells [4]. In particular, crosslinking is induced on two length scales within the hierarchical bundle structures, both between the outer shells of adjacent DWNTs as well as between the outer and inner shells within each DWNT. By tailoring this irradiation induced crosslinking, we have observed order of magnitude increases in both the effective strength and modulus of the individual DWNT bundles to ~17 GPa and ~700 GPa, respectively. In-situ TEM imaging during tensile testing of the crosslinked DWNT bundles revealed distinct failure mechanisms for low and highly crosslinked bundles, confirming the beneficial effects of bridging adjacent shells and tubes.

We have also developed a continuum based shear-lag model that successfully predicted the saturation regime in the shear force as a function of overlap length for the SEM experiments of shear between MWNTs [5]. In this study, the data from shear experiments performed on un-functionalized MWNTs fell into the region between two theoretical curves with shear strengths of 30 and 60 MPa representing arm-chair and zig-zag tubes, respectively. This suggests that the shear between two MWNTs is dependent on chirality. Furthermore, through the model we demonstrated that CNT alignment, although required, is not sufficient for optimal mechanical performance of CNT yarns. Rather, the average overlap lengths between CNTs needs to be chosen properly, based on the mechanical properties of the constituents and the shear interactions between CNTs, to achieve the highest mechanical performance, such as the highest elastic energy density and full utilization of the CNT strength. Likewise, to achieve ductility and associated high-failure energies, spreading the localization of sliding and deformation delay is needed.

The next level of hierarchy in CNT fibers is the bundle-bundle interaction level. At this level, we have combined nanomechanical shear experiments between functionalized bundles of CNTs with multiscale simulations to reveal the role of nanotube surface functionalization on CNT-CNT interactions [6]. We found that in-situ CVD functionalization of CNT bundles by PMMA-like oligomers enhances the shear strength of bundle junctions by approximately an order of magnitude compared to “bare” van der Waals interactions between pristine CNTs. Through multiscale simulations, we have shown that the enhancement of shear strength is attributed to an interlocking mechanism of polymer chains in the bundles, dominated by van der Waals interactions, and stretching and alignment of chains during shearing. Unlike covalent bonds, weak bonds can reform upon failure, resulting in strong, yet robust fibers.

[1] H.D. Espinosa, T. Filleter, and M. Naraghi, “Multiscale Experimental Mechanics of Hierarchical Carbon-based Materials” Adv. Mater., In Press, 2012.

[2] M. Naraghi, T. Filleter, A. Moravsky, M. Locasio, R. O. Loufty, and H. D. Espinosa, "A multi-scale study of high performance DWNT-polymer fibers," ACS Nano, vol. 4, pp. 6463-6476, 2010.

[3] T. Filleter, S. Yockel, M. Naraghi, J. T. Paci, O. C. Compton, M. L. Mayes, S. T. Nguyen, G. C. Schatz, and H. D. Espinosa, "Experimental-Computational Study of Shear Interactions within Double-Walled Carbon Nanotube Bundles" Nano Letters, vol. 12, pp. 732-742, 2012.

[4] T. Filleter, R. Bernal, S. Li, and H.D. Espinosa, "Ultrahigh Strength and Stiffness in Cross-Linked Hierarchical Carbon Nanotube Bundles" Advanced Materials, Vol. 23, No. 25, p. 2855-2860, 2011.

[5] X. Wei, M. Naraghi, and H. D. Espinosa, "Optimal Length Scales Emerging from Shear Load Transfer in Natural Materials: Application to Carbon-Based Nanocomposite Design" ACS Nano, vol. 6, pp 2333–2344, 2012.

[6] M. Naraghi, G. H. Bratze1, T. Filleter, Z. An, X. Wei, S. T. Nguyen, M. J. Buehler, H. D. Espinosa, "Atomistic Investigation of Load Transfer Between DWNT Bundles Crosslinked by PMMA-Oligomers" In Preparation, 2012.

ID: 536

Two - dimensional Green's Function for anisotropic bimaterial with imperfect interface

Les Sudak
Department of Mechanical and Manufacturing Engineering,
University of Calgary, Calgary, Alberta, Canada

A general method is presented for the rigorous solution for the two-dimensional Green's function for an anisotropic bimaterial subject to a line force or a line dislocation. Bonding along the bimaterial interface is considered to be homogeneous imperfect. Using complex variable techniques the basic boundary value problem for two analytic vector functions is reduced to a coupled linear first-order differential equation for a single analytic vector function defined in the lower half space. The coupled linear differential equation for the single analytic vector function can be subsequently decoupled into three independent linear first-order differential equations for three newly defined analytic functions. Closed-form solutions for the two dimensional Green's function are subsequently derived.

Missing Abstract

ID: 616

ID: 639

The Novel Mechanical Structure and Function of the Inner Ear

Charles R. Steele
Stanford University
USA

Sunil Puria
Stanford University
USA

Abstract:
The cochlea of the inner ear serves well in processing sound information, transforming a sound signal input into a neural excitation output. This is a consequence of novel composite design with distributed piezoelectric sensing and actuation. The cochlea acts as a real-time Fourier analyzer with a mapping of each frequency of the sound to a place along the cochlea. This mapping can be explained by a simplified "box model", containing only water and a highly orthotropic elastic partition. This "passive" fluid-elastic response is close to the actual response for high intensity of sound. However, for low intensity in the living mammal, the response is amplified by around two orders of magnitude, due to an "active" process. This is due to piezoelectric behavior of the mammalian outer hair cell. This leads to a "feed-forward/negative feed backward" model for the active process. This requires no tuning, i.e., an "open loop" system, which produces remarkable agreement with the measurements.

For a fixed input frequency, experiments have shown that a traveling wave on the basilar membrane (BM) builds to a peak at a certain point and then rapidly decays beyond that point. The location of the peak depends on the frequency, so each location on the BM is said to have a “best frequency” (BF), associated with it, which produces the maximum response amplitude at that point on the BM. A sensory epithelium attached to the BM, called the organ of Corti (OC), contains the sensory hair cells, which respond to the BM motion and initiate the neural excitation. Three rows of outer hair cells (OHC) most likely use a piezoelectric-like mechanism to provide an amplification of the wave for low input amplitudes, an effect that is known as the active amplifier mechanism (1). A large scale model of the organ of Corti (Volderich) emphasized the intriguing spatial arrangement of the components. In particular, the apical inclination of the OHC was shown to provide a spatial “feed-forward” that greatly enhances the wave amplitude near BF. The approach has been utilized in one-dimensional (1-D), two-dimensional (2-D) and three-dimensional (3-D models. These have few parameters, each of which has a clear physical interpretation. However, the BM velocity simulation disagreed with in-vivo measurements in showing i) an excessive phase excursion and ii) a best frequency (BF) shift from passive to active of around an octave, instead of the measured half octave. In recent work, it is found that returning to the time-averaged Lagrangean alleviates the phase problem.

The Lagrangean is valid only for conservative systems. However, using the Mazwell reciprocity is found to yield the equivalent result for the system with viscous damping.

Furthermore another prominent feature of the OC is included, namely the inclination of the phalangeal process of the Deiters cell. The OHC motility causes a positive spatial “feed-forward” of force on the BM (the “push”) as well as a negative “feed-backward” of force (the “pull”) from the phalangeal process. The push and pull work together to provide a two order of magnitude increase in the amplitude of the wave for short wavelengths, but they cancel each other out for long wavelengths. For very short wavelengths, the viscosity of the fluid dominates. Thus, the significant enhancement occurs for a narrow band of spatial wavelengths, without the need for special filtering or tuning of parameters at each BF. The relationship between BF, BM sensitivity, and BM sharpness of tuning are not well established. In the present work, we elucidate relationship between these quantitative outputs and model inputs for the low frequency cochleas, human and chinchilla, and the high frequency cochleas, cat and gerbil. Extensive BM measurements are available for one in each group. The calculations for the simple box model of the cochlea with the push-pull mechanism and the time-averaged Lagrangian method yield results very similar to animal measurements of the BM velocity (VBM) for gerbil and chinchilla. In addition to the simulations of VBM, BM vibration thresholds and the sharpness of cochlear tuning curves are calculated from the present cochlear model, and the model results are compared with animal BM vibration, auditory neural threshold, and the sharpness measurements of animal cochlear neurons for animals and predicted auditory-nerve fibers frequency-threshold curves (ANFTCs) for human.

ID: 653

The Influence of Large Deformation on a Bio-membrane Undergoing Thermal Fluctuations

L B Freund
University of Illinois
USA

Abstract:
Thermal fluctuations of bio-membranes immersed in water, which are driven by Brownian motion, have been a topic of active interest for decades. Even though the materials are soft and susceptible to large deformation, nearly all quantitative studies of the phenomenon have relied on the use of small deformation plate theories for describing the internal energy of the membrane, an energy which is necessary for a statistical description. Here, we describe the use of simple models that retain the essential features of bio-membrane response -- in-plane isotropy, zero in-plane shear stress and conserved area, for example -- but that admit the possibility of large deformation so as to assess the circumstances under which this effect might influence behavior to a consequential degree.

ID: 723

The Effective Thermoelectric Properties of Composite Materials

Jiangyu Li
University of Washington

Abstract:
Vast amount of efforts have been devoted to nanostructured thermoelectric materials for enhanced conversion efficiency, yet there have been very limited theoretical understanding toward the effective behavior of thermoelectric composites. At issue is whether the effective figure of merit of a thermoelectric composite can be higher than all its constituents, and how we can take advantages of the size and interfacial effects of composite materials to further enhance their thermoelectric conversion efficiency. In this work, we develop a rigorous mathematical analysis of the electric conduction and heat transfer in heterogeneous thermoelectric composites using asymptotic homogenization theory, from which the effective thermoelectric conversion efficiency is derived, showing that higher conversion efficiency than all its constituents is possible in the composites even in the absence of size and interfacial effects. This points to a new route for high efficiency thermoelectric materials.

ID: 739

Role of Surface Roughness in Hysteresis During Adhesive Elastic Contact

Haneesh Kesari
Brown University
USA

Joseph Doll

Abstract:
In experiments that involve contact with adhesion between two surfaces, as found in atomic force microscopy or nanoindentation, two distinct contact force (P) vs. indentation-depth (h) curves are often measured depending on whether the indenter moves towards or away from the sample. The origin of this hysteresis is not well understood and is often attributed to moisture, plasticity or viscoelasticity. We present experiments [1] and continuum mechanics models [2] that will show that hysteresis can exist without these effects, and that its magnitude depends on surface roughness. We explain the observed hysteresis as the smeared out effect of a large series of surface instabilities that are induced by the surface roughness and adhesion. These instabilities cause the size of the nominal contact region to be significantly different during the loading and the unloading phases of the contact experiment. We also demonstrate that when this is the case material properties can be estimated uniquely from contact experiments even when the measured P-h curves are not unique. The hysteresis energy loss during contact is also a measure of the adhesive toughness of the contact interface. We show experimentally that roughness can both increase and decrease the adhesive toughness of the contact interface. We show through numerical simulation of continuum adhesive contact models that the contact interface is optimally tough at conditions at which the contact region is at the cusp of the transition at which it turns from being mostly simply connected to being predominantly multiply connected. This insight is useful in increasing interface toughness by modifying its small scale structure through microfabrication techniques.

References [1] H. Kesari, J. Doll, W. Cai, B. Pruitt, and A. Lew. Role of surface roughness in hysteresis during adhesive elastic contact. Philosophical Magazine Letters, 90(12):891–902, 2010. [2] H. Kesari and A. J. Lew. Effective macroscopic adhesive contact behavior induced by small surface roughness. Journal of the Mechanics and Physics of Solids, 59:2488–2510, 2011.

ID: 745

Phase-Field Models for Dynamic Brittle Fracture

Michael J. Borden
The University of Texas at Austin
United States

Thomas J.R. Hughes
The University of Texas at Austin
United States

Chad M. Landis
The University of Texas at Austin
United States

Abstract:
The phase-field approach to predicting fracture supplements the usual linear momentum equation with an additional scalar valued phase-field equation. In this approach, discontinuities are not introduced into the geometry or displacement field. Instead, the fracture surface is approximated by a phase-field, which smoothes the boundary of the crack over a small region (see Figure 1). A major advantage of using a phase-field is that the evolution of fracture surfaces follows from the solution of a coupled system of partial differential equations. Implementation does not require additional ad hoc rules to determine crack initiation, propagation direction, or bifurcation.

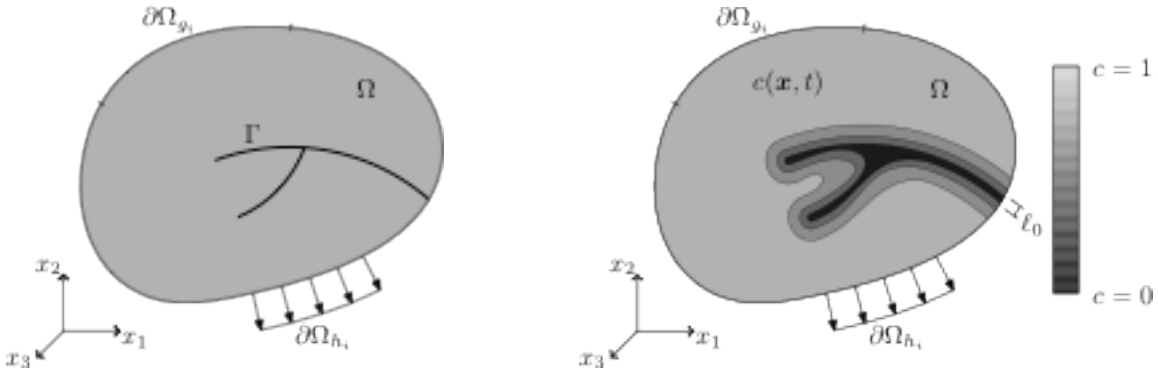

Figure 1. The sketch on the left shows a schematic representation of a solid body Ω with internal discontinuity Γ. The sketch on the right shows an approximation of the discontinuity by the phase-field $c(x,t)$. The model parameter ℓ_0 controls the width of the approximation.

In this presentation, we discuss our recent work on the numerical implementation of phase-field models for dynamic brittle fracture. These models are based on the variational formulation for Griffith-type fracture models [2]. The total potential energy of the discrete problem is written as

$$\Psi = \int_{\Omega} \psi_e(\varepsilon) d\Omega + \int_{\Gamma} G_c \, d\Gamma \tag{1}$$

where ε is the infinitesimal strain tensor, ψ_e is the elastic strain energy function, G_c is the critical fracture energy, and Γ is the unknown crack path. The phase-field approximation to this energy is stated as

$$\Psi \approx \int_{\Omega} g(c)\psi_e^+(\varepsilon) + \psi_e^-(\varepsilon) d\Omega + \int_{\Omega} G_c \left(\frac{(1-c)^2}{4l_0} + l_0 |\nabla c|^2 \right) d\Omega \tag{2}$$

where ψ_e^+ and ψ_e^- are an additive decomposition of the elastic strain energy function into tensile and compressive components respectively, and g is a degradation function that reduces the contribution from ψ_e^+ as c goes to zero. In the second term of (2), the length scale parameter, l_0, controls the width of the approximation. As part of our work, we make use of the smooth basis functions provided by isogeometric analysis [3] and study the effect of adding terms to the potential energy approximation that involve higher-order derivatives of the phase-field. This leads to an approximation that is stated as

$$\Psi \approx \int_{\Omega} g(c)\psi_e^+(\varepsilon) + \psi_e^-(\varepsilon) d\Omega + \int_{\Omega} G_c \left(\frac{(1-c)^2}{4l_0} + \frac{l_0}{2} |\nabla c|^2 + \frac{l_0^3}{4} |\Delta c|^2 \right) d\Omega. \tag{3}$$

Starting from (2) and (3) we will derive the corresponding strong form statements. We will then present results that show that the higher-order model (3) is a better approximation to the discrete potential energy (1). To conclude this presentation, we will show the results of a number of numerical benchmark experiments for crack propagation and branching. These experiments show that the phase-field model can capture complex crack behavior in both two and three dimensions without introducing any ad hoc criteria for crack nucleation and branching.

References:

[1] M.J. Borden, C.V. Verhoosel, M.A. Scott, T.J.R. Hughes, C.M. Landis, "A phase-field description of dynamic brittle fracture," Comp. Meth. in Appl. Mech. Engng. **217-220,** 77-95 (2012).

[2] B. Bourdin, G.A. Francfort, J-J. Marigo, "The variational approach to fracture," J. Elast. **91**, 5-148 (2008).

[3] J.A. Cottrell, T.J.R. Hughes, Y. Bazilevs, *Isogeometric Analysis: Toward Integration of CAD and FEA.* Wiley:Chichester (2009).

ID: 765

The Simulation of Hydraulic Fracture Problems with Universal Meshes

Adrian Lew

Michael Hunsweck

Abstract:
We describe our approach to simulating hydraulic fractures based on the use of Universal Meshes. This problem is challenging to simulate because of the non-linear coupling between the fluid pressure and the crack opening, and also because of the presence of two moving boundaries, the crack tip and the fluid front. Often in simulating hydraulic fracture, the rock is modeled as a homogeneous, isotropic, infinite elastic medium. This has the advantage of bypassing the 2D elastostatics equations for the rock and instead solving a 1D integral relation between the fluid pressure and crack opening. While this approach has been highly successful for this simplified case, there would be great difficulty in extending it to more general problems, for example when it is desired to model the effects of poroelasticity or the intersection of hydraulic fractureswith pre-existing natural fractures. Finite-element-based approaches are attractive in the simulation of hydraulic fractures because of their ability to easily handle inhomogeneities in the material and more general geometries. To this end, we have devised one such algorithm to simulate plane-strain, curvilinear hydraulic fractures. The algorithm is capable of handling the non-linear coupling between the pressure and crack opening profile, and to separately track the evolution of the fluid front and the crack tip.

I.4

Awards Lecture - Taylor Medal (Joe D. Goddard)

Awards Lecture by Taylor Medalist

(Joe D. Goddard)

ID: 750

Playing in Sand for Science, Engineering and Fun

2012 G.I. Taylor Medalist Lecture
Society of Engineering Science

Joe Goddard
Department of Mechanical and Aerospace Engineering
University of California, San Diego

Abstract

"[Granular media] are omnipresent: from the rings of Saturn to the snow of our mountains. [They] represent a major object of human activities: as measured in tons, the first material manipulated on earth is water; the second is granular matter."
P.-G. de Gennes "From Rice to Snow", *2008 Nishina Foundation Nobelist Lectures*, In *Lect. Notes Phys.* **746**, 297-318 (2008).

The past forty years or so have witnessed a resurgence and continuous growth of interest in the mechanics of granular materials, whose scientific origins go back at least to the 18th Century. The subject is relevant to a number of geotechnical and technological processes, such as stability of slopes and natural avalanches, mechanics of desert sands, and vibratory conveying and compaction. The challenge of understanding and mathematically modeling these materials and processes has attracted researchers from a wide array of disciplines, ranging from soil mechanics to theoretical physics, who bring complementary but sometimes opposing philosophies and methodologies to the table.

This lecture provides a broad overview of the field, including the distinguished flow régimes of elastoplastic solid, viscoplastic fluid and viscous gas. The focus here is on the first two, which involve several fascinating phenomena such as Reynolds dilatancy, seismic liquefaction, mesoscopic force chains, shear bands and Faraday patterns on vibrated layers. An effort is made to relate these qualitatively to the geotechnical and technological processes mentioned above.

As a second aspect of the lecture, a discussion is given of the challenges and puzzles associated with the mathematical modeling of granular media. In contrast to molecular solids and fluids, whose relatively small particles are governed by reversible ("frictionless") intermolecular forces and strong thermal motion ("kT"), the typical granular material consists of particles ranging in size from microns to meters, whose individual and collective motion is dominated by frictional contacts and external forces such as gravity. This severely limits the traditional approaches of molecular-kinetic theory and statistical mechanics, yet the typical number of particles in such systems renders a brute-force numerical description by the so-called "distinct element method" (DEM) impracticable for many purposes. Hence, one important challenge is the development of continuum models of the kind that have proved indispensable for traditional solid and fluid mechanics.

A brief summary is given of some of the more promising phenomenological continuum models for the elastoplasticity and viscoplasticity of non-cohesive granular media. One conclusion is that multiscale or "multipolar" continuum models involving additional kinematic degrees of freedom and conjugate "hyperstresses", may be essential to the rheology of granular media, particularly the elastoplatic behavior. Because of the typical particle sizes, this becomes much more compelling for granular media than for other complex solids and fluids.

I.5

Awards Lecture - SES Young Investigator (Markus Buehler)

Awards Lecture by SES Young Investigator Medalist (Markus Buehler)

ID: 096

From atoms to structures – how spiders turn weakness into strength

Markus J. Buehler
Laboratory for Atomistic and Molecular Mechanics (LAMM), Department of Civil and Environmental Engineering, Massachusetts Institute of Technology
United States

Abstract:
This talk will explain how materials in biology are synthesized, controlled and used for a variety of purposes—structural support, force generation, catalysis, or energy conversion—despite severe limitations in available energy, quality and quantity of building blocks. We demonstrated that the chemical composition of biology's materials plays a minor role in achieving functional properties. Rather, the way components are connected at different length-scales defines what material properties can be achieved, how they can be altered to meet functional requirements, and how they fail in disease states. We have achieved this by using the world's fastest supercomputers to predict properties of complex materials from first principles, in a multiscale approach that spans orders of magnitude in scale. This method, combined with experimental studies, allows us to build virtual "*in silico*" material models that provide unseen insight into the workings of natural and synthetic materials from the bottom up.

We demonstrate this approach in a case study of spider silk, one of the strongest yet most flexible materials in Nature, despite being made out of some the simplest, most abundant and intrinsically weak proteins, including weak hydrogen bonding. We discovered that the great strength and flexibility of spider silk—exceeding that of steel and other engineered materials—can be explained by the material's unique structural makeup that involves multiple hierarchical levels. These hierarchical levels span from the genetic information that defines the protein sequence to the structural scale of an entire spider web. Thereby, each level contributes to the overall properties, but the remarkable properties emerge because of the synergistic interaction across the scales where the sum is more than its parts. We showed that the nonlinear material behavior of silk fibers, softening at the yield point to dramatically stiffen during large deformations until point of failure, is what allows for localization of deformation upon loading, and is precisely what makes spider webs robust and extremely resistant to defects, as compared to other linear-elastic or elastic-plastic materials. Through *in situ* experiments on webs of a European garden spider, we confirm the prediction that locally applied loading results in minimal damage. We further show that under global loads such as wind, the material behavior of silk under small-deformation is crucial to maintaining the web. By translating this insight gained from the study of natural materials such as spider silk to engineered materials such as carbon nanotube fibers, graphene composites or metal-polymer films, our research has resulted in an engineering paradigm that facilitates the design of sustainable materials starting from the molecular level, leading to the formation of hierarchical structures that span all scales from nano to macro.

[1] T. Knowles, M.J. Buehler , "Nanomechanics of functional and pathological amyloid materials," *Nature Nanotechnology*, Vol. 6(7), 2011

[2] M.J. Buehler, “Tu(r)ning weakness to strength,” *Nano Today*, Vol. 5 , pp. 379-383, 2010
[3] S. Keten, Z. Xu, B. Ihle, M.J. Buehler, “Nanoconfinement controls stiffness, strength and mechanical toughness of beta-sheet crystals in silk,” *Nature Materials*, Vol. 9, pp. 359-367, 2010
[4] S. Cranford, A. Tarakanova, N. Pugno, M.J. Buehler, “Nonlinear material behaviour of spider silk yields robust webs,” *Nature*, doi:10.1038/nature10739, 2012

Track II

Mechanics of Biological Systems

II.1

Mechanics of Biological Systems - Cell and Tissue Mechanics

ID: 249

Damage and Solid-Fluid Interactions during Transient Large Deformation of Rat Brain Tissue

Henry W. Haslach, Jr.
Department of Mechanical Engineering
University of Maryland, College Park, MD
United States

Lauren Leahy
Department of Mechanical Engineering
University of Maryland, College Park, MD
United States

Abstract:

Physical impact, shock wave, or sudden acceleration may induce mild traumatic brain injury (mTBI), but the mechanisms that underlie the cause and effect are not well understood even though the mechanical behavior of the non load-bearing brain tissue is critically important during the initial insult. Brain tissue is composed of water and solid phases so that the mechanical properties of rat brain tissue are strongly influenced by the high water content of the tissue and its flow within the tissue under internal pressure induced by a mechanical load. We seek the mechanical cause of the initial injury leading to mTBI, but the physical mechanism that transmits the insult to inner brain substructures, such as the hippocampus or the corpus callosum, is unknown. One candidate medium is the extracellular fluid (ECF). So our hypothesis for the immediate mechanical cause of tissue damage that may lead to mTBI is that pathological extracellular fluid flow disrupts tissue substructures. For example not only may axons be stretched, but the adhesions between glia and axons may be disrupted. In particular, we hypothesize that intercellular fluid flow in the tissue is the immediate cause of tissue damage by rearranging substructures such as axonal tracts as the applied load opens passageways for fluid transport.

Rat models have been routinely used for investigating the initial mechanical causes of mTBI. But in order for mechanisms to be elucidated, the characterization of mechanical properties of rat brain tissue must be improved. Small-sized specimens of fresh rat brain tissue tested under confined compression, that enforces uniaxial fluid flow, elucidate the solid - internal fluid interaction, and others under a combination of translational shear and fixed compression represent the passage of a pressure wave in the tissue. Damage indicators are identified at much lower strains than the consensus 20% strain damage threshold on quasi-static stress-stretch curves, on those at constant slow (0.001/s) and moderate (1/s) strain rates to at least 30% strain in both types of tests, and on confined compression curves for several cycles of linear deformation to 5% strain followed by stress relaxation. The damage indicators on the quasi-static curves are sudden temporary drops in the stress magnitude due to substructure rearrangement, on the faster deformation rate curves are peaks in the stress magnitude, and on the stress-relaxation curves is the relaxation to zero stress. The general consensus is that the shape of an undeformed

brain in vivo is maintained by the balance between the hydrostatic pressure in the extracellular fluid and the tension in dendrites, axons and glial processes. Mechanical damage may disrupt this balance and open passageways for pathological extracellular fluid flow. Therefore permeability is proposed as a damage parameter in nonlinear viscoelastic modeling.

Tests that combine compression and translational shear investigate the tissue large deformation response to the longitudinal and shear components of a pressure wave seen in blast injuries. Translational shear is employed because it is a more likely loading of the brain than rotational shear. The tests at constant translational stretch rates of 0.001, 1, and 100/s were performed at normal compressions of either 16.7% or 33% of the 3 mm thickness. The specimens are attached to the grips with surgical glue to prevent slip on the grips. The shear stress-stretch curves, obtained for a range beyond the point at which the tissue begins to tear in shear, are monotonic until reaching a stress peak, which is interpreted as the point at which significant damage initiates. Video images of the damage process visible on the side surface of the specimen have been recorded. The interaction of compression and translational shear involves the extracellular fluid carrying hydrostatic pressure load and therefore applying a local force to the solid component of the tissue that can result in mechanical damage.

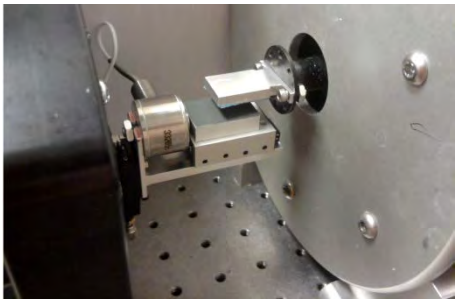

Translational Shear Fixture for 12x6x3 mm specimens

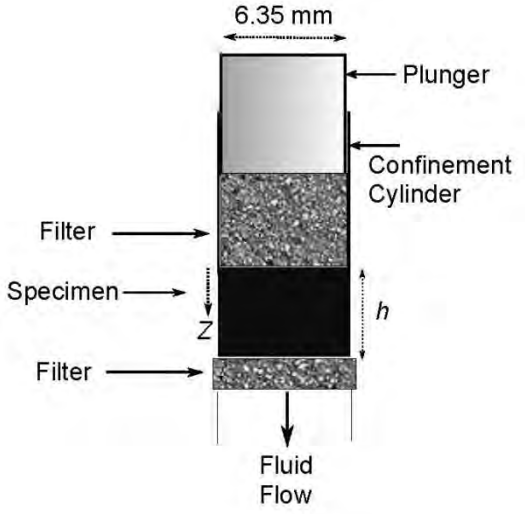

Schematic of the confined compression apparatus, with 6.35 mm (0.25 inch) inner diameter of the confinement cylinder where *h* is the specimen length and *Z* is the coordinate in the reference system.

ID: 317

3D Neutrophil Tractions in Changing Microenvironments

Christian Franck
Brown University
USA

Jennet Toyjanova
USA

Abstract:
Neutrophils are well-known as first responders to defend the body against life threatening bacterial diseases, infections and inflammation. The mechanical properties and the local topography of the surrounding microenvironment play a significant role in the regulating neutrophil behavior including cell adhesion, migration and generation of tractions. In navigating to the site of infection, neutrophils are exposed to changing microenvironments that differ in their composition, structure and mechanical properties. Our goal is to investigate neutrophil behavior, specifically migration and cellular tractions in a well-controlled 3D in vitro system. By utilizing an interchangeable 2D-3D sandwich gel structure system with tunable mechanical properties neutrophil migration and cell tractions can be computed as a function of gel stiffness and geometric dimensionality.

Missing Abstract

ID: 541

ID: 597

Mechanics of Cell Division in 3D Investigated with Traction Force Microscopy

Jacob Notbohm
Division of Engineering and Applied Science
United States

Ayelet Lesman
Division of Chemistry and Chemical Engineering
United States

David A. Tirrell
Division of Chemistry and Chemical Engineering
United States

Guruswami Ravichandran
Division of Engineering and Applied Science
United States

Abstract:
Cell division is a mechanical process wherein a single mother cell, actuated by internal forces alone, splits into two daughter cells. While previous studies have investigated the interior mechanics and biological pathways of division, there is a lack of understanding of the way in which a cell interacts with its surroundings during division. A more thorough understanding of cell-matrix interactions during division will lead to a better understanding of processes such as cellular growth and development. To better understand the way in which a cell interacts with its surroundings during division, this work studies cell geometry and mechanics during division in a 3D matrix using high resolution time-lapse confocal microscopy. To quantitatively measure how the cell interacts with the matrix, 3D traction force microscopy is used, wherein fluorescent particles are suspended into the matrix and imaged as the cell divides. Digital volume correlation is applied to compute the 3D cell-induced matrix displacements during division.

ID: 598

Nonlinear Viscoelastic Model for Tendon Creep

Frances Davis
Virginia Tech

Raffaella De Vita

Abstract:
This study presents a transversely isotropic viscoelastic model for the creep behavior of tendons developed within the nonlinear integral framework proposed by Pipkin and Rogers [1]. The proposed model represents a departure from the popular quasi-linear viscoelastic (QLV) model [2] by including the dependence of the creep rate on stress. Creep data at different stress levels were collected on rat-tail tendon fascicles using the load frame of a TA Instruments Q800. The creep load applied was 0.5 N, 1.3 N, 2.0 N, or 2.8 N and was held for 10 minutes. The current model is compared with the experimental data and predictions for the QLV model. [1] Pipkin, A.C. and Rogers, T.G. (1968) J Mech Phys Solids, 16(1), pp. 59-72. [2] Fung, Y.C. (1993) Springer-Verlag, New York.

ID: 628

A Solid-Fluid Reacting Mixture Theory Model for Bone

Stephen Cull
Graduate Student
Department of Mechanical and Manufacturing Engineering, University of Calgary
Canada

Marcelo Epstein
Professor
Department of Mechanical and Manufacturing Engineering, University of Calgary
Canada

Abstract:
Biological materials such as bone provide an interesting application for the continuum theory of chemically reacting mixtures. The reactions that occur in bone continually replace old bone mineral with new bone mineral in a process called remodeling. Remodeling allows bone to both repair damage and to optimize its structure to loading conditions. In addition to chemical signals, the remodeling rate of bone is affected by mechanical factors. A solid-fluid mixture is used to model bone, with the addition of an evolution equation that provides a coupling between mechanical and chemical events. Thus, the rate of remodeling is constitutively tied to both the extent of reaction and the deformation gradient. Numerical examples for the proposed mixture theory model of bone are presented and discussed.

ID: 632

Factors that Influence the Mechanical Response of Degrading Swine Neural Tissue at Low Strain Rates

Sarah A. Bentil
The Ohio State University
United States

Rebecca B. Dupaix
The Ohio State University
United States

Abstract:
The ability to characterize the material response of brain tissue is invaluable in medicine. Applications include robotic surgery, where prediction of brain deformation is needed and surgeon training systems, where force feedback data is needed. The literature shows that experimental tests have been performed using many different animals (i.e. swine, macaque, rats, etc.), strain rates, and deformation modes (i.e. compression, shear, tension, etc.) to extract the material behavior [1-4]. Yet the mechanical properties of brain tissue can vary between samples, despite using identical experimental conditions. Some of the variability is attributed to temperature, sample preparation, and *post mortem* age of the tissue [5-6].

The purpose of this study is to add to the limited knowledge in the literature describing brain tissue property variability given a particular experimental protocol. Specifically, swine neural tissue was used to conduct *in vitro* unconfined compression tests at low strain rates. During these tests, all tissue samples were subjected to a ramp-hold displacement input. The experiments were designed such that the variation of mechanical properties attributed to the following factors: *post mortem* age (several hours to a week), compressive rate (1 mm/min, 5 mm/min, and 10 mm/min), brain hemisphere (left and right), and brain lobe (frontal, temporal, and occipital) could be explored using statistical methods.

An analysis of variance (ANOVA) performed on a linear mixed effects statistical model yielded the factors that significantly affected the mechanical behavior of the tissue. The model also considered the variability in the mechanical behavior that was attributed to the pig used in each experiment. The factors that significantly influenced the material properties of the swine neural tissue were *post mortem* age, compressive rate, brain lobe, and the interaction between *post mortem* age and compressive rate.

References:

1. Bilston, L.E., Z.Z. Liu, and P.T. Nhan, *Linear viscoelastic properties of bovine brain tissue in smear.* Biorheology, 1997. **34**(6): p. 377-385.
2. Cheng, S., E.C. Clarke, and L.E. Bilston, *Rheological properties of the tissues of the central nervous system: A review.* Medical Engineering & Physics, 2008. **30**(10): p. 1318-1337.
3. Gefen, A. and S.S. Margulies, *Are in vivo and in situ brain tissues mechanically similar?* Journal of Biomechanics, 2004. **37**(9): p. 1339-1352.
4. Miller, K. and K. Chinzei, *Constitutive modelling of brain tissue: Experiment and theory.* Journal of Biomechanics, 1997. **30**(11-12): p. 1115-1121.
5. Bilston, L.E., *Brain Tissue Mechanical Properties*, in *Biomechanics of the Brain*, K. Miller, Editor. 2011, Springer New York. p. 69-89.
6. Rang, E.M., Lippert, S. A., and Grimm, M. J., *The degradation of the material properties of brain tissue as a function of time postmortem.* Proceedings of the 2001 ASME Bioengineering Conference BED, 2001. **50**: p. 887-888.

ID: 647

Mechanics of Specific Adhesion of Bio-Membranes to Compliant Substrates

Alireza Sarvestani
University of Maine
USA

Abstract:
We have outlined a framework to investigate the thermodynamic equilibrium adhesion of a bio-membrane to a compliant substrate functionalized with immobilized bio-adhesive ligands. The membrane is modeled as a soft elastic shell, subjected to surface tension and reconstituted with mobile receptors and a repelling layer on the ventral side. The free energy function of the system is assumed to be comprised from the following contributions: the membrane-substrate non-specific interactions, stored elastic energy (in deformed membrane and substrate), binding enthalpy, and mixing entropy of mobile receptors. Assuming a van der Waals form for the interfacial non-specific potential, the equilibrium configuration of the system is studied in detail. We have shown that the equilibrium spread area of the adherent membrane is very sensitive to the rigidity of the underlying substrate and decreases as the surface compliance increases. This prediction is reminiscent of the experimental observations of spread area of cells attached to soft substrates. This is an interesting result considering the lack of contribution of intracellular signaling or actively regulated cytoskeleton in the proposed physical model for the adhesion. This suggests that the mechanistic pathways inherent to membrane-substrate thermodynamic interactions can be equally important as intracellular signaling pathways to mediate the process of rigidity sensing by cells.

Missing Abstract

ID: 698

ID: 722

PROBING NANOSCALE BILOGICAL FERROELECTRICITY IN AORTIC WALLS BY PIEZORESPONSE FORCE MICROSCOPY

Jiangyu Li
University of Washington

Abstract:

We report the discovery of biological ferroelectricity in aortic walls, the first observation of such phenomena in soft tissues. While many biological tissues are piezoelectric and pyroelectric with spontaneous polarization, ferroelectricity has not been reported in any of the soft biological tissues yet. Using piezoresponse force microscopy, we discovered that the porcine aortic walls are not only piezoelectric, but also ferroelectric, with the piezoelectric coefficient in the order of 1pm/V, and switching coercive voltage approximately 10V. It was also found that the polarization of the aortic walls is internally biased outward, and the inward polarization switched by a negative voltage is unstable, reversing spontaneously to the more stable outward orientation shortly after the switching voltage is removed. The discovery of ferroelectricity in soft biological tissues adds an important dimension to their biophysical properties and physiological functions, and its implications in cardiovascular and other diseases are discussed as well.

ID: 756

A Theoretical Study of Lamellipodia Dynamics

Sefi Givli
Technion – Israel Institute of Technology
Faculty of Mechanical Engineering
Israel

Yair Adler
Technion – Israel Institute of Technology
Faculty of Mechanical Engineering
Israel

Abstract:
The lamellipodia, a motility mechanism in motile cells, is a thin and wide region in the cell front. Inside this region lies a crowded network of polymers, mainly polarized actin filaments. These filaments depolymerize at their rear and polymerize at the other end which is directed towards the cell leading edge. This process affects the shape of the cell membrane and forces the lamellipodia edge to protrude in a crawl-like manner. In this work, we study the mechanical processes underlying the lamellipodia behavior by means of a coarse grained mechanical model. The model accounts for the membrane shape and its mechanical interaction with an active network of actin filaments. Fig.1 provides a schematic description of the model, and illustrates how the membrane shape and the actin concentration construct a closed feedback loop.

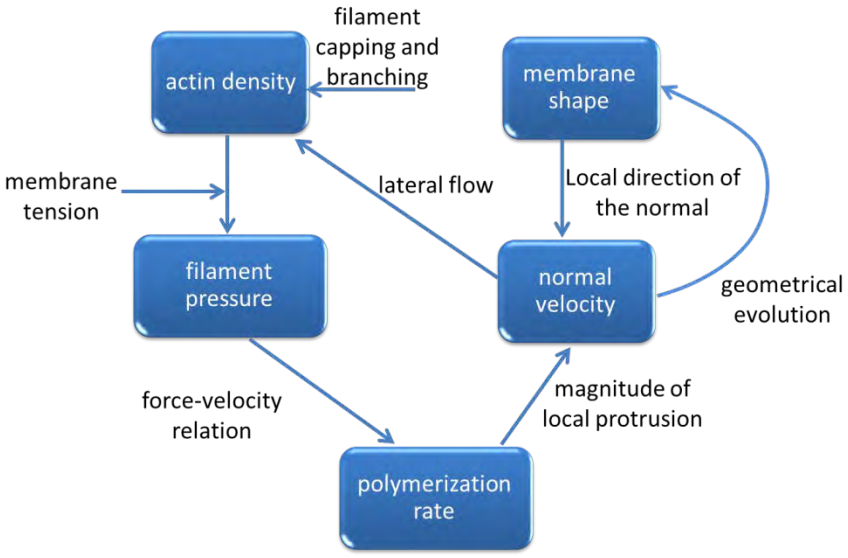

Fig.1: A schematic illustration of the model

We hypothesize that tension in the plasma membrane is dictated by the interrelation between actin polymerization which pushes the cell membrane from within, the contraction at the cell rear and anchorage to the substrate. Here, we focus our attention to the geometrical evolution of the

leading edge setting aside the detailed description of how each of these three processes affects the tension in the membrane. In particular, membrane tension is presumed to be a control parameter that manifests the coordination between protrusion, adhesion, and contraction. The governing equations consist of a non-linear integro-differential PDE to describe the shape dynamics, and a non-linear conservation law for the actin concentration along the edge of the lamellipodia. The model parameters, such as capping and branching rates of the actin filaments, are in accordance with recent experimental reports.

The numerical results of our model are compared with experimental observations. Special focus is put on comparison with quantitative measurements of steady state configurations (Keren et al., 2008) and with qualitative observations of lamellipodia dynamics (Barnhart et al., 2011). The results, e.g. Fig.2, are in very good agreement with these experiments, and suggest that the mechanical coupling between the membrane shape and the actin network is an important feature of the lamellipodia, which dominates its dynamic behavior. In addition, we show that the maximal crawling velocity is limited by dynamics stability rather than polymerization rate.

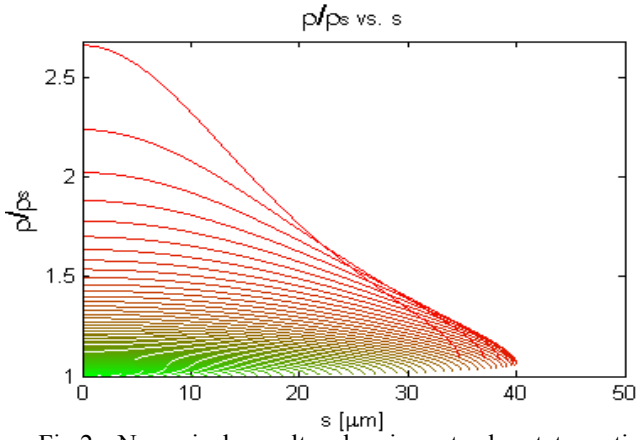

Fig.2: Numerical results showing steady state actin concentration along the leading edge for different crawling velocities.

References:

Barnhart, E.L., Lee, K.-C., Keren, K., Mogilner, A., Theriot, J.A., 2011. An Adhesion-Dependent Switch between Mechanisms That Determine Motile Cell Shape. PLoS Biol 9, e1001059.

Keren, K., Pincus, Z., Allen, G.M., Barnhart, E.L., Marriott, G., Mogilner, A., Theriot, J.A., 2008. Mechanism of shape determination in motile cells. Nature 453, 475-U471.

II.2

Mechanics of Biological Systems - Mechanics of Biomaterials and Biomolecules

ID: 106

Nanomechanics of Tropocollagen and Hydroxyapatite Biomaterials With an Account of Collagen Mutations and Varied Hydroxyapatite Textures: Implications for Bioinspiration, Disease Mechanics, and Material Mechanics

Devendra Dubey
Not specified

Vikas Tomar
Perdue University

Abstract:
Hierarchical nanocomposite materials such as bone, dentine, nacre etc. are primarily composed of organic (polymeric polypeptide Tropocollagen (TC) chains) and inorganic (calcium hydroxyapatite (HAP) and calcium carbonate) phases. Interfacial interactions between the organic phase and the mineral phase as well as the structural effects arising due to the staggered arrangement, TC mutations, and varied HAP textures significantly affect the strength of such biomaterials. In addition, the above factors also influence the pathology of a biological tissue. The effect of such factors is intricately intertwined with the chemical environment of such materials. In the present investigation, different idealizations of TC-HAP composite biomaterial system under tensile and compressive loadings are analyzed using explicit three dimensional (3-D) molecular dynamics (MD) simulations to develop an understanding of these factors. The analyses focus on understanding the correlations among factors such as the structural arrangement, the peak stress during deformation, the Young modulus, the peak interfacial strength, and the length scale of the localization of peak stress during deformation. Analyses show that maximizing the contact area between the TC and HAP phases result in higher interfacial strength as well as higher fracture strength. Due to the staggered arrangement, the orientation of HAP crystals has insignificant effect on the biomaterial strength in comparison the effect observed when a series of HAP-TC interfaces could be formed in parallel. Analyses based on strength scaling as a function of structural hierarchy reveal that while peak strength follows a multiscaling relation, the fracture strength does not. The peak strain for failure was found to be independent of the level of structural hierarchy. Analyses include effect of collagen mutation to different types of residues as well as genetically affected variations. Analyses are extended into quantum mechanical domain to elucidate role of electronic contributions. Results are discussed in terms of possibility of motivating bio-inspired materials and well as to explore possible disease mechanics issues.

ID: 168

Mechanics of biopolymer-reinforced thin rod buckling

Wanliang Shan
Department of Mechanical & Aerospace Engineering, Princeton University, Princeton, NJ 08544, USA
Princeton Institute for the Science and Technology of Materials (PRISM), Princeton, NJ 08544, USA

Winston Soboyejo
Department of Mechanical & Aerospace Engineering, Princeton University, Princeton, NJ 08544, USA
Princeton Institute for the Science and Technology of Materials (PRISM), Princeton, NJ 08544, USA

Zi Chen
Department of Biomedical Engineering, Washington University in St. Louis, St. Louis, MO 63130, USA

Clifford P. Brangwynne
Department of Chemical & Biological Engineering, Princeton University, Princeton, NJ 08544, USA

Abstract:
Fiber composite networks of hard fibers within a soft matrix are ubiquitous in biology, from the biopolymer cytoskeleton within living cells to bone and extracellular matrix supporting tissues. However, mechanics of these structures remains poorly understood. We have studied the buckling force and rod profile of a hard-soft fiber composite model system. We show that the buckling rod follows an exponentially decaying profile and that the transverse and longitudinal coupling between the rod and the surrounding elastic medium determines the profile. Surprisingly, upon mechanical disruption of this longitudinal coupling, force transmission remains localized and the buckling profile retains its finite penetration depth into the network. The residual longitudinal coupling arises from friction that sensitively depends on the microstructure of the rod-network interface. This biologically inspired system may provide insights into force propagation in cells and tissues, and suggests novel biomimetic materials with highly tunable stress responses.

ID: 183

The dependence of Plectonemic DNA on solution Electrostatics

David Argudo
University of Pennsylvania
United States

Prashant Purohit
University of Pennsylvania
United States

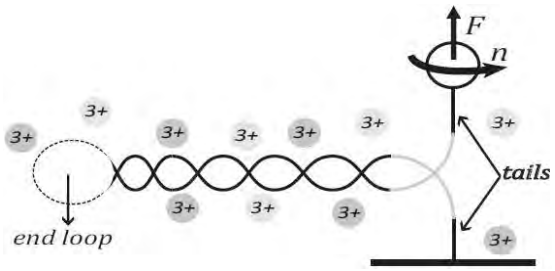

Figure 1: Sketch from [9] representing single molecule experiments.

Abstract:
The bending and torsional properties of DNA affect in a direct way various cellular processes, such as replication, transcription, compaction and protein-DNA binding. This is our motivation behind the study of DNA supercoils which are also known as plectonemes. Supercoils are present in cellular DNA, and several molecular machines manipulate them during key processes such as transcription and DNA repair [1]. In several scenarios, the action of these molecular machines or enzymes on DNA has been found to depend on the mechanical stress present in the molecules. Consequently, DNA supercoiling remains a subject of study for theorists and experimentalists alike. Experimentally, DNA supercoiling has been investigated using several biochemical and biophysical methods, including single molecule experimental techniques. In these experiments, it is possible to apply a force and/or moment parallel to the filament axis of a DNA molecule, and measure the elastic response in terms of elongation and angle of twisting about the filament axis. The vertical extension of the filament and the external applied moment are recorded as a function of the number of turns. These experiments have been performed under a wide range of monovalent and multivalent salt concentrations because of their physiological relevance [2,3]. Recent single molecule experiments using multivalent ions have shown that condensation into toroids occurs when the DNA molecule is subjected to tensile forces. Here we show that the combined tension and torsion of DNA in the presence of condensing agents dramatically modifies this picture by introducing supercoiled DNA as a competing structure in addition to toroids. We develop an elastic-isotropic rod model for twisted DNA in the plectonemic regime that can be applied to DNA single molecule experiments. We account for DNA elasticity, entropic effects due to thermal fluctuations and electrostatic interactions in the presence of monovalent and multivalent ions.

1. General Description of the Model

Figure 1 gives a sketch of the single molecule experiments. A vertical pulling force F is applied coaxially to the center-line of the space curve describing the tails of the DNA filament and the DNA molecule is rotated n turns by a torsional moment M_{ext}. Under these conditions the DNA forms plectonemes once $n > n_{critical}$. The rod model is made up of three regions [4]:

• **Plectoneme**: Two identical helical curves with constant curvature and torsion and length L_p.
• **Tails**: The extended section of the DNA molecule with total length L_t. The tails are not completely straight and the centerline follows a writhing path due to thermal fluctuations [5].
• **End loop** (Length L_o): It is an approximation based on the localizing solution of a rod [6].

The free energy of the DNA molecule $V(l_p, \theta, r, M_{ext}, x_i)$ is minimized subject to the imposed end rotations n = twist +writhe and the geometrical constraint $L = L_p+L_t+L_o$. The variable x_i represents any auxiliary parameters or internal variables that may appear in the free energy of the system depending on the model picked to describe the electrostatics and entropic free energy [7].

2. Results

Trends observed in the extension rotation experiments are captured by an elastic rod model but exact quantitative agreement with different experiments can only be obtained by a careful choice of entropic and electrostatic parameters.

2.1. Monovalent ions dominate: We use our theoretical framework to test several DNA-DNA interaction models [4]. Understanding the effects of each of the model led us to pick the model of Ubbink and Odijk [7], where we treat the effective linear charge ν as a fitting parameter. We obtained simple analytical formulae for ν as a function of the salt concentration for both monovalent and multivalent (in low concentrations) that result in strong agreement with different sets of experimental data and Monte Carlo simulations for a wide range of forces [4]. We also include the end loop energetic contributions and obtain estimates for the jumps in the external torque and extension of the molecule seen in single molecule experiments [2]. Our methods also allow us to consider scenarios where we have a series of loops forming in the DNA instead of plectonemes. This happens when the energetic cost of forming a loop is lower than that of forming a turn of helix. However, for a given choice of electrostatic and entropic interactions we find there is a range of forces in which both regimes can co-exist due to thermal motion. Furthermore we show that our model for plectonemic DNA can reproduce experimental data from single DNA molecule experiments were low concentration of polyvalent ions are added to a high concentration of monovalent salt solution. We found that as polyvalent ions concentration c_{mu} increases the radius of the helix approaches the inter-axial equilibrium distance [8].

2.2. Multivalent ions dominate

We combine a fluctuating elastic rod model of DNA with phenomenological models for DNA interaction in the presence of condensing agents to compute the minimum energy configuration for a given tension and end rotations [9]. We constrained our analysis to the most likely DNA configurations straight, supercoiled and toroidal. We found that there are no equilibrium supercoiled solutions below a threshold force F_T and show that for each tension $F > F_T$ there is a critical number of end rotations above which the supercoiled solution is preferred. Our results closely match recent extension rotation experiments on DNA in the presence of spermine and other condensing agents. Motivated by this we construct a phase diagram for the preferred DNA states as a function of tension and applied end rotations and identify a region where new experiments or simulations are needed to determine the preferred state [9].

References

[1] P. Nelson, Biological Physics, New York, 2004.
[2] H. Brutzer *et al.*, *Biophys. J.*, 2010, **98**, 1267.
[3] K. Besteman *et al.*, *Phys. Rev. Lett.,* 2007, **98**, 058103.
[4] D. Argudo and P. Purohit, *Acta Biomater.*, 2012, **8**, 2133.
[5] J. Moroz and P. Nelson*, Macromolecules,* 1998, **31**, 6333.
[6] J. Coyne*, IEEE J. Oceanic Eng.*, 1990, **15**, 72.
[7] J. Ubbink and T. Odijk, *Biophys. J.*, 1999, **76**, 2502.
[8] B. Todd *et al.*, *Biophys. J.,* 2008, **95**, 4775.
[9] D. Argudo and P. Purohit, *Biophys. J.,* 2012, DOI: 10.1016/j.bpj.2012.05.033

ID: 336

Snap-Through Instability in the Venus Flytrap: From Biomechanics to Biomimetics

Qiaohang Guo
College of Materials Science and Engineering, Fuzhou University,
China

Huang Zheng
Fujian Radio and Television University
China

Wei Li
College of Materials Science and Engineering, Fuzhou University,
China

Wenzhe Chen
College of Materials Science and Engineering, Fuzhou University,
China

Zi Chen
Department of Biomedical Engineering, Washington University in St. Louis
Department of Mechanical & Aerospace Engineering, Princeton University
United States

* Qiaohang Guo and Zi Chen contributed equally to this work.

Abstract:
Plants are usually perceived as slow movers, but some plants can move relatively fast-in some case, faster than insects. For example, the Venus flytrap can close the leaves in a blink of an eye to capture insects, even though it does not have nerves or muscles. This type of phenomena has intrigued researchers for centuries. Darwin first systematically studied the rapid closure mechanism, and commented that this plant is "one of the most wonderful in the world". Afterwards, several mechanisms were proposed, including the rapid loss of turgor pressure, an irreversible acid-induced wall loosening mechanism, and the snap-through instability mechanism, but with little unanimous agreement among researchers. Here we propose a coupled mechanical bistable mechanism that explains the rapid closure of the Venus flytrap in a comprehensive manner, supported a series of experimental observations. Such bistable behaviors are theoretically modeled and validated with table-top experiments. Based on the principles learnt from the Venus flytrap, a "flytrap robot" is designed as a proof of concept. From our study, promises hold to design smart bio-mimetic materials and devices with controllable instabilities to be used as sensors, actuators, artificial muscles and biomedical devices.

ACKNOWLEDGEMENT
This work has been supported by National Science Foundation of China (No. 11102040), the Sigma Xi Grants-in-Aid of Research (GIAR) program, American Academy of Mechanics Founder's Award from the Robert M. and Mary Haythornthwaite Foundation, and Society in Science – Branco Weiss fellowship.
Correspondence: chen.z@seas.wustl.edu.

REFERENCES
1. Y. Forterre, J. M. Skothelm, J. Dumais and L. Mahadevan. Nature **433**, 421-425 (2005).
2. Z. Chen, C. Majidi, D. J. Srolovitz and M. Haataja. Appl. Phys. Lett. **98**, 011906 (2011).
3. A. Pavlovič, V. Demko and J. Hudák. Ann Botany **105**, 37-44 (2010).
4. M. Colombani and Y. Forterre. Comput. Meth. Biomech. Biomed. Eng. **14**, 115-117 (2011).
5. M. Shahinpoor. Bioinspiration Biomimetics **6**, 046004 (2011).
6. Z. Chen, et al. submitted to Phys. Rev. Lett. (arXiv:1206.4739v4).
7. I.S. Chun, et al. Nano Lett. **10**, 3927-3932 (2010).
8. D. P. Holmes and A. J. Crosby. Adv. Mater. **19**, 3589-3593 (2007).
9. R. Yang, S. C. Lenaghan, M. Zhang and L. Xia. Plant Signaling & Behavior **5**, 968-978 (2010).

ID: 405

Mechanotransduction is Enhanced by the Synergistic Action of Heterotypic Cell Interactions and TGF-beta1

Vivek Shenoy
USA

Abstract:
With the use of planar substrates and collagen gels, the field of mechanotransduction has focused on the role of extracellular matrix stiffness, mechanical tension, and TGF-beta 1 in generating a more contractile fibroblast. However, little is known about the role of cell-cell interactions in inducing cellular contraction. We used 3-dimensional self-assembled microtissues, in which cell-cell interactions dominate, and a recently developed cell power assay (an assay for mechanotransduction) to quantify the effects ofTGF-beta 1 vs. the heterotypic cell interface on the power exerted by pure normal human fibroblast (NHF) and pure rat hepatocyte 35 (H35) microtissues and their rmixes. As a control, we found that TGF-beta 1 only doubled the power output of pure NHF and pure H35microtissues, whereas the heterotypic environment resulted in a 5-fold increase in cell power (0.24-0.05 to1.17-0.13 fJ/h). Seeding TGF-beta1-treated NHFs with untreated H35 cells demonstrated that the hetero typic environment and TGF-beta1 synergistically increase cell power by 22 x by maximizing heterotypic cell interactions. Using a mathematical simulation of stress generation, we showed that tensile forces can be enhanced by heterotypic cell interactions. These data render a new understanding of how heterotypic cell interactions may increase cellular force generation during wound healing.

ID: 421

The Existence and Function of DNA Buckling in Tailed Bacteriophages

Andrew D. Hirsh
University of Michigan, Ann Arbor
United States

Noel C. Perkins
University of Michigan, Ann Arbor
United States

Abstract:
Double stranded DNA (dsDNA) bacteriophages are remarkable biochemical machines that pack their micron-length genome into a preassembled capsid only tens of nanometers wide. Driving the packing process are the most powerful known biological motors capable of generating forces around 100 pN [1-2]. Under the large compressive forces inside the capsid, DNA is highly bent below the persistence length of the molecule.

A recent high (7.8Å) resolution cryo-electron microscopy (cryo-EM) reconstruction of bacteriophage φ29 also revealed the existence of DNA inside the viral tail [3]. In particular, the reconstruction revealed an intriguing toroidal DNA supercoil (thought to be 30-40 basepairs) lodged in a small protein cavity outside the capsid in the tail. It appears that DNA under high compression is able to adopt a buckled conformation in a volume only 3.5 times wider and 2 times taller than the width of the molecule. In previous work, we have employed a continuum elastic rod model and all-atom molecular dynamics to simulate the atomic structure of the toroid and its subsequent dynamic ejection from the cavity. Exploring how DNA responds to extreme compression represents a relatively unexplored regime.

Given the evidence of DNA buckling in φ29, we now use theoretical methods to explore the existence of buckling in other dsDNA bacteriophages. During packaging, DNA is guided into the capsid through a "portal system" typically composed of a series of stacked cylindrical protein subunits which extend into the capsid. Often possessing different internal diameters, these proteins create cavities in an otherwise straight channel tube, a feature observed in φ29 and across a number of well-studied bacteriophages (as reviewed in e.g. [4]). Unlike φ29, these cavities are formed prior to genome packaging.

As packaging nears completion, the packing motor generates significant compressive force on straight DNA which may build until DNA buckles. The height of these cavities essentially dictates the length of a DNA column which can be buckled. Using analytic and numerical approaches, we compute the forces required at the onset and during buckling. As the three dimensional post-buckled conformation develops, we predict lower forces required to maintain equilibrium. We postulate that a buckling event could mechanically provide the "head-full" signal to the packing motor to terminate DNA packaging or signal a conformational change in

the portal protein required to seal the capsid. In the case of bacteriophage T7, cryo-EM (albeit at lower resolution than φ29) reveals a taller cavity than φ29 as well as a conformational change in the portal system upon reaching maturity [5].

References:

[1] Smith, D., S. Tans, S. Smith, S. Grimes, D. Anderson, and C. Bustamante. 2001. The bacteriophage phi 29 portal motor can package DNA against a large internal force. Nature. 413(6857), 748–752.

[2] Rickgauer, J. P., D. N. Fuller, S. Grimes, P. J. Jardine, D. L. Anderson, and D. E. Smith. 2008. Portal motor velocity and internal force resisting viral DNA packaging in bacteriophage phi 29. Biophys. J. 94(1), 159–167.

[3] Tang, J., N. Olson, P. J. Jardine, S. Grimes, D. L. Anderson, and T. S. Baker. 2008. DNA poised for release in bacteriophage phi 29. Structure. 16(6), 935–943.

[4] Tavares, P., S. Zinn-Justin, and E. V. Orlova. 2012. Genome gating in tailed bacteriophage capsids. Adv. Exp. Med. Biol., 726, 585-600

[5] Agirrezabala, X, J. Martin-Benito, J. R. Caston, R. Miranda, M. Valpuesta, and J. L. Carrascosa. 2005. Maturation of phage T7 involves structural modification of both shell and inner core components EMBO J. 24(21), 3820-3829.

ID: 429

Molecular Origin of the Sawtooth Behavior and the Toughness of Nacre

NING ZHANG
University of Florida MAE-B 223

Youping Chen

Abstract:
We present in this paper a method to build a computer model that mimic the mineral-protein composite structure of a nacre tablet. Motivated by the interesting observations in AFM experiments of nacre, protein chains stretching out from grain boundaries are simulated by steered molecular dynamics (SMD) to gain an insight into the effect of protein-aragonite interaction on the mechanical properties of nacre and the molecular mechanisms of the sawtooth behavior. Force-extension curves are obtained and the key characteristics of sawtooth behavior are observed in SMD simulations in agreement with existing AFM experiments of nacre. The effect of water on protein-mineral interaction is investigated through including and excluding water molecules in the grain boundaries of the models. Different from the existing belief that protein unfolding is the origin of the sawtoot behavior, we have found that the electrostatic interactions between the protein and aragonite mineral are responsible for the sawtooth behavior and hence the high toughness of nacre.

ID: 463

Capillary Forces as a Mechanism of Action in Microporous Scaffolds

Samantha Polak
University of Illinois - Urbana-Champaign

Amy Wagoner Johnson

Abstract:
Research shows significant improvements in bone formation in CaP scaffolds containing microporosity. However, the mechanism controlling improvements has yet to be determined. We also demonstrated the presence of cells and bone throughout microporous (MP) scaffold rods containing 5µm pores. We have identified a mechanism by which bone formation improves in these scaffolds and by which cells and bone remain viable in such small pores. We propose that MP CaP scaffolds with cells and growth factors relevant to bone formation through capillary forces upon implantation. Theoretical calculations show capillary forces are large enough to draw in a variety of cell types into the micropore network. In experiments, we demonstrate that cells are in the micropores minutes after implantation. In contrast, scaffolds treated with PBS or that are contaminated by particulates in the micropores, showed no cell infiltration. This is the first demonstration of a specific mechanism that enhances bone formation in these scaffolds.

ID: 508

Prediction and Control of 3D Shape and Mechanical Properties of DNA-based Nanostructures

Do-Nyun Kim
Laboratory for Computational Biology & Biophysics, Department of Biological Engineering, Massachusetts Institute of Technology
United States

Mark Bathe
Laboratory for Computational Biology & Biophysics, Department of Biological Engineering, Massachusetts Institute of Technology
United States

Abstract:

Recent advances in DNA nanotechnology enable the construction of complex one, two, and three-dimensional structures at the nanometer-scale with diverse engineering and scientific applications. In particular, scaffolded DNA origami has proven to be a versatile and robust approach to self-assembling individual DNA strands into bundles with precise control over their final solution shape and mechanical properties [1-4]. However, the design of these structures largely relies on designer intuition and experience without feedback based on a physical model, which hinders the use of this technology by the broader scientific community and unnecessarily increases the financial cost and time required to achieve target design specifications. For these reasons we are developing an integrative computational design and analysis approach for DNA-based nanotechnology called CanDo (Computer-aided engineering for DNA origami, http://cando-dna-origami.org). In this work, we demonstrate that CanDo predicts complex equilibrium solution shape and mechanical flexibility due to thermal energy from basepair connectivity maps [5]. Recently, we additionally extended CanDo to model nicks in the DNA double-helix and single-stranded DNA mechanics, also validated experimentally [6]. We demonstrate the capabilities of CanDo by comparing predicted shapes and flexibilities with experimental observations for various three-dimensional DNA origami objects including structures with significant bend and/or twist, tensegrity structures, and wireframe structures. In addition, we briefly introduce our ongoing efforts to model salt-dependent electrostatic interactions between DNA helices and to develop a lattice-free design strategy.

Methods:

CanDo employs the finite element method to model DNA at the basepair resolution and predict the three-dimensional shape in equilibrium and thermally induced fluctuations of the folded structure. Each DNA double helix is modeled as a series of finite element beams with experimentally determined stretching (1,100 pN), bending (230 pN nm^2), and torsional (460 pN nm^2) stiffness of average B-form DNA helix. Basepairs connected by strand crossovers are assumed to be rigidly constrained to each other in their motions. The three-dimensional solution shape in equilibrium is computed via the mechanical perturbation analysis using the commercial

Finite Element software ADINA (ADINA R&D, Inc.) to compute the minimum energy structure that satisfies axial and torsional constraints of DNA basepairs at crossover positions (Figure 1). Equilibrium thermal fluctuations at this free energy minimum are then computed by using normal mode analysis, as previously demonstrated for proteins using the finite element method [7-8]. Additional details on the model are available in [6].

Figure 1 Snapshots of a spherical wireframe structure [3,6] during the mechanical perturbation analysis performed by CanDo. CanDo computes the equilibrium solution shape (yellow) from the initial design (blue) that is based on a two-dimensional basepair connectivity map (left corner in the plane) via several intermediate solution steps (purple, orange, and green).

References:

1. Rothemund, P.W.K. Folding DNA to create nanoscale shapes and patterns. *Nature*, 440: 297-302 (2006).
2. Douglas, S.M., Dietz, H., Liedl, T., Högberg, B., Graf, F., Shih, W.M. Self-assembly of DNA into nanoscale three-dimensional shapes. *Nature*, 459: 414-418 (2009).
3. Dietz, H., Douglas, S.M., Shih, W.M. Folding DNA into twisted and curved nanoscale shapes. *Science*, 325: 725-730 (2009).
4. Han, D., Pal, S., Nangreave, J., Deng, Z., Liu, Y., Yan, H. DNA origami with complex curvatures in three-dimensional space. *Science*, 332: 342-346 (2011).
5. Castro, C.E., Kilchherr, F., Kim, D.N., Lin Shiao, E., Wauer, T., Wortmann, P., Bathe, M., Dietz, H. A primer to scaffolded DNA origami. *Nature Methods*, 8: 221-229 (2011).
6. Kim, D.N., Kilchherr, F., Dietz, H., Bathe, M. Quantitative prediction of 3D solution shape and flexibility of nucleic acid nanostructures. *Nucleic Acids Research*, 40: 2862-2868 (2012).
7. Bathe, M. A finite element framework for computation of protein normal modes and mechanical response. *Proteins: Structure, Function, and Bioinformatics*, 70: 1595-1609 (2008).
8. Kim, D.N., Nguyen, C.T., Bathe, M. Conformational dynamics of supramolecular protein assemblies. *Journal of Structural Biology*, 173: 261-270 (2011).

ID: 520

The Multiscale Mechanics of Scaled Fish Skin

Francois Barthelat
McGill University

Lawrence Szewciw

Abstract:
The scaled skin of fish is a high-performance protective system which has been evolving for 500 millions of years. While scales from ancient; fish were thick and heavy, the vast majority of today; teleost fish have evolved towards an elegant compromise between light weight, flexibility and resistance to puncture. In this work we have investigated the performance and mechanics of the scaled skin of striped bass Morone saxatilis, a relatively common fish found in the Atlantic Ocean. Individual scales of this fish consist of dense crossplies of collagen type I fibrils, which are mineralized with hydroxyapatite in the outermost layer. We have showed that the puncture resistance of individual scales is superior to that of high performance engineering polymers (polycarbonate and acrylic). The mechanics of puncturing several overlapping scales was also explored with experiments and models. The effects of the friction between scales and of the stiffness of the substrate were of particular interest. The stiff collagenous layer underlying the scales (stratum compactum) was found to be critical by providing a stiff and strong backing material for the scales. Bending of the skin is a typical deformation mode which occurs during swimming and also locally in the event of a puncture. Through bending experiments on whole fish as well as modeling, we have demonstrated that the scales contribute to stiffening the skin at high bending curvatures. The scales can therefore store strain energy at the end of each stroke, which can be recovered to initiate the next stroke for highly efficient swimming. We also show that stiffening of the skin in bending contributes to delaying localization in the event of a sharp puncture, by spreading deformations over a large surface of the skin. Implications for biomimetic lightweight and flexible protective systems are discussed.

ID: 567

DYNAMIC FORCE SPECTROSCOPY OF SPECIFIC BINDING BETWEEN PROTEIN AND DNA APTAMER

Xiao Ma
Department of Mechanical Engineering, Iowa State University
United States

Pranav Shrotriya
Department of Mechanical Engineering, Iowa State University
United States

Introduction

Nowadays the interest and need on the development and modulation of biotic-abiotic interface keep increase, one of the essential challenges on this objective is the detection of binding specificity and strength between bio-molecules, which requires a thorough understanding of the mechanism governing the binding interaction. Research on force interaction between the complimentary pair of bio-molecules or functional groups contributes to implement the above objectives.

This research aims at the measurement of binding forces between human thrombin and its complementary DNA aptamer, which is an example of protein/DNA interaction. The specific single-stranded DNA aptamer that binds to thrombin has a hairpin structure with the specific base sequence $GGNTGGN_{2\text{-}5}GGNTGG$, known as G-quadruplex. Thrombin aptamer can fit into thrombin heparin binding site and has high binding specificity with thrombin [1]-[2].

The objective of this research is to confirm the highly specific binding between thrombin and its aptamer and measure the binding strength between the pair through Atomic Force Microscopy (AFM).

Method

In order to implement binding force measurement bet-ween the complementary pair via AFM, thrombin is immobilized to the AFM tip and aptamer is attached to the gold substrate. The functionalized AFM tip with thrombin then is brought into contact with aptamer to establish a ligand/receptor bond, and then pulled away at a controlled rate to subsequently break the bond [3]. The measurements of this bond break force are performed a large number of times in order to obtain a statistically significant measure of the force interaction.

Force curve experiments were performed via Dimension 3100 AFM in binding buffer at two nominal displacement rates (200nm/s and 2000nm/s) to test loading rate effect. Thousands of force curves experiments were taken to construct force spectrum. Since the last binding event is more likely to have fewest bond breakages, only that data were used for analysis.

Results

The typical force curve of thrombin-aptamer pair is shown in Fig.1. Discrete drops in forces have been suggested to be associated with sequentially unbinding interactions between thrombin and aptamer. The stepwise trend and large magnitude of binding forces show the binding specificity between thrombin and aptamer. The last rupture force distributions are categorized into 4 different loading rate levels, as shown in Fig.2.

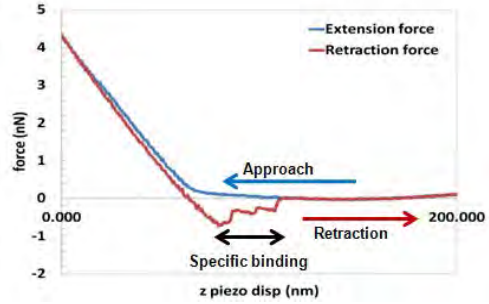

Fig.1 Typical force curve

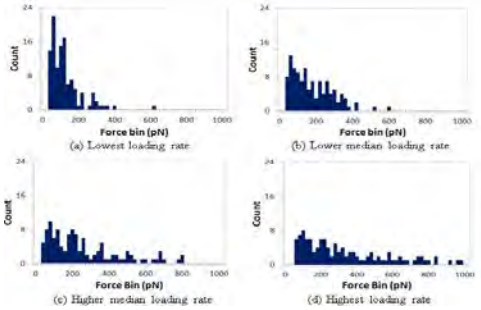

Fig.2 Last rupture force distribution

The last rupture force spans a very broad range, which implies most last bind forces comprise of several multiples of the "single-bond" binding. In order to find out this single-bond binding force, autocorrelation function was performed on the last rupture force distribution, as shown in Fig.3. The repeated pattern and period show the most frequent rupture force for a single binding event. This most frequent rupture force, defined as force quantum, can then be determined as 19.5, 25.8, 33.0 and 39.9pN from low to high loading rate levels.

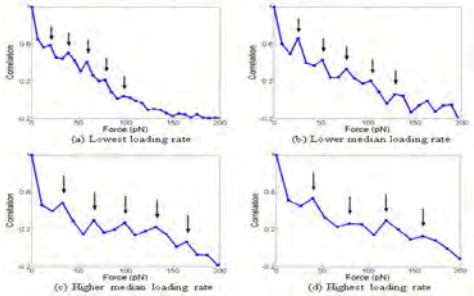

Fig.3 Autocorrelation function

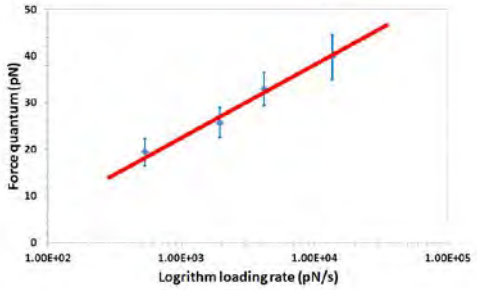

Fig.4 Binding force as a function of loading rates

As shown in Fig.4, force quantum has a linear dependence on the logarithm of loading rate, which explicitly demonstrated the binding strength and loading rate effect of thrombin-aptamer pair, and can be well explained by the single energy barrier model proposed by Evans, et al. [4]. The good agreement between experiment and theory implies that single energy barrier is the governing mechanism of binding and dissociation behavior between thrombin and its aptamer.

References

[1] Bode. The refined 1.9 Å crystal structure of human a-thrombin. *The EMBO Journal,* 1989, *8*(11), 3467-3475.

[2] Bock. Selection of single-stranded DNA molecules that bind and inhibit human thrombin. *Nature,* 1992, *355*, 564-566.

[3] Basnar, B., Elnathan, R., and Willner, I.. Following aptamer-thrombin binding by force measurements. *Analytical Chemistry,* 2006, 78, (11), 3638-3642.
[4] Evans. Dynamic Force Spectroscopy - Physics of Bio-Molecules and Cells.169

ID: 603

Large Deformations of Lipid Bilayers Induced by Protein-Like Inclusions

Raffaella De Vita
Virginia Tech

Iain Stewart

Abstract:
A new energy for the description of large deformations of lipid bilayers is formulated with mathematical rigor. This energy is derived by considering the Smectic A liquid crystalline nature of lipid bilayers and the coupling between the deformations of the layers and comprising lipid molecules. The analogies between Smectic A liquid crystals, with an infinite number of layers, and lipid bilayers, with a finite number of layers, are further discussed. The novelty of the energy density is demonstrated by studying the large deformations of planar lipid bilayers induced by cylindrical protein-like inclusions. The results of this study are directly compared with the results obtained using May's theoretical framework (2000) in which small deformations are assumed. As expected, the proposed energy density predicts larger distortions of the lipid molecules and deformations of the lipid bilayers close to the inclusion.

ID: 643

Critical Scales Govern the Mechanical Fragmentation Mechanisms of Biomolecular Assemblies

Sinan Keten
Northwestern University
USA

Abstract:
Mechanical perturbations such as ultrasonication-induced cavitation alter the formation and fragmentation of biomolecular materials, providing a new route to manipulate emergent size and order of assemblies. However, how fragmentation of assemblies occurs in the vicinity of a shock front remains to be understood, since the molecular mechanisms are challenging to discern directly from experiments. Through an atomistically informed coarse-grained model that leverages the capability of rapidly simulating microscopic length and time scales while retaining low-level details, we present a comprehensive investigation of the fragmentation mechanisms of protein assemblies under shock deformation. These simulations illustrate for the first time that the fragmentation pathways depend strongly on the shock front radius and impact energy relative to fibril size and strength. A transition between two competing mechanisms is observed at a critical impact velocity, leading to a stark contrast in the size scaling of fragmentation at low and high strain rates. These findings establish and classify key fragmentation mechanisms based on their dependence on the characteristic length and time scales of deformation and relaxation processes, thereby explaining a broad range of recent experiments that suggest a strong dependence of the fragmentation processes on perturbation conditions. Our results facilitate a broader perception of how molecular assemblies can be broken down by force for the functional mechanoassembly and manipulation of nanomaterials.

ID: 705

Multi-Scale Study of Hydrogels: from Nano to Meso

Hossein Salahshoor

Abstract:
Recently, hydrogels have found a variety of applications in biomedical engineering since their porous structure and hydrophilicity enables them to absorb a large amount of water. However, strength and toughness of hydrogels is not well understood. As a result, multi-scale modeling will lead to a better understanding of their properties. In this study, hydrogel is studied using ab-initio molecular dynamics (MD) and coarse-grained (CG) framework, considering Condensed-Phased Optimized Molecular Potential (COMPASS) and Martini force fields. PEDGE and Jeffamine are the epoxy and curing agent used as hydrogel. The crosslinking process is modeled using cyclic NPT and NVT simulations starting from a high temperature, cooled down to a lower one to simulate the curing process. Mechanical properties of hydrogels are studies by applying a strain to the unit cell and the results show that the CG model leads to a more accurate Young Modulus and Strength. The simulation results are in excellent agreement with the experimental data in comparison with conventional molecular dynamics. Also, diffusivity of water in the hydrogel structure is studied in the CG framework and the swelling mechanism is studied.

ID: 717

Multiscale Modeling of Protein Dynamics

Michael Leamy
Georgia Institute of Technology
USA

Kyle Karlson
USA

Abstract:
Two multiscale continuum models for simulating protein dynamics are developed which allow for resolution of protein peptide planes in a beam-like finite element. A curvature and strain-based finite element formulation is utilized. This formulation is advantageous in simulating proteins since amino acid chains may be described by a single element, even when the protein segment considered exhibits large curvature and twist such as in the α-helical shapes prominent in many proteins. Concurrent and hierarchical multiscale models are developed for the curvature and strain-based beam formulation. The hierarchical multiscale continuum model utilizes a novel shooting method to calculate the deformed configuration of the protein. An optimization algorithm determines the requisite stiffness parameters by varying the beam stiffness used in the shooting method until deformed configurations of test cases correspond to those produced by the LAMMPS molecular dynamics software. Additionally, a concurrent multiscale method is detailed for evaluating protein inter-atomic potential parameters from the curvature and strain degrees of freedom employed in the model. This allows internal forces and moments to be calculated using nonlinear protein potentials. Proof of concept testing and model verification for both models includes comparing the multiscale techniques to all-atom molecular dynamics solutions. Specifically, the models are verified by simulating a polypeptide in a vacuum and comparing the predicted results to those computed using LAMMPS.

ID: 725

New Insight into the Toughening Mechanisms of Nacre

Barton Prorok
Auburn University
USA

Marianne Sullivan

Abstract:
Many living organisms form biogenic minerals or biominerals, which are composite materials containing an organic matrix and nano- or micro-scale minerals assembled in a hierarchical architecture. These biogenic composites possess excellent mechanical properties in comparison to their abiogenic architectures (on the order of 3000 times greater), which make them attractive for mechanically protective applications. One biogenic material that has garnered a lot of attention is Nacre, or Mother of Pearl; found in many Mollusk shells. The Nacre architecture has been well studied the past decade, however little work has focused on the fact that the Nacre composite is also itself a component of another composite architecture in the shells. In between thick layers of Nacre is a thin layer of an organic matrix that marks the seasonal growth patterns of the shells, analogous to tree rings. No work has focused on how these two layers interact to determine mechanical properties, which are likely as important as the tablet sliding itself. Determining this relationship would have a great impact on designing composite architectures that can improve the performance of mechanically protective armor.

ID: 830

MECHANICAL PROPERTIES AND STRUCTURE OF CONTINUOUS DNA NANOFILAMENTS

Kaspars Maleckis
Department of Mechanical and Materials Engineering
University of Nebraska-Lincoln
USA

Yuris Dzenis
Department of Mechanical and Materials Engineering
University of Nebraska-Lincoln
USA

Abstract:
DNA is used as self-assembling multifunctional building material for novel technologies, such as nanostructured sensing materials and field-effect transistors, or nanosized computers and functioning devices. While having the unique advantage of forming complex structures, the self-assembly process is hard to control. Electrospinning is an alternative top-down nanomanufacturing method, by which polymer nanofibers can be produced in high electric fields. Unlike self-assembly, electrospinning can provide continuous nanofibers, with ability to bridge the nano and micro scales.

This study presents the first systematic investigation of continuous electrospun DNA nanofibers. Two types of fibers from single stranded (ss) and double stranded (ds) DNA solutions with wide range of diameters were produced by electrospinning. Tensile tests of single DNA nanofibers were performed for the first time, revealing very high mechanical properties – exceeding 1GPa strength and 300MPa toughness for the best results. Mechanical tests also showed size effect on strain at failure and toughness which increase significantly as fiber diameters decrease. Based on mechanical response the differences of molecular networks were proposed. Structural studies using Raman spectroscopy, X-ray diffraction (XRD) and other methods provided additional insight on DNA nanofiber structure.
Electrospun collagen scaffolds are widely used in tissue engineering, with aim to replicate natural environment of the extracellular matrix (ECM). However, due to organic solvents used in production, the artificial collagen scaffolds are unable to mimic the mechanical properties and structure of the natural ECM. Fibers from collagen-DNA hybrid solutions were made to enhance the processing, structure, and properties of tissue engineering fibers. It was found that as little as 0.2% of DNA enabled electrospininning collagen fibers from aqueous solutions. XRD and thermogravimetric analyses exhibited close correspondence to natural collagen fiber results, unlike the results from conventionally produced fibers. Moreover, higher DNA concentrations produced extraordinary increases in ultimate strain and toughness up to three orders of the magnitude in the hybrid nanofibers.

The results of this study show that continuous DNA and collagen-DNA nanofibers can serve as building blocks for novel high-performance biodegradable and biocompatible materials for tissue engineering and other bionanotechnology devices and applications.

Missing Abstract

ID: 343

II.3

Mechanics of Biological Systems - Experimental Methods in Biomechanics

ID: 347

Micro-Mechanics of Neuronal Compression

Adam Fournier
Johns Hopkins University

KT Ramesh
USA

Abstract:
Traumatic axon injury (TAI) can be characterized as focal or multi-focal damage to the white matter tracts of the central nervous system and has been linked to spinal cord injury and traumatic brain injury. Degenerative responses to TAI have been linked to disruption of the cytoskeleton of neural axons. To investigate the dynamics of how constituents of the cytoskeleton respond to focal loading, superior cervical ganglia were removed from mice, dissociated, fluorescently labeled, and imaged during focal compression. Using a previously developed microcompression platform, compatible with confocal microscopy, visualization of the axon deformation was achieved prior to, during, and immediately after injury. Three dimensional imaging of the cytoskeletal deformation response provides insight to the structural roles and responses of cytoskeletal constituents under focal loading.

ID: 523

A New Method to Determine the Cohesive Behavior of Soft Biological Interfaces

Francois Barthelat
McGill University

Ahmad Khayer Dastjerdi

Abstract:
Virtually all organisms ranging from micron-sized bacteria through to larger-scale vertebrates benefit, to different extents, from remarkable properties of high-performance biological adhesives. These adhesives are also extensively used in surgery procedures, in tissue reconstruction and in tissue engineering. Therefore, the mechanical performance particularly fracture behavior of these; is crucial to the strength, toughness, reliability and performance of the repaired tissues in which they are used. Single-molecule force spectroscopy using the atomic force microscope has recently shown that these biological adhesives can dissipate a considerable amount of energy through protein unfolding/refolding processes. However, how this nano-scale energy dissipation relates to macroscopic performance is currently unknown. Here we present a new interfacial fracture technique which provide the cohesive law (traction-separation curve) of biological adhesives in the fracture mode (mode I), and without any prior assumption on its shape. The technique is based on the standard double-cantilever beam used for measuring interfacial toughness of industrial adhesives, which was adapted to take into account the high compliance of the biological adhesives compared to the beams. Using this novel technique, the adhesion of a fibrin network a biological adhesive which is used as a bio-glue in surgery to hydroxyapatite and collagen substrates was investigated. The effect of calcium concentration and fibrin crosslinking on the fracture behavior of the fibrin network was studied. Examination of the cohesive laws for different calcium concentrations provides hints on how the progressive failure of the fibrin network can be associated to the disruption of calcium salt bridges. It is also shown that covalent crosslinking highly increases the interfacial toughness of the network. This method can be applied to other soft biological adhesives of importance in the biomedical field, and it can also be used to assess and optimize the effect of various parameters on fracture toughness.
Supported by the Fonds de Recherche du (FRQS) and The Network for Oral and Bone Health Research.

ID: 711

Lipid Bilayer Mechanics in a Pipette with Glass-Bilayer Adhesion

Ashutosh Agrawal
University of Houston
USA

Tristan Ursell

Abstract:
Electrophysiology is a central tool for measuring how different driving forces (e.g. ligand concentration, transmembrane voltage, or lateral tension) cause a channel protein to gate. Upon formation of the high resistance seal between a lipid bilayer and a glass pipette, the so-called `giga-seal', channel activity can be recorded electrically. In this work, we explore the implications of giga-seal formation on the mechanical state of a lipid bilayer patch. We employ a mechanical model for the free energy of bilayer geometry in the presence of glass-bilayer adhesion to draw three potentially important conclusions. First, we use our adhesion model to derive an explicit relationship between applied pressure and patch shape that is consistent with the Laplace-Young Law, giving an alternative method of calculating patch tension under pressure. With knowledge of the adhesion constant one can precisely calculate the patch tension as a function of pressure, without the difficulty of obtaining an optical measurement of the bilayer radius of curvature. Second, we employ data from previous electrophysiological experiments to show that over a wide range of lipids, the resting tension on a electrophysiological patch is highly variable and can be 10-100 times higher than estimates of the tension in a typical cell membrane.

II.4

Mechanics of Biological Systems - Computational Modeling in Biomechanics

ID: 338

Analytical and Numerical Analyses of the Micromechanics of Soft Fibrous Connective Tissues

Gal deBotton
Ben-Gurion University
USA

Tal Oren
USA

Abstract:
State of the art research and treatment of biological tissues require accurate and efficient methods for describing their mechanical properties. Indeed, micromechanics motivated approaches provide a systematic method for elevating relevant data from the microscopic level to the macroscopic one. In this presentation the mechanical responses of hyperelastic tissues with one and two families of collagen fibers are analyzed by application of a new variational estimate accounting for their histology and the behaviors of their constituents. The resulting, close form expressions, are used to determine the overall response of the wall of a healthy human coronary artery. To demonstrate the accuracy of the proposed method these predictions are compared with corresponding 3-D finite element simulations of a periodic unit cell of the tissue with two families of fibers. Throughout, the analytical predictions for the highly nonlinear and anisotropic tissue are in agreement with the numerical simulations.

ID: 431

Nanoscale Plastic Deformation Mechanism in Single Crystal Aragonite

NING ZHANG
University of Florida MAE-B 223

Youping Chen

Abstract:
Molecular dynamics simulations have been performed to study the dynamic behaviors of single crystal aragonite under indentation, tension and compression. The elastic modulus and hardness of single crystalline aragonite measured in our simulations are found in good agreement with experimentally measured values. Our simulation results show that the mechanical properties of aragonite crystal, including the elastic modulus, hardness, strength, and toughness, strongly depend on the crystallographic orientations and loading conditions. We have identified that this dependence is resulted from different deformation mechanisms, i.e., phase transformation, amorphous phase formation, dislocation, and twining. This work is an attempt to identify the deformation mechanisms in aragonite and to establish the relationship between the dominant deformation mechanisms and its crystallographic orientations and loading conditions.

Missing Abstract

ID: 443

ID: 544

Computational Structural Model of the Atrium in Healthy and Arrhythmic Condition

Chiara Bellini
Department of Mechanical and Manufacturing Engineering, The University of Calgary
Canada

Elena Di Martino
Department of Civil Engineering, The University of Calgary
Canada

Salvatore Federico
Department of Mechanical and Manufacturing Engineering, The University of Calgary
Canada

Abstract:
This work was aimed at implementing a structural model of the atria, based on previously performed experimental measurements. Characterization of the mechanical behaviour of tissues from healthy human atria represents a necessary reference point to assess the effect of atrial pathologies, such as atrial fibrillation, a form of sustained cardiac arrhythmia, on the mechanics of the atrium, and provides the specifications for the design of tissue engineered cardiac patches that are capable of substituting malfunctioning regions of the atrium.

Mechanical Characterization of the Atrium

The local mechanical response of tissues from healthy human atria was assessed by means of planar biaxial tests performed following Sacks (2000). Square tissue specimens were excised and mounted on the testing device by means of nylon sutures and surgical staples to allow free shearing and ensure homogeneous distribution of the loads. Loads were applied as distributed tension forces per unit of length to optimize motor accuracy. Five loading protocols were performed on each specimen, each characterized by a specific ratio between the distributed tensions in the two in-plane directions of loading. Local deformations were computed from the position of five graphite markers glued on the surface of the specimens and tracked with a video extensometer. Experimental data were processed to obtain second Piola-Kirchhoff stress tensor components versus Green-Lagrange strain tensor components curves.

Structurally Motivated Fung-Type Potential for the Atrium

Fung-type elastic strain energy potentials are given by the composition of a function g with a quadratic form $\mathcal{Q}(\boldsymbol{E}) = \frac{1}{2}\boldsymbol{E} : \mathbb{Q} : \boldsymbol{E}$ in the Green-Lagrange strain $\boldsymbol{E}$:

$$W(\boldsymbol{E}) = a\, g(\mathcal{Q}(\boldsymbol{E})) = a\, g(\tfrac{1}{2}\boldsymbol{E} : \mathbb{Q} : \boldsymbol{E}) \tag{1}$$

It is possible to prove (Federico et al., 2008) that the fourth-order tensor $\mathbb{Q}$ of the quadratic form $\mathcal{Q}$ is proportional to the (material) linear elasticity tensor $\mathbb{L}$, i.e.,

$$\mathbb{Q} = a^{-1}\mathbb{L} \tag{2}$$

and that W is convex if, and only if, function g is monotonically increasing and convex, and the quadratic form $\mathcal{Q}$ is convex, which is automatically verified if $\mathcal{Q} = a^{-1}\mathbb{L}$ is definite positive, i.e., if constant a is positive, and the linear elasticity tensor $\mathbb{L}$ is positive definite.

From the fundamental relation expressed by Eq. (2), a clear structural interpretation can be given to Fung-type potentials, once a structural description of the linear elasticity tensor $\mathbb{L}$ is available. We propose to express $\mathbb{L}$ for the atrium by means of the Theory of Mixtures. If indices 0, 1, and 2 denote the matrix and the two families of fibres, respectively, then tensor $\mathbb{L}$ is given by

$$\mathbb{L} = \phi_0 \mathbb{L}_0 + \phi_1 \mathbb{L}_1 + \phi_2 \mathbb{L}_2 \tag{3}$$

where ϕ_α are the volumetric fractions. We assume $\mathbb{L}_0$ to be isotropic, and $\mathbb{L}_1$ and $\mathbb{L}_2$ to be transversely isotropic, each in the direction of one of the two families of fibres, and the two directions of transverse isotropy to be mutually orthogonal and orthogonal to the direction of the normal to the plane of the biaxial test. Hence, the overall tensor $\mathbb{L}$ is orthotropic in the three named directions.

The figure on the right shows how the proposed structural Fung-type potential is able to discern the test protocols described above.

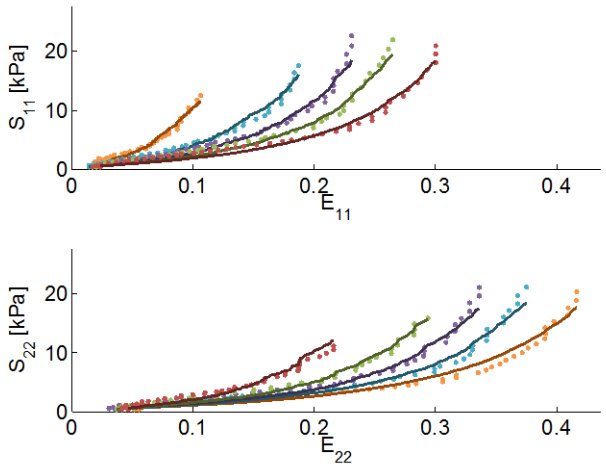

Numerical Implementation

The structural Fung-Type potential was implemented into ABAQUS as a user-defined material. This required the spatial elasticity tensor providing the power-conjugation of the Green-Naghdi rate $\boldsymbol{\tau}^{\square}$ of the Kirchhoff stress $\boldsymbol{\tau}$ with the deformation rate $\boldsymbol{d}$. The procedure outlined by Simo and Hughes (1998) was followed, and the special tensor products introduced by Curnier et al. (1995) were used to find a covariant, coordinate free expression of the sought elasticity tensor as

$$\mathbb{B} = J\,\mathbb{C} + 2\,\boldsymbol{\tau}\,\underline{\otimes}\,\boldsymbol{g}^{-1} + [\boldsymbol{i}\,\underline{\otimes}\,(\boldsymbol{\tau}\boldsymbol{g}) - (\boldsymbol{\tau}\boldsymbol{g})\,\underline{\otimes}\,\boldsymbol{i}] : \mathbb{V} \tag{4}$$

where $J = \det \boldsymbol{F}$, $\mathbb{C}$ is the standard spatial elasticity tensor, $\boldsymbol{g}$ is the spatial metric, $\boldsymbol{i}$ is the spatial second-order identity and, $\boldsymbol{V}$ and $\boldsymbol{b}$ being the left stretch and left Cauchy-Green tensors,

$$\mathbb{V} = \frac{1}{I_1(V)I_2(V) - I_3(V)}\left[(I_1(V))^2(\boldsymbol{V}\,\underline{\otimes}\,\boldsymbol{g}^{-1} - \boldsymbol{g}^{-1}\,\underline{\otimes}\,\boldsymbol{V}) - I_1(V)\,(\boldsymbol{b}\,\underline{\otimes}\,\boldsymbol{g}^{-1} - \boldsymbol{g}^{-1}\,\underline{\otimes}\,\boldsymbol{b}) + (\boldsymbol{b}\,\underline{\otimes}\,\boldsymbol{V} - \boldsymbol{V}\,\underline{\otimes}\,\boldsymbol{b})\right] \tag{5}$$

References

Curnier, A., He, Q.-C., Zysset, P. 1995, *J. Elasticity*, 37, 1-38

Federico, S., Grillo, A., Giaquinta, G., Herzog, W., 2008, *Meccanica*, 43 (3), 279-288

Fung, Y.C., 1967, *Am. J. Physiol.,* 213, 1532-1544

Sacks, M.S., 2000, *J. Elasticity*, 61, 199-246

Simo, J.C., Hughes, T.J.R., 1998, *Computational Inelasticity*, Springer

ID: 551

An Immersed Finite Element Method Approach for Brain Biomechanics : An Application to Hydrocephalus

Saswati Roy
The Pennsylvania State University
USA

Luca Heltai
USA

Abstract:
The immersed element method (IFEM) is a computational method for analyzing structure interaction (FSI) problems. Immersed methods have gained wide use in the analysis of biomechanical systems. In this paper, we use the fully variational formulation of the IFEM [1] to develop a biomechanical model of the brain duringhydrocephalus. Hydrocephalus is a pathological condition of the brain during which the lateral ventricles of the brain become distended due to the excessive accumulation of the cerebrospinal (CSF) in them. We analyze the hydrocephalic brain as an FSI problem in which parenchyma, modeled as an incompressible neo-Hookean material, interacts with the surrounding CSF, modeled as a Newtonian. We generate the mesh for the structure from the MRI scan of an actual hydrocephalic brain and analyze the effect of varying the physical parameters, like viscosity, of the encephalic system within realistic ranges on the deformation of the brain during hydrocephalus. References [1] Luca Heltai and Francesco Costanzo. Generalized immersed element method. To appear in Computer Methods in Applied Mechanics and Engineering.

ID: 641

An X-FEM Based Eulerian Formulation to Model the Mechanics of Lipid Membranes

Louis Foucard
University of Colorado at Boulder
USA

Abstract:
The cell membrane-cortex complex is an important structure that not only provides a barrier between intra and extra-cellular environments, but also plays a large role in cell mechanics and function. For instance, membrane/cortex mechanics is of critical importance in processes such as cell blebbing, endocytosis or cell division, processes that all involve extreme deformations and changes of morphology. From a modeling viewpoint, the classical method that consists of modeling a membrane within the lagrangian formalism is neither suited to describe such severe deformations (100%) nor to capture the dynamics of the cytosol in the intracellular space. To address this issue, we present a fully Eulerian approach that describes the large deformations of an elastic membrane and its interactions between with the intracellular fluid. The membrane is modeled as a two-dimensional elastic surface, defined by a level set function in a three-dimensional space, across which discontinuities of continuum fields such as pressure and fluid velocity can naturally be enforced using the extended finite element method (X-FEM). The motion of the membrane is then described with the traditional level-set evolution equation, which follows from a balance of between internal and external forces in the membrane. We show that this method is ideal to enforce volume constraints; Dirichlet and Neumann type boundary conditions on the membrane, and to numerically evaluate the membrane curvature. The validity of the model is then assessed by computing equilibrium shapes, membrane strains as well as pressure jumps across the membrane in several biologically relevant situations, such as membrane adhesion, cell blebbing and endocytosis.

ID: 644

Simulation Based Design Approach to Tuning the Assembly, Selective Transport and Mechanical Properties of Cyclic Peptide Nanotubes

Sinan Keten
Northwestern University
USA

Luis Ruiz

Abstract:
Cyclic peptide nanotubes (CPNs) have unique chemical and mechanical features that make them squarely positioned to tackle persistent challenges in novel biomaterials, sensors, and selective membranes. These self-assembled hierarchical nanostructures are highly organized at the nanoscale and feature exceptional thermodynamical stability arising from the collective action intersubunit hydrogen bonds networks. Understanding the elasticity and fracture behavior of CPNs through a multi-scale analysis is crucially important for developing science-based approaches to designing the molecular subunits and hierarchical assemblies of these materials. In pursuit of addressing this need, here we propose a methodology for linking atomistic simulation results into coarser descriptions of these self-assembling soft nanostructures. Our approach involves estimation of the free energy landscape of the system along the deformation reaction coordinate from atomistic simulation trajectories using nonequilibrium statistical thermodynamics formulations, which enables bridging scales through mapping to coarse-grain or continuum descriptions. We demonstrate the basic multi-scale approach for investigating the mechanics of cyclic peptide based organic nanotubes (CPNs), mapping out the elastic range of intersubunit interactions along with the large deformation and fracture regimes (Ruiz and Keten, Int. J. of Applied Mechanics, 2011,Journal of Engineering Mechanics, 2012). This work illustrates the potential of atomistically informed methods for predicting elastic as well as large deformation behavior of high aspect ratio self-assembling nanostructures. The key outcome of our efforts is that chemical modifications carefully selected by predictive simulations (Hourani et al. JACS, 2011) enhance the transport, self-assembly and mechanical behavior of peptide nanotubes simultaneously, enabling a science based approach to the synthesis of novel nanotubes with highly tunable properties.

ID: 662

Stiffness Homogenization of Damaged Teeth Repaired by Resin Injection

Elsa Vennat
Laboratory of Soil Mechanics, Structures and Materials, Ecole Centrale Paris, Châtenay Malabry
France

Chloé Arson
School of Civil and Environmental Engineering, Georgia Institute of Technology
Center for Tectonophysics, Texas A&M University
United States

Dental caries are the most common human disease. They are usually treated by removing the carious lesion, and substituting the mineral components of a micrometric layer of sane dentin by a resin composite. Tooth reparation thus consists in a demineralization phase followed by an injection phase. *A homogenization scheme is proposed in order to predict the elastic properties of intact, demineralized and injected dentin.* Dentin is a biological composite material (Figure 1) made of tubules, Peri-Tubular Dentin (PTD) and Inter-Tubular Dentin (ITD). Tubules can be considered as pipes full of fluids. PTD is highly mineralized dentin located in periphery of tubules. ITD is a collagen rich mesh filled with apatite crystals. At the nanoscale level, inter-tubular dentin is a composite made of collagen fibrils (CF) and hydroxyapatite crystals (HA).

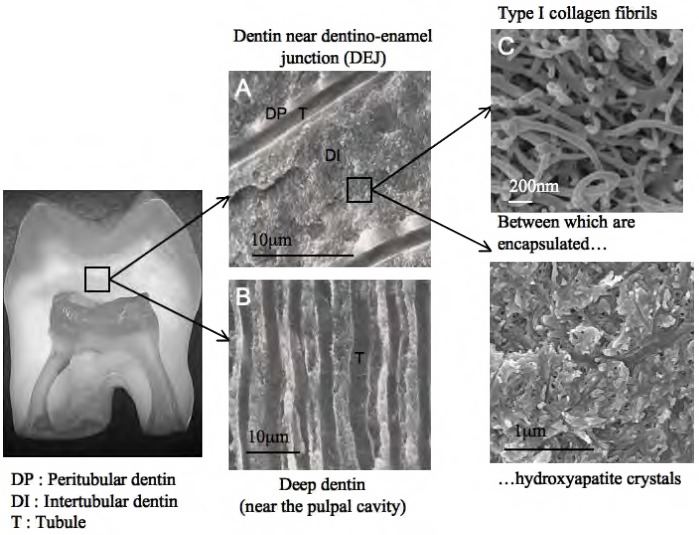

Figure 1.
Dentin Microstructure
(Vennat, 2009).

Demineralization results in tubule enlargement (by quasi-total removal of PTD) and inter-tubular dentin collagen fiber network uncovering. Although HA minerals were observed in the inter-fibrilar space by Vennat (2009), there is no consensus on the location of the crystals in dentin microstructure. In particular, Bar-On and Wagner (2012) only account for HA crystals contained in CFs in their homogenization scheme, whereas Pashley et al. (2011) consider that CFs are encapsuled in a mineral, in addition to containing intra-fibrilar HA crystals. As a result, several scenarios can be envisaged to explain the evolution of dentin microstructure during demineralization. In this research work, it is assumed that CFs contain ellipsoidal HA inclusions.

Intervowen CFs are viewed as a porous matrix, in which each pore is considered as an inclusion: either made of extra-fibrilar protein, or of an extra-fibrilar HA crystal. Based on the assumptions made on dentin microstructure, dentin stiffness tensor is homogenized in three steps (Figure 2).

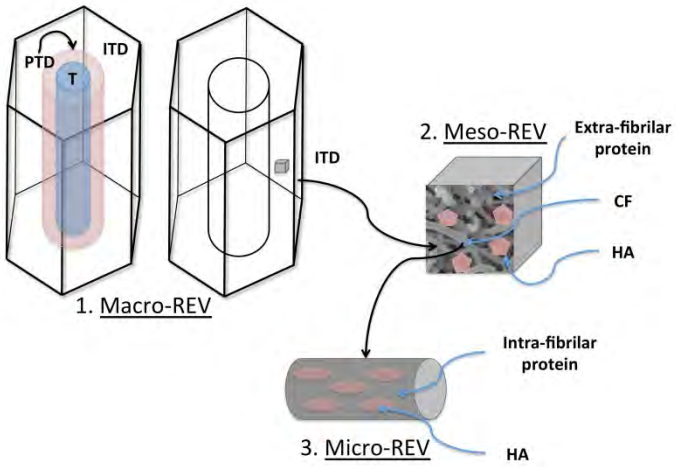

Figure 2. Three-Step Homogenization Procedure Proposed to Determine Dentin Stiffness.

1. A cylinder with a hexagonal basis constitutes the periodic unit cell defining the "macroscopic" Representative Elementary Volume (REV). It contains a fraction of tubule surrounded by PTD and ITD. PTD is viewed as a hollow inclusion in an ITD matrix, and the self-consistent method is applied. It is thus possible to test various rheologies at the interface between ITD and PTD - as opposed to the composite approach proposed by Bar-On and Wagner (2012). The porosity mode associated to dentin tubules is of the order of 0.35 (Vennat, 2009). The fraction of tubule contained in the macroscopic REV is assumed to be a cylinder with a circular basis. In intact dentin, the diameter of tubules is about 2 microns, which imposes a REV size of about 9 microns. Tubules and PTD are considered as homogeneous materials. In demineralized (resp. injected) dentin, the elastic moduli of tubules and PTD are replaced by those of the demineralizing fluid (resp. by those of resin).

2. The "mesoscopic" REV is a fraction of ITD containing CFs, HA crystals and inter-fibrilar proteins. Its size should be about 10 microns in order to satisfy the statistical homogeneity requirements (Nemat-Nasser & Hori, 1993). This is approximately the size of the macroscopic REV, which is determined by dentin tubular porosity. It is thus impossible to use a homogenization scheme based on random distributions of inclusions. A smaller mesoscopic REV needs to be defined. That is the reason why ITD is modeled as a layered composite (Bar-On and Wagner, 2012). A formula based on the volume fraction of HA and inter-fibrilar protein inclusions (e.g., Halpin-Tsai model) is used in order to compute ITD mesoscopic stiffness tensor. Inter-fibrilar protein and HA crystals are modeled as homogeneous materials. In demineralized (resp. injected) ITD, HA crystals properties are replaced by fluid (resp. resin) properties.

3. *The "microscopic" REV is a portion of CF, made of protein matrix containing ellipsoidal HA inclusions*. Both the matrix and the HA crystals are considered as homogeneous materials, and the self-consistent method is used to compute CF microscopic stiffness tensor. In both demineralized and injected dentin, HA crystals are replaced by void inclusions, i.e. it is assumed that capillary effects prevent the penetration of resin in CF microscopic pores.

ID: 701

Mechanical Feedback during Early Brain Development

Zi Chen
Department of Biomedical Engineering, Washington University in St. Louis
United States

Benjamen A. Filas
Department of Ophthalmology and Visual Sciences, Washington University School of Medicine
United States

Larry A. Taber
Department of Biomedical Engineering, Washington University in St. Louis
United States

Abstract:
Mechanical feedback plays an important role in morphogenesis during embryonic development. The brain starts as a simple tube, which subdivides into three primary vesicles (forebrain, midbrain, and hindbrain) and then undergoes a period of rapid expansion. This growth is known to depend on the increasing pressure generated by the cerebrospinal fluid (CSF) filling the lumen. Interestingly, if the brain is punctured during this period, it collapses and then re-inflates rapidly after the wound heals. The mechanisms of this response have not been previously reported. To study this problem, we are measuring fluid pressure, wall strains, and geometry (via optical coherence tomography). This information is used to develop a computational model for the collapse and growth process, with stress-based growth laws implemented in the model to simulate the experiments. Our study shows that the early-stage brain is more prone to collapse but in a more gradual manner than in older embryos. Our results also suggest that the brain may have a latent ability to re-inflate (often with overshooting) to counteract congenital malformations, the mechanism of which warrants further investigation. Our work will fit in the theme of how epigenetic factors (e.g., mechanical feedback) regulate morphogenesis in embryonic development, and will also benefit the ongoing efforts in understanding the origins of congenital brain disorders.

ACKNOWLEDGEMENT
This work has been supported by NIH/NINDS grant, R01 NS070918, and Society in Science – Branco Weiss fellowship.
Correspondence: lat@wustl.edu.

REFERENCES
1. M. A. Wyczalkowski, Z. Chen, B. Filas, V. Varner and L. A. Taber, Birth Defects Res., Part

C 96, 132 (2012).
2. L.A. Taber. Philos. T. R. Soc. A 367:3555–3583 (2009).
3. B.A. Filas, V.D. Varner, D.A. Voronov, and L.A. Taber. J. Vis. Exp., e3129 (2011).
4. B.A. Filas, P.V. Bayly, and L.A. Taber. Ann. Biomed. Eng. **39**, 443-454 (2010).
5. B.A. Filas. PhD thesis, 2012.

ID: 786

Towards Multi-Scale Modeling of Muscle Fibers with Sarcomere Non-Uniformities

Sefi Givli
Technion – Israel Institute of Technology
Faculty of Mechanical Engineering
Israel

Gregory Domeshek
Technion – Israel Institute of Technology
Faculty of Mechanical Engineering
Israel

Abstract:
The muscle is a hierarchical structure with structural components that span over several scales. The basic contractile unit of the muscle is the half-sarcomere that has a length of one micron. Myofibrils, typically several millimeters long, are composed of thousands of sarcomeres connected in series. In turn, the muscle fiber contains a large number of aligned myofibrils. There is a wide evidence for the existence of sarcomere non-uniformities in skeletal muscles. However, the importance of sarcomere non-uniformities to muscle function is still under debate. There is some indirect evidence that these non-uniformities play a significant role in muscle function and in phenomena such as creep, sensitivity of muscle tension to fiber length, and damage due to eccentric contraction. Importantly, these intriguing behaviors cannot be explained by classical cross-bridge theories (e.g.[4]). The main goal of this work is to develop a theoretical framework that enables a systematic and quantitative analysis of the role of non-uniformities in muscle function.

Applying the strategy of a discrete system of sarcomeres must involve thousands of sarcomeres in a single myofibril. This is computationally expensive, and perhaps impractical for a fiber which involves the collective behavior of millions of sarcomeres. Since several length scales are involved (sarcomere, myofibril, fiber) it is desirable to utilize a multi-scale modeling approach. In this contribution, we present a theoretical framework for studying the collective behavior of a large ensemble of half sarcomeres in a myofibril. The approach is based on transforming the large system of discrete elements (half-sarcomeres) into a continuum for which macro-behavior is dictated by micro-properties. Specifically, we consider statistical properties of the ensemble rather than solving for each degree of freedom [1,2]. We show that adopting a model with a non-physiological number of sarcomeres can lead to a non-realistic behavior and therefore to erroneous interpretation. Further, we utilize our approach in order to address controversial phenomena, such as residual force enhancement.

Residual force enhancement (RFE) is a phenomenon where the steady-state isometric force after stretch remains higher than the corresponding force obtained at the same final length for a

purely isometric contraction. The two leading hypotheses for explaining RFE are Passive force mechanism [3], and Sarcomere non-uniformities [5]. The question which of these mechanisms dominates RFE is still open. Thus, a theoretical approach that accounts for a physiological number of sarcomeres with non-uniformities and physiological variability, such as the one proposed here, can be very useful in addressing this question quantitatively. In a recent review [3], it was argued that sarcomere non-uniformities probably play a minor role in residual enhanced tension (RFE). The two key arguments were that (i) RFE has been observed on the ascending limb, and (ii) RFE has been observed to lead to forces higher than the optimal force. Nevertheless, we claim that the aforementioned observations can be explained by sarcomere non-uniformities (see Fig.1), provided that the number of sarcomeres involved is very large, as occurs in physiological conditions.

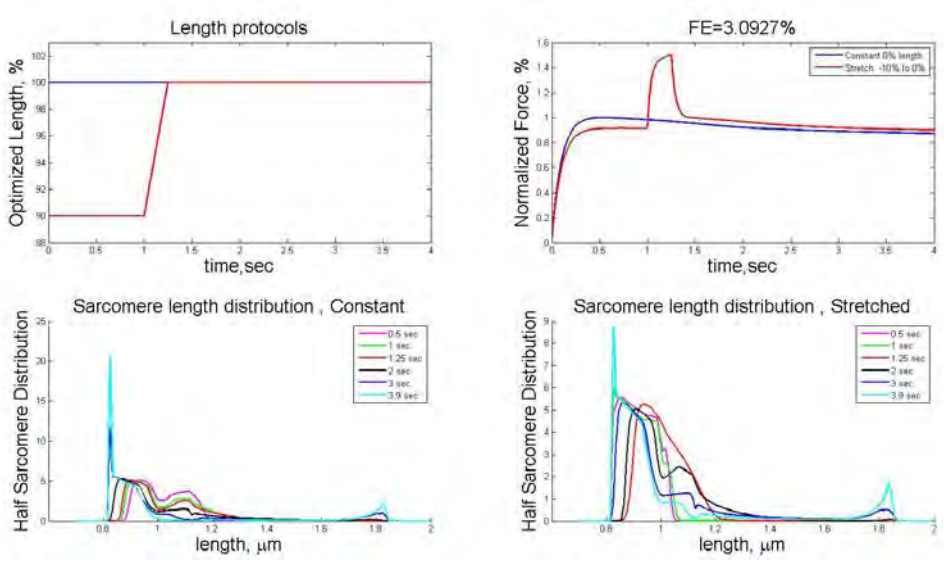

Figure 1: Numerical simulations demonstrating residual force enhancement on the ascending limb.

Acknowledgement. This work was supported by the Israel Science Foundation (ISF 1500/10).

References:

[1] S. Givli, "Towards multi-scale modeling of muscle fibers with sarcomere non-uniformities". Journal of Theoretical Biology, 2010. 264: p. 882-892.

[2] S. Givli, K. Bhattacharya, "A coarse-grained model of the myofibril: Overall dynamics and the evolution of sarcomere non-uniformities". Journal of the Mechanics and Physics of Solids, 2009. 57(2): p. 221-243.

[3] W. Herzog, E.J. Lee, D.E. Rassier, "Residual force enhancement in skeletal muscle". Journal of Physiology-London, 2006. 574(3): p. 635-642.

[4] A.F. Huxley, "Muscle Structure and Theories of Contraction". Progress in Biophysics & Molecular Biology, 1957. 7: p. 255-&.

[5] D.L. Morgan, U. Proske, "Can all residual force enhancement be explained by sarcomere non-uniformities?". Journal of Physiology-London, 2007. 578(2): p. 613-615.

Track III

Multifunctional Materials and Multiphysics Problems

III.1

Multifunctional Materials and Multiphysics Problems - Soft Materials and Structures

ID: 129

Exploring the Chain Length Dependence of the Thermal Responsive Solubility of poly(N-isopropylacrylamide) Oligomer via Simulation

Ashley Tucker
Not specified

Mark Stevens

Abstract:
Aqueous solutions of poly(N-isopropylacrylamide) (PNIPAM) exhibit temperature responsive solubility. With increasing temperature, the solubility of the polymer transitions from good to poor, inducing a structural change in the polymer backbone. Molecular dynamics of aqueous solutions of single chain PNIPAM oligomers of varying lengths have been completed over a wide range of temperatures in order to elucidate the effect of oligomer length on the transition temperature. Short oligomer chains show negligible change in the chain structure with increasing temperature and no transition due to the chain stiffness. Upon increasing oligomer length, a transition is observed, and the transition temperature decreases. The solvent accessible surface area decreases, showing an increase in shielding of the hydrophobic groups with increasing oligomer length in the collapsed state. Thus, structure of the chain directly affects the temperature at which a transition occurs. The single chain structure relates to the behavior of temperature responsive surfactants and coatings on nanoparticles.

In this presentation, we formulate this coupled problem in which the Kuhn-Tucker condition is accommodated through a variational inequality with respect to the liquid pressure. The resulted numerical methods (finite element method or displacement discontinuity method for the solid): (a) allow modeling the evolution of both fronts with a resolution consistent with the mesh size, and (b) eliminate the need of explicitly tracking the fluid front which leads to substantial saving in computational cost.

Numerical examples with a fixed fracture and a propagating fracture are used to verify the proposed methods

ID: 140

Macroscopic and Microscopic Instabilities in Soft Layered Electroactive Polymers

Stephan Rudykh
Massachusetts Institute of Technology
United States

Gal deBotton
Ben-Gurion University
Israel

Kaushik Bhattacharya
California Institute of Technology
United States

Abstract:

The developments of microscopic and macroscopic instabilities in soft electroactive composites under coupled electro-mechanical loadings are investigated. We focus on the materials with layered microstructures and analyze the role of the electric field and spatial configurations and material properties on the onset of both microscopic and macroscopic instabilities. To determine the response of the multilayered structure to electrostatic excitation and mechanical loadings, an analytical solution is derived in terms of electric field and deformation gradient. The determined from the exact solution local fields are used in the Bloch-Floquet analysis to predict the onset of microscopic instabilities. The onset of macroscopic instabilities is identified by analyzing the homogenized tensor of electroelastic moduli. The results for global bifurcation modes agree with these of the limit of infinite wavelengths in the microscopic instability analysis.

References:

1. S. Rudykh and G. deBotton, *Stability of Anisotropic Electroactive Polymers with Application to Layered Media*. Z. Angew. Math. Phys.(ZAMP) **62**, 1131–1142 (2011)

2. S. Rudykh and G. deBotton, *Instabilities of Hyperelastic Fiber Composites: Micromechanical Versus Numerical Analyses*. Journal of Elasticity **106**, 123–147 (2012).

3. S. Rudykh, K. Bhattacharya and G. deBotton, *Snap-through actuation of thick-wall electroactive balloons*. International Journal of Non-Linear Mechanics, **47**, 206–209 (2012).

ID: 143

Evaluation of Director Distortion Tensor for Nematic Liquid Crystals with Defect

Hossein Pourmatin
Carnegie Mellon University

Amit Acharya

Abstract:
The characteristics of line defects in Nematic liquid crystals have been studied. In this presentation, I will introduce the Director Distortion Tensor and the way we evaluate it, using Stokes-Helmholtz decomposition and Volterra process. This will propose a unique non-singular representation for Frank-Oseen energy in the presence of defects in the structure of the material. At the end, I will present some examples of integer and half-integer defects, evaluated with this method.
.

ID: 156

The nonlinear elastic response of suspensions of rigid inclusions in rubber

Oscar Lopez-Pamies
University of Illinois at Urbana-Champaign
USA

Taha Goudarzi
University of Illinois at Urbana-Champaign
USA

Toshio Nakamura
State University of New York at Stony Brook
USA

Abstract:

In the first part of the talk, we present a solution for the fundamental problem of the overall elastic response of ideal (Gaussian/Neo-Hookean) rubber reinforced by a dilute isotropic distribution of rigid particles under arbitrarily large deformations. The derivation makes use of a novel iterative homogenization technique in finite elasticity that allows to construct exact solutions for the homogenization problem of two-phase nonlinear elastic composites with particulate microstructures. The solution is fully explicit for axisymmetric loading, but is otherwise given in terms of an Eikonal partial differential equation in two variables for general loading conditions. In the limit of small deformations, it reduces to the classical Einstein-Smallwood result for dilute suspensions of rigid spherical particles. The solution is further confronted to 3D finite-element simulations for the large-deformation response of a rubber block containing a single spherical rigid inclusion of infinitesimal size.

In the second part of the talk, we make use of the dilute solution as a fundamental building block to derive in turn a simple explicit approximate solution for non-Gaussian rubber reinforced by an isotropic distribution of rigid particles at finite concentration. This is accomplished by means of two different techniques in two successive steps. First, the dilute solution is utilized together with a differential scheme in finite elasticity to generate a solution for Neo-Hookean rubber filled with an isotropic distribution of rigid particles of polydisperse sizes and finite concentration. This non-dilute result is then employed within the context of a new comparison medium method — derived as an extension of the Talbot-Willis (1985) variational framework to the non-convex realm of finite elasticity — to generate in turn a corresponding solution for filled non-Gaussian rubber wherein the underlying elastomeric matrix is characterized by any I_1-based stored-energy function $g(I_1)$ of choice. The solution is fully explicit and remarkably simple. Its key theoretical and practical merits are discussed in detail.

Additionally, the constructed analytical solution is confronted to 3D finite-element simulations of the large-deformation response of Neo-Hookean and non-Gaussian rubber reinforced by

isotropic distributions of rigid spherical particles with the same size, as well as with different sizes. Specifically, we consider the cases of infinite periodic media where the repeated unit cells contain a large number of monodisperse and polydisperse spherical particles that are randomly distributed as dictated by a sequential adsorption algorithm; full 3D computations of this sort have been previously considered in the context of infinitesimal elasticity by a number of authors, but the finite elasticity simulations performed in this paper appear to be the first of their kind in the literature. Good agreement is found among all three sets of results. The implications of this agreement are discussed.

ID: 185

Bursting drops in solids

Qiming Wang[1], *Zhigang Suo*[2] *and Xuanhe Zhao*[1]*

[1] Soft Active Materials Laboratory, Department of Mechanical Engineering and Materials Science, Duke University, Durham, NC 27708, USA. [2] School of Engineering and Applied Science, Harvard University, Cambridge, MA 02138, USA.

Abstract

Droplets in air or liquids under electrical voltages appear in diverse processes from thunderstorm cloud formation, ink-jet printing, electrospinning nanofibers to electrospray ionization. In these processes, the electrostatic energy competes with surface energy of the drops and causes sharp tips to form on the ends of the drops. Here, we report a physically distinct scenario for droplets in solid matrices under voltages. We show that water drops in elastic polymers can form sharp tips and surprisingly burst into long tubes under applied voltages. The new phenomenon is governed by the elasticity and fracture of the solids, instead of the drops' surface energy as in previous cases. A new scaling is derived for the critical electrical field of the voltage-induced instability of drops in solids. The observations and analyses have significant practical impacts, as they illustrate the mechanism of a major failure mode, defect-induced breakdown, of dielectric polymers, which are widely used as insulating cables and polymer capacitors and transducers.

*To whom correspondence should be addressed. E-mail: xz69@duke.edu

ID: 213

Dynamic Electrostatic Lithography

Qiming Wang
Duke University
USA

Jianfeng Zang
USA

Abstract:
Dynamic Electrostatic Lithography is invented to dynamically generate various patterns on large-area and curved polymer surfaces under the control of electrical voltages. The shape of the pattern can be tuned from random creases and craters to aligned creases craters and lines, and the size of the pattern from millimeters to sub-micrometers. This technology has potential applications on on-demand super-hydrophobicity, tunable adhesion, switchable optics, controlled drug release, anti-fouling coatings, and transfer printing.

ID: 234

Rupture of a Highly Stretchable Acrylic Dielectric Elastomer

Matt Pharr
Harvard University

Jeong-Yun Sun

Abstract:
Dielectric elastomer transducers are often subject to large tensile stretches and are susceptible to rupture. Here we carry out an experimental study of the rupture behavior of membranes of an acrylic dielectric elastomer. Pure-shear test specimens are used to measure force-displacement curves, using samples with and without pre-cracks. We find that introducing a pre-crack into a membrane drastically reduces the stretch at rupture. Furthermore, we measure the stretch at rupture and fracture energy using samples of different heights at various stretch-rates. The stretch at rupture is found to decrease with sample height, and the fracture energy is found to increase with stretch-rate.

ID: 239

Abnormal Fragmentation of Hyperelastic Sheets under Extreme Deformation

Qing Tu
Duke University
USA

Qiming Wang

Abstract:
Fragmentation, the generation of multiple cracks, occurs in various phenomena ranging from drying mud and paints, shattering window shields, failed computer chips, to intraplate fracture of the Earth crust. Most of current works on fragmentation are focused on brittle materials. On the other hand, fragmentation of hyperelastic materials such as rubbers has been rarely studied. Here, we report a combined experimental and theoretical study on the fragmentation in a layer of a silicone rubber under extremely high deformation (e.g. up to 600% strain). In the experiment, we bonded a rubber sheet with low stretchability to another sheet with high stretchability. The bilayer was then subjected to uniaxial tension, while the fragmentation process in the sheet with low stretchability was recorded. We find the fragmentation of hyperelastic materials does not follow the classical two-scaling theory even qualitatively. For example, the average size of fragments does not decrease monotonically with the applied strain, due to the large deformation of fragments before fracture. A new theory has been formulated to explain the abnormal fragmentation of hyperelastic sheets under extreme deformation. The theoretical prediction matches consistently with the experimental results. The study has a significant implementation on failure of many medical devices, tissues, and biomaterials.

ID: 241

The Mechanics of Curly Hair

J.T. Miller
Department of Civil and Environmental Engineering
Massachusetts Institute of Technology
Cambridge, MA USA

A. Lazarus
Department of Mechanical Engineering
Massachusetts Institute of Technology
Cambridge, MA USA

B. Berry
Department of Mechanical Engineering
Massachusetts Institute of Technology
Cambridge, MA USA

B. Audoly
Institut d'Alembert
CNRS and University Paris 6
Paris, France

P.M. Reis
Department of Civil and Environmental Engineering
Department of Mechanical Engineering
Massachusetts Institute of Technology
Cambridge, MA USA

Abstract:
We explore the oft-neglected role of intrinsic natural curvature on the mechanics of elastic rods. Our testbed, a hanging hair, is a deceivingly simple system that exhibits complex mechanics and geometrically nonlinear behavior (as can be seen in Figure 1).

Figure 1: Custom-fabrictated 20-cm-long elastomeric rods hanging under the influence of gravity. Intrinsic curvature increases (left to right) from approximately 0 to 60 m^{-1}. The first three rods exhibit planar behavior while the last two exhibit non-planar behavior.

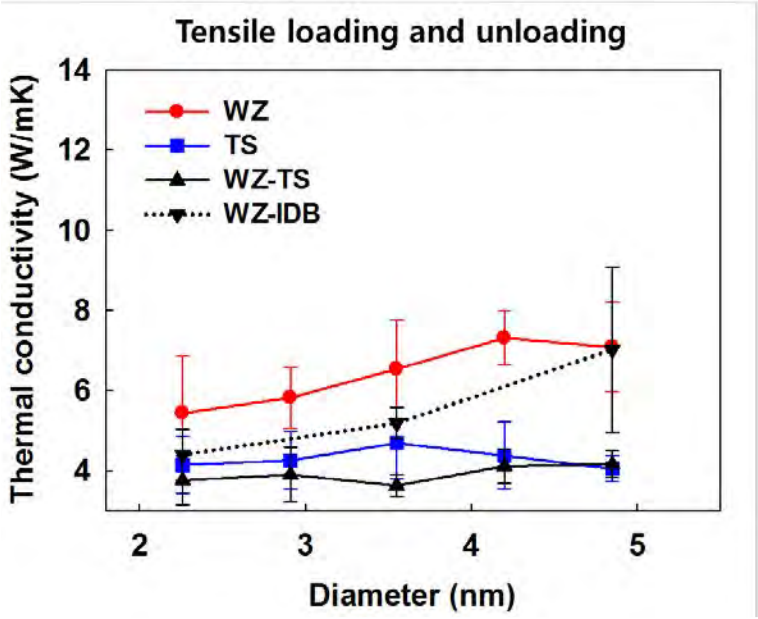

Fig. 5 Thermal conductivities of WZ-structured, TS-structured, WZ-TS structured, and WZ-IDB structured nanowires as functions of diameter during tensile loading and unloading.

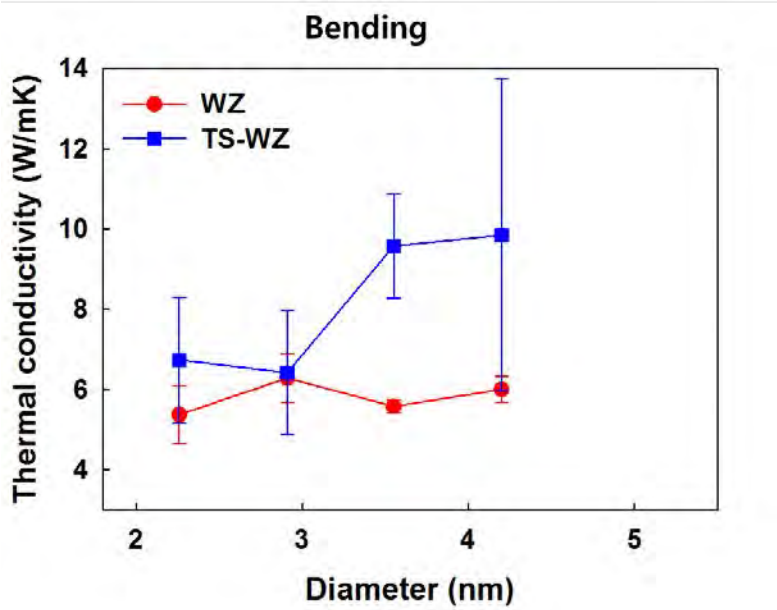

Fig. 2 Thermal conductivities of initial WZ-structured nanowires and TS-WZ structured nanowires as functions of diameter during bending.

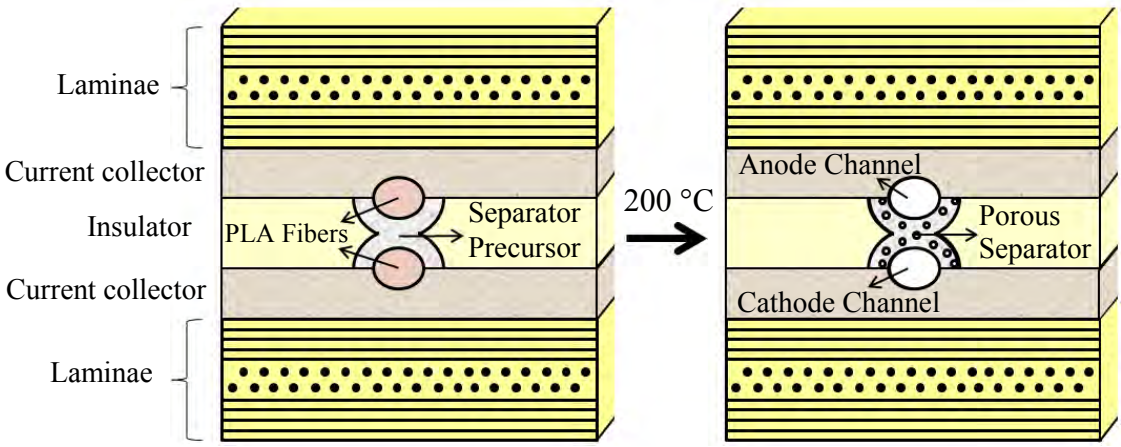

Figure 1. Schematic of the composite flow battery manufacturing process. The left image shows the initial layup and the right image shows the vascular composite formed after PLA vaporization.

As the first research thrust, semi-solid electrodes were synthesized and characterized to assess their usability in a flow battery composite. Electrodes were prepared by mixing non-aqueous electrolytes and carbon black with micron-scale particles of either lithium cobalt oxide (LCO) for the cathode or lithium titanate (LTO) for the anode. Rheometry tests run on the fluids show that they are strongly shear-thinning, suggesting they contain a network of carbon black that stabilizes a suspension of active material. The electrochemical activity of the fluids was confirmed with galvanostatic cycling and cyclic voltammetry tests on a flow cell made of metal current collectors and a commercial separator. Work is ongoing to find electrode compositions that provide both optimal electrochemical performance and workable viscosity.

As the second research thrust, dual polymer films were studied to develop a film that would transform into a porous separator upon PLA vaporization. Films containing PLA and a surviving polymer, either PET or PI, were prepared by co-dissolving the polymers and casting films using a doctor blade or spin coater. The PLA phase could then be removed using etching, dissolution, or high temperature. Optical microscopy and scanning electron microscopy (SEM) of the films before and after PLA removal show that the cast films contain phase-separated PLA domains that can be removed to form porous networks. Work is underway to optimize the morphology of these networks by controlling solution composition and film casting technique.

Future work will involve the use of PLA fibers and a separator precursor film to create composites with the channel architecture described in Figure 1. Semi-solids will then be loaded into the composites and the multifunctional performance of the system will be tested.

1. Thomas J. P. QMA (2005) The Design and Application of Multifunctional Structure-Battery Material Systems. *JOM* 57(3):18-24.
2. Duduta M*, et al.* (2011) Semi-Solid Lithium Rechargeable Flow Battery. *Advanced Energy Materials* 1(4):511-516.
3. Esser-Kahn AP*, et al.* (2011) Three-Dimensional Microvascular Fiber-Reinforced Composites. *Advanced Materials* 23(32):3654-3658.

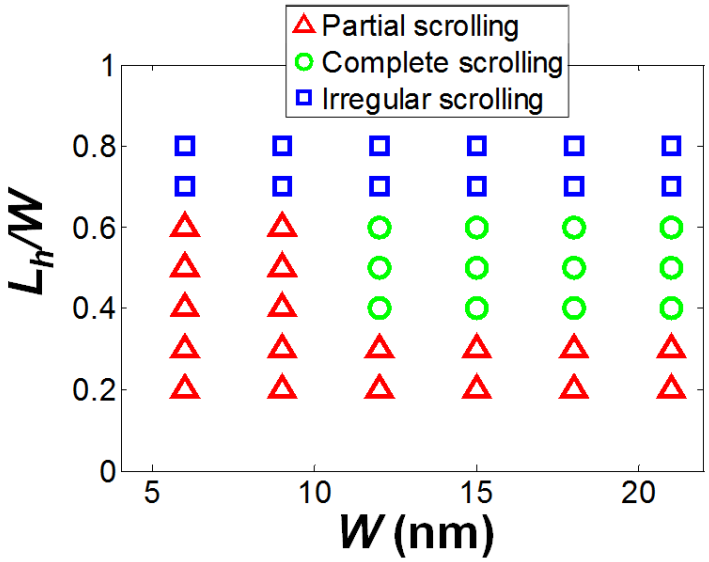

Figure 2. *A phase diagram in the space of the width of hydrogenated region and the width of graphene shows three different possible scrolling processes. Complete scrolling cases are denoted by green circles.*

ID: 254

Constitutive Models for Magneto-Elastic Composites at Finite Strains: The Effects of Particle Rotations and Magnetic Torques

Pedro Ponte Castaneda

Evan Galipeau

Abstract:
This presentation is concerned with the application of a finite-strain homogenization framework to develop constitutive models for magnetorheological elastomers (MREs) consisting of initially aligned, rigid magnetic particles distributed randomly in an elastomeric matrix. The effective electro-elastic energy of the composite is written in terms of a purely mechanical component, together with a magnetostatic component evaluated in the deformed configuration of the composite, as estimated by means of the purely mechanical solution of the problem. It is argued that the resulting constitutive model for the material, which can account for the initial volume fraction, average shape, orientation and distribution of the generally anisotropic and non-spherical particles, should be accurate when the matrix is stiff compared to the magnetic forces and torques on the particles. The theory predicts the existence of certain ``extra" stresses---arising in the composite beyond the purely mechanical and magnetic (Maxwell) stresses---which can be directly linked to changes in the effective magnetic permittivity of the composite with the deformation. For the special case of isotropic distributions of magnetically isotropic, spherical particles, the extra stresses are due to changes in the particle two-point distribution function with the deformation, and are of order volume fraction squared, arising from dipole interactions between the particles. On the other hand, for the case of aligned, ellipsoidal particles, the effect can be of order volume fraction, when changes are induced in the orientation of the particles, as a consequence of magnetic torques on individual particles. The theory is capable of handling the strongly nonlinear effects associated with finite strains and magnetic saturation of the particles at sufficiently high deformations and magnetic fields, respectively. It will be shown that particle rotations can be used to produce relatively large magnetostrictive strains and actuation stresses.

ID: 257

On the Macroscopic Response of Deformable Dielectric Composites and Applications to Electrostriction

Pedro Ponte Castaneda

Morteza Siboni

Abstract:
In this paper, we provide Hashin-Shtrikman (HS) estimates for the effective response of particulate Deformable Dielectric Composites (DDCs) consisting of rigid dielectric particles, which are embedded in an ideal dielectric elastomer matrix. The derivation of the results for the electro-mechanical response assumes linearized deformations but includes non-linear (quadratic) terms in the electric fields. We investigate three different physical mechanisms contributing to the macroscopic electro-mechanical response of the composite: the intrinsic electro-mechanical coupling of the dielectric matrix, the inter-particle interactions which are accounted for by making use of the two-point probability distribution functions, and the effect of the electric torques on anisotropic particles. Several illustrative examples are provided to emphasize the relative importance of the different effects. In particular, it is shown that inter-particle interactions can have synergistic effects with the intrinsic electro-mechanical coupling of the matrix, and significantly enhance the electro-mechanical coupling of DDCs, while the electric torque on the particles has an opposing effect. However, microstructures with non-spherical particles can still be designed leading to improved electrostriction for the composite.

ID: 264

Stretch-Induced Wrinkling Instability in thin Sheets

Rui Huang
University of Texas at Austin
USA

Vishal Nayyar
USA

Abstract:
Wrinkles are commonly observed in stretched thin sheets and membranes. This paper presents a numerical/experimental study on stretch-induced wrinkling of hyperelastic and plastic thin sheets. The model problem is set up for uniaxial stretching of a rectangular sheet with two clamped ends and two free edges. A two-dimensional stress analysis is performed first under the plane-stress condition to determine stretch-induced stress distribution patterns in the elastic sheets, assuming no wrinkles. As a prerequisite for wrinkling, development of compressive stresses in the transverse direction is found to depend on both the length-to-width aspect ratio of the sheet and the applied tensile strain. Next, an eigenvalue analysis is performed to find the potential buckling modes of the elastic sheet under the prescribed boundary conditions. A nonlinear post-buckling analysis is performed to show evolution of stretch-induced wrinkles. The wrinkle wavelength decreases with increasing strain, in good agreement with the prediction by a scaling analysis. However, as the tensile strain increases, the wrinkle amplitude first increases and then decreases eventually flattened beyond a moderately large strain, in contrast to the scaling analysis. Experimental measurements with rubber and polyethylene sheets are presented in comparison with the numerical results. Finally, the effects of plasticity on the stress patterns and the wrinkling instability are discussed.

ID: 281

Extremely Stretchable and Tough Hydrogels

Jeong Yun Sun
Harvard University
USA

Xuanhe Zhao

Abstract:
Hydrogels are pervasive in nature and technology, but the scope of applications is often severely limited by the mechanical behavior of hydrogels. Most synthetic hydrogels are much more brittle than natural hydrogels such as cartilage. Despite intense efforts to synthesize hydrogels of enhanced mechanical behavior, much of the property space of hydrogels remains uncharted. Here we report extremely stretchable and tough hydrogels made of polymers forming networks via ionic and covalent crosslinks. Although the gel contains ~ 90% water, it can be stretched beyond 20 times its initial length, and has fracture energy of ~9000 J/m2. We envision that gels of much improved mechanical behavior will open up applications such as artificial tissues and soft machines.
.

ID: 288

Buckling-Induced Tunable Chirality in Rationally-Designed Surface-Attached Cellular Structures

Sicong Shan
Harvard University
USA

Sung Kang

Abstract:
Chirality is crucial in understanding and controlling the behavior of living and non-living systems since the presence or absence of chirality in the structures plays important roles in their interactions with molecules, enzymes, light, and mechanical stress. Processes that induce chirality have been extensively studied at the molecular and macroscopic scales, but are relatively unexplored at the mesoscale. By rational design based on modeling, we experimentally demonstrate the controlled reversible switching between achiral and chiral configurations using swelling/de-swelling of surface-attached cellular structures. Importantly, the buckling patterns and the associated symmetry reduction of the initially achiral centrosymmetric structures could be tuned, simply by changing their dimensions. This approach opens the way to deterministically select to select the appearance of either mixed (racemic) or chiral phases. In the case of chiral transformations, spontaneous symmetry breaking resulted in the formation of large uniform areas of structures of single handedness. The fundamental understanding of this process provides a general route to designing deterministically deformable structures with dynamically switchable mechanical and/or optical properties.
.

ID: 296

Synthetic Papillae through Reversible and Controlled Surface Textures

Sourav Chatterjee
University of Pittsburgh
United States

Sachin Velankar
University of Pittsburgh
United States

Abstract

Machines in nature, unlike traditional engineering structures, are often soft, and hence highly adaptive. There has been a recent interest in mimicking the functionalities of such soft machines [1]. Examples of such machines include soft robots, bioinspired lenses with tunable focal length and gecko inspired artificial adhesives.

We are interested in particular, in the creation of actively tunable textured surfaces, using soft substrates. Our designs are motivated by the unique capabilities of the cuttlefish, which camouflage themselves by rapidly switching from smooth to textured skin by expressing protuberances called papillae [2]. We will show, in this study, an implementation of a simple device, which is able to change surface texturing at the flip of a switch in the timescales of a few seconds. We will further demonstrate ways to control both the response times as well as spatial locations of the texturing.

The buckling of thin films attached to soft substrates is an well-known phenomenon, and has been studied extensively. [3]. Our objective is in achieving the buckling transition reversibly in response to an external stimulus, in a simple and robust fashion, and hence, we use shape memory alloy (SMA) as a reversible actuator. These smart materials shrink when heated beyond their transition temperature, produce strains of about 3.5% and on cooling, they return back to the original shape when they are loaded.

Our setup consists of an SMA wire, embedded in a PDMS elastomer matrix. A polyester film is adhered to the PDMS matrix. On actuation through electrical heating, the wire deformation leads to the buckling of the film, shown in Figure 1. Figure 2 shows the growth in buckling amplitude corresponding to the transition. A reverse transition on cooling the sample leads to a complete reversal of the surface texturing. The cycle can be carried out multiple times, thus making it a robust active surface whose texture can be turned on and off in the flip of a switch.

The response times for the surface transition are of the order of a few seconds, as shown in Figure 2, and we demonstrate the ability to control the timescales for both the growth and decay of the amplitude. Spatial control of buckling is important for adaptive, tunable surfaces.

Using our setup, we are able to program the spatial location of the wrinkles by creating a local strain field in the location of the wrinkles.

We have shown a simple, flip-of-a-switch implementation of a bio-inspired responsive surface, which is able to both create and control changes in topography in small timescales. The phenomenon used is scale-free i.e. with suitable device design the texture of the surface can range from a few microns to many cm. Even though the strains achievable by the SMA are modest (a few percent), by using those strains to drive an elastic instability, large change in surface texture can be realized. Possible applications include novel adhesive surfaces, rapidly switchable optical devices and soft robots.

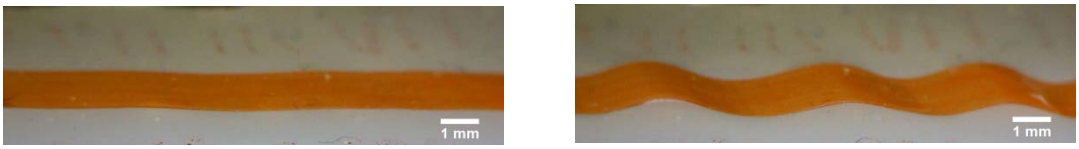

(a) (b)

Figure 3 (a) An initially flat film before actuation and (b) sinusoidal bucklesafter actuation

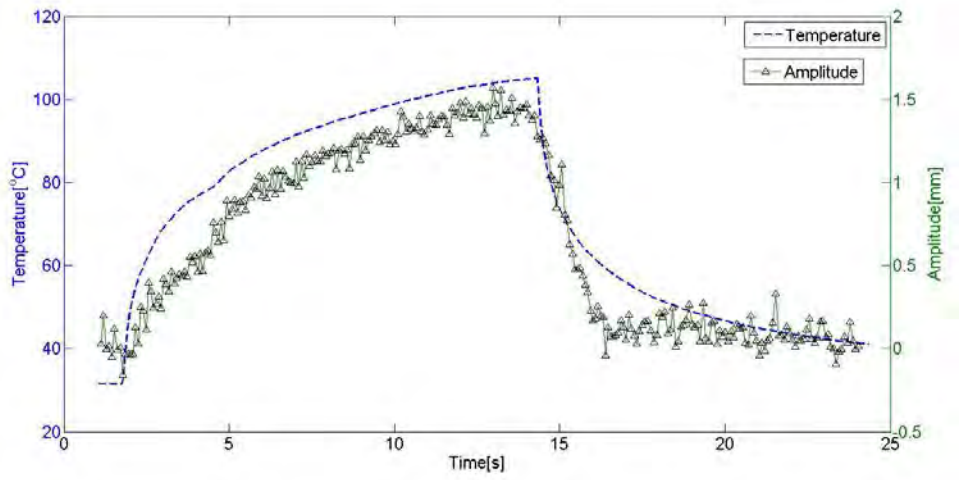

Figure 4 Evolution of wire temperature and buckling amplitude with time

References

[1] Z. Suo, MRS Bulletin **37**, 218-225 (2012).
[2] J. J. Allen, L. M. Mäthger, A. Barbosa, and R. T. Hanlon, Journal of Comparative Physiology. A, Neuroethology, Sensory, Neural, and Behavioral Physiology **195**, 547-55 (2009).
[3] J. Genzer and J. Groenewold, Soft Matter **2**, 310-323 (2006).

ID: 308

Nonlinear Elastic Networks

Bastiaan Florijn
Leiden University/LION

Abstract:
We study the linear and nonlinear behavior of random 2D elastic networks at the desktop scale. I will demonstrate how to fabricate random networks and characterize them with the lattice connection number Z. We investigate experimentally if there is a relation between the mechanical response and the lattice connection number Z of the network.Bastiaan Florijn, M. van Deen, H. Imthorn, M. van Hecke

ID: 312

Following the Equilibria of Slender Elastic Rods

Arnaud Lazarus
Department of Mechanical Engineering
Massachusetts Institute of Technology
USA

James T. Miller
Department of Civil and Environmental Engineering
Massachusetts Institute of Technology
USA

Pedro M. Reis
Department of Mechanical Engineering
Department of Civil and Environmental Engineering
Massachusetts Institute of Technology
USA

Abstract:
We present a novel continuation method to characterize and quantify the equilibria of slender elastic rods under large geometrically nonlinear displacements and rotations. The rod is discretized into finite segments and its 3D kinematics is represented by the position of the nodes and a set of unit quaternions at each segment to take the material frame orientation into account. The equilibrium equations are derived from the geometrically constrained mechanical energy of the rod due to internal moments (bending and torsion), external forces and torques. Thanks to the mathematical properties of quaternions, the obtained algebraic nonlinear system of equilibrium equations is at most polynomial cubic and efficiently solved with an asymptotic numerical continuation method. Based on the asymptotic expansion of the unknown kinematics, Lagrange parameters and control parameter in a path-parameter variable, this method gives access to analytical equilibrium branches, a.k.a bifurcation diagrams. This is in contrast with the individual solution points attained by classic energy minimization or predictor-corrector techniques. Finally, the stability of the equilibrium is assessed by analyzin the Lyapunov exponents of the Jacobian of the Lagrangian along the branches. This original numerical method is implemented in the open source software MANLAB: a user-friendly, interactive and object-oriented Matlab path-following and bifurcation analysis program.

We challenge our numerics for the specific problem of an extremely twisted naturally curved rod and perform a detailed comparison against a precision desktop-scale experiment. The quantification of the underlying 3D buckling instabilities and the characterization of the resulting complex configurations are in excellent agreement be- tween numerics and experiments (see Fig 1.).

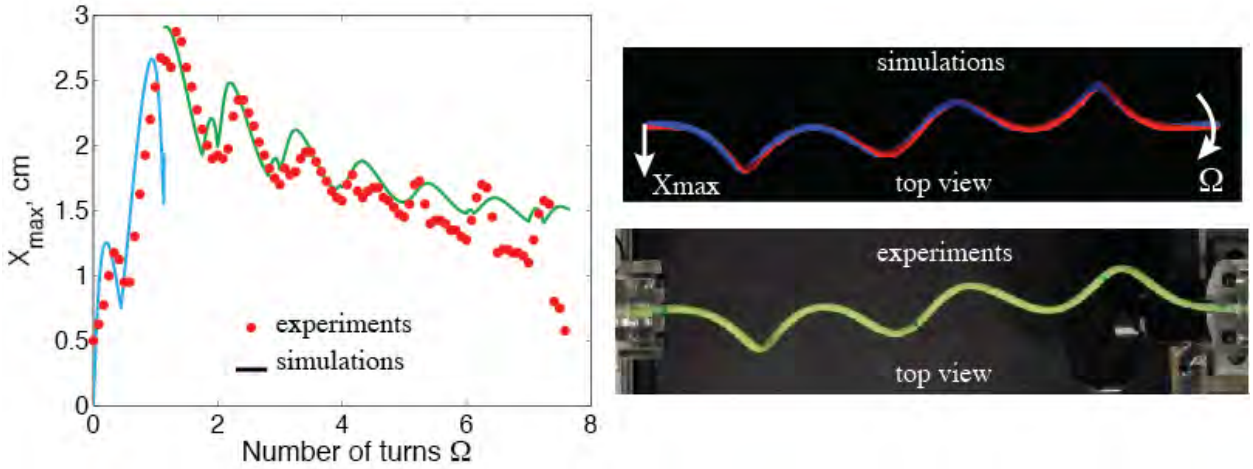

Fig. 1: (a) Bifurcation diagram of a quasi-statically twisted naturally curved elastic rod hanging under its own weight. (b) Numerical and experimental top view of the equilibrium configuration at four turns of the clamped right end.

ID: 315

Dynamic Stiffness and Damping in Viscoelastic Structures and Composites: Stability of Negative-Stiffness Based Extreme Behavior

Dennis Kochmann
California Institute of Technology
USA

Charles Wojnar
USA

Abstract:
The development of composite materials and structures containing metastable negative-stiffness elements has resulted in tunable extreme stiffness and damping of viscoelastic composites and structures in recent years. Prominent examples comprise composites with phase-transforming constituents (whose transformation behavior gives rise to significant viscoelastic softening) or prestressed (visco)elastic structural systems (where snap-through mechanisms facilitate the negative-stiffness effect). While independent studies of the stability and performance of such systems have been carried out, the correlation between their stability and overall properties is not well understood at present. Here, we present a stability analysis of the fundamental examples of two-phase composites and prestressed viscoelastic structures to demonstrate the link between stability and performance. In particular, we show that in the static case extreme stiffness cannot be achieved due to overall instability, whereas dynamic systems promise to stabilize and thus allow for extreme dynamic stiffness and damping based on negative-stiffness effects.

ID: 321

Bistable Morphing Structures: Geometric and Mechanical Determinations

Zi Chen
Department of Biomedical Engineering, Washington University in St. Louis
Department of Mechanical & Aerospace Engineering, Princeton University
United States

Qiaohang Guo
College of Materials Science and Engineering, Fuzhou University
Department of Mathematics and Physics, FuJian University of Technology
China

Carmel Majidi
Department of Mechanical Engineering, Carnegie Mellon University
United States

Wenzhe Chen
Department of Mechanical Engineering, Carnegie Mellon University
United States

David J. Srolovitz
Institute of High Performance Computing, 1 Fusionopolis Way
Singapore

Mikko Haataja
Department of Mechanical & Aerospace Engineering
Princeton Institute for the Science and Technology of Materials (PRISM)
Program in Applied and Computational Mathematics, Princeton University
United States

Abstract:
Multistable structures feature more than one stable shapes, and can quickly transform from one to another upon a certain mechanical stimulus. Engineering applications include the design of mechanical or electromechanical devices, ranging from bio-inspired robotics to deployable aerospace components. Although there have been many modeling efforts on such large shell deformations, the nonlinear geometric effects still remain incompletely understood.
Here, we present a theoretical framework, by combing differential geometry, linear elasticity and variational principles, to model large shell deformation and the associated geometric nonlinear effects. This theoretical framework is then applied to give the geometric and mechanical conditions for bistable behaviors, due to geometric nonlinearity. Specifically, we identify two dimensionless parameters, one related to geometry and mechanical stresses, and the other associated purely with the mechanical stresses, that control bistability and show then non-negligible role of edge effects in setting the energy preferences between the two locally stable

shapes for a plate of finite width. This work classifies the conditions for bistability and defines the design space for bistable, morphing structures, with theoretical predictions validated by bench-top experiments. The results will also advance the understanding of nonlinear behaviors in large deformations of plates and shells.

In a broader sense, the results of this work will also promote understanding of morphology formation in a variety of natural and engineered systems, and benefit the engineering design of functional devices, as sensors, actuators, artificial muscles and bio-inspired robots.

ACKNOWLEDGEMENT

This work has been supported by National Science Foundation of China (No. 11102040) and the Sigma Xi Grants-in-Aid of Research (GIAR) program, American Academy of Mechanics Founder's Award from the Robert M. and Mary Haythornthwaite Foundation, and Society in Science – Branco Weiss fellowship.

Correspondence: chen.z@seas.wustl.edu.

REFERENCES

1. Y. Forterre, J. M. Skothelm, J. Dumais and L. Mahadevan. Nature **433**, 421-425 (2005).
2. Z. Chen, C. Majidi, D. J. Srolovitz and M. Haataja. Appl. Phys. Lett. **98**, 011906 (2011).
3. I.S. Chun, et al. Nano Letters **10**, 3927-3932 (2010).
4. C. Majidi C, Z. Chen, D.J. Srolovitz and M. Haataja. J. Mech. Phys. Solids 58:73-85 (2010).
5. S. Daynes, C.G. Diaconu, K.D. Potter, P.M. Weaver. J. Compos. Mater. 44:1119-1137 (2010).
6. S. Armon, E. Efrati, R. Kupferman, E. Sharon. Science **333**: 1726-1729 (2011).
7. Z. Chen, et al. submitted to Phys. Rev. Lett. (arXiv:1206.4739v4).
8. M. A. Wyczalkowski, Z. Chen, B. Filas, V. Varner and L. A. Taber, Birth Defects Res., Part C 96, 132 (2012).

ID: 325

Stretchable and Flexible Ferroelectrics

Xue Feng

B.D. Yang

Abstract:
NO ABSTRACT

ID: 328

Shape Selection in Hyperbolic Non-Euclidean Plates

John Gemmer
University of Arizona
USA

Shankar Venkataramani

Abstract:
We present a theoretical study of free non-Euclidean plates with disc geometry and prescribed growth that corresponds to a deformation with constant negative Gaussian curvature. We take the equilibrium configuration taken by these sheets to be a minimum of a Foppl-von type functional. In this model there are two reduced theories, the small slope approximation and the Kirchhoff model. In the small slope approximation we show that equilibrium deformations converge in the vanishing thickness limit to a saddle shape. For the Kirchhoff model we show that for all radii there exists low bending energy configurations free of any in plane stretching that obtain a periodic profile. The number of periods in these configurations is set by the condition that the principle curvatures of the surface remain finite and grows approximately exponentially with the radius of the disc. We discuss the implications of our work to modeling hydrogels.

ID: 339

On the Coupled Response of Electro-Active Polymer Chains

Noy Cohen
Ben-Gurion University
Israel

Gal deBotton
Ben-Gurion University
Israel

Abstract

Electro-active polymers (EAPs) are materials capable of undergoing large deformations when stimulated by an electric field. At the present there are models describing the polymer's uncoupled electrostatic response under the influence of an electric field at both the macroscopic and the microscopic levels [1]. Similarly, there are models describing the polymer's reaction to a purely mechanical loading, macroscopically [2] as well as through its micro-structure [3]. The connection between the micro and the macro analyses shed light on the overall response of polymers and provide tools for optimizing their performances [4]. In recent years, the electro-mechanical coupling in EAPs has been characterized and modeled at the macroscopic-continuum level [5]. To the best of our knowledge, the corresponding analysis of the coupling at the microscopic level is not available of yet. Our work is aimed towards understanding and analyzing the relation between the structure of electro-active polymers and the forces and stresses that develop due to electrostatic excitations.

We introduce a microscopic model that assumes known geometries of the chains before and after the deformation. In addition, a variational approach is used following McMeeking et al. [6], which leads to the development of an expression for the internally stored electrical enthalpy in the polymer and the corresponding stresses that develop.

In a way of an example a polymer with specific structure of its chains under constant electric excitation and axial deformation is examined and compared with corresponding macroscopic model proposed by Dorfmann and Ogden [7].

[1] Tiersten, H. F. (1990). A Development of the Equations of Electromagnetism in Material Continua, Vol. 36 of Springer Tracts in Natural Philosophy, Springer-Verlag, New York.

[2] Ogden, R. W. (1997). Non-Linear Elastic Deformations, Dover Publications, New York.

[3] Treloar, L.R.G. (1975). The Physics of Rubber Elasticity (third edition), Oxford University Press, London.

[4] Tian, L., Tevet-Deree, L. deBotton, G., Bhattacharya, K. (2012). Dielectric Elastomer Composites, Journal of the Mechanics and Physics of Solids, Vol. 60, pp. 181-198.

[5] Toupin, R. (1956). The Elastic Dielectric, J. Rational Mech. Anal., Vol. 5 (6), pp 849–915.

[6] McMeeking, R., Landis, C. and Jimenez, S. (2007). A principle of virtual work for combined electrostatic and mechanical loading of materials, International Journal of Non-Linear Mechanics, Vol. 42, pp 831-838.

[7] Dorfmann, A. and Ogden, R.W. (2005). Nonlinear Electroelasticity, Acta Mechanica 174, pp167-183.

Missing Abstract

ID: 362

ID: 367

Sinusoidal to Helical Buckling of an Elastic Rod under a Cylindrical Constraint

Tianxiang Su
Harvard University
USA

James Miller
USA

Abstract:
We investigate the buckling and post-buckling behavior of an elastic rod loaded under cylindrical constraint. Our precision desktop-scale experiments comprise of axially compressing a hyper-elastic rod inside a transparent acrylic pipe. These experiments are also modeled using a discrete elastic rod simulation that includes frictional effects. Under imposed displacement, the initially straight rod first buckles into a sinusoidal mode and eventually undergoes a secondary instability into a helical buckling regime. The buckling and post-buckling behavior is found to be highly dependent on the systems' geometry, in particularly the aspect ratio of the rod to pipe diameter. We quantify the wavelength and pitch of the periodic patterns through direct digital imaging and record the reaction forces at both ends of the pipe. The observed behavior is rationalized through scaling arguments and captured by numerical simulations.

ID: 373

Physical Aging can Improve the Recovery Behavior of Shape Memory Polymers

Thao Nguyen
Johns Hopkins University

Alicia Ortega
USA

Abstract:
Shape-memory behavior in polymers describes the ability to store a deformed shape and recover fully to an original shape in response to an environmental trigger. Shape-memory polymers (SMPs) are attractive for medical applications because they can be designed for biocompatibility, biodegradability, and controlled drug delivery. Moreover, they can store and recover large deformation, which is desirable for minimally invasive surgery. Despite their numerous advantages, SMPs have not been widely adopted for surgical applications, primarily because of their slow recovery times. In this study, we suggest a novel, counterintuitive method for achieving faster shape recovery by the simple act of storage at an optimal temperature and time. We measured the effects of aging on the unconstrained recovery response of two tBA-co-PEGDMA amorphous networks with different crosslink densities for different aging times, 0-180 days. Aging delayed the activation of shape recovery and produced a faster initial recovery response with negligible effect on the strain performance. A thermoviscoelastic model, recently developed for amorphous networks near the Tg , was applied to study the effect of aging temperature and time on the activation temperature and initial recovery rate. The aging temperature had a dramatic but non-monotonic effect on the recovery response. There was an optimal aging temperature below Tg that maximized the initial recovery rate and activation temperature. At the optimal temperature, the chain mobility was low enough to inhibit viscoelastic strain recovery and prevent loss of programmed shape, but still high enough to permit structural relaxation to achieve faster recovery rates. Overall, this newly proposed method of increased shape-recovery performance as a function of physical aging could potentially help solve some inherent challenges in the design SMP biomedical devices.

ID: 385

Mechanical Tunable Metamaterials

Shengqiang Cai

Abstract:
Metamaterials have been recently used to manipulate electromagnetic waves, acoustic waves as well as elastic waves. The properties of metamaterials highly depend on their internal structures. In the talk, I will present some results showing how to use mechanical deformation, especially mechanical instabilities, to tune the properties of metamaterials.

ID: 408

Large, Uni-Directional Actuation In Dielectric Elastomers Achieved by Fiber Stiffening

David Clarke
Harvard University
USA

Jiangshui Huang
USA

Abstract:
Very large voltage-induced strains can be produced with dielectric elastomers when they are first pre-strained. The requirement of pre-straining and maintaining it complicates the fabrication of actuators made from dielectric elastomers. Furthermore, only small strains can be produced with uni-directional actuators because of premature dielectric breakdown. In this contribution we show that very large, unidirectional strains can be produced without pre-straining if the elastomer is stiffened in the perpendicular direction using a parallel array of fibers. The resulting composite elastomeric material is an unusual composite since the fibers not only amplify the attainable deformation when an electric field is applied but also suppress electrical breakdown in their immediate vicinity.

ID: 410

Shape Transitions in Elastomeric Bistrips From the Hemi-Helix to the Jelly-Roll

David Clarke
Harvard University
USA

Jiangshui Huang
USA

Abstract:
A variety of three-dimensional shapes can be produced from elastomer strips by the simple operation of straining one, attaching it side-by-side to a second unstrained strip and then releasing. In addition to the well-known simple helix and the jelly-roll that can be created this way, we have discovered a new shape that exists when the cross-section is small and deformation by twisting can dominate. This new shape, termed a hemi-helix, consists of alternating helical sections of opposite chirality along the length of the bi-strip. The region where the chirality switches sign is a perversion and we find that the number of perversions depends on the pre-strain as well as other parameters. In this contribution, we show by combined experiment and simulation how the transition from hemi-helix to simple helix to jelly roll depends on both the value of pre-strain as well as other geometric parameters.

ID: 441

Finite Element Analysis of Some Common Boundary Value Problems of Light Activated Shape Memory Polymers

Jaskirat Sodhi
Department of Engineering and Technology
Lake Superior State University
Sault Ste. Marie
USA

I. Joga Rao
Department of Mechanical and Industrial Engineering
New Jersey Institute of Technology
USA

Abstract:
Shape memory polymers (SMP's) belong to a large family of shape memory materials, which are defined by their capacity to store a deformed (temporary) shape and recover an original (parent) shape. SMP's have the ability to change size and shape when activated through a suitable trigger. This trigger, which can be heating the polymer or exposing it to light of a specific frequency, is responsible for the new temporary shape. Return to the original shape can be achieved by a suitable reverse trigger. Light Activated Shape Memory Polymers (LASMP) are recently developed smart materials, which are synthesized with special photosensitive molecules. These molecules when exposed to Ultraviolet (UV) light at specific wavelengths, form covalent crosslinks that are responsible for providing LASMP with their temporary shape. Light activation removes temperature constraints faced by thermoresponsive SMP's for medical applications and also brings the added advantage of remote activation.

The authors have introduced a constitutive model to model the mechanics of these LASMP in the past [1]. The modeling is done using a framework based on the theory of multiple natural configurations. The authors have also used the developed model to solve a few cases of homogeneous and inhomogeneous deformations with uniform and non-uniform exposure to light in the past. In this paper, this model is implemented into a finite element program (ABAQUS) to simulate the behavior of light activated shape memory polymers in realistic geometries and conditions.

ABAQUS is a highly sophisticated, general purpose finite element program, designed primarily to model the behavior of solids and structures under externally applied loading. ABAQUS is one of the few commercial finite element softwares which allows a user to include a user-defined finite element module for a new material. A material module facilitates a user to input different physical properties and related constants associated with material used to form the real object. LASMPs are recently developed polymers and using a material module that is made for

commonly used polymers is not appropriate for this purpose. Hence, a new material module based on the constitutive model derived is developed. A user subroutine (UMAT) is created in FORTRAN for LASMP and finite element analysis is carried out in ABAQUS/CAE. The required test to validate the developed user subroutine (UMAT) based on the current model is also performed. In this study, results are presented for the finite element analysis carried out on a few common boundary value problems such as uni-axial stretching, inflation of a cylinder and twisting of a cylinder. These cases will portray deformations such as stretching and shearing which will cover a broad range of boundary value problems, where a LASMP may find application in the biomedical and aerospace industries.

1. J.S. Sodhi and I.J. Rao, "Modeling the Mechanics of Light Activated Shape Memory Polymers," International Journal of Engineering Science, Volume 48, Issue 11, November 2010, Pages 1576-1589

.

ID: 447

Evaporation-Induced Self-Organization of Polymer Nanorod Arrays: When Structured Solids Met a Liquid

Sung Hoon Kang
Harvard University
United States

Boaz Pokroy
Israel Institute of Technology
Israel

L. Mahadevan
Harvard University
United States

Joanna Aizenberg
Harvard University
United States

Abstract:
Soft materials and structures provide new opportunities for designing multifunctional materials systems from their responsiveness to various stimuli. Among many stimuli-responsive behaviors, we have studied evaporation-induced self-organization of polymer nanorod arrays because of its potential to make dynamically tunable patterns that be utilized as smart functional surfaces. We will present our understanding about the pattern formation mechanisms and some of applications of the phenomena including trapping and releasing micro objects, non-chemical glue, and security features from optical effects (Fig. 1). Our approach can be also utilized as a simple and energy-efficient method for fabricating multifunctional materials with novel properties.

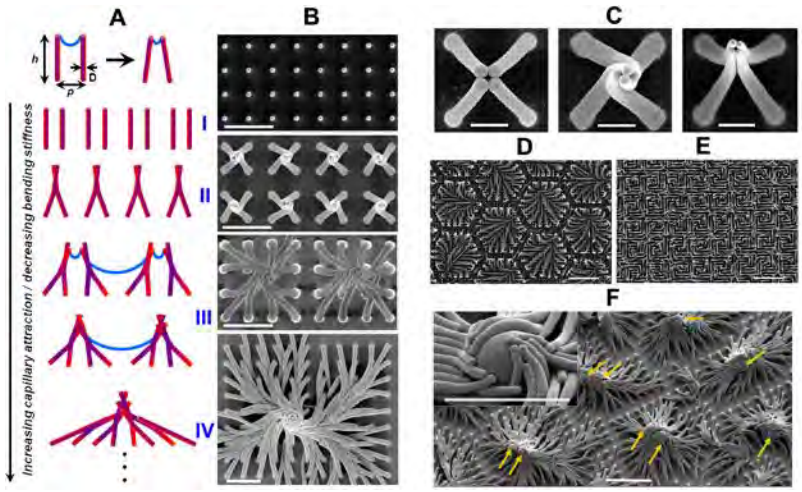

Figure 1. Assembly of polymer nanorods into diverse shapes and hierarchical architectures. (A) Schematic and (B) corresponding SEM images showing the hierarchical assembly of nanorod arrays into higher order chiral structures. Blue lines in the schematics indicate menisci forming as a liquid evaporates (scale bar = 4 μm). (C) Clusters of nanorods connected at the tips (left), twisted into a chiral bundle (center), or zipped together (right) (scale bar = 1 μm). (D) SEM image of nanorods assembled under a honeycomb mask (scale bar = 20 μm). (E) SEM image of nanorods self-organized into a Moiré pattern by an evaporating liquid sandwiched between two periodic nanorod arrays (scale bar = 20 μm). (F) Low-magnification SEM showing the capture of the 2.5 μm polystyrene spheres (indicated by arrows) (scale bar = 10 μm). The inset shows a magnified view depicting a single sphere trapped through the conformal wrapping of the nanorods (scale bar = 2 μm).

References:

1. B. Pokroy, S. H. Kang, L. Mahadevan, and J. Aizenberg, "Self-Organization of a Mesoscale Bristle into Ordered, Hierarchical Helical Assemblies," Science, 323, 237-240 (2009).

2. S. H. Kang, B. Pokroy, L. Mahadevan, and J. Aizenberg, "Control of Shape and Size of Nanopillar Assembly by Adhesion-Mediated Elastocapillary Interaction," ACS Nano, 11, 6323-6331 (2010).

3. S. H. Kang, N. Wu, A. Grinthal, and J. Aizenberg, "Meniscus Lithography: Evaporation-Induced Self-Organization of Pillar Arrays into Moiré Patterns," Physical Review Letters, 107, 177802 (2011).

4. A. Grinthal, S. H. Kang, A. K. Epstein, M. Aizenberg, M. Khan, and J. Aizenberg, "Steering Nanofibers: An Integrative Approach to Bio-Inspired Fiber Fabrication and Assembly," Nano Today, 7, 35-52 (2012).

ID: 448

Highly Sensitive Skin-Mountable Strain Gauges Based Entirely on Elastomers

Nanshu Lu
Department of Aerospace Engineering and Engineering Mechanics
University of Texas at Austin
United States

John Rogers
Department of Materials Science and Engineering
University of Illinois at Urbana-Champaign
United States

Abstract

Quantifying naturally occurring strains in soft materials, such as those of the human body, requires strains gauges with equal or greater mechanical compliance. We report materials and mechanics for an all-elastomer strain measurement device with gauge factor as high as 29 and with Young's modulus that approaches that of the human epidermis. These systems combine thin, carbon black doped poly(dimethylsiloxane) (CB-PDMS) as the strain gauges due to their high resistivity and strong dependence on strain, with carbon nanotube doped PDMS (CNT-PDMS) as the interconnects due to their comparatively low resistivity and weak dependence on strain. Devices comprised of molded, straight resistors of CB-PDMS joined by serpentine-shaped interconnects of CNT-PDMS, both in a common matrix substrate of PDMS, have electrical responses that depend almost entirely on the strain in the CB-PDMS. Integrated structures of this type have Young's moduli of 224 kPa, which lies within the range of values for the human epidermis. Such sheets can be readily laminated on and form conformal contact to the human skin, with only modest mechanical constraints on natural motions. Strains measured in this mode on the wrist are between 11.2% and 22.6%.

References

[1] D. Kim, N. Lu, R. Ma, *et al*, 2011, *Science*, 333, 838.
[2] T. Yamada, Y. Hayamizu, Y. Yamamoto, Y. Yomogida, A. Izadi-Najafabadi, D. N. Futaba, K. Hata, 2011, *Nat Nanotechnol*, 6, 296.
[3] C. Liu, 2007, *Adv Mater*, 19, 3783.
[4] S. R. Quake, A. Scherer, 2000, *Science*, 290, 1536.
[5] S. Rwei, F. Ku, K. Cheng, 2002, *Colloid Polym. Sci.*, 280, 1110.
[6] X. Niu, S. Peng, L. Liu, W. Wen, P. Sheng, 2007, *Adv Mater*, 19, 2682.
[7] K. S. Ryu, X. Wang, K. Shaikh, C. Liu, 2004, *J Microelectromech S*, 13, 568.
[8] D. Kim, N. Lu, R. Ghaffari, *et al*, 2011, *Nat Mater*, 10, 316.
[9] L. Bokobza, 2007, *Polymer*, 48, 4907.

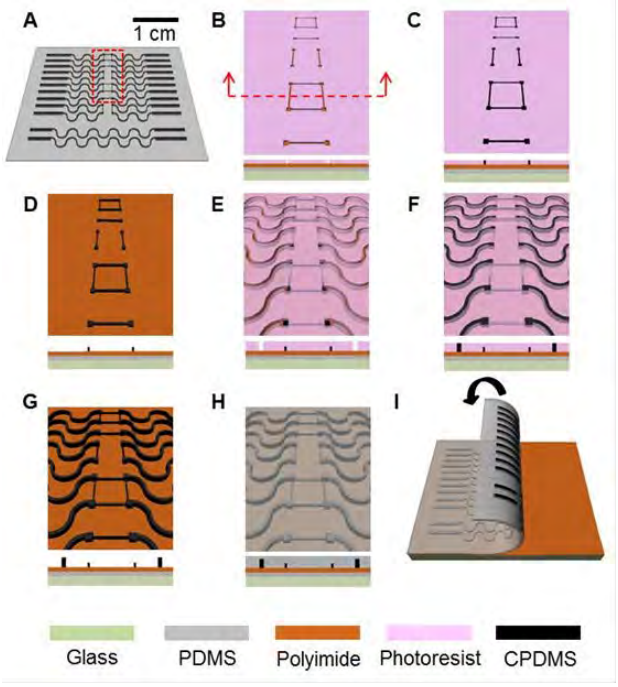

Figure 1 Schematic illustrations of fabrication procedures for all-elastomer strain gauges. (A) Full-sized completed device. Tilted top views and cross-sectional views of the red dotted box in Frame A are provided in Frames B through H. (B) Positive photoresist patterned in the form of trenches with layouts matching desired resistors and Wheatstone bridge geometries, on a film of polyimide. (C) CB-PDMS squeezed into the trenches with excess removed by a razor blade. (D) Photoresist rinsed off after curing the CB-PDMS. (E) Thick layer of photoresist patterned in the form of trenches with layouts matching the interconnects. (F) CNT-PDMS squeezed into the trenches with excess removed by a razor blade. (G) Photoresist rinsed off after curing the CNT-PDMS. (H) Cast PDMS to cover all of the patterned features. (I) Peeling the entire integrated structure from the polyimide to yield a device shown in Frame A.

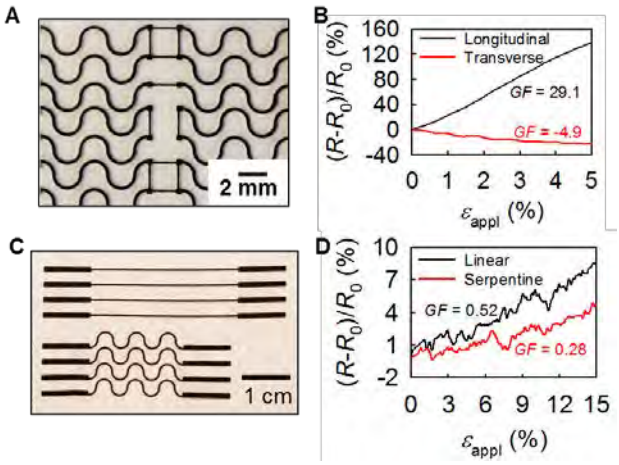

Figure 2 Tensile tests of all-elastomer strain gauges. (A) Top view of an as-fabricated strain gauge. (B) Change of resistance for longitudinal and transverse resistors as a function of tensile strain. Gauge factor as high as 29 has been achieved. (C) Top view of as-fabricated linear and serpentine structures of CNT-PDMS embedded in a PDMS substrate. (D) Change in resistance of linear and serpentine structures of CNT-PDMS as a function of applied tensile strain. Linear CNT-PDMS is more strain-sensitive than serpentine ones.

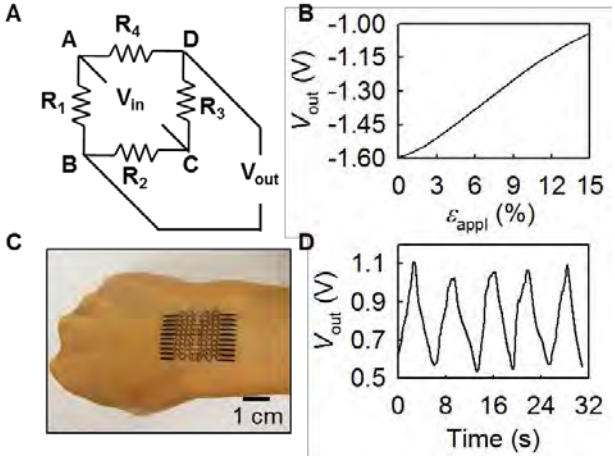

Figure 3 Using all-elastomer strain gauges in Wheatstone bridge configurations to quantify strain associated with deformations in human skin. (A) Schematic diagram of a Wheatstone bridge. (B) Output voltage of the Wheatstone bridge as a function of uniaxial tensile strain. (C) Device laminated on the human wrist. Device is as soft as human skin and therefore imposes minimal mechanical constraint. (D) Output voltage when the wrist is undergoing cyclic bending. Strains measured in this mode are between 11.2% and 22.6%

Missing Abstract

ID: 457

Missing Abstract

ID: 473

ID: 478

Design of Soft Dielectric Composites: Instabilities and Effects of Anisotropy

Massimiliano Gei
Department of Mechanical and Structural Engineering, University of Trento
Italy

Roberta Springhetti
Department of Mechanical and Structural Engineering, University of Trento
Italy

Abstract:
Dielectric elastomers are an important class of materials currently employed to design and realize electrically-driven, highly-deformable actuators and generators which find application in several fields of engineering (Carpi et al., 2008). The use of composites may improve the performance of such systems as a thorough design may lead to a substantial increase of the dielectric constant of the material and then of the coupling between electrical input and mechanical response (Ponte Castañeda and Siboni, 2012; Tian et al., 2012). However, the mechanics of electroelastic soft dielectric composites is still under development and a number of problems are still open in this field.
In the talk, results related to the following issues will be presented and discussed:

i) *the effect of the microstructure on the overall behavior of layered composite actuators*. Sensitivity of the performance in terms of layering angle and electromechanical properties of phases will be highlighted;

ii) *the difference between charge-controlled and voltage-controlled type of actuation in anisotropic electroelastic material*. A layered composite turns out to be macroscopically anisotropic in terms of both mechanical and electrical responses. Now, electric field and electric displacement field are no longer aligned and this means that the control of the former depends on the voltage while to set the latter the charge distribution must be imposed. Interestingly, the two ways may give, for the same composite, strongly different macroscopic behaviors;

iii) *the role of instabilities in limiting large-strain performance in soft layered composites.* Electromechanical instability and band-localization instability are considered in this investigation as well as microbuckling (Bertoldi and Gei, 2011). It is shown that, depending on the properties of the phases, all types may become important to limit the range of applicability of a layered electroelastic composite.

iv) *how to exploit instabilities to conceive unusual operation principles*. It is shown that, under certain conditions, snap though instabilities can be induced in layered composites made of ideal dielectrics modeled with a neo-Hookean free energy; this may be useful in the design of release-

actuated devices. Moreover, playing with the geometry of the composite, a counter intuitive thickening effect can be induced in electrode-membrane-electrode actuator configurations.

Acknowledgement:
The financial support of Italian MIUR, grant PRIN no. 2009XWLFKW, and of EU, COST Action no. MP1003, is gratefully acknowledged.

References:

Bertoldi, K. and Gei, M. (2011). Instability in multilayered soft dielectric. *J. Mech. Phys. Solids*, 59, 18-42.

Carpi, F., De Rossi, D., Kornbluh, R., Pelrine, R., and Sommer-Larsen, P. (Eds.) (2008). *Dielectric Elastomers as Electromechanical Transducers*, Elsevier, Oxford, UK.

Gei, M., Colonnelli, S., and Springhetti, R. (2012). The role of electrostriction on the stability of dielectric elastomer actuators. *Submitted*.

Ponte Castañeda, P. and Siboni, M.N. (2012). A finite-strain constitutive theory for electro-active polymer composites via homogenization. *Int. J. Non-Linear Mech.*, 47**,** 293-306.

Tian, L., Tevet-Deree, L., deBotton, G., and Bhattacharya, K. (2012). Dielectric elastomer composites. *J. Mech. Phys. Solids*, 60, 181–198.

ID: 482

Self-Assembled Biological Structures

Devin M. Ridgley
Virginia Tech
United States

Elizabeth C. Claunch
Virginia Tech
United States

Justin R. Barone
Virginia Tech
United States

Abstract:
Biological systems self-assemble into flat structures such as tapes and sheets. The size of the tape or sheet can be controlled through molecular choice and self-assembly is observed from the nanometer to the micrometer scale. Short peptides and substituted amino acids are employed as self-assembling molecules. In solution and upon drying, the sheets and tubes twist and roll into cylinders and tubes. Molecular features relative to experimental conditions influence deformation of the tapes and sheets and determine final morphology and properties.[1,2] Morphological development is observed with atomic force microscopy (AFM) and scanning electron microscopy (SEM). Molecular spectroscopy delineates interactions necessary to build the structures. Nanoindentation results quantify the modulus of the structures, which can be related back to morphology and molecular interactions. Self-assembling polymer molecules from the molecular to the macroscopic scale is the next natural step in materials design. Reaching the macroscopic scale is challenging but useful engineered products can be constructed with properties and structure controlled from the molecular scale. Eventually, we will be able to conceptualize a product that has inherent function, shape, and color and design molecules to self-assemble into that product.

1 Athamneh, A. & Barone, J. R. Enzyme-mediated self-assembly of highly ordered structures from disordered proteins. *Smart Materials and Structures* **18**, 104024 (2009).
2 Ridgley, D. M., Ebanks, K. C. & Barone, J. R. Peptide mixtures can self-assemble into large amyloid fibers of varying size and morphology. *Biomacromolecules* **12**, 3770-3779 (2011).

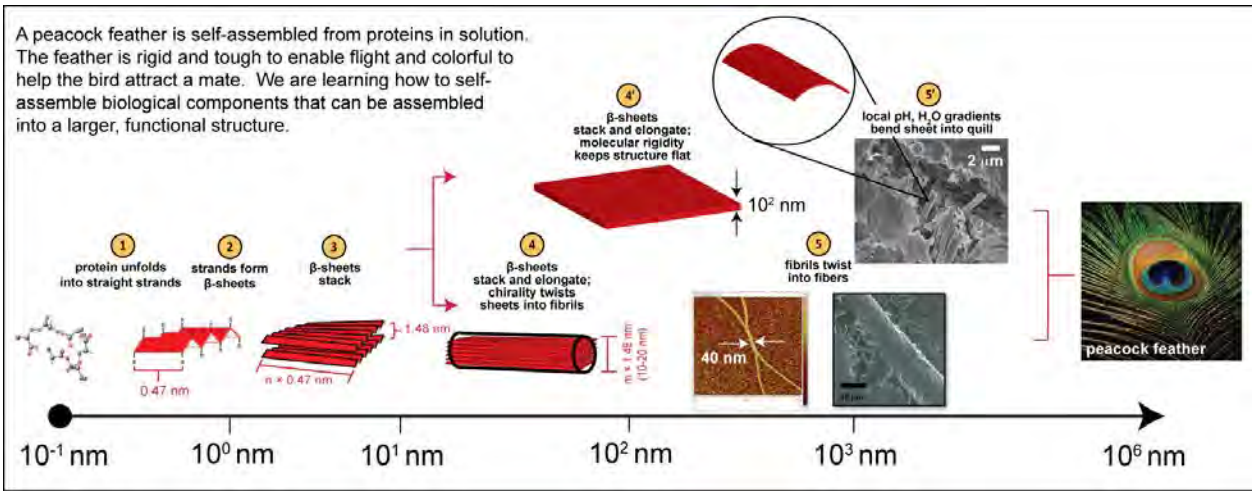
A peacock feather is self-assembled from proteins in solution. The feather is rigid and tough to enable flight and colorful to help the bird attract a mate. We are learning how to self-assemble biological components that can be assembled into a larger, functional structure.
1
protein unfolds into straight strands
2
strands form β-sheets
3
β-sheets stack
4
β-sheets stack and elongate; chirality twists sheets into fibrils
4'
β-sheets stack and elongate; molecular rigidity keeps structure flat
5'
local pH, H2O gradients bend sheet into quill
5
fibrils twist into fibers
0.47 nm
n × 0.47 nm
1.48 nm
n × 1.48 nm (10-20 nm)
10² nm
2 μm
40 nm
peacock feather
10⁻¹ nm
10⁰ nm
10¹ nm
10² nm
10³ nm
10⁶ nm

ID: 502

On the Mechanics of Soft Multilayered Composites

Stephan Rudykh
Massachusetts Institute of Technology
United States

Ashley Browning
Massachusetts Institute of Technology
United States

Mary C. Boyce
Massachusetts Institute of Technology
United States

Abstract:

Mechanical properties of flexible armors inspired by the design of overlapping scales present on teleost fish species (*e.g.*, zebrafish *Danio rerio* and *Arapaima gigas*) are investigated. The overlapping stiff scales are embedded in a soft tissue such that the composite material can provide protection while also undergoing large deformations when subjected to blunt or predatory loading. Here, we consider the influence of geometric structure of the mineralized scales and soft tissue on the mechanical performance of the composite. To this end, we first derive an analytical solution for the multilayered structure accounting for large deformations. The solution predicts the mechanical response of the media as a function of scale inclination angle, constituent volume fractions, and the stiffness ratio of phases. To capture the edge effects and account for the scales overlapping and, consequently, to inhomogeneity of the phase deformation field, we develop a finite element based numerical model of the structure and loading conditions. In these approaches we use neo-Hookean model to define the behavior of the tissue phase.

Physical prototypes of the composite armor are fabricated by a combination of 3-D printing and molding methods. The manufactured specimens cover a large variety of geometrical arrangements (constituent volume fractions, scale inclination angles, and scale overlapping). The prototypes are subjected to mechanical loading and the local deformation mechanics of the scale/soft tissue structure are measured using digital imaging correlation. The measured mechanical response, macroscopic as well as local, is found to be in good agreement with the simulations as well as with analytical predictions for the corresponding laminates. Moreover, the results provide a detailed picture of the composite deformation mechanisms which consist of tissue shear, scale rotation, and scale bending, depending on the microstructural parameters. The understanding of the key mechanisms and parameters is an important step towards designing materials balancing protection and flexibility.

References:

4. B.J.F. Bruet, J.H. Song, M.C. Boyce, C. Ortiz, *Materials design principles of ancient fish armour*. NATURE MATERIALS 7**,** 748-756 (2008)

5. M.C. Boyce and C. Ortiz , *Materials science - Bioinspired structural materials*, SCIENCE **319**, 1053-1054 (2008)

6. S. Rudykh and G. deBotton, *Stability of Anisotropic Electroactive Polymers with Application to Layered Media*. Z. Angew. Math. Phys.(ZAMP) **62**, 1131-1142 (2011)

7. S. Rudykh and G. deBotton, *Instabilities of Hyperelastic Fiber Composites: Micromechanical Versus Numerical Analyses*. Journal of Elasticity **106**, 123–147 (2012).

ID: 511

Active Programmable Shape Memory Polymer-based Cellular Materials

David Restrepo
School of Civil Engineering, Purdue University
United States

Nilesh D. Mankame
Smart Materials & Structures, General Motors Global Research and Development
United States

Pablo D. Zavattieri
School of Civil Engineering, Purdue University
United States

Abstract:
A cellular material refers to the group of materials formed by the connection of struts or faces grouped together in arrays of geometric elements to fill space. Cellular materials combine properties inherent from the base material with those imparted by its cellular microstructure yielding in a unique combination of properties not seen in its solid counterpart.

Once a cellular material is manufactured its properties are fixed. In this work we present some initial studies on the feasibility of modifying the effective mechanical properties of cellular materials after they have been manufactured by the imposition of controlled morphological imperfections at the cell level. Changes in the effective properties of cellular materials without complete reprocessing of the material will allow customized instances of cellular material to be derived cost-effectively form a common mass-produced cellular primitive. In this talk, we present some initial progress on the study, analysis, design and mechanical testing of periodic cellular smart materials with the aim to develop programmable materials.

"Programming" of the cellular material is achieved using the ability of Shape Memory Polymers (SMPs) to freeze a temporary deformation for an extended period of time. Programming and recovery of the cellular material is obtained using the typical programming-recovery process for SMPs (Fig. 1). The programming process starts at the point **1** where the material is under zero stress and is in its rubbery state at a uniform temperature of 70^{o}C. It is then deformed under displacement control to **2** where a defined range of compressive strain is imposed on it according to the desired programming. The applied strain is then held fixed to hold the strain constant while the material is cooled uniformly to 25^{o}C. The increase in modulus corresponding to the transition from the rubbery to the glassy regime causes the stress in the sample to increase sharply at point **3**.

Thermal contraction and stress relaxation in the viscoelastic material counteract this stress increase leading to a moderate jump in stress from point **2** to **3**. The material is then unloaded at a uniform temperature of 25^{o}C to **4**. Some elastic strain recovery occurs during the unloading

resulting in a material with a Y-periodic geometric imperfection at **4**. The material with imperfect cell geometry is now ready for evaluation of its effective properties at 25°C. A different magnitude of the imperfection can be imposed on the material subsequently by heating it to 70°C under zero stress (point **5**) and repeating the programming process described above.

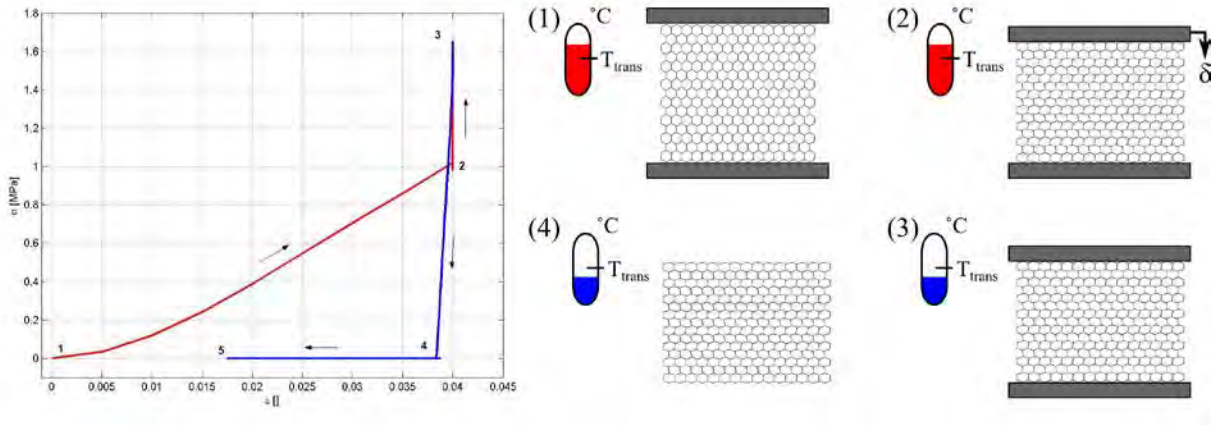

Fig. 1 – Process for programming a geometrical imperfection in an SMP-based cellular material

Nonlinear FEA simulations and experiments shows that small geometric imperfections (2% global strain) produce variations up to 20% in the effective initial compressive storage modulus in the prototypical material (Fig. 2).

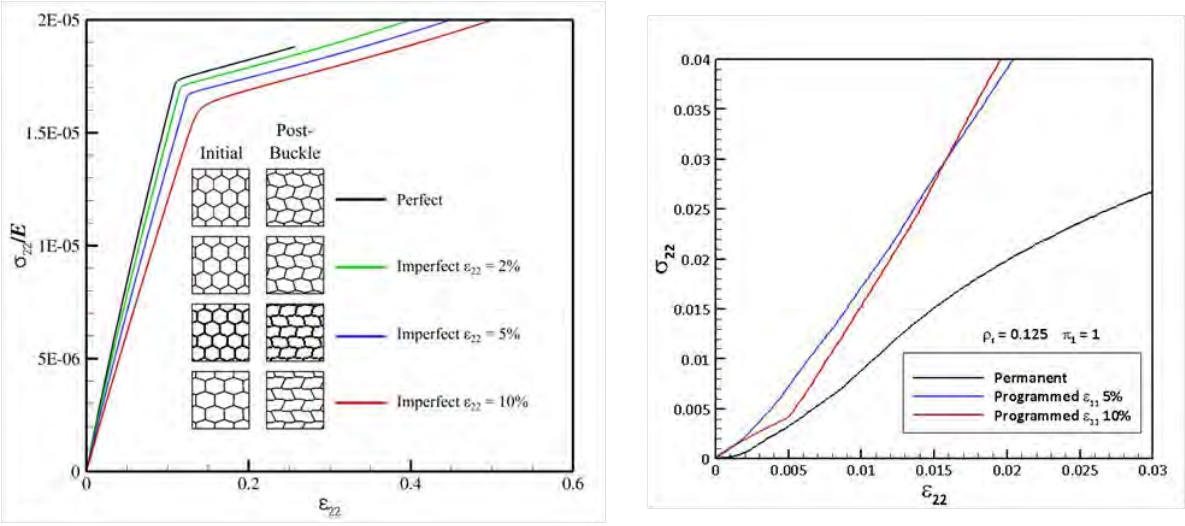

(a) **(b)**

Fig. 2 – Initial compressive storage modulus change after programming. (a) Nonlinear FEA simulations. (b) Initial experiments

In this talk, we will present the analysis of the effect of the various geometrical and material parameters involved in the mechanics of these cellular materials, as well as some discussion about scalability of this approach and alternative strategies for achieving controllable geometry changes at the cell level.

ID: 513

Exploiting buckling Buckling to design structures with negative Thermal Expansion

Jia Liu

Abstract:
Thermal expansion characterizes the tendency of materials to change in volume in response to a change in temperature. Materials with unusual thermal expansion behavior such as negative thermal expansion are of interest from both a technological and fundamental standpoint. Here, we exploit buckling in periodic structures to design materials which shrink spontaneously upon heating. Materials with positive thermal expansion ratio are laminated to construct a sandwich structure. Remarkably, by properly selecting the material and geometric properties, upon buckling the structure is observed to decrease in its macroscopic dimensions. These results open avenues for the fabrication of structures with unusual thermal expansion behaviors over a wide range of length scales.

ID: 515

Collapse of Non-Rectangular Microchannels in an Elastic Halfspace: Theory, Simulation, and Experiment

Carmel Majidi
Carnegie Mellon University

Tong Lv

Abstract:
Lab-on-a-chip microfluidics and liquid-phase metal electronics are typically composed of an elastomeric sheet embedded with a network of fluidic microchannels. Pressing the surface of the elastomer can change the cross-sectional area of the embedded microchannel and alter the fluid flow-rate, conductivity, and threshold for particulate filtration. In this work, we examine the relationship between surface pressure and area for a variety of cross-sectional geometries, from rectangles to isosceles and concave triangles. In addition to performing finite element simulations and experimental measurements, we introduce a predictive model that uses classical solutions from contact mechanics to establish an algebraic mapping between surface pressure and change in cross-sectional area. These algebraic estimates are in reasonable agreement with both simulation and experiment and can be generalized to address a broad range of design challenges in soft microfluidics, from pressure-controlled protein filtration to measuring surface tractions with electric resistance.

ID: 524

SNAP-BUCKLING INSTABILITY OF BEAMS AND SHELLS

Anupam Pandey*, Douglas P. Holmes*, Callan Gillespie*

Dominic Vella**, Derek Moulton**

Tarun Sinha***, & Howard A. Stone***

*Department of Engineering Science & Mechanics, Virginia Tech, Blacksburg, VA, USA

** Oxford Centre for Collaborative Applied Mathematics, Oxford University, UK

***Mechanical and Aerospace Engineering Department, Princeton University, Princeton, NJ, USA

Plants and animals utilize the rapid snap-through instability for pollen emplacement, seed dispersal, nutrition and defense. Snap-buckling of curved beams, plates, and shells presents an interesting experimental paradigm due to the ability for one structure to rapidly change between two stable configurations. While snapping, geometric arches and spherical shells exhibit a highly non-linear response dictated by the geometry and material properties of the system. In this presentation, we examine the dynamics of snap-through of an arch under point load, snapping of hemispherical shells and impact of geometric parameters that affect the relevant snap-through timescale. Our results show that snapping of an arch under a point occurs when displacement of its midpoint is zero. The single most important parameter α which defines the coupling between bending and stretching energy dictates the snap-through timescale. Decreasing α leads to an increase in snap-through dynamics of over an order of magnitude greater than the inertial timescale.

ID: 529

Use of Mechanical Actuations for Control and Manipulation of Microfluidic Flow

Behrouz Tavakol

In this work, we manipulate and direct fluid flow toward a desired path by controlling the deformation of an elastic arch within a flexible microfluidic channel using mechanical actuation. The flexible arch can be prepared by buckling an elastic film and its deflection can be predicted by classical theory of Euler buckling. The effect of arch thickness and shape was investigated numerically and verified experimentally. The flow rate was predicted analytically using a perturbation of lubrication theory and confirmed by simulation and experimental results. Good agreement was obtained between higher orders of analytical solutions and both simulation and experimental results. We demonstrate how the device can be used to move fluids towards regions of high-stress as a way to prepare portable, flexible microfluidics for chemical mixing, self-healing, and in situ diagnostics.

ID: 545

Experimental and Numerical Studies of Wrinkling in Network of Soft and Stiff Materials

Narges Kaynia
Massachusetts Institute of Technology
United States

Yaning Li
Massachusetts Institute of Technology
United States

Mary C. Boyce
Massachusetts Institute of Technology
United States

Abstract:

This research was motivated by the undulating patterns observed in the epidermis cells of some plants in nature. Analytical and finite element models were developed to capture the underlying wrinkling mechanisms. The characteristics of the undulation patterns were found as functions of model geometry and material composition. Experiments were designed to further explore the modeling results. The composite samples were made from different types of elastomers by varying the geometry and the material properties. External loads were applied to these samples to trigger the wrinkling patterns. Extensive mechanical experiments of these samples were conducted to observe the onset and progression of the wrinkling patterns. The experimental and numerical results were consistent with the analytical predictions. This research has potential for designing active or actuating composite materials or devices which are responsive and reversible.

ID: 553

Numerical Modeling of the Nonlinear Elastic Response of Filled Elastomers via Hashin Microstructures

Taha Goudarzi
University of Illinois at Urbana-Champaign
USA

Celia Reina Romo

Abstract:
In this talk, I will present an effective numerical method to generate approximate solutions for the overall non-linear elastic response of isotropic filled elastomers subjected to arbitrary finite deformations. The basic idea is first to idealize the random microstructure of filled elastomers as a composite sphere assemblage of Hashin, and then to generate approximate (statically admissible) solutions for these material systems by solving numerically the response of a single composite sphere subjected to affine stress boundary conditions. The key theoretical and practical strengths of the proposed variational approach are discussed. As a first application, results are presented for Neo-Hookean elastomers reinforced with rigid particles, both in 2D and 3D. Comparisons with new exact analytical solutions and full 3D FE results for isotropic filled elastomers will also be presented to assess the accuracy of the proposed method.

ID: 565

Drag Control through Wrinkling on Curved Surfaces

Pedro M. Reis
Department of Mechanical Engineering
Department of Civil and Environmental Engineering
Massachusetts Institute of Technology,
02139 Cambridge, USA

Denis Terwagne
Department of Civil and Environmental Engineering
Massachusetts Institute of Technology,
02139 Cambridge, USA

Abstract:
Wrinkling patterns correspond to modes of undulatory out-of-plane surface deformation that occur when a structure that is comprised of a thin stiff film adhered to a softer thick substrate is compressed (see Fig. 1a). We present the results of an experimental investigation on the wrinkling of positively curved surfaces and explore their use towards drag reduction applications.

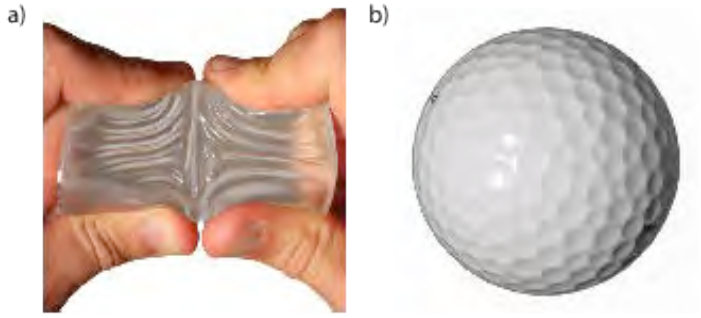

Fig. 1: (a) Wrinkles emerge when a structure made of a stiff film on a soft foundation is compressed. (b) The dimples on a golf ball delay the flow separation around the ball and reduce its drag when moving through a fluid.

In our precision desktop-scale experiments we make use of rapid prototyping techniques to fabricate samples that have custom geometry and material properties, using silicone-based elastomers. Our structures consist of a thin stiff shell that is chemically bonded to a thicker soft core substrate. This substrate contains a spherical cavity that can be depressurized, under controlled volume conditions, to homogeneously compress the ensemble. Under this loading, the initially smooth outer-shell develops a complex wrinkling pattern. We systematically characterize and quantify the morphology of the various patterns and map out the phase diagram of the system. Both geometric and material quantities are considered in the parameter space. Motivated by the similitude between the quasi-hexagonal wrinkling patterns we observe in some of our samples and the dimples on a golf ball (see Fig. 1b), we systematically characterize the aerodynamic behavior of our structures in the context of fluid drag reduction. An added advantage of the novel mechanism we introduce is that it allows for both dynamic switching and tuning of the surface morphology, thereby opening paths for drag control.

ID: 635

Non-linear Response of Soft Porous Structures: Effect of Pore Shape on Their Response

Johannes Overvelde

Nature makes extensive use of structures characterized by well defined microstructures often either regular or periodic to achieve different properties and attributes. Recently it has been shown that by introducing a microstructure in a soft matrix, microscopic instabilities can be triggered. Interestingly these instabilities can be utilized to design porous materials whose response is characterized by multiple phases with highly varying properties. As an example, a square array of circular pores has been shown to strongly influence the material stiffness and Poisson ratio. Expanding on these findings, in this study we will investigate both numerically and experimentally the effect of pore shape on the nonlinear response of a square array of holes in a soft matrix. Our results show that the pore shape can be used effectively to design material with desired properties and pave the way for the development of a new class of soft, active and reconfigurable devices over a wide range of length scales.

ID: 657

Atomistic Investigation of the Giant Flexoelectricity in Polymers

Qian Deng
University of Houston
United States

Pradeep Sharma
University of Houston
United States

Abstract:
Flexoelectricity, which couples inhomogeneous deformation to electric polarization, has been attracting scientific attention since 1960s. Different from the case of solid crystalline dielectrics, the flexoelectricity in polymers is nonlinear and the mechanism might be more complicated. Recent studies have shown that giant flexoelectricity may exist in certain polymers. We believe that this giant flexoelectricity is close related to the microstructure of these polymers. To investigate this mechanism, in this work, a series of atomistic simulations are conducted on both amorphous and crystalline polyvinylidene fluoride (PVDF) films. As an application of this study, we propose a microstructure based constitutive law for polymers with flexoelectricity. At last, the polarization-strain gradient relationship for an α-phase PVDF film is calculated using the proposed constitutive law and the results is compared with that reported in previous experiments.

ID: 684

Characterizing Functional Glass Transition in Polymers from Molecular Simulations

Sinan Keten
Northwestern University
USA

Luis Ruiz

Abstract:
Multifunctional materials such as shape memory polymers undergo critical transitions from the glassy to the rubbery state by the introduction of external cues such as temperature and moisture. The mechanical properties of the polymer are distinctly different at below and above the glass-transition temperature and the triggering mechanisms can be specific to the chemical structure of the polymers as well as moisture and solvent effects in the service environment. Discerning these effects are challenging to carry out experimentally, however, they remain crucially important for applications of these materials as biomaterials, sensors, actuators, as well as self-healing phases in complex composites. Here we present a general multi-scale modeling approach that involves tracking variation in the motion of atoms and molecules from atomistic trajectories, which provides direct insight into the mechanical behavior and glass-transition of polymer materials under a broad range of polymer chemistries and solvent conditions. Implications of the findings for the mechanical behavior of shape memory and multifunctional polymers will be discussed. Our methodology provides a means for linking chemistry into mechanical behavior, paving the way for simulation based design approaches to new nanomaterials and nanocomposites with multifunctional properties that can be tuned by chemistry and confinement effects that emerge at the nanoscale.

ID: 692

An Analytic Theory of Planar Creasing Patterns

Evan Hohlfeld
Lawrence Berkeley Natl. Lab
USA

Abstract:
Strained soft elastomers can spontaneously form patterns of sharply-creased folds, called sulci, via a strongly sub-critical, yet scale-free instability. Treating the threshold for non-linear instability as a non-linear critical point, we explain the formation and near-threshold development of sulcus patterns in terms of the scale and translation symmetries which are broken by the formation of an isolated, small sulcus. Our analytic theory and simulations show that, relative to this non-linear critical point, sulcus formation can arise either as a super-critical or as a weakly sub-critical bifurcation in a thick, compressed slab, depending on the boundary conditions. An infinite number of competing, equilibrium patterns simultaneously emerge at this critical point, but the one selected has the lowest energy. We give a simple, physical explanation for the formation of sulcification patterns using an analogy to a solid-solid phase transition with a finite energy of transformation.

ID: 748

Harnessing Responsive Gels to Design Synthetic Microswimmers

Hassan Masoud
Georgia Institute of Technology
United States

Alexander Alexeev
Georgia Institute of Technology
United States

Abstract:

Swimming microdevices that are able to carry payloads and navigate autonomously through highly viscous environments have the potential to revolutionize drug delivery systems, microsurgery, lab-on-a-chip devices, and micro/nano fabrication. Recent advances in the MEMS technology have enabled researchers to design and employ different swimming microrobots, many of them biomimetic, to perform tasks in microfluidic systems. However, despite recent notable progress in creating microswimmers, the development of miniature self-propelling robots that can effectively navigate along arbitrary trajectories within microchannels remains to be a challenge.

Herein, we use computational modeling to design a synthetic microswimmer that not only self-propels, but also navigates in a low-Reynolds-number environment. Our simple swimmer consists of a cubic gel body with two rectangular stiff flaps attached to its opposite sides and a stimuli-sensitive flexible flap at the body front end (see Figure 1a). The responsive gel undergoes periodic expansions and contractions (see Figure 1b), which can be experimentally triggered by an oscillatory chemical reaction or by oscillating magnetic and electric fields. Periodic volumetric changes of the body lead to the time-irreversible beating motion of the propulsive flaps which propel the microswimmer through the inertialess fluid. We examine the effect of body elasticity and length of propulsive flaps on the locomotion of our swimmer and show how they can be tailored to optimize the swimming speed and efficiency. We also demonstrate that our swimmer can successfully turn in the desired direction following the application of an external stimulus to the responsive steering flap. In this scenario, the steering flap bends and flutters around its curved profile resulting in a rotating torque that deflects the

swimmer trajectory. Our simulations indicate that the magnitude and direction of swimmer turning action can be regulated by the strength of the external stimulus.

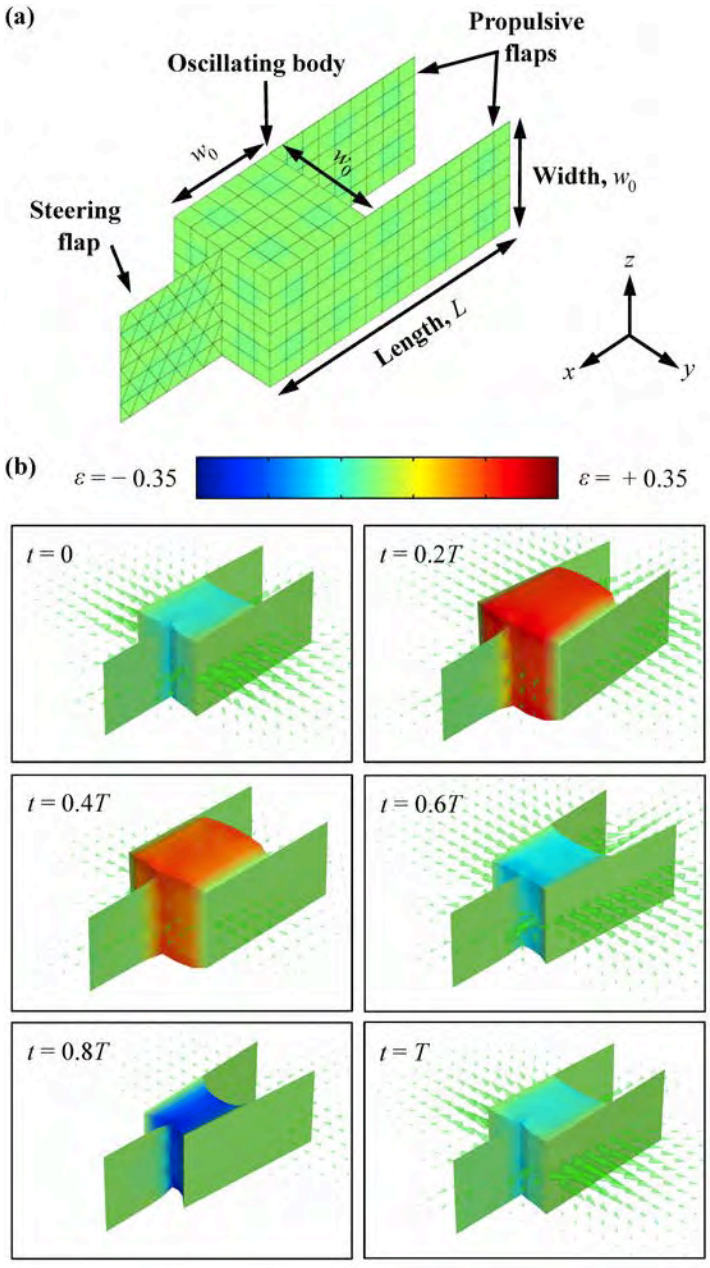

Figure 1 Panel (a) shows a schematic of the microswimmer. Panel (b) shows snapshots illustrating the swimmer motion during one period of the gel body oscillations. Colors in panel (b) represent the material strain ε. Green cones represent velocity vectors in the xy plane through the middle of the swimmer body.

III.2

Multifunctional Materials and Multiphysics Problems - Modeling and Simulation of Cellular Functions

ID: 787

Towards Modeling Mechanical Effects Arising During Cyclic Adenosine Monophosphate Release in Human Trophoblast Cells

Luca Deseri[0]
Department of Mechanical and Structural Engineering,
University of Trento, via Mesiano 77, I-38123 Trento, Italy
and
visiting at CNA-Carnegie-Mellon University
15213 Pittsburgh PA-USA

Laura Lunghi
Department of Biology and Evolution,
University of Ferrara, via Mortara, 44100 Ferrara, Italy

June 28, 2012

Conformational changes of transmembrane domains of beta-adrenergic receptors have been observed at the onset of the cyclic Adenosine Mono Phosphate (cAMP) pathway [8]. Often times such changes may be accompanied by shortening or elongating of lipids forming the cell membranes ([5]) and/or shearing of them across the thickness of the membrane. This suggests some conformational-mechanical coupling.

The pathway mentioned above may be detected through measurements of cAMP. This is an intracellular second messenger that transduce the effects of extracellular ligands inside the cell, since such ligands cannot get through the cell membrane. The ligands bind to a specific receptor, following the so called "lock and key mechanism". Beta-adrenergic receptors are integral membrane proteins embedded in the lipid bilayer and they belong to the G protein-coupled receptor (GPCR) family, which is characterized by seven transmembrane helices, denoted by $TM1TM7$ (see e.g. [4]). The conformational changes cited above may involve both a rotation about the axis of $TM6$ and a shear of $TM6$ towards $TM5$. Once the adrenergic ligand (i.e. epinephrine) is recognized, the receptor changes conformation and, thus, activates the G protein. This detaches from the receptor and, in turn, activates another membrane protein, called adenylyl cyclase. This enzyme transforms adenosine triphosphate (ATP) in cAMP. The cyclic nucleotide is involved in the regulation of several important cell functions, including proliferation and migration. This may be observed in human trophoblast cells (see e.g. [9], [1], [2]) forming the fetal site of the placenta. The response of aggregates of such cells to epinephrine is detected through enhancement of intracellular cAMP. During the process, part of it is transported to the extracellular medium through membrane proteins called MRP1 (see e.g.[3]).

Predictions about the cell response to a given ligand and, hence, the associated conformational and mechanical changes are sought. The second messenger effects are conjectured to be directly linked to the coupling of conformational and mechanical effects arising in the receptors and in the cell membrane.

[0]Corresponding author: Luca Deseri - fax: +39 0461 282599; tel.: +39 0461 282503; web-site: http://www.ing.unitn.it/~deseril/; e-mail: deseril@ing.unitn.it. Additional e-mail address: lnglra1@unife.it (Laura Lunghi).

III.3

Multifunctional Materials and Multiphysics Problems - Synthesis and Characterization of Multifunctional Materials

ID: 105

Computational Modeling and Design of Actively-Cooled Microvascular 3D Woven Glass/Epoxy Composites

Soheil Soghrati
Civil and Environmental Engineering Department, University of Illinois at Urbana-Champaign
United States

Ahmad R. Najafi
Mechanical Science and Engineering Department, University of Illinois at Urbana-Champaign
United States

C. Armando Duarte
Civil and Environmental Engineering Department, University of Illinois at Urbana-Champaign
United States

Nancy R. Sottos
Materials Science and Engineering Department, University of Illinois at Urbana-Champaign
United States

Scott R. White
Aerospace Engineering Department, University of Illinois at Urbana-Champaign
United States

Philippe H. Geubelle
Aerospace Engineering Department, University of Illinois at Urbana-Champaign
United States

Abstract:
The current work is inspired by recent advances in the fabrication of microvascular fiber-reinforced composites with the sacrificial fiber technique [1]. In this technique, catalyst-impregnated polylactic (PLA) sacrificial fibers are introduced to the woven microstructure of the composite and then evacuated to form the hollow microchannels. The embedded microchannels are employed to actively cool the microvascular composite for high-temperature applications.

To evaluate the thermal/structural response of these actively-cooled composite, we introduce a novel Interface-enriched Generalized Finite Element Method (IGFEM) [2,3]. The IGFEM has the ability to yield a similar level of accuracy and rate of convergence as the standard FEM with finite element meshes that do not conform to the geometry of the microchannels or the fiber tows. Moreover, the proposed scheme presents several advantages in terms of reducing the number of additional degrees of freedom, applying Dirichlet boundary conditions, and computing the enrichment functions over conventional GFEM. We perform a detailed convergence study, validate the computational models, and show the application of the IGFEM to design the embedded microchannels in the woven composite.

The computational design of the actively-cooled microvascular composite is a challenging task due to the existence of multiple constraints and objective functions. We employ the allowable temperature of the composite and the maximum temperature of the coolant as the design constraints. The void volume fraction of the microvascular composite and the pressure drop required for circulating the coolant in the microchannels are adopted as the objective functions.

In addition to incorporating multiple constraints and objective functions, this optimization problem is governed by a large number of design parameters. These parameters include the microchannels configuration, spacing between the microchannels, length of the domain, type and flow rate of the coolant, and type and magnitude of the applied thermal loads. We perform a thorough study on the impact of each design parameters on the objective functions and constraints and present a general framework for the design of actively-cooled microvascular composite skin panels to be used in hypersonic aircraft applications.

References:

[1] A. P. Esser-Kahn, P. R. Thakre, H. Dong, J. F. Patrick, N. R. Sottos, J. S. Moore, and S. R. White. Three dimensional microvascular fiber-reinforced composites. Advanced Materials, 23(32): 3654-3658, 2011.

[2] S. Soghrati and P. H. Geubelle. An interface-enriched generalized finite element method for 3D weakly-discontinuous problems with complex internal geometries. Computer Methods in Applied Mechanics and Engineering, 217-220: 46-57, 2012.

[3] S. Soghrati, A. M. Aragón, C. A. Duarte, and P. H. Geubelle. An interface-enriched generalized finite element method for problems with discontinuous gradient fields. International Journal for Numerical Methods in Engineering, 89(8): 991-1008, 2012.

ID: 196

Coupling of thermal conduction and mechanical deformation of GaN nanowires due to structural transformations

Kwangsub Jung
Seoul National University
Republic of Korea

Maenghyo Cho
Seoul National University
Republic of Korea

Min Zhou
Georgia Institute of Technology
United States

Abstract:
Molecular dynamics simulations with the Green-Kubo approach are carried out to analyze the mechanical and thermal responses of [0001]-oriented GaN nanowires with hexagonal cross sections. The nanowires undergo tensile and bending deformations. The focus is on the effect of deformation and the phase transformations on the thermal conductivity of the nanowires. The wurtzite (WZ) structure of nanowires transforms to a tetragonal structure (TS) under tension, causing the thermal conductivity to decrease as the strain increases. Unloading of the transformed wires is associated with a reverse transformation from the TS structure to the WZ structure. During the reverse transformation, the nanowires consist of both TS regions and WZ-structured regions. For particular sizes, an inversion domain boundary (IDB) is observed in the intermediate states. Thermal conductivities of the nanowires in the intermediate states (WZ-TS and WZ-IDB) are lower than those of WZ-structured nanowire as shown in Fig. 1. During bending, a different phase transformation process is observed. Specifically, the WZ structure transforms to the TS structure only on the surface of the nanowires. In contrast to what is observed for tensile loading, the thermal conductivity of the wires with diameters below 2.91 nm remains essentially unchanged during bending, but the conductivity of the wires with larger diameters increases with the structural change as shown in Fig. 2. The size dependence of thermal conductivity is also analyzed for wires with different structures. As the lateral size increases, the thermal conductivity of WZ-structured nanowires increases, but the conductivity of TS-structured nanowires and wires in the intermediate states during unloading decreases. The different trends in changes of thermal conductivity appear to result from phonon behavior changes primarily associated with the different states. Specifically, the relaxation time of phonons decreases as strain increases and the group velocity of phonon depends on the stiffness of the nanowires.

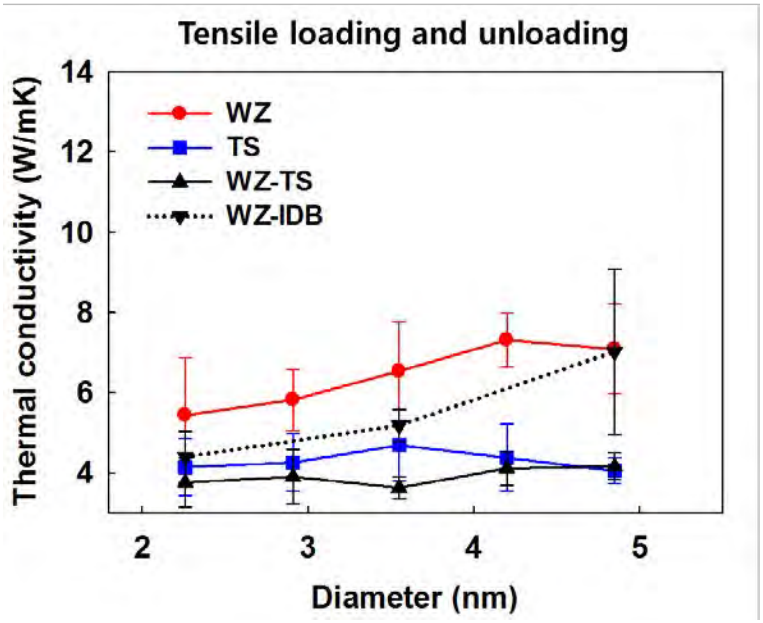

Fig. 5 Thermal conductivities of WZ-structured, TS-structured, WZ-TS structured, and WZ-IDB structured nanowires as functions of diameter during tensile loading and unloading.

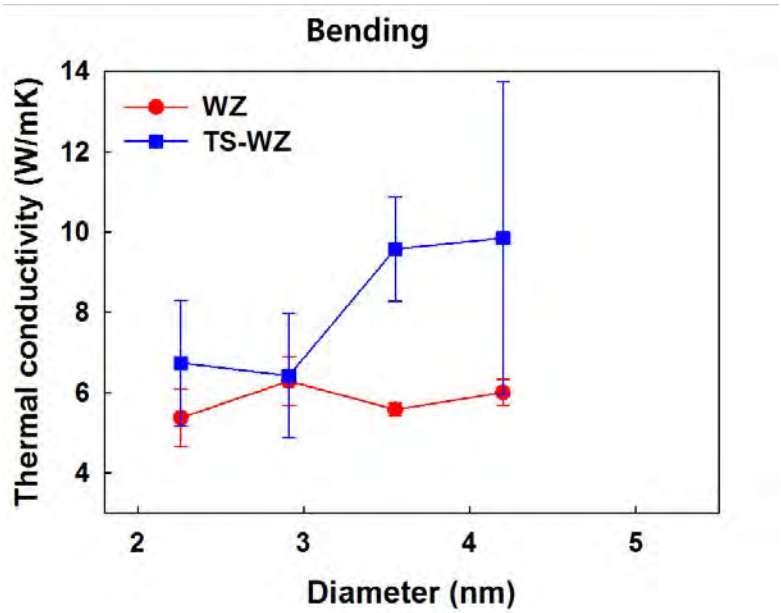

Fig. 2 Thermal conductivities of initial WZ-structured nanowires and TS-WZ structured nanowires as functions of diameter during bending.

ID: 311

Flexoelectricity in ferroelectric thin films: thermodynamic theory and experiments

Daining Fang
Peking University
China

Hao Zhou
Peking University
China

Jiawang Hong
Tsinghua University
China

Yihui Zhang
Tsinghua University
China

Faxin Li
Peking University
China

Yongmao Pei
Peking University
China

Abstract:
Flexoelectricity describes the coupling between strain/stress gradient and polarization, which is responsible for many novel physical phenomena in ferroelectrics (high flexoeletric coupling coefficient) and become remarkable at the nanoscale (high strain gradient). Especially, interface misfit strain relaxation in epitaxial thin films and nanoindentation are two important origins of large strain gradient, and thus flexoelectricity emerges in these two situations.

Within the Landau-Ginsburg-Devonshire phenomenological approach, we studied the flexoelectric effects on the nanoscale polarization behaviour of epitaxial ferroelectric thin films. It is found that flexoelectricity can induce the increase of theoretical critical thickness, below which the switchable spontaneous polarization vanishes. This increase is remarkable in tensile films while trivial in compressive films due to the electrostriction caused decrease of ferroelectric-paraelectric potential barrier, which can be easily destroyed by the flexoelectricity in tensile films. What's more, a uniform electric field is found to be valid in removing the imprint effect resulted from flexoelectricity.

Besides, it is also found that mechanical bending can eliminate the pre-existing electrical imprint behaviour of ferroelectric thin films by use of piezoresponse force microscopy.

Preliminarily, a nanoindentor platform with functions of applying electric field, magnetic field and thermal field was designed and can be constructed to study the external fields' impacts on the ferroelectrics' mechanical properties (e. g. elastic modulus, yield strength and fracture toughness) and their multi-physical-field coupling properties (e. g. magnetostriction, piezoelectricity and flexoelectricity) through nanoindentation, microbridge and microcantilever experiments.

ID: 411

Direct Fabrication of Arbitrary-Shaped Ferroelectric Nanostructures on Hard and Soft Substrates

Suenne Kim
Georgia Institute of Technology
United States

Yaser Bastani
Georgia Institute of Technology
United States

Nazanin Bassiri-Gharb
Georgia Institute of Technology
United States

Elisa Riedo
Georgia Institute of Technology
United States

Abstract:
Due to their ferroelectric switching and enhanced piezoelectric responses, ferroelectric oxides can be utilized in a variety of nanometer scale applications, such as non-volatile memory and energy harvesting devices. However, the processing temperatures required for their manufacturing are high and incompatible with other on-chip components in most of the reported techniques.
We fabricated $Pb(Zr_{0.52}Ti_{0.48})O_3$ (PZT) and $PbTiO_3$ (PTO) ferroelectric-oxide nanostructures in repeated (disk, line or sphere arrays) or in arbitrarily-designed shapes on platinized silicon and soda-lime glass substrates.[1] Thermochemical Nanolithography (TCNL), a versatile atomic force microscope (AFM) based chemical nanopatterning technique, was incorporated into the sol-gel process to create PTO/PZT ferroelectric nanostructures directly on the substrates. Nanoscale crystallization of the sol-gel precursor film can be also achieved on a substrate having low-melting point by this method. In particular, using heated thermal AFM tips as a local heat source, nanoscale transformation was achieved from the sol-gel precursor film deposited on a flexible polyimide (Kapton) substrate.
Ferroelectric lines with width as narrow as ~25 nm, spheres with diameter as small as ~10 nm, and nanospheres at the density of 213 Gb in^{-2} have been produced. Micro-Raman spectroscopy, piezo-response force microscopy, and Kelvin probe force microscopy results indicate that the TCNL technique is, in fact, capable of producing of high-temperature perovskite oxide ferroelectrics. This could facilitate production of high-density complex ferroelectric structures for energy harvesting arrays, sensors and actuators in nano-electromechanical systems (NEMS).

References:

1 Kim, S. *et al.* Direct Fabrication of Arbitrary-Shaped Ferroelectric Nanostructures on Plastic, Glass, and Silicon Substrates. *Advanced Materials* **23**, 3786-3790, doi:10.1002/adma.201101991 (2011).

ID: 413

Self-Sensing Fibers and Thermal Sprayed Electrodes for Health Monitoring of Composites

Toshio Nakamura
Department of Mechanical Engineering, State University of New York at Stony Brook, NY USA

Abstract:
Development of novel damage assessment devices for carbon fiber-reinforced composite structures utilizing carbon fibers as multifunctional elements is presented. Here the fibers act as not only load carrying components but also sensors through their electrical conductivity. Two key features are the fabrications of electrodes required to measure electrical resistivity changes due to damage, and the robust data interpretation scheme to diagnose the damage states. The former takes the advantage of new technology based on the thermal spray process where molten copper particles are directly deposited onto composite laminate surfaces to form network of electrodes. The latter task relies on the optimization/inverse analysis to estimate damage location and size through processing of measured data. Initial experimental measurements with artificially made damage indicate increased resistivity in among electrodes.

Introduction

Carbon fiber reinforced polymer (CFRP) is being increasingly used as primary components of aerospace structures. However, there is yet to be an effective tool to monitor structural integrity and assess possible damage. Utilizing the electrical conductivity of carbon fibers in CFRP laminates, an alternate concept in health monitoring of composite was emerged. The idea is to conduct electricity through fibers and measure potential or resistivity changes between multiple points (i.e., electrodes). Since damage or straining of composite can impede current pathways through some fibers, it results in the increased resistance of a circuit made of carbon fiber network (distributed throughout the structure). Hence, this monitoring concept relies on the fibers themselves to act as the sensing elements which should minimize any structural attrition due to sensor incorporations. An advantage of this method is that any fiber loss/breakage, which lowers structural integrity, is closely tied to the resistance changes of fibers. In other words, the damage is directly captured as an increased electrical resistance in the fiber network. In addition, since a resistance is taken over two locations, a damage located away from electrodes is still detectable as long as the electrical passage between the electrodes is affected.

Damage Identification Process

The proposed sensor system measures resistances among electrodes attached to composite structures and estimate its size and location within each grid formed by 4 (or 9) electrodes. These electrodes serve as input/output of electrical current, and also identify the approximate location of local damage. The process is repeated grid by grid throughout the electrode network. The damage is evaluated according to the following steps. First, the relationship between damage state and electrical resistance changes is established as the reference solution. Second, changes in electrical resistances due to damage are measured. Third, the measurements are processed by an inverse analysis to obtain estimated damage parameters. In the present study, the downhill

simplex method, which is a multi-dimensional minimization algorithm, is used to find the best estimates.

Fabrication of Thermal Spray Electrodes

To demonstrate the proposed system, actual test specimens with electrodes deposited by the thermal spray (TS) process are fabricated. Then resistances between the electrodes are measured with and without damage. Eight-ply composite laminates with [0/90]2s arrangements and ~2 mm thickness were cut to 12" by 9" dimensions. Their surfaces were initially grit-blasted to remove excess epoxy layer (~50 μm). Then, copper powder was fed to Atmospheric Plasma Spray (APS) and sprayed over a mask with holes for electrodes. In this experiment, the twelve circular shaped electrodes with 12 mm diameter as well as two base electrodes were fabricated. On every electrode, two electric wires were soft-soldered to measure resistances by the 'four-point probe' method, which offsets instrumental contact resistances. In an initial step toward monitoring actual damage in composite laminate with thermal sprayed electrodes, 10 mm diameter hole was drilled through-thickness to represent damage in the current feasibility study. The size and depth of the hole were chosen arbitrary but made large enough to detect resistance measurements beyond measurement errors. Thus through-thickness hole, unlike a part-through damage as described in the simulation study was made. The measured contact resistances (between fibers and electrodes) are relatively large compared to expected resistance changed due to part-through damage. Thus the present aim is to simply verify the changes in resistances due to an existence of a hole in this preliminary phase.

Conclusions

A novel health monitoring approach, which utilizes the electrical conductivities of carbon fibers, is proposed to identify damage on the CFRP laminate. Two key features of the procedure are the robust data processing scheme based on an inverse analysis technique to identify damage state, and the thermal spray technique to fabricate multiple electrodes. In the inverse analysis, the downhill simplex technique is adopted to determine the best estimate of damage parameter. Here an error objective function is introduced to search its global minimum in the four parameter space representing damage location and size. Several damage models are constructed for the finite element simulations to test the accuracy of estimated parameters. In summary, the present simulation study indicate that to identify the damage size within a reasonable accuracy (±20%), the electrode density or spacing to be about 10 times the expected size of damage. A smaller damage may be still detected but with less accuracy.

In order to prove the feasibility of proposed technique, a network of copper electrodes were deposited on actual composite laminate. First, resistance measurements were made without damage to verify the electrical conductance among electrodes. From various electrode pairs, somewhat scattered results were observed. Next, as a preliminary step toward establishing damage monitoring system with thermal sprayed electrodes, a 10 mm diameter hole was drilled through-thickness. The size and depth of the hole was chosen arbitrary but chose to be large enough to detect resistance changes. The measured results indicated promising results with the increased resistances due to the hole. Although much refinement is needed before reliable estimates in damage size can be established, these measurements support the capability of self-sensing fibers with thermal spray electrodes to detect damage.

ID: 419

Heating in Microstructures of HMX/Estane PBX during Dynamic Deformation

Ananda Barua
Georgia Institute of Technology
USA

Min Zhou
Georgia Institute of Technology
USA

Abstract:
We report the results of a study of the thermomechanical response of HMX/Estane PBX system during impact loading. The focus is on the dynamic response of confined specimens over the range of strain rates of 104 & 105 s-1. The materials analyzed have HMX volume fractions between 0.69 and 0.82. A recently developed cohesive finite element method is used to track and analyze the contributions to heating from different constituents, interfaces, deformation and fracture mechanisms, and internal friction. In particular, energy dissipations due to viscoelastic deformation, grain fracture, interfacial debonding, and friction along crack faces are quantified for the range of grain volume fractions and strain rates considered. In order to obtain a quantitative characterization of the heating processes, the results are compared with the predictions of the gamma probability distribution function which represents the heating process of materials with spatially randomly varying but temporally constant internal heating sources. This comparison allows insight to be gained regarding the intensity, spatial and temporal distributions, and mechanisms of the impact-induced heating in the heterogeneous materials.

ID: 458

Sliding on a Nanotube: Interplay of Friction, Deformations and Structure

Hsiang-Chih Chiu
School of Physics
Georgia Institute of Technology
United States

Suenne Kim
School of Physics
Georgia Institute of Technology
United States

Elisa Riedo
School of Physics
Georgia Institute of Technology
United States

Abstract:
Carbon nanotubes (CNT) have potential applications in micro and nano-electro-mechanical devices such as actuators and sensors, as well as mechanical reinforcement in composite materials. For most CNT applications, CNTs are in contact with their supporting surfaces. Therefore it is important to understand their tribological properties and the influences of surface chemistry or structural defects. In this work, we study the frictional properties of individual CNT by sliding a nanosize Atomic Force Microscopy (AFM) tip along and across its principal axis. This direction-dependent friction force is found to strongly correlated with the CNT chirality, surface chemistry and structural defects present in the nanotube. Our finding provides a better understanding of the frictional properties of individual CNTs and might assist manipulations of nano-objects at the nanoscale.

Reference:
[1] Hsiang-Chih Chiu, Beate Ritz, Suenne Kim, Erio Tosatti, Christian Klinke, and Elisa Riedo, *Advanced Materials* **24**, 2879 (2012)

ID: 485

Structural Composite Flow Batteries

Stephen J. Pety
University of Illinois at Urbana-Champaign
United States

Hefei Dong
University of Illinois at Urbana-Champaign
United States

Jeffrey S. Moore
University of Illinois at Urbana-Champaign
United States

Nancy R. Sottos
University of Illinois at Urbana-Champaign
United States

Scott R. White
University of Illinois at Urbana-Champaign
United States

Abstract:

Integrating batteries into structural composites allows for the creation of energy storage devices with good mechanical properties and low weight[1]. The goal of this work is to integrate a flow battery into a composite where anode and cathode fluids are pumped through microvascular channels. This design is attractive in that it allows for rapid "recharging" of the battery since discharged fluid can be quickly pumped out and replaced with charged fluid. The fluids to be used are recently developed semi-solid Li-ion electrodes[2] that have a large energy density due to their high operating voltage and high loading of active material.

To produce the flow battery composite, a manufacturing technique is required that will create composites with two channels (one for the cathode and one for the anode) connected by a porous separator film. Our approach is to use sacrificial polylactide (PLA)[3] to form the channels and to assist in the creation of the separator. The scheme is as follows (see Figure 1): first, a two-fiber strand of PLA is prepared where the fibers are separated by a dual polymer precursor film. The precursor consists of a bicontinuous distribution of PLA and a surviving polymer such as polyethylene terephthalate (PET) or polyimide (PI). The strands are woven into a fiber preform, the composite is infiltrated and cured, and high temperature is applied to trigger vaporization of the PLA. Anode and cathode fluids can then be pumped into the newly formed channels with the surviving polymer film serving as a porous separator.

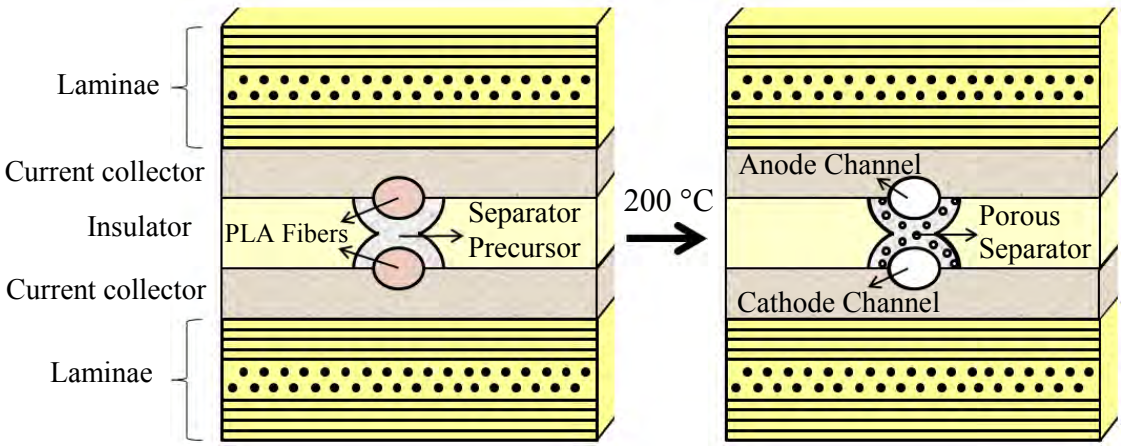

Figure 1. Schematic of the composite flow battery manufacturing process. The left image shows the initial layup and the right image shows the vascular composite formed after PLA vaporization.

As the first research thrust, semi-solid electrodes were synthesized and characterized to assess their usability in a flow battery composite. Electrodes were prepared by mixing non-aqueous electrolytes and carbon black with micron-scale particles of either lithium cobalt oxide (LCO) for the cathode or lithium titanate (LTO) for the anode. Rheometry tests run on the fluids show that they are strongly shear-thinning, suggesting they contain a network of carbon black that stabilizes a suspension of active material. The electrochemical activity of the fluids was confirmed with galvanostatic cycling and cyclic voltammetry tests on a flow cell made of metal current collectors and a commercial separator. Work is ongoing to find electrode compositions that provide both optimal electrochemical performance and workable viscosity.

As the second research thrust, dual polymer films were studied to develop a film that would transform into a porous separator upon PLA vaporization. Films containing PLA and a surviving polymer, either PET or PI, were prepared by co-dissolving the polymers and casting films using a doctor blade or spin coater. The PLA phase could then be removed using etching, dissolution, or high temperature. Optical microscopy and scanning electron microscopy (SEM) of the films before and after PLA removal show that the cast films contain phase-separated PLA domains that can be removed to form porous networks. Work is underway to optimize the morphology of these networks by controlling solution composition and film casting technique.

Future work will involve the use of PLA fibers and a separator precursor film to create composites with the channel architecture described in Figure 1. Semi-solids will then be loaded into the composites and the multifunctional performance of the system will be tested.

1. Thomas J. P. QMA (2005) The Design and Application of Multifunctional Structure-Battery Material Systems. *JOM* 57(3):18-24.
2. Duduta M*, et al.* (2011) Semi-Solid Lithium Rechargeable Flow Battery. *Advanced Energy Materials* 1(4):511-516.
3. Esser-Kahn AP*, et al.* (2011) Three-Dimensional Microvascular Fiber-Reinforced Composites. *Advanced Materials* 23(32):3654-3658.

ID: 707

Synthesis of Carbon Nanoscrolls from Hydrogenated Graphene

Shuze Zhu
Department of Mechanical Engineering, University of Maryland
USA

Teng Li
Department of Mechanical Engineering, University of Maryland
USA

Abstract:
The surge of interest in graphene, as epitomized by the Nobel Prize in Physics in 2010, is largely attributed to its exceptional properties. Graphene's two-dimensional structure exposes its entire volume to its surrounding, rendering highly amenable surface chemistry. Tremendous efforts have been placed on the chemical functionalization of pristine graphene by adsorbing foreign atoms, molecules and functional groups on its surface. Among various forms of chemical functionalization, hydrogenation of graphene (e.g., attaching atomic hydrogen to the carbon atoms in graphene) receives the most attention. Hydrogenation of graphene changes the hybridization of carbon atoms from sp^2 into sp^3. As a result, the 2D atomic structure of pristine graphene is distorted into 3D locally at each adsorbed hydrogen atom. As a result, when a pristine graphene is hydrogenated, it is found that the resulting graphene is rippled. The rippling can be explained by the local distortion of the atomic structure of graphene due to hydrogenation. These observations open up the possibility to tailor the morphologic properties of graphene in a bid to facilitate the formation of nanostructures of interest.
In this research project, we aim to demonstrate the hydrogenation-assisted self-assembly of graphene. In particular, we focus on the hydrogenation-assisted formation of a carbon nanoscroll (CNS) from a freestanding graphene, using molecular dynamics simulations.
A CNS is formed by rolling up a monolayer graphene into a spiral multilayer nanostructure, and thus is topologically open (e.g., the core size of a CNS is highly tunable by relative sliding between adjacent layers). By contrast, a CNT is topologically closed, thus its core size can only be changed slightly by stretching the carbon-carbon bonds. The open and highly tunable structure of CNSs, together with the exceptional mechanical and electronic properties inherited from the basal graphene, has inspired potential applications of CNSs, such as hydrogen storage medium, water and ion channels, nano-oscillators, and nanoactuators.
Enthusiasm aside, the realization of these promising applications hinges upon feasible and reliable fabrication of high quality CNSs, which remains as a significant challenge. A completely rolled-up CNS is energetically more favorable than its basal graphene in a planar form. Formation of a CNS, however, requires a sufficiently large driving force to overcome the energy barrier of initial curling and rolling of the basal graphene before its continuous scrolling into a

CNS. Existing chemical approaches to overcoming such an initial energy barrier to form CNSs include applying high-energy sonication to exfoliated graphite sheets or immersing a SiO_2-supported graphene monolayer immersed in isopropyl alcohol solution. In general, these chemical approaches to fabricating CNSs suffer from the possible contamination of chemical residue, and also the difficulty in controlling the rolling initiation and rolling direction.

Here we show that hydrogenation helps overcome the energy barrier to form an overlap in the non-hydrogenated part in the graphene. Once that energy barrier is overcome, the graphene can spontaneously roll up into a CNS. The successful formation of a CNS depends on the width of the free standing graphene and the hydrogenation aspect ratio (Figure 1). A phase diagram obtained from this study elucidates the key parameters that govern the successful scrolling of graphene into CNSs (Figure 2). With the ever maturing nanopatterning technique to hydrogenate graphene at high precision, the hydrogenation-assisted self-assembly of graphene holds great potential leading to a feasible fabrication technique of high quality and well controlled graphene-based novel nanostructures.

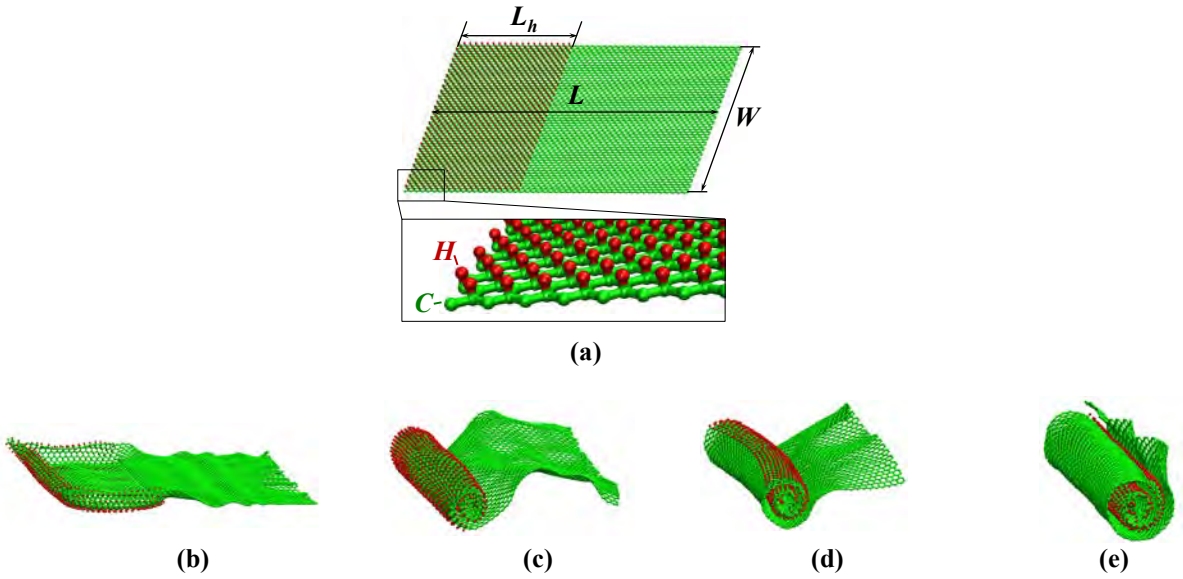

Figure 1. *(1) Schematic of a monolayer graphene that is partially hydrogenated at one side. (b)-(e) The hydrogenated portion of the graphene tends to fold and roll up, helping overcoming the energy barrier of further steady rolling up of the whole graphene into a CNS. Temperature in the molecular dynamics simulation is 300K.*

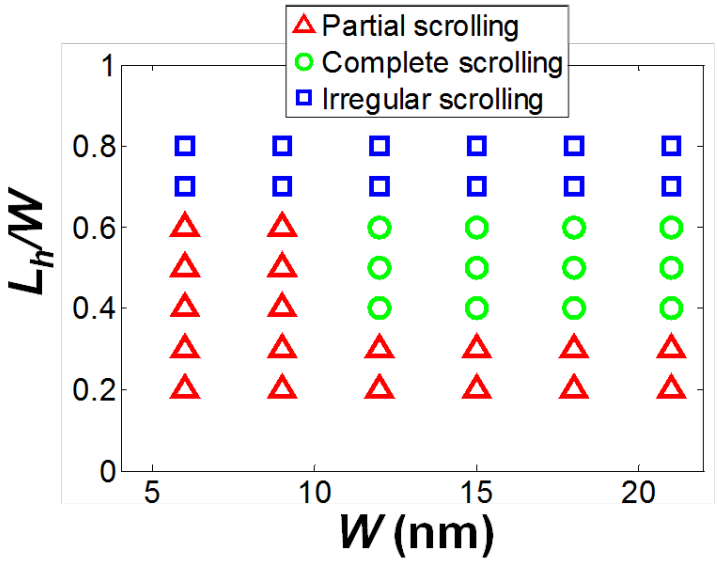

Figure 2. *A phase diagram in the space of the width of hydrogenated region and the width of graphene shows three different possible scrolling processes. Complete scrolling cases are denoted by green circles.*

III.4

Multifunctional Materials and Multiphysics Problems - Mechanics of Phase Transforming and Multifunctional Materials

ID: 107

Experimental Measurement of Coupled Thermo mechanics in Silicon With An Account of Length Scale, Stresses, and Quantum Scale Thermodynamics

Ming Gan
Not specified

Vikas Tomar
Perdue University

Abstract:
Silicon micro- and nano-structures are the essential parts of many integrated circuits and sensors. The functioning and performance of these devices are highly affected by the thermal properties of the silicon structures. Due to the size effect, the thermal properties of bulk silicon cannot represent those of silicon micro-structures. Furthermore, stress/strain inside the silicon structures also has an effect on their thermal properties. In this presentation first ever experimental measurements of coupling between mechanical strength and thermal conductivity in silicon micro and nanostructures are presented. Such measurements are coupled with surface stress measurements to show that its strain not the phase transformation that is playing a significant role in coupled multiphysics behavior of silicon nano- and microstructures.

ID: 158

Electromechanical behavior of soft electrostrictive composites: A novel microscopic theory for their analysis and bottom-up design

Oscar Lopez-Pamies
University of Illinois at Urbana-Champaign
USA

Abstract:

In this talk, I will present a "microscopic" theory with the capability to provide constitutive models for the macroscopic response of soft electrostrictive composites directly in terms of the coupled and nonlinear electromechanical behavior of their underlying constituents and their microstructure. This will be accomplished by means of an innovative iterated homogenization method that allows for the construction of exact solutions for the response of nonlinear elastic dielectric composites subjected to finite deformations and finite electric fields. These include solutions for the local fields in the underlying phases, from which — in addition to the macroscopic response — the onset of instabilities can be determined. In spite of its generality, the analysis of the proposed formulation reduces to the study of tractable Hamilton-Jacobi equations in which the initial volume fractions of the constituents play the role of "time" and the applied mechanical and electrical loads play the role of "space".

ID: 201

Multiphysics model of semiconducting ferroelectrics and its application to memory devices

Nathaniel Ng
Institute of High Performance Computing
Singapore

Kaushik Bhattacharya
California Institute of Technology
United States

Abstract:
Ferroelectrics are used in many electronic devices, and is recently being developed for ferroelectric random access memory applications. The behavior of ferroelectrics is classically described using the Devonshire-Ginzburg-Landau (DGL) model. In this model, ferroelectrics are treated as insulators. On the other hand, it is well known that ferroelectrics are in fact wide band-gap semiconductors. Hence, the natural question to ask is: how can we capture the key aspects of semiconductor physics--band bending at the interface, Fermi levels, depletion layers? In fact, recent progress has been made in models that treat ferroelectrics as semiconductors, and these methods make no a priori assumptions on the space charge or polarization distributions. However, these methods are often restricted to equilibrium profiles and may not necessarily bridge the time scales between charge-carrier dynamics and domain wall motion. In this work, we introduce a model that addresses these difficulties, yet at the same time is consistent with both the DGL model and the classic drift-diffusion model in semiconductors. Here, we demonstrate that charge carriers migrate to neutralize electric fields across 90 degree domain walls. A full simulation of a ferroelectric transistor is also attempted, with current flow, electric field and polarization distributions. In the simulation, we find that charge accumulates at the ferroelectric-semiconductor interface and the polarization vectors form closure domains at the interfaces.

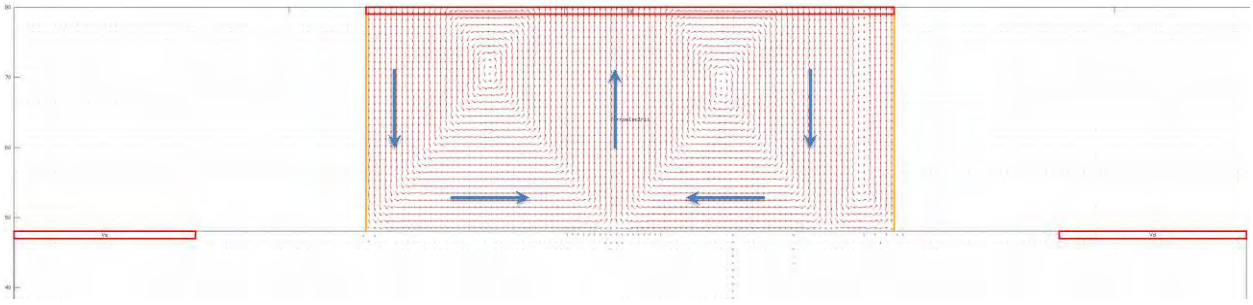

Fig 1. Polarization vectors in a ferroelectric transistor ($BaTiO_3$ on silicon), forming closure domains at the interface.

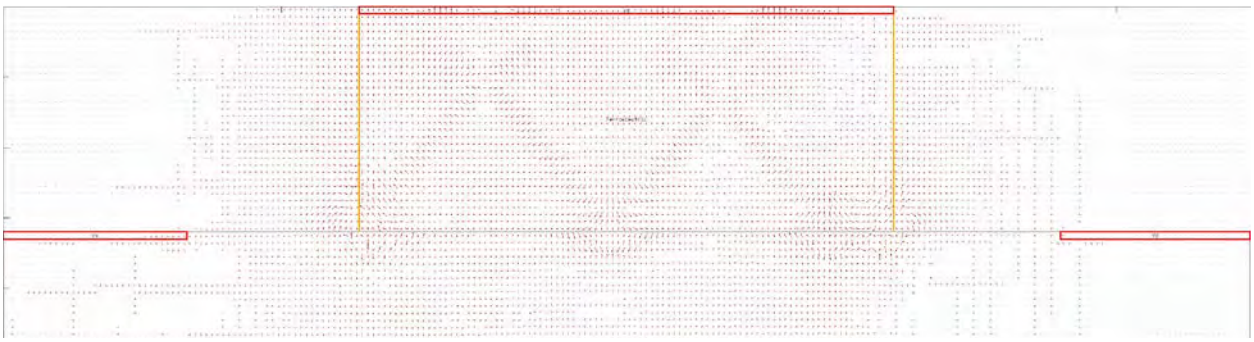

Fig 2. Corresponding electric field distribution, including stray fields

References:

[1] Y. Xiao, V. B. Shenoy and K. Bhattacharya, *Phys. Rev. Lett.*, **95**, 247603 (2005).
[2] P. Suryanarayana and K. Bhattacharya, *J. Appl. Phys.*, **111**(3), 034109.

ID: 223

A Quasi-Harmonic Lattice Dynamic Analysis of 180 Domain Walls in PbTiO3

Arzhang Angoshtari
Georgia Institute of Technology
USA

Arash Yavari
Georgia Institute of Technology
USA

Abstract:
We first briefly describe a quasi-harmonic lattice dynamics approach to approximate the Helmholtz free energy of defective crystals at finite temperatures. We then show how to obtain the structure of a defective crystal by minimizing its free energy and using its partial symmetries. We then obtain the finite-temperature structure of 180o ferroelectric domain walls in PbTiO3 from zero to room temperature. We observe that both Pb-centered and Ti-centered 180o domain walls are thicker at room temperature. Moreover, our calculations show that the Ti-centered domain walls have a lower free energy than Pb-centered domain walls and hence are more likely to be seen at finite temperatures.

ID: 253

On Metric Independent Aspects of Electromagnetism

Reuven Segev
Ben-Gurion University
Israel

Lior Falach
Ben-Gurion University
Israel

Abstract:
We consider here a theoretical formulation of objects and equations of electromagnetism on differentiable manifolds devoid of a Riemannian metric. A metric independent formulation of continuum physics is advantageous because it applies to classical mechanics as well as to the special and general theories of relativity. Another advantage of a metric independent formulation of continuum mechanics is that the various fields and equations may be defined over the body independently of the configuration in space. In other words, the description of the fields is automatically Lagrangian and does not depend on any particular reference configuration.

The framework we use is integration theory of differential forms on differentiable manifolds. The fundamental object is an n-dimensional manifold S that may be thought of as either a body or as the physical space or as spacetime.

A density of an extensive property, for example, the electric charge density, is represented mathematically as an n-form on S rather than a scalar field. It is recalled that an n-form on an n-dimensional manifold has only one component so no extra information is added. A flux field is represented as an $(n-1)$-form on S rather than a vector field. Again, it is recalled that an $(n-1)$-form has n components. As an $(n-1)$-form, the flux form may be restricted to the boundaries of n-dimensional regions in S and may be integrated over them. The restriction of an $(n-1)$-form on S to an $(n-1)$-dimensional submanifold of , provides the generalization of Cauchy's formula for scalar valued fluxes.

The divergence of the vector field representing a flux field is generalized to the exterior derivative dJ of the $(n-1)$-form J. This way, both the integral and differential equations of balance may be formulated. Noting that in a spacetime framework and using a Lorentzian frame, the flux of an extensive property contains the density of the property, the differential balance equation becomes $dJ = 0$. By the Poincarè lemma, for each point $\in S$, there is an $(n-2)$-form g in a neighborhood of x such that $J = dg$. Depending on the topology of S, the form g may be defined globally. In the context of electromagnetism in 4-dimensional spacetime, the flow potential g is the Maxwell 2-form and the condition $J = dg$ makes up the first two Maxwell equations.

In the metric independent formulation of mechanics, a force on a particle is modeled by its action on a virtual velocity vector to produce virtual power, linearly. As a virtual velocity vector is an element $w \in TS$, a force F on a particle is an element of the cotangent bundle T^*S. A second basic property of electromagnetism, is the existence of a 2-form f on spacetime, the Faraday 2-form. In terms of the Faraday form, the Lorentz force that the electromagnetic field exerts on a particle having charge Q and 4-velocity v is $F = -Qv \dashv f$. Here, $\dashv$ denotes the contraction operation so that $(v \dashv f)(u) = f(v,u)$. Thus, the virtual power that the Lorentz force produces for the virtual velocity w is given by $F(w) = -Qf(v,w) = Qf(w,v)$.

The basic property of the Faraday form is given by $df = 0$. This condition provides the second couple of Maxwell's equation. A potential for the Faraday form f is the 1-form α, i.e., the form such that $d\alpha = f$. The form α is a generalization of the vector potential of electromagnetism.

Force densities, such as body forces and surface forces of continuum mechanics, are fields that operate on virtual velocity fields to produce the corresponding densities of virtual power. Thus, the value $b(x)$ of a body force b at $x \in S$ is a linear mapping $T_xS \to \bigwedge^n T_x^* S$ and the value $t_R(y)$ of the surface force at a point y in the boundary ∂R of a region R is a linear mapping $T_yS \to \bigwedge^{n-1} T_y^* \partial R$.

Subjected to some natural conditions, one can prove the generalization of the Cauchy theorem asserting the existence of a *traction-stress* field σ over S whose value $\sigma(x)$ at a point $x \in S$ is a linear mapping $T_xS \to \bigwedge^{n-1} T_x^* S$. The generalization of Cauchy's formula for stresses may be written simply as

$$t_R(y)(w)(v_1,\ldots,v_{n-1}) = \sigma(y)(w)(v_1,\ldots,v_{n-1}).$$

In particular, the force density of the Lorentz force is given in terms of its action on a virtual velocity field w as $b(w) = (w \dashv f) \wedge J$, where a wedge denotes the exterior product of differential forms.

The Maxwell stress, regarded as a traction stress is given by

$$\sigma(w) = (w \dashv g) \wedge f - (w \dashv f) \wedge g.$$

It is noted that so far no constitutive assumptions have been made between f and g. It may be shown that in case the aether relations are used in a Lorentzian spacetime, one has

$$d\big(\sigma(w)\big) = (w \dashv f) \wedge J.$$

It follows that

$$\int_{\partial R} \sigma(w) = \int_R (w \dashv f) \wedge J,$$

as expected.

ID: 293

Thermodynamics of direct energy conversion using multiferroic materials

Yintao Song
Department of Aerospace Engineering and Mechanics, University of Minnesota
110 Union Street S. E., 107 Akerman Hall, Minneapolis, MN 55455, USA
Email: ytsong@umn.edu

Vijay Srivastava
Aerospace Engineering and Mechanics, University of Minnesota, Minneapolis, MN

Kanwal Bhatti
Chemical Engineering and Materials Science, University of Minnesota, Minneapolis, MN

Chris Leighton
Chemical Engineering and Materials Science, University of Minnesota, Minneapolis, MN

Richard D. James
Aerospace Engineering and Mechanics, University of Minnesota, Minneapolis, MN

Abstract:

The discovery of new technologies for the production of electricity without significant greenhouse gas emission is one of the most important environmental imperatives of the twenty-first century. A recently demonstrated method of converting heat to electricity based on first order phase transformations in multiferroic materials [1, 2] provides a possible route to this goal, potentially applicable to energy conversion using the waste heat from power plants, automobile exhaust systems, and computers, as well as natural sources such as solar-thermal conversion from the deserts and polar regions of the world. The general idea makes use of the fact that electromagnetic properties such as magnetization and polarization, and many other electromagnetic properties, are sensitive to a change of lattice parameters [3]. Structural phase transformations have an abrupt change of lattice parameters, and therefore can lead to abrupt changes of these properties. Using standard methods of electromagnetic conversion, such as induction and charge separation, the abrupt change of a suitable electromagnetic property can be converted into electricity. The energy for this purpose arises from a fraction of the latent heat absorbed. An attractive feature of this method is the elimination of the generator: the heat is converted directly to electricity. What fraction of the latent heat is converted to electricity, how best to design the device, and how to quantitatively compare this method with other methods of energy conversion rest on thermodynamic arguments? The purpose of this study is to present a thermodynamic model [4] for energy conversion using a first order phase transformation with an abruptly changing magnetization.

In thermodynamics, the phase transformation is governed by the free energy landscape in the Gibbs' sense. The Gibbs free energy can be explicitly evaluated for the alloy Ni44Co6Mn40Sn10, which has been the subject of a detailed characterization study by

calorimetry, wide angle x-ray diffraction, SQUID magnetometry and small angle neutron scattering [5]. (The alloy used in the demonstration [2] was the nearby alloy Ni45Co5Mn40Sn10.) We start with describing how the simple free energy used in the paper is related to more general thermodynamic/micromagnetic models that account for magnetic domains, twinning and martensitic phase transformation. This comparison sharply defines the domain of application and transferability of our model. Then we introduce our procedure for determining the free energy based on magnetic and calorimetric measurements: a simple spin-1 Brillouin function is found to work remarkably well. This section fully accounts for phase transformation. The comparison between the predictions of this free energy and further experimental observations (not used in the evaluation of the free energy) involves field and temperature induced phase transformation. The model can be used to study thermodynamic cycles that are possible according to the theory and which are interesting from the point of view of the direct energy. It suggests the conditions under which the new energy conversion can be optimized. Under such optimal conditions, the efficiency and power density compares favorably with the best thermoelectrics. We also postulate several related new methods for direct conversion of heat to electricity suggested by the underlying theory.

[1] V. Srivastava, X. Chen, and R. D. James, "Hysteresis and unusual magnetic properties in the singular Heusler alloy NiCoMnSn". *Appl. Phys. Lett.*, **97(1)**:014101, 2010

[2] V. Srivastava, Y. Song, K. Bhatti, and R. D. James. "The direct conversion of heat to electricity using multiferroic alloys". *Adv. Energy Mater.*, **1**:97, 2011.

[3] R. D. James and Z. Zhang. "A way to search for multiferroic materials with "unlikely" combinations of physical properties". In A. Planes, L. Manosa, and A. Saxena, editors, "*The Interplay of Magnetism and Structure in Functional Materials*", volume 79, page 159, New York, 2005. Springer.

[4] Y. Song, K. Bhatti, V. Srivastava, C. Leighton, and R. D. James. "Thermodynamics of energy conversion via first order phase transformation in low hysteresis magnetic materials". *In preparation*.

[5] K. P. Bhatti, S. El-Khatib, V. Srivastava, R. D. James, and C. Leighton. "Small-angle neutron scattering study of magnetic ordering and inhomogeneity across the martensitic phase transformation in $Ni_{50-x}Co_xMn_{40}Sn_{10}$ alloys". *Phys. Rev. B*, **85**:134450, 2012.

ID: 318

Cofactor Conditions For Twinned Martensite and Austenite Interface

Xian Chen
Aerospace Engineering and Mechanics, University of Minnesota
110 Union St. SE, Minneapolis, MN 55455, US

Richard D. James
Aerospace Engineering and Mechanics, University of Minnesota

Abstract:
For martensitic phase transformations, the middle eigenvalue of the transformation stretch matrix **U** has been directly linked to the high degree of reversibility and low hysteresis of a transforming material [1, 2]. Microscopically, it is associated with a perfect interface between austenite and a single variant of martensite. The interface normal is calculated by geometric nonlinear theory and was characterized in NiTiPd alloys [3]. For polycrystalline materials, laminated martensite stripes merging with austenite appear at grain boundaries, triple junctions and around crystal defects. Materials spend energy on formation of these microstructures and result in hysteresis during transformation.

To examine the compatibility condition for laminated martensite twins and uniform austenite interfaces, we propose the *Cofactor Conditions*, which restrict not only on the transformation stretch matrix itself but also the pair of twin variants. Even for those who satisfy middle eigenvalue of **U** equal to 1, the martensite variants form twinned laminated microstructures because it reduces the strain energy locally due to the defects. There are three types of martensitic twins. Due to their individual geometric characteristics, Cofactor Conditions have different forms.

For Type I twins, the twinning plane normal is parallel to one of the 2-fold symmetry axes of austenite. The Cofactor Conditions require that $|\mathbf{U}^{-1}\hat{\mathbf{e}}|=1$ and $\mathbf{v}_2 \cdot \hat{\mathbf{e}} \neq \mathbf{1}$ where $\hat{\mathbf{e}}$ denotes 2-fold symmetry axis, $\mathbf{v}_2$ is the eigenvector of **U** associated with the middle eigenvalue 1. By energy minimization, the twinned martensitic laminates are curved to fit the austenite lattice by a set of zig-zag interfaces without transition layer while varying twinning volume fractions between 0 and 1.

For Type II twins, the relative twin shear is parallel to the 2-fold symmetry axis but the twinning plane becomes an irrational plane in R^3. The Cofactor Conditions require that $|\mathbf{U}\hat{\mathbf{e}}|=1$ and $\mathbf{v}_2 \cdot \hat{\mathbf{e}} \neq \mathbf{1}$. The Type II twin laminates are always parallel to austenite/martensite interface so as to minimize the local elastic energy.

For Compound twins, both twinning plane and twin shear are both rational. The Cofactor Conditions require that the eigenvector of **U** is perpendicular to the 2-fold symmetry axis, which results in a stress-free microstructure in the plane with normal $\mathbf{v}_2$.

[1] J. Ball, R. D. James, Fine Phase Mixtures as Minimizers of Energy, *Arch. Rat. Mech. Anal.* 100 (1987): 13.

[2] V. Srivastava, X. Chen, R. D. James, Hysteresis and unusual magnetic properties in the singular Heusler alloy $Ni_{45}Co_5Mn_{40}Sn_{10}$, *Appl. Phy. Lett.,* 1 (2010): 014101.

[3] R. Delville, D. Schryvers, Z. Zhang, R. D. James, Transmission electron microscopy investigation of microstructures in low-hysteresis alloys with special lattice parameters, *Scripta Mater.*, 5 (2009): 293.

ID: 330

Thermo-Mechanical Coupling in Polycrystalline Shape Memory Alloys

Reza Mirzaeifar
Georgia Institute of Technology

Reginald DesRoches

Abstract:
The martensitic phase transformation in Shape Memory Alloys (SMAs) is associated with generation or absorption of latent heat. In this work, the coupled thermo-mechanical response of polycrystalline SMAs is studied using a micromechanical constitutive model. A three-dimensional Voronoi tessellation is used to model the grain geometries in a polycrystalline SMA. By assigning appropriate crystal orientations to the grains in the model, the effect of preferred crystallographic texture on the temperature changes in the material due to the phase transformation latent heat is studied. In addition to the uniaxial loading of a cube with periodic boundary conditions, the thermo-mechanical response of polycrystalline SMA micro beams subjected to bending is also investigated. In order to experimentally study the micro-macro linkage, an infrared thermovision camera is used to capture the temperature changes due to phase transformation latent heat in large SMA polycrystalline bars and beams subjected to uniaxial tension and bending.

ID: 359

Fracture Toughness of Superelastic Shape Memory Alloys

Theocharis Baxevanis
Department of Aerospace Engineering
Texas A&M University

Chad Landis
Department of Aerospace Engineering and Engineering Mechanics
The University of Texas at Austin,

Dimitris Lagoudas
Department of Aerospace Engineering
Texas A&M University

Abstract:
Shape Memory Alloys (SMAs) are desirable in a wide range of applications due to a reversible diffussionless solid to solid transformation – from austenite to martensite and vice-versa – that results in large reversible strains. As SMAs are increasingly used in the aeronautics and the medical industries, it is essential to understand their fracture properties for estimating maximum tolerable loads in the presence of cracks and improving their overall functional and structural performance. To this end, the fracture toughness enhancement due to phase transformation near a crack growing both stably and steadily is analyzed for mode I loading under plane-strain conditions using the finite element method. A substantial fracture toughening is observed associated with closure stresses placed on the crack tip by the transformed material left behind in the wake of the advancing crack tip.

The analysis assumes isothermal loading at constant temperature above the martensitic-start temperature and below the austenitic-start temperature for an initially austenitic material. The constitutive law used adopts the classical rate-independent small-strain flow theory for the evolution equations of the transformation strains. The small-scale transformation condition is modeled by a boundary layer approach, wherein the actual boundary conditions have been replaced by the requirement of an asymptotic approach to the mode I asymptotic elastic K-field at large distances from the crack tip.

The stable crack growth is assumed to start and progress quasi-statically with the crack tip energy release rate maintained at a critical value; this is accomplished by means of the Virtual Crack Closure Technique. Under steady-state conditions, it is imagined that the crack has grown at constant level of applied energy release rate, denoted as G_{ss}, while crack growth proceeds at a critical level, G_{tip}, of the crack-tip energy release rate.

According to the numerical results for both stable and steady crack growth, the crack tip is surrounded by a fully transformed, elastically deformed zone, which is itself surrounded by a partially transformed zone, before the untransformed material is reached. The results suggest that very close to the crack tip, inside the region of elastically deformed martensite, the stresses have

ID: 396

Modeling the Behaviour of Crystallizable Shape Memory Polymers with Triple Shape Effect

Swapnil Moon

Jaskirat Sodhi

Abstract:
Shape Memory Polymers are actively moving materials with the capability to remember their original shape even after undergoing significant deformation, when triggered by an external stimulus. Triple-shape polymers are a promising class of SMP with an ability to switch between three different shapes when triggered by heat. Where the temporary shape is fixed by formation of two different crystalline phases and return to the original shape is due to melting of these phases. Our research is focused upon modeling the mechanics associated with these triple-shape SMPs. The model is developed using a framework based upon theory of multiple natural configurations. In order to model the mechanics, different aspects of this material need to be characterized. This includes developing a model for the amorphous phase and the subsequent semi-crystalline phases, with different stress free states and melting of these phases. The model is then used to simulate results for typical boundary vale problems.

ID: 407

Thermomechanics of Phase Transformation Kinetics in Molecular Dynamics

CHAN-TSAN LU
Carnegie Mellon University
United State

KAUSHIK DAYAL
Carnegie Mellon University
United States

Abstract:
A phase-transforming material is modeled in continuum mechanics by a multi-well elastic energy density. Such an energy typically leads to problems with microstructural interfaces. In dynamics, the evolution of these solutions with interfaces is not unique. Uniqueness can be restored by additionally imposing kinetic relations that relate the velocity of interfaces to the thermodynamic conjugate driving force.

Recent attention has focused on obtaining kinetic relations from molecular dynamics simulations. Previous works, e.g. [1], concerning phase transformation interfaces in atomic chains assume that the phase boundary moves as a traveling wave to compute the kinetic relation. However, this procedure provides a one-parameter family of kinetic relations. In other words, the driving force and interface structure for a given phase boundary velocity is not unique. The so-called "radiation condition" is then used to select a unique kinetic relation. In this work, we re-examine these results in the framework of continuum thermomechanics, unlike the previous works that have interpreted the results in continuum mechanics. Our key finding is that inclusion of thermal effects resolves the issue of non-uniqueness of the kinetic relation in that we find that the kinetic relation is now dependent on the heat flux as well as mechanical quantities such as stress.

We simulate Riemann-type problems in the one-dimensional chain of atoms and observe the evolution of energy content at different wavelengths ahead and behind the microstructural interface. Our key findings include (A) the change in energy content ahead and behind the phase boundary occurs at a distinguished wavelength that is directly related to the velocity of the interface; and (B) the interface kinetics and increase in thermal energy at the distinguished wavelength is almost insensitive to the energy content at other wavelengths.

The thermomechanical implications of these findings is as follows. The finding (A) implies that the thermomechanical dissipation can be written as a product of the interface velocity and a quantity that we identify as the conjugate driving force, thereby fitting the atomic calculations into the framework of adiabatic interface motion. The finding (B) implies the unusual conclusion that the kinetics is not a function of temperature, but instead is a function of the heat flux across the interface. Together, these findings provide a closure for the full continuum thermodynamic

set of equations that include both momentum balance (elastodynamics) as well as energy balance (heat transfer).

[1] H. Schwetlick and J. Zimmer, Kinetic Relations for a Lattice Model of Phase Transitions, Arch. Rat. Mech. Anal., Submitted, Under Revision

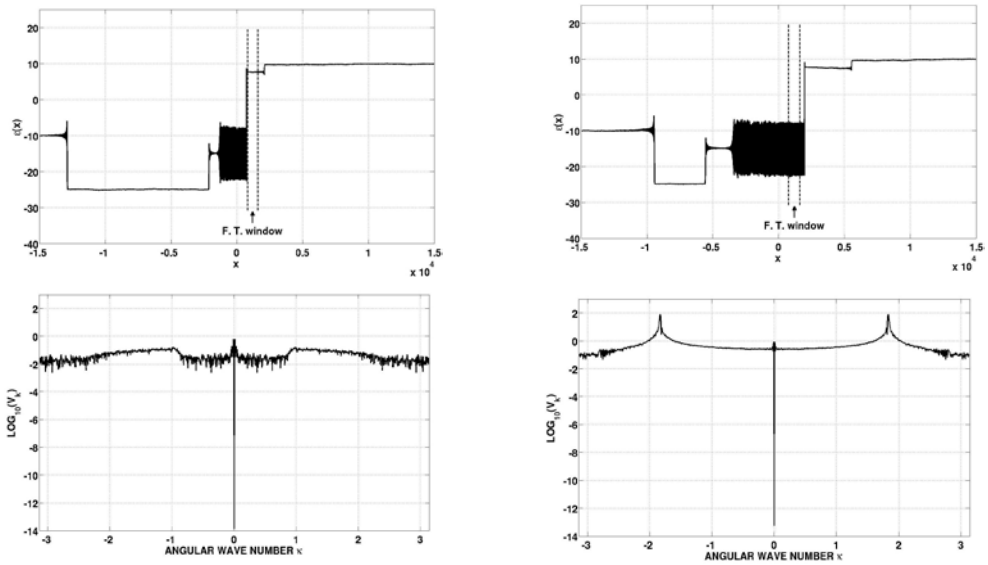

Fig 1. Fourier transform at a fixed point in space as the phase interface sweeps through it.

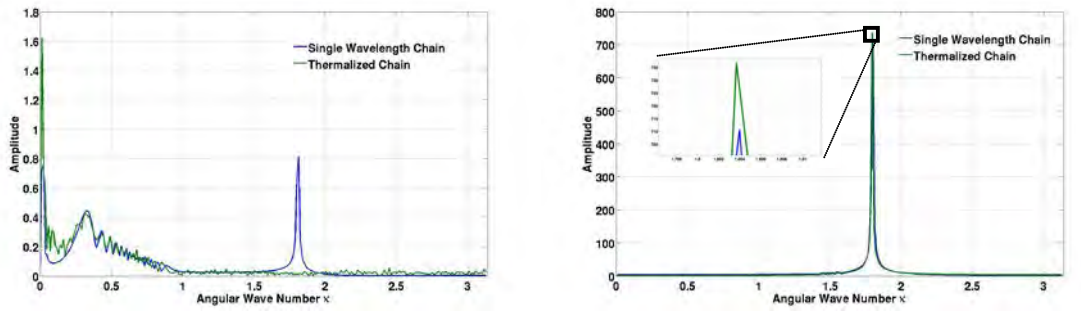

Fig 2. (Note the extremely different scales). Left: energy content before the interface moves through in 2 atomic chains, one with energy in the distinguished wavelength and the other completely thermalized; right: energy content after the interface moves through, showing that the energy transfer to the distinguished wavelength is independent of temperature.

ID: 430

Parallel Edge Cracks due to a Phase Transformation

Bharat Penmecha
California Institute of Technology
USA

Kaushik Bhattacharya
California Institute of Technology
United States

Abstract:
Solid to solid phase transformations are accompanied by a change of crystal structure. This results in a change of shape or volume or both as one phase nucleates within the other and grows into it. If this change of shape is kinematically incompatible, and if the interface is (at least partially) coherent, leads to internal stress. When the material is brittle this stress field could be high enough to nucleate or grow pre-existing cracks. Examples range from martensitic phase transformation as in Tin and Zirconia to diffusional phase transformations as in Nickel superalloys to (Lithium) iron phosphate. The resulting cracks could grow as the phase boundary propagates in the sample in a directional nature giving rise to specific patterns. Examples of this include the well-known phenomenon of tin pest and some recent observations in oxy-acids of interest as solid oxide fuel cells. These observations serve as our motivation.

In the current work we investigate the growth of a set of parallel edge cracks due to a martensitic phase transformation. The variation of the stress field set up during a martensitic phase transformation is rather sharp unlike that in a diffusion driven situation. As observed in the phenomena of thermal cracking, the crack pattern in the case of a smooth stress field is susceptible to period doubling instabilities [1, 2]. But in the situation where the stress variation is sharp, experimental evidence points to a set of parallel equi-sized cracks which grow as the front progresses [3]. With this as the motivation we examine the growth of cracks in the case of a solid-solid phase transition and arrive at the conclusion that the preferred configuration for the cracks is uniform growth without any instability.

In this work we analyze a set of parallel equi-spaced edge cracks in a half-plane growing in the wake of a phase boundary as it moves quasi-statically from the edge to the interior; see Figure 1. We assume that the elastic moduli are identical on either side of the phase boundary. The stress field is evaluated using superposition, see Figure 1. We use a thin film approximation and distributed dislocation technique to evaluate the stress field and the stress intensity factors. We perform this analysis for two cracks in a unit cell. We also examine the effect of the cracks on the interface. By calculating the driving force on an arbitrary interface and setting it to zero, we determine the equilibrium shape of the interface.

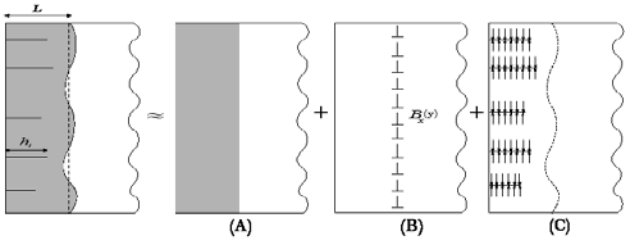

Figure 9: Set-up of the problem and solution by superposition

Next, using the equilibrium condition for crack growth, $K = K_c$, we determine the equilibrium length of a set of equi-spaced cracks of equal length, see Figure 2. The equilibrium length of the crack crosses over the interface. The stability condition for the homogenous growth of equal sized cracks, $\frac{\partial K}{\partial a} < 0$, holds in this case and so the cracks can continue to grow uniformly. The stability of this equilibrium configuration against period doubling (every other crack stops and the rest continue to grow) is also examined. In this case the stability condition is $\frac{\partial K_1}{\partial a_2} < 0$. Figure 3 shows that this condition is satisfied. From this we conclude that cracks initiate, grow all the way to the interface at equal spacing, and continue to grow as the interface progresses without any instability.

The conclusion from theory is verified by performing a large number of simulations with different number of initial notches in a unit cell. It is seen that at various transformation strains different number of notches develop into cracks there by resulting in different spacing. Figure 4 shows an example where out of a set of eight notches every other notch developed into a crack and these cracks continued to grow without any instability at a uniform spacing.

In conclusion we have a theory for crack growth during a solid-solid phase transition with a sharp front based on linear stability analysis. This theory is substantiated through a series of simulations.

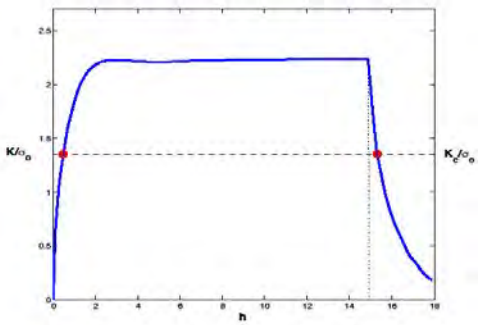

Figure 2: Variation of SIF of a set of equi-spaced equal size cracks with length. Equilibrium length is indicated by the red dots.

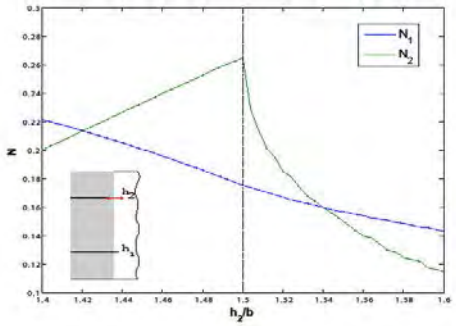

Figure 3: Variation of SIFs of the two cracks with length of one crack fixed and the other varies. The negative slope indicates stability against period doubling.

Figure 4: Simulation with 8 notches. Only 4 develop into cracks at the applied strain. These 4 cracks grow uniformly without any instability.

[1]. S. Nemat-Nasser, L.M. Keer, and K.S. Parihar. Unstable growth of thermally induced interacting cracks in brittle solids. *International Journal of Solids and Structures*, 14(6):409 - 430, 1978.

[2]. Z.P. Bazant, H. Ohtsubo, and K. Aoh. Stability and post-critical growth of a system of cooling or shrinkage cracks. *International Journal of Fracture*, 15(5):443-456, 1979.

[3]. L. Pauchard, M. Adda-Bedia, C. Allain, and Y. Couder. Morphologies resulting from the directional propagation of fractures. Phys. Rev. E, 67:027103, Feb 2003.

ID: 471

Effect of Temperature and Material Direction on the Deformation-Induced Martensite Formation in Austenitic Stainless Steel Sheets

Allison Beese
Northwestern University
USA

Dirk Mohr

Abstract:
The deformation-induced phase transformation in temper rolled austenitic stainless steel 301LN sheets is analyzed computationally and experimentally. Metastable austenitic steels provide both high strength and ductility due to their ability to undergo deformation-induced phase transformation. The face-centered cubic (FCC) austenite to body-centered cubic (BCC) martensite phase transformation has a first order effect on the macroscopic strain hardening behavior. Isothermal experiments at different stress states have shown that transformation kinetics depends on the stress triaxiality and the Lode angle, in addition to material direction and temperature, which led to the development of a new anisotropic temperature and stress state dependent transformation kinetics law. Here, this law is coupled with a new phenomenological anisotropic plasticity model that describes the strain hardening behavior as a function of plastic strain and martensite volume fraction. Furthermore, experimental results are presented to validate the computational model.

ID: 486

Modeling of Field-Induced Phase Transformation in Magnetic Shape Memory Alloys

Krishnendu Haldar, Dimitris C. Lagoudas

Department of Aerospace Engineering,
Texas A&M University, College Station, TX 77843, USA.

Abstract

Magnetic Shape Memory Alloys (MSMAs) exhibits reorientation (Ni_2MnGa) and field induced phase transformation (NiMnCoIn). A major drawback for the variant reorientation is the comparatively low blocking stress, while a high available magnetic energy in the field induced phase transformation can lead to large strain and high actuation stresses. In this work, a continuum based modeling of field induced phase transformation is developed.

1. Modeling and results

The *Zeeman Energy* (ZE), which depends on the difference between the saturation magnetizations of the austenitic and martensitic phases, is converted to mechanical energy through magnetic field induced phase transformation. In the NiMnCoIn material system, the Zeeman energy can be substantial as the austenitic phase is ferromagnetic while the martensitic phase is antiferromagnetic. For the NiMnCoIn system, Kainuma et al. (2006) found that a 4 Tesla magnetic field can recover 3% pre applied strain in martensite at room temperature.

We aim to propose a phenomenological modeling for Field Induced Phase Transformation (FIPT), where a magnetic field $\mathbf{H}_a$ is applied coaxially with the mechanical load. Initially, the specimen is in antiferromagnetic martensitic phase. After a critical applied magnetic field is reached, ferromagnetic austenitic phase nucleates and phase transformation completes with further increase in magnetic field. We denote the Gibbs free energy of the austenitic phase and the martensitic phase by G^A and G^M respectively. The Gibbs free energy of the of the system can be written as

$$\begin{aligned} G(\boldsymbol{\sigma}^E, \mathbf{H}, T, \boldsymbol{\varepsilon}^t, \mathbf{M}^t, \xi, g) &= G^A(\boldsymbol{\sigma}^E, \mathbf{H}, T) + \xi[G^M(\boldsymbol{\sigma}^E, \mathbf{H}, T) - G^A(\boldsymbol{\sigma}^E, \mathbf{H}, T)] \\ &+ G^I(\boldsymbol{\sigma}^E, \mathbf{H}, \boldsymbol{\varepsilon}^t, \mathbf{M}^t) + G^{mix}(g). \end{aligned}$$

G^I and G^{mix} are the Gibbs free energy due to the magneto-inelastic deformation and the energy due to the mixing of the two phases during transformation. The set of internal state variables are as follows: $\boldsymbol{\varepsilon}^t$ is the *transformation strain* tensor, $\mathbf{M}^t$ is the *transformation magnetization* vector, ξ is the *martensitic volume fraction* and g is the *mixing energy* of the two phases during transformation. $\mathbf{M}^t$ takes into account the phenomenological effect of different micro-magnetical mechanisms e.g. rotation of magnetization vector and evolution of magnetic domain walls. More detailed modeling description can be obtained in Haldar et al. (2012).

1.1. Model predictions

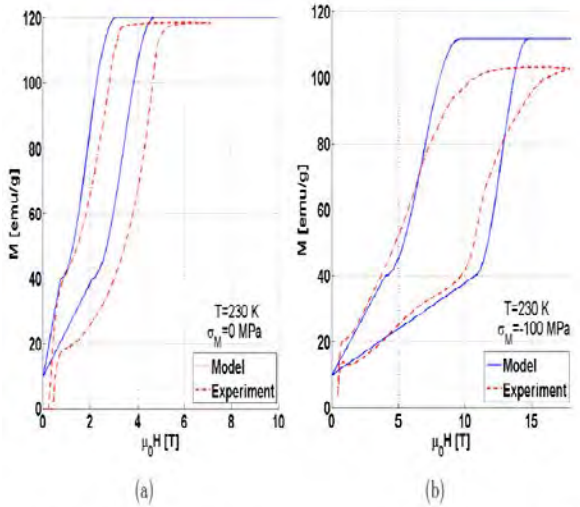

Figure 1: Model predictions of magnetization responses (a) at 230 K and σ_M=-57 MPa and (b) at 230K and σ_M=-100 MPa.

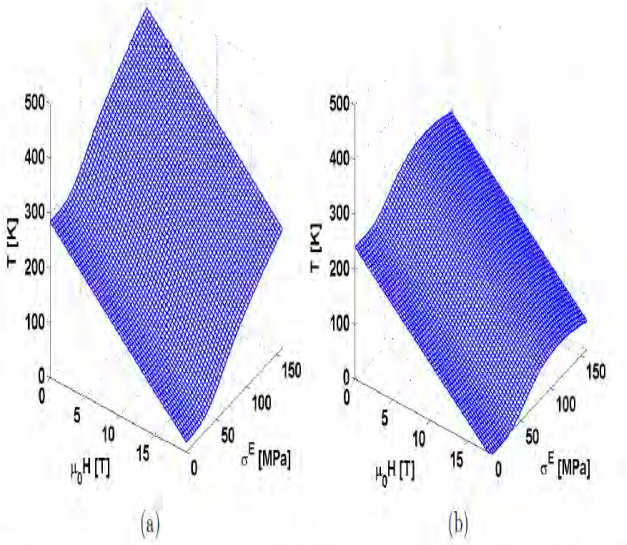

Figure 2: 3D phase diagram: (a) austenitic finish surface and (b) martensitic finish surface.

References

Kainuma, R., Imano, Y., Ito, W., Sutou, Y., Morito, H., Okamoto, S., Kitakami, O., Oikawa, K., Fujita1, A., Kanomata, T., Ishida, K., 2006. Magnetic-field-induced shape recovery by reverse phase transformation. Nature 439, 957–960.

Haldar, K., Lagoudas, D. C., Karaman, I.,2012. Magnetic Field-Induced Martensitic Phase Transformation in Magnetic Shape Memory Alloys: Modeling and Experiments. Submitted: Journal of Mechanics and Physics of Solids.

ID: 494

A Finite Element Based Phase Field Model for Martensitic Phase Transformation in Shape Memory Alloys

Harshad Paranjape
The Ohio State University
United States

Sivom Manchiraju
The Ohio State University
United States

Peter M. Anderson
The Ohio State University
United States

Abstract:

Experimental studies of martensitic transformation in Shape Memory Alloys (SMAs) have repeatedly shown complex interactions between individual variants of martensite and between the variants and the matrix. This interaction can result in many interesting experimental observations such as that of dislocation plasticity in the matrix during transformation [1]. However, most continuum level finite element method based models ignore this interaction at the individual variant level and can at best capture the interaction at the grain level. An attractive alternative is to use phase-field method to model individual variants of martensite explicitly. But present phase field model implementations are based on small deformation approximations and cannot handle arbitrary boundary and loading conditions.

A new microstructural model is developed to capture interactions at the martensite variant scale by solving the traditional phase field equations for martensitic phase transformation using finite element method. Specifically, the approach models the phase transformation between austenite and several possible martensite variants and also the reorientation between different variants. Martensite volume fraction ν_t of variant *t* is taken as the order parameter. The evolution of the order parameter follows the Ginzburg-Landau kinetic equation.

$$\dot{\nu}_t = L_{tu} f_t^{\text{drive}} + \zeta(x,t)$$

Here L_{tu} is the mobility matrix, f_t^{drive} is the driving force for phase transformation or variant reorientation and $\zeta(x,t)$ is the Langevin noise term. The driving force consists of contributions from a gradient based interface energy term, work of external stress and Landau polynomial based chemical free energy term.

$$f_t^{\text{drive}} = k_{tu}\nabla^2\nu_u + F^{eT}F^eT^*S_t - \frac{\partial\Psi_R}{\partial\nu_t}$$

Here k_{tu} is the interfacial energy coefficient, F^e is the elastic deformation gradient, T^* is the second Piola-Kirchhoff stress, S_t is the Bain transformation strain matrix for t^{th} martensite variant. Ψ_R is the chemical (Helmholtz) free energy density defined in terms of a Landau polynomial commonly used in the phase field literature [2].

$$\Psi_R = \frac{1}{2} E^e \cdot C E^e + \Delta f(\theta) \left[\frac{a}{2} \left(\sum_{t=1}^{N_{\text{variants}}} v_t^2 \right) - \frac{b}{4} \left(\sum_{t=1}^{N_{\text{variants}}} v_t^4 \right) + \frac{c}{2} \left(\sum_{t=1}^{N_{\text{variants}}} v_t^2 \right)^3 \right]$$

Here E^e is the elastic strain, C is the stiffness and a, b, c are three parameters defining the Landau polynomial. Temperature dependent barrier for phase transformation ($\Delta f(\theta)$) is defined in terms of the latent heat of transformation (λ_T) and the transformation temperature (θ_T).

$$\Delta f(\theta) = \frac{\lambda_T}{\theta_T} (\theta - \theta_T)$$

The transformation temperature is approximated as the mean of austenite-start and martensite-start temperatures.

The mechanical and thermal equilibrium equations are solved using finite element method with displacement and temperature being the primary solution variables. The phase transformation equations detailed above dictate the material state and hence the stress field at a material point and are implemented as user material subroutine in commercial finite element software (ABAQUS). This finite element based phase field model is advantageous over spectral methods based phase-field models since it can capture large rotations and deformations and has the ability to handle any arbitrary boundary condition. Some preliminary results of the model showcasing its ability to capture the variant-variant and variant-matrix interaction are presented.

[1] Norfleet DM, Sarosi PM, Manchiraju S, Wagner MFX, Uchic MD, Anderson PM, Mills MJ. Transformation-induced plasticity during pseudoelastic deformation in Ni-Ti microcrystals. Acta Materialia 2009;57:3549.

[2] Artemev A, Jin Y, Khachaturyan AG. Three-dimensional phase field model of proper martensitic transformation. Acta Materialia 2001;49:1165.

ID: 535

Mechanical Properties of Thermoelectric Materials Via Molecular Dynamics and Coarse-Grained Simulations

Yongtao Li

Abstract:
Thermoelectric (TE) materials (PbTe and Bi2Te3) are well known for their thermoelectric properties, while their mechanical properties are usually overlooked. For application as well as production of TE materials, the mechanical properties of TE materials are very crucial in determining the performance of TE materials. In this work, atomistic simulations were first employed to examine the plastic deformation of PbTe during nanoindentation tests. The simulation results, for the first time, revealed the plastic deformation mechanism for PbTe under nanoindentation. The estimation of hardness and modulus are in reasonably good agreement with the experimental data. The effect of system size, loading rate and indenter size on hardness were discussed. Based on the molecular dynamics (MD) simulation results, a new element of tetragonal shape was used to investigate the plastic deformation of PbTe via the coarse-grained (CG) simulations. The CG simulations have reproduced the dislocation nucleation and migration. The threshold stress value for dislocation nucleation under compression tests from the CG simulations was in good agreement with the corresponding MD simulations. At last MD simulations have been performed to study edge dislocations in bulk Bi2Te3. The dislocation core structure, migration mechanism and mobility are identified. The critical resolved shear stress (CRSS) for dislocation glide at 0 K was evaluated and compared to the experimental data. The comprehensive understanding of mechanical properties of TE materials will further enable us to study the effect of mechanical issues, i.e. plastic deformation and dislocations, on their thermoelectric properties.

ID: 614

Flexoelectricity

Pradeep Sharma

Abstract:
In this presentation, I will present an overview of the phenomenon of flexoelectricity. I will briefly discuss its atomistic origins, a simple phenomenological theoretical framework and highlight the size-effects in electromechanical coupling that emerge at the nanoscale. I will argue, through computational examples, the possibility of coaxing graphene to be piezoelectric i.e. creating apparently piezoelectric; materials without piezoelectric materials, emergence of piezoelectricity at the nanoscale, and the possibility of high temperature energy harvesting. Finally, I will present evidence indicating the crucial role of flexoelectricity in a major bottleneck underpinning the use of ferroelectric based nanocapacitors used for energy storage.

ID: 636

A Hybrid Crystal Plasticity and Phase Transformation Model for High Carbon Steel

R. W. Neu
Georgia Institute of Technology
United States

E. S. Alley
Naval Surface Warfare Center
United States

Abstract:
Presence of retained austenite in high-carbon, martensitic steels, shown in Fig. 1, can have a significant effect on the stress-strain response. A hybrid constitutive model is presented that accounts for both the plastic deformation of martensite and stress-assisted transformation of austenite to martensite.

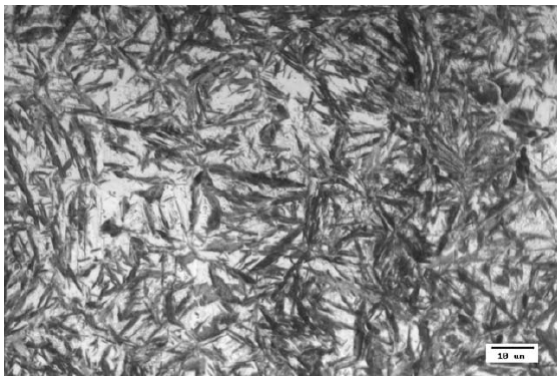

Fig. 1. High carbon steel microstructure contain 35% retained austensite (light phase) and martensite.

The two-phase hybrid model is built around a triple multiplicative decomposition of the deformation gradient $\underset{\sim}{\mathbf{F}}$,

$$\underset{\sim}{\mathbf{F}} = \underset{\sim}{\mathbf{F}}^{\mathbf{e}} \cdot \underset{\sim}{\mathbf{F}}^{\mathbf{p}} \cdot \underset{\sim}{\mathbf{F}}^{\mathbf{tr}} \tag{6}$$

where $\underset{\sim}{\mathbf{F}}^{\mathbf{tr}}$ accounts for the volumetric strain produced by the austenite-to-martensite phasetransformation, $\underset{\sim}{\mathbf{F}}^{\mathbf{p}}$ accounts for polycrystalline plasticity in the martensite, and $\underset{\sim}{\mathbf{F}}^{\mathbf{e}}$ accounts for the elastic deformation and rigid body rotations. Plastic deformation and transformation occur along slip and transformation systems, respectively, associated with the lattice structures of the martensite and austenite. The evolution of crystal plasticity follows the work of Asaro [1]. The model uses the 48 BCC slip systems to approximate the behavior of BCT tempered martensite. The stress-assisted transformation formulation is based on the work of Suiker and Turteltaub [2] that includes an internal state variable to track the volume fraction of retained austenite.

The model is implemented as a user material (UMAT) subroutine for ABAQUS [3]. Because the distribution of retained austenite and martensite is generally finer than the element size of interest in structural analyses, the microstructural representation of each element is a homogenization of the initial percentages of austenite and martensite. The parameters of the model are calibrated to the experimental stress-strain and volumetric transformation strain data with different initial retained austensite percentages. The model correctly captures the tension-compression asymmetry in the stress-strain response observed experimentally, shown in Fig. 2, as well as the experimentally measured amounts of transformed volume fraction. An example application of this model is the design of a bearing steel microstructure for rolling contact fatigue performance [4,5]. In these exercises, increasing the amount of initial retained austenite results in higher accumulations of ratcheting plastic strain, suggesting reduced fatigue resistance, as well as large compressive residual stresses, blunting the effect of inhomogeneities such as inclusions.

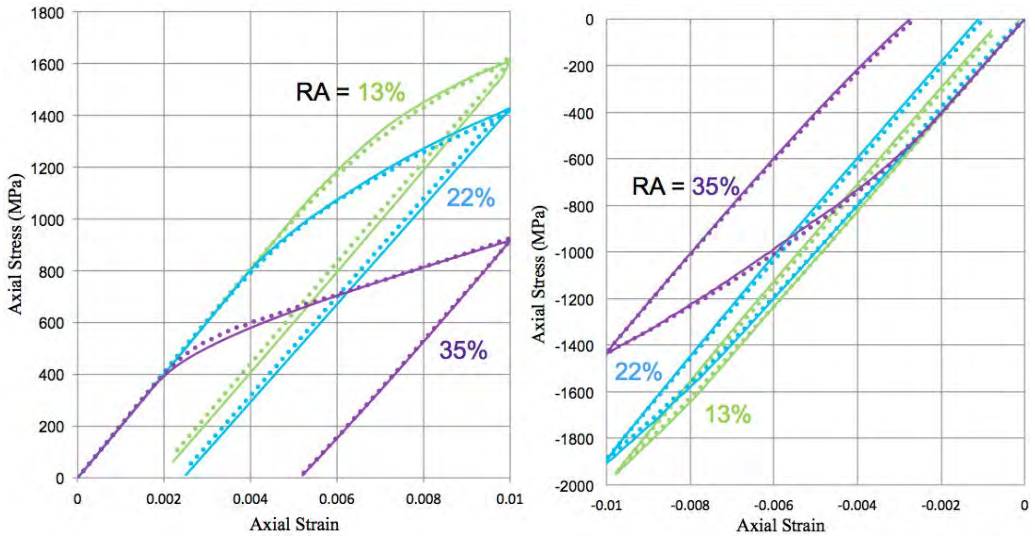

(a) (b)

Fig. 2. Comparison of model response (solid) and experiments (dashed) for varying amounts of initial retained austenite (RA) in (a) tension and (b) compression.

References

[1] **Asaro RJ (1983) Micromechanics of crystals and polycrystals. *Advances in Applied Mechanics* Vol. 23, San Diego: Academic Press.**

[2] Suiker A, Turteltaub S (2005) Computational modelling of plasticity induced by martensitic phase transformations. *Int. Journal for Numerical Methods in Engineering* 63:1655–1693.

[3] Alley ES, Neu RW (2012) A hybrid crystal plasticity and phase transformation model for high carbon steel. *Computational Mechanics* (in press).

[4] Alley ES, Sawamiphakdi K, Anderson PI, Neu RW (2010) Modeling the influence of microstructure in rolling contact fatigue. *Journal of ASTM International* 7(2).

[5] Alley ES, Neu RW (2010) Microstructure-sensitive modeling of rolling contact fatigue. *International Journal of Fatigue* 32(5):841-850.

Track IV

Multiscale Mechanics of Materials

IV.1

Multiscale Mechanics of Materials - Modeling of Microstructure Evolution

ID: 102

Isotropic Rate--Dependent Finite Plasticity Using the Theory of Material Evolution

Ben Nadler
University of Victoria

Abstract:
The theory of material evolution is a general framework to model materials that show time dependency, where plastic deformation is one example. In the case of plastic deformation the stress- strain relations are not fixed in time, as for elastic material, but rather time dependent for an external observer measuring the deformation from some fixed reference configuration. The theory of material evolution naturally emerges from the theory of material inhomogeneities, which addresses the question whether two material points are made of the same material. For a body made of the same material one can define material uniformity, homogeneity and inhomogeneity. Material evolution can be viewed in a similar way where the constitutive response of a particular material point is compared at different times. If the constitutive response is different at different times, we say that the material evolves. The underling assumption in the theory of material evolution is that the material stays the same with respect to some intrinsic configuration rather than with respect to the fixed reference configuration.In this work the theory of material evolution is utilized to model isotropic plastic-like evolution, where it is shown that the Mandel stress tensor plays important role since it emerges as the thermodynamically dual configurational force to the evolution. A simple evolution models that satisfies the assumptions used in the classical theory of plastic deformation, such as volume preserving and the existence of yield criterion, are introduced. This plastic-like evolution law is rate-dependent and thus dissipative, while for low deformation rates the response is rate-independent. Examples are provided to demonstrate the inelastic evolution (plastic) response that emanate from this theory.

ID: 126

Joule Heating in Graphene Nanoribbon

Yanbiao Chu
Electronic Packaging Laboratory, University at Buffalo
University at Buffalo

Cemal Basaran
Electronic Packaging Laboratory, University at Buffalo
University at Buffalo

Abstract:
Since was firstly isolated in 2004[1], graphene has been proposed for promising application in electronics [2-6], as its unique electrical [7], thermal [8], and mechanical properties [9]. Especially, graphene nano-ribbon (GNR), tailored from the 2D graphene lattice with finite size, has been found to possess interesting electronic structures with dependence on its width and edge shapes[10, 11]. This opens an opportunity to construct circuit all of graphene[12].

Understanding energy dissipation and transport in nanoscale structures is important to design energy-efficient circuits and energy-conversion systems. As for GNRs, experiments demonstrate Joule heating as main failure mechanism [13-16]. The dissipated power can raise the operating temperature to a point where thermal management becomes critical. Although preliminary models present [17, 18], detailed picture can only be got through microscopic analysis. According to quantum mechanics, Joule heating is due to the transfer of kinetic energy from electron to lattice. In this work, the interaction between electron and longitudinal phonons is studied by Ensemble Monte Carlo (EMC) simulations.

References

1. Novoselov, K.S., et al., *Electric Field Effect in Atomically Thin Carbon Films.* Science, 2004. **306**(5696): p. 666-669.
2. Geim, A.K. and K.S. Novoselov, *The rise of graphene.* Nat Mater, 2007. **6**(3): p. 183-191.
3. Han, M.Y., et al., *Energy Band-Gap Engineering of Graphene Nanoribbons.* Physical Review Letters, 2007. **98**(20): p. 206805.
4. Li, X., et al., *Chemically Derived, Ultrasmooth Graphene Nanoribbon Semiconductors.* Science, 2008. **319**(5867): p. 1229-1232.
5. Geim, A.K., *Graphene: Status and Prospects.* Science, 2009. **324**(5934): p. 1530-1534.
6. Schwierz, F., *Graphene transistors.* Nat Nano, 2010. **5**(7): p. 487-496.
7. Meric, I., et al., *Current saturation in zero-bandgap, top-gated graphene field-effect transistors.* Nat Nano, 2008. **3**(11): p. 654-659.
8. Balandin, A.A., et al., *Superior Thermal Conductivity of Single-Layer Graphene.* Nano Letters, 2008. **8**(3): p. 902-907.
9. Lee, C., et al., *Measurement of the Elastic Properties and Intrinsic Strength of Monolayer Graphene.* Science, 2008. **321**(5887): p. 385-388.
10. Nakada, K., et al., *Edge state in graphene ribbons: Nanometer size effect and edge shape dependence.* Physical Review B, 1996. **54**(24): p. 17954-17961.

11. Son, Y.-W., M.L. Cohen, and S.G. Louie, *Half-metallic graphene nanoribbons.* Nature, 2006. **444**(7117): p. 347-349.
12. Lin, Y.-M., et al., *Wafer-Scale Graphene Integrated Circuit.* Science, 2011. **332**(6035): p. 1294-1297.
13. Liao, A., et al., *Thermal dissipation and variability in electrical breakdown of carbon nanotube devices.* Physical Review B, 2010. **82**(20): p. 205406.
14. Liao, A.D., et al., *Thermally Limited Current Carrying Ability of Graphene Nanoribbons.* Physical Review Letters, 2011. **106**(25): p. 256801.
15. Murali, R., et al., *Breakdown current density of graphene nanoribbons.* Applied Physics Letters, 2009. **94**(24): p. 243114-3.
16. Wang, P.C. and R.G. Filippi, *Electromigration threshold in copper interconnects.* Applied Physics Letters, 2001. **78**(23): p. 3598-3600.
17. Bae, M.-H., et al., *Scaling of High-Field Transport and Localized Heating in Graphene Transistors.* ACS Nano, 2011. **5**(10): p. 7936-7944.
18. Fertig, H.A. and L. Brey, *Nanophysics in graphene: neutrino physics in quantum rings and superlattices.* Philosophical Transactions of the Royal Society A: Mathematical, Physical and Engineering Sciences, 2010. **368**(1932): p. 5483-5497.

ID: 163

Gradient Material Mechanics Across the Scale Spectrum

Elias Aifantis
Aristotle University of Thessaloniki
USA

Abstract:
Gradient material mechanics as developed by the author and his co-workers in the last two decades for elasticity, plasticity and dislocation dynamics is extended to problems of diffusion and heat flow, as well as to electroplasticity and photoplasticity. The role of non-convexity, heterogeneity and stochasticity in the evolution of microstructure and their relation to propagating material instabilities and size effects is discussed.

Missing Abstract

ID: 187

ID: 255

Microstructure Evolution and its Effect on the Macroscopic Response and Stability of Porous Metals

Pedro Ponte Castaneda

Michalis Agoras

Abstract:
Homogenization estimates will be given for the effective response and the evolution of the underlying microstructure in viscoplastic porous media. In particular, improved bounds of the Ponte Castañeda-Willis type will be given for the class of porous materials consisting of ellipsoidal voids distributed randomly with ``ellipsoidal’’ two-point statistics in a viscoplastic matrix. For this purpose, a novel strategy has been used based on the theory of iterated homogenization. The basic idea is to make use of available bounds for porous materials in the limit when the porosity is large in an incremental fashion to generate corresponding results for general values of the porosity. The new bounds obtained by the above-mentioned ``iterated'' procedure can be shown to be much improved relative to earlier bounds, especially at low values of the porosity and high triaxialities. In addition, comparisons will be made with the Gurson-type and other homogenization estimates for ideally plastic porous material, demonstrating the accuracy of the new estimates. Finally, the new estimates will be used to model the evolution of the average size, shape and orientation of the voids, as well as its effect on the macroscopic response, including on the possible development of shear-localization instabilities.

ID: 279

Role of Dislocation Transmission Across Interfaces on Microstructural Evolution

Irene Beyerlein

Abstract:
Here we study the microstructural evolution in bulk nano-layered bi-metallic composites under mechanical deformation. As a result of their ultra-high density of bi-metal interfaces, they exhibit extraordinary strength, hardness, and thermal stability, far exceeding those of the individual constituents by orders of magnitude. Such superior damage tolerance is a consequence of how well these bi-metal interfaces can [illegible] dislocations, that is, nucleate, store, transmit, or annihilate them. This presentation will focus on the particular properties of the bi-metal interface that permit or hinder the transmission of slip or twinning dislocations. We will present models that are being used or newly developed to link the influence of interface transmissibility to the relative activities of slip and twinning in the layers and ultimately microstructural evolution in the bulk composite material.

ID: 307

Continuum dislocation theory and formation of microstructure in ductile single crystals

KHANH CHAU LE
(joint work with D. Kochmann and B.D. Nguyen)

The characteristics of plastic deformation of engineering materials depend to a high degree on the material microstructure comprising all structural characteristics on the microscale. Along with the properties of the periodic crystal lattice, the microstructural defects are integral components to determine the macroscopic mechanical response of the material. The most important mechanism for plastic yielding is the nucleation and motion of dislocations in crystals. Dislocation sliding and climbing accomodate plastic deformation, cross-slip or pile-up of dislocations are only two examples of mechanisms responsible for work hardening. Furthermore, dislocations are not only a key microstructural defect for plastic slip but also the core ingredient for forming microstructural patterns and substructures. The formation of microstructure like deformation twinning, polygonization, recrystalization, grain growth, texturing etc. exhibits various rearrangements of dislocation patterns. The aim of this talk is to show that the continuum dislocation theory can be used to describe such formation of microstructure, where we focus just on two continuum models of deformation twinning and of polygonization.

Slip and twinning are the major deformation modes which accomodate a change of shape under the action of applied tractions or displacements. Experimental evidence for deformation twinning was found long time ago and has been reported to occur especially in b.c.c., h.c.p. and lower symmetry metals and alloys but also in many f.c.c. metals and alloys with low stacking-fault energy, or other intermetallic compounds as well as in geological materials such as calcite or quartz. Twinning becomes particularly important in metals with only a limited number of slip systems, as it can operate to provide the five slip systems required to satisfy the criterion for a general slip deformation. Deformation twinning basically divides the originally uniform single crystal into two volumetric parts – a parent phase (with unaltered crystal lattice) and a twin phase (with a different crystal lattice orientation). Both phases normally occur in the form of lamellar structures, where a bicrystal consisting of neighboring parent and twin phase is commonly referred to as a *twin*. The twin lattice can be generated either by a rotation of the original crystal lattice by 180^0 about some axis (mode I) or by reflection in some plane (mode II) so that in both cases – when joint with the undistorted parent phase – an unfaulted single crystal is formed, which exhibits a twin boundary with coincident lattice positions at the interface.

A new ingredient of our theory (see [1]) is the so-called twinning shear produced by the existing dislocations in the already active slip system, which plays a similar role as Bain's strain in the theory of martensitic phase transformations, see e.g. [2]. This twinning shear followed by a rotation enables the initially homogeneous crystal to form the twin phase from the parent phase. The underlying mechanism of twin formation is closely related to that of [3], where a decomposition of

ID: 383

EVALUATION OF STRENGTH-HARDENING COEFFICIENT THROUGH ELECTRICAL CONDUCTIVITY MEASUREMENTS

Igor Sevostianov
NMSU

Abstract:
The paper addresses the problem of quantitative connections between strength hardening coefficient (incremental stiffness) and electrical resistance in a fatigued material. The physical mechanism providing the background of this connection is dislocation density growth induced by cyclic loading. The dislocation density leads to increase in both electrical resistivity and incremental compliance of the material. Experimental data are in a good agreement with the analytical cross-property connection derived from the theory of plastic hardening and the theoretical estimation of the effect of dislocation density on electrical resistivity. Such a cross-property connection can be used for development of a new methodology of structural health monitoring based on electrical conductivity measurements.

ID: 391

Morphological Transformations of Heterogeneous Particles in Elastically Stressed Solids

JIANMIN QU
Northwestern University
USA

Xujun Zhao
USA

Abstract:
Morphological evolution of the microstructure in heterogeneous materials is of great interest in material design and mechanics of materials. For example, it is experimentally observed that second phase particles in Ni-base superalloys undergo shape changes from spheres to cuboids with round corners, to platelets aligned along crystallographic directions when superalloys are annealed at constant temperature. Phenomena such as splitting of a single large particle into a group of small cuboids or a pair of gamma precipitate doublets are also observed experiments experimentally. In this work, we present a general approach to determine the equilibrium morphologies of microstructures by minimizing the total system energy using a hybrid extended finite element/level set method. The geometry of the material interface is implicitly described by the level set and the morphological transformation of microstructures, such as merging and splitting and creating sharp cusps, can be accurately captured. We found that the equilibrium morphology of the heterogeneities is strongly dependent upon the elastic anisotropy of the system, the elastic mismatch between the particle and matrix, as well as the particle size.

ID: 449

Kinetic Monte Carlo Simulation of Plastic Strain Recovery in Nanocrystalline Materials

Yuesong Xie
Purdue University
United States

Marisol Koslowski
Purdue University
United States

Abstract:
It is observed that nanocrystalline thin films recover between 50% and 100% of plastic deformation after unloading[1], [2]. Several models have been developed to explain this time dependent, thermally activated process. Koslowski [3] and Mompiou *et al.* [4] suggest that it is reverse dislocation motion that causes this phenomenon. Koslowski attributes this to the internal stress imbalance resulted from heterogeneous microstructure and Mompiou *et al.* to interactions with grain boundaries. On the other hand, Wei *et al.*[5] show that for nanocrystalline materials, with grains under 5nm. Most grains would be dislocation free and then creep is governed by grain boundary diffusion and sliding. Grain boundaries of higher diffusivity will diffuse and slide during loading, yet perform reverse diffusion due to the traction exerted by the grain boundaries of lower diffusivity.

Here we present simulations and analytical models to show that plastic strain recovery can be explained as a result of reverse motion of dislocations driven by heterogeneous internal stresses due to grain size distribution. Dislocation dynamics simulations coupled to a Kinetic Monte Carlo method are performed. We study a large distribution of grain configurations using Voronoi diagrams to generate the grains. These simulations predict that the percentage of recovered strain increases with the volume fraction of large grains and that the percentage of recovered strain is affected by the grain size distribution.

We compare our simulations to two analytical models i) an elastic-perfect plastic response model and ii) and elastic-linear hardening response model coupled to creep models to predict recovery. This allows the calculation of the stress dependent exponent and strain rate constant used in creep models. We find a stress exponent in the range 4 to 5 in good agreement with dislocation mediated creep process.

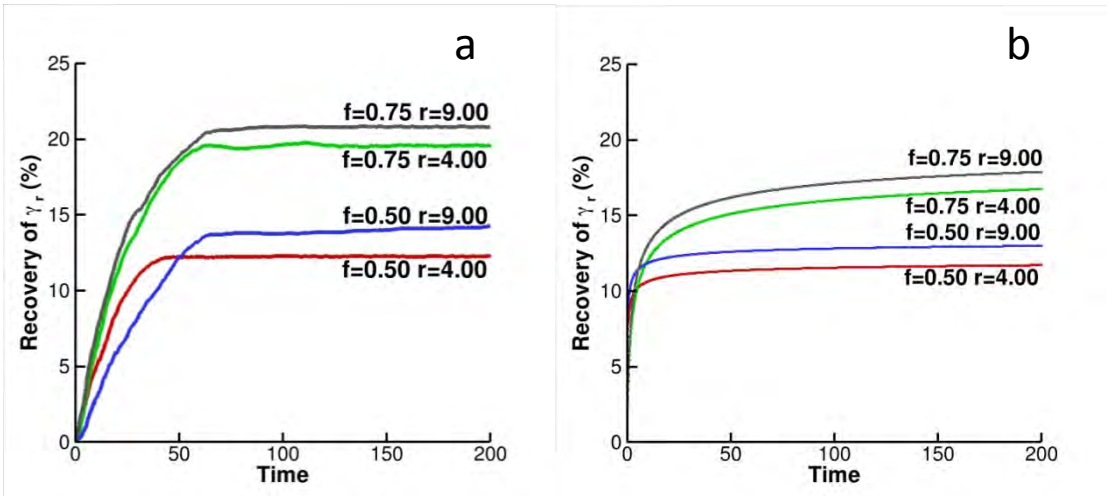

Figure 1. (a) Time evolution curves of strain recovery for square grids from KMC simulation. (b) Time evolution curves of strain recovery from analytical models.

Figure 1 shows the calculated strain recovery curves for a range of large grains volume fraction f and grain size ratio r.

Keywords: Kinetic Monte Carlo, Plastic strain recovery, Nanocrystalline structure, Thermally activated process.

References:

[1] J. Rajagopalan, J. H. Han, and M. T. A. Saif, "Plastic Deformation Recovery in Freestanding Nanocrystalline Aluminum and Gold Thin Films," *Science*, vol. 315, no. 5820, pp. 1831–1834, Mar. 2007.

[2] I. Lonardelli, J. Almer, G. Ischia, C. Menapace, And A. Molinari, "Deformation behavior in bulk nanocrystalline-ultrafine aluminum: in situ evidence of plastic strain recovery," *Scripta Materialia*, vol. 60, no. 7, pp. 520–523, Apr. 2009.

[3] M. Koslowski, "Effect of grain size distribution on plastic strain recovery," *Phys. Rev. B*, vol. 82, no. 5, Aug. 2010.

[4] F. Mompiou, D. Caillard, M. Legros, and H. Mughrabi, "In situ TEM observations of reverse dislocation motion upon unloading in tensile-deformed UFG aluminium," *Acta Materialia*, vol. 60, no. 8, pp. 3402–3414, May 2012.

[5] Y. Wei, A. F. Bower, and H. Gao, "Recoverable creep deformation due to heterogeneous grain-boundary diffusion and sliding," *Scripta Materialia*, vol. 57, no. 10, pp. 933–936, Nov. 2007.

Missing Abstract

ID: 484

ID: 504

ANALYTICAL AND EXPERIMENTAL DETERMINATION OF RATE, AND TEMPERATURE DEPENDENT NANOINDENTATION SIZE EFFECT IN METALS

George Voyiadjis
Louisiana State University

Danial Faghihi

Abstract:
NO ABSTRACT

ID: 506

Modelling of Martensitic Phase Transformation and Plastic Slip in Polycrystalline Materials

A.W. Richards
California Institute of Technology
United States

R.A. Lebensohn
Los Alamos National Laboratory
United States

K. Bhattacharya
California Institute of Technology
United States

Abstract:

Inelastic deformations due to a combination of plastic slip and martensitic phase transformations are observed in a variety of polycrystalline materials, including steels and shape-memory alloys (SMAs), but resolving the fine microstructures generated by slip (e.g. dislocation structures) and phase transformation becomes prohibitively expensive for a macroscopic polycrystalline model. Consequently, the interplay between these two mechanisms and their combined effects on the macroscopic response of polycrystalline materials remains poorly understood. Since both mechanisms originate as lattice-scale deformations constrained along slip- and habit-planes of single crystals, it seems natural to develop a model that treats the two similarly; that is, as competing constraint sets on lattice-scale deformations. Beginning with a non-convex energy potential at the micro-scale, we relax this potential using well-established homogenization techniques to coarse-grain over the subgranular microstructure, producing an analytical model for the effective response of an inelastic single crystal. We then extend this model numerically to polycrystals. Preliminary computational results are discussed, investigating the effects of the relative transformation- and flow-stress, as well as the influence of various kinetic laws.

ID: 558

Ginzburg-Landau-Type Models in Mechanics

Dmitry Golovaty
The University of Akron
United States

Shlomo Ta'asan
Carnegie Mellon University
United States

Abstract:
The structure of a Ginzburg-Landau (GL) model originally introduced to model superconductivity can be extended to describe a variety of other physical phenomena that involve ordered systems. The GL theory is particularly useful for understanding the behavior of structural defects - the regions of disorder that appear, e.g., for topological reasons. In my talk, I will discuss GL-type models that arise in continuum mechanics and describe their connection to underlying atomistic configurations.

ID: 563

Dislocation Mean Free Path Length Determination by Measurement of Geometrically Necessary Dislocation (GND) Density in Crystal Plasticity

Jeffrey Kysar
Columbia University

Muin Oztop

Abstract:

We describe measurements of the lower bound on the total density of Geometrically Necessary Dislocations (GND) on individual slip systems of a nickel crystal indented by a wedge. The GND content is measured by high-resolution electron backscatter diffraction (EBSD) with spatial resolutions of 2500 nm, 500 nm, 200 nm, 100 nm, and 50 nm. The multiple length scale measurements demonstrate that the GND density varies quasiperiodically, and the period of the GND variation is a characteristic length scale of crystal plasticity. Since the physical consequence of the formation of the quasiperiodic GND dislocation structure is to limit the mobility of dislocations, the dislocation mean free path length is assumed to scale with the period of the varying GND density. Our results demonstrate that the dislocation mean free path length evolves with increasing plastic deformation.

ID: 566

Thermodynamics of Microstructure Evolution

Victor Berdichevsky

Abstract:
It is gradually getting clear that there is "one more law of thermodynamics" that controls evolution of microstructures: in a closed thermodynamically stable system entropy of microstructure decays for positive temperatures of microstructure and grows for negative temperatures of microstructure. In a sense, this evolution is opposite to the law of evolution of usual thermodynamic entropy. Entropy of microstructure has appeared under different names in theory of glassy materials, granular matter, composite materials and polycrystals. In this talk I consider entropy of microstructure and the law of its evolution for two examples: grain growth in polycrystals and deformation of granular materials

ID: 596

Simulating Morphology Evolution of Precipitates in Elastic Media

Ravindra Duddu
Department of Civil and Environmental Engineering, Vanderbilt University, Nashville, TN
United States

Abstract:
We present a numerical formulation to investigate the morphology evolution of second phase precipitates(γ') in binary ($\gamma - \gamma'$) superalloys [1]. These superalloys or high-performance alloys exhibit excellent mechanical strength, creep resistance at high temperatures, and corrosion and oxidation resistance; hence, they are commonly used in gas turbines, turbine blades of jet engines and engine valves in automobiles. The superior mechanical properties of these superalloys depend mainly on the microstructure's morphology, that is, on the size and distribution of the secondary phase (γ') precipitates, which impede the movement of dislocations and defects in crystal lattices leading to strengthening. Therefore, understanding the physics of precipitation is an important step in materials modeling for design; and, numerical simulation can help shed new light onto the underlying evolution mechanisms. The broader goal of computational modeling is to aid in the development of new manufacturing technologies and precipitation strengthening techniques that lead to optimal material performance and energy efficiency.

Typically, the precipitation process consists of three stages: nucleation, growth, and coarsening or Ostwald ripening, of second phase (γ') particles. Herein, we restrict our attention to the latter two stages of growth and coarsening in two phase systems via diffusional phase transformation in anisotropic elastic media [2]. The two phases, namely, the matrix phase and the particle phase, are separated by the particle–matrix interface. The governing equations of elasticity and substrate diffusion are subject to different body forces and boundary conditions in the two phases. The interfacial substrate concentration is given by the stress modified Gibbs–Thompson equation and the evolution velocity is given by the substrate concentration jump at the particle–matrix interface. The computational challenges associated with simulating the particle–matrix interface evolution are significant due to the presence of: discontinuous strains across the interface due to misfit eigenstrains, cubic elastic anisotropy, discontinuous substrate concentration gradients across the interface, moving interfaces, and inter-particle interactions. Also, computing the interfacial curvature and the evolution velocity present a significant challenge. Therefore, specialized methods for handling moving boundaries and for solving diffusion and elasticity equations on irregularly shaped domains are needed for producing accurate simulations.

The existing approaches for simulating microstructure morphology evolution can be broadly classified on the basis of how the interface is resolved (sharp vs. diffused interface) and how it is represented (Lagrangian vs. Eulerian). The phase field method, which is a diffused interface Eulerian formulation, has yielded interesting results; however, it solves the evolution equations with a large number of parameters. On the other hand, the boundary integral method, which is a sharp interface Lagrangian formulation, is computationally efficient; however, it cannot handle, quite well, complex topological transitions such as particle merging, splitting and vanishing. Herein, we employ a new sharp interface Eulerian formulation based on the extended finite

element method (XFEM) and the level set method [1], which is capable of capturing topological transitions of arbitrarily shaped particles without introducing any additional smoothing parameters. Furthermore, the proposed formulation eliminates the need for the finite element mesh to conform to the particle–matrix interface and so no remeshing is required. We adopt a staggered explicit numerical scheme, wherein the governing of elasticity and substrate diffusion are solved using the XFEM and the particle interface evolution equation is solved using the explicit level set method. A regular finite element mesh consisting of rectangular bilinear element and a matching finite difference grid were used for computations. A random grid rotation scheme is employed so as to alleviate the mesh directional bias (or mesh anisotropy) of finite element calculations. Numerical examples simulating both equilibrium and dendritic morphologies of microstructures are considered to demonstrate the viability of the formulation.

Figures 1(a) and 1(b) show the initial and final morphology of a rectangular particle with rounded corners that is misaligned by 45^{o} from the elastically soft directions. The computation is performed on a 2 µm × 2 µm domain using a 200 × 200 element mesh. The competition between the elastic energy and the interfacial energy provides a mechanism to explain the ``arrowhead'' precipitate morphology in Fig. 1(b) that is observed in the experimental micrographs.

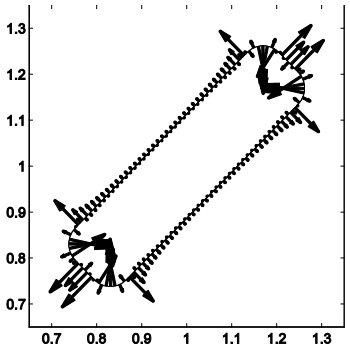

Figure 1(a)

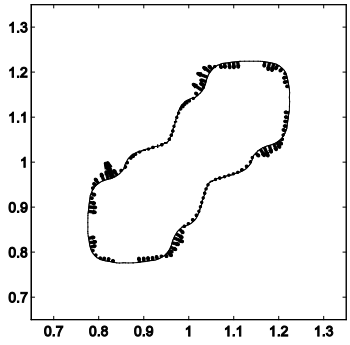

Figure 1(b)

Figures 2(a) and 2(b) show the diffusional evolution of a four-fold symmetric shape due to a misfit dilatational eigenstrain and isotropic interfacial energy. The computations are performed on a 2 µm × 2 µm square domain using a 400 × 400 mesh. The random grid rotation scheme helps ameliorate the evolution results and so the final particle shapes obtained from two different initial interface–to–mesh alignments are consistent illustrating mesh independence of the method, reasonably.

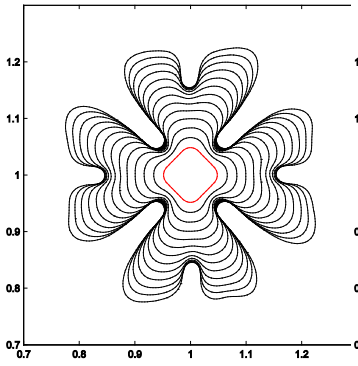

Figure 2(a)

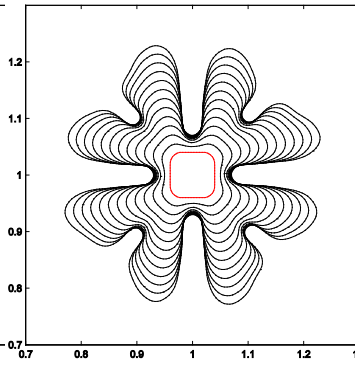

Figure 2(b)

References

3. R. Duddu, D. L. Chopp, P. W. Voorhees and B. Moran, "Diffusional evolution of precipitates in elastic media using the extended finite element and the level set methods." *Journal of computational Physics*, 230(4): 1249-1264, 2011, doi: 10.1016/j.jcp.2010.11.002.
4. C.H. Su and P.W. Voorhees. The dynamics of precipitate evolution in elastically stressed solids .1. Inverse coarsening. *Acta Materialia*, 44(5):1987–1999, 1996.

ID: 747

A Coupled Model for Phase Transformations and Dislocation Plasticity

Ido Regev
Los Alamos National Laboratory

Turab Lookman

Abstract:
We propose a model which couples the effects of irreversible plastic deformation and reversible phase transformations in shear deformation of polycrystals. Plastic deformation is described by a recently introduced model which involves two internal variables: the density of dislocations and a variable that describes the complexity of the arrangement of dislocations in the material called the ``effective temperature''. The phase transformation is modeled as an activated process with an activation barrier that is calculated analytically from a Landau free-energy. The irreversible structural changes that occur due to plastic deformation are incorporated in the free-energy and result in sensitivity of the phase diagram to cycling history. The stress-strain curves show qualitative agreement with experimental results.

ID: 758

Interfaces and Microstructure Evolution in Ferroelastics

Turab Lookman

Abstract:
The nucleation and growth of ferroelastic twin boundaries is of particular interest as twin boundaries can be superconducting, have high ionic mobilities or assume other functionalities. A common method of producing high twin wall densities is by fast temperature quench from a paraelastic phase into a ferroelastic phase. I will review some recent progress based on driving a single domain crystal by shear strain in the low temperature phase. The use of driven systems to generate high twin densities is motivated by the experimental observation of noise generation by moving twin boundaries and the crossover from classical criticality to self-organized criticality.
Collaborators: X. Ding, Z. Zhao, E.K.H. Salje, A. Saxena

IV.2

Multiscale Mechanics of Materials - Defects in Materials

Missing Abstract

ID: 87

ID: 109

Exploring Interfacial-Mediated Plasticity and the Deformation Mechanisms in Nanocrystalline Materials

Garritt Tucker
Sandia National Laboratories

Shreevant Tiwari
Georgia Institute of Technology

Abstract:
Grain boundaries (GBs), and their associated deformation processes, become increasingly influential on polycrystalline material behavior as the average grain size is reduced to the nanometer length-scale. In nanocrystalline (NC) face-centered cubic metals, such as copper, a transition from dislocation-dominated to GB-mediated strain accommodation coincides with a maximum in material strength. Therefore, it is imperative to understand the cooperative role of GBs and other deformation mechanisms, such as dislocation nucleation and lattice strain, in NC metals with grain sizes in this regime. We use atomistic simulations in this work to investigate the deformation of GBs and explore their contribution in the behavior of NC copper at low temperature. Dislocation nucleation from GBs, as well as GB sliding and migration are shown to be important mechanisms in nanograined systems. We also show how fundamental kinematic information is obtained from atomistic data using non-local microscale metrics computed from nearest neighbor lists. In addition, we can resolve the role of different deformation mechanisms in the total strain of NC systems using the metrics, and quantitatively confirm the transition to GB-mediated plasticity in NC metals.

* Sandia National Laboratories is a multi-program laboratory managed and operated by Sandia Corporation, a wholly owned subsidiary of Lockheed Martin Corporation, for the U.S. Department of Energyfs National Nuclear Security Administration under contract DE-AC04-94AL85000.

ID: 161

Atomistic Simulations of Grain Boundaries in Metallic Materials

Douglas E. Spearot
University of Arkansas
United States

Shawn P. Coleman
University of Arkansas
United States

Abstract:
The objective of this work is to explore the atomic-level structure of grain boundaries in metallic materials and their role during mechanical deformation via the use of atomistic simulations. First, molecular dynamics (MD) simulations are used to study dislocation nucleation and motion in nanocrystalline Cu with grain boundaries that have been doped with antimony (0.0-1.0 at.%Sb) for the purpose of increasing the thermal stability of the nanocrystalline microstructure. MD simulations of tensile deformation show that grain boundary doping causes an increase in the flow stress of nanocrystalline Cu but does not shift the grain diameter associated with maximum strength, as shown in Figure 1 from Rajgarhia *et al.* [1]. The increase in flow stress is caused by the Sb atoms which prevent relative sliding between grains in the nanocrystalline sample. Overall, the presence of the Sb dopants positioned at the grain boundaries impacts grain boundary mediated deformation, but does not appreciably influence the heterogeneous sources for partial dislocations during tensile deformation.

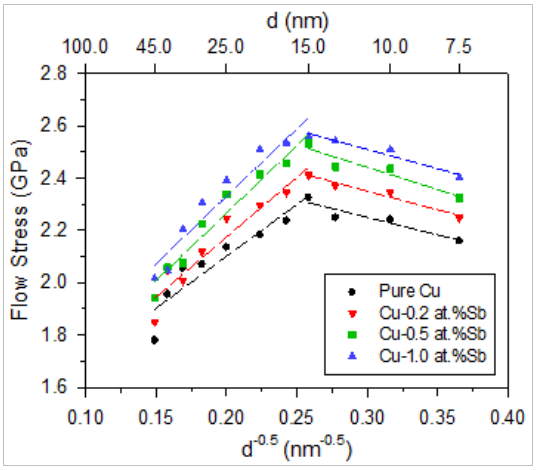

Figure 1. Flow stress as a function of grain diameter in nanocrystalline Cu samples doped with Sb [1].

Second, virtual diffraction patterns for <100> symmetric tilt grain boundaries (STGBs) are computed directly from molecular dynamics simulations via the structure factor equation. Virtual x-ray diffraction line profiles show peak broadening, peak shifting and the emergence of secondary peaks about the {200} scattering angle, analogous to that observed experimentally. Virtual electron diffraction patterns reveal peak streaking whose position and intensity are unique for each grain boundary model, as shown in Figure 2 from Coleman *et al.* [2].

Diffraction patterns computed from atomistic simulations illuminate new experimentally verifiable routes to characterize the nanoscale deformation gradients created by grain boundaries in metallic materials and may ultimately provide a hierarchical route to link with continuum models of plasticity in nanocrystalline materials.

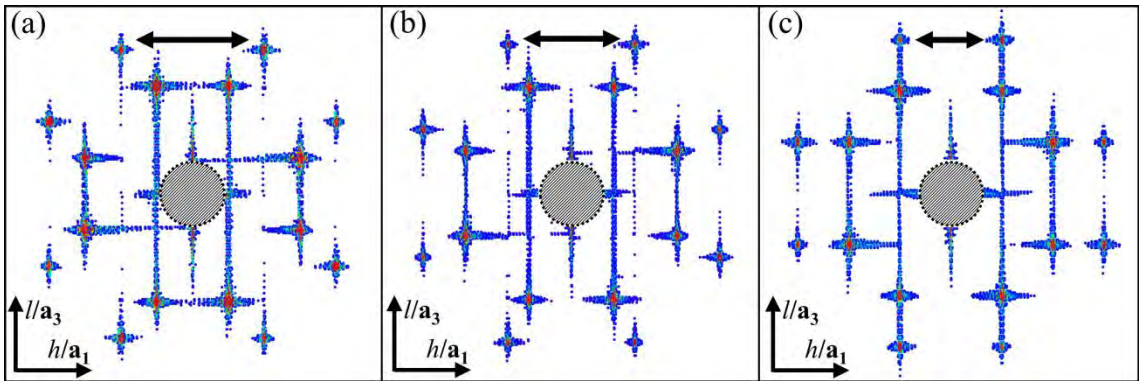

Figure 2. Virtual electron diffraction patterns viewed along the misorientation axis for the (a) Σ5 (310), (b) Σ29 (520), and (c) Σ5 (210) STGBs in Ni [2]. Misorientation of the opposing lattice regions in the bicrystal models influences the peak locations as indicated by the arrows.

References:

[1] Rajgarhia, R.K., Spearot, D.E., Saxena, A. (2010) Plastic deformation of nanocrystalline copper-antimony alloys, Journal of Materials Research, 25, 411-421.

[2] Coleman, S.P., Spearot, D.E., Capolungo, L. (2012) Grain boundary structure analyzed via virtual diffraction patterns computed from molecular dynamics simulations, Scripta Materialia, submitted for publication.

ID: 176

Hierarchical multi-scale modelling of full-field evolution of deformation texture and plastic anisotropy in sheet metal forming

P. Van Houtte
Department MTM, K.U.Leuven
Belgium

J. Gawad
Department of Computer Science, K.U.Leuven
Belgium

P. Eyckens
Department MTM, K.U.Leuven
Belgium

B. Van Bael
Department MTM, K.U.Leuven
Belgium

G. Samaey
Department of Computer Science, K.U.Leuven
Belgium

D. Roose
Department of Computer Science, K.U.Leuven
Belgium

Abstract:
Focus is on the implementation of texture-induced plastic anisotropy in FE simulations of metal forming. The crystallographic texture [1] is introduced as a state variable in every integration point. A multi-scale model could then called to calculate the stress-strain response and the local texture evolution in every integration point and strain increment (Fig. 1). The present authors prefer the Advanced Lamel Model [2] for this task because it is a good compromise between accuracy of deformation texture predictions and calculation speed. However, the model needs to be called very often, which leads to prohibitive calculation times. This can be reduced by using an anisotropic analytical constitutive model (in this case: the FACET model [3]), identified in advance using the results of virtual mechanical tests. The latter are also performed by the ALAMEL model, taking the measured texture of the material into account. However, texture evolution is not automatically taken into account in this way. This has recently been remediated by using an adaptive scheme for updating the texture and the anisotropy. Texture and anisotropy

were updated by the ALAMEL-model. Results for cup drawing of aluminum and steel sheet are shown. The calculation times had been reduced from months to days. Predicted fields of plastic anisotropy and textures are discussed including experimental validation. Reference [4] gives a more detailed description of this method and its results.

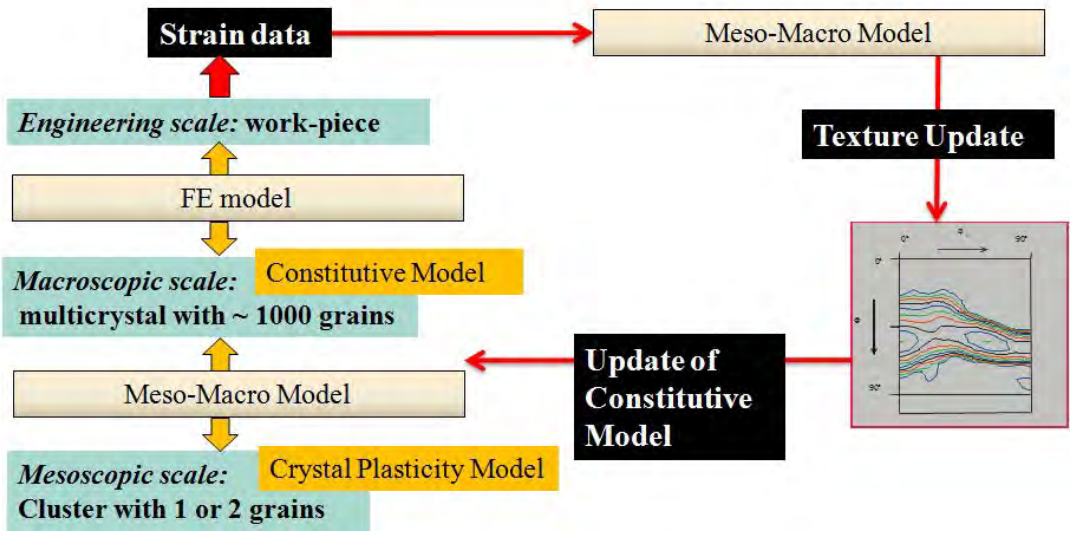

Fig. 1. FE simulation of metal forming with texture updating without optimization. Updating is done in each integration point at the end of each time increment.

Acknowledgements

Financial support from K.U.Leuven is acknowledged (contract IDO/08/09), as well as form the Belgian Federal Science Policy agency (contracts IAP6/4 and IAP7/21). Thanks also to the companies TataSteel, ArcelorMittal and Aleris for the sheet materials and cup drawing experiments. GS is Postdoctoral Fellow of the Research Foundation – Flanders (FWO).

References

1. U.F. Kocks, C.N. Tomé and H.-R. Wenk. *Texture and Anisotropy: Preferred Orientations and their Effect on Materials Properties* (Cambridge University Press, 1998), ISBN 0 521 46516 8.

2. P. Van Houtte, S. Li, M. Seefeldt, L. Delannay *Int. J. Plasticity*, 21 (2005), pp. 589-624.

3. P. Van Houtte, S.K. Yerra, A. Van Bael. *Int. J. Plasticity*, 25 (2009), pp. 332-360.

4. P. Van Houtte, J. Gawad, P. Eyckens, B. Van Bael, G. Samaey, D. Roose. A full-field strategy to take texture induced anisotropy into account during FE simulations of metal forming processes. *JOM,* 63/11 (November 2011) 37-43.

ID: 178

Continuum Mechanics of Coupled Displacement, Strain, and Rotation Discontinuities and Singularities

Amit Acharya
Carnegie Mellon University
USA

Abstract:
The duality between terminating discontinuities of fields and the incompatibilities of their gradients is used to define a coupled dynamics of the discontinuities of the elastic displacement field and its gradient. The theory goes beyond standard translational and rotational Volterra defects (dislocations and disclinations) by introducing and physically grounding the concept of generalized disclinations in solids without a fundamental rotational kinematic degree of freedom (e.g. directors). All considered incompatibilities have the geometric meaning of a density of lines carrying appropriate topological charge, and a conservation argument provides for natural physical laws for their dynamics. Thermodynamic guidance provides the driving forces conjugate to the kinematic objects characterizing the defect motions, as well as admissible constitutive relations for stress and couple stress. It is shown that even though higher-order kinematic objects are involved in the specific free energy, couple stresses may not be required in the mechanical description in particular cases. The resulting models are capable of addressing the evolution of defect microstructures under stress with the intent of understanding dislocation plasticity in the presence of phase transformation and grain boundary dynamics. This is joint work with Claude Fressengeas.

ID: 180 LA-UR-12-22947

Impact of grain size effects on stacking fault widths and deformation twins using 3D phase field dislocation dynamics (PFDD) simulations

Abigail Hunter
Los Alamos National Laboratory
United States

Timothy C. Germann
Los Alamos National Laboratory
United States

Irene J. Beyerlein
Los Alamos National Laboratory
United States

Abstract:
Due to the small length scales (< 100nm), plasticity is mediated differently in nanomaterials. For example, fcc metals plastically deform through the motion of extended dislocations due to energetic benefits found while shifting through the crystal lattice. In bulk and large-grained materials, these extended dislocations stay close together (on the order of 1-10 nm) and are often assumed to be a single unit (i.e. a perfect dislocation). However, when the internal microstructure (i.e. grain size, film thickness) approaches tens of nanometers plasticity is primarily mediated through the motion and interaction of partial dislocations, resulting in large stacking fault widths (on the order of the grain size) and can no longer be described as a perfect dislocation.

As characteristic length scales shrink and plasticity is accommodated differently, alternative deformation mechanisms not seen in the bulk and course-grained material counterparts emerge, such as deformation twinning. While deformation twinning is a well-known phenomenon in many nanoscale fcc metals and it is well established that partial dislocations are the basic defect responsible for deformation twins [1], the material parameters that control the inclination to twin, or twinnability, is not well understood. Experimental results and numerical simulations demonstrate that the formation of twins in nanocrystalline fcc metals is due to the nucleation of partial dislocations from grain boundaries and interfaces [2, 3, 4, 5]. Hence, a firm understanding of extended dislocations and their interactions at interfaces and grain boundaries is key to understanding deformation twins and their impact on the mechanical behavior of nanomaterials.

Traditionally, the intrinsic stacking fault energy (SFE) has been used as an indicator for a material's twinnability, with a low intrinsic SFE corresponding to a high probability of twin formation. In fact, most analytical and numerical models only consider the intrinsic SFE when describing the extension of partial dislocations and twin formation [6, 7, 8, 9, 3, 10, 11, 12, 13].

Conversely, some modeling studies on nucleation phenomena propose that additional energy parameters from the γ-surface (a material dependent energy landscape that describes the energy maxima and minima that atoms must overcome as they shear pass one another on {111} planes), in particular, the unstable and unstable twin SFEs play an important role in the nucleation of partial dislocations and twins forming from crack tips and grain boundaries [14, 15, 16, 17, 18]. This suggests that to accurately model partial dislocations, interactions with interfaces, and deformation twins, more aspects of the γ-surface must be accounted for.

This research uses a 3D phase field dislocation dynamics (3D PFDD) model to investigate the effects of grain size and confined plasticity on partial dislocation motion and stacking fault widths, with a specific focus on the nucleation and propagation of deformation twins at grain boundaries and interfaces in varying nanoscale grain sizes. The phase field approach is centered on energy minimization and, hence, evolution of the phase field variables and plastic deformation has a direct dependence on system energetics. This is advantageous for investigating extended dislocations and stacking faults because the PFDD model describes these defects using a parameterized γ-surface that is developed for specific materials using points from a γ-surface as simulated by either *ab initio* density functional theory (DFT) or molecular dynamics (MD). This incorporates a dependence on unstable SFEs in addition to the commonly used intrinsic SFE. Additionally, this establishes a link between atomic-scale numerical methods and the PFDD model that enables us to follow the dynamics of several nucleating and interacting dislocations based on appropriate calculation of their stacking fault widths and accurately probe the physics that underlies plastic deformation of even the smallest volumes.

1. J.W. Christian, S. Mahajan, Progress in Materials Science 39 (1995) 1-157.
2. V. Yamakov, D. Wolf, S.R. Phillpot, A. K. Mukherjee, H. Gleiter, Nature Materials, 1 (2002) 1-4.
3. M. Chen, E. Ma, J. Hemker, H. Sheng, Y. Wang, X. Cheng, Science 300 (2003) 1275-1277.
4. X.Z. Liao, F. Zhou, E. J. Lavernia, D.W. He, Y.T Zhu, APL 83(24) (2003) 5062-5064.
5. X.Z. Liao, F. Zhou, E. J. Lavernia, S.G. Srinivasan, M.I. Baskes, D.W. He, Y.T Zhu, APL 83(4) (2003) 632-634.
6. Z.Q. Wang, I. J. Beyerlein, PRB 77 (2008) 184112-1-14
7. V. Yamakov, D. Wolf, M. Salazar, S.R. Phillpot, H. Gleiter, Acta Mat. 49 (2001) 2713-2733.
8. E. Martinez, J. Marian, A. Arsenlis, M. Victoria, J. M. Perlado, J. Mech. Phys. Solids 56 (2008) 869-895.
9. R.J. Asaro, P. Krysl, B. Kad, Philosophical Magazine Letters 83(12) (2003) 733-743.
10. P. Gu, B. Kad, M. Dao, Scripta Mat. 62 (2010) 361-364.
11. J. Douin, F. Pettinari-Sturmel, A. Coujou, Acta Mat. 55 (2007) 6453-6458.
12: M.A. Meyers, D. J. Benson, O. Vohringer, B. K. Kad, Q. Xue, H.-H. Fu, Materials Science and Engineering A322 (2002) 194-216.
13. Hirth and Lothe, "Theory of dislocations" 1968.
14. J. R. Rice, J. Mech. Phys. Solids 40(2) (1992) 239-271.
15. E. B. Tadmor, S. Hai, J. Mech. Phys. Solids 51 (2003) 765-793.
16. S. Kibey, J. B. Liu, D. D. Johnson, H. Sehitoglu, APL 89 (2006) 191911-1-3.
17. N. Bernstein, E. B. Tadmor, PRB 69 (2004) 094116-1-10.
18. H. Van Swygenhoven, P. M. Derlet, A. G. Froseth, Nature Materials 3 (2004) 399-403.

ID: 197

Symmetries of continuous and discrete defective crystals

Rachel Nicks (née Sigrist)
University of Nottingham
UK

Gareth Parry
University of Nottingham
UK

Abstract:
We generalize, to the case of a class of crystals with uniform distributions of defects, symmetry considerations which are well known in the case of perfect crystals.

In the case of perfect crystals, the geometrical symmetries that are relevant to continuum mechanics relate to the various changes of basis that preserve a point lattice L, and this leads to material symmetries of strain energy functions invariant under transformations associated with the classical crystal classes (triclinic, tetragonal, cubic, etc.).

For defective crystals, one has first of all to decide on an appropriate generalization of the perfect lattice L, and then consider the geometrical symmetries of that discrete point set. We do this as follows:

i. We use the simplest constitutive assumption that accounts for the existence of defects in a continuum model of a crystal, allowing the strain energy function to depend on the value of the dislocation density tensor, denoted S. We indicate how this constitutive assumption leads to the consideration of crystal continua where S is constant in space.

ii. We note the connection between S and the Lie bracket of certain vector fields, and note that (material) points in the continuum can be interpreted as elements of a Lie group G determined by the value of S. These vector fields are considered to be lattice vector fields in Davini's [1] model for a continuum theory of defective crystals.

iii. We show that certain discrete subgroups D of G provide an appropriate generalization of the perfect lattices, and confine attention to the case where the value of S determines that G is a nilpotent group, corresponding (it turns out) to a uniform distribution of screw dislocations. Cermelli and Parry [2] consider the structure of these discrete subgroups in detail. The cases where G is solvable have also been treated in [5,6].

iv. We determine the set of all generators of D, which allows us to give the material symmetries of the corresponding strain energy function, in generalization of the argument which takes one from the set of all bases of L to the discrete, classical symmetries of a perfect crystal.

Finally we invoke results of Mal'cev [3] to make a connection between the symmetries of the discrete group D and the symmetries of the continuous group G. It turns out that, for choices of S such that G is nilpotent, the symmetries of D extend uniquely to the symmetries of G, and this gives the prospect of an explicit description of the connection between continuous and discrete models of defective crystals.

This work (the nilpotent case) is reported in reference [4] below and the solvable cases are treated in [5,6].

Acknowledgment

We are grateful for the support of the UK Engineering and Physical Sciences Research Council (grant number EP/G047162/1).

References

[1] C.Davini, A proposal for a continuum theory of defective crystals. *Arch. Rational Mech. Anal.,* **96**, 1986, 295-317.

[2] P.Cermelli and G.P.Parry, The structure of uniform discrete defective crystals. *Continuum Mech. Thermodyn.,* **18**, 2006, 47-61.

[3] A.Mal'cev, On a class of homogeneous spaces. Isvestiya Akad. Nauk SSSR Ser., Mat **13**, 9-32. Am.Math.Soc.Translation **39**, 1949.

[4] G P Parry and R Sigrist, Reconciliation of local and global symmetries for a class of crystals with defects. *J Elasticity,* **107**, 2012, 81-104.

[5] R.Nicks and G.P.Parry, On symmetries of a crystals with defects related to a class of solvable groups (S_1). *Math.Mech.Solids.* DOI: 10.1177/1081286511427485

[6] R.Nicks and G.P.Parry, On symmetries of a crystals with defects related to a class of solvable groups (S_2). *Mathematical Methods in the Applied Sciences.* DOI: 10.1002/mma.2571

ID: 209

Atomistic Simulations of Defect Nucleation & Intralayer Fracture in Molybdenum Disulphide (MoS_2) During Nanoindentation

James A. Stewart
University of Arkansas
United States

Douglas E. Spearot
University of Arkansas
United States

Abstract:
Molybdenum disulphide (MoS_2) is a layered, hexagonal crystal that has a very low coefficient of friction and consequently has been used widely as a solid lubricant and liquid lubricant additive. Recently, nanoparticles of MoS_2 have been proposed as a friction modifier additive to traditional liquid lubricants for the purpose of imparting sensitivity to specific temperature and pressure regimes. To properly develop these nanoparticles with temperature and pressure sensitivities, it is necessary to understand the mechanical response of crystalline MoS_2 under mechanical loading conditions; specifically, the fundamental mechanisms associated with the nucleation and interaction of defects. This work addresses this issue by simulating the mechanical response of MoS_2 during nanoindentation, which is representative of the loading conditions experienced by these nanoparticles during synthesis and application.

This work has two main objectives. First, an interatomic potential for Mo-S systems developed by Liang *et al.* [1,2] is implemented into the classical molecular dynamics simulation code, LAMMPS [3]. Liang *et al*. [1, 2] parameterized a potential for Mo-S systems combining the reactive empirical bond-order (REBO) and Lennard-Jones potentials and utilized this potential to study the tribological properties of MoS_2. The REBO potential captures the covalent bonding that occurs within a MoS_2 tri-layer while the Lennard-Jones potential captures the long-range and interlayer S-S van der Waals interactions. In this work, this potential was refined to provide improved overall predictions for the mechanical properties of MoS_2 via molecular statics calculations. Second, using this newly implemented Mo-S potential, nanoindentation simulations are performed using three indenter tip radii to investigate the mechanical response of MoS_2 with specific focus on initial defect nucleation. Nanoindentation force - displacement curves are created and compared to predictions using Hertzian contact theory. It is shown that MoS_2 does not follow the Hertzian prediction due to its anisotropic nature (C_{11} = 238 GPa and C_{13} = 52 GPa [1]). In addition, it is shown that the initial sudden force drop event in the force - displacement curve corresponds to an energetically stable plastic deformation. The mechanism associated with plastic failure of MoS_2 has been hypothesized to be the occurrence of broken bonds with the fracturing of MoS_2 tri-layers. However, it is proven in this work that the initial plastic yield is not a result of bond breaking. Instead, the mechanism for plastic yield of crystalline MoS_2 is a relative slip within or between the MoS_2 tri-layers. A slip vector analysis [4] is used to gain insight into the permanent slip occurring within the MoS_2 lattice below the indenter. The

magnitude of the permanent slip that occurs within the MoS_2 lattice as a result of nanoindentation is shown in Figure 1.

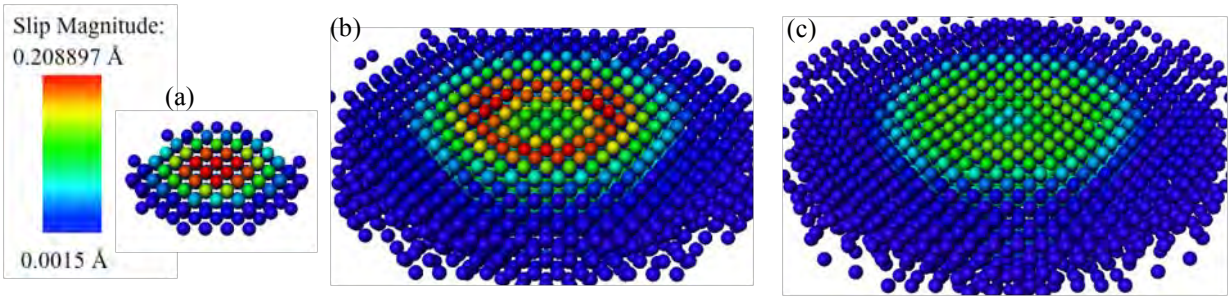

Figure 1: Atomic configurations and slip magnitude (a) before sudden force drop, (b) after sudden force drop and (c) with indenter fully retracted.

References:

[1] Liang, T., Phillpot, S.R. and Sinnott, S.B. (2009). Parameterization of a reactive many-body potential for Mo-S systems. Physical Review B, **79**, 245110 (1-14).

[2] Liang, T., Phillpot, S.R. and Sinnott, S.B. (2012). Erratum: Parameterization of a reactive many-body potential for Mo-S systems [Physical Review B, **79**, 245110 (2009)]. Physical Review B, **85**, 199903(E).

[3] Plimpton, S. (1995). Fast Parallel Algorithms for Short-Range Molecular Dynamics, Journal of Computational Physics, 117, 1-19. < http://lammps.sandia.gov >.

[4] Zimmerman, J.A., Kelchner, C.L., Klein, P.A., Hamilton, J.C. and Foiles S.M. (2001). Surface Step Effects in Nanoindentation. Physical Review Letters, **87**, 165507(1-4).

ID: 211

Mesoscale Dislocation-Defect Dynamics Plasticity

Hussein Zbib
Washington State University
USA

Abstract:
In this work we investigate, using molecular dynamics and discrete dislocation dynamics analyses, how dislocation mechanisms and interactions contribute to strength, accumulation of damage and fatigue in crystalline materials. Guided by these results, we develop a dislocation-based continuum crystal plasticity model, including dislocation densities, hardening laws based on dislocation-dislocation interaction, and a set of mechanisms-based evolution laws. The evolution laws consists of a set of terms each corresponding to a physical mechanisms that can be explicitly evaluated from the discrete dislocation analyses, including dislocation growth, annihilation, junction formation, junction breaking, dislocation-defect interaction and cross-slip. It is shown that the discrete events of cross-slip of screw dislocations can be explicitly incorporated in the continuum theory based on a probability distribution function defined by activation energy and activation volume of cross-slip, which is analogous to the one used for the discrete system. This enables the redistribution of dislocations and dislocation density patterning due to the effect of stacking fault energy. The formulation is employed for explaining the cross-slip phenomena during uniaxial tensile deformation of fcc and bcc single crystals.

ID: 214

Weyl Geometry and the Nonlinear Mechanics of Distributed Point Defects

Arash Yavari
School of Civil and Environmental Engineering
Georgia Institute of Technology

Abstract:

In this seminar we show how to obtain the residual stress field of a nonlinear elastic solid with a spherically-symmetric distribution of point defects. The material manifold of a solid with distributed point defects -- where the body is stress-free -- is a flat Weyl manifold, i.e. a manifold with an affine connection that has non-metricity but both its torsion and curvature tensors vanish. Given a spherically-symmetric point defect distribution, we construct its Weyl material manifold using the method of Cartan's moving frames. Having the material manifold the anelasticity problem is transformed to a nonlinear elasticity problem; all one needs to calculate residual stresses is to find an embedding into the Euclidean ambient space. In the case of incompressible neo-Hookean solids we calculate the residual stress field. We then consider the example of a finite ball of radius R_o and a point defect distribution uniform in a ball of radius R_i and vanishing elsewhere. We show that the residual stress field inside the ball of radius R_i is uniform and hydrostatic. We then compare the nonlinear and classical linear solutions. We also prove a nonlinear analogue of Eshelby's celebrated inclusion problem for a spherical inclusion in an isotropic incompressible nonlinear solid.

ID: 220

Understanding the role of grain boundaries during deformation using spherical nanoindentation and orientation imaging microscopy

Shraddha J. Vachhani
Georgia Institute of Technology, Atlanta, GA
United States

Roger D. Doherty
Drexel University, Philadelphia, PA
United States

Surya R. Kalidindi
Drexel University, Philadelphia, PA
United States

Abstract:
Grain boundaries play a significant role in the deformation of polycrystalline materials. Since the discovery of the Hall-Petch effect [1-2] more than sixty years ago, it is well known that the yield strength of a polycrystalline material can be connected to its average grain size by an inverse power-law relationship. The dislocation pile-up model [3] proposed to explain this strengthening effect implicitly assumes that the grain boundaries are poor dislocation sinks. An alternate model proposes the presence of a hardened region in the vicinity of the grain boundary [4] as a result of the increased dislocation density in the area. These concepts are still a topic of debate in literature, mainly due to the lack of experimental protocols for reliably extracting information about the material behavior at the sub-micron length scale.

Nanoindentation technique [5], with its high resolution load and depth sensing capabilities, provides an excellent opportunity to quantify the mechanical properties at the length scales smaller than an individual grain in a polycrystalline sample. Our recently developed analysis protocols [6-7] transform the load-displacement data obtained from a spherical nanoindentation test into a meaningful indentation stress-strain (ISS) curve. These ISS curves have been shown to capture various aspects of the elastic-plastic material response more reliably [8], compared to conventional nanoindentation data analysis protocols. This capability now provides a means to quantify subtle changes in the mechanical properties at a sub-micron length scale. Combining spherical nanoindentation data with complementary structure information obtained locally at the indentation site using orientation imaging microscopy permits detailed investigations of the changes in the structure and mechanical properties occurring as a result of the imposed macroscale deformation. This combination to techniques makes an effective tool for studying the underlying hardening mechanisms in the grain boundary regions.

In this work, we will apply this novel approach to systematically study the changes in the structure and mechanical properties of high purity aluminum in the annealed and deformed (to varying strain levels) conditions. One of the reasons for choosing pure aluminum is that it

exhibits very little elastic anisotropy and the plastic deformation mechanisms at the single crystal level are already well understood. This knowledge aids in the data analysis and interpretation. Also, in the fully annealed condition, the aluminum samples can be produced to exhibit extremely large grain sizes (of the order of several millimeters) making it possible to investigate individual grains and specific grain boundaries while avoiding contributions from the neighbors.

As a first step in the study, the inherent dependence of the indentation yield strength (Y_{ind}) on the local crystal orientation [9] was documented by measuring the mechanical response at various locations of known crystal lattice orientation on a fully annealed aluminum sample. In spite of a negligible difference in the dislocation density in the differently oriented grains in the fully annealed sample, it was seen that the Y_{ind} can vary by as much as 40% depending on the local crystal orientation. Quantifying the contribution of lattice orientation to the measured indentation yield strength is necessary to reliably estimate the specific contribution of the changes in dislocation density to the $Y_{ind.}$

Following this, the local yield properties within the grains and close to the grain boundaries were characterized on samples deformed to increasing levels of strain. The microstructure that develops during deformation is highly complex and the dislocation density can vary significantly from one location to another within the grain. A novel approach [8] to investigate the role of grain boundaries during the imposed macroscale deformation by monitoring the changes in local properties as a function of distance from the grain boundary will be presented. It will be demonstrated that these newly developed protocols provide valuable new research tools for studying the precise role of grain boundaries in plastic deformation of polycrystalline metals.

References

[1] E. O. Hall, "The Deformation and Ageing of Mild Steel: III Discussion of Results " *Proceedings of the Physical Society. Section B* vol. 64, 1951.

[2] N. J. Petch, "Cleavage strength of polycrystals," *Iron and Science Institure-journal,* vol. 173, 1953.

[3] A. H. Cottrell, "Theory of brittle fracture in steel and similar metals," *Metallurgical Society of American Institute of Mining, Metallurgical and Petroleum Engineers -- Transactions,* p. 212, 1958.

[4] A. E. Meyers MA, "A model for the effect of grain size on the yield stress of metals," *Philosophical Magazine A,* vol. 46, p. 737, 1982.

[5] J. L. Hay and G. M. Pharr, "Instrumented indentation testing," vol. 8-03D, ed: ASM Handbook.

[6] S. R. Kalidindi and S. Pathak, "Determination of the effective zero-point and the extraction of spherical nanoindentation stress-strain curves," *Acta Materialia,* vol. 56, pp. 3523-32, 2008.

[7] S. Pathak*, et al.*, "Determination of an effective zero-point and extraction of indentation stress-strain curves without the continuous stiffness measurement signal," *Scripta Materialia,* vol. 60, pp. 439-42, 2009.

[8] S. Pathak*, et al.*, "Studying grain boundary regions in polycrystalline materials using spherical nano-indentation and orientation imaging microscopy," *Journal of Materials Science,* vol. 47, pp. 815-823, 2012.

[9] S. Pathak*, et al.*, "Measurement of the local mechanical properties in polycrystalline samples using spherical nanoindentation and orientation imaging microscopy," *Acta Materialia,* vol. 57, pp. 3020-8, 2009.

ID: 222

Elastic twinning in transparent single crystals: phase field modeling and indentation experiments

J.D. Clayton, M.A. Grinfeld
Impact Physics, RDRL-WMP-C, US Army Research Laboratory, USA

C.D. Hilton, J.J. Swab
Transparent Materials, RDRL-WMM-E, US Army Research Laboratory, USA

J. Knap
Computational Sciences, RDRL-CIH-C, US Army Research Laboratory, USA

Background:
This work investigates elastic twinning in calcite ($CaCO_3$), a transparent mineral with trigonal symmetry, using theory, simulation, and experiment. Elastic twinning in calcite single crystals has been studied since the early 20th century in the former USSR [1-3] and more recently in Europe [4] and the US [5-9]. Pertinent descriptions are available elsewhere for thermodynamics of structural transformations [10] and mechanics of anisotropic single crystals [3, 11].

Phase Field Theory and Numerical Results:
A phase field theory for twinning, which accounts for large deformations and anisotropy, is developed in [6-8]. Letting $\mathbf{F}=\nabla\boldsymbol{\chi}$ denote the deformation gradient, a free energy functional is

$$\Phi(\boldsymbol{\chi},\eta) = \int \psi(\mathbf{F},\eta,\nabla\eta)\, d\Omega \qquad (1)$$

Order parameter η distinguishes among original crystal ($\eta=0$), twins ($\eta\rightarrow1$), and interfaces ($0<\eta<1$) in reference domain Ω. Minimization of the sum of elastic and surface energies, subject to boundary constraints, determines an equilibrium configuration of a stressed body. Indentation of a calcite single crystal with a rigid indenter of diameter 1 mm is shown on the left of Fig. 1; shearing of a slab of calcite single crystal [5] is shown on the right. Results are similar to experiment [1-5, 9]: twins terminate in sharp cusps and increase in length with increasing force.

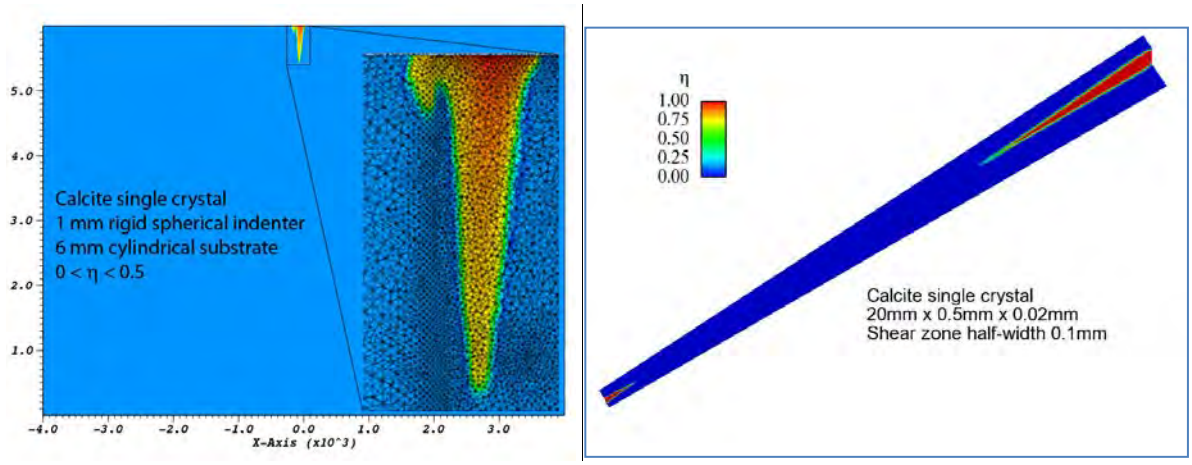

Fig 1 Phase field simulation of spherical indentation (left) and direct shear (right)

Indentation Experiments:

Spherical indentation into (100) cleavage planes is performed with a spherical diamond indenter of tip diameter 3 mm, as discussed in [9]. High resolution photographs provide in situ evidence of twinning and de-twinning processes (Fig. 2, left). The resolved shear stress on the twinning plane in the direction of shear, τ, at load P where twinning is first observed in experiments ($50<P<75$ N) is computed from nonlinear elastic anisotropic simulation [10] as $G/65<\tau_c<G/50$, where G=36.7 GPa is a representative shear modulus for calcite at room temperature [8].

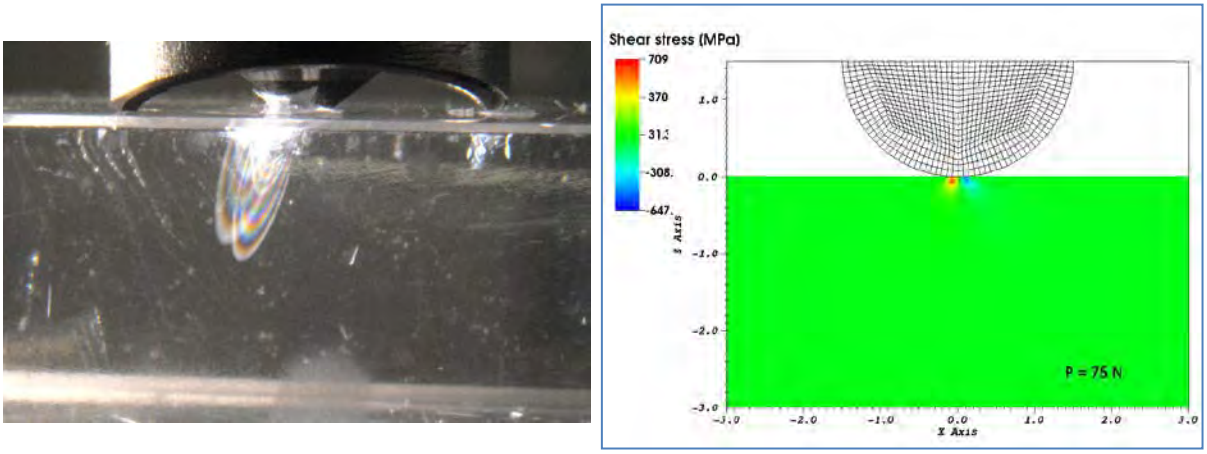

Fig. 2 Elastic twin at P=325N (left) and τ from nonlinear elastic simulation at P=75N (right)

References:

[1] R.I. Garber. Dokl. Akad. Nauk SSSR 21, 233 (1938)

[2] I.M. Lifshitz. Macroscopic description of the phenomenon of crystal twinning, Zh. Eksp. Teor. Fiz. 18, 1134-1143 (1948)

[3] V.S. Boiko, R.I. Garber, A.M. Kosevich. Reversible Crystal Plasticity. AIP Press, New York (1994)

[4] R.E. Cooper. Kinetics of elastic twinning in calcite. Proc. R. Soc. A 270, 525-537 (1962)

[5] H. Kaga, J.J. Gilman. Twinning and detwinning in calcite. J. Appl. Phys. 40, 3196-3207 (1969)

[6] J. Knap, J.D. Clayton. A computational framework for phase-field modeling. US Army Res. Lab. Tech. Rep. ARL-MR-0760, Aberdeen Proving Ground, MD (2011)

[7] J.D. Clayton, J. Knap. A phase field model of deformation twinning: nonlinear theory and numerical simulation. Physica D 240, 841-858 (2011)

[8] J.D. Clayton, J. Knap. Phase field modeling of twinning in indentation of transparent crystals. Modelling Simul. Mater. Sci. Eng. 19, 085005 (2011)

[9] C.D. Hilton, J. Yu, J.J. Swab. Elastic twinning and cleavage fracture in calcite materials: experimental methods and preliminary results. US Army Res. Lab. Tech. Rep. (forthcoming), Aberdeen Proving Ground, MD (2012)

[10] M.A. Grinfeld. Thermodynamic Methods in the Theory of Heterogeneous Systems. Longman, Sussex (1991)

[11] J.D. Clayton. Nonlinear Mechanics of Crystals. Springer, Dordrecht (2011)

[12] J.D. Clayton, R. Becker. Elastic-plastic behavior of cyclotrimethylene trinitramine single crystals under spherical indentation: modeling and simulation. J. Appl. Phys. 111, 063512 (2012)

ID: 232

Anisotropy of Thin Web Materials

John M. Considine
US Forest Service, Forest Products Laboratory
USA

Fabrice Pierron
University of Southampton, Faculty of Engineering and the Environment
UK

David Vahey
US Forest Service, Forest Products Laboratory
USA

Kevin T. Turner
University of Pennsylvania, Mechanical Engineering and Applied Mechanics
USA

Abstract:
Unexpected presence of anisotropy, often caused by misalignment of reinforcing fiber, is considered a defect in thin webs like paper and paperboard. These webs are frequently converted to final products by drawing them through rollers where printing, embossing, slicing and die-cutting operations occur. Tensile straining of anisotropic thin webs can produce wrinkles and other distortions creating problems in converting systems and significant financial loss through equipment downtime and product loss.

Characterization of anisotropy within thin webs is complicated by the inability of the web to remain in-plane in presence of appreciable compressive stress. Additionally, most thin webs exhibit some specimen size effect that influences the magnitude of measured stiffnesses. Nonlinear stress-strain behavior is common for paper and paperboard and most thin webs, but converting issues related to anisotropy occur at small strains.

A novel method of anisotropy evaluation is presented. A circular thin web of material, approximately 24 cm in diameter, is held under tension by eight grips, located 45° apart, where four consecutively-located grips are fixed and the other four consecutively-located grips are movable such that known forces may be applied. A fixture schematic is shown in Figure 1. Different in-plane tensile force conditions ($F_1 \neq F_2 \neq F_3 \neq F_4$) are applied and stereo DIC (digital image correlation) is used to capture full-field strains. Anisotropic in-plane Q_{ij} are determined from the measured in-plane strain field with use of VFM (Virtual Fields Method).

Two paper materials were examined for presence of anisotropy: a filter paper made with 100% cotton linters, grammage 187 g/m^2 and density 603 kg/m^3, and a paperboard commonly used for corrugated containers, grammage 209 g/m^2 and density 688 kg/m^3. Table 1 shows Q_{ij} for each

material. Filter paper had very low Q_{16} and Q_{26} and is effectively orthotropic; paperboard had very high Q_{26}, especially as compared to Q_{12}, and was significantly anisotropic.

This presentation will summarize the development of the load fixture, DIC system and application of VFM to this geometry. Validation of the methodology was accomplished with FEM. In-plane Q_{ij} determined by VFM will be compared with those measured ultrasonically and by tensile coupons. Effect of shear-coupling, a form of anisotropy, will be demonstrated by presence of Q_{16} and Q_{26} stiffnesses.

Figure 1: Fixture schematic of device used to determine anisotropy in thin web materials.

Table 1: Q_{ij} for each material in this study. Units are in specific stiffness, km^2/s^2.

	Q_{11}	Q_{22}	Q_{12}	Q_{66}	Q_{16}	Q_{26}
Filter	2.95	1.54	0.17	1.76	-0.10	-0.05
Paperboard	10.75	3.95	0.94	4.76	-0.16	-1.50

ID: 273

High Temperature Mechanical Behaviour of Nanoscale Multilayers

J.M. Molina-Aldareguia, M. Monclús and S. Lotfian
IMDEA Materials Institute
Spain

J. Llorca
IMDEA Materials Institute and Department of Materials Science, Polytechnic University of Madrid, Spain

K.E. Yazzie and N. Chawla
Materials Science and Engineering, Arizona State University
USA

N.A. Mara and I. Beyerlein
Los Alamos National Laboratory
USA

Abstract:

Nanoscale multilayers exhibit extremely high strength and toughness. However, little is known about their high temperature behavior due to the difficulty on testing thin-films at high temperature. In this paper we discuss the high temperature mechanical behavior of metallic-ceramic (Al/SiC) and metallic-metallic (Cu/Nb) nanoscale multilayers. The high temperature mechanical properties were characterized using two different techniques: nanoindentation and micropillar compression at temperatures up to 400 ºC. The former can be carried out without intensive sample preparation but analysis of the results is difficult due to the complex stress state imposed by the indenter. The latter requires the use of complex micromachining techniques but the results are easier to interpret. In view of this, the results obtained using both techniques will be compared and discussed. Finally, post-deformation microstructural analysis was carried by FIB and atomic force microscopy (AFM) to provide insight into the deformation mechanisms.

For instance, in the case of Al/SiC nanolaminates, the high temperature nanoindentation response in the range between 25 ºC to 300 ºC, showed that the Al/SiC nanolaminates were stable at temperatures up to 200ºC, after which extensive chemical reaction between Al and SiC induced a large reduction in the hardness, as can be seen in Figure 1. However, micropillar compression testing has revealed far more insights into the deformation mechanisms of this type of multilayers, as shown in Figure 2 for micropillars compressed at room temperature and 100 ºC. The results will be discussed as a function of the plastic deformation of the Al layers constrained by the elastic SiC layers and the role of interfacial sliding.

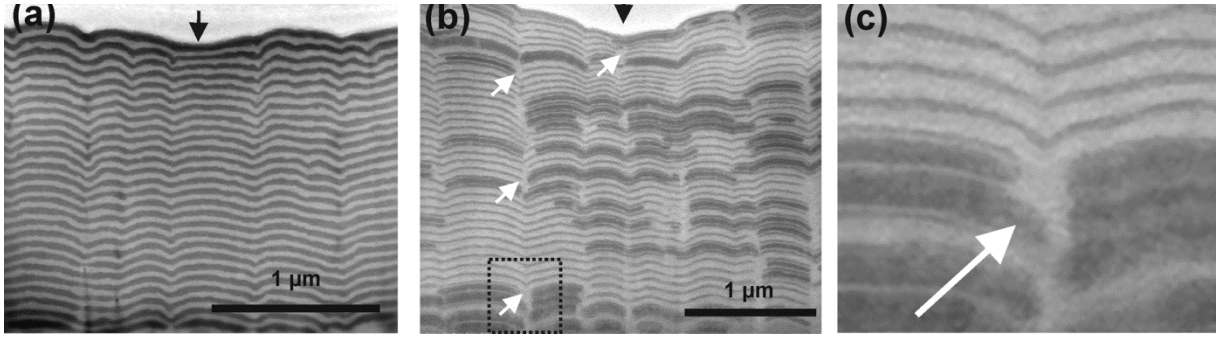

Figure 1: SEM images of indentation cross-sections: (a) at room temperature (dark gray: SiC; light gray: Al) and (b) at 300 ºC. Some reaction between Al and SiC can be observed at 300ºC (dark areas). The white arrows in (b) indicate areas where the SiC layers have broken and the Al has plastically flown to heal the cracks, as shown in more detail in (c).

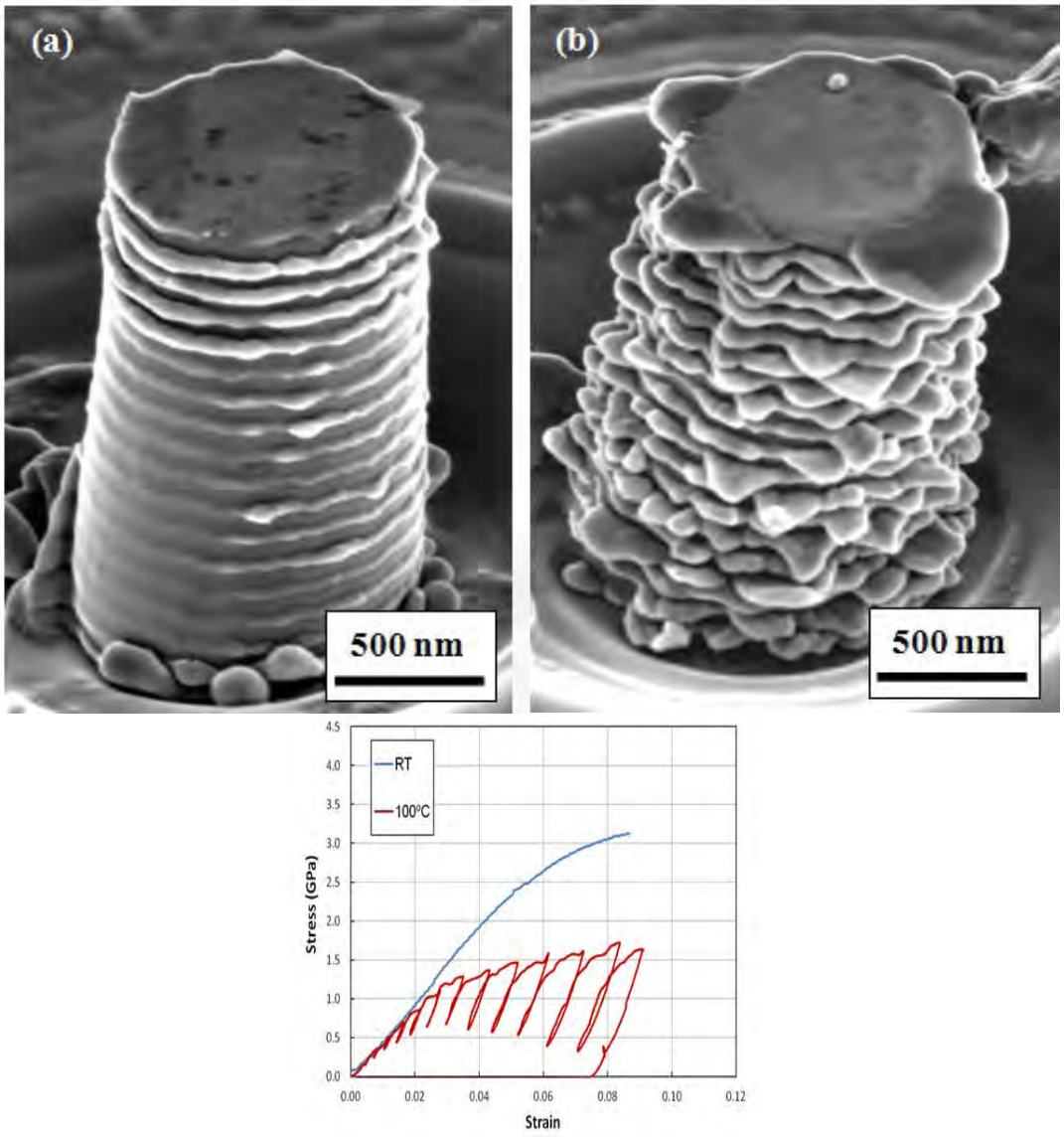

Figure 2: (a) Micropillar compression test at (a) room temperature and (b) 100 ºC. (c) Corresponding stress-strain curves

Acknowledgement. We acknowledge the financial support of the Spanish Ministry of Science and Innovation (MAT2009-14396-C02), the US National Science Foundation Materials World Network, the Comunidad de Madrid through the program ESTRUMAT (S2009/MAT-1585) and the European Commission through the European Project RADINTERFACES.

References

[1] Lotfian S, Molina-Aldareguia JM, Yazzie E, Llorca J, Chawla N. Philosophical Magazine Letters (2012), in press.

ID: 292

Twin Formation in Polycrystals -- 3D Grain-Resolved Simulations and Comparison to HEDM Measurements

Nathan Barton
Lawrence Livermore National Laboratory

Shawn Chester

Abstract:
Twinning is an important deformation mechanism in many materials, particularly for lower symmetry materials and for deformation at relatively high rates or low temperatures. Due to challenges both in modeling twin formation and in conducting experiments that quantitatively measure twinning, many questions remain regarding the mechanistic details of twinning. Even conceptually simple models of twinning behavior can be challenging to implement and computationally expensive to use in simulations. We present results from recent simulations for twinning in polycrystals, with finite elements used to resolve discrete twin formation. Effects of interest include the role of stress concentrations in the initiation to twinning, interaction among twin systems, and competition with dislocation glide mediates plasticity. Features of the model are highlighted using idealized two dimensional simulations, and fully three dimensional simulations are used to investigate complexities arising in polycrystals. Comparisons are made to experimental data from far-field high energy diffraction microscopy (HEDM) for a magnesium alloy. We will also discuss prospects for calibrating twinning kinetics from molecular dynamics simulations. This work was performed under the auspices of the U.S. Department of Energy by Lawrence Livermore National Laboratory under Contract DE-AC52-07NA27344 (LLNL-ABS-543380).

ID: 294

Modeling the Crystallographic Texture of Cu/Nb Layered Composites by Accumulated Roll Bonding

Curt Bronkhorst
USA

Benjamin Hansen
USA

Abstract:

Nano-multilayered composites of Copper and Niobium have demonstrated extraordinary ability to withstand both mechanical and radiation induced damage nucleation when the layer thicknesses have become less than one micron thickness. Although the bi-metallic interfaces are believed to play a role in the enhanced performance, we have yet to demonstrate an explanation. The accumulated roll bonding process is used to manufacture these materials. During this process, the individual Copper (fcc) and Niobium (bcc) layer thicknesses begin at 1mm and continue until the layer thicknesses become on the order of 10’s of nanometers. We present a new local single crystal model for the potential influence of the bi-material interface on dislocation motion in the near vicinity of the interface and apply this model to polycrystal multi-layer simulations in an attempt to predict the dominant experimentally observed orientation relationships across the interface. Direct comparison to experimental results will be made.

ID: 350

Multiscale Simulation of Dislocation Grain Boundary Interaction in fcc Materials

Zhiqiang Wang
University of North Texas
USA

Abstract:
Dislocation-grain boundary interactions play important roles in polycrystal plasticity. However, many detailed mechanisms are still unclear. Recently, we applied quasi-continuum method to carry out multiscale simulations of lattice dislocations interacting with tilt grain boundaries in face-centered cubic (FCC) materials. Lattice dislocation transmission, pile-up, and reflection are analyzed along with grain boundary dislocation activities and interaction residue evolutions. It is found that "positive" and "negative" interactions between dislocation and grain boundary show different dislocation transmission behavior, which is greatly affected by dislocation pile-up. Based on microscale understanding, a geometrical rule is developed to differentiate the grain boundaries for dislocation transmission. This physics-based rule can be used in mesoscale computational tools, such as discrete dislocation dynamics method, to incorporate grain boundaries into plasticity modeling.

ID:369

Effect of Void-Growth on Shear-Band-Spacing in Metals

Kubair, D. V., Ramesh, K. T.
Mechanical Engineering
The Johns Hopkins University
Baltimore, MD

P.K. Swaminathan
The Johns Hopkins University Applied Physics Laboratory
Laurel, MD

Abstract

In most large strain-rate loading scenarios fragmentation initiates at strain-localized sites (shear-bands). In order for the fragmentation size to alter the shear-band-spacing needs to be altered. Multiple shear-band formation simulations under pure-shear loading conditions are performed to understand the effect of void-growth on the shear-band-spacing. We use the phenomenological modified Gurson yield function that accounts for void-growth under shear-loading. The void-growth leads to an additional competing strain-softening mechanism on top of the existing thermal softening in the material. The interplay between the competing mechanisms lead to a reduction in the shear-band-spacing and the triggering of the inhomogeneous strains around the localized bands. For a linear void-growth-rate law described in the literature we found that the localization always triggered due to the thermal softening.

ID: 400

Modeling Deformation-Induced Orientation Fragmentation

Marc Seefeldt
KU Leuven, Department of Metallurgy and Materials Engineering

Abstract:
Bulk ultra-fine grained materials are mostly made through severe plastic deformation involving simple shear as predominant deformation mode. Microstructurally, large plastic deformation leads to grain subdivision through formation of new grain boundaries. Two basic mechanisms can be distinguished: a) formation of intragranular misorientation bands, usually micro shear bands localizing a variable amount of shear, and b) lattice curvature along existing GBs leading to polygonization. It will be discussed how micro shear bands can be formed as a result of dislocation elementary processes transferring slip to closely neighbouring parallel slip planes and allowing dislocation multiplication. Both will result into localization of slip. Models for grain subdivision are presented for plastic deformation of copper and niobium up to large strains. Finally, it is discussed how such models can efficiently be formulated in terms of partial disclinations, and how well-established phenomenological scaling laws from large strain plasticity can be understood in this framework.

Missing Abstract

ID: 428

ID: 444

Strength in Nanocrystalline Cu: Role of Grain Boundary Relaxation

Nhon Q. Vo
Northwestern University, Evanston, IL
United States

Robert S. Averback
University of Illinois, Urbana Champaign, Urbana, IL
United States

Pascal Bellon
University of Illinois, Urbana Champaign, Urbana, IL
United States

Jonathan Schäfer
Technical University of Darmstadt, Darmstadt
Germany

Alfredo Caro
Los Alamos National Laboratory, Los Alamos, NM
United States

Abstract:
Contrary to the often reported findings from molecular dynamics (MD) computer simulation that metals soften as their grain sizes fall below 10-15 nm, we do not observe such flow-strength softening when specimens are first thermally relaxed (Fig. 1) [[1]]. Moreover, the yield strength of all samples scales with the degree of grain boundary (GB) relaxation [[2]]. With addition of impurities decorating GBs, it is found to lower GB energy and dramatically increase the yield strength of the alloy (Fig. 2), with the dilute Cu-Nb alloys approaching the theoretical yield strength of Cu [[3]]. These observations suggest a new scaling behavior for the onset of plasticity in nanocrystalline materials, controlled not by the grain size alone, but by a combination of both grain size and the degree of GB relaxation. We offer a simple model that illustrates the increased hardening is a consequence of the GB relaxation, which suppresses GB accommodation and forces the material to deform by dislocation glide [[4]],1,2]. The new model provides an explanation for why some experiments observe an inverse Hall-Petch relationship at grain sizes below 10-15 nm while others do not. It also sheds light on recent findings of the exceptionally high-strength nanocrystalline alloys, where GB strengthening cannot fully explain it [[5]],[[6]].

[[1]] N.Q. Vo, R.S. Averback, P. Bellon, A. Caro, Phys. Rev. B **78** (2008) 241402.
[[2]] N.Q. Vo, R.S. Averback, P. Bellon, A. Caro, Scr. Mater. **61** (2009) 76.
[[3]] N.Q. Vo, J. Schaefer, R.S. Averback, K. Albe, Y. Ashkenazy, P. Bellon, Scr. Mater. **65** (2011) 660.
[[4]] N.Q. Vo, R.S. Averback, P. Bellon, A. Caro, Phys. Rev. B **77** (2008) 134108.
[[5]] S. Ozerinc, K. Tai, N.Q. Vo, P. Bellon, R.S. Averback, W.P. King (In Press, Scr. Mater.)

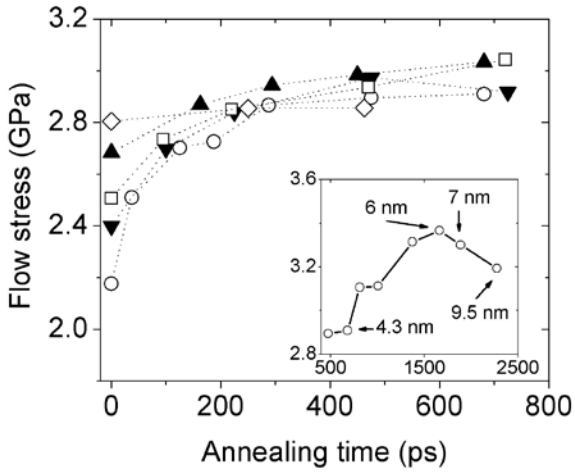

Figure 1. Flow stress as a function of annealing time for samples of different grain size: 2.5 nm (○), 4 nm (▼), 5 nm (□), 10 nm (▲), and 15 nm (◊). The inset shows the flow stress of the 2.5 nm sample versus annealing time. The grain size of this sample is indicated at various annealing times [1].

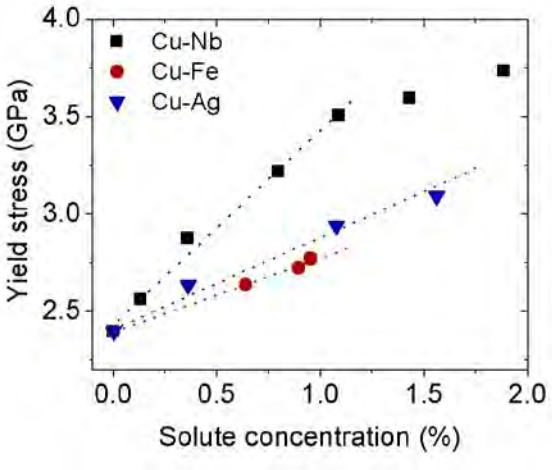

Figure 2. Yield stress of nanocrystalline Cu alloys as a function of solute concentration at constant strain rate 1 x 10^9 s^{-1} [3].

[6] T.J. Rupert, J.R. Trelewicz, C.A. Schuh, J. Mater. Res. **27** (2012) 1285.

ID: 474

Microstructure Effects on Shock-Induced Slip and Twinning: Large-scale Molecular Dynamics Studies

Timothy C. Germann
Los Alamos National Laboratory
United States

Irene J. Beyerlein
Los Alamos National Laboratory
United States

Christian Brandl
Los Alamos National Laboratory
United States

Ellen Cerreta
Los Alamos National Laboratory
United States

Xiang-Yang Liu
Los Alamos National Laboratory
United States

Alex Perez-Bergquist
Los Alamos National Laboratory
United States

Ramon Ravelo
University of Texas – El Paso
United States

Jian Wang
Los Alamos National Laboratory
United States

Ruifeng Zhang
Los Alamos National Laboratory
United States

Abstract:
Large-scale molecular dynamics (MD) simulations are used to study grain size and interface effects on dislocation slip and twinning under high strain-rate (e.g. shock) loading. In particular, I will discuss recent examples from our work on three different systems. (a) Homophase

interfaces, namely grain boundaries in shocked copper which serve as dislocation sources, sinks, storage, and transmission sites. The role of atomic interface structure in each of these processes may be elucidated using high-resolution TEM analysis of pre- and post-shock samples [1], and atomistic studies of selected grain boundaries in a bicrystal geometry [2]. (b) Nanocrystalline Ta, whose deformation involves a delicate competition between slip and twinning mechanisms, and is strongly dependent upon shock pressure, grain size, and texture [3]. (c) Cu/Nb nanolayered composites, in which the Cu-Nb interfaces serve both as dislocation sources during shock compression, and dislocation sinks upon release. Here we describe the development of an embedded atom method (EAM) interatomic potential which provides an accurate description of deformation twinning in bcc Nb under compression and the structure and energetics of Cu-Nb interfaces [4,5]. Using this potential, MD simulations provide insight into the role of atomic Cu-Nb interface structures on the nucleation, transmission, absorption, and storage of dislocations during shock loading of Cu-Nb nanolayered composites. The key role which interface structure plays is demonstrated by both MD simulations and post-mortem transmission electron microscopy (TEM) of shock-recovered samples [6], which indicate that deformation twinning in Cu is preferentially nucleated from Cu(112)//Nb(112) interface habit planes, as opposed to the more common Cu(111)//Nb(110) interfaces.

1. A.G. Perez-Bergquist, E.K. Cerreta, C.P. Trujillo, G.T. Gray III, C. Brandl, and T.C. Germann, Scripta Mat. **67**, 412 (2012).
2. C. Brandl and T.C. Germann, AIP Conf. Proc. **1426**, 1299 (2012).
3. R. Ravelo, Q. An, T.C. Germann, and B.L. Holian, AIP Conf. Proc. **1426**, 1263 (2012).
4. R.F. Zhang, J. Wang, I.J. Beyerlein, and T.C. Germann, Phil. Mag. Lett. **91**, 731 (2011).
5. R.F. Zhang, J. Wang, X.Y. Liu, I.J. Beyerlein, and T.C. Germann, AIP Conf. Proc. **1426**, 1251 (2012).
6. W.Z. Han, A. Misra, N.A. Mara, T.C. Germann, J.K. Baldwin, T. Shimada, and S.N. Luo, Phil. Mag. **91**, 4172 (2011).

ID: 500

Twin Boundary Motion in Pure Magnesium

Neha Dixit
Johns Hopkins University

Leslie Lamberson

Abstract:
Magnesium is of great interest to the automobile and aerospace industries due to its low density. Extensive use of this metal as a structural material is limited by our poor understanding of its deformation and failure mechanisms. Magnesium has a hexagonal close packed crystal structure, and twinning is a dominant mode of deformation under many loading conditions. The understanding of the basic morphology of deformation twinning has grown over the years. The connections between deformation twinning, stacking faults and partial dislocations have also been established but there is no understanding of the dynamics of twinning. As a result, it has been difficult to model the development of twins during deformation. In order to investigate the twin dynamics, normal plate impact experiments are performed with microsecond pulse durations. A stationary pre-twinned magnesium target is subjected to a short, high amplitude stress pulse by impacting it with a flyer plate carried on a projectile. The stress state is deduced from the particle velocity measured at the rear end of the target with a normal velocity interferometer (NVI). The intent is to develop estimates of twin boundary velocity under measured stresses.

ID: 507

A STRAIN GRADIENT PLASTICITY FRAMEWORK FOR CRYSTALS AND LOCALIZATION PROBLEMS

George Voyiadjis
Louisiana State University

Danial Faghihi

Abstract:
NO ABSTRACT

ID: 509

Multiscale Perspective of Understanding the Role of Interfaces in Solids

Jian Wang
Los Alamos National Laboratory

Irene Beyerlein

Abstract:
Interfaces in crystalline solids have enormous technological importance in determining mechanical properties of composites and morphologies of nanostructures. For example, interfaces may block slip even when dislocations move easily in both of the bounding crystals; Interfaces may be sinks for impurities and point defects. On the other hand, twin interface may change kinetics of adatom diffusion during nanostructured materials synthesis, resulting in sophisticated nanostructures. In this talk, from a multi-scale perspective, I will discuss the recent effort in developing multi-scale materials modeling tools that incorporate atomistic findings regarding interface physics into the high length scale models. The potential applications in designing materials by tailoring interfaces are also discussed.

ID: 581

Influence of Grain Boundaries on Shock Wave Propagation in Polycrystalline Copper

D. J. Luscher
Theoretical Division, Fluid Dynamics and Solid Mechanics

C. A. Bronkhorst
Theoretical Division, Fluid Dynamics and Solid Mechanics

E. K. Cerreta
Materials Science and Technology Division, Structure/Property Relations

Abstract:
High-rate large deformation response of polycrystalline metals is often accompanied by the nucleation and subsequent evolution of voids in a ductile process. Appropriately modeling this behavior at a macroscale has proven difficult without a better understanding of the physics of the nucleation process at finer scales. Flyer plate experiments have been conducted to characterize the influence of grain boundaries on the nucleation of voids in polycrystalline copper samples up through incipient spallation. A deeper understanding of these results can be achieved by mesoscale (polycrystal) numerical simulations to resolve features of heterogeneous response fields. In this talk, a mesoscale modeling framework is presented with emphasis on details of single crystal plasticity applicable to large deformation at high strain rates in shock loading regimes. Of particular importance is incorporating the nonlinear pressure-volume-temperature equation of state in a manner consistent with other aspects of the model. Simulation results highlighting the influence of grain boundaries on non-uniformity of a shock wave are presented.

ID: 599

Crystal Plasticity Modeling of the Interfacial Stability of CuNb Bicrystals

Jason Mayeur

Abstract:
The synthesis of nanoscale polycrystalline CuNb bimetallic layered composites via accumulative roll bonding leads to the development of a predominant interface orientation relationship and textures that are distinct from the rolling textures that are expected from rolling Cu and Nb individually. The interfacial constraints on plastic deformation at diminishing layer thicknesses are the source of these observed differences. This work studies the effects of kinematic constraints on interfacial stability for various CuNb bicrystal configurations via single crystal plasticity. Attention is focused on the slip system activity and the evolution of crystallographic orientation in the quantification of the deformation behavior of the bicrystals. The results are compared to single crystal Cu and Nb simulation results with the same orientations to assess the influence of the kinematic constraints on the deformation behavior.

Missing Abstract

ID: 648

ID: 658

High-Temperature Discrete Dislocation Dynamics

Amine Benzerga
Texas A&M University
USA

Shyam Keralavarma

Abstract:
At low homologous temperatures, the plastic deformation of metals is controlled by the glide of dislocations and a host of a thermal interactions with other dislocations, precipitates and grain boundaries. In discrete dislocation dynamics simulations of such deformation processes, temperature effects may enter through dislocation mobility and lattice friction as well as cross-slip. At temperatures greater than about 1/3 of the melting point, the climb of dislocations becomes increasingly important leading to phenomena such as creep and dynamic recovery. The modeling of climb as a nonconservative motion generally requires the concurrent modeling of dislocation motion and the diffusion of point defects into the cores of the dislocations. In this paper we report on a self-consistent formulation of high-temperature discrete dislocation plasticity in finite bodies, which couples dislocation dynamics with vacancy diffusion theory. To address the issue of disparate time scales related to glide and climb mechanisms, an adaptive multi-time stepping algorithm is used in the numerical implementation of the theory. We then present a series of deformation analyses at constant applied stress in single crystals. We show that two regimes of power-law creep naturally emerge in the simulations, as affected by the applied stress and test temperature. We also systematically quantify the power law exponent in eitherregime and the part of the strain rate that results from mass transport through the diffusive flow of vacanciesdue to pressure gradients.

ID: 762

Deformation-Induced Lattice Intra-Grain Misorientations in Polycrystals

Paul Dawson

Matthew Miller

Abstract:
Intra-grain lattice misorientations develop quickly with plastic straining in polycrystalline solids. Lattice misorientations occur as a consequence of the heterogeneity of deformation within and among crystals and can be traced to the anisotropic properties, both elastic and plastic, of crystals that comprise a polycrystal. Misorientations can be observed directly from orientation maps generated by electron-back scattered diffraction (EBSD) methods and indirectly through broadening of diffraction intensity images obtain by x-ray or neutron diffraction. Coordinated experiments and simulations offer an avenue to observe the development of misorientations and to understand the origins and causes of their evolution with deformation. In this talk we present a methodology, called a virtual diffractometer, for generating diffraction images from information embedded in finite element simulations of deforming polycrystals. We compare these with measured images and demonstrate that changes in intensity patterns are connected to intra-grain misorientation development in the simulation. Further, we discuss the connection between the misorientations structure within crystals and the deformation mode that a polycrystal is subjected to during the deformation. Together, these provide an insight link between the material, its anisotropic properties at the crystal scale, the mode of deformation acting on the material, and its derived misorientation structure.

ID: 766

Dislocation Dynamics Simulations of Materials with Interfaces

First Author: Caizhi Zhou
Los Alamos National Laboratory
United States

Second Author: Jian Wang
Los Alamos National Laboratory
United States

Third Author: Irene J. Beyerlein
Los Alamos National Laboratory
United States

Forth Author: Curt A. Bronkhorst
Los Alamos National Laboratory
United States

Abstract:
Extensive investigations over the past decade indicate that nanoscale metallic composites have unprecedented levels of strengths, ductility and damage tolerance in extreme environments. Atomic-scale modeling of unit processes suggests that the mechanical properties of nanoscale metallic composites under deformation are dominated by defect-interface interactions. To understand the role of interface structures and properties during deformation and design ultra-high strength, damage-tolerant nanoscale composite, we develop a mesoscale model, interface dislocation dynamics model, based on experiment observation and atomic scale simulations to study the dislocation-interface interactions at micro- and nanoscales and provide a generic bi-metal interface model that represents the key characteristics of the structure and properties of the interface. In order to capture the fundamental physics of dislocation-interface interactions, dislocation annihilation, nucleation and emission from the interface are all considered in our simulations, which is different from traditional DD simulations on single-phase materials.

IV.3

Multiscale Mechanics of Materials - Multiscale Characterization of Materials

Missing Abstract

ID: 103

ID: 104

Multi-scale Analysis for Solder Alloys using Velocity Averaging Method

Yongchang Lee
University of Buffalo

Cemal Basaran

Abstract:
The solder joint is an interesting system for the application of both continuum mechanics and molecular dynamics due to its own material behaviors such as mass transport and creep. In computational mechanics, molecular dynamics (MD) and finite element (FE) analysis have been used for solder alloys on microscale and macroscale analysis, respectively. MD has been used to determine the material properties such as diffusivity. FE has been used for continuum mechanics problems such as mean-time-to-failure analysis. Developing nanotechnologies and minimization of electronics require for the analysis of solder alloy to use multi-scale simulation method which has both advantages of MD and FE. This present work uses a velocity averaging method to couple MD with FE analysis for solder alloy. A velocity averaging technique shows excellent coupling results through the transfer of the energy and displacement between MD and FE. This approach has benefits on the simulation time by using staggered time integration algorithm, on reducing computational cost by using a short handshake region, and on a simple way to link MD with FE. In this simulation, we use the most common solder alloy, SAC405, 94.5Sn, 4.0Ag, 0.5Cu by weight. Using molecular dynamics simulations with the conditions determined by FE analysis, we obtain material properties of the solder alloy. FE analysis is conducted using the updated material properties by MD simulation. The result of velocity averaging method is compared with the result of FE analysis to show the effect of multi-scale analysis.

ID: 267

A study of Platinum Group Elements (PGEs) in Chondrites

Narendra Kumar Agrawal (E-Mail: *research.nka@gmail.com*)
Department of Physics, Malaviya National Institute of Technology, Jaipur, India.

Priti Agarwal
Department of Botany, University of Rajasthan, Jaipur, India.

Ravi Agarwal
Centre for Converging Technologies, University of Rajasthan, Jaipur.

Keywords: ICP-MS (Inductively Coupled Plasma Mass Spectrometer), Chondrite, PGE.

Abstract: Strong Siderophile, chalcophile affinity, high résistance to form oxygenated compounds and refractory nature of platinum-group elements (PGE: Ru, Rh, Pd, Os, Ir, and Pt) makes them important geochemical and cosmochemical tracers. The abundances of elements in meteorite are, to a large extent controlled by their volatility (inverse of refractory). The abundances of platinum-group elements (PGEs) can put a strong constrain on the nature and timing of chemical fractionation of meteorite and early solar system. So it is very important to precise determination of platinum-group elements, even also in very small fragments of meteorite (like chondrules, CAI etc.) and other object in order to significantly increase our understanding about formation of solar system. Hence we have worked out and develop the procedure for the precise determination of platinum-group elements in ≈ 1 mg sample of bulk meteorite by ICP-MS (Inductively Coupled Plasma Mass Spectrometer). Here we detail the procedure and demonstrate the feasibility and reproducibility by analyzing several aliquots of Allende standard.

Introduction: Platinum group elements (PGE: Pt, Pd, Rh, Ir, Ru and Os) have similar physical and chemical properties to one another in many respects but their behavior differs markedly from their congeners (the transition metals Fe, Ni and Co) Group 8b of the periodic table [1, 2]. PGEs are distinguished by their refractory nature (except for Pd), high résistance to form oxygenated compounds and siderophile character. These make PGEs a useful geochemical and cosmochemical tracer. The PGEs together with Au constitute a coherent group of siderophile and chalcophile elements with lower vapor pressures then Fe therefore having a strong repulsion to form oxygenated compound - the so-called 'noble' character. The resistance of PGE to oxidation is important for understand their cosmochemistry, within a wide range of oxygen and sulfur fugacities PGEs commonly exhibit siderophile and chalcophile behavior which together control the condensation behavior of PGEs in solar system as pure metal or alloys instead of forming oxygenated compounds. The PGEs are much important as they have distinctive cosmochemical behavior that helps to reconstruct some evolutionary aspects of the meteorite and planets. In only addition, they have a great economical relevance also.

Experimental and analysis Technique: Conventional ICP-MS (its sample introduction system) involves the analysis of sample in solution form for the analysis; these imply that the meteorite sample should be brought in the solution form by chemical dissolution. Standard calibration curve is prepared between counts and standards concentration (with correlation coefficient 0.99998 of all PGEs). Fig 1a, b plotted calibration curve of PGEs.

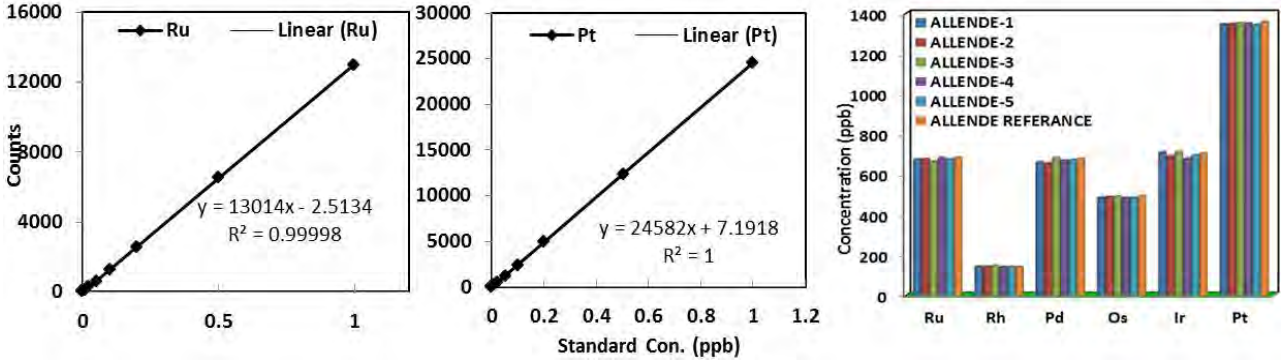

Fig. 1 Calibration curve of Ru (Fig a) and Pt (Fig b) used for the determination of sample concentration. Linearity of the calibration line show the detection ability (Limit) of ICP-MS, accuracy in measurement. Slop of the celebration line and correlation coefficient is given with the curve. The absolute concentration Platinum Group Element (PGEs) in Allende standard as sample (fig c). Reproducibility of the curve shows the feasibility of the analysis with ≈ 1 mg sample amount.

Discussion: As a test of the overall reproducibility of the adopted method, five different aliquots (all ≈ 1 mg) of Allende standard as sample are analyzed. Absolute abundances of PGEs in all aliquot of Allende standard analysed by this technique is plotted with reference values [3] are plotted in fig. 1c. Plot shows PGEs abundance in Allende standard powder determined by this technique is reproducible within 0.4-3.5% (2σ) for all PGEs. The novel method for the analysis of meteorite by conventional ICP-MS, documented in this work, presently many advantages by the analysis of small fragments in meteorite like chondrule, CAI (Ca- Al rich inclusion) mineral and metal phases can be conveniently exploited to improve our knowledge of these materials, from chemical classification to cosmochemical evolution.

Result and Conclusion : We have demonstrated the capability to measure the abundances of PGEs in ≈1 mg amount specimen of meteorites with sufficient precision by ICP-MS. Using this technique the abundances of the highly siderophile elements (HSE) Os, Ir, Ru, Pt, Rh and Pd are determined in carbonaceous CV3 chondritic meteorite Allende by developing an analytical technique that permits the precise and accurate measurement of all HSE from the same digestion aliquot. Feasibility and reproducibility of the analysis with 1 mg sample by ICP-MS, five Allende standard are analyzed as sample (≈ 1 mg). Fig 1c demonstrate the reproducibility of analyzed PGEs in five aliquots of ≈ 1 mg Allende standard as sample, close agreement with the reference values shows the feasibility of analysis with ≈ 1 mg sample by ICP-MS.

References

[1] Agrawal N K, Suruchi Goel, Murty S V S 2010 A Study of Platinum Group Elements (PGE's) in Meteorites; 16th National Space Science Symposium 2010 (NSSS-2010) **PS-4** P28 159.

[2] Westland A D 1981 Inorganic chemistry of the platinum-group elements; CIM Special Volume **23** 5-18.

[3] Jochum K P 1996 Rhodium and other platinum-group elements in carbonaceous chondrites; Geochim. Cosmochim. Acta **60** 3353-3357.

Missing Abstract

ID: 343a

ID: 360

Mechanical Response of a Particle Filled Elastomer Subject to Biaxial Loading

Francesco Pancheri
Tufts Mechanical Engineering dpt.

Abstract:
In this presentation we show new experimental results obtained using a particle filled elastomer subjected to plane stress uniaxial, equibiaxial and biaxial periodic loading-unloading tests. All tests are performed using real time strain control of the sample's gage region. Taking a phenomenological approach, we demonstrate the vital role played by using a comprehensive set of experimental data to perfect the constants of Ogden's hyperelastic model representative of the first loading of the material. Through a novel biaxial test procedure, we show that when the material is first subject to uniaxial extension the material undergoes isotropic softening but the damage imparted by periodic loading and unloading is stored only in the direction of stretch and does not alter the Mullins type effect in the orthogonal axis. The material becomes transversely isotropic. Finally, the new biaxial experimental results also validate the stress softening typical of the Mullins effect does not depend on peak stress but on the maximum stretch experienced by the material.

ID: 549

Multi-scale Characterization of Novel Aluminum-Carbon Nanocomposites Called Covetics

Iwona Jasiuk
Department of Mechanical Science and Engineering
University of Illinois at Urbana-Champaign
United States

Sabrina Nilufar
Department of Mechanical Science and Engineering
University of Illinois at Urbana-Champaign
United States

Abstract:

Nanocarbon metals called "covetics" are a new class of materials which consist of a metal (copper, aluminum, zinc, silver, gold, or other metal) and carbon nanofillers. In these materials, a carbon nanosized phase is combined with a metal in a new way not yet observed in the currently known materials. This leads to new and often improved properties of these materials compared with the corresponding pure metals and alloys.

We characterized the composition, structure, and mechanical properties of 7075 aluminum covetics with 0, 3 and 5 wt% carbon (C), which were manufactured by Third Millennium Metals, Inc. The materials were in the T0 condition and cold-rolled ten times to a thickness of 1.0 mm (0.04 in) from the as-cast 1.0 cm (0.40 in) thick sheets. All three billets were cast in the same durance and rolled in the same batch after side by side homogenization.

Multi-scale characterization techniques included density measurement, structure imaging using scanning electron microscopy (SEM), composition measurements using SEM-energy dispersive spectroscopy (SEM-EDS), and mechanical testing including tensile and indentation tests.

Densities of 7075 Al covetics were obtained by measuring the weight and volume of at least five samples. Theoretical densities were predicted by applying the following formula: theoretical density = $\rho_f \nu_{f+} \rho_m \nu_m$, where, ρ_f = filler density, ρ_m = matrix density, ν_f = volume fraction of filler, and ν_m = volume fraction of matrix. In calculations we assumed the density of amorphous carbon as 1.8-2.1 g/cm^3 and the density of 7075 Al as 2.81 g/cm^3 and no voids. Measured densities, which agreed with theoretical predictions, were slightly lower for covetics.

Tensile specimens were prepared in accordance with the ASTM Standard E-8/E8M-09 sub-size specifications with a 25 mm (1.0 in) gauge length. The tensile test was performed in air at room temperature using an MTS servo hydraulic materials testing machine (MTS 22 kips load cell) operated at a constant crosshead speed of 0.0254 mm/s (0.001in/s). Four samples of each kind were machined to the same length in three different orientations (0^0, 45^0, 90^0) to the direction of

rolling. Load-displacement data were recorded and used to obtain stress-strain curves and calculate Young's modulus E, ultimate tensile strength UTS, 0.2% yield strength YS and % elongation %EL. The results show considerable increase in UTS and 0.2% YS with carbon content increase. The UTS increased by 40% (from 0 to 5% C) for a 0 degree orientation, from about 400 MPa to nearly 600 MPa. Similarly, 0.2% YS increased by 41% (from 0 to 5% C) for covetics as compared to base Al alloy at 0^0 orientation as shown in Figures 1 and 2. Note that strength increased significantly higher than the strain hardening created by the rolling process alone. From Al data from the Aluminum Association's Engineering Data for Aluminum Structures, standard Al 7075-0 as cast has a UTS = 275 MPa. Ductility also increased for covetics but elastic modulus E remained unchanged (about 70 GPA for all cases).

Vickers and Rockwell hardness tests also showed improved properties for covetics. More specifically, for 5wt% C covetics Vickers hardness increased by 33% and Rockwell hardness increased by 32%. In addition, nanoindentation was performed on the same rolled sheets as used for tensile and hardness tests in the plane parallel to the rolling direction. Indentations were conducted using a Hysitron TI 950 TriboIndenter® with a diamond Berkovich tip. For all test areas, 8000 μN load-controlled indents were applied using a 5 sec load, 2 sec hold and 5 sec unload function. Measured quantities were the reduced elastic modulus E_r and hardness H. Both E_r and H increased for covetics. Reduced modulus (Er) and hardness increased by 8% and 43% respectively for covetics (5 wt%) as compared to 0 wt%C 7075 Al alloy.

The SEM micrographs of fractured tensile samples of the covetics and 7075 Al alloy were also analyzed. No significant differences were observed at lower magnifications, but higher magnifications (20,000X) revealed less ductile local failure behavior for covetics. It was observed from the SEM images show that carbon was dispersed very well in the Al matrix and not visible. EDS data provided qualitative chemical composition of the covetic materials.

These experimentally obtained data serve as inputs for multi-scale modeling of covetics.

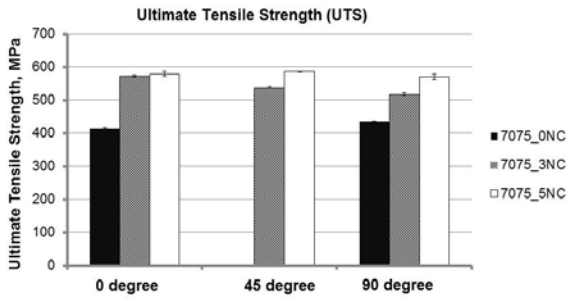

Figure 1. Ultimate tensile strength.

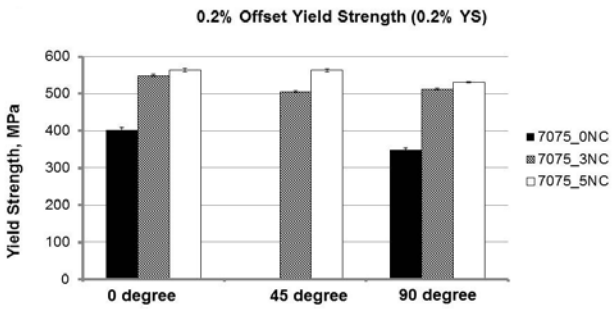

Figure 2. 0.2% yield strength.

Missing Abstract

ID: 588

ID: 703

Direct Measurements of the Carbon Nanotube-Polymer Interfacial Strength

Xiaoming Chen
SUNY at Binghamton
USA

Meng Zheng

Abstract:
Understanding the interfacial stress transfer between carbon nanotubes (CNTs) and polymer matrices is of great importance to the development of CNT-reinforced light-weight and high-strength polymers. In this paper, we present our recent work on studying the interfacial strength between Poly(methyl methacrylate) (PMMA) and the embedded individual CNTs. The mechanical strength of the CNT-PMMA interface is quantitatively characterized by using an in-situ scanning electron microscopy single-tube pull-out testing scheme. By pulling out individual tubes from the polymer matrix using atomic force microscopic force sensors inside a high resolution electron microscope, the pull-out force and the embedded tube length are measured with resolutions of sub-nN and nm, respectively. Our results reveal the dependence of the pull-out force on the embedded tube length. Our work contributes directly to a better understanding of the failure mechanism of the nanotube-polymer interface and the mechanical properties of nanotube-reinforced polymer composites.

ID: 754

Temperature Dependence of Thermal Expansion Coefficient, Effective Elastic Modulus and Electrical Conductivity of Porous YSZ-Ni Composites

S. Ali Tabei
Georgia Institute of Technology
USA

Majid Baniassadi

Abstract:
Yittria-Stabilized Zirconia (YSZ)-Ni composite is amongst the top candidates for anode material in solid oxide fuel cells (SOFCs). Functioning temperatures of SOFCs could be up to 1000°C, therefore investigation of temperature dependence of mechanical and electrical properties of the constituting materials is crucial. A Three-dimensional (3D) reconstruction of the microstructure of a three phase composite (Ni, YSZ and voids) is already accomplished by using a Monte Carlo method based on two-point statistical correlation functions. In this study, the previously reconstructed microstructure is exploited to investigate the effects of temperature on the effective elastic modulus, electrical conductivity and thermal expansion coefficient of the virtual microstructure. Finite elements simulation was used to derive the temperature dependence of the aforementioned properties. Analytical calculations of mechanical and thermal properties are also made which in addition to comparison to experimental results, makes the FEM simulations acceptable.

ID: 763

Characterization of Residual Stress Distributions at the Continuum Scale Using Diffraction-Based Lattice Strain Data at the Crystal Scale

Paul Dawson

Matthew Miller

Abstract:
In this talk, we present a computational framework for evaluating residual stress distributions in engineering components manufactured with polycrystalline structural alloys. The framework is designed to fully utilize lattice strain data from spatially-resolved diffraction measurements taken over the domain of the component, such as those possible with either high energy x-ray or neutron sources. A key attribute of the framework is the definition of two, coexisting stress fields: a continuum field and a crystal scale field. The continuum field satisfies the constraints from equilibrium and surface tractions; the crystal scale field is derived from the lattice strains measured using by diffraction. To effectively handle the distinct demands required of the two fields, the framework combines a traditional, element-based discretization for the continuum stress field with an element-free discretization for the crystal scale stress field. Parameters used in the discretization of the two fields are evaluated by minimizing a weighted residual defined by the difference between these fields over the full domain of the component. The framework thereby links the continuum scale field across the dimensions of a component to the elastic strains measured at the crystal scale. As an example, we present the residual stress field imparted by an interference fit of a disk onto a circular shaft. Using lattice strain data generated by high energy x-ray diffraction, residual stress distributions are determined for two different cases, one having a two-dimensional and the other a three-dimensional stress field.

ID: 774

Atomic Structure Determination by Fusing Atomic Probe Tomography and Scanning Transmission Electronic Microscopy

Dongsheng Li
Pacific Northwest National Lab

Zhijie Xu

Abstract:
With the development of Local Electrode Atomic Probe (LEAP), the atomic structure determination is expanding from metallic alloys to heterogeneous materials with complex structure and compositions. This makes the 3D atomic structure determination possible for most energy materials applied in battery, fuel cell, semiconductors, and nuclear science. However, the traditional structure reconstruction introduces false magnification and large errors due to the assumption of uniform and isotropic evaporation. New efficient and accurate reconstruction algorithms enhanced by spatial and chemical information from STEM are crucial for next generation atomic structure reconstruction. We proposed an efficient and accurate method combining numerical simulations and experiments to determine 3D atomic structures from APT for complex heterogeneous materials with anisotropic and heterogeneous evaporation behavior. Novelty of this approach is to apply a Level Set evaporation model and iterative algorithms to reconstruct 3D structure using the structure information obtained from STEM. Current evaporation models for APT widely utilize the approach of finite element method, which is computational expensive and inaccurate when interface normal is involved in the calculation for atomic evaporation. Our preliminary results in evaporation model demonstrated an increase of efficiency with no sacrifice of accuracy comparing with the standard FE method. This established a solid foundation for the further iterative algorithm in
comparing with simulation using microstructure information obtained by discrete chemical imaging modality. Simultaneously, we also applied crystal plasticity finite element method to predict the microstructure evolution during thermomechanical processing after large strain. Combining this with microstructure reconstruction and crashworthiness model, we developed the capability.

IV.4

Multiscale Mechanics of Materials - Advances in the Study of Defects through Atomistic/Continuum Coupling Methods

ID: 122

Objective Density Functional Theory: A First Principles Method for the Simulation of Objective Structures

Amartya Banerjee
University of Minnesota

Ryan Elliott

Abstract:
Objective structures are atomic/molecular configurations which generalize the notion of crystals and are such that all the constituent atoms/molecules of the structure see the same environment up to orthogonal transformations and translations. Some of the most widely studied atomic/molecular structures in materials science and nanotechnology fall into the category of objective structures. The list of objective structures includes nanotubes, bucky balls, tail sheaths and capsids of viruses, graphene sheets and molecular bilayers. Due to the presence of high degrees of symmetry, objective structures are likely to be associated with remarkable material properties - particularly, collective material properties such as ferromagnetism and ferroelectricity. A systematic study of objective structures therefore, is likely to lead to the discovery of novel materials. At the same time, formulation of computational methods specifically designed for studying objective structures, is likely to lead to the development of novel nanomechanicssimulations methodologies. Following this line of thought, we have been developing Objective Density Functional Theory - a suite of rigorously formulated quantum mechanical theories and numerical algorithms for carrying out abinitio simulation studies of objective structures. In this work, we discuss the essential ingredients of objective density functional theory. First, using tools from Group Representation Theory, we demonstrate how the equations of Kohn-Sham Density Functional Theory for objective structures admit symmetry adapted cell problems. Then, we discuss spectral discretization strategies for these cell problems as well as the efficient implementation of the resulting numerical schemes. We highlight the role played by symmetry in the choice of basis functions, the computation of electrostatic potentials through series expansions and the block-diagonalization of the hamiltonian. Finally we discuss our usage of objective density functional theory for carrying out symmetry adapted abinitio molecular statics and moleculardynamics computations of specific objective structures.
.

ID: 147

Three-dimensional Quasicontinuum Simulations of Fracture Initiation Under Mixed Modes in Fe

Jaime Marian
Lawrence Livermore National Laboratory

Inga Vatne

Abstract:
Simulations of fracture initiation and crack propagation under modes I and II are translationally invariant and thus typically performed in 2D to simulate a semi-infinite solid. When out-of-plane mode III or mixed modes are considered, however, the crack responds three-dimensionally in terms of the growth mechanism and/or the plastic features observed. In addition, in real crack fronts, dislocations are emitted as loops with a characteristic length-scale. To capture this length scale and faithfully represent materials behavior, 3D simulations must be employed. Because crack growth is mediated by processes operating at the atomic scale, atomistic resolution is desirable near the crack tip. However, far away from it the laws of elasticity are sufficient to describe the material response and a continuum representation of the material is adequate. The Quasicontinuum method (QC) suggests itself as an ideal technique to bridge both of these limits, yet providing a seamless and consistent description between them. Here, we perform QC simulations of crack growth in static conditions for bcc Fe and compare 2D to fully 3D conditions. We calculate the critical stress intensity factors under both scenarios and identify the growth mechanisms operating in each case. We analyze and categorize the dislocation structures emitted and compare the QC results to expected solutions from analytical models.

ID: 182

Multiscale Atomistics with Electrostatic Interactions

Jason Marshall
Carnegie Mellon University
United States

Kaushik Dayal
Carnegie Mellon University
United States

Abstract:

Atomic-scale defects in ionic solids play a central role in enabling their properties: for example, the electromechanics of multifunctional ferroelectrics occurs by the nucleation and motion of domain wall defects. Additionally, complex geometric features such as cracks and free surfaces play a crucial role in the structure and interaction of these defects.

I will describe a multiscale atomistic method that accurately and efficiently models defects in these materials. A key challenge is atoms in these materials interact through long-range electrostatic forces, leading to different mechanics than in structural materials where interactions are primarily short-range. The long-range interactions are intractable to existing atomistic multiscale methods that are geared towards short-range interactions. Our method, based on rigorous ideas of continuum limits of dipole lattices, deals with this challenge by exploiting the atomic-scale polarization density as a multiscale mediating quantity. We demonstrate the method on examples of ferroelectrics under complex electrical and mechanical loading.

Below are results of an externally applied electric field to an electromechanical material. The picture on the left shows the change in polarization in the x direction. The picture on the right shows the equivalent stress.

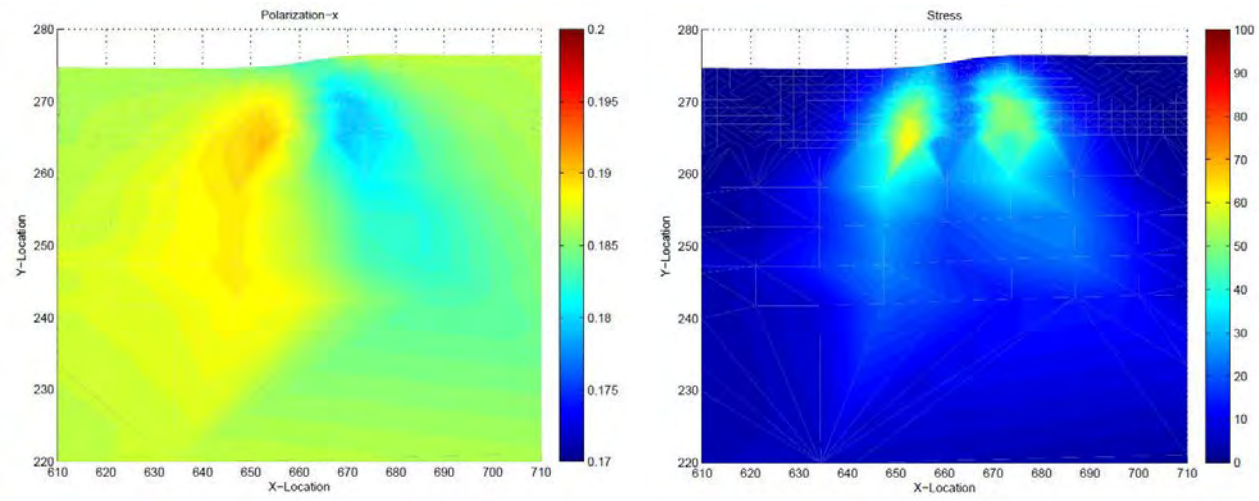

ID: 235

A Gamma-Convergence Analysis of the Quasicontinuum Method

Malena I. Español
University of Akron
United States

Dennis M. Kochmann
California Institute of Technology
United States

Sergio Conti
University of Bonn
Germany

Michael Ortiz
California Institute of Technology
United States

Abstract:

The quasicontinuum (QC) method was introduced in [1, 2] to overcome the practical limitations of classical atomistic modeling in terms of simulating time and space, by combining a fully atomistic description with approximation methods of the finite element technique commonly applied to problems of continuum mechanics. In this work, we investigate the convergence of quasicontinuum approximations of harmonic atomistic models by means of Gamma convergence [3, 4]. We consider an infinite harmonic crystal in n dimensions, belonging to an arbitrary crystal class and governed by general force constants, deforming under applied loads. The deformations of the crystal are constrained by a general interpolation (not necessarily uniform or periodic) defined from a restricted set of atoms, and the energy sums are approximated by means of a general summation rule (not necessarily uniform or periodic). Using the tools of Gamma-convergence (a variational notion of convergence which, in particular, implies convergence of energy minimizers), we identify general conditions on the interpolation scheme for the sequence of approximating energies to be convergent. This type of convergence shows that the potential energy computed from the discrete atomistic description and the quasicontinuum formulation coincide in the limit of infinite refinement (in other words, both representations yield identical crystal energies when viewed from a macroscopic viewpoint). We also propose a numerical patch test to confirm the veracity of our conclusions, which does not require mesh refinement but is based on the rescaling of an external force field: as the oscillatory field becomes smoother and smoother, the equilibrated energy of the QC-discretized body converges towards the limit of the atomistic model for an affine deformation. We report results for such a numerical patch test for a three-dimensional mesh-free quasicontinuum model that confirms our findings.

References:

[1] E. B. Tadmor, M. Ortiz, and R. Phillips. Quasicontinuum analysis of defects in solids. *Philosophical Magazine A,* 73 (6):1529-1563, 1996.

[2] J. Knap and M. Ortiz. An analysis of the quasicontinuum method. *Journal of the Mechanics and Physics of Solids,* 49:1899-1923, 2001.

[3] G. Dal Maso. *An Introduction to Gamma-convergence.* Progress in Nonlinear Differential Equations and their Applications, 8. Birkhäuser Boston Inc., Boston, MA, 1993.

[4] A. Braides. *Gamma-Convergence for Beginners,* Oxford Lecture Series in Mathematics and its Applications, Oxford University Press, Oxford, 2002.

ID: 262

Quasicontinuum modeling of coupled mechanical/diffusion problems

Ignacio Romero
Technical University of Madrid
Spain

María P. Ariza
University of Seville
Spain

Mauricio Ponga
University of Seville
Spain

Michael Ortiz
California Institute of Technology
United States

Abstract:

The Quasicontinuum method (QC) was proposed more than fifteen years ago [1] as a modeling approach for the solution of mechanical problems where atomistic resolution is required in a localized subset of the analysis domain. Initially, the QC was applied to the solution of mechanical problems in solids with defects. More recently, the method has been extended to encompass coupled thermo-mechanical problems [2,3] and mass-diffusion problems [4], enabling the full analysis of continuum/atomistic domains of alloys, at finite temperature, and even kinetic phenomena.

The development of QC formulations for multi-species solids with non-homogeneous temperature distributions relies on three aspects. First, a theory is required that describes equilibrium and away-from-equilibrium thermodynamics of many-particle solids. Second, a kinetic theory governing the rate problem must be provided to describe the evolution of the system. Third, a coarse-graining of the full thermodynamic problem must allow bridging the continuum and atomistic scales.

The third feature, the atomistic-to-continuum coupling, need not be different than the standard coarse-graining scheme in the purely mechanical QC. In this talk we will focus on the other two aspects: we will present a theory on non-equilibrium thermodynamics suitable for many particles bodies based on Jaynes' maximum entropy principle, and we will describe a kinetic theory which adapts Onsager's to the type of system under study.

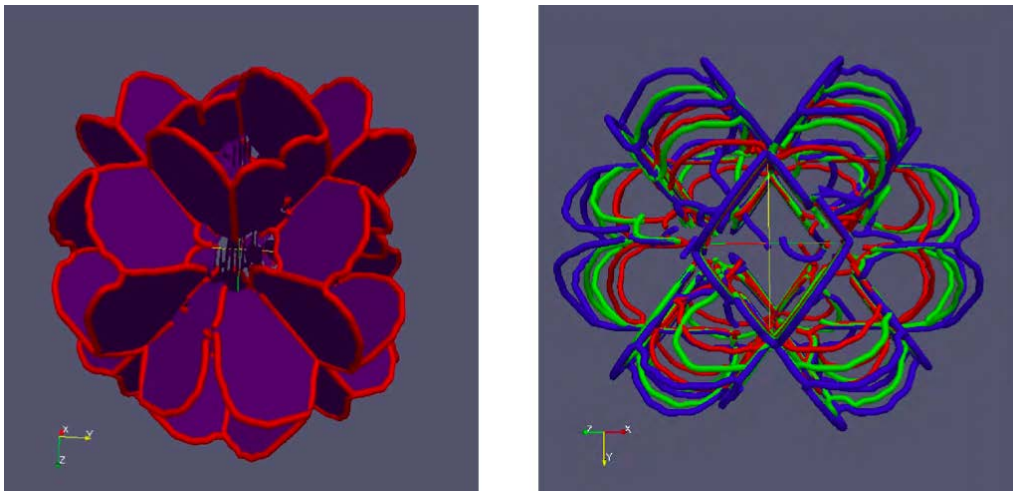

Cu crystal (with nanovoid) subjected to triaxial loading. Loop structures (left) and loop evolution (right)

Two aspects are particularly noteworthy in the approach proposed. First, by recourse to meanfield theory and the use of variational updates [5], the solution to the fully coupled transient problem will be identified as the stationarity point of a single functional, hence simplifying the formulation of numerical methods. Second, using ideas from Discrete Exterior Calculus, the kinetic model that we propose would discrete from the outset, hence sidestepping the need for discretizing Fourier and Fick's laws.

Numerical examples will be presented for coupled thermo-mechanical and mechano-diffusive problems. For the thermal proble, we will describe the simulation of nanovoid growth in copper under uni- and tri-axial loading, including heat effects. For the second, several validation examples will be shown of mass transfer in Cu-Ni alloys.

[1] E B Tadmor, M Ortiz, and R Phillips. "Quasicontinuum Analysis of Defects in Solids." *Philosophical Magazine A* 73, no. 6 (1996): 1529–1563.

[2] Y Kulkarni, J Knap, and M Ortiz. "A Variational Approach to Coarse Graining of Equi Librium and Non-Equilibrium Atomistic Description at Finite Temperature." *Journal of the Mechanics and Physics of Solids* 56. (2008): 1417–1449.

[3] L. Dupuy, E. Tadmor, R. Miller, and R Phillips. "Finite-Temperature Quasicontinuum: Molecular Dynamics Without All the Atoms." *Physical Review Letters* 95, no. 6. (2005): 1–4.

[4] Venturini, G. Topics in Multiscale Modeling of Metals and Metallic Alloys. PhD Thesis. California Institute of Technology, 2011.

[5] Q Yang, L Stainier, and M Ortiz. "A Variational Formulation of the Coupled Thermo-Mechanical Boundary-Value Problem for General Dissipative Solids." *Journal of the Mechanics and Physics of Solids* 54 (2006): 401–424.

ID: 309

Atomistics based multiscale predictions of age hardening curves in Al-Cu alloys

Chandra Veer Singh
University of Toronto
Canada

Abstract:

Precipitation hardening is one of the most commonly used ways of achieving high strength structural alloys. Precipitates restrict dislocation motion, thereby increasing alloy strength. The first historic flight by Wright Brothers inadvertently utilized this phenomenon, but it was not understood until 1930's and 40's when the theory of dislocation was developed by Taylor [1], Orowan [2] and Polanyi [3]; and the observation of nanometer-sized solute clusters by X-ray scattering by Guinier [4] and Preston [5]. In the later part of 20th Century, precipitation hardening has significantly progressed in achieving higher and higher alloy strengths, and industrial usage, especially the aerospace industry wherein about 50% of external structure is made from Al-xxx alloys. Nonetheless, the design process to achieve strong precipitation hardened alloys has remained largely empirical in nature. This is because direct investigation of precipitation hardening process was out of reach mainly due to the complexity of the hardening mechanisms and their atomistic nature until recently when exponential improvements in computational power and the accuracy of atomistic modelling techniques. Consequently, now it is possible to quantitatively investigate the inherent mechanisms of dislocation-precipitate interactions and its role in the resultant hardening contribution.

With this theme in mind, here we present a hierarchical multiscale model that combines atomistic simulations, dislocation line tension simulations, and analytic modeling to predict age hardening. As the foundation of our multiscale approach, atomistic modeling serves two purposes: (1) computation of solute-dislocation interactions energies for input into a semi-analytic solute hardening model and (2) evaluation of precipitate strengths for use in continuum dislocation line tension simulations. The precipitate microstructure in the dislocation line tension simulations is obtained from simple analytic precipitate kinetics relations. The proposed model is employed to predict aging curves in binary Al-Cu alloys. The model predictions are found to correspond quite well with experiments. As a whole, this work aims to better illuminate the current state of physics-based plasticity modeling and highlight important challenges that remain.

At first, large scale atomistic simulations were performed to investigate dislocation interactions with Guinier-Preston (GP) zones [6] and θ''-precipitates using LAMMPS software. The code was modified to use a recently developed Angular Dependent Potential (ADP) [7]. A variety of dislocation bypass mechanisms, including well known Friedel and Orowan mechanisms were found to occur depending on the orientation of GP zone with respect to the dislocation glide plane, GP zone and θ''-precipitate sizes, offset of the precipitates from dislocation glide plane, temperature [7], and dislocation character [8]. Critical resolved shear stresses (CRSS) were measured from the atomistic calculations for different combinations of parameters affecting

dislocation-precipitate interactions. This serves as an input for the line tension dislocation dynamics model which calculates the overall precipitation hardening contribution to the flow strength of the alloy due to specific precipitation microstructure in the alloy at a given aging time, i.e. accounting for the distribution of precipitate sizes, types, their random placement in the microstructure following the kinetics of the aging process. Finally, after combining both solute and precipitation hardening contributions at different aging times, the age hardening curves are drawn. Since this data corresponds to 0K atomistic simulations, the role of thermal activation is investigated for a specific GP zone-dislocation interaction. The relation between precipitation hardening at 0K and 300K is found and the age hardening curves are re-scaled to correspond to room temperature data. The comparison of our predictions with experiments is shown in Fig. 1.

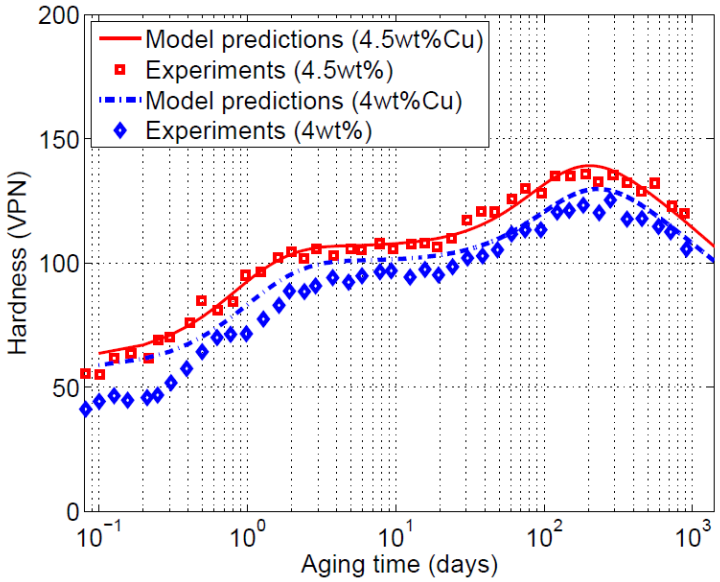

Figure 10: 300 K hardness vs. aging time predictions for Al-Cu aged at Tage = 110◦C. Experimental data is from Silcock et al. [9].

References

[1] Taylor, G. I., 1934. The mechanism of plastic deformation of crystals. Part I. Theoretical. Proc R Soc Lond A 145 (855), 362–387.

[2] Orowan, E., 1934. Z Phys 89, 634.

[3] Polanyi, M., 1934. Z. Phys. 89, 660.

[4] Guinier, A., 1939. Ann. Phys. 12, 161 .

[5] Preston, G. D., 1938. Philos Mag 26, 855.

[6] Singh, C. V., Warner, D. H., 2010. Mechanisms of Guinier-Preston zone hardening in athermal limit. Acta Mater 58 (17), 5797–5805.

[7] Apostol, F., Mishin, Y., 2011. Interatomic potential for the Al-Cu system. Phys Rev B 83, 054116.

[8] Singh, C. V., Mateos, A., Warner, D. H., 2011. Atomistic simulations of dislocation-precipitate interactions emphasize importance of cross-slip. Scripta Mater 64, 398–401.

[9] Silcock, J. M., Heal, T. J., Hardy, H. K., 1953-54. Structural ageing characteristics of binary al-cu alloys. J Inst Metals 82, 239–248.

ID: 314

A New Quasicontinuum Formulation Based on Local Maximum-Entropy Interpolation

Dennis Kochmann
California Institute of Technology
USA

Abstract:
Modeling the mechanical behavior of solids at the micro- and nanometer scale is challenging as the discrete nature of the crystal becomes apparent: simulations using molecular dynamics provide the required accuracy but come with prohibitively high computational expenses severely limiting the simulation capabilities. Continuum models are much more attracting yet not suitable at those scales where the continuum hypothesis breaks down. Hence, multiscale techniques are needed to bridge the scales from atomistics to the continuum. The quasicontinuum (QC) method was introduced to overcome the practical limitations of classical atomistic modeling in terms of simulation time and space. The QC methodology employs a combination of full atomistic resolution in regions of high variations and an approximate continuum model in the major part of the simulation domain away from those regions. As the continuum description is based on discrete lattice statics with atomic positions constrained by an interpolation scheme, the model can be solely based on atomistic potentials without the need for phenomenological continuum models. Here, we present a new quasicontinuum formulation that is based on a meshfree interpolation scheme (making use of local maximum-entropy shape functions) to result in tunable accuracy and efficiency and to pave the road towards improved model adaption capabilities. In addition, we demonstrate sample applications of the new technique.

ID: 366

Hyper-QC: Accelerated Finite-Temperature Quasicontinuum Simulations Using Hyperdynamics

Ellad Tadmor
University of Minnesota
USA

Woo Kyun Kim
USA

Abstract:
The quasicontinuum (QC) method is a spatial multiscale method which extends the length scales accessible to fully-atomistic simulations (like molecular dynamics (MD)) by several orders of magnitude. While the recent development of the so-called hot-QC method enables dynamic simulations at finite temperature, the times accessible to these simulations remain limited to the sub-microsecond time scale (like those of traditional MD) due to small time step required for stability of the numerical integration. As a result, the loading rates in hot-QC and MD simulations are much larger than those in typical experiments, which can distort the resulting deformation mechanisms. In recent years several accelerated MD schemes such as hyperdynamics, parallel replica dynamics, and temperature-accelerated dynamics have been developed to simulate systems with extended time scales. In this study, we develop a novel finite-temperature QC method which can treat much longer time scales by coupling the hot-QC method with hyperdynamics, one of the accelerated MD schemes. We refer to this approach as hyper-QC. As in the original hyperdynamics method, hyper-QC utilizes a characteristic evolution of dynamical systems with a separation of time scales between short atomic vibration periods and long waiting times at each metastable state. Therefore, the hot-QC potential energy is modified such that the energy barriers are reduced to shorten waiting times while the characteristic dynamics are preserved. The methodology is validated by comparing hyper-QC results with those of full MD for 1D and 2D example problems.

ID:376

Higher-Order Adaptive Finite-Element Methods for Kohn-Sham Density Functional Theory

Phani Motamarri
Graduate Student, Department of Mechanical Engineering,
University of Michigan, Ann Arbor

Vikram Gavini
Assistant Professor, Department of Mechanical Engineering,
University of Michigan, Ann Arbor

Abstract:
Many macroscopic properties of solids are influenced by complex interplay of defects. A mathematical model which accurately describes such defects must include both the electronic structure of the defect core at the quantum mechanical length scale and also elastic and electrostatic interactions at the coarse (micrometer and beyond) scale. One of the most popular electronic structure theories derived from first principles is the widely used Kohn-Sham density-functional theory (DFT). However, the complexity of the Kohn-Sham DFT calculations still restricts the computation to a few hundreds of atoms. To extend the DFT calculations to realistic sample sizes that can accurately capture the long ranged fields generated by defects, an efficient multi-scale approach that can seamlessly connect quantum mechanical and continuum scales is highly desirable. Development of real-space electronic structure calculations using a finite-element discretization of DFT is an important step in this direction. The ability to handle complex geometries, arbitrary boundary conditions and more importantly the coarse graining nature of the basis sets makes finite-elements highly desirable especially in problems involving defects. As a first step towards developing a multi-scale method with Kohn-Sham DFT as the sole input physics, it is desirable to develop a robust and an efficient computational framework for the real-space finite-element discretization of the Kohn-Sham DFT problem.

One of the recent works in the above direction is the development of a real-space, non-periodic, finite element formulation for the Kohn-Sham DFT problem [1]. However, it is observed linear finite-elements require a large number of basis functions—of the order of 100,000 basis functions per atom—to achieve chemical accuracy in electronic structure calculations, and this compares very poorly with plane-wave basis or other real-space basis functions. Prior investigations [2] have demonstrated that higher-order finite-element discretizations can alleviate this degree of freedom disadvantage of linear finite-elements. However, the use of higher-order elements increases the per basis-function computational cost due to the need for higher-order accurate numerical quadrature rules. Furthermore, the bandwidth of the matrix increases cubically with the order of the finite-element, which in turn increases the computational cost of matrix-vector products. In addition, since a finite-element basis is non-orthogonal, the discretization of the Kohn-Sham DFT problem results in a generalized eigenvalue problem, which is more expensive to solve in comparison to a standard eigenvalue problem resulting from using an orthogonal basis (for e.g. plane-wave basis). Thus, the computational efficiency

afforded by using a finite-element basis in electronic structure calculations, and its relative performance compared to plane-wave basis and other real-space basis functions (for e.g Gaussian basis), has remained an open question to date. A recent investigation [3] in the context of orbital-free DFT has indicated that the use of higher-order finite-elements can significantly improve the computational efficiency of the calculations. We extend this investigation to study the Kohn-Sham DFT problem in the present work.

In this work [4], we present an efficient computational approach to perform real-space electronic structure calculations using an adaptive higher-order finite-element discretization of Kohn-Sham density-functional theory (DFT). We use the self-consistent field formulation of the Kohn-Sham DFT problem as our starting point. In order to aid our study, we first develop estimates for the discretization error in the ground-state energy in terms of the ground-state electronic fields (wavefunctions and electrostatic potential) and characteristic mesh-size. These error estimates and the *a priori* knowledge of the asymptotic solutions of far-field electronic fields are used to construct mesh coarsening rates for the various benchmark problems considered in this work. Since the finite-element discretization of the Kohn-Sham problem results in a generalized eigenvalue problem, which is computationally expensive to solve, we propose an efficient solution strategy for solving the discrete eigenvalue problem by using spectral finite-elements in conjunction with Gauss-Lobatto quadrature, and a Chebyshev acceleration technique for computing the occupied eigenspace. Using the proposed solution procedure, our numerical investigations suggest that staggering computational savings—of the order of 1000−fold—can be realized, for both all-electron and pseudopotential calculations, by using higher-order finite-element discretizations. On all the benchmark systems studied, we observe diminishing returns in computational savings beyond the sixth-order for accuracies commensurate with chemical accuracy, suggesting that the hexic spectral-element may be an optimal choice for the finite-element discretization of the Kohn-Sham DFT problem. A comparative study of the computational efficiency of the proposed higher-order finite-element discretizations suggests that the performance of finite-element basis is competing with the plane-wave discretization for non-periodic pseudopotential calculations, and is comparable to the Gaussian basis for all-electron calculations. Further, we demonstrate the capability of the proposed approach to compute the electronic structure of materials systems containing a few thousand atoms using modest computational resources, and good scalability of the current implementation up to a few hundred processors.

References:

[1] P. Suryanarayana, V. Gavini, T. Blesgen, K. Bhattacharya, M. Ortiz, Non-periodic finite-element formulation of Kohn-Sham density functional theory, J. Mech. Phys. Solids 58 (2010) 256–280.

[2] L. Lehtovaara, V. Havu, M. Puska., All-electron density functional theory and time-dependent density functional theory with high-order finite elements, J. Chem. Physics. 131 (2009) 054103.

[3] P. Motamarri, M. Iyer, J. Knap, V. Gavini, Higher-order adaptive finite-element methods for orbital-free density functional theory, J. Comp. Phys (2012) (To Appear).

[4] P. Motamarri, M. R. Nowak, K. Leiter, J. Knap, V. Gavini, Higher-order adaptive finite-element methods for Kohn-Sham density functional theory, J. Comp. Phys (under review).

ID: 377

Coarse-Graining Kohn-Sham Density Functional Theory

Phanish Suryanarayana
Georgia Institute of Technology
USA

Abstract:
Defects, though present in relatively minute concentrations, play a significant role in determining macroscopic properties. Even vacancies, the simplest and most common type of defect, are fundamental to phenomena like creep, spall and radiation ageing. This necessitates an accurate characterization of defects at physically relevant concentrations, which is typically in parts per million. This represents a unique challenge since both the electronic structure of the defect core as well as the long range elastic field need to be resolved simultaneously. Unfortunately, accurate ab-initio electronic structure calculations are limited to a few hundred atoms, which is orders of magnitude smaller than that necessary for a complete description. Thus, defects represent a truly challenging multiscale problem. Density functional theory developed by Hohenberg, Kohn and Sham (DFT) is a widely accepted, reliable ab-initio method for computing a wide range of material properties. Traditional implementations of DFT solve for the wavefunctions, a procedure which has cubic-scaling with respect to the number of atoms. This places serious limitations on the size of the system which can be studied. Further, they are not amenable to coarse-graining since the wavefunctions need to be orthonormal, a global constraint. To overcome this, we have developed a linear-scaling method for DFT where the key idea is to directly evaluate the electron density without solving for the individual wavefunctions. Based on this linear-scaling method, we have developed a numerical scheme to coarse-grain DFT derived solely based on approximation theory, without the introduction of any new equations and resultant spurious physics. This allows us to study defects at a fraction of the original computational cost, without any significant loss of accuracy. We demonstrate the efficiency and efficacy of the proposed methods through examples.

ID: 434

On the Meaning of Polarization in Crystalline Solids

Kaushik Bhattacharya
California Institute of Technology
United States

Saurabh Puri
UES Inc.
United States

Abstract:
Electrically polarized materials like ferroelectrics play a central role in a variety of technological applications, and this has motivated a large body of work in understanding its microscopic origins. This in turn raises a seemingly innocent question about the meaning of polarization. College physics defines electrical polarization as the first moment of charge. Unfortunately the first moment of a periodic distribution over an unit cell is not translation invariant, and thus this elementary definition does not allow us to define the polarization density of a crystalline solid. This talk explores this question by considering the large body limit of a crystalline solid.

ID: 442

High Temperature Response of Twin Boundaries in FCC Metals

Yashashree Kulkarni
University of Houston
USA

Tanushree Sinha

Abstract:
Nanotwinned structures have shown strong promise as optimal motifs for strength, ductility and grain stability in fcc metals in sharp contrast to their nano-grained counterparts where gains in strength are disappointingly offset by loss of ductility. Furthermore, it has been well established that nanocrystalline metals exhibit structural instability at ambient and higher temperatures via grain growth and grain boundary mediated processes such as migration, sliding and defect nucleation. However, the high temperature response of twin boundaries and nanotwinned structures has remained relatively unaddressed. This talk will present our studies on the high temperature response of coherent twin boundaries in fcc metals by way of molecular dynamics simulations. At low and intermediate temperatures, the twin boundaries exhibit normal motion coupled to shear deformation as expected. However, our simulations at higher temperatures (above 0.5-0.7 homologous temperature) reveal considerable deformation twinning, an occurrence that has not been observed before in fcc metals. We discuss a possible conjecture for this anomalous behavior based on the energetics of the competing deformation modes.

ID: 490

Illuminating the Chemo-Mechanics of Crack Tip Processes via Quantum Mechanics Based Concurrent Multiscale Modeling

Derek Warner
Cornell University

Rick Zamora

Abstract:
NO ABSTRACT

ID: 512

Hydrogen Assisted Cracking in Aluminum: A QCDFT Study

Gang Lu
University of Michgan, Ann Arbor

Yi Sun

Abstract:
Hydrogen (H) embrittlement is one of the most important problems in materials science and engineering as almost all metals and their alloys suffer to some extent of H-induced brittleness. Despite the progress in the last four decades, a complete mechanistic understanding of H embrittlement still eludes us. In this talk, I will present a quantum mechanics based multiscale modeling of H embrittlement in Al using Quasi-continuum density functional theory (QCDFT). QCDFT method concurrently couples finite-element and electronic structure calculations, and is ideally suited for this task. A complex interplay between H enhanced local plasticity and H-assisted cracking is observed in the QCDFT simulations, depending on H positions at the crack tip. The crack tip with H atoms at the front surface is much more vulnerable to cracking than that with H atoms on the crack surfaces. The top-site H atoms are particularly more corrosive in breaking Al-Al bonds comparing to the bridge sites. Dislocation nucleation and deformation twinning at the crack tip compete with the cracking and the overall embrittlement behavior depends on H position, concentration and loading conditions. The atomistic mechanism and electronic structure underlying the observed behavior will be discussed. The work was supported by the Office of Naval Research.

ID: 525

Numerical Analysis of Atomistic-to-Continuum Methods for Defects

Mitchell Luskin
University of Minnesota

Alexander Shapeev

Abstract:
Many materials problems require the accuracy of atomistic modeling in small regions, such as the neighborhood of a crack tip. However, these localized defects typically interact through long-range elastic field switch a much larger region that cannot be computed atomistically. Materials scientists have proposed many methods to compute solutions to these multiscale problems by coupling atomistic models near a localized defect with continuum models where the deformation is nearly uniform on the atomistic scale. During the past several years, a mathematical structure has been given to the description and formulation of atomistic-to-continuum coupling methods, and corresponding numerical analysis has clarified the relation between the various methods and their sources of error. This lecture will present recent developments for the numerical analysis of atomistic-to-continuum coupling methods.

ID: 610

Electronic Structure Calculations of an Edge Dislocation in Aluminum

Balachandran Radhakrishnan
University of Michigan
United States

Vikram Gavini
University of Michigan
United States

Abstract:
Dislocations play a pivotal role in mechanisms governing the plastic deformation of materials. While a qualitative understanding of the dislocation behavior has long been established, current efforts are towards quantitatively predicting the characteristics of dislocations. Continuum models can predict the long ranged elastic fields produced by dislocations, but cannot describe the defect core. Atomistic calculations have been used to study the core structure of a dislocation, but the transferability of interatomic potentials to regions of extreme deformations is yet to be ascertained. The present work uses electronic structure calculations to study an edge dislocation in Aluminum.

While electronic structure calculations have provided significant insights into the bulk properties of materials, their applicability to the study of defects in materials has been limited by the restrictive geometries and cell-sizes accessible through conventional electronic structure codes. In particular, there are vast spans of interacting length scales which govern the behavior of defects--from the electronic structure of the defect core to the long ranged elastic fields--which require electronic structure calculations at macroscopic scales. Further, in the context of dislocations, the elastic fields produced are incompatible with periodic boundary conditions that are required in a Fourier-based formulation. In the present work, we use Quasi-Continuum reduction of *orbital-free* Density Functional Theory (QCOFDFT) [1] which is a seamless multi-scale technique that uses a single electronic structure theory as its sole input physics. The key ideas used in QCOFDFT are

(i) a real-space formulation;
(ii) finite element discretization, and
(iii) an adaptive mesh retaining full discretization near the defect core and coarse graining in regions away from the core.

In the present work, using QCOFDFT, we study various aspects of an edge dislocation in Aluminum, which include the electronic-structure of a single dislocation, the associated energetics, and the dependence on macroscopic deformations. As a first step, in order to understand the electronic structure of the dislocation core, we consider a perfect edge dislocation (a/2[110]) in Aluminum with the ionic positions determined from the continuum theory. We hold the ionic positions fixed in order to first determine the appropriate cell-size required to accurately account for the electronic-structure effects of the dislocation core. In this study, we employ

periodic boundary conditions on the electronic fields along the dislocation line (<112>) and apply Dirichlet boundary conditions on the electronic fields, determined from the Cauchy-Born hypothesis, in the other two directions. Figure 1 shows the electron density contours of a perfect edge dislocation in Aluminum.

Figure 1: Electron density contour of a perfect edge dislocation in Aluminum

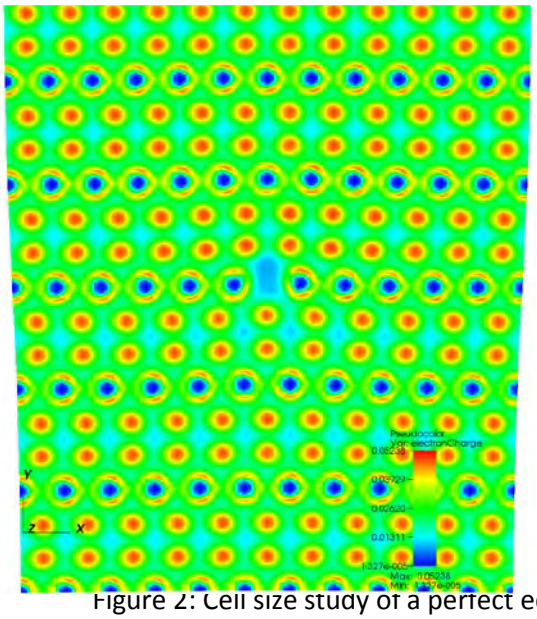

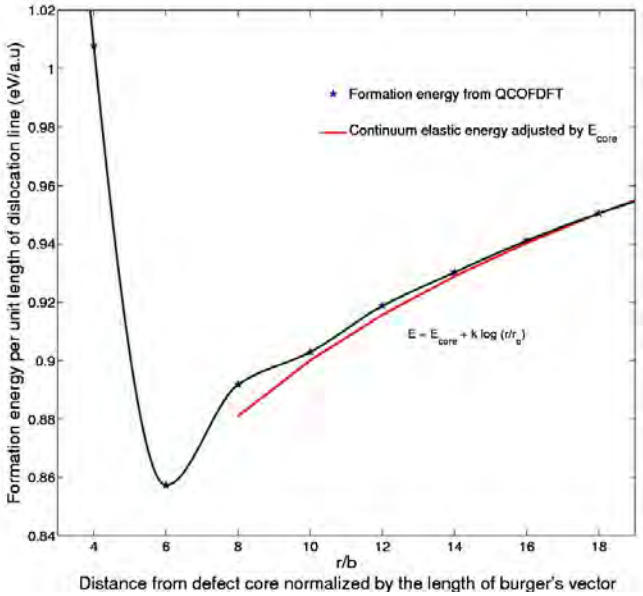

Figure 2: Cell size study of a perfect edge dislocation

In order to determine the appropriate simulation cell-size, we progressively increase the cell-size from 4|**b**| to 18|**b**| (**b**: Burgers vector) and compute the energetics of electronic relaxations. Figure 2 shows that the formation energy of the edge dislocation asymptotes to the expected logarithmic behavior for large cell-sizes as described by continuum theories. However, the formation energy significantly deviates from this logarithmic behavior upto 12|**b**| predominantly due to electronic-structure effects. This suggests that quantum-mechanical interactions play an important role in the energetics of a dislocation upto the order of 10|**b**|, which is much larger than most of the previous electronic structure studies on dislocation cores.

As a next step, we are currently relaxing the ionic positions of the edge dislocation to see formation of Shockley partials and studying the associated energetics. As a further step we will investigate the effect of macroscopic deformations on the energetics and core structure of Shockley partials.

IV.5

Multiscale Mechanics of Materials - Crystal Plasticity Across the Scales

Missing Abstract

ID: 142

ID: 159

Three-dimensional Continuum Dislocation Microplasticity FE-Simulation

Stephan Wulfinghoff
Karlsruhe Institute of Technology (KIT)
Germany

Thomas Böhlke
Karlsruhe Institute of Technology (KIT)
Germany

Abstract:
Modern continuum approaches for micro-plasticity applications try to fill the gap between size-independent, phenomenological plasticity models for macroscopic simulations and micro-plasticity models based on discrete objects like ab-initio methods or discrete dislocation dynamics. The formulation of phenomenological nonlocal hardening models based on plastic

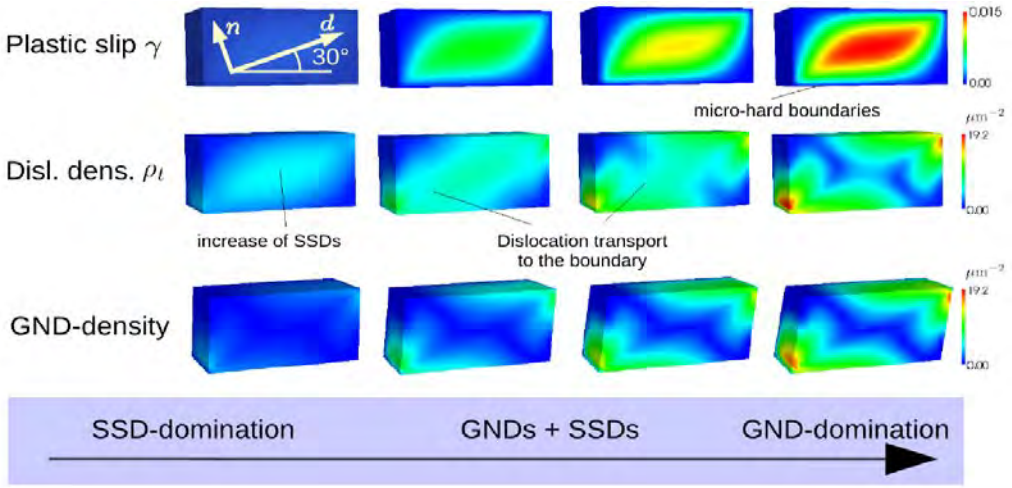

strain gradient measures like Nye's dislocation density tensor [3] is the most popular approach for continuum mechanical micro-plasticity theories and allows to reproduce many of the experimentally observed size-effects at least qualitatively.
Additionally, several dislocation density-based theories have emerged that account explicitly for dislocation transport and production. The kinematical theory of Hochrainer et al. [1] averages the collective motion of three-dimensional discrete, connected and curved dislocation lines.
As the theory is numerically expensive in three-dimensional multislip applications, a simplified version (by Hochrainer et al. [2]) of the kinematical continuum mechanical dislocation-density framework is considered in the presentation based on two evolution equations for the dislocation density and the average dislocation curvature. The dislocation velocity couples the dislocation field problem to the elasto-visco-plastic crystal plasticity framework via Orowan's equation. The kinentic coupling based on phenomenological hardening approaches like the Taylor-relation is also discussed.

Simulation results show the performance of the theory in three dimensional applications. The findings are compared to gradient plasticity predictions.

References

[1] T. Hochrainer, M. Zaiser and P. Gumbsch, A three-dimensional continuum theory of dislocations: kinematics and mean field formulation. Philosophical Magazine 87:1261–1282, 2007.
[2] T. Hochrainer, M. Zaiser and P. Gumbsch, Dislocation transport and line length increase in averaged descriptions of dislocations. arXiv:1010.2884v1
[3] J. F. Nye, Some geometrical relations in dislocated crystals. Acta Metallurgica 1:153–162, 1953.

ID: 212

Riemann-Cartan Geometry and the Nonlinear Mechanics of Dislocations

Arash Yavari
School of Civil and Environmental Engineering
Georgia Institute of Technology

Abstract:

In this seminar we will show that the nonlinear mechanics of solids with distributed dislocations can be formulated as a nonlinear elasticity problem provided that the material manifold – where the body is stress-free − is chosen appropriately. Choosing a Weitzenböck manifold (a manifold with a flat and metric-compatible affine connection that has torsion) with torsion tensor identified with the given dislocation density tensor the body would be stress-free in the material manifold by construction. For classical nonlinear elastic solids in order to calculate stresses one needs to know the changes of the relative distances, i.e. a metric in the material manifold is needed. For distributed dislocations this metric is the metric compatible with the Weitzenböck connection. We will present exact solutions for the residual stress field of several distributed dislocation problems in incompressible nonlinear elastic solids using Cartan's method of moving frames. We will also discuss zero-stress dislocation distributions in nonlinear dislocation mechanics.

ID: 240

Simulation of Size effects in the Growth of Cylindrical Voids by Means of Dislocation Dynamics and Molecular Dynamics

Javier Segurado
Polytechnic University of Madrid. IMDEA-materials

Javier LLorca

Abstract:
The overall ductility of metals is mainly controlled by the ability of the material to withstand the growth of micron-sized voids up to the point in which fracture is triggered by the sudden coalescence of neighbor voids into a crack. Most of the models developed to quantify and understand the void growth process did not take into account two important factors: the anisotropic nature of plastic flow in single crystals and the size effects that appear when plastic flow is confined into very small regions. These limitations can be overcome using discrete dislocation dynamics, which includes naturally both effects and that has already been successfully to study voids growing inside single crystals, Segurado and LLorca, 2009. However, from a more fundamental viewpoint, some of the normal considerations made for the DD simulations are not physically clear. This is the case of the dislocation nucleation in the presence of a void: DD normally considers bulk nucleation via Frank-Read sources although a big effect is suspected of the free void surfaces in the dislocation nucleation. In this investigation, the mechanical response and void growth of a model 2D material with circular voids will be studied using both a discrete dislocation dynamics technique and a molecular dynamics approach. The considered Representative Volume Element (RVE) will be a square with a circular hole inside. In the DD case, simulations were based on the methodology developed by Van der Giessen and Needleman, 1995, which was extended by the authors to non-convex domains through the use of finite elements with embedded discontinuities (Romero et. al. 2008). In the case of MD, a glue potential was adapted and applied to a pure 2D model, in order to allow the comparison with DD and the use of crystal sizes close to the micron. The results suggest that for the atomistic 2D model, dislocation nucleation in the free boundary plays a fundamental role. Finally, 3D DDD simulations based on the code Tridis (Verdier et at 1998) have been performed. The DDD model was used together with FEM in order to solve the boundary conditions in an exact manner at each increment of the process. The effect of dislocations abandoning the sample is studied using different approaches. In this case simulations of void growth were based on cubic RVEs with a spherical void inside. As in 2D, different void sizes have been studied and, qualitatively, the size effect obtained was very similar to the 2D case. Segurado J, Llorca J. Acta Materialia 2009, 57:1427 Van der Giessen E, Needleman A. Modell Simul Mater Sci Eng 1995;3:689. Romero I, Segurado J, LLorca J. Modell Simul Mater Sci Eng 2008;16:035008. Verdier M, Fivel M.C., Groma I.,Simul. Mater. Sci. Eng. 6 (6) (1998) 755;770.

ID: 265

Crystal plasticity simulations using discrete Fourier transforms

Hamad F. Al-Harbi
George W. Woodruff School of Mechanical Engineering
Georgia Institute of Technology, Atlanta, GA 30332, USA

Surya R. Kalidindi
Department of Mechanical Engineering and Mechanics
Drexel University, Philadelphia, PA 19104, USA

Abstract:

In recent work [1, 2], we have demonstrated the viability and computational advantages of using a compact database of discrete Fourier transforms (DFTs) for facilitating crystal plasticity solutions in cubic polycrystalline materials subjected to arbitrary deformation paths. This new DFT approach allows for compact representation and fast retrieval of crystal plasticity solutions which is found to be able to speed up the calculations by about two orders of magnitude. In this paper, we present the first successful implementation of this spectral approach to perform crystal plasticity computations in a commercial finite element code. More specifically, the spectral approach to crystal plasticity solutions was successfully integrated with the commercial finite element package ABAQUS through a user materials subroutine, UMAT. Details of this new crystal plasticity FE approach are demonstrated and validated through a few example case studies involving the simulation of bulk deformation processing operations on face centered and body centered cubic metals. The evolution of the underlying crystallographic texture in the work-piece and its associated macroscale anisotropic properties predicted from this new approach are compared against the corresponding results from the conventional crystal plasticity finite element method [3]. It will be shown that implementing the spectral approach to crystal plasticity computations in a FE code produced excellent predictions similar to the classical crystal plasticity FE method, but at a significantly faster computational speed and much lower computational cost.

As an example, we show in Figure 1 a comparison of the stress-strain curves and deformed texture predicted from implementing the spectral approach to crystal plasticity computations in the FE package, ABAQUS, against the corresponding predictions from the conventional crystal plasticity FE approach for plane strain compression of a copper polycrystalline material subjected to 70% height reduction. The three-dimensional FE model consisted of 500 C3D8 elements with one single crystal orientation per integration point. It is seen that the spectral approach accurately reproduced all of the features of the classical method at a significantly faster computational speed. In this case study, the classical crystal plasticity FE simulation required 110 minutes, whereas the spectral approach based on 500 dominant DFTs took only 6 minutes. In addition, a particularly attractive feature of this new spectral approach is that it provides the user with tremendous flexibility in making trade-offs between accuracy and computational speed. This approach allows the user to perform a large number of very quick

simulations at a lower than desired accuracy, identify the specific ones that appear to produce promising results, and redo these much more accurately (at a higher computational cost).

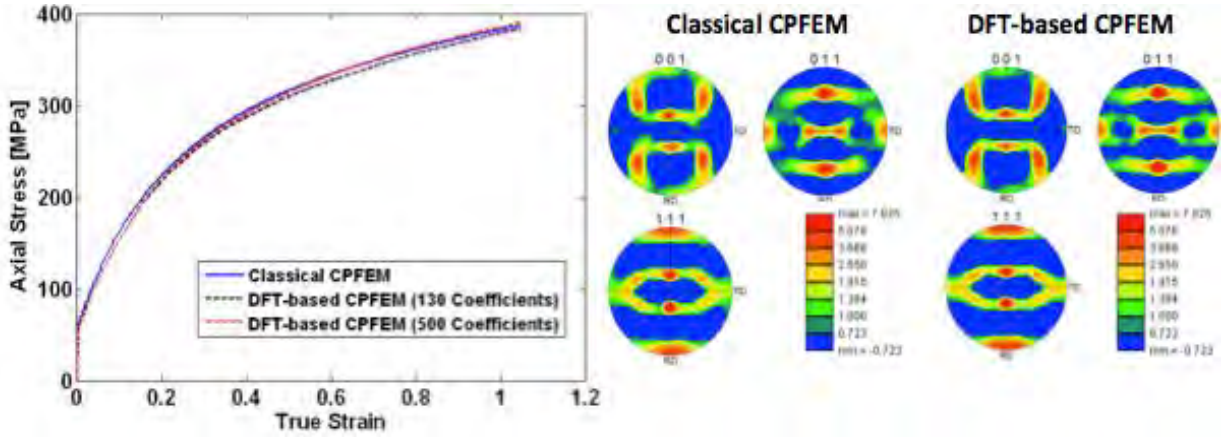

Figure 11: Comparison of the predictions from the spectral approach to crystal plasticity computations implemented in the FE package, ABAQUS, against the corresponding predictions from the conventional crystal plasticity FE approach for plane strain compression of copper polycrystalline material: (a) stress-strain curves, and (b) pole figures.

References

1. Hamad F. Al-Harbi, M.K., and Surya R. Kalidindi, *Spectral Approaches for the Fast Computation of Yield Surfaces and First-Order Plastic Property Closures for Polycrystalline Materials with Cubic-Triclinic Textures.* Computers, Materials, & Continua (CMC), 2010. **15**(2): p. 153-172.
2. Knezevic, M., H.F. Al-Harbi, and S.R. Kalidindi, *Crystal plasticity simulations using discrete Fourier transforms.* Acta Materialia, 2009. **57**(6): p. 1777-1784.
3. Kalidindi, S.R., C.A. Bronkhorst, and L. Anand, *Crystallographic texture evolution in bulk deformation processing of FCC metals.* Journal of the Mechanics and Physics of Solids, 1992. **40**(3): p. 537-569.
4. Landi, G., S.R. Niezgoda, and S.R. Kalidindi, *Multi-scale modeling of elastic response of three-dimensional voxel-based microstructure datasets using novel DFT-based knowledge systems.* Acta Materialia, 2010. **58**(7): p. 2716-2725.

5. Fast, T. and S.R. Kalidindi, *Formulation and calibration of higher-order elastic localization relationships using the MKS approach.* Acta Materialia, 2011. **59**(11): p. 4595-4605.
6. Fast, T., S.R. Niezgoda, and S.R. Kalidindi, *A new framework for computationally efficient structure-structure evolution linkages to facilitate high-fidelity scale bridging in multi-scale materials models.* Acta Materialia, 2011. **59**(2): p. 699-707.

ID: 275

A Physically-Based BCC Crystal Plasticity Model Incorporating Non-Schmid Yield Behavior

Hojun Lim
Sandia National Laboratories
USA

Corbett Battaile

Abstract:
Despite the technological importance of body-centered cubic (BCC) metals, models of their plastic deformation are less common than those of face-centered cubic (FCC) metals, due in part to the complexity of slip in BCC crystals. In order to study the effect of microstructure on low-temperature plasticity in BCC metals, we have developed a single crystal plasticity model that captures non-Schmid yield behavior based on the atomistic results of Groger et al. [1, 2] for molybdenum and tungsten. At the atomic scale, non-Schmid stresses influence deformation by altering the dislocation core structure, which allows the motion of screw dislocations to be assisted by shear stresses that do not lie on the slip plane. This leads to not only a non-associative flow law, but also the well-known tension/compression asymmetry in the yield surface.

The model is implemented in a BCC polycrystal finite element formulation to reproduce continuum response as well as individual grains responses via stress, strain, and crystallographic rotation. It is shown that the non-Schmid effects create tension/compression asymmetry as well as different crystallographic rotation and crystal orientation dependent mechanical behavior compared to conventional plasticity models.

Sandia is a multi-program laboratory operated by Sandia Corporation, a wholly owned subsidiary of Lockheed Martin, for the United States Department of Energy National Nuclear Security Administration under contract DE-AC0494AL85000.

ID: 276

Incorporating Limited Slip into Crystal Plasticity to Improve Stress-Strain and Texture Prediction

Jeffrey Lloyd
Georgia Institute of Technology
USA

David McDowell
Georgia Institute of Technology
USA

Abstract:
Crystal plasticity simulations traditionally incorporate strengthening mechanisms through phenomenological hardening relations similar to those in macro-scale plasticity, which do not adequately predict stress-strain and texture behavior of complex loading paths. This work examines the ability of a mantle-core crystal plasticity model to predict stress-strain and texture evolution of polycrystalline copper subjected to compression, torsion, and compression-torsion sequencing tests. The mantle-core model is based on experimental observation that limited slip activity initially occurs in the grain interior while multislip is more prevalent near grain boundaries. The model is compared to traditional crystal plasticity data, and more satisfactory prediction of stress-strain as well as texture evolution is observed using the mantle-core model, where limited slip activity promotes subgrain formation, and rotation, as experimentally observed. These results suggest that crystal plasticity models that use limited slip activity to promote subgrain formation can be used to more accurately predict stress-strain and texture evolution data.

ID: 299

Modeling Localized Deformation in Irradiated bcc Metals Using Continuum Crystal Plasticity

Anirban Patra
School of Materials Science and Engineering, Georgia Institute of Technology, Atlanta, GA 30332
USA

David L. McDowell
School of Materials Science and Engineering, GWW School of Mechanical Engineering, Georgia Institute of Technology, Atlanta, GA 30332
USA

Abstract:
Structural materials used in nuclear applications are subjected to significant doses of radiation, resulting in the formation of point defect clusters, dislocation loops and complex dislocation networks. The deformation behavior of irradiated metals is greatly affected by these defects serving as obstacles in the path of glide dislocations. Combined phenomena of increase in yield strength, decrease in ductility, flow localization and lower strain to failure are typically observed. The deformed microstructure after quasi-static tensile loading shows the formation of defect-depleted dislocation channels which are ~50-200 nm wide, wherein majority of the inelastic strain is localized.

The present work extends a defect density based continuum finite deformation crystal plasticity framework [1] to model the said localization phenomena in irradiated bcc materials. The crystal plasticity model accounts for climb-assisted glide of mobile dislocations trapped in the field of immobile (forest) dislocations and irradiation-induced defects at the level of slip systems. This framework tracks the evolution of irradiation-induced defects, i.e., point defects (interstitials and vacancies) and defect dislocation loops (interstitial loops in bcc metals), in addition to the mobile and immobile dislocations that govern the inelastic deformation behavior.

The crystallographic shearing rate (which is tensorially summed over all slip systems to give the inelastic velocity gradient) is the additive sum of contributions due to cooperative dislocation glide and climb. This is based on the following physical picture: mobile dislocation segments that are pinned at irradiation-induced obstacles (during their glide on preferred slip planes) climb by absorbing point defects; thus enabling the unpinned mobile dislocation segments to glide further. This type of approach allows us to model not just dislocation glide-dominated deformation (e.g. quasi-static tensile loading), but also climb-dominated deformation, such as irradiation creep governed by stress-induced preferential absorption of interstitials (SIPA) in a crystal plasticity framework.

A rate-theory based formulation is used to model the evolution of point defects due to generation, mutual recombination and absorption by dislocations. Models for evolution of

irradiation-induced interstitial loops due to absorption of point defects by mobile dislocations, and annihilation due to interaction with gliding mobile dislocations have also been developed. The dislocations evolve by multiplication, trapping, mutual annihilation, cross-slip, climb and dynamic recovery processes. See Ref. [1] for details.

This 'local' framework is used to simulate the mechanical behavior and deformed microstructure of an irradiated 9Cr-1Mo ferritic/martensitic steel loaded quasi-statically in tension using 2D generalized plane strain finite elements. A reasonable fit to the experimental stress-strain curves (from Maloy et al. [2]) is obtained for various radiation and temperature histories (Figure 1(a)), at least until geometric necking instabilities set in at the later stages of deformation. In the present form of simulations, the applied boundary conditions cannot handle geometric instabilities. Softening observed in the simulated stress-strain response of the irradiated samples in Figure 1(a) is solely due to 'constitutive' material softening.

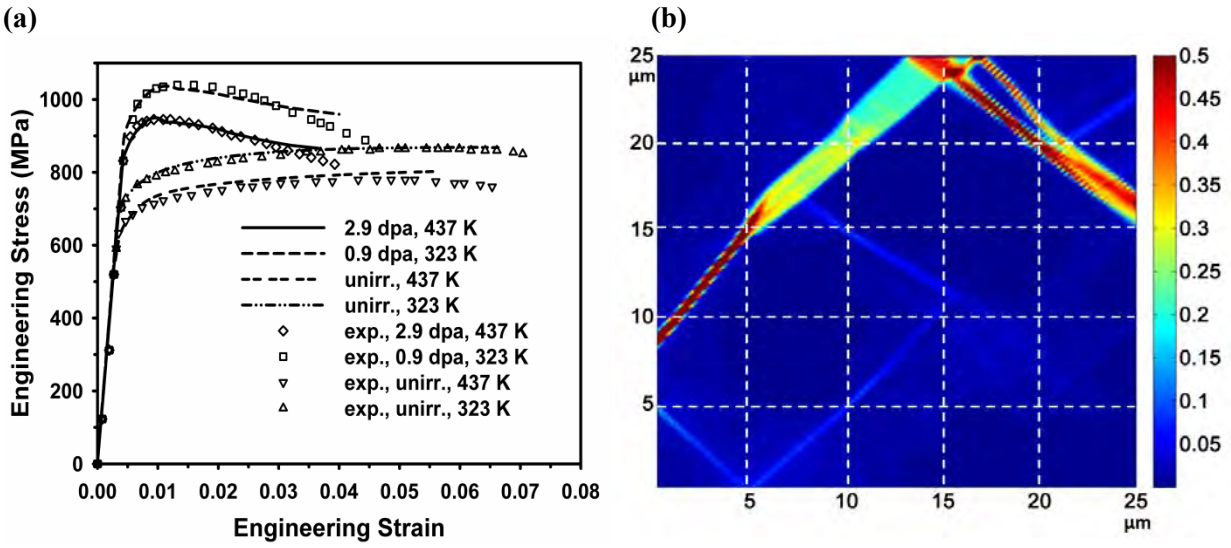

Figure 1.(a) Comparison of simulations calibrated to experiments over a range of temperature and radiation dpa doses. Open symbols represent experimental engineering stress-strain curves. (b) Distribution of effective inelastic strain in a sample loaded in tension to 4% engineering strain at 437 K, after being irradiated to 2.9 dpa dose. Dotted white lines indicate grain interfaces.

A refined mesh with 200 nm element size is used to model the deformed microstructure in a material with idealized square-shaped grains. This mesh size serves as the limit of continuum field approximation for representing a statistical ensemble behavior of dislocations; at a mesh size of 200 nm, we will have ~2-4 dislocations per finite element (given a dislocation density of $5x10^{7}$-$1x10^{8}$ mm^{-2} in the present material). As seen in the effective inelastic strain plot in Figure 1(b), the deformation is localized along narrow shear bands (defect-depleted dislocation channels), which are ~200-500 nm in width. The localized inelastic strain in channels is ~0.5-0.7. These values differ from the experimentally observed channel widths (50-200 nm) and in-channel strains (1.0-5.0). The mesh size in our simulations limits the channel widths to a minimum of 200 nm. However, it is pointed out that the net localized shear strain (product of in-channel strain and channel width) is more or less invariant and within 100-200% of the experimentally measured values. As an example, for a simulated channel width of 200 nm, the

in-channel strain should be multiplied by a factor of 4 to compare with the experimentally measured localized strain in channels of width 50 nm. Further, it should be noted that irrespective of the simulated channel width, the effect of localization on the polycrystalline stress-strain behavior would remain the same provided the 'constitutive' crystal plasticity model phenomenologically captures the underlying mechanisms of strain localization (via defect annihilation). This has been verified using simulations with larger mesh size.

The spatial arrangement of dislocation channels and the degree of localization is found to be strongly dependent on the crystallographic orientation distribution of the grains. The spacing between channels varies as a function of the grain size in the material. Further, maximum inelastic strain in the channels increases linearly with increasing radiation dose for the same initial crystallographic orientations of grains. Reorientation and bifurcation of channels takes place at the interfaces of idealized square grains in our simulations. It is also found that the channels widen with increasing degree of cross-slip. Effect of geometry and simulation cell size on the localization behavior is also studied to verify that the observed dislocation channels are not an artifact of the geometry and boundary conditions.

References

1. A. Patra, D.L. McDowell, "Crystal plasticity-based constitutive modeling of irradiated bcc structures", Philosophical Magazine, Vol. 92 (2012), pp. 861-887.
2. S.A. Maloy, M.R. James, G. Willcutt, W.F. Sommer, M. Sokolov, L.L. Snead, M.L. Hamilton, F. Garner, "The mechanical properties of 316L/304L stainless steels, Alloy 718 and Mod 9Cr-1Mo after irradiation in a spallation environment", Journal of Nuclear Materials, Vol. 296 (2001), pp. 119-128.

ID: 368

Unique Scale-Dependent Definition for Stress at the Atomic Scale

Ellad Tadmor
University of Minnesota
USA

Nikhil Admal
USA

Abstract:
At the molecular level there are atoms and forces, whereas continuum theories deal with fields and stress. To connect between these models of reality it is necessary to obtain expressions for continuum variables, such as stress and heat flux, at the molecular level. To date, many different expressions have been proposed and some confusion exists in the literature as to which is "correct". We show that a unified framework based on the work of Irving and Kirkwood and later Noll, can be established from which all other expressions can be derived. Interestingly, it turns out that subtle arguments related to the nature of interatomic potentials play an important role in the derivation and point to the existence of a unique scale-dependent stress tensor. This definition is intimately tied to the existence of residual stresses in materials. The theoretical framework as well as numerical results will be presented.

ID: 370

Microcanonical Entropy and Mesoscale Dislocation Mechanics

Amit Acharya
Carnegie Mellon University
USA

Abstract:
In classical equilibrium statistical mechanics, there is a formula for the entropy of a finite dimensional, constrained Hamiltonian system. It seems that this idea can be combined in a systematic way with space-time averaged, kinematically rigorous PDE models to produce mesoscale models physical phenomena. In doing so, the idea of local equilibrium in non-equilibrium thermodynamics of extended systems can be given a specific operational meaning at the level of generating useful algorithms from it. The energetics and driving forces for dissipative mechanisms in these models can be precisely linked to atomistic behavior through well-defined, material-specific, one-time calculations that are expected to be possible on modern computers. This presentation will discuss the details of this formalism and illustrate it in the context of mesoscale dislocation plasticity.

ID: 455

A Versatile Microelectromechanical System for Fatigue Testing of Nanostructures

Ehsan Hosseinian
Georgia Institute of Technology
United States

Olivier N Pierron
Georgia Institute of Technology
United States

Abstract
Microelectromechanical systems (MEMS) were recently described as superior mechanical testing systems for nanomaterials. Currently, the most advanced MEMS setups are best suited for *in-situ* SEM or TEM studies, since they require high magnification images to measure strain. Here we present a MEMS material testing setup, shown in figure1, that relies on electronic measurements of nanospecimen elongation. Compared to previously demonstrated MEMS devices that rely on high magnification images to measure elongation, this MEMS is more versatile, allowing both *in situ* TEM testing and *ex situ* (e.g., in an environmental chamber) testing of nanomaterials with high accuracy and precision (sub nm). The MEMS device comprises two identical capacitive sensors on each side of the nanospecimen that are used to electronically measure the specimen gap change. The mode of operation of the MEMS setup is illustrated with *ex-situ* uniaxial tensile and fatigue tests of nanocrystalline nickel nanobeams.

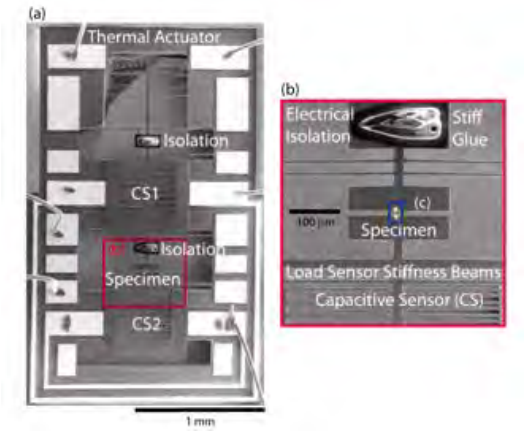

Figure 12. SEM images of the MEMS device

Additionally we have fabricated nanocrystalline dog-bone samples, specifically designed for easy manipulation. The geometry of samples enables us to manipulate the sample and fix it with epoxy instead of FIB deposited platinum (see figure2). It is expected that the combination of ex-

situ and in-situ nanomechanical tests will enable a thorough investigation of mechanical properties of nanocrystalline FCC metals at the nanoscale.

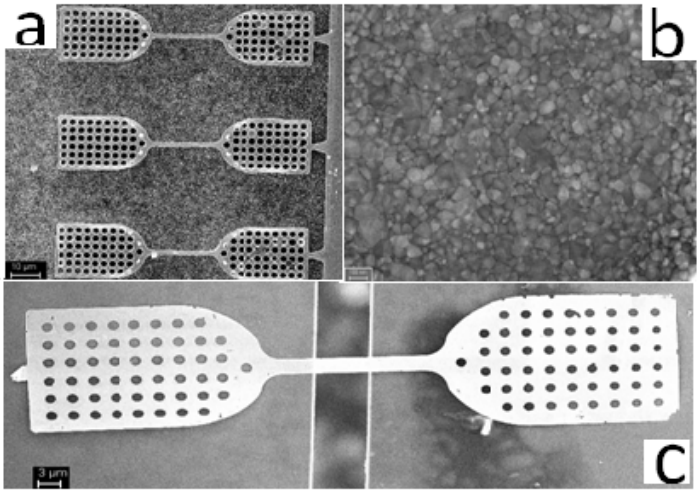

Figure 13: a) SEM micrograph of gold Nc specimens with b) average grain size of 50 nm c) manipulated specimen, mounted in between two sides of the gap

Missing Abstract

ID: 467

ID: 514

Coarse-grained Molecular Dynamics through Quasicontinuum

Jeff Amelang
Caltech

Dennis Kochmann

Abstract:
The Quasicontinuum (QC) technique has been largely successful at overcoming simulation time and memory limitations encountered when solving lattice statics problems by combining a fully atomistic material description with the finite element technique. QC is effective in problems where inhomogeneities are localized and behavior in major portions of the computational domain can be approximated. However, in dynamic problems it is just this disparity in length scales that creates artificial material interfaces and hampers the application of QC because high-frequency oscillations at wavelengths unsupportable by the coarse regions become trapped in the fine regions. In this talk we will present our progress on the development of a new, parallel implementation of dynamic QC intended for high performance computing. We will also discuss early results in applying a novel time integration technique (Replica Time Integrators) that transmits (instead of suppresses) high-frequency oscillations through coarse regions.

ID: 538

A Size-dependent Plasticity Model as the Gamma-limit of Dislocation Activity in the Finite Kinematic Framework

Celia Reina
Lawrence Livermore National Laboratory

Sergio Conti

Abstract:
This talk will present a size-dependent plasticity model in the finite kinematic framework that is directly obtained as the limit of the dislocation activity. The project intends to provide a physically-based model of strain gradient plasticity that can be directly used at the continuum level in standatd engineering models and simulations. At the same time, the model gives the dependencies of the continuum plastic energy on the plastic part of the deformation gradient and relates the material properties to the underlying microstructure.

ID: 554

Modeling Pore Collapse and Chemical Reactions in Crystalline Energetic Materials

Ryan Austin
Lawrence Livermore National Laboratory
USA

Nathan Barton
USA

Abstract:
The collapse of micron-sized pores in crystalline energetic materials is the primary route to initiating thermal decomposition reactions under shock wave loading. The processes involved in pore collapse localize energy and generate temperatures that enable chemical reaction. Given the difficulty of probing such small-scale dynamic events in experiments, it has been useful to study the problem using numerical simulation. However, few numerical investigations have considered the anisotropic nature of crystal deformation or included the effects of highly-exothermic chemical reactions. The details of deformation at this length scale are important because the crystal mechanics influence the character of strain localization around the pore. In this work, we focus on simulating the collapse of a single air-filled pore in crystalline HMX (octahydro-1,3,5,7-tetranitro-1,3,5,7-tetrazocine) under shock wave loading. The simulations are preformed using a multiphysics arbitrary-Lagrangian-Eulerian finite element code (ale3d) wherein coupled responses of the HMX crystal are defined by a dislocation-dynamics based model of thermoelasto-viscoplasticity and a reactive equation-of-state. In this regard, a multistep reaction network is specified for the thermal decomposition of HMX. A small parametric study is undertaken to assess model sensitivities to shock strength, pore size, crystal orientation, and selected aspects of the material model. Results relevant to the shock initiation of HMX are presented. p, li { white-space: pre-wrap; } This work performed under the auspices of the U.S. Department of Energy by Lawrence Livermore National Laboratory under Contract DE-AC52-07NA27344 (IM release #: LLNL-ABS-546512).

ID: 608

The Use of Crystal Plasticity Finite Element Method to Investigate Slip and Twinning in Pure Magnesium

Matthew W. Priddy
Woodruff School of Mechanical Engineering, Georgia Institute of Technology
United States of America

David L. McDowell
Woodruff School of Mechanical Engineering, Georgia Institute of Technology
School of Materials Science and Engineering, Georgia Institute of Technology
United States of America

Abstract:
Magnesium is 75% less dense than steel and 33% less dense than aluminum and has the highest strength-to-weight ratio of all structural metals, making it an ideal material for transportation systems. However, magnesium has a hexagonal close-packed (HCP) crystal structure and deforms by a combination of slip and twinning, making it difficult to predict magnesium's macroscopic response to plastic deformation. The contribution of combined slip and twinning to the deformation of single crystal and polycrystalline magnesium is assessed in this work.

Table 1. Deformation modes of magnesium.

Slip/Twin System	No. of Systems	Slip Direction	Plane Normal
Basal Slip $\langle a \rangle$	3	$\langle 11\bar{2}0 \rangle$	$\{0001\}$
Prismatic Slip $\langle a \rangle$	3	$\langle 11\bar{2}0 \rangle$	$\{1\bar{1}00\}$
Pyramidal Slip $\langle c+a \rangle$	6	$\langle 11\bar{2}3 \rangle$	$\{11\bar{2}2\}$
Extension Twin	6	$\langle \bar{1}011 \rangle$	$\{\bar{1}012\}$
Contraction Twin	6	$\langle \bar{1}01\bar{2} \rangle$	$\{\bar{1}011\}$

To gain insights into the relevant modes of deformation of magnesium, this research introduces a temperature and strain-rate dependent, single crystal constitutive law for multiple slip and twinning modes for magnesium and its alloys, which is employed in a crystal plasticity 3D finite element method (CPFEM) framework via a user material subroutine (UMAT) in Abaqus/Standard. Deformation by slip is modeled using an Arrhenius type, thermally activated flow law for the α^{th} slip system,

$$\dot{\gamma}^{(\alpha)} = \dot{\gamma}_0 \exp\left\{-\frac{\Delta F}{kT}\left[1-\left(\frac{\left|\tau^{(\alpha)}-\chi^{(\alpha)}\right|-\kappa^{(\alpha)}}{D^{(\alpha)}}\right)^{p}\right]^{q}\right\}\operatorname{sign}\left(\tau^{(\alpha)}-\chi^{(\alpha)}\right).$$

The directional hardening term, $\chi^{(\alpha)}$, is initially zero and employs the Armstrong-Frederick direct hardening/dynamic recovery relation to capture slip-slip interactions. The nondirectional hardening term, $\kappa^{(\alpha)}$, is equal to the critical resolved shear stress (CRSS) at the onset of

deformation and models slip-slip interactions through the evolution of statistical stored (forest) dislocations. The nondirectional hardening term also employs a relation to account for size effects during slip-twin interactions, by modeling the reduction in mean-free path for dislocation motion when twins are present in the parent material. In this particular flow rule, the drag stress, $D^{(\alpha)}$, is the upper bound for the Peierls resistance, which is estimated as the CRSS for screw dislocations in pure magnesium at 0 K.

Deformation by twinning employs a similar flow law as slip, but accounts for the density of available nucleation sites and the activation free energy to nucleate a twin. This relationship is coupled with a stress-based relation for twin nucleation and growth. To account for the crystal reorientation due to twinning, the crystal lattice of a twinned region is rotated according to,

$$\boldsymbol{R}^{tw} = 2\mathbf{n} \otimes \mathbf{n} - \mathbf{I} \ ,$$

where $\mathbf{n}$ is the twin plane normal and $\mathbf{I}$ is the identity tensor.

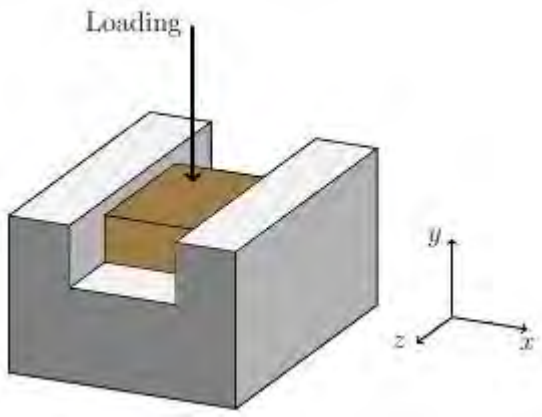

Figure 14. (a) Schematic view of channel-die compression test.

The constitutive model is calibrated and validated to single crystal and polycrystalline channel-die compression experimental data of pure magnesium, respectively [1,2]. A schematic of channel-die compression is shown in Figure 1. The seven calibration simulations match the stress-strain response of the physical experiments with reasonable agreement, as well as the active deformation modes of each calibration simulation match the deformation modes observed by Kelley and Hosford in the physical experiments.

References:

[1] Kelley, E. W., & Hosford, J. W. F. (1968). Plain-strain compression of magnesium and magnesium alloy crystals. *Metallurgical Society of American Institute of Mining, Metallurgical and Petroleum Engineers -- Transactions*, 242(1), 5-13.

[2] Kelley, E. W., & Hosford, J. W. F. (1968). Deformation characteristics of textured magnesium. *Metallurgical Society of American Institute of Mining, Metallurgical and Petroleum Engineers -- Transactions*, 242(4), 654-661.

IV.6

Multiscale Mechanics of Materials - Multiscale Mechanics

ID: 208

Multi-Scale Quasistatic Damage Evolution for Polycrystalline Materials

Robert Lipton
Louisiana State University, Baton Rouge, LA
United States

Michael Stuebner
Global Engineering and Materials Inc., Princeton, NJ
United States

Yuanjie Lua
Global Engineering and Materials Inc., Princton, NJ
United States

Abstract:
We present a new multi-scale model for linking higher order microstructure descriptions to failure initiation and damage propagation in polycrystalline media. The model gives an accurate local field description for predicting damage nucleation at the length scale of the polycrystalline texture. The new method allows the recovery of the local damage microstructure inside domains of microtexture and has the capability to capture the conditions for component failure through the propagation of damage across macroscopic length scales. Computational examples for damage evolutions for different load cases demonstrate the potential of this model. In the simulations component level failure is seen in the form of damage appearing along ligaments with length scales comparable to the structural component.

Modeling and Simulation:
The damage parameter for this model is given by the local damage volume fraction $\theta = \theta(x)$. The average stress over each grain is obtained through the solution of a global or homogenized problem posed in terms of an effective elastic tensor depending locally on the damage volume fraction and the orientation of the principle slip plane within each crystal grain.

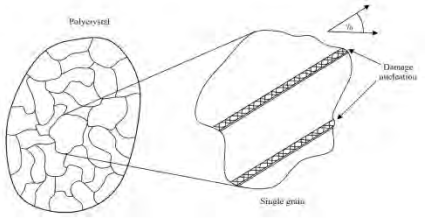

We carry out a simulation for a matrix material containing multiple textured sub-domains. This example is motivated by the TI-AL alloy system. Here the textured domains are modeled by ellipses of different shapes and orientations. A randomly generated geometry with elliptic inclusions is shown below. Here a random number generator is used to assign the centroid of

each ellipse together with the aspect ratios for each ellipse. A random number generator is also used to assign the damage plane inside each ellipse. The matrix material between inclusions has a uniform damage plane direction fixed at 0 degrees. The specimen is subjected to uniaxial tension loading.

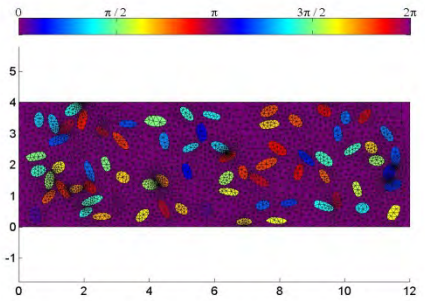

On the left and right side the traction loads are monotonically increasing over time. The Young's modulus of the inclusion is assumed to be twice the one of the matrix. The Poisson's ratio is the same for both damaged and undamaged material and is 0.3333. The damage evolution is displayed for six different times. The evolution starts with the top left frame and proceeds from left to right along the first row, then proceeds left to right along the second row. The brown areas contain damaged material, the blue ones undamaged. The damage progression is seen to depend on the shape and location of the textured regions.

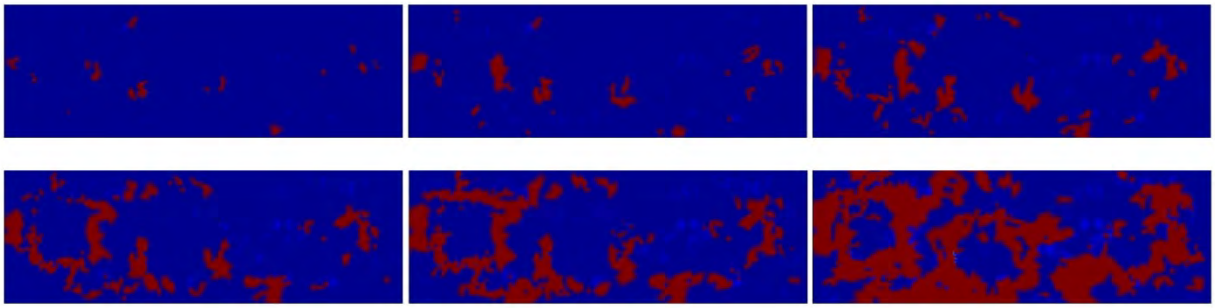

Conclusion:

A new multi-scale model for linking micro-structure to component level mechanical response and damage evolution is developed. A set of simulations are carried out to illustrate the model. The effects of damage accumulation at the length scale of the single crystal grains have been modeled through the nucleation of thin layers of soft elastic material oriented along the slip plane of each grain. The locally resolved stress deviator inside each grain is related to an average stress field over the grain via a stress amplification tensor that depends upon the direction of the slip plane inside the grain and the local volume fraction of the damage layers inside the grain.
This article will appear in IJES 58, pp. 85–94 (September 2012).

Acknowledgment: The authors gratefully acknowledge the support from AFOSR under the STTR Phase I contract FA9550-10-C-0100

ID: 245

DEM Calculations of Radial Stresses in a Column of Granular Materials

Aleksandr O. Spiridonov
New Jersey Institute of Technology, Granular Science Laboratory
United States

Anthony D. Rosato
New Jersey Institute of Technology, Granular Science Laboratory
United States

Abstract:

This paper focuses on assumptions implicit in Janssen's model for a column of granular material - uniformity of stresses across the width, and the proportionality of axial and radial stresses - as well as an examination of the influence of the size of the sub-domains (annular rings) used to determine averages. Stresses [3] in the column were computed via discrete element simulations, in which particles are modeled are inelastic, frictional soft spheres. Results were validated through force balances at the boundaries, by comparing boundary pressures to local sub-domain stresses, and by making comparisons against the literature where possible. The axial and radial stresses across the column diameter had an average variance of less than 20%; however, the shear stress variance was irregular resulting in average of approximately 200% over the entire depth of a column. Moreover, the data did not reveal any clear proportionality of the axial and radial stresses averaged in the column.

Computed axial stresses $\sigma_{zz}(z)_{sim}$ closely approximated the exponential saturation behavior of Janssen's theory [1], $\sigma_{ZZ}(z) = \sigma_{sat}\left(1 - e^{-\beta z}\right)$, that has been observed in experiments [4,5,6]

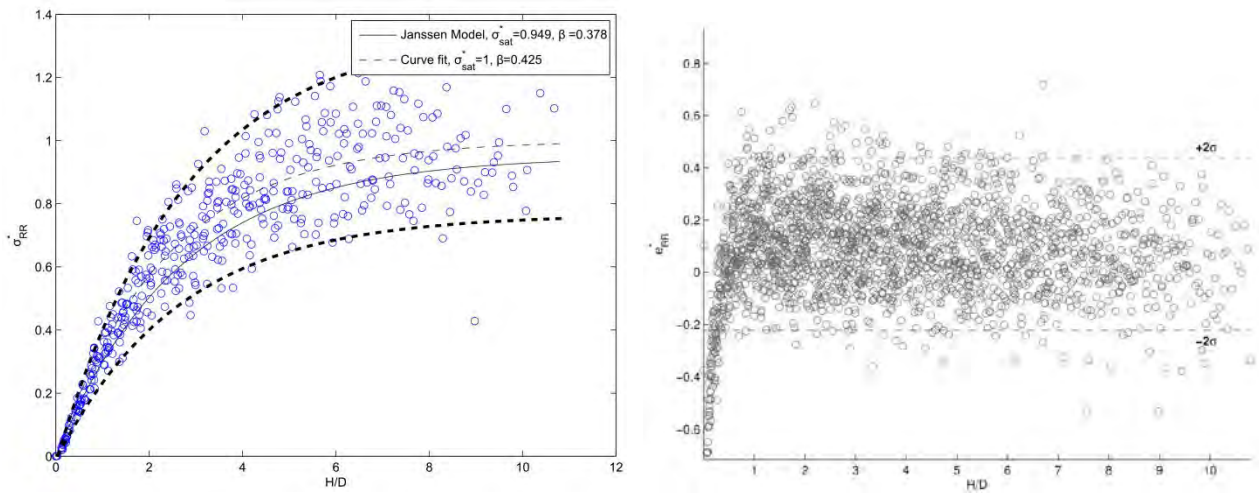

(a) (b)

Figure 1. (a) Normalized radial stress at the wall vs. depth in cylinder diameters and (b) Normalized deviations from theoretical values.

and in computer simulations [7] in the literature. However, calculated stresses were

approximately 13% smaller than theoretical values. When the radial stresses (Fig. 1a, circles) in an annular subdomain at the cylinder wall were compared against Janssen's predictions (Fig. 1a, solid line), significant deviations, within $\pm 30\%$ of the trend line (Fig. 1a, thin dashed line), were observed, in addition to the saturation stress being larger than predicted by 5%. Axial shear stresses showed similar behavior, but with larger deviations of up to 100%. Deviations $e^* = (\sigma_{simulation} - \sigma_{theory})/\sigma_{theory}$ for both cases were approximately normally distributed within a band proportional to the local stress (Fig. 1b). In the latter expression, σ_{theory} denotes either radial $\sigma_{RR} = K\sigma_{zz}$ or shear stress $\sigma_{RZ} = \mu\sigma_{RR}$ from Janssen's theory, in which μ is the coefficient of friction, and K is a constant [2] that depends on μ. As the stresses reach a plateau value, it is expected that the proportional behavior of the deviations should also limit the amplitude of the deviations. The local particle-scale stress at the cylinder wall can then be bound with a certain degree of confidence by an envelope delimited by the bold dashed lines in Fig. 1 and defined by: $(1 - nS)\sigma_{\text{theory}}(z) \leq \sigma(z) \leq (1 + nS)\sigma_{\text{theory}}(z)$, where S is the sample standard deviation (different for radial and shear stresses), and n is a free parameter that controls the amount of data that is likely to fall within the envelope. In Fig. 1a, $n = 2$, selected to cover 95% of the data. The dependence of S on the system dimensions and physical parameters is currently under investigation. Increases in size of the annular stress calculation zones to several particle diameters resulted in a noticeable reduction in deviations from values predicted by the theory, thus suggesting a transition to macro-scale behavior as predicted by Janssen's model.

Further studies are planned to examine the transition to macro-scale behavior, the identification of weak force chains in the system and their effect on the relationship between axial and radial stress in the material.

References

[1] Janssen, H. A. and Z. Vereins. Deutsh Eng., 1895. 39: p. 1045.

[2] Nedderman, R.M. 1992, Cambridge, U.K.: Cambridge University Press. p. 86.

[3] Bagi, K. Mechanics of Materials, 22(3), 1996: pp. 165-167

[4] Vanel, L. and E. Clement. European Physical Journal B, 1999. 11: pp. 525-533.

[5] Bertho, Y., F. Giorgiutti-Dauphine, and J.-P. Hulin. Phys. Rev. Lett., 2003. 90: p.144301.

[6] Walton, O.R. SAE 2004 Transactions: J. Aerospace, 2004. 2004-01-2329: pp. 1-14.

[7] Chester, S., Cui, M., Rosato, A. and O.R. Walton. Powders & Grains 2008. 1145, 2009:pp. 309-312.

ID: 246

Multiscale Experiments on Stress Projection Parameters in BCC Tantalum

Jay Carroll
Sandia National Laboratories
USA

Brad Boyce
USA

Abstract:
Simple stress projection factors commonly used for FCC metals, such as the Schmid factor, are not strictly valid for BCC metals. Nevertheless, the tension experiments shown here demonstrate some correlation between Schmid factor and strain accumulation. For a tantalum oligocrystal with millimetric-sized grains, Schmid factors, obtained through electron backscatter diffraction (EBSD), were compared to local strain fields obtained through digital image correlation (DIC). A strong correlation was found between Schmid factor and strain within each grain. A similar experiment on polycrystalline tantalum with more typical grain sizes (~40 mum) showed a reduced, but still significant, correlation. These two cases highlight the effects of neighboring grains on local grain deformation. In future work, more refined stress projection measures will be compared to material deformation and the effects of neighboring grains will be investigated. These experiments are currently being used to develop crystal plasticity models for BCC metals and evaluate their fidelity.

ID: 355

Multi-scale Modeling of Autonomous ODE systems

Likun Tan
Carnegie Mellon University
United States

Amit Acharya
Carnegie Mellon University
United States

Kaushik Dayal
Carnegie Mellon University
United States

Abstract:
Given an autonomous system of ordinary differential equations (ODE), we consider developing practical models for the deterministic, slow/coarse behavior of the ODE system. The coarse variables are defined as running finite time averages of phase functions. Approaches to construct the coarse evolution equation are discussed and implemented on a 'Forced' Lorenz system, a singularly perturbed system whose fast flow does not necessarily converge to an equilibrium and a one-dimensional atomic chain undergoing phase transition. We explore two strategies. In one, we compute (locally) invariant manifolds of the fast dynamics, parametrized by the slow variables. In the other, the choice of our coarse variables automatically guarantees them to be 'slow' in a precise sense. This allows their evolution to be phrased in terms of averaging utilizing limit measures (probability distributions) of the fast flow. Coarse evolution equations are constructed based on these approaches and coarse features of the model problems are observed.

ID: 379

Coupling Between Failure-Time Variability and Macro-Strain Distributions in a Multiscale Damage Model

Arjun Roy[1] Joseph P. Cusumano
Department of Engineering Science and Mechanics
The Pennsylvania State University
University Park, PA

We study the failure-time statistics for a previously developed [1] coupled-field model for damage evolution in a 1-D bar. The dimensionless boundary value problem for this system is

$$\left((1-\phi)\,u'\right)' - \ddot{u} + c\dot{u}'' = 0 \tag{1a}$$

$$\dot{\phi} = \eta\phi\left[\frac{1}{2}(u')^2 - \alpha\phi^{-\frac{1}{3}}\right]^+ \tag{1b}$$

with boundary conditions $u(0,t) = 0$ and $(1-\phi(1,t))u'(1,t) + c\dot{u}'(1,t) = F_0 e^{i\omega t}$. Here, $u(x,t)$ is the macroscopic displacement field and $\phi(x,t)$ is a scalar microscopic field variable representing damage that varies between 0 (undamaged) and 1 (completely damaged). F_0 and ω are the amplitude and frequency, respectively, of the periodic end-load, c is the damping factor, η and α are two parameters that control the average damage growth rate and the intensity of the damage growth threshold, respectively, and $b^+ = (b+|b|)/2, \forall b \in \mathbb{R}$. We use the finite-element method to discretize the problem spatially and obtain the following sets of ordinary differential equations

$$\mathbf{M}^{\mathbf{u}}\ddot{\mathbf{u}} + \mathbf{C}\dot{\mathbf{u}} + \mathbf{K}(\phi)\mathbf{u} = \mathbf{f}^{\mathbf{u}} \tag{2a}$$

$$\mathbf{M}^{\boldsymbol{\phi}}\dot{\boldsymbol{\phi}} = \mathbf{f}^{\boldsymbol{\phi}}, \tag{2b}$$

where, $\mathbf{M}^{\mathbf{u}}$ and $\mathbf{M}^{\boldsymbol{\phi}}$ are the mass matrices corresponding to u and ϕ, respectively, $\mathbf{C}$ is the damping matrix, $\mathbf{K}(\phi)$ is the stiffness matrix and $\mathbf{f}^{\mathbf{u}}$ and $\mathbf{f}^{\boldsymbol{\phi}}$ are the forcing vectors for the macroscopic and microscopic system. Here we assume only that the source of variability observed in failure-time data is the initial unknown damage state and take the initial damage to be uniformly distributed for each x. We thus performed Monte-Carlo life-cycle simulations for ensembles of initial damage states to obtain failure-time statistics. However, we found that the computational time required for such simulations is enormous and have therefore developed a numerical scheme based on the method of averaging [2] that reduces computational time by orders of magnitude.

For this we note that damage evolution occurs at a much slower time-scale in comparison to the macroscale dynamics and set η to be our smallness parameter. We can therefore assume that the macroscopic strain ($u'(x,t)$) stays within $\mathcal{O}(\eta)$ of its unperturbed ($\eta = 0$) steady-state at any given damage level. We thus calculate the unperturbed macroscopic steady-state, using Eq. (2a), at every time-step and substitute it into damage evolution equations Eq. (2b). The resulting equations are in standard form for averaging. Thus, we calculate averaged "slow flow" damage evolution equations, at each damage degree-of-freedom (ϕ_i), as

$$\dot{\phi}_i = \frac{2\pi}{\omega}\eta F^2 \int_0^{\frac{2\pi}{\omega}} \phi_i\left[\frac{V_{ss,i}^2}{2} - \alpha\phi_i^{-1/3}\right]^+ dt + \mathcal{O}(\eta^2), \tag{3}$$

where $V_{ss,i}$ is the unperturbed steady-state macroscopic strain at the i-th element.

ID: 437

Coupled 3D Multiscale Modeling of Failure in Thin Material Layers

Matthew Mosby
University of Notre Dame

Karel Matous
USA

Abstract:
The microstructure of material layers, such as in adhesively bonded joints, is complex, often requiring detailed numerical simulations to resolve microscale damage effects. Here, we reduce the computational cost by modeling the composite layer in the spirit of FE2 computational homogenization, attaching a representative computational domain to each integration point and linking the micro- and macro-scales by the variational energy equivalence. The fully coupled, three dimensional, finite strains model with damage mechanics at the microscale is formulated. Multiscale simulations of failure in a model adhesive layer using multiple microstructure configurations are shown. Our model system consists of homogeneous adherends connected by a layer of epoxy embedded with spherical particles. The effect of microstructure configuration and particle stiffness on the microscale damage initiation and propagation in the 3D setting is examined. Additionally, details regarding efficient parallel implementation of the method in the computational setting are discussed.

ID: 472

Concurrently Coupled Atomistic and Continuum Simulation of Strontium Titanate

Shengfeng Yang
University of Florida
United States

Youping Chen
University of Florida
United States

Abstract:
A concurrent atomistic-continuum methodology (CAC) is presented to simulate the dynamic processes of dislocation nucleation and migration as well as crack initiation and propagation in complex crystals. The CAC method is based on a unified formulation of atomistic and continuum representation of balance laws and a modified FE method to numerically solve the governing equations.

Motivated by Kirkwood's idea of molecule possessing internal degrees of freedom as well as the lattice dynamics description of internal deformation, Chen [J Chem Phys 2009;130:134706] have proposed a new description of crystalline materials as a continuous collection of lattice cells but embedded within each lattice cell is a group of discrete atoms. This concurrent two-level description of crystal structure and deformation results in a new link between the continuously-distributed local density function in the physical space and the phase space dynamical function. As exact consequences of the new definition of local density functions and Newton's laws, Chen [J Chem Phys 2009;130:134706] obtained the field representation of microscopic balance laws.

To numerically solve the governing equations, we discretize a crystalline solid with finite elements. Since the only constitutive law is the interaction force between atoms and no space derivative is involved, the inter-element connectivity is not required. In critical region with atomic-scale structural features or behavior, the governing equations can be discretized by finest mesh and solved with atomic resolution; in regions away from the critical region, coarse-scale FE discretizaiton can be used to eliminate the majority of degrees of freedom, and the displacement of atoms within the coarse elements can be mapped back through interpolation of FE nodal displacements. The same set of governing equations of the entire computer model provide a smooth interface between for the atomistic and the continuum regions, leading to a concurrently coupled atomistic-continuum model under a same single set of governing equations.

We choose the perovskite oxides strontium titanate in this work because perovskite oxides in general have a broad application on electronic devices and in particular it is one of the most commonly used substrates for the growth of complex oxide thin films and superlattices and also

a potential thermoelectric material. The rigid-ion potential for STO developed by Thomas et al. [Nucl. Instrum. Methods Phys. Res. B 2005; 228:288-92] is employed in this work to describe the force field in the CAC model. This potential includes short-range pair interactions represented by Born-Mayer model and long-range Coulomb interactions.

CAC simulation results have demonstrated a smooth passage of discontinuities, including cracks and dislocations, through the atomistic-continuum interface without the need of additional constitutive rules or special numerical treatment. Although some of the accuracy is lost in CAC simulations as a consequence of a 98.4% reduction in the degrees of freedom, the CAC results such as the stress-strain responses, the mechanisms of cracks propagation and dislocation migration, and the dissociation of dislocations all are qualitatively and quantitatively comparable with that of MD results. The stacking fault width and nanoindentation hardness measured in the CAC simulations also agree well with existing experimental data.

In distinction with existing multiscale methods, CAC method solves both the deformation of lattice cells and the internal deformation within each lattice cell. In this work we show that it is necessary to include the internal degrees of freedom of atoms from the three sublattices in STO into the methodology in order to describe the actual dissociation process and resolve the dislocation core structure. This dislocation dissociation process has been reproduced in both the CAC and the MD simulations, which justifies the need of including the internal degrees of freedom of atoms in the CAC formulation and explains why most existing concurrent multiscale methods cannot be applied to simulate mechanical behavior of polyatomic crystalline materials.

Compared with metals, the criteria for cleavage planes and slip planes are different in ionic material. The zigzag fracture pattern with crack surface being {1 0 0} neutral planes produced in both MD and CAC simulation confirms that the neutrality condition criterion for cleavage planes holds true for STO crystalline materials. The nanoindentation simulation shows that the maximum shear stress does not appear at the {1 1 0} planes due to the Schmidt factor, nevertheless the dislocations only nucleate and propagate in {1 1 0} planes that prevent bringing the cations close to each other. This thus verifies the criterion for easy glide systems in ionic materials.

ID: 481

Nanoparticle Effect on Entangled Polymer Chain Dynamics

Ying Li
Department of Mechanical Engineering, Northwestern University
United States

Martin Kröger
Polymer Physics, Department of Materials, ETH Zurich
Switzerland

Wing Kam Liu
Department of Mechanical Engineering, Northwestern University
United States

Abstract:
In polymer nanocomposites (PNCs), fillers with dimensions on the nanometer scale added into polymers offer a huge enhancement on the mechano–viscoelastic properties of polymers. Understanding the nanoparticle (NP) effect on the polymer chain dynamics has a broad impact on determining the shear elasticity and viscosity of PNCs. Even though extensive investigations have been done to explore chain dynamics inside PNCs, widely different and often conflicting results are reported. On the small scale of local chain dynamics, both experimental and computational results demonstrated that a mobility gradient existed in the direction of NPs [1–3]. On the other hand, the NPs show no influence on local segmental dynamics of the chains adjacent to silica particles, compared with motions of the bulk chains [4].

More recently the dynamics of entangled polymer chains in PNC had been explored by neutron spin echo (NSE) experiments [5], from the initial Rouse dynamics to entanglement controlled motion, by filling hydrophobically modified (nonattractive) silica particles into a poly(ethylene-alt-propylene) (PEP) matrix. Authors reported several key findings: (i) the polymer behaves Gaussian even at high filler volume fractions, ϕ, (ii) the fillers are found to have no influence on the basic Rouse relaxation rate of PEP, (iii) the effective lateral confinement length or apparent tube diameter of PEP is decreasing with increasing ϕ, and (iv) a crossover from polymer chain entanglements to 'NP entanglements' (chain motion is hindered by NPs) is observed, with the critical ϕ_c determined to be 35% [5]. At the same time, both contour length fluctuation (CLF) and constraint release (CR) effects are suppressed by these NPs [6]. However, a rigorous link between the polymer chain dynamics and its entanglement status inside PNCs is still missing.

In this paper, we performed large scale isobaric molecular dynamics (MD) on a conventional finite-extensible non-linear elastic (FENE) spring model for polymer melts, filled by spherical non-attractive NPs of diameter D, with ϕ ranging from 0% to 42% (Figs. 1a-c). Our normal mode analysis, primitive path (PP) and dynamic structure factor results on this simple model support the above key findings (i), (iii) and (iv). We find ϕ_c=31%, agreeing reasonably well with the experimental result (ϕ_c=35%) [6]. While below ϕ_c, the normal mode relaxation can be accelerated by NPs due to the disentanglement behavior of polymer chains, adding NPs above ϕ_c

slows down the relaxation processes. The basic Rouse relaxation rate is thus greatly affected by NPs. To our knowledge, the present study provides the first observation of disentanglement behavior within highly entangled polymer chains filled with NPs. Moreover, when $\phi<\phi_c$, the observed reduction of disentanglement time τ_d is linearly proportional to the reduction of entanglements per chain $<Z_{kink}>$ (Fig. 1d) or tube diameter $<a_{pp}>^{-2}$, in agreement with the tube theory [7] which also indicates the polymer chain entanglement-dominated regime. However, if $\phi>\phi_c$, such a relationship will be broken down, due to the 'NP entanglements'.

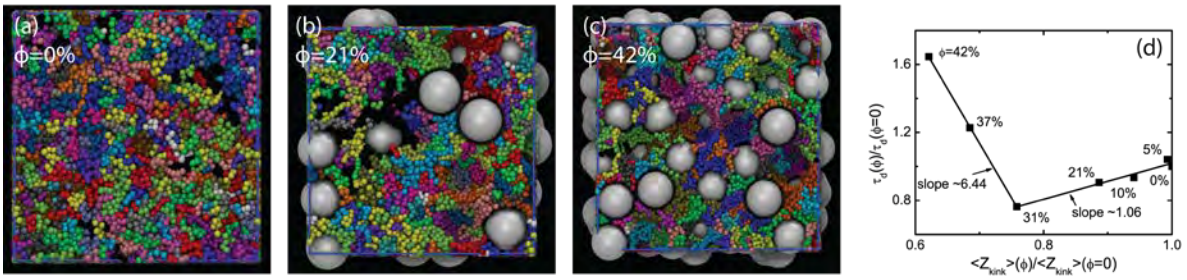

FIG. 1: (a)-(c) Snapshots of simulated systems at three different volume NP concentrations. Each chain has a randomly selected color, including black. (d) Reduced disentanglement time τ_d vs. reduced number of entanglements per chain $<Z_{kink}>$ for PNCs with different ϕ. Below ϕ_c=31%, the τ_d is found to be linearly proportional to $<Z_{kink}>$, which indicates the 'polymer entanglements'-dominated regime. Beyond ϕ_c=31%, the $<Z_{kink}>$ continues diminishing while τ_d increases with ϕ, characterizing the 'NP entanglements'-dominated regime.

[1] H. Montes, F. Lequeux, and J. Berriot, Macromolecules 36, 8107 (2003).
[2] A. Papon, K. Saalwachter, K. Schaler, L. Guy, F. Lequeux, and H. Montes, Macromolecules 44, 913 (2011).
[3] F. W. Starr, T. B. Schroder, and S. C. Glotzer, Macromolecules 35, 4481 (2002).
[4] R. B. Bogoslovov, C. M. Roland, A. R. Ellis, A. M. Randall, and C. G. Robertson, Macromolecules 41, 1289 (2008).
[5] G. J. Schneider, K. Nusser, L.Willner, P. Falus, and D. Richter, Macromolecules 44, 5857 (2011).
[6] K. Nusser, G. J. Schneider, and D. Richter, Soft Matter 7, 7988 (2011).
[7] M. Doi and S. Edwards, The Theory of Polymer Dynamics (Oxford, Clarendon, 1986).

ID: 487

A Coarse-Grained Atomistic Method for 3D Dynamic Fracture Simulation

Qian Deng
University of Florida
United States

Youping Chen
University of Florida
United States

Abstract:

In this work, a new coarse-grained (CG) method is presented. The new method combines an atomistic formulation of balance equations and a modified finite element method. Through three numerical examples, we demonstrate that the new method is able to predict the dynamic fracture behavior of crystalline materials. Firstly, the stress wave propagation is simulated through the CG method and the stress response is found to be identical with that of the corresponding atomic-level molecular dynamics (MD) simulation. Then, 3D dynamic crack propagation in a notched thin film under tension is simulated through both CG and MD simulations. Simulation results show that not only the crack propagation paths but also the local and average stresses calculated from CG simulations agree well with that from the corresponding MD simulations. Most importantly, although large number of degrees of freedoms has been eliminated, the CG models capture the atomic scale phenomenon such as the dislocation emission and migration accompanied with the crack propagation. In addition, through CG simulations of a plate under impact lading, the CG method is demonstrated to be able to simulate both stable crack propagation problems and the fragmentations of materials under high strain rate dynamic loading.

ID: 601

Generalized Viscoelastic Model for Dynamic Nanoindentation Analysis

Nimitt G. Patel
Clarkson University
United States

Philip A. Yuya
Clarkson University
United States

ABSTRACT:

In dynamic nanoindentation, the conventional analysis model for contact stiffness and damping is based on the two-parameter Voigt solid. However, the two-parameter model oversimplifies the response of most viscoelastic materials. Because it only incorporates a single relaxation time, it is limited to modeling material response at a single frequency. Furthermore, it cannot account for instantaneous elasticity and therefore underestimates contact forces. Here, we present a more general model that is applicable to more compliant viscoelastic materials. Using natural latex rubber as a test material, dynamic nanoindentation experiments were performed with a 107 μm radius diamond cono-spherical tip at ambient conditions. The results were analyzed using conventional Voigt model and contrasted to analysis done using Maxwell standard linear solid (M-SLS) model. System calibrations were performed prior to nanoindentation testing in order to ensure that material measurements are quantitative and accurate. A least-square nonlinear fit was performed on the experimental data (compliance and phase) to obtain the model constants (Fig.1). The material stiffness and damping were calculated from the material constants obtained from curve fitting. For the Voigt model, the storage stiffness is given by the stiffness of the sample ($k_1 s$) while the loss stiffness is given by the product of the frequency by the damping

constant value ($\omega C_1 s$). In the limit of linear viscoelasticity, the elastic–viscoelastic correspondence principle is used to relate the dynamic stiffness and damping of the contact to modulus values (Fig.2). The results clearly show that analysis based on a Voigt two parameter model, which works well for most glassy polymers, overestimates the material stiffness for soft compliant materials and thus, results in higher values for the storage modulus. Consequently, we can deduce a conclusion that a refined model incorporating more elements should be used for analyzing dynamic nanoindentation data for such materials. Because the measured frequency response is a combination of both the indenter parameters and tip-sample contact forces, proper systems calibration is necessary to ensure accurate measurements. The analysis will prove useful for quantitative nanoindentation property measurements of viscoelastic materials such as compliant polymers and soft biological materials.

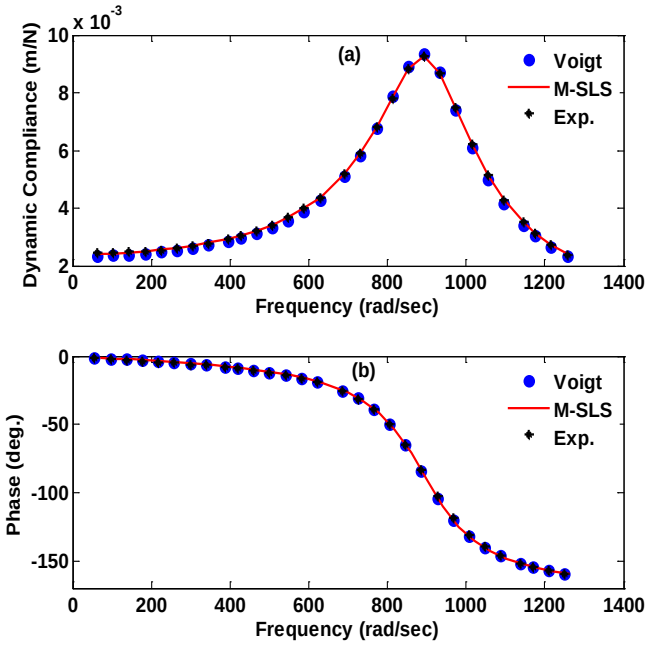

Fig. 1. Example of frequency response of the indenter tip in contact with latex showing, (a) dynamic compliance and (b) phase shift.

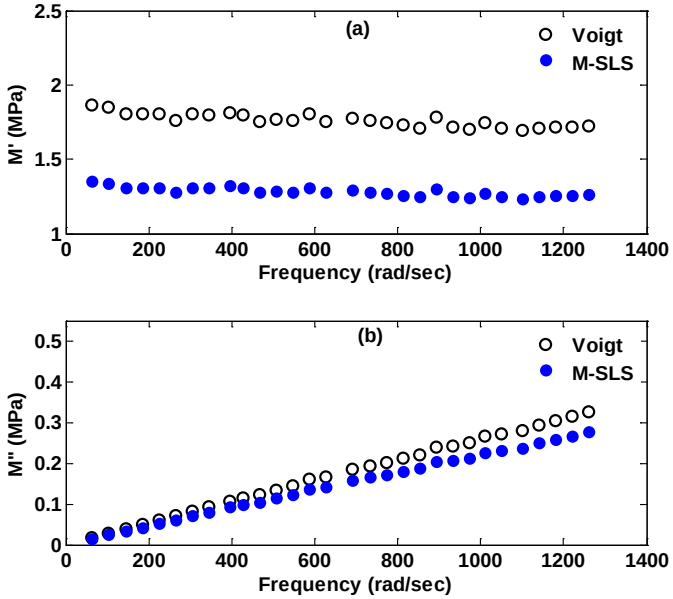

Fig. 2. The storage and loss indentation moduli for latex as a function of frequency when modeling the tip-sample forces as a Maxwell standard linear solid and as a Voigt solid.

ID: 609

A Linearly Elastic Model for a Peridynamic Body

Adair R. Aguiar, aguiarar@sc.usp.br
Department of Structural Engineering, University of São Paulo
São Carlos, SP, Brazil

Roger L. Fosdick, fosdick@aem.umn.edu
Department of Aerospace Engineering and Mechanics, University of Minnesota
Minneapolis, MN, United States

Abstract:
The peridynamic theory is an extension of the classical continuum theory in which a material point interacts directly with other material points separated from it by a finite distance. The main strength of the peridynamic theory is to apply its basic equations directly on either a surface of discontinuity, such as a crack, or a continuum in which discontinuities may appear as a result of deformation. Away from these places, the deformation is smooth, causing the peridynamic theory to yield the same governing equations as the classical theory in the limit of vanishing distances between material points. Constitutive modeling within the peridynamic theory considers the collective deformation at each time of all the material within a δ-neighborhood of any point. The assignment of the parameter δ, called the horizon, is treated as a material property. The difference displacement field quotient in this neighborhood, rather than the extension scalar field, is used to generate a three dimensional state-based linearly elastic peridynamic theory. This yields an enhanced interpretation of the kinematics between bonds that includes both length and relative angle changes. A strain energy function for a linearly elastic isotropic peridynamic material which contains four material constants is proposed as a model, and it is used to obtain the force vector state and the associated modulus state for this material. These states are analogous to, respectively, the stress field and the fourth-order elasticity tensor in the classical linear theory. In the limit of small horizon, we find that only three of the four peridynamic material constants are related to the classical elastic coefficients of an isotropic linear elastic material, with one of the three constants being arbitrary. The fourth peridynamic material constant, which accounts for the coupling effect of both bond length and relative angle change, has no effect in the limit, but remains a part of the peridynamic model. It is a matter of concern that, in spite of the fact that the peridynamic model is isotropic and reproduces the classical elasticity model in the limit of small horizon, two peridynamic constants are left undetermined. The determination of these two constants is the subject of future investigation.

1. The Linear Peridynamic Model

Let $\mathsf{B} \subset \mathsf{E}^3$ be the undistorted reference configuration of an elastic solid body at time $t = 0$ and let $\boldsymbol{\chi}(\mathbf{x},t)$ be the position of the particle $\mathbf{x} \in \mathsf{B}$ at time $t \geq 0$. Constitutive modeling within the peridynamic theory considers the collective deformation at each time t of all the material within a neighborhood of an arbitrary point $\mathbf{x}_0 \in \mathsf{B}$. We shall omit writing the time variable t. Here, this neighborhood is the sphere $\mathsf{N}_\delta \subset \mathsf{B}$ centered at $\mathbf{x}_0$ of radius δ, called the *horizon*. For any $\mathbf{x} \in \mathsf{B}$ such that $|\,\mathbf{x} - \mathbf{x}_0\,| < \delta$, the vector $\boldsymbol{\xi} := \mathbf{x} - \mathbf{x}_0$ is called a bond to $\mathbf{x}_0$. The displacement field $\mathbf{u}(\mathbf{x})$ associated with the motion $\boldsymbol{\chi}(\mathbf{x})$ at $\mathbf{x} \in \mathsf{B}$ is defined by $\mathbf{u}(\mathbf{x}) := \boldsymbol{\chi}(\mathbf{x}) - \mathbf{x}$. We define the difference displacement state at $\mathbf{x}_0$ as $\underline{\mathbf{u}}\langle\boldsymbol{\xi}\rangle := \mathbf{u}(\mathbf{x}) - \mathbf{u}(\mathbf{x}_0)$.

The strain energy function in the standard peridynamic theory defines the value of the free energy at each $\mathbf{x}_0 \in \mathsf{B}$ in terms of the deformation state at $\mathbf{x}_0$ in the neighborhood N_δ. Here, we take the strain energy as

$$W_{\mathbf{x}_0}[\underline{\mathbf{h}}] = \int_{\mathsf{N}_\delta}\int_{\mathsf{N}_\delta} \omega(|\boldsymbol{\xi}|,|\boldsymbol{\eta}|)\Big[\frac{\alpha_1}{2}\big(\underline{\varepsilon}[\underline{\mathbf{h}}]\langle\boldsymbol{\xi}\rangle\big)^2 + \alpha_2\, \underline{\varepsilon}[\underline{\mathbf{h}}]\langle\boldsymbol{\xi}\rangle\, \underline{\varepsilon}[\underline{\mathbf{h}}]\langle\boldsymbol{\eta}\rangle + \frac{\alpha_3}{2}\big(\underline{\underline{\gamma}}[\underline{\mathbf{h}}]\langle\boldsymbol{\xi},\boldsymbol{\eta}\rangle\big)^2 + \alpha_4\, \underline{\underline{\gamma}}[\underline{\mathbf{h}}]\langle\boldsymbol{\xi},\boldsymbol{\eta}\rangle\, \underline{\varepsilon}[\underline{\mathbf{h}}]\langle\boldsymbol{\xi}\rangle\Big] dv_{\boldsymbol{\eta}}\, dv_{\boldsymbol{\xi}}, \tag{1.7}$$

where $\underline{\mathbf{h}}\langle\boldsymbol{\xi}\rangle = \underline{\mathbf{u}}\langle\boldsymbol{\xi}\rangle/|\boldsymbol{\xi}|$, $\omega(\cdot,\cdot)$ is a given weighting function satisfying $\omega(|\boldsymbol{\xi}|,|\boldsymbol{\eta}|) = \omega(|\boldsymbol{\eta}|,|\boldsymbol{\xi}|)$, $\alpha_i, i = 1,\ldots,4$, are peridynamic constants to be specified, $\underline{\varepsilon}[\underline{\mathbf{h}}]\langle\boldsymbol{\xi}\rangle = \underline{\mathbf{e}}\langle\boldsymbol{\xi}\rangle \cdot \underline{\mathbf{h}}\langle\boldsymbol{\xi}\rangle$ defines an infinitesimal normal strain state with $\underline{\mathbf{e}}\langle\boldsymbol{\xi}\rangle = \boldsymbol{\xi}/|\boldsymbol{\xi}|$, and $\underline{\underline{\gamma}}[\underline{\mathbf{h}}]\langle\boldsymbol{\xi},\boldsymbol{\eta}\rangle = \big(\underline{\underline{\mathbf{e}}}\langle\boldsymbol{\xi},\boldsymbol{\eta}\rangle \cdot \underline{\mathbf{h}}\langle\boldsymbol{\xi}\rangle + \underline{\underline{\mathbf{e}}}\langle\boldsymbol{\eta},\boldsymbol{\xi}\rangle \cdot \underline{\mathbf{h}}\langle\boldsymbol{\eta}\rangle\big)/2$, $|\boldsymbol{\xi}| < \delta, |\boldsymbol{\eta}| < \delta$, defines an infinitesimal shear strain state, with $\underline{\underline{\mathbf{e}}}\langle\boldsymbol{\xi},\boldsymbol{\eta}\rangle = \big(\mathbf{1} - \underline{\mathbf{e}}\langle\boldsymbol{\xi}\rangle \otimes \underline{\mathbf{e}}\langle\boldsymbol{\xi}\rangle\big)\underline{\mathbf{e}}\langle\boldsymbol{\eta}\rangle / \sin\alpha$ and α being the smallest included angle between $\boldsymbol{\xi}$ and $\boldsymbol{\eta}$.

In the limit of small horizon, $\delta \to 0$, we use an expression from Silling (2010) to show that $\mathbf{H}_0 \cdot \big(\mathbf{C}_{\mathbf{x}_0}\mathbf{H}_0\big)\big/2 = W_{\mathbf{x}_0}[\mathbf{H}_0\,\underline{\mathbf{e}}]$, where $\mathbf{C}_{\mathbf{x}_0}$ is the elasticity tensor at $\mathbf{x}_0$ from the classical linear theory and $\mathbf{H}_0 = \mathbf{H}_0(\mathbf{x}_0)$ is the displacement gradient field evaluated at $\mathbf{x}_0$, which is assumed to be small. Using (1.1) to evaluate $W_{\mathbf{x}_0}[\mathbf{H}_0\,\underline{\mathbf{e}}]$, we find that the term multiplying α_4 does not contribute to the proposed form of the free energy $W_{\mathbf{x}_0}[\underline{\mathbf{h}}]$ when $\underline{\mathbf{h}} = \mathbf{H}_0\,\underline{\mathbf{e}}$. We also find that the the classical linear material is isotropic and that the peridynamic constants α_1, α_2, and α_3 satisfy the relations $2\alpha_1 + \alpha_3 = 15(C_{1111} - C_{1122})/(16\hat{\omega})$, $\alpha_1 + 2\alpha_2 = 3(C_{1111} + 2C_{1122})/(16\hat{\omega})$, where $\hat{\omega} = \pi^2 \lim_{\delta\to 0}\int_0^\delta\int_0^\delta \omega(\zeta,\eta)\, d\zeta\, d\eta$ and C_{1111}, C_{1122} are components of $\mathbf{C}_{\mathbf{x}_0}$ in a fixed orthonormal basis $\{\mathbf{e}_i\}$, $i = 1,2,3$. Given one of the three peridynamic coefficients α_1, α_2, or α_3, the remaining two are determined in terms of the elastic constants of an isotropic material from the classical linear theory. Thus, there are two undetermined peridynamic coefficients, which remain part of the enhanced theory proposed here in which both bond stretch and relative bond angles are taken into account, and their fundamental relationship to the deformation and force response state needs further explanation.

Acknowledgements

Financial support from the Brazilian funding agencies FAPESP, CNPq, and CAPES are gratefully acknowledged. The first author is also very grateful to both MSI and the AEM/UMN department for their hospitality and to the SET/EESC/USP department for the 6-month sabbatical to conduct this research abroad.

ID: 631

Effective Electromechanical Properties of a Medium Containing Unidirectional Cylindrical Holes Embedded in a 622 Piezoelectric Matrix

Adair Roberto Aguiar, aguiarar@sc.usp.br
Uziel Paulo da Silva, uziel@sc.usp.br
Programa de Pós-Graduação Interunidades Bioengenharia–EESC-FMRP-IQSC / USP
São Carlos, SP, Brazil

Julián Bravo Castillero, jbravo@matcom.uh.cu
Reinaldo Rodríguez Ramos, reinaldo@matcom.uh.cu
Facultad de Matemática y Computación, Universidad de La Habana San Lázaro y L. Vedado
Habana 4, CP-10400, Cuba

Abstract:
Bones are heterogeneous solids with highly complex structures that require multiple scale analysis. Experimental evidence indicates that bones present the piezoelectric effect and that this effect accelerates bone growth and remodeling, which is very useful in the consolidation of bone fracture. The Asymptotic Homogenization Method (AHM) yields a two-scale procedure to analyze the electromechanical behavior of these complex structures. To obtain their effective properties, bones are modeled as composite materials containing a periodic distribution of unidirectional circular cylindrical holes in a linear, transversely isotropic piezoelectric matrix whose constituent material belongs to the symmetry crystal class 622. The holes are centered in a periodic cell of square cross section and the periodicity is the same in two perpendicular directions. The composite state is antiplane shear piezoelectric, that is, a coupled state of out-of-plane shear deformation and in-plane electric field. A set of local problems arises from the two-scale analysis using the AHM. Complex variable methods are used to obtain solutions to these problems. These solutions are expanded in a power series of Weierstrass elliptic functions containing coefficients that are determined from the solutions of systems of infinite linearly algebraic equations. Truncating the infinite systems, we obtain analytical formulae for elastic, piezoelectric and dielectric effective properties, which depend on the volume fraction of the holes and an electromechanical coupling factor of the matrix. To compare these formulae with formulae available in the literature, the effective properties are plotted against volume fraction, showing good agreement.

NUMERICAL RESULTS

Using the Asymptotic Homogenization Method (AHM), we have obtained analytical formulae for the effective properties of a periodic distribution of unidirectional circular cylindrical holes in a linear, transversely isotropic piezoelectric matrix whose constituent material belongs to the symmetry crystal class 622. The formulae are given by

$$\frac{p_e}{p}=\frac{\left[(1+V_1-L)(V_2-L)(1+\sigma)\right]}{\chi},\qquad \frac{s_e}{s}=\frac{(V_2-L)^2(1+\sigma)}{\chi},\qquad \frac{t_e}{t}=\frac{(1+V_1-L)(V_2-L)(1+\sigma)}{\chi}, \tag{1}$$

where p, s, and t are the elastic, piezoelectric, and dielectric material constants of the matrix, respectively, p_e, s_e, and t_e are the effective elastic, piezoelectric and dielectric material

constants of the composite, V_1 is the area fraction of the holes, V_2 is the area fraction of the matrix, $\sigma = s^2/(pt)$ is the electromechanical coupling factor of the matrix,

$$\chi = (1+V_2-L)^2 + \sigma(V_1-L)^2, \quad \text{and} \quad L = \sum_{g=1}^{N_0}\sum_{i=1}^{N_0}\eta_{1\,4g-1}\left(\delta_{4g-1\,4i-1} - \sum_{t=1}^{N_0}\eta_{4g-1\,4t+1}\eta_{4t+1\,4i-1}\right)^{-1}\eta_{4i-11}. \tag{2}$$

In (2.b), $\eta_{kl} = -C^l_{l+k-1}r^{l+k}S_{k+l}$, no sum on l, $C^l_k = \dfrac{k!}{l!(k-1)!}$, $S_{k+l} = \sum_{m=-\infty}^{\infty}\sum_{n=-\infty}^{\infty}(m\omega_1 + n\omega_2)^{-(k+l)}$, $m^2+n^2 \neq 0$, $k+l \geq 3$, and $S_2 = 0$. For the square array of holes considered in this work, $\eta_{kl} \neq 0$ if $k+l = 4n$. Otherwise, $\eta_{kl} = 0$. Note that η_{kl} may not be equal to η_{lk}.

In Fig. 1 we show curves for the ratio between the effective coupling factor $\sigma_e = s_e^2/(p_e t_e)$ and σ versus the area fraction V_1 using both the expressions (1) for increasing values of N_0 in (2.b) and expressions obtained via the Mori-Tanaka approach. Observe from this figure that the curves obtained via the AHM become indistinguishable for large values of N_0 and all of these curves lie below the curve obtained via the Mori-Tanaka approach, which is represented by the stars. The curves have the same qualitative behavior. The good agreement among all the curves obtained via the AHM suggests that the expression corresponding to $N_0 = 0$ yields a very simple formula to calculate the effective coupling factor of the composite.

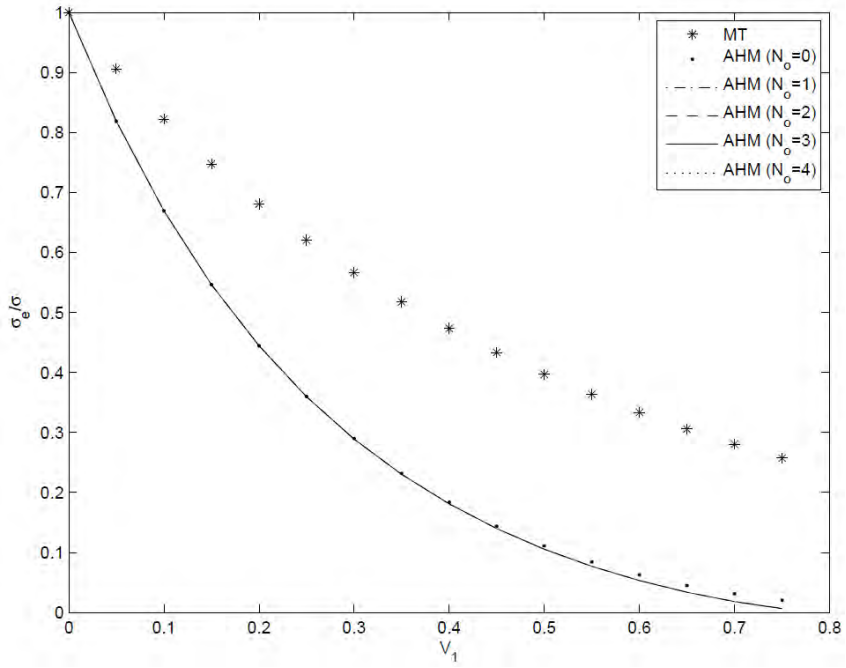

Figure 1: The ratio σ_e/σ versus the area fraction V_1.

Acknowledgements

This work is dedicated to Professor B.E Pobedrya for his 75th anniversary. Financial support from the National Council for Scientific and Technological Development (CNPq) and the Coordination for the Improvement of Higher Education Personnel (CAPES) is gratefully acknowledged.

ID: 664

Microstructural Modeling of Polymer Nanocomposites using a Coupled Viscoelastic-Viscoplastic-Viscodamage Constitutive Model

Rashid K. Abu Al-Rub
Zachry Department of Civil Engineering, Texas A&M University
USA

Ardeshir H. Tehrani
Zachry Department of Civil Engineering, Texas A&M University
USA

Abstract:

There have been very few attempts for conducting more realistic large scale simulations of nano-composites with random distribution of nano particles with different morphologies (e.g. carbon nanotubes/nanofibers, nanoclays), which is the focus of this study. Many experimental studies revealed the enhancement in the multifunctional properties of nanocomposites strongly depends on the morphology and properties of the nano-inclusions. The volume fraction, aspect ratio, size, distribution, and mechanical properties of inclusions affect the mechanical responses of polymer nanocomposites. Although there are many experimental studies on nanoclays and nanotubes/ fibers polymer-based composites, very little research has been done in the three-dimensional micromechanical computational modeling of these nanocomposites. In this study, damage evolution in nanocomposites containing the PMMA polymer embedded with silicate nanoclay (NC) particles and carbon nanotubes (CNT) of various microstructures is simulated by using coupled thermo-nonlinear-viscoelastic-viscoplastic-viscodamage constitutive model. Three-dimensional microstructure-based RVEs (representative volume elements) have been arbitrarily generated with different random distributions and structures of dispersed nano-inclusions.

1. Constitutive Model

A summary of the main constitutive equations are presented here. For more details, one can refer to Tehrani and Abu Al-Rub (2011). The Eluerian strains ε_{ij} are decomposed into viscoelastic and viscoplastic components:

$$\varepsilon_{ij} = \varepsilon_{ij}^{ve} + \varepsilon_{ij}^{vp} \tag{1}$$

Schapery's nonlinear viscoelastic model is used to model the viscoelastic response as:

$$\varepsilon_{ij}^{ve,t} = g_0 \bar{D}_0 \bar{\tau}_{ij}^{t} + g_1 \int_0^t \Delta\bar{D}^{\left(\psi^t - \psi^\xi\right)} d\left(g_2 \bar{\tau}_{ij}^{\xi}\right) \tag{2}$$

where $\bar{D}_0$ and $\Delta\bar{D}$ are the instantaneous and transient compliances, respectively, g_0, g_1, and g_2 are nonlinear parameters that are functions of stress and temperature, $\psi^t = t / a_T$ is the reduced time with a_T being the time-temperature-shift factor, and $\bar{\tau}_{ij} = \tau_{ij} / (1-\phi)$ is the Kirchhoff stress components in the undamaged (effective) configuration with $0 \le \phi \le 1$ being the damage density. The rate of viscoplastic deformation, d_{ij}^{vp}, is given by:

$$d_{ij}^{vp} = \Gamma^{vp} \left\langle f / \tau_y^0 \right\rangle^N \frac{\partial g}{\partial \bar{\tau}_{ij}} \tag{3}$$

where Γ^{vp}, τ_y^0, and N are material parameters, and g is a Drucker-Prager-Type viscoplastic potential. The damage evolution is modeled using the following viscodamage evolution law:

$$\dot{\phi} = \Gamma^{vd} \left[\left(\left(\bar{Y} - Y_{ref} \right) / Y_{ref} \right) (1-\phi)^2 \right]^q \exp\left(k \varepsilon_e \right) \tag{4}$$

where Γ^{vd}, Y_{ref}, q, and k are material parameters, $\bar{Y}$ is the energy release rate, and $\varepsilon_e = \| \varepsilon_{ij} \|$ is the total effective strain.

2. Mesomechanical Simulations

Figure 1 shows virtually created three-dimensional RVEs with dispersed and perfectly bonded NC and CNTs in a PMMA polymer matrix.

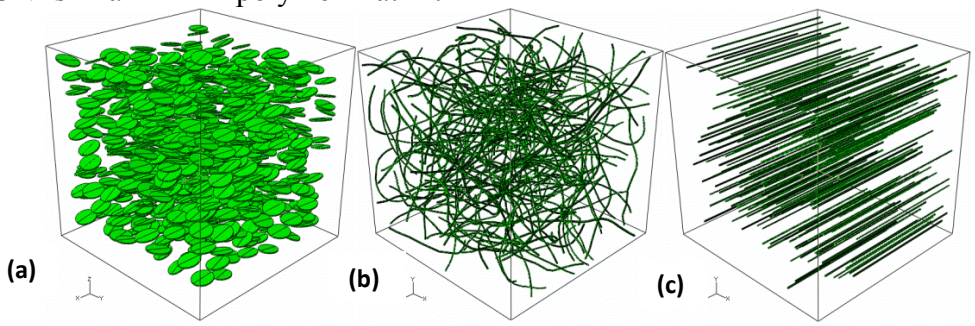

Figure 1. RVEs with: (a) 2 wt% of NC particles, (b) 0.5 wt% of curved CNTs, and (c) 0.5 wt% of straight CNTs.

Several finite element simulations under displacement control test (tension and compression) were conducted. Figure 2 shows the stress-strain responses of the composites with different weight fractions of nano-particles. The composites' Young's moduli, strain hardening rates, and ultimate strength increase as the weight fraction of CNTs/NC increases. The enhancement is more pronounced for the straight CNT/PMMA composite.

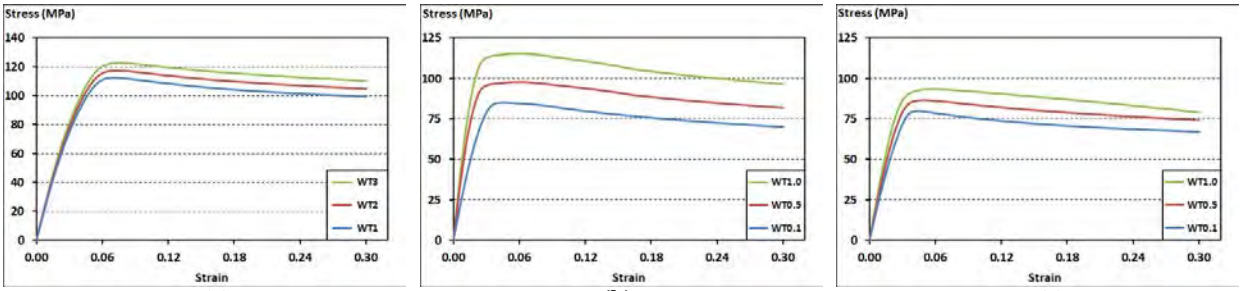

Figure 2. Stress-strain responses of RVEs subjected to tension with a rate of 0.001/sec : (a) NC/PMMA composite (1, 2, and 3 wt%), and CNT/PMMA composite (0.1, 0.5, and 1.0 wt%); (b) straight and (c) curved.

Reference

Tehrani, A.H., Abu Al-Rub, R.K., "Mesomechanical modeling of polymer/clay nanocomposites using a viscoelastic-viscoplastic-viscodamage constitutive model," ASME Journal of Engineering Materials and Technology, Vol. 133, No. 4, 011017, 2011.

ID: 732

Atom-Based Continuum Method via Generalized Gauss Quadrature

Xianqiao Wang
The George Washington University
USA

James Lee

Abstract:

Multiscale material modeling has evolved into predictive tools that complement experimental investigations at comparable length- and time-scales, with the explosive growth of interest in different kinds of theories. However, literature in this topic has struggled to strike a reliable balance over years between the computational efficiency and the accuracy of results involved in systems. Here we present a novel atom-based continuum methodology [1] coupling with thermal, mechanical, and electrical mechanism, aiming at a seamless transition from the atomistic to the continuum description of multi-element crystalline material. Taking both efficiency and accuracy into consideration, we adopt a modified finite element method with generalized Gauss quadrature based on interatomic potentials. Since the interatomic potential is the only constitutive law needed to characterize the mechanism of the materials in question and no spatial derivative is involved in the governing equation, the connectivity between neighboring elements is not required, thereby permitting and facilitating simulation of the initiation and evolution of discontinuities. By implementing the disparate discretization or adopting various number of Gauss integral points, the simulation model of interest can be evolved from a nodal-based simulation to a full-blown molecular dynamics simulation. With significantly less degrees of freedom than that of a fully atomistic model and without additional constitutive law to govern the system, the atom-based continuum method with generalized Gauss quadrature offers the potential to reproduce key physical phenomena while maintaining the reliable accuracy of the results in quest.

REFERENCES [1] Xianqiao Wang and J.D. Lee, "An Atom-Based Continuum Method for Multi-element Crystals at Nano Scale," CMES: Computer Modelling in Engineering & Sciences, 69(3):199-222, 2010.

ID: 735

Modeling of the Acoustic Radiation Force Produced in Tissue-Like Solids by a Modulated Ultrasound Field

Egor Dontsov
University of Minnesota
United States

Bojan Guzina
University of Minnesota
United States

Abstract:
The acoustic radiation force (ARF) is a phenomenon that stems from the nonlinear effects of finite-amplitude wave propagation. It represents the *mean* transfer of momentum, associated with the sound waves, to the medium, and allows for an effective computation of the *mean* motion induced by high-intensity sound waves, e.g. acoustic streaming in fluids. The concept of the ARF bears relevance to a number of emerging biomedical applications [1], where the focused ultrasound beam is typically modulated with a low-frequency signal as a tool to facilitate the *local* reconstruction of tissue's viscoelastic properties [1-3]. As an illustration, Fig. 1 shows the schematics of the shear-wave motion generated by the ARF, and the numerical simulation of the axial displacement, produced by a short pulse-modulated ultrasound field.

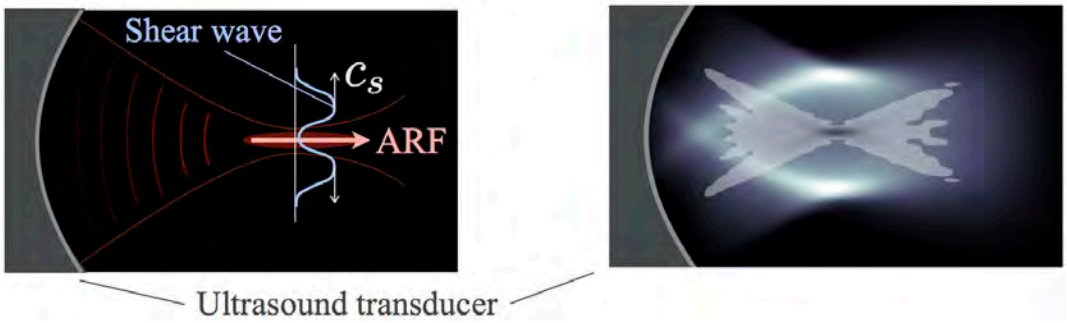

Figure 1: Left panel: schematics of the shear wave motion produced by the radiation force push; right panel: simulation of the intensity field (foreground image) and ARF-induced displacement (background image).

The complete modeling of the ARF-generated shear motion can be split into three independent tasks (see Fig. 2): i) computation of the ultrasound-scale acoustic solution, ii) derivation of the formula for the ARF, which allows the computation of the body force distribution for a given ultrasound field, and iii) solution of the linear viscoelastic problem with the ARF body force. This study focuses exclusively on the second task, i.e. on the derivation of the formula for the ARF. To cater for biomedical applications of the radiation force, the developments consider the situations when the high-intensity focused ultrasound field is modulated by either steady-state or transient signal whose dominant frequency is small relative to the ultrasound frequency.

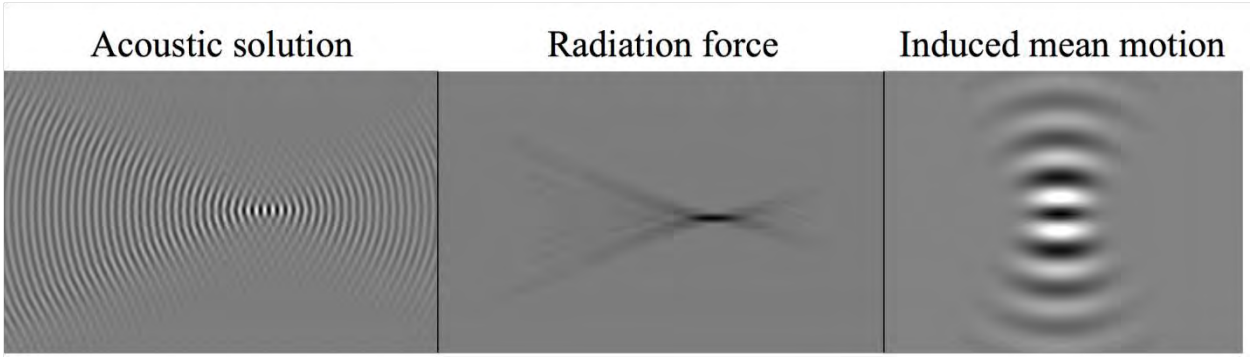

Figure 2: Three components that are required to model the ARF-induced deformation: i) model for the ultrasound-scale wave motion, ii) formula for the ARF, and iii) solution of the linear viscoelastic problem with ARF as a body force (picture corresponds to the time-harmonic modulation).

To expose the mechanics of ultrasound-based tissue palpation, the analysis of the nonlinear wave motion at hand is simplified by taking the ratio between the modulation and ultrasound frequency, the Mach number, the ratio of the shear to bulk modulus, and the dimensionless attenuation coefficient each to be small and commensurate in magnitude. A scaling approach that is driven by the geometry of the focused ultrasound beam demonstrates that the waves are nearly planar within the region of interest (i.e. the focal zone, where the nonlinear effects are most pronounced). Following a recent plane-wave study [4], the computation of the ARF due to modulated focused ultrasound is next facilitated by the introduction of "fast" and "slow" time variables, which allows the analysis to parse individually the ultrasound- and modulation-rate variations in the solution. To expose the mean motion induced by the ARF, the "fast" time average, computed over the period of ultrasound vibrations, is deployed to filter out the ultrasound-scale oscillations and extract the sought mean motion. On approximating the constitutive response of soft tissues as that of an isotropic nonlinear viscoelastic solid with heat conduction, the governing equations for the mean tissue motion, featuring the new formula for the ARF [5], are obtained by taking the "fast" time average of the nonlinear field equations dictating the original ultrasound-scale problem. Thus obtained radiation force is shown to consist of two qualitatively different terms: i) the *potential* body force term, which is proportional to the gradient of the intensity and generates compressional waves, and ii) the *directional* body force term, which acts along the transducer's axis and generates predominantly shear wave motion (as shown in Fig.1). A comparison with the existing theory reveals a number of key features that are brought to light by the new formulation, including the contributions to the ARF of ultrasound modulation and thermal expansion, as well as the precise role of the third-order elastic moduli in generating the sustained radiation body force in tissue-like solids by a focused ultrasound beam.

References:

[1] A. P. Sarvazyan, O. V. Rudenko, and W. L. Nyborg. Biomedical applications of radiation force of ultrasound: historical roots and physical basis. Ultras. Med. Biol., 36:1379–1394, 2010.
[2] B. B Guzina, K. Tuleubekov, D. Liu, and E. Ebbini. Viscoelastic characterization of thin tissues using acoustic radiation force and model-based inversion. Phys. Med. Biol., 54:40894112, 2009.
[3] M. Fatemi and J. Greenleaf. Vibro-acoustography: An imaging modality based on ultrasound-stimulated acoustic emission. Proc. Natl. Acad. Sci., 96:6603–6608, 1999.
[4] E.V. Dontsov and B. B. Guzina. Effect of low-frequency modulation on the acoustic radiation force in Newtonian fluids. SIAM J. Appl. Math., 71:356–378, 2011.
[5] E.V. Dontsov and B. B. Guzina. Acoustic radiation force in tissue-like solids due to modulated sound field. JMPS, doi: 10.1016/j.jmps.2012.04.006.

ID: 737

Multiple Time Scale Algorithm for Simulation of Multiphysics

James D. Lee
The George Washington University, Washington, DC, United States

Jiaoyan Li
The George Washington University, Washington, DC, United States

Xianqiao Wang
Georgia University, Athens, GA, United States

Abstract:
Consider a crystalline material system consisting of two regions (1) an atomic region: modeled by MD simulation and a relatively small time step is used to update the solutions and (2) an atom-based continuum region: modeled by CG-MD simulation and a relatively large time step is employed to reduce the computational efforts, and thereby it leads to an acceleration of simulations (cf. Figure 1). Since the crystalline material is distinguished from other states of matter by a periodic arrangement of the atoms, it can then be represented as a collection of repeated unit cells and a group of discrete and distinct atoms situated within each unit cell.

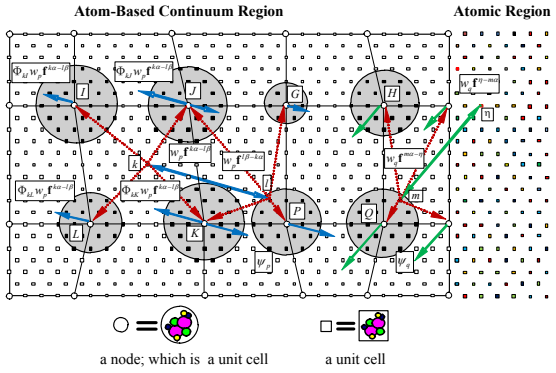

Fig. 1 Multiple length scale modeling

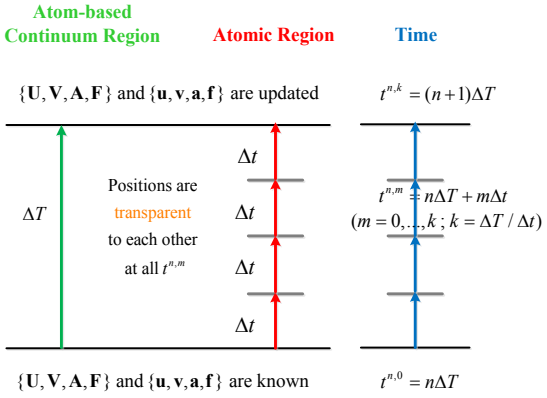

Fig. 2 Multiple Time scale Algorithm

The key point is how to calculate the interatomic force for both atomic region and atom-based continuum region (cf. Figure 1). In the atom-based continuum region, we assume the generic displacement field can be related to the nodal values through shape function.

$$\mathbf{u}^{k\alpha} = \Phi_N^k \mathbf{U}_N^\alpha \tag{5}$$

One may prove that the nodal force contributed by $\mathbf{f}^{k\alpha}$ can be obtained as

$$\mathbf{F}_N^\alpha = \Phi_N^k \mathbf{f}^{k\alpha} \tag{6}$$

Figure 2 shows the time steps, ΔT *and* Δt, and the marching for both atom-based continuum region and atomic region, respectively.

To control the temperature in a specific region through which the thermal effects are brought into picture, the atomistic system is regulated by a Nosé-Hoover thermostat:

$$m^i \ddot{\mathbf{u}}^i = \mathbf{f}^i + \boldsymbol{\varphi}^i - m^i \chi(t)(\mathbf{v}^i - \overline{\mathbf{v}}) \tag{7}$$

where $\chi(t)$ is a friction coefficient controlled by

$$\frac{d\chi(t)}{dt} = \frac{1}{\tau^2}\{\frac{T}{T_{eqb}} - 1\} \tag{8}$$

and the temperature T is calculated as a space-averaged variable of the velocity field

$$3Nk_B T = \sum_{i=1}^{N} m^i (\mathbf{v}^i - \overline{\mathbf{v}})^2 \tag{9}$$

In eq. (3), $\boldsymbol{\varphi}^i$ is the Lorentz force due to the external electromagnetic field

$$\boldsymbol{\varphi}^i = q^i (\mathbf{E}^{ext} + \mathbf{v}^i \times \mathbf{B}^{ext} / c) \tag{10}$$

It is noticed that one may calculate the electrical quantities, including polarization, voltage, and electrical field, based on atomic motions

$$\mathbf{P}^{ind}(\mathbf{x}^k, t) = \frac{1}{V_{cell}} \sum_{\alpha=1}^{N_a} q^\alpha \Delta \mathbf{x}^{k\alpha} \tag{11}$$

$$V^{ind}(\mathbf{x}^k, t) = \sum_{l=1, l\neq k}^{N_l} \sum_{\alpha=1}^{N_a} q^\alpha \Delta \mathbf{x}^{l\alpha} \cdot \frac{(\mathbf{x}^k - \mathbf{x}^l)}{\left|\mathbf{x}^k - \mathbf{x}^l\right|^3} \tag{12}$$

$$\mathbf{E}^{ind}(\mathbf{x}^k, t) = \sum_{l=1, l\neq k}^{N_l} \sum_{\alpha=1}^{N_a} q^\alpha \Delta \mathbf{x}^{l\alpha} \cdot [\frac{3(\mathbf{x}^k - \mathbf{x}^l) \otimes (\mathbf{x}^k - \mathbf{x}^l)}{\left|\mathbf{x}^k - \mathbf{x}^l\right|^5} - \frac{\mathbf{I}}{\left|\mathbf{x}^k - \mathbf{x}^l\right|^3}] \tag{13}$$

In this presentation, we will also address how some of the conceptual problems and numerical difficulties associated with non-equilibrium MD simulation are resolved. Through the simulation, we will demonstrate some thermomechanical-electromagnetic coupling phenomena. These include propagation of wave with optical modes, mechanically induced voltage, electric field and temperature, effects of electromagnetic wave, and wave passing through interface between atoms and continuum.

ID: 768

Multi-scale Contact Evolution Analysis between Cellular Polymeric Pad and Rigid Substrate for Applications in Microelectronics Machining

Ashraf Bastawros
Iowa State University

Tianyu Yu

Abstract:
NO ABSTRACT

IV.7

Multiscale Mechanics of Materials - Size Scale Effects in Micro/Nano Structured Materials and Composites

ID: 198

SES 2012 – October 10-12, 2012 – Atlanta, GA
Symposium on 'Size Scale Effects in Micro/Nano Structured Materials and Composites'

Exploring the Deformation and Mechanics of Twinned Nanocrystalline Copper with Atomistic Simulations

Garritt J. Tucker, Stephen Foiles, Henry Padilla, and Brad Boyce
Sandia National Laboratories, Albuquerque, NM 87185

The influence of twin boundaries (TBs) on the mechanics of materials has been an active area of research in the last decade due to potential improvements in functional properties. In metallic materials, such as copper, higher strengths have been obtained without sacrificing other beneficial bulk properties with the addition of TBs in the microstructure. However, questions still remain pertaining to the influence of TBs on the deformation and microstructural evolution in nanocrystalline (NC) materials. Therefore, we leverage large-scale molecular dynamics simulations and a textured columnar NC copper structure with different TB densities, to elucidate the affect of TBs on both the mechanical properties and underlying deformation mechanisms. The results show that TBs do influence the mechanics of columnar NC copper under uniaxial loading at room temperature. Furthermore, by incorporating various densities of TBs in the columnar microstructure, differences are computed in the underlying deformation mechanisms controlling plasticity, and TBs could potentially be favored pathways for dislocation migration. Our results show that the role of deformation twinning, TB migration, and the propensity of the NC grains to nucleate dislocations, varies with initial TB density. We also study microstructural evolution and grain growth with varying densities of TBs. The role of grain boundaries, as dislocation sources and carriers of plasticity, is also investigated as a function of loading and TB density.

* *Sandia National Laboratories is a multi-program laboratory managed and operated by Sandia Corporation, a wholly owned subsidiary of Lockheed Martin Corporation, for the U.S. Department of Energy's National Nuclear Security Administration under contract DE-AC04-94AL85000.*

ID: 274

Micropillar compression of LiF between room temperature and 400 ºC

R. Soler and J.M. Molina-Aldareguia
IMDEA Materials Institute
Spain

J. Segurado and J. Llorca
IMDEA Materials Institute and Department of Materials Science, Polytechnic University of Madrid, Spain

J.M. Wheeler and J. Michler
EMPA-Swiss Federal Laboratories for Materials Science and Technology
Switzerland

Abstract:
Micropillar compression tests have become popular in recent years to study the effect of specimen size (in the range of micron and sub-micron pillar diameter) on the mechanical properties of single-crystals in the absence of strain gradients. The first studies were carried out in face-centred-cubic (fcc) metals [1-3] and reported a strong increase in the flow stress as the micropillar diameter decreased below ≈10 □m. Recently, the method has been used to study other singe-crystal materials like ceramics and oxides [4-5] as means of studying plasticity of hard materials at room temperature, and typically little size effects have been observed.

LiF constitutes a striking example, as results are very dependent on crystal orientation [6]. Micropillar compression of [111] oriented LiF single crystal micropillars were carried out in the temperature range 25-400 ºC, for micropillar diameters between 1 and 5 □m. The pilla
obtained by etching the matrix in directionally-solidified NaCl–LiF and KCl-LiF eutectic compounds, as shown in Fig. 1(a). Previous studies in [100] oriented LiF micropillars reported a strong size effect [7], while our studies [8] in [111] oriented LiF micropillars show no size effects at room temperature. One explanation for this is the large lattice resistance of the operating slip system, {100}<100>, for the [111] orientation, as opposed to the low lattice resistance of the operating slip system, {110}<110> for the [100] orientation. This size independent behavior has also been found in other materials in which the lattice resistance is so high, that size effects are non-existent, or at least, negligible [4].

However, the evolution of flow stress with temperature in LiF was found to depend on the micropillar diameter, which can result on a marked size effect as the temperature increases, as shown in Fig. 1(b). This behavior can be attributed to the drop in the Peierls stress due the thermal activation of dislocation glide in this temperature range. These results will be thoroughly discussed in the light of 3D Discrete Dislocation Dynamics simulations.

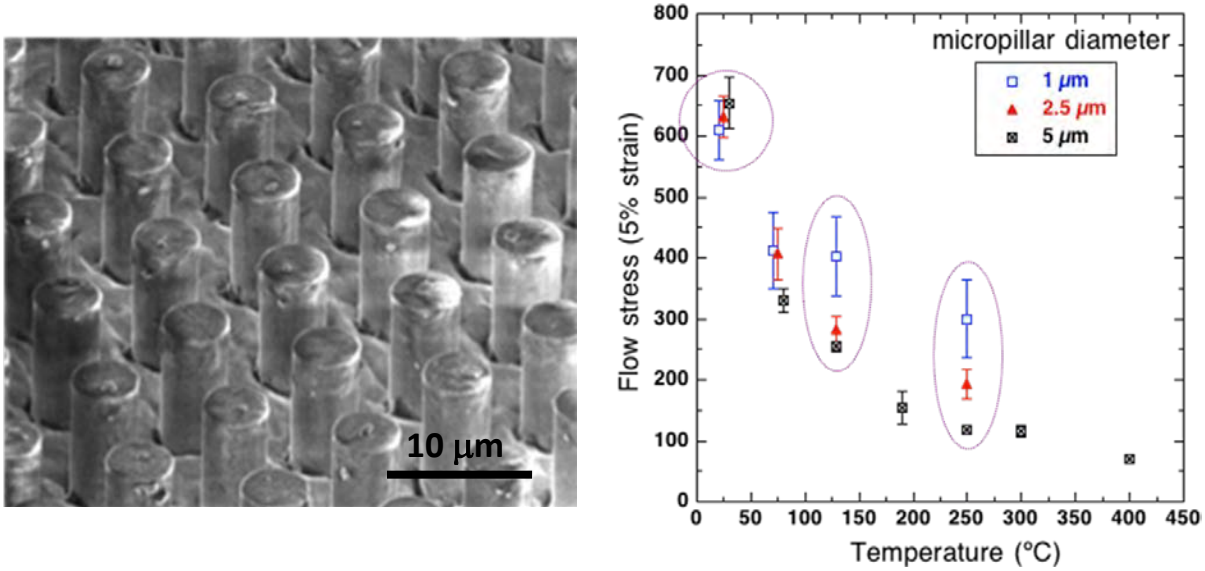

Figure 1. (a) Forest of 5 mm diameter LiF micropillars after etching away the matrix in the directionally solidified eutectic NaCl-LiF. (b) Flow stress versus temperature for three different pillar diameters.

Acknowledgement. The authors acknowledge the financial support of the Spanish Ministry of Science and Innovation (MAT2009-14396) and the Comunidad de Madrid through the program ESTRUMAT (S2009/MAT-1585).

References

[1] Uchic MD, Dimiduk DM, Florando JN, Nix WD. Science 2004;305:986-989.

[2] Greer JR, Oliver WC, Nix WD. Acta Mater 2005;53:1821-1830.

[3] Volkert CA, Lilleodden ET. Philos Mag 2006;86:5567-5579.

[4] Michler J, Wasmer K, Meier S, Ostlund F, Leifer K 2007; Appl. Phys. Lett. 90: 043123.

[5] Korte S, Clegg WJ, Philos Mag 2010;91:1150-1162.

[6] Nadgorny EM, Dimiduk, DM, Uchic, MD, 2008. Size effects in LiF micron-scale single crystals of low dislocation density. J. Mater. Res. 23, 2829-2835.

[7] Soler R, Molina-Aldareguia JM, Segurado J, LLorca J, Merino RI, Orera VM. Int. J. Plasticity 2012: 36, 50-63.

[8] Soler R, Molina-Aldareguia JM, Segurado J, LLorca J, Adv Eng Mat 2012: In press

ID: 304

Size Effects on Mechanical Properties of Silver Nanowires

Yong Zhu
North Carolina State University
USA

Qingquan Qin

Abstract:
We report the quantitative measurement of a full spectrum of mechanical properties of fold twinned silver (Ag) nanowires (NWs), including Young modulus, yield strength, and ultimate tensile strength. In-situ tensile testing of Ag NWs with diameters between 34 and 130 nm was carried out inside a scanning electron microscope (SEM). Young modulus, yield strength, and ultimate tensile strength all increased as the NW diameter decreased. The maximum yield strength in our tests was found to be 2.64 GPa, which is about 50 times the bulk value and close to the theoretical value of Ag in the <110> orientation. The size effect in the yield strength is mainly due to the stiffening size effect in the Young& modulus. Yield strain scales reasonably well with the NW surface area, which reveals that yielding of Ag NWs is due to dislocation nucleation from surface sources. Pronounced strain hardening was observed for most NWs in our study. The strain hardening, which has not previously been reported for NWs, is mainly attributed to the presence of internal twin boundaries.

[1] T. Knowles, M.J. Buehler , “Nanomechanics of functional and pathological amyloid materials,” *Nature Nanotechnology*, Vol. 6(7), 2011
[2] M.J. Buehler, “Tu(r)ning weakness to strength,” *Nano Today*, Vol. 5 , pp. 379-383, 2010
[3] S. Keten, Z. Xu, B. Ihle, M.J. Buehler, “Nanoconfinement controls stiffness, strength and mechanical toughness of beta-sheet crystals in silk,” *Nature Materials*, Vol. 9, pp. 359-367, 2010
[4] S. Cranford, A. Tarakanova, N. Pugno, M.J. Buehler, “Nonlinear material behaviour of spider silk yields robust webs,” *Nature*, doi:10.1038/nature10739, 2012

ID: 319

Large strain deformation of Cu-Nb laminar nanocomposites produced vis Accumulative Roll Bonding

Nathan A. Mara
Los Alamos National Laboratory
Los Alamos, New Mexico, USA

John Carpenter
Los Alamos National Laboratory
Los Alamos, New Mexico, USA

Shijian Zheng
Los Alamos National Laboratory
Los Alamos, New Mexico, USA

Weizhong Han
Los Alamos National Laboratory
Los Alamos, New Mexico, USA

William Mook
Los Alamos National Laboratory
Los Alamos, New Mexico, USA

Thomas Nizolek
Los Alamos National Laboratory
Los Alamos, New Mexico, USA

Jian Wang
Los Alamos National Laboratory
Los Alamos, New Mexico, USA

Irene Beyerlein
Los Alamos National Laboratory
Los Alamos, New Mexico, USA

Abstract:
In this presentation, we report on the plastic deformation of Cu-Nb lamellar nanocomposites processed via Severe Plastic Deformation as a function of decreasing layer thickness. We utilize Accumulative Roll-Bonding (ARB) to process bulk Cu-Nb nanolamellar composites from 1 mm thick high-purity polycrystalline sheet down to layer thicknesses of 10 nm. This processing technique has the advantage of producing bulk quantities of nanocomposite material, and also

exposes the interface and bulk constituents to large strains (1000's of percent). These extreme strains result in rolling textures, interfacial defect structures, and deformation mechanisms very different from those seen in nanolamellar composites grown via Physical Vapor Deposition methods. Results will be discussed in terms of the effects of interfacial content on deformation processes at diminishing length scales, and defect/interface interactions at the atomic scale. It is found that material behaviors such as enhanced thermal stability, mechanical strength and ductility, and mechanical anisotropy are strongly dependent upon the specific interfaces formed during processing.

ID: 324

Super Plastic Deformation in Metallic Nanowires sized Ranging from 10 Atomic Layers to 20 nm

Scott Mao
University of Pittsburgh
USA

He Zheng

Abstract:
Although deformation processes in submicron-sized metallic crystals are well documented, the direct observation of deformation mechanisms in crystals with dimensions below the sub-10-nm range is currently lacking. Here, through in situ high-resolution transmission electron microscopy (HRTEM) observations, we show that (1) in sharp contrast to what happens in bulk materials, in which plasticity is mediated by dislocation emission from Frank-Read sources and multiplication, partial dislocations emitted from free surfaces dominate the deformation of gold (Au) nanocrystals; (2) the crystallographic orientation (Schmid factor) is not the only factor in determining the deformation mechanism of nanometre-sized Au; and (3) the Au nanocrystal exhibits a phase transformation from a face-centered cubic to a body-centered tetragonal structure after failure. These findings provide direct experimental evidence for the vast amount of theoretical modelling on the deformation mechanisms of nanomaterials that have appeared in recent years. The talk will be focused on in-situ TEM investigation on discrete plasticity in gold nanowires based on the publication: H. Zheng, Ajing Cao, C. Weinberger, J. Y. Huang, K. Du, J. Wang, Y. Ma, Y. Xia, S. X. Mao, Nature Communication (2010).

ID: 394

Modeling Plasticity of BCC Micro-Pillars using Dislocation Dynamics

William Nix
Stanford University
USA

Ill Ryu
USA

Abstract:
We describe a three-dimensional, dislocation dynamics (DD) model of dislocation plasticity in BCC micro-pillars and use it to study size effects and the effects of initial dislocation density and strain rate on strength. The model is based on the molecular dynamics (MD) simulations of Weinberger and Cai who discovered a surface-controlled cross-slip process leading to dislocation multiplication without the presence of artificial pinning points. We find a smaller stronger size effect that can be understood in terms of the dependence of the mobile dislocation density on pillar size, through the balance between the multiplication rate and depletion rate (from the surface). In this respect, neither the single-arm source model nor the starvation/nucleation model accounts for the size effect. Instead, it is controlled by the multiplication/loss competition. Although DD simulations still require higher strain rates than those found in experiments, the DD simulations incorporating the surface multiplication mechanism predict the dependences of flow stress on pillar size, initial dislocation density and strain rate that are largely consistent with experiments. An analytical model is constructed to rationalize the behavior of the DD model at such high strain rates.

ID: 397

Mechanical Properties of Bi-Crystalline, Aluminum Nano-Pillars containing - 3 and 5 Boundaries

Zachary Aitken
California Institute of Technology
USA

Siddhartha Pathak
USA

Abstract:
Numerous studies on deformation of sub-micron, single-crystalline pillars have furthered our understanding of confined plasticity dominated by a free surface revealing a ubiquitous size effect. While this is of fundamental importance, most structural materials contain interfaces, such as grain boundaries in homogeneous polycrystalline structures, which have important effects on their mechanical properties and serve as sites for damage initiation. The behavior of lattice defects during post-elastic straining in such materials is thus complicated by the influence of boundaries. We present experimental and computational results of the influence of a single highly-coincident, low-energy (Sigma;-3 and Sigma;-5) grain boundary within individual Al nano-pillars subjected to uni-axial compression and tension. We discuss their deformation in the framework of stochastic stress-strain signature indicative of nucleation controlled plasticity, as also revealed by molecular dynamics simulations and post-mortem TEM analysis.

ID: 398

Hybrid Stochastic and Deterministic Approach for Realistic Time-scale Fully Atomistic Simulations using SISYPHUS

Pratyush Tiwary
School of Engineering, Brown University
USA

Axel van de Walle
School of Engineering, Brown University
USA

Abstract:
We use our recently proposed accelerated dynamics algorithm [1,2] to study various aspects of dislocation nucleation and movements in FCC Gold nanopillars under realistic strain rates and loads. This algorithm reaches such low-strain rates by minimizing the time Molecular Dynamics (MD) spends in low-lying energy basins. A Monte Carlo (MC) scheme is used to accelerate the transitions out of such basins [1-2]. An open-source software package implementing these ideas is expected to be released soon, named SISYPHUS (Stochastic iterations to strengthen yield of path hopping over upper states).

We perform compression tests on Gold nanopillars for strain rates varying between 7 orders of magnitudes, reaching as low as 400/s. Our calculations show the quantitative effects on the yield point of unrealistic strain-rate Molecular Dynamics calculations. We find that the failure mechanism for <001> compression of Gold nanopillars remains the same across the entire strain-rate range. It happens through twin formation and propagation (see figure 1). However the elastic limit (defined as stress for nucleation of the first dislocation) depends significantly on the strain-rate (see figure 2). This is in accordance with the high strain rate sensitivity for surface nucleation of dislocations, as seen in experiments.

We then calculate temperature and stress dependence of activation free energy for surface nucleation of dislocations in pristine Gold nanopillars under realistic loads. While maintaining fully atomistic resolution, we achieve the fraction of a second time-scale regime. We find that the activation free energy depends significantly on the driving force (stress or strain) and temperature, leading to very high activation entropies.

We also use our method to study the dependence of dislocation velocity on the applied stress field at strain-rate of 400/second [3]. SISYPHUS is used to perform simulations of Au nanopillars with different internal stress fields (implemented by changing the vacancy concentration), where it is shown how the dependence of the dislocation velocity on the applied stress reduces with increasing internal stress components. Low-strain simulations such as ours are needed here because it is important that the external driving force be lower than the intrinsic dislocation velocity so that there is no bias because of the applied strain-rate. Thus the transverse

displacement of the nanoindenter tip (as one applies compression) in a unit time should be much less than the distance moved by the dislocation in this much time.

We also propose a new methodology that overcomes some of the limits in our original accelerated dynamics scheme (and accelerated dynamics methods in general). We expect our method to be used for understanding and predicting deformation mechanism under realistic driving forces for various problems.

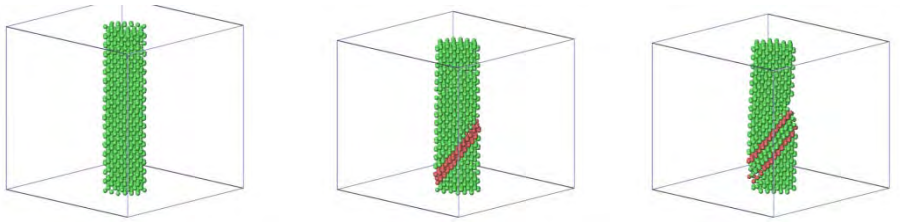

(a) (b) (c)

Figure 1: Perspective view of nanopillar (a) before compression and (b), (c) at various stages of compression showing twin nucleation and propagation. Strain rate is 400/sec. We find that the twin formation and propagation mechanism persists irrespective of applied strain-rate. Green denotes FCC, red denotes HCP. The surface atoms have been removed for clarity.

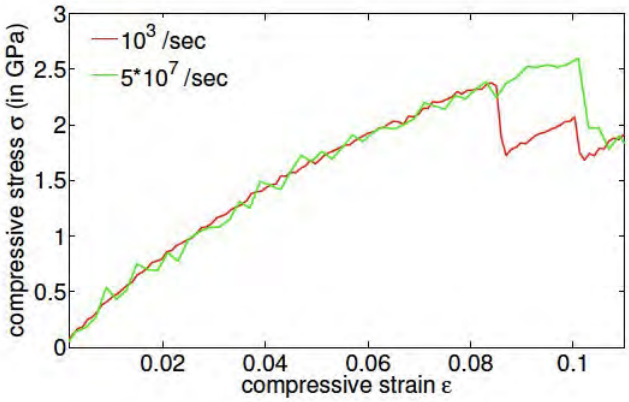

Figure 2: The stress versus nominal strain curve of Au nanowire under <001> compression.The stress-strain plots are shown for two different strain rates: $5x10^7$/sec (green) and 10^3/sec (red).

References:

[1] P. Tiwary, A. van de Walle, Physical Review B 2001, **84**, 100301.

[2] P. Tiwary, A. van de Walle, Journal of Mechanics & Physics of Solids 2012, under review.

[3] R. Maaß, P.M. Derlet, P. Tiwary, A. van de Walle and J.R. Greer, in preparation.

ID: 436

Deformation Mechanisms in Gradient Nano-grained Metals

Ting Zhu
Georgia Institute of Technology
USA

Zhi Zeng
USA

Abstract:
We perform large molecular dynamics simulations to study the mechanical behavior of gradient nano-grained copper. In a system with the gradient size of nano-grains that are confined by the coarse-grained substrate, the mechanically driven grain growth evolves progressively from the surface into substrate, giving rising to the extraordinary tensile ductility of gradient nano-grained structures. Our detailed molecular dynamics simulations reveal the underlying deformation mechanisms that well correlate the experimental measurements.

ID: 466

Plasticity in Penta-Twinned Silver Nanowires

Horacio D. Espinosa
Northwestern University
United States

T. Filleter
Northwestern University
United States

S. Ryu
Stanford University
United States

K. Kang
Stanford University
United States

J. Yin
Stanford University
United States

R. A. Bernal
Northwestern University
United States

K. Sohn
Northwestern University
United States

S. Li
Northwestern University
United States

J. Huang
Northwestern University
United States

W. Cai
Stanford University
United States

Missing Abstract

ID: 475

ID: 522

The Importance of Stress-Dependent Generalized Stacking Fault Energies on Accurate Prediction of Dislocation Nucleation

Seok-Woo Lee
California Institute of Technology

Andrew Jennings

Abstract:

As material dimensions are reduced to nanometer length scale, dislocation nucleation-governed plasticity becomes dominant deformation mechanism, which determines crystalline strength. For example, as-grown metallic nanowires are usually defect-free with their incipient plasticity occurring via dislocation nucleation at free surfaces. While it is common to utilize atomistic simulations to predict the nucleation stresses, a classical dislocation theory-based analytical approach is powerful in that it provides physical insight into understanding thermodynamics of dislocation nucleation process. To ensure accuracy of such continuum-based models, several physical quantities like dislocation line energy, work-done by loading mechanism, and stacking fault energy must be obtained. Here, we demonstrate that stacking fault (SSF) energy, commonly assumed to be constant in continuum models, requires accounting for stress tensor dependence, leading to the formulation of generalized stacking fault (GSF) energy as a necessary step towards accurately capturing dislocation nucleation physics. We present the stress-dependent GSF energies as calculated under various straining condition using atomistic simulations and postulate their connection to the continuum-based dislocation theory. We subsequently apply this hybrid method to address both homogenous and heterogeneous dislocation nucleation problems, specifically focusing on uniaxial straining of single crystalline metallic nanowires. We discuss virtues and limitations of this hybrid method within the framework of dislocation nucleation driven plasticity in nano crystals and highlight the critical role of stress-dependent GSF in accurate prediction of dislocation nucleation energies.

ID: 556

Nanoindentation of Conformally-coated Carbon Nanotube Forests

Parisa Pour Shahid Saeed Abadi

Abstract

Carbon nanotube (CNT) forests grown by low pressure chemical vapor deposition (CVD) on Si substrates were conformally coated with metal oxides using atomic layer deposition. The mechanical response and recoverability of the material were measured using micro-indentation testing. The deformation mechanism and the permanent deformations within the forest were investigated. Comparisons were made to CNT forests with no coating. Overall, the addition of the coatings was found to significantly increase the stiffness of the CNT forests. For instance, an addition of 5 nm Alumina coating increased the stiffness from 2 to 20 kN/m. In addition, higher buckling loads were found due to the increased critical buckling load of the coated CNTs within the forest. This study clarifies the effects of tailored mechanical constraints by CNT coating on the mechanical response of CNT forests. The impact of such coatings for applications involving large loads or extended material cycling will be discussed.

ID: 744

The Origin of Tensile Ductility in Metallic Glass Nanowires

Daniel Gianola
University of Pennsylvania
USA

Roman Ehrbar

Abstract:
Metallic glasses have long been recognized as promising structural materials. Despite exhibiting excellent properties such as high strength and elasticity, low internal friction, and plastic-like formability, their Achilles heel is the lack of tensile ductility. Recent experiments on nano-sized samples have shown exceptions to the conventional wisdom of poor ductility of metallic glasses, although the mechanism responsible for this behavior is debated. One prevailing view supporting observations of the suppression of catastrophic shear bands is that nanoscaled volumes of material do not release sufficient elastic strain energy during the embryonic stages of shear band formation to counter the energy penalty of creating a shear band. Here, we present results using quantitative in situ tensile testing of nano-molded and thereby damage-free $Pt_{57.5}Cu_{14.7}Ni_{5.3}P_{22.5}$ metallic glass nanowires that, in contrast to previous findings, show clear shear localization down to 60 nm. However, we found that focused Ga^+ ion irradiation serves to modify the glass structure allowing ductile flow to occur. We also show that this effect is reversible through annealing below the glass transition temperature, which structurally relaxes the glass into a brittle state. Our findings provide rationale for observations of homogeneous plastic deformation in submicron metallic glass fabricated by focused ion beam machining, and suggest strategies for circumventing the poor ductility that has long plagued widespread proliferation of metallic glasses in structural settings.

ID: 772

Source-Based Strengthening of Sub-Micron Al Crystals

Marc Legros
CEMES-CNRS

Früic Mompiou

Abstract:
Whiskers, thin films, and micro pillars display an increase of their strength as an inverse power law of their size. Today, several points of view have been brought forward to explain this trend: classical strain hardening, dislocation exhaustion or multiplication and nucleation. For sub-micrometer single crystalline pillars and fibers, where no external boundaries or interfaces are confining the dislocations, knowing the initial dislocation microstructure has become a key point. This is for example what differentiates whisker behavior (brittle fracture up to theoretical shear strength) from regular single crystal (plastic deformation at lower stress). Observing the dislocation structure under stress provides even further insight to understanding the basic mechanisms in small-scale plasticity. Here, we have combined TEM and SEM tensile tests on fibers with diameters in the micron range and below. These Al fibers were fabricated by selective chemical etching of an eutectic lamellar Al/Al2Cu alloy, thus avoiding a modification of their initial structure by FIB. For SEM tests, the microstructure was characterized before, and when possible after the test, revealing a persistent increase in dislocation density close to necking or fracture zones. In situ TEM, performed with a classical but rigid straining holder revealed the activation of single arm sources, operating individually or in bunches. In the simpler cases, without inserting a load cell in series with the sample, we directly probed the local resolved shear stress, by measuring the radius of curvature of the dislocation sources. These combined experiments outline a complete picture of the plasticity in these small objects[1], directly linked to the size of these intermittent spiral sources. As they operate closer to the surface, increasing stress values are needed, giving rise to the size effect. [1] Mompiou F, Legros M, Sedlmayr A, Gianola DS, Caillard D, Kraft O. Source-based strengthening of sub-micrometer Al fibers. Acta Materialia 2012;60:977.

IV.8

Multiscale Mechanics of Materials - Multiscale Characterization and Modeling of Geomaterials

ID: 133

Granular Element Method for Computational Particle Mechanics

Keng-Wit Lim
Jose E. Andrade
California Institute of Technology
United States

Abstract:
Particle morphology can be characterized, in general, by three properties: sphericity, roundness, and roughness [1]. These properties measure morphological characteristics at different length scales, with increased spatial resolution needed to measure roughness, for example. Particle morphology has been shown to be crucially important for macroscopic properties in granular materials. In the case of macroscopic strength, it has been determined that lack of sphericity, sharper angularity and increased roughness all lead to increased mobilized strength in granular materials.

We present a method within the family of the Discrete Element Method (DEM) capable of accurately capturing grain shape using Non-Uniform Rational Basis Splines (NURBS). The new method, called the Granular Element Method (GEM) [2], accurately accounts for grain sphericity and roundness. As such, the need for complicated and ad-hoc approaches to construct three-dimensional grain geometries (e.g. clustering) is entirely bypassed. GEM maintains compatibility with standard DEM technology [3] and provides several significant advantages for accuracy in discrete mechanics computations. Furthermore, the applicability of GEM is enhanced by its tight integration with existing computer aided geometric design and modeling tools and ability to provide a seamless transition from binary images of real grain shapes (e.g., from X-ray computed tomography (CT)) to modeling and analysis.

As an example, we use GEM to simulate two 15-grain assemblies to showcase its ability to capture irregular shapes and to illustrate the importance of shape in the macroscopic response. The two assemblies, one using GEM and the other using discs, are subjected to uniform compression in several stages followed by a constant volume distortion. Figures 1 and 2 show that the macroscopic average stresses and interparticle contact forces are significantly different because of the different contact topologies in the two assemblies. This example shows the ability of GEM to account for complicated load paths through a granular assembly because of the geometrical enhancement of the grain shapes provided by GEM.

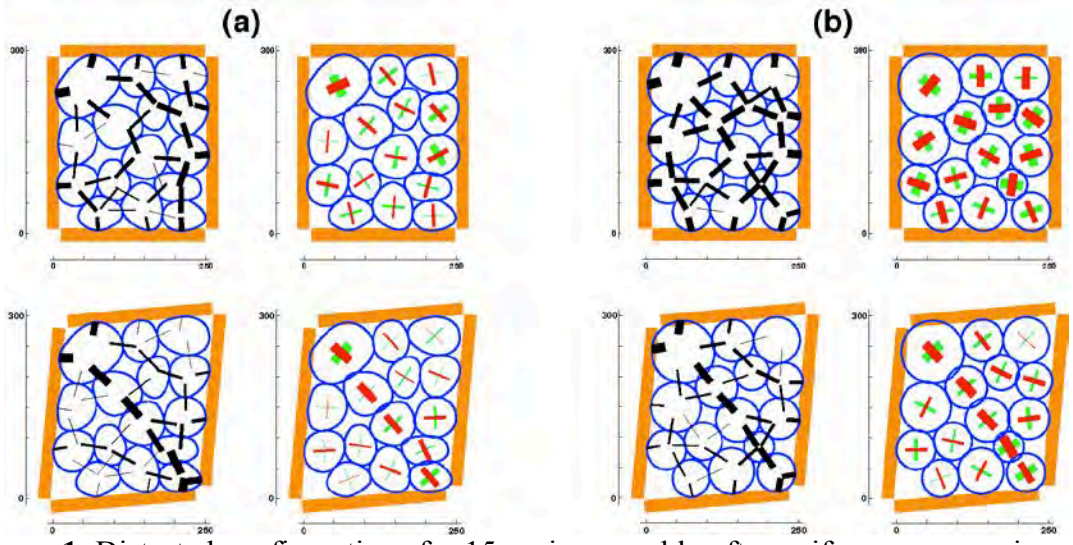

Figure 1. Distorted configurations for 15-grain assembly after uniform compression and distortion. (a) GEM (b) Discs. Each subfigure shows interparticle forces (thickness proportional to force magnitude) and average principal stresses and directions in each particle (red for most compressive; green for least compressive). After [2].

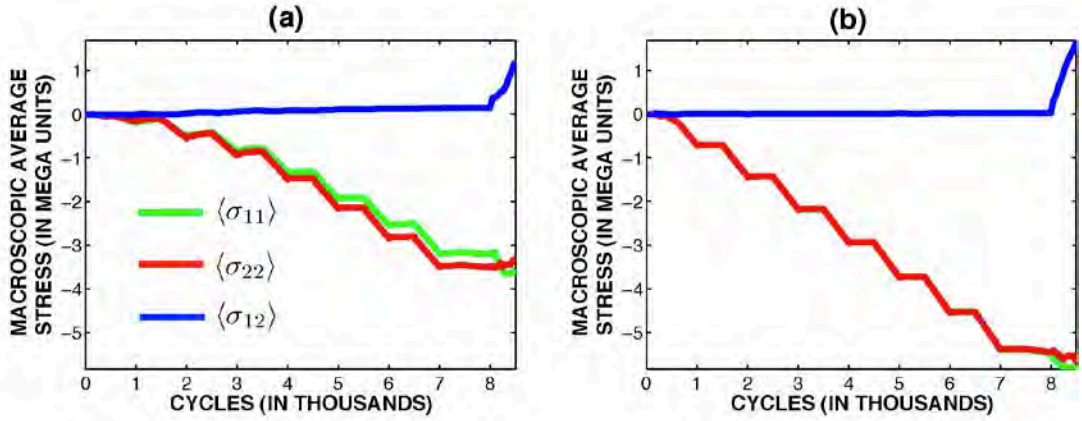

Figure 2. Evolution of average macroscopic stress components. (a) GEM (b) Discs. After [2].

References

1. Cho G. C., Dodds J. and Santamarina J. C.: Particle shape effects on packing density, stiffness, and strength: Natural and crushed sands. Journal of Geotechnical and Geoenvironmental Engineering, 132 (5): 591–602, 2006.
2. Andrade J. E., Lim K.-W., Avila C. F. and Vlahini´c I.: Granular Element Method for computational particle mechanics. Computer Methods in Applied Mechanics and Engineering (in press).
3. Cundall P. A. and Strack O. D. L.: A discrete numerical model for granular assemblies. Géotechnique, 29: 47–65, 1979.

ID: 190

Three dimensional ellipsoidal discrete element modeling of X-ray CT sand assemblies in triaxial compression

Richard A. Regueiro, Yevgeniy Kaufman, Austin Nossokoff, Beichuan Yan
Department of Civil, Environmental, and Architectural Engineering
University of Colorado at Boulder, 428 UCB, Boulder, CO 80309
United States of America

Mehmet Cil, Khalid Alshibli
Department of Civil and Environmental Engineering
University of Tennessee, Knoxville, TN 37996-2010
United States of America

Abstract:
There are various ways to generate initial particle assemblies of granular materials for discrete element (DE) modeling, three of which are mentioned here: (i) random generation to achieve specified particle size gradation and assembly porosity; (ii) random generation to achieve specified particle size gradation and then settle by gravity into a container; or (iii) directly from X-ray computed tomography (CT) images. This paper addresses method (iii). We approximate the sand grains as two-axis ellipsoids, with radii, position, and orientation provided by the X-ray CT images. Because the ellipsoids are approximations of sand grain geometry, there are overlaps or gaps between particles provided by the algorithm that in turn interprets the raw X-ray CT volume data. In order not to lose the "fabric" of the sand assemblies provided by the CT images, we isotropically compress the assemblies to a dense state before compressing in triaxial compression, and also consider gravity deposition. Results are compared to measured stress versus strain experimental data, but only for the elastic-plastic portion of the loading curve before shear banding is observed. This DE modeling is a precursor to overlap finite element/DE coupling for multiscale modeling of the interfacial mechanics between deformable solids and dense granular materials.

Results:
DE simulations of conventional triaxial compression (CTC) tests were performed on the following RVE assemblies of ASTM 20/30 quartz Ottawa sand: (a) 4201 particles (7.9mm x 7.7mm x 19.5mm) trimmed from the full cylindrical specimen (20.2mm in height, 9.5mm in diameter), (b) 897 particles (5.8mm x 5.4mm x 5.3mm) trimmed from the 4201 particle RVE, and (c) the 4201 particle assembly after gravity deposition (see top and middle figures). The initial configuration involving particle size, orientation, and centroid position is taken directly from the CT image after applying an algorithm that approximates the particle shapes as two-axis ellipsoids. The experimentally-measured principal stress ratio (PSR) plotted versus axial strain for the 9.5mm diameter by 20mm in height cylindrical specimen, with confining stress of 70kPa, is shown in the bottom figure up to 2% strain, the strain level to which we attempt to simulate

without accounting for strain localization (i.e., needing a membrane BC). The RVE after gravity deposition is denser than those taken from the CT images and isotropically compressed. The representation of particle shapes from CT data is work in progress. The comparison of PSR for DE simulations and experimental data shows the difference in results for the different DE RVEs.

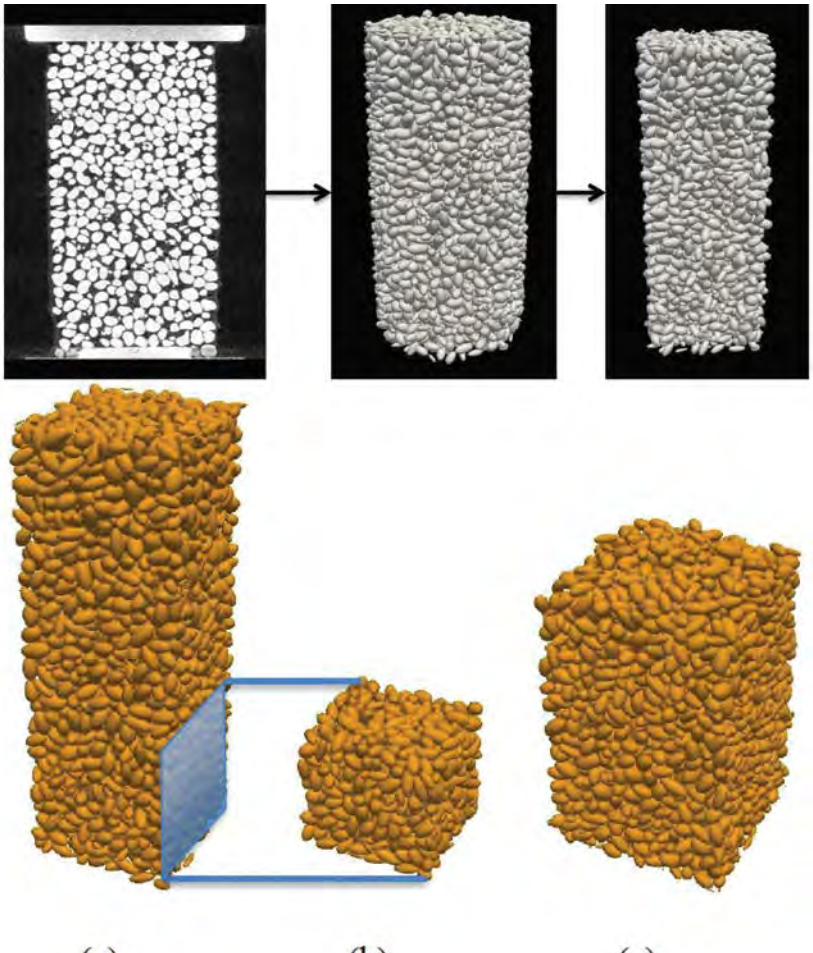

(a) (b) (c)

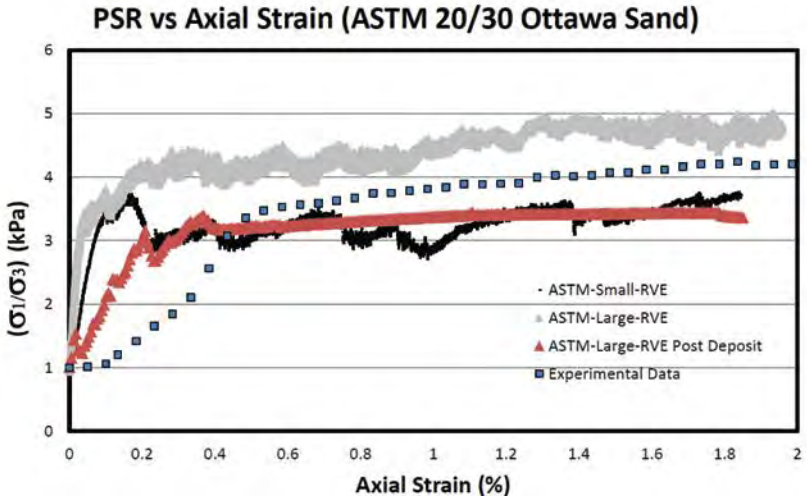

Acknowledgements:
Funding for this research was provided by National Science Foundation grant CMMI-0700648, and Office of Naval Research grant N00014-11-1-0691. This funding is gratefully acknowledged. The CT data were collected using the X-ray Operations and Research Beamline Station 13-BMD at the Advanced Photon Source (APS), Argonne National Laboratory. We thank Dr. Mark Rivers of the APS for assistance in performing the scans. Use of the Advanced Photon Source was supported by the U.S. Department of Energy, Office of Science, Office of Basic Energy Sciences under Contract No. DE-AC02-06CH11357. This support is gratefully acknowledged.

ID: 191

Microscopic origin of macroscopic strength in granular media: Friction

Alex X. Jerves
California Institute of Technology
United States

José E. Andrade
California Institute of Technology
United States

Abstract:
In the last decade, micro-scale physics has become a fundamental object of study in the attempt of developing a strong theory in granular mechanics capable of filling the lack of a more general (physics based) theoretical framework in the field (e.g.) (Dascula and Cambow, 2008), (Oda and Iwashita, 1999). Furthermore, understanding (from the micro mechanical point of view) the evolution and physical meaning of the experimental results (macro-scale) promises to give a deeper insight into the behavior of these complex materials.

This work attempts to introduce a rigorous treatment of the micro-mechanical behavior of granular materials by connecting the mechanics of micro and macro scales in a general way. This would contribute to the quest for a broader understanding of the relation between micro and macro scales without the need to rely on particular cases and experimental data, which have been used as bench mark examples to illustrate the existence and main features of chain forces and macro-mechanics (e.g., photo-elasticity in 2D discs, phenomenological constitutive laws). Hence, this work introduces a general and rigorous treatment of the aforementioned subject, pursuing as its ultimate goal the development of physics-based constitutive models.

In order to reach the mentioned objectives we depart from Christoffersen's expression (Christoffersen et al., 1981) for the average stress in an assembly of particles, which defines stress as a function of inter-particle contact forces and fabric. Then, using spectral decomposition of the stress tensor, and local coordinates for the contact forces (normal and tangent components at each contact point) (see Figure 1), as well as, relying on Mohr's circle to extract mechanics and physics, we arrive to an expression that enables us to compute Mohr-Coulomb's friction angle (see Figure 2) (constitutive parameter of a continuum, macro-scale, model) in terms of the contact forces and the fabric (micro-mechanical topology and kinetics) for an array containing arbitrary shape and size particles in two dimensions.

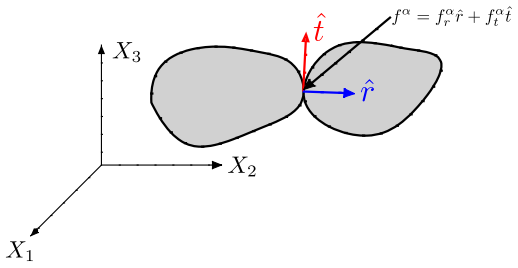

Figure 1: Inter-particle contact forces expressed in local (normal and tangent) coordinates.

Having derived such an expression, we specialize it for arbitrary size discs, and using Karush-Kuhn-Tucker conditions we find the limit (maximum) Mohr-Coulomb's friction angle, that (at the macro-scale level) tells us when an array of particles looses stability in the quasi-static sense. Finally, these analytical results are validated by deriving (from our equations) Rowe's expression (P.W. Rowe, 1962) for the limit (maximum) ratio between the two principal-stresses for two-dimensional regular packings (discs with the same size, a single angle defining the topology of the array, and inter-particle Coulomb friction coefficient constant throughout the array).

From this general theoretical two-dimensional framework we are able to extract meaningful mechanics and draw some interesting conclusions. First, at the regular packing level, our analysis gives (when limit state) null horizontal inter-particle normal forces (and as consequence null corresponding tangent forces). This may explain buckling in this type of arrays as a consequence of the lost of contact. Furthermore, all the non-zero tangent inter-particle forces reach the limit state (in the Coulomb's friction law sense), these physical features are consistent with the fact that (in this kind of arrays) sliding, rotation, and rolling of particles can yield the same macro-strain measures.

Finally, further analysis of the analytical expressions unravel another important result: Coulomb's friction law arises naturally from the equations, implying that the inter-particle friction coefficient may be a function of geometrical, constitutive and topological features of the particles but it does not depend on the inter-particle contact forces.

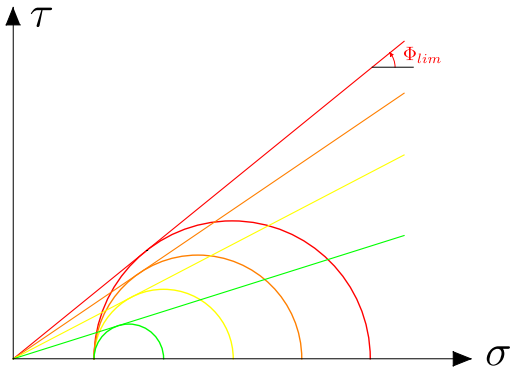

Figure 2: Mohr-Coulomb limit (maximum) friction angle.

References:

Christoffersen, J., Mehrabadi, M. M., Nemat-Nasser, S. (1981). *A Micromechanical Description of Granular Material Behavior*. Journal of Applied Mechanics **48**, 339-344.

Dascalu, C., Cambou, B., (2008). *Multiscale Approaches to Geomaterials*. Acta Geotechnica **3**.

Oda, M. & Iwashita, K., editors. Mechanics of granular materials: an introduction.
Taylor & Francis, 1999.

Rowe, P. W. (1962). *The Stress-dilatancy Relation for Static Equilibrium of an Assembly of Particles in Contact*. Proceedings of the Royal Society of London **269**, 500-527.

ID: 238

On The Flow of a Generalized Reiner-Rivlin Type Fluid

Wei-Tao Wu
Department of Mechanical Engineering, Carnegie Mellon University, Pittsburgh, PA

Nadine Aubry
Department of Mechanical Engineering, Carnegie Mellon University, Pittsburgh, PA

Mehrdad Massoudi
U. S. Department of Energy, National Energy Technology Laboratory (NETL), Pittsburgh, PA

Abstract:
In this paper, we use the model developed by Massoudi [1] to study the simple shear flow of granular materials between two horizontal plates, with the lower plate fixed and the upper plate moving at a constant speed. This model is a generalized volume fraction dependent non-Newtonian model for granular materials, which is also shear rate dependent.
We assume that there is no thermo-chemical and electromagnetic effects, so the governing equations consist of the conservation of mass, linear momentum and angular momentum. The conservation of mass in the Eulerian form is,

$$\frac{\partial \rho}{\partial t} + div(\rho \boldsymbol{u}) = 0 \tag{1}$$

For incompressible flows, this equation is automatically satisfied when the flow is steady. The linear momentum equation reads,

$$\rho \frac{d\boldsymbol{u}}{dt} = div(\boldsymbol{T}) + \rho \boldsymbol{b} \tag{2}$$

where $\boldsymbol{T}$ is the Cauchy tensor stress which will be given by the constitutive equations, and $\boldsymbol{b}$ is the body force. In the absence of couple stresses, the angular momentum equation implies that the Cauchy stress is symmetric.
Based on the Reiner-Rivilin model [2, 3] and the model developed by Rajagopal and Massoudi [4], Massoudi suggested a new generalized Reiner model [1]:

$$\boldsymbol{T} = [-k\phi + \beta_2{}^*(\phi + \phi^2) tr\boldsymbol{D}]\boldsymbol{I} + \beta_3{}^*(\phi + \phi^2)\boldsymbol{D}\Pi^{\mathrm{m}/2} + \beta_5{}^*(\phi + \phi^2)\boldsymbol{D}^2 \tag{3}$$

where $\boldsymbol{D}$ is the symmetric part of velocity gradient, ϕ is the volume fraction and $\boldsymbol{\Pi} = \frac{1}{2} tr[2\boldsymbol{D}]^2$. In this model, m is a power-law exponent. When m is positive, the fluid is shear-thickening, and when m is negative, the fluid is shear-thinning. It can be found that when m is zero, this model reduces to the Reiner-Rivlin model.
In this work, we study the simple shear flow of granular materials between two horizontal plates, with the lower plate fixed and the upper plate moving with a constant speed. We also assume that the flow is laminar and fully developed. Substituting equation (3) into the governing equation (2), the balance of momentum equations is obtained:

$$\frac{d}{d\bar{y}}\left[(\phi + \phi^2)\left|\frac{d\bar{u}}{d\bar{y}}\right|^{\mathrm{m}/2}\frac{d\bar{u}}{d\bar{y}}\right] = 0 \tag{4}$$

$$\frac{d}{d\bar{y}}\left[R_1\phi + R_5(\phi + \phi^2)\left(\frac{d\bar{u}}{d\bar{y}}\right)^2\right] - \phi = 0 \tag{5}$$

$$\bar{y} = \frac{y}{H}, \bar{u} = \frac{u}{U}, R_1 = -\frac{k}{H\rho_{10}g}, R_5 = \frac{\beta_{50}U^2}{H^3\rho_{10}g} \tag{6}$$

where H is the distance between the two plates and U is the reference velocity. It can be seen that R_1 is the ratio of the pressure force caused by the gradient of the volume fraction to the gravity, and R_5 is the ratio of normal stress difference effects to the gravity [5]. The boundary conditions are assumed to be,

$$\begin{cases} \bar{u} = 0, \bar{y} = 0 \\ \bar{u} = 1, \bar{y} = 1 \end{cases} \tag{7}$$

$$\int_0^1 \phi \, d\bar{y} = N \tag{8}$$

The effect of R_1 on the distribution of the volume fraction and dimensionless velocity are shown in Figure 1. It can be seen that an increase of the magnitude of R_1, namely the pressure gradient, which is caused by the difference of volume fraction along the y direction, leads to a decrease of the slope of the volume fraction along the y direction. Furthermore, from Figure 1(b), it is observed that as the absolute value of R_1 increases, the dimensionless velocity increases slightly approaching a straight line when R_1=-2.6.

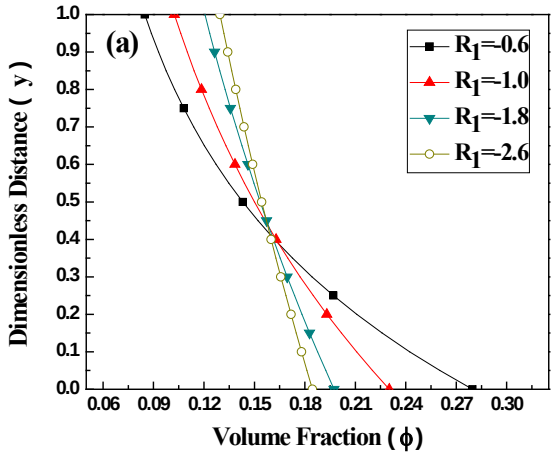

Figure 1 (a) Effect of R_1 on the volume fraction profile for R_5=0.2, m=0.3, and N=0.15.

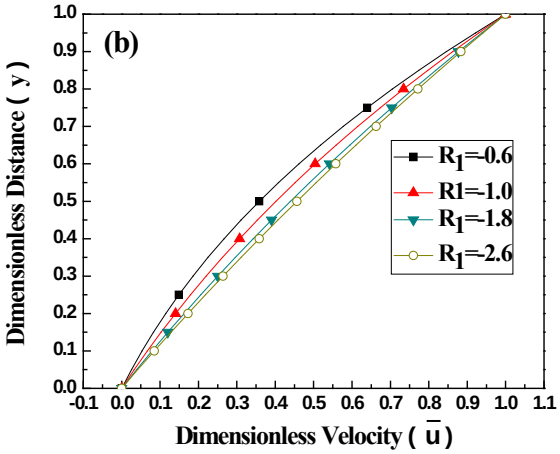

Figure 1(b) Effect of R_1 on the dimensionless velocity profile for R_5=0.2, m=0.3, and N=0.15.

REFERENCES

1. Massoudi, M., 2011. A generalization of Reiner's mathematical model for wet sand. *Mech. Research Comm*. **38**, 378-381.
2. Reiner, M, 1945. A mathematical theory of dilatancy. *Am. J. Math*. **67**, 350– 362.
3. Rivlin, R.S., 1948. The hydrodynamics of non-Newtonian fluids. *Proc. R. Soc*. Lond. **193**, 260-281.
4. Rajagopal, K.R. and Massoudi, M., 1990. A Method for Measuring Material Moduli of Granular Materials: Flow in an Orthogonal Rheometer. Topical Report, DOE/PETC/TR-90/3.
5. Massoudi, M., 2011. "Heat Transfer in Complex Fluids," pp. 497-520. In *Two Phase Flow, Phase Change and Numerical Modeling*. Edited by: A. Ahsan, ISBN 978-953-307-584-6. InTech Open, September 2011. http://www.intechopen.com/articles/show/title/heat-transfer-in-complex-fluids

ID: 244

Flow of drilling fluids in a pipe

Minglun Gu
Department of Mechanical Engineering,
Carnegie Mellon University,
United States

Nadine Aubry
Department of Mechanical Engineering,
Carnegie Mellon University,
United States

Mehrdad Massoudi
U. S. Department of Energy
National Energy Technology Laboratory
United States

Abstract:

In the past half-century, conventional rheological models such as the power-law ($\tau = k\dot{\gamma}^n$), Bingham-plastic ($\tau = \tau_0 + k\dot{\gamma}$), and Herschel-Bulkley (H-B) ($\tau = \tau_0 + k\dot{\gamma}^n$) models have been widely used for flow simulation of drilling muds. However, all these prevalent models overlooked the fact that drilling muds as suspension systems exhibit shear-induced particle migration, which has been long observed for concentrated suspensions (Karnis, et al., 1966; Leighton & Acrivos 1987a; Abbott et al. 1991; Phillips et al. 1992). As the requirement for engineering applications becomes increasingly stringent, drilling muds might be expected to assume a prescribed concentration at a specific location, so the fact that shear-induced particle migration exist and affect the flow behavior cannot afford to be neglected. We hereby model drilling fluids as concentrated suspensions and conduct a numerical study on the behavior and effect of shear-induced particle migration.

Leighton and Acrivos (1987b) identified three causes for shear-induced particle migration, namely shear-rate gradients, relative viscosity gradients and concentration gradients. Based on their proposal, various numerical studies were conducted on suspension flows in Couette devices and pipe geometries (Phillips et al. 1992, Fang & Phan-Thien 1995, Zhang & Acrivos 1994, Subia et al. 1998), and the numerical results are all in good agreement with experimental data.

Hence, in this study, we also model concentrated suspensions as an effective continuum and incorporate the convection-diffusion equation proposed by Phillips et al. (1992) in the simulation of suspension flow of a generalized power-law fluid. Our main purpose is to examine the behavior of particle migration and its effect on the rheological behavior of shear-rate dependent suspensions, and to identify new properties of such fluids in conventional flow conditions such as Couette flows and Poiseuille flows. With this in mind, we limit our attention to flows of neutrally buoyant particle suspensions under normal pressure and temperature,

without the presence of an electric or magnetic field, and also neglect the normal-stress induced particle migration.

Upon describing the governing equations and constitutive equations, benchmark numerical results will be provided in terms of fully developed pressure-driven pipe flow. Several adjustable parameters arise in the constitutive equations, including the shear-rate dependency coefficient, mean volume fraction, concentration dependency coefficient, normalized pressure gradient and Reynolds number. Considering their potential importance for flow characterization, a parametric study will be carried out for each of these parameters.

References:

Boyer, F., Pouliquen, O., and Guazzelli, É. 2011 Dense suspensions in rotating-rod flows: normal stresses and particle migration. J. Fluid Mech. 686-703.

Fang, Z. & Phan-Thien, N. 1995 Numerical simulation of particle migration in concentrated suspensions by a finite volume method. J. Non-Newtonian Fluid Mech. 58, 67-81.

Karnis, A., Goldsmith, H. L. & Mason, S. G. 1966 The kinetics of flowing dispersions I. Concentrated suspensions of rigid particles. J. Colloid Interface Sci. 22, 531-553.

Leighton, D. & Acrivos, A. 1987a Measurement of shear-induced self-diffusion in concentrated suspensions of spheres. J. Fluid Mech. 177, 109-131.

Leighton, D. & Acrivos, A. 1987b The shear-induced migration of particles in concentrated suspensions. J. Fluid Mech. 181, 415-439.

Phillips, R. J., Armstrong, R. C., Brown, R. A., Graham, A. L. & Abbott J. R. 1992 A constitutive equation for concentrated suspensions that accounts for shear-induced particle migration. Phys. Fluids A 4, 30-40.

Subia, S. R., M. S. Ingber, L. A. Mondy, S. A. Altobelli and A. L. Graham 1998 Modelling of concentrated suspensions using a continuum constitutive equation. J. Fluid Mech. 373, 193-219.

Zhang, K. & Acrivos, A. 1994 Viscous resuspension in fully developed laminar pipe flows. Intl. J. Multiphase Flow 20, 579-591.

ID: 258

Numerical solution to the heat transfer and flow of granular materials using a non-linear heat flux vector

Hyunjin Yang
Department of Mechanical Engineering, Carnegie Mellon University, Pittsburgh, PA, USA

Nadine Aubry
Department of Mechanical Engineering, Carnegie Mellon University, Pittsburgh, PA, USA

Mehrdad Massoudi
U. S. Department of Energy, National Energy Technology Laboratory (NETL), Pittsburgh, PA, USA

Abstract:

In many chemical processes and engineering applications such as drying or the design of thermally insulating materials, it is crucial to derive an accurate and reliable formulation for the heat flux vector. In this paper, we consider the one dimensional fully developed flow of granular materials down a heated inclined plane using the non-linear constitutive equation of the heat flux vector developed by Massoudi [1, 2].

We use the conservation of mass, the conservation of linear momentum, and the energy equation as the governing equations. In these equations, the stress tensor and the heat flux vector are expressed by the constitutive relations that were derived by Rajagopal & Massoudi [3] (stress tensor **T**) and Massoudi [1, 2] (heat flux vector **q**), where

$$\mathbf{T} = [\beta_0(\phi) + \beta_1(\phi)\nabla\phi\cdot\nabla\phi + \beta_2(\phi)\mathrm{tr}\,\mathbf{D}]\mathbf{I} + \beta_3(\phi)\mathbf{D} + \beta_4(\phi,\nabla\phi)\nabla\phi\otimes\nabla\phi + \beta_5(\phi)\mathbf{D^2} \quad (1)$$

where

$$\beta_0 = -f\phi,\ \beta_1 = \beta_1{}^*(1+\phi+\phi^2),\ \beta_2 = \beta_2{}^*(\phi+\phi^2),\ \beta_3 = \beta_3{}^*(\phi+\phi^2),$$
$$\beta_4 = \beta_4{}^*(1+\phi+\phi^2),\ \beta_5 = \beta_5{}^*(\phi+\phi^2) \quad (2)$$

and

$$\mathbf{q} = a_1\mathbf{n} + a_2\mathbf{m} + a_3\mathbf{Dn} + a_4\mathbf{Dm} + a_5\mathbf{D^2n} + a_6\mathbf{D^2m} \quad (3)$$

with $a_1 = -$k(thermal conductivity) and $a_2 - a_6$ being scalar functions of

$$\phi, \theta, \mathbf{m}.\mathbf{m}, \mathbf{n}.\mathbf{n}, \mathbf{m}.\mathbf{n}, \mathbf{n}.\mathbf{Dn}, \mathbf{n}.\mathbf{D^2n}, \mathbf{m}.\mathbf{Dm}, \mathbf{m}.\mathbf{D^2m}, \mathbf{n}.\mathbf{Dm}, \mathbf{n}.\mathbf{D^2m},$$
$$I_1 = \mathrm{tr}\mathbf{D}, I_2 = \mathrm{tr}\mathbf{D}^2, I_3 = \mathrm{tr}\mathbf{D}^3 \quad (4)$$

where ϕ is the volume fraction which is a function of time and position, and is related to the density through the relation $\rho = \rho_{10}\phi$, with ρ_{10} being the reference density. In addition, $\mathbf{m} = \mathrm{grad}\,\phi$, $\mathbf{n} = \mathrm{grad}\,\theta$, $\mathbf{D} = \frac{1}{2}[\nabla\mathbf{u} + (\nabla\mathbf{u})^{\mathbf{T}}]$.

Since we consider the fully developed flow of dense granular materials down a heated inclined plane, the velocity, volume fraction and temperature profiles are assumed to be functions of y only (normal to the direction of the flow). That is,

$$\mathbf{u} = u(y)\mathbf{i}, \phi = \phi(y), \theta = \theta(y) \tag{5}$$

To perform a parametric study, we consider the dimensionless form of the equations using:

$$\bar{y} = \frac{y}{H}, \bar{u} = \frac{u}{u_0}, \bar{\theta} = \frac{\theta - \theta_\infty}{\theta_w - \theta_\infty} \tag{6}$$

The boundary conditions are:

$$\text{At } \bar{y} = 0 : \bar{u} = 0, \bar{\theta} = 1$$

$$\text{At } \bar{y} = 1 : \frac{d\bar{u}}{d\bar{y}} = 0, \bar{\theta} = 0, \; R_1\phi + \frac{R_2}{2}(1 + \phi + \phi^2)\left(\frac{d\phi}{d\bar{y}}\right)^2 + \frac{R_5}{4}(1 + \phi + \phi^2)\left(\frac{d\bar{u}}{d\bar{y}}\right)^2 = 0, N = \int_0^1 \phi \, d\bar{y}$$

The differential equations are solved numerically through the Gauss-Seidel method and the Newton-iteration. In the energy equation, in addition to the viscous dissipation parameter Γ, there are three independent dimensionless numbers, P_2, P_5 and P_6. Among these parameters, the effect of the dimensionless parameter P_2 on the temperature profile is displayed in Fig. 1.

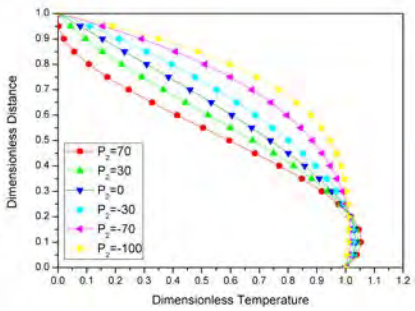

FIGURE 1. EFFECT OF P_2 ON THE DIMENSIONLESS TEMPERATURE PROFILE FOR THE PARAMETER VALUES $R_1 = -3, R_2 = 10, R_3 = 0.05, R_5 = 0.01, \Gamma = 0.5, P_5 = P_6 = 0$

P_2 is related to the distribution of the volume fraction due to diffusion and gravity. It can be observed that the overall temperature of the flow approaches the value of the temperature at the lower wall and the maximum temperature in the lower region decreases as $|P_2|$ increases when P_2 is negative. On the other hand, when P_2 is positive, the maximum temperature near the lower wall rises with $|P_2|$, while the temperature in the upper region of the flow decreases.

[1] Massoudi, M., 2006a, "On the heat flux vector for flowing granular materials, Part 1: Effective thermal conductivity and background," Math. Methods Applied Sci., Vol. 29, pp. 1585-1598

[2] Massoudi, M., 2006b, "On the heat flux vector for flowing granular materials, Part 2: Derivation and special cases," Math. Methods Applied Sci., Vol. 29, pp. 1599-1613

[3] Rajagopal, K. R. & M. Massoudi., 1990, "A Method for Measuring Material Moduli of Granular Materials: Flow in an Orthogonal Rheometer," Topical Report, DOE/PETC/TR-90/3, 1990.

ID: 266

EPMA and ENVI a Potential Tool for Materials and Structure Analysis

Narendra Kumar Agrawal (E-Mail: *research.nka@gmail.com*)
Department of Physics, Malaviya National Institute of Technology, Jaipur, India.

Priti Agarwal
Department of Botany, University of Rajasthan, Jaipur, India.

Ravi Agarwal
Centre for Converging Technologies, University of Rajasthan, Jaipur.

Abstract: The prime objective of our study is to determine the mineralogy and Petrology in individual chondrules. These (Mineralogy and Petrology) are used for determination of the formation histry (how they form, when they form etc.) and other process regarding formation of chondrule as well as chondrite, meteorite and parent body like Mineralogy can tell thermal alteration histry of chondrule, peak temperature, re-melting/ partial malting and explain structure of chondrule etc. Spherical objects of about few mm sizes and few mg weights are called chondrules that are major constituent of most chondrites. Chondrules are one of first solids to form in the solar system. So we have planned to make study of Mineralogy, Petrology, Elemental Abundance in individual chondrule by using EPMA. With EPMA we are able to make analysis with <1mg sample it only depend on sample surface and preparation of mount for EPMA analysis [Agrawal et.al NSSS2010, Suruchi et.al ISMAS2009]. We have separated and selected few chondrules from Dhajala meteorite. A split of chondrule is used for determination of major elemental composition (Si, Ti, Al, Fe, Mg, Mn, Ca, Na, K, P, Ni, and Cr) by EPMA. EPMA elemental composition is used for the determination of Mineralogy using standard geological formula, method and reasonable assumptions. EPMA elemental composition for each point (determine on the basis of gray scale of each phase) is converted in bulk chondrule composition (only surface) by using ENVI software. Few of these results are discussed in this paper.

Introduction: Meteorites are fragments of asteroids-the leftover material in the formation of large solar system objects. Material from asteroids is pristine as it represents the most primitive solid matter of the solar system. Meteorites can be generally classified into two broad categories: Undifferentiated and Differentiated. Undifferentiated meteorites are also called chondrites, meteorites containing chondrules. Most of the meteorites that fall on the earth are chondrites. Chondrites are those solid objects, which have been subjected to minimum secondary processing (e.g. aqueous alteration and thermal metamorphism) since their formation and preserve primitive signatures in the form of elemental and isotopic compositions. Thus, chondrites and their components are the logical places to search for survived signatures of early stages of nebular history and solar system.

Experimental and analysis Technique: Chemical and characterization of chondrules by EPMA: Chemical characterization of chondrules has also been done by Electron Probe Micro Analysis (EPMA) method. By this non-destructive method, chemical composition of Major and Some minor in the form of their oxides analyzed. All 10 Chondrule, Fusion crust and bulk have been characterized By EPMA. EPMA (Electron Probe Micro Analysis) is a crucial technique for the non-destructive chemical analysis of the solid sample. The operating principles of EPMA is

divided into four main parts (i) Source or electron gun (generation of the electron) (ii)Electromagnetic lenses (controlling the electron current and focusing of the electron beam (iii) Interaction of the electron beam with sample (various energy exchange processes) and finally, (iv) collection and detection of several entities that produced during interaction.

Chemical Composition and Mineralogy by EPMA and ENVI

Major element compositional data are determined for samples using Electron Microprobe (EPMA). Using back scattered electron (BSE) image the different topography present on chondrule sections are first determined. X-Ray Florence technique is used for the determination of elemental composition by EPMA. Using a focused (~1 µm diameter) beam in point mode, 15kV accelerating voltage, and 15 nA gun current, spot analysis performed for each topography and gray scale which is determined by the processed BSE image by ENVI software. This helped in (1) deciding the mineral present in the sample (for determination of mineral present the standard geological norm calculation method is used). (2) Composition of mineral (using ENVI analysis). Usually 5-10 spots were taken per topography and grayscale in a given chondrule on average 200 spote per chondrule. By using ENVI (environment for visualizing images) data from these spot analyses used to calculate the mineral composition.

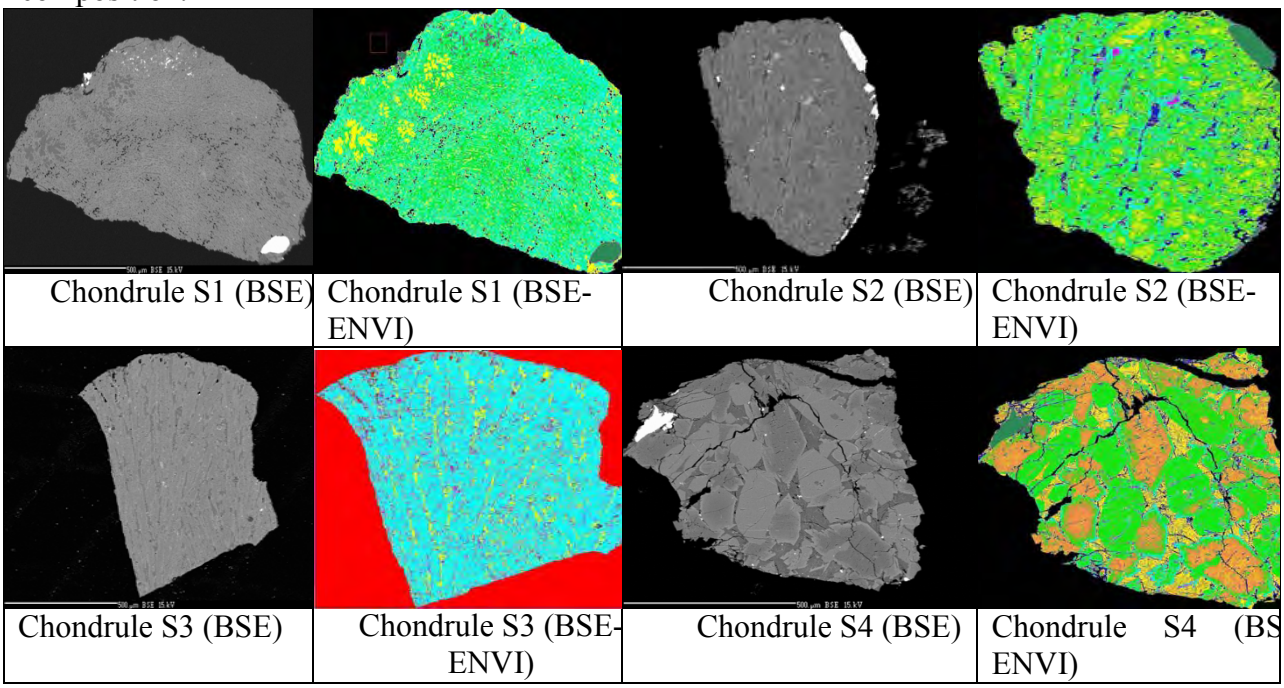

Fig. 1: BSE (Backscattered Electron image) and ENVI Processed coluor mapped BSE (Backscattered Electron image) of Dhajala T-20 Chondrule.

Table 1. Classification of Dhajala chondrule on the basis of their Textural and Compositional

SAMPLE	Textural	Textural Classification	FeO (%)	Compositional Classification
CHONDRULE R4	Cryptocrystalline	Porphyritic, dominated by olivine	12.68	IIA
CHONDRULE R10	Cryptocrystalline (disterbed Barred)	Porphyritic, dominated by olivine	18.68	IIA
CHONDRULE R12	Radial	Porphyritic,olivine and pyroxene	7.21	IIA
CHONDRULE R11	Cryptocrystalline	Non Porphyritic,olivine and pyroxene	30.56	IIAB

CONCLUSIONS

1. The BSE ((Backscattered Electron image) is taken by EPMA and Processed By ENVI to determine gray scale and topology of surface of each chondrule(Fig.1).
2. X-Ray analysis is done for each gray scale to Determine Major elemental composition by EPMA of each chondrule. Mineral composition, and BSE ((Backscattered Electron image) are used to classified the each chondrule on the basis of Texture and Composition (table 1).

Reference

Agrawal N K, Suruchi Goel, Murty S V S 2010 A Study of Platinum Group Elements (PGE's) in Meteorites; 16th National Space Science Symposium 2010 (NSSS-2010) **PS-4** P28 159.

ID: 392

Inter-Particle Forces in Granular Media Inferred by the Granular Element Method (GEM)

Eloüüse Marteau

Jose Andrade

Abstract:
By providing a connection between continuum and granular scales, assessment of inter-particle contact forces is of major interest for the development of multiscale methods. The Granular Element Method (GEM) is a computational technique capable of inferring inter-particle contact forces in granular materials under macroscopic loading. The method takes as input the particle average stresses and the structure of the assembly, extracted from experimental techniques. The key of the proposed approach is to combine GEM with Digital Image Correlation (DIC). DIC is applied to sequences of optical images to measure in plane full-field strain from which average particle stresses are deduced. Additionally, information about location of contact points and particle shape are obtained from digital images using segmentation algorithms. This experimental data is then passed to GEM to reconstruct the force distribution. We present here the combined results of DIC and GEM that demonstrate the applicability and the potential of combining advanced experimental techniques with GEM.

Missing Abstract

ID: 503

ID: 561

Transitioning from 3d Imaging to Computational Methods in Granular Media

Ivan Vlahinić
California Institute of Technology
Pasadena, CA, United States

José Andrade
California Institute of Technology
Pasadena, CA, United States

Edward Andó
Université Joseph Fourier
Grenoble, France

Gioacchino Viggiani
Université Joseph Fourier
Grenoble, France

Abstract:
Computed tomography (e.g. X-ray CT) continues to provide unprecedented 3D images of microstructures (e.g. sand), with the scale of individual voxels on the order of a few micrometers. The experiments are by design full-field and non-destructive. In the scientific and mechanistic context, CT experiments enable a deep insight into the behavior of granular materials, in-situ and as a function of macroscopic states (e.g. loads). If utilized to full capacity, the experiments promise to substantially advance the fundamental understanding of granular materials.

A significant bottleneck in this paradigm is that CT ultimately yields 3D images of microstructure (unlike classic triaxial tests, for instance, that return macroscopic strains and/or stresses). Thus far, a challenge has been to quantify the data, i.e. to transfer images into 'quantities' that are palatable for mechanical analysis. In this presentation, we propose a method that substantially reduces this bottleneck. Specifically, we propose a novel way to extract grain topology from loose and/or dense discrete systems via level sets.

Classically, segmentation of individual grains and decoding of grain kinematics, is performed after the raw CT images are converted into their binary or lego-brick counterparts. This greatly reduces or even strips valuable resolution from the raw CT images. ‘Damage’ or image over-segmentation is particularly apparent in the regions of grain contacts. This is problematic because grain contact evolution (i.e. grain fabric) in natural materials (e.g. sand) has an outsized influence on the macroscopic stress-strain response. It is also at the heart of micro-mechanical sources of macroscopic phenomena, including material hardening and softening, as reported by DEM and experimental data over the last 3 decades.

In this presentation, we show how level sets can be used to extract the topology from tomographic images. The method can accurately resolve grain surfaces near to and far from the grain-grain contact regions with sub-voxel resolution, turning images into ‘quantitative’ descriptions of segmented grains.

That we can perform the grain extraction directly in 3D removes a need for reconstruction of grains from individual tomographic slices. We validate the method on 3D X-Ray CT images of highly spheroidal (Caicos Ooid) and highly angular (Hostun Sand) natural materials, with excellent results.

ID: 587

Edelen's dissipation potentials in the mechanics of particulate media

J.D. Goddard
Department of Mechanical and Aerospace Engineering
University of California, San Diego
9500 Gilman Drive
La Jolla, CA 92093-0411, USA

Abstract

This paper is concerned with the role of "dissipation potentials" in various theories of viscoplasticity. As generalizations of the classical Rayleigh-Onsager forms, such potentials have found extensive use in conventional plasticity theories and are readily generalized to multi scale continuum model. In a remarkable work, largely neglected in literature on continuum mechanics, Edelen (*Int. J. Eng. Sci.*, **10**,481, 1972) offers a purely mathematical construct of such potentials, along with non-dissipative terms that are omitted from the classical theories.

The present work revisits Edelen's theory and considers the Legendre-Fenchel duality of convex potentials. The implications are explored for maximum-dissipation principles and related plastic-normality rules. It is conjectured that Edelen's non-dissipative terms may serve to represent the (Reynolds) dilatancy constraint, as a special case of more general non-dissipative couplings.

ID: 665

A Multiscale Model for Coal Reservoir Geomechanics

D Nicolas Espinoza
Laboratoire Navier

Jean-Michel Pereira

Abstract:
Coal gas reservoirs are fractured geomaterials which containvast amounts of adsorbed gas. An accurate determination of the reservoir total amount of gas and hydro-mechanical behavior requires a thorough understanding of the coupling between adsorption, mechanical stresses, and deformation. For example, this knowledge would help predict and remediate the decrease in permeability observed in coal seams upon CO2 injection. We present a thermodynamically-derived poroelastic multiscale modelrelevant for fractured transversely-isotropic microporous media. A salient feature of this model includes the possibility of handling fluids in nanometer-sized pores, in which fluids do not behave as inbulk conditions. The adsorption-strain coupling at the matrix scale canbe modeled in terms of a pressure-dependent 'tangent Biot coefficient'. The application of the theoretical model enables the prediction of several phenomena observed at laboratory scale and the simulation of reservoir scale stress distribution and fluid flow.

ID: 679

Micromechanical Description of Strain in a Granular Material due to Fabric Evolution

Mehdi Pouragha, Richard Wan, Barthelemy Harthong

Civil Engineering Department, University of Calgary
Canada

Abstract:
The deformation of a granular material under externally applied loads involves three different length scales, i.e. the micro-scale, the meso-scale and the macro-scale. The state of the material is believed to be captured by statistical descriptions of the granular assembly through evolving fabric (contact normals at the micro-scale) and connectivity (interaction with immediate neighbouring particles at the meso-scale) during the course of loading. While the overall stress tensor is typically expressed in terms of a fabric tensor based on the distribution density of contact forces at the micro-scale, a description of deformations requires a proper characterization of geometrical configurations at the meso-scale through a network of deforming cells (herein, Dirichlet cells) representing nearest neighbours (Fig. 1a). Herein, the formulation will be pursued in 2D and hence surface area (average) will be confused with volume (average) in 3D.

In the proposed scheme, we consider the probability distribution of contacts $P(\theta)$ for a given particle and search for every direction θ, the nearest contact in its neighbourhood $[\theta-\delta\theta,\theta+\delta\theta]$ which inevitably controls the size of the Dirichlet cell. Accordingly, the most probable outcome for the associated cell volume along θ can be found by considering all possible contact locations in the neighbourhood. Any subsequent changes in contact topology would change the Dirichlet cell, and hence deformations (volumetric and deviatoric) can be ultimately computed by finding the change in mean volume associated with the direction θ under consideration.

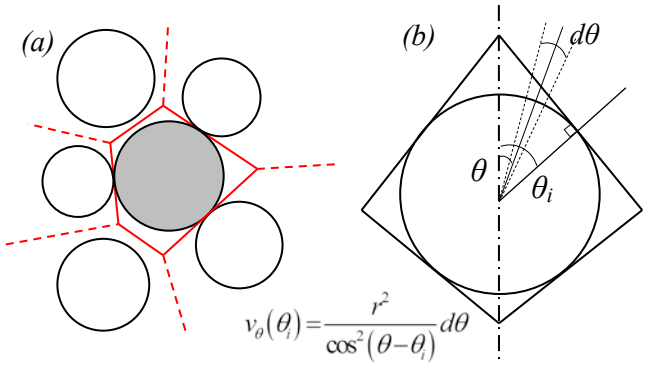

Fig 1. (a) Dirichlet cell, (b) Volume of the cell along θ

If for a given particle we know the coordination number z as well as the anisotropy a of the contact distribution, then $P(\theta)$ can be written as:

$$P(\theta)=\frac{z}{2\pi}\left(1+a\cos 2\theta\right) \text{ with } \int_{\theta-\delta\theta}^{\theta+\delta\theta}P(\vartheta)d\vartheta=1 \qquad (1)$$

Referring to Fig. 1b, the mean cell volume $\langle v_\theta \rangle$ associated to θ can be readily calculated as:

$$\langle v_\theta \rangle = \int_{\theta-\delta\theta}^{\theta+\delta\theta} P(\vartheta).v_\theta(\vartheta)\, d\vartheta = A_z r^2 - ar^2 \cos 2\theta.B_z,\ A_z = \frac{z}{\pi}\tan\frac{\pi}{n},\ B_z = \left(\frac{2z}{\pi}\tan\frac{\pi}{z} - 2\right) \quad (2)$$

Furthermore differentiating Eq. (2) with respect to z and a, herein considered as two state variables, the strain along direction θ emerges as:

$$\varepsilon(\theta) = \left[\varepsilon_v - \varepsilon_s \frac{\cos 2\theta}{2}\right];\ \varepsilon_v = \frac{1}{A_z}\frac{\partial A_z}{\partial z}\delta z \text{ and } \varepsilon_s = \frac{2}{A_z}\left(a.\frac{\partial B_z}{\partial z}\delta z + \delta a.B_z\right) \quad (3)$$

with ε_v and ε_s being volumetric and deviatoric strains associated with the Dirichlet cell. It is seen that this strain reaches a limiting value given that the contact density around a particle cannot exceed $3/\pi$ for particles of sensibly the same size with the upper bound of a being $(6/z - 1)$. The final step involves considering a REV consisting of Dirichlet cells of volume $V(z)$ following a normal probability distribution $P^*(z)$ so that the associated deviatoric and volumetric strains can be calculated by homogenization, i.e.

$$\langle \varepsilon \rangle = \frac{1}{V_{REV}} \int_{z_{\min}}^{z_{\max}} \varepsilon V(z) P^*(z) dz;\ V_{REV} = \int_{z_{\min}}^{z_{\max}} V(z) P^*(z) dz \quad (4)$$

Fig. 2 shows proposed model results of a biaxial test for which the evolution of anisotropy (a) and coordination number (z) was available from discrete element (DEM) computations [1]. The proposed model reproduces fairly well the DEM results given that no systematic calibration was conducted. This is indeed the first step towards developing a micromechanical model based on a statistical description of the granular material requiring only a few parameters of physical significance.

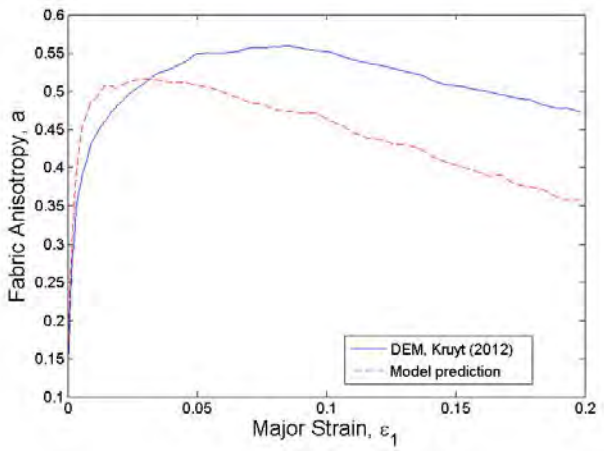

Fig 2. Comparing model prediction with DEM simulation (Kruyt, 2012)

References:

[1] N. P. Kruyt, "Micromechanical study of fabric evolution in quasi-static deformation of granular materials," Mechanics of Materials, vol. 44, pp. 120-129, 2012.

ID: 688

Study of the Influence of Pore and Crack Sizes on Unsaturated Rock Permeability by a Mechanical Damage Model

Jean-Michel Pereira
Laboratoire Navier - éq. Géotechnique (CERMES)
Ecole des Ponts ParisTech
France

Chloé Arson
School of Civil and Environmental Engineering, Georgia Institute of Technology
Center for Tectonophysics, Texas A&M University
United States

Abstract:
The probabilistic definition of Pore Size Distribution (PSD) has been used to formulate a multi-scale permeability model for unsaturated damaged rock (Arson & Pereira, 2012). Natural pores and cracks are considered as two separate sets of pores, characterized by two different size distributions ($\mathbf{p_p(r)}$ and $\mathbf{p_c(r)}$ respectively):

$$\begin{aligned} \mathrm{Tr}\left(\boldsymbol{\varepsilon}^{el}\right) = V_p = \int_{r_p^{min}}^{r_p^{max}} \alpha_p(r)\pi r^2\,dr = \pi N_p \int_{r_p^{min}}^{r_p^{max}} p_p(r) r^2\,dr \\ \mathrm{Tr}\left(\boldsymbol{\varepsilon}^{ed} + \boldsymbol{\varepsilon}^{id}\right) = V_c = \int_{r_c^{min}}^{r_c^{max}} \alpha_c(r)\pi r^2\,dr = \pi N_c \int_{r_c^{min}}^{r_c^{max}} p_c(r) r^2\,dr \end{aligned} \quad (1)$$

in which $\mathbf{N_p}$ and $\mathbf{N_c}$ denote the number of natural pores and cracks in the Representative Elementary Volume (REV). The bounds of the integrals in Eq. (1) define the ranges of values that can be taken by natural pore and crack sizes. PSD curves are coupled to the mechanical behavior of the rock by updating microscopic parameters (such as average pore size) with deformation and damage. In addition, PSD parameters are related to intrinsic permeability, through Hagen-Poiseuille flow equation and Darcy's law. The capillary pore radius ($\mathbf{r}_{sat}$) is related to capillary pressure by Laplace equation and to the PSDs by the pore volume saturated by water. Microscopic PSD parameters are thus updated with macroscopic thermodynamic variables. This allows updating permeability and retention properties (Pereira & Arson, 2012).

In the present work, the model is used to predict rock microstructure changes and the consequent impact on intrinsic permeability and drainage-imbibition paths. A triaxial compression test is simulated under controlled capillary pressure with several ranges of values for the sizes of pores and cracks (Tab.1). In virtue of Laplace law, it is verified that for a given natural porosity mode and a fixed minimum crack size, an increase of the upper bound of crack sizes originates drying (Fig.1.a). In the PSD-permeability model, crack shape is only controlled by an internal length parameter, and the evolution of the mesoscopic damage variable determines the number density of cracks in the REV. As a result, longer cracks are associated to a larger void volume fraction, and have a stronger impact on intrinsic permeability enhancement (Fig.1.b). For a given pore and crack size range, the typical size separating the two porosity modes drastically affects the water retention curve (Fig.2.a), and also influences the relative permeability (Fig.2.b). In this particular problem, a reduction of the crack size range makes it easier for the material to dry, which can be

explained by a general increase of the volume fraction of larger pores (natural or crack-induced). In this set of simulations, the number density of natural pores is likely to be much larger than the number density of cracks forming in the REV. As a conclusion, the authors advocate using both the average pore size and the pore number density as microscopic dissipation variables.

Table 1. Ranges of value of the pore and crack sizes in the simulated compression tests.

Test	r_p^{min} (	r_p^{max} (	r_c^{min} (	r_c^{max} (
Influence of the maximum crack size	**0.01**	**1**	**1**	**10**
	0.01	1	1	100
	0.01	1	1	1000
	0.01	1	1	10000
Influence of the size separating the two porosity modes	**0.01**	**1**	**1**	**10**
	0.01	0.1	0.1	10
	0.01	0.5	0.5	10
	0.01	5	5	10

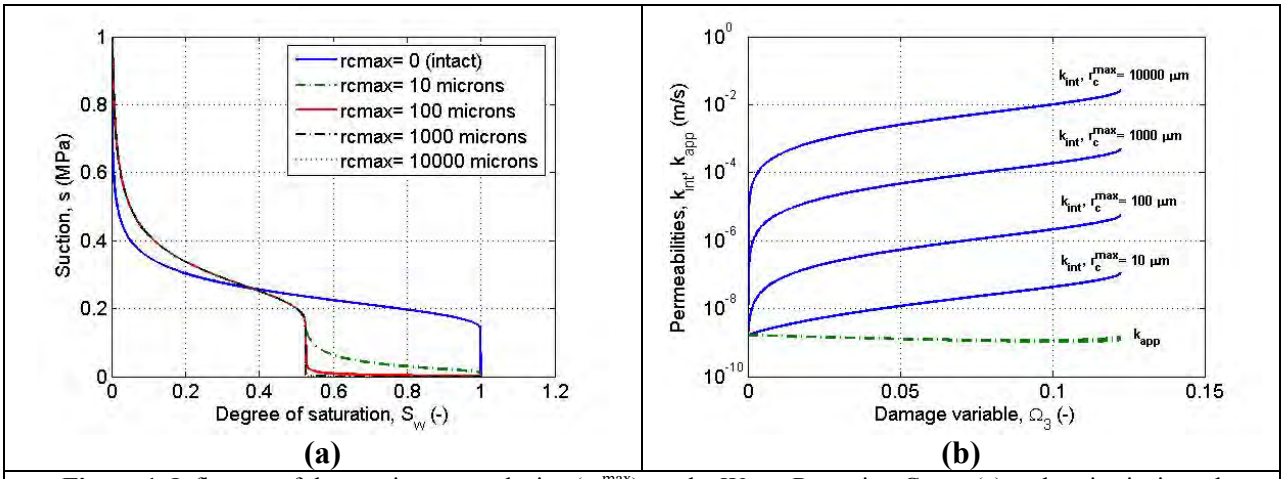

Figure 1. Influence of the maximum crack size (r_c^{max}) on the Water Retention Curve (a) and on intrinsic and apparent permeabilities (b) during a triaxial compression test.

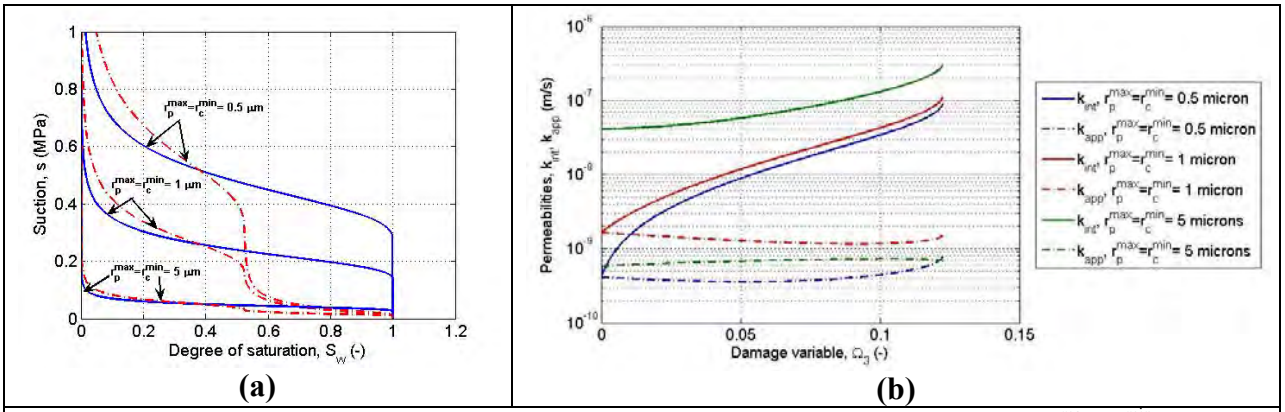

Figure 2. Influence of the size separating the natural and the crack-induced porosity modes (r_p^{max}=r_c^{min}) on the Water Retention Curve (a) and on intrinsic and apparent permeabilities (b) during a triaxial compression test. *Water Retention Curves: solid lines = non-damaged states, dashed lines = damaged state at the end of the test.*

IV.9

Multiscale Mechanics of Materials - Multiscale Mechanics of Energy Storage Materials

ID: 150

Skin Effect and Material Degradation of Lead-free Solder Joint under AC

Wei Yao
University of Buffalo
USA

Cemal Basaran

Abstract:
In this study, alternating current (AC) electromigration (EM) degradation simulations were carried out for SAC405 solder joints Square, sine and triangle current wave forms were used as input signals. DC and pulsed DC (PDC) electromigration analysis were conducted for comparison purposes. The maximum current density ranged from to, frequency ranged from 0.05 Hz to 5 Hz, and ambient temperature from 350K to 450 K. It was observed that MTF was inversely proportional to ambient temperature T1.1 in Celsius, and also inversely proportional to current density j0.27 in A/cm2. Higher frequency will lead to a shorter lifetime with in the frequency range we studied, and a relationship is proposed as. Lifetime of a solder joint subjected to AC is longer compared with DC and PDC loading conditions. AC skin effect was investigated experimentally. Skin effect was investigated as well.

ID: 233

Concurrent Reaction and Plasticity during Lithiation of Crystalline Silicon in Lithium-ion Batteries

Matt Pharr
Harvard University
USA

Kejie Zhao
USA

Abstract:

In an electrochemical cell, crystalline silicon and lithium react at room temperature, forming an amorphous phase of lithiated silicon. The reaction front-the phase boundary between the crystalline silicon and the lithiated silicon-is atomically sharp. Evidence has accumulated recently that the velocity of the reaction front is limited by the rate of the reaction at the front, rather than by the diffusion of lithium through the amorphous phase. We present a model of concurrent reaction and plasticity. We identify the driving force for the movement of the reaction front, and accommodate the reaction-induced volumetric expansion by plastic deformation of the lithiated silicon. The model is illustrated by an analytical solution of the co-evolving reaction and plasticity in a spherical particle. We derive the conditions under which the lithiation-induced stress stalls the reaction. We also show that fracture is averted if the particle is small and the yield strength of lithiated silicon is low. Furthermore, we have recently measured the velocity of the phase boundary at various potentials for three orientations in silicon. Using our experimental values, we show that our model accounts for recently observed lithiated silicon nanowires of anisotropic morphologies. We also model fracture of these nanowires, and compare to these experiments.

Missing Abstract

ID: 237

ID: 351

Lithium Intercalation Induced Deformation and Dislocation Nucleation in SnO2 Nanowires

Scott Mao
University of Pittsburgh
USA

Li Zhong
USA

Abstract:
Although the lithium intercalation, one of the lithiation mechanisms, has been investigated by theoretical simulation over a wide range of different electrode materials, there is a lack of experimental evidence and fundamental understanding on formation and evolution of the lithium intercalation atomistically. It is critical to explore the dynamic process of lithiation intercalation, distortion of lattice structure and amorphous evolution by use of combined transmission electron microscope (TEM) and Computational DFT. In this talk, we report the atomic scale lithiation mechanism of SnO2 nanowires in a lithiation process. The lithiation initiated multiple stripes with width of a few nanometer parallel to (020) planes transversing the entire wires, serving as multiple reaction fronts for late stage of lithiation. The lithium intercalation can induce large lattice stress leading to formation of a high density of dislocations with Burgers vectors of <100> along the strips. Inside the stripes, we identified high density dislocations and enlarged inter-planar spacing which provide effective path for lithium ion transport. This multiple strips and multiple reaction fronts lithiation mechanism is unexpected and differs completely from the expected core shell lithiation mechanism.

ID: 361

Coupled Mechano-Diffusional Driving Forces for Fracture in Electrode Materials

Y. F. Gao
Georgia Institute of Technology
United States

M. Zhou
Georgia Institute of Technology
United States

Abstract:
Electrode degradation due to internal stress build-up during cycling has been one of the key challenges for secondary battery designers. When guest atoms are inserted or extracted from the host in the electrode, the material in the electrode expands or shrinks, by up to ~300% in some Li-alloy based electrodes, inducing stresses that may cause material cracking. Here, we investigate the coupled mechano-diffusional driving forces for fracture in electrode materials using a mixed finite element framework. The simulation shows that when a pre-crack is loaded by a tensile stress, either induced by charging/discharging or applied externally, guest atoms will accumulate in front of the crack tip due to the stress triaxiality, in a fashion similar to the hydrogen accumulation seen in the context of hydrogen embrittlement in metals. The accumulation of guest atoms is so significant that a saturation zone in which the guest concentration reaches the full-charging limit can develop, and the size of the saturation zone depends on the remote loading and the average concentration in the whole electrode. In order to establish the correlation between the guest atom accumulation effect and the cracking conditions, the energy release rate J of the crack has been calculated. By treating the crack tip as a separate thermodynamic system, we used the non-equilibrium thermodynamics to prove that the standard form of J-integral for energy release is no longer path-independent when coupled mechano-diffusion driving force is present. Instead, an area integral similar to that found in hygrothermal problems must be included. Indeed, numerical results show that J calculated by contour integral alone can be negative for certain paths; while J calculated by taking both the contour and path integrals into account differ only by less than 2% for all the paths considered up to the point of full-scale yielding. Interestingly, although the hydrostatic stress is relaxed when guest atoms accumulate in front of the crack tip, the energy release rate can be up to 80% larger than that when the accumulation effect is not considered, at least for the loading conditions considered in this study. Our results indicate that the guest accumulation due to the two-way coupling significantly affects the driving forces for fracture.

Recent experimental evidences suggest that the elastic modulus and yield stress of Li/Si undergo significant softening when the lithium concentration increases. In order to investigate how this lithiation-induced softening affects the fracturing conditions, galvanostatic discharge processes of thin-film Li/Si electrodes with surface pre-cracks are considered. Starting with a uniformly charged thin film (ξ_{init} Li per Si), a constant surface outflux of Li is prescribed in order to mimic

the galvanostatic discharging conditions. During the initial stages, J increases quadratically with respect to $\Delta\overline{\xi} \equiv \xi_{init} - \overline{\xi}$ [cf. fig. 1]. When $\Delta\overline{\xi}$ reaches a certain critical value, however, the slope of $\Delta\overline{\xi} \sim \mathrm{J}$ curve suddenly decreases, as a result of the initiation of full-scale yielding which releases mechanical energies. The effect of lithiation-induced softening on fracturing conditions is investigated through parametric studies. It is found that for the same discharge level of $\Delta\overline{\xi}$, J is always lower when the initial concentration ξ_{init} is higher. On the other hand, since critical energy release rate $\mathrm{J_{cr}}$ usually increases when yield stress decreases in engineering materials, it is expected that $\mathrm{J_{cr}}$ in Li/Si would be higher at higher $\overline{\xi}$. Even under the assumption of concentration-independent critical energy release rate of $\mathrm{J_{cr}}$~10 J/m^2, the maximum allowable of $\Delta\overline{\xi}$ is 1.28 when $\xi_{init} = 0.99\xi_{\max}$ and 0.16 when $\xi_{init} = 0.2\xi_{\max}$, a ~780% difference in the maximum allowable $\Delta\overline{\xi}$. Our results clearly indicate that operation at higher concentrations can significantly mitigate fracture failure in Li/Si electrodes.

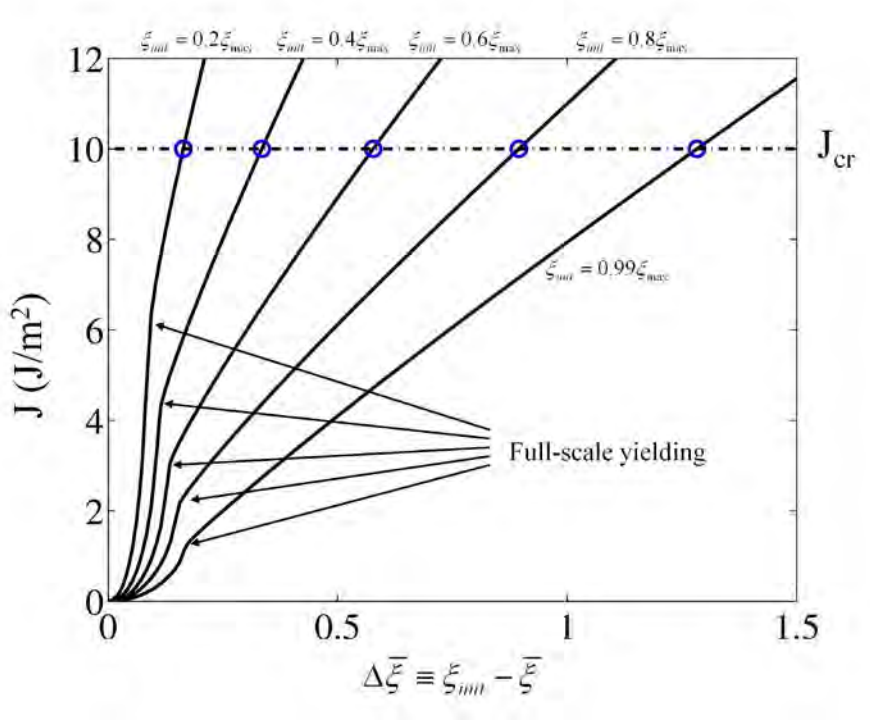

Fig. 1 Energy release rate J in a Li/Si thin-film electrode during galvanostatic discharge (at the discharge rate of C/50). The film has a thickness of 200 nm when fully delithiated and a surface crack of 20 nm. For the same discharge level of $\Delta\overline{\xi}$, J is significantly lower when ξ_{init} is higher.

ID: 388

A Coupled Electro-Chemo-Mechanical Framework for Diffusion and Deformation in Solids

JIANMIN QU
Northwestern University
USA

Zhiwei Cui
USA

Abstract:
Solid materials used in energy conversion and storage devices are often subjected to multiple driving forces (electrical, chemical, radiological, thermal, mechanical, etc.). The interactions among these different driving forces often impact the efficiency, reliability and durability of the devices. Understanding of how the different driving forces interact requires theories and models that are capable of accounting for the coupling of multi-physics processes. In this talk, a framework is presented that couples the mechanical and chemical (or electrochemical) fields in solids via the use of stress-dependent chemical potentials. To illustrate the development and applications of this coupled electro-chemo-mechanical theory, two examples of practical interest will be discussed, namely, solid oxide fuel cells and lithium ion batteries. Our interest is to understand how solid diffusion generates mechanical stresses, and how such mechanical stresses affect the diffusion. The first example is concerned with the interactions between mechanical stresses and ionic transport in the electrolyte of a solid oxide fuel cell. It is found that the non-uniform oxygen vacancy concentration in the electrolyte can generate significant stresses whose amplitude is comparable to the thermal mismatch induced stress in the cell stack. More importantly, significant stress concentration near processing defects (voids and microcracks) occurs due to the presence of ionic fluxes. The second example is on the insertion of lithium into silicon in silicon anodes in lithium batteries. Using input from ab initio and molecular dynamic simulations, we investigated the mechanisms of lithium insertion and how the process is affected by mechanical stresses.

ID: 406

Pressure-Gradient Dependent Diffusion and Crack Propagation in Lithiated Silicon Nanowires

Vivek Shenoy
USA

Abstract:
Silicon is a promising material for use in lithium-ion battery electrodes due to its extremely high theoretical capacity. The difficulty associated with using silicon in these applications is due to the fact that it undergoes large volumetric expansions of up to 400% during lithiation; such extreme expansions generate high stresses that can lead to fracture and capacity loss. Previous attempts at modeling cracking in lithiated materials have entirely ignored or simplified the effects of pressure-gradients on the diffusive flux, which leads to an overestimation of the stress-state within the material. We have developed a method of studying lithiation-induced crack propagation in silicon nanowires that accounts for the effects of pressure-gradients within the material on the flux. Our approach consists of finite element simulations in which the pressure-gradients are computed numerically and used to calculate the flux vector. This method allows us to capture the effect of the crack-tip on the localized diffusion, which plays an important role in arresting crack growth. We have used our method to study the effects of charging rate and particle size on crack propagation in silicon nanowires. Three crack growth regimes have been observed depending on the charging rate and nanowire diameter - no growth, arrested growth, and complete growth - and they have been tabulated in a failure diagram.

[1].[1] R. Grantab and V. B. Shenoy, J. Electrochem. Soc., Volume 159, Issue 5, pp. A584-A591 (2012
cellular force generation during wound healing.

ID: 415

Understanding and Mitigating Diffusion-Induced-Stresses and Fracture in Lithium ion Battery Electrodes

Yang-Tse Cheng
University of Kentucky
USA

Abstract:
Most lithium ion battery electrodes experience large volume changes caused by concentration changes within the host particles during charging and discharging. Electrode failure, in the form of fracture or decrepitation, can occur as a result of repeated volume changes. In this presentation, we will provide an overview of our recent work on modeling the evolution of concentration, stress, and strain energy within a spherically- or cylindrically-shaped electrode element under various charging-discharging conditions. We show that a dimensionless parameter, the electrochemical Biot number, may be used to characterize stress and strain energy evolution in an electrode. In particular, the electrochemical Biot number determines the maximum stress and strain energy. Based on analytic solutions, we propose tensile stress and strain energy based criteria for the initiation and propagation of cracks in insertion electrodes. These criteria may help guide the development of new materials for lithium ion batteries with enhanced durability and performance. We will also discuss other effects, such as moving phase boundaries, surface and interface energies, and concentration-dependent elastic modulus, on stress and strain energy evolution in insertion electrodes, as well as stress-induced whisker growth in lithium ion battery electrodes and crack pattern formation in silicon thin film electrodes. Finally, we will discuss our recent work on liquid metal alloys as self-healing electrodes for lithium ion batteries.

ID: 424

Degradation and Life prediction of Large Format Li-ion Cells

Wei Lu
Department of Mechanical Engineering
University of Michigan
United States

Abstract:
The electrification of the drivetrain is crucial to solve our energy problems and fill the gap to sustainable and zero emission mobility. We are now within reach of mass-marketed vehicles using Li-based batteries. Full engineering analysis of batteries and battery systems must be regularized, and engineering development is needed to allow creation of products and tools for integration of battery systems into vehicles. Electric Vehicles (EV) and Hybrid Electric Vehicles (HEV) face significant battery-related challenges, including limited driving range and high battery cost resulting from the capacity fade of batteries during usage. The prediction of capacity fade and lifetime of batteries is important for cell design, determination of the optimal operation condition and control, and cell maintenance, and eventually the successful implementation of HEVs and EVs. Various mechanisms contribute to capacity fade, especially in large format cells which use multiple-material electrodes to enhance the performance. An integrated approach considering different aspects of the fading mechanisms is necessary. In this talk I will present some of our recent works on modeling the fading mechanisms in Li-ion batteries together with experimental investigations. Specifically, I will focus on those mechanisms that are not well understood before, such as stress evolution in lithium manganese dioxide particles due to coupled phase transition and intercalation, facture of active material particles, ion diffusion and percolation, dissolution of active material, heat generation under various operational and environmental conditions, effects of face pressure on cell performance. We have developed a life prediction framework that will integrate multiple physics across different scales — including electrochemical, transportational, thermal, mechanical and thermodynamic processes. Assisted with experimental measurements, we are incorporating realistic three dimensional electrode microstructures in our models for high fidelity simulation and prediction.

The figures below illustrate some of these topics.

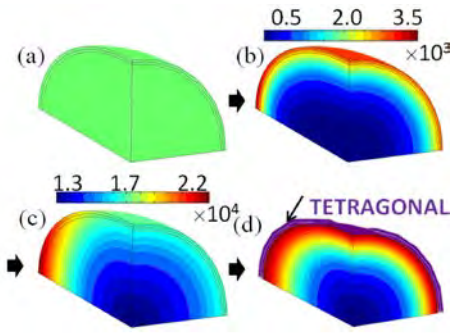

Figure 1. Lithium concentraion profile at representative steps. (a) initial manganese dioxide particle (b) Li-ion diffuses into the particle, forming a concentration profile (c) the tip of the long axis reaches the stoichiometric maximum and phase transition starts to occur (d) formation of a tetragonal phase shell.

Figure 2. Intercalation and phase transition induced stress in a particle with an aspect ratio of 1.95. Shown is comparison of the maximum principal stress σ_1 before and after phase transition without and with intercalation. The 3D images show σ_1 distribution in the particle.

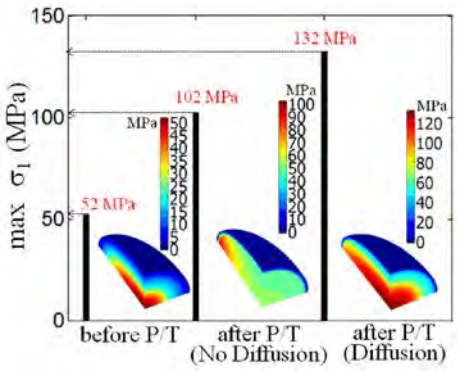

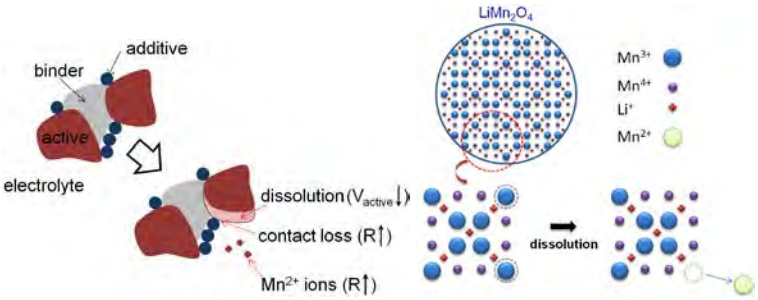

Figure 3. Schematic diagram of the effect of dissolution and schematic diagram of the dissolution process: two Mn3+ cations convert into one Mn4+ and one Mn2+, then Mn2+ ions leave the solid phase.

Figure 4. Calculation shows relative capacity decrease due to dissolution with (a) different temperature (b) different voltage range

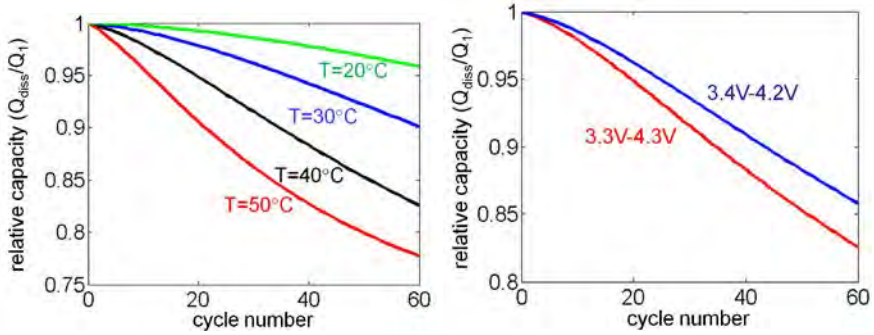

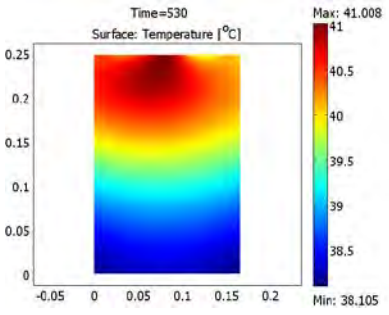

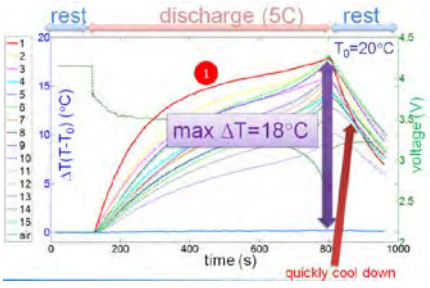

Figure 5. Calculation shows heat generation during charge and discharge.

ID: 435

Mechanical Behavior of Lithiated Silicon Alloys: An Molecular Dynamics Study

Feifei Fan

Shan Huang

Abstract:
Understanding the mechanical behavior of amorphous Li-Si alloys is crucial to preventing the mechanical degradation in the negative electrodes of lithium-ion batteries. By using a reactive force field potential, we perform the molecular dynamics simulations of tension and compression in amorphous LixSi alloys. We find these alloys with low and high Li concentrations exhibit drastically different atomic structures, which are characteristic of the covalent network glass and metallic glass, respectively. Those structure differences underlie the asymmetry in plastic yield stresses between tension and compression that depends sensitively on the lithium concentrations. Implications regarding to the coarse-grained constitutive modeling of lithiated silicon alloys are discussed.

ID: 438

Mechanical Degradation During Lithium Intercalation in Nanostructured Anodes Materials for Li-ion Batteries

Reza Shahbazian Yassar
Michigan Technological University

Abstract:
Silicon and titanate are promising materials for Lithium-ion batteries. This report focuses on the in-situ observation of lithiation and delithiation in Si nanorods and TiO2 nanotubes. The intercalation of Li ions in Si nanorods was monitored during charging and the fracture of nanorods was quantified in terms of size. The electrochemical testing of these low dimensional structures was conducted inside a transmission electron microscope equipped with a novel in-situ electrical probing holder. In addition, the intercalation of crystalline anatase and amorphous TiO2 was studied and their fracture events were monitored in real time.

Missing Abstract

ID: 456

ID: 461

Understanding the Mechanical Degradation of High Energy Density Electrode Materials for Next Generation Lithium Ion Batteries

Xingcheng Xiao
General Motors Global R&D Center

Abstract:
The diffusion induced stress has been believed to be one of the major driving forces responsible for the mechanical degradation especially for electrode materials with high capacity in lithium ion batteries. On the other hand, due to the coupling effect, the stress can also affect the diffusion and therefore change the cycling efficiency, which has not been fully understood yet. In this talk, we will first introduce how to in situ characterize the diffusion induced stress, combining the in-situ observation of the crack generation and propagation in the Si thin film based electrode. We will then discuss different approaches to tailor the nanostructure for mitigating the mechanical degradation of Si electrode to improve its capacity retention and cyclic life, including pattering Si to relax the stress relaxation, applying surface coatings to modify the stress gradient and providing the energy barrier for crack nucleation.

ID: 470

Morphological Changes in Magnesium Nanoblades under Cyclic Hydrogenation

Bo Yang
University of Texas at Arlington

Yuping He

Abstract:
Magnesium nanoblades turn into powder upon cyclic hydrogenation. In this work, we carry out an analytical study of hydrogen diffusion and induced stresses to interpret the morphological changes in Mg nanoblades. By assuming the H diffusion coefficient and H adsorption rate to be exponentially and linearly dependent on concentration, a physical model is developed to first predict the hydrogenation process of Mg nanoblades. The predicted H uptake curves agree well with the experimental data from V-coated Mg nanoblades. The obtained H diffusion coefficients in MgHx between Mg and MgH2 have nearly three orders of magnitude variation. In both one- and two-dimensional simulations, it is shown that a hydride shell is not formed during hydrogenation but that a hydride core is formed during dehydrogenation. The strong concentration dependence of H diffusion constant throws profound influence on the stability and instability of a diffusion front such that it tends to corrugate forming islands of hydride during dehydrogenation. The uneven diffusion field leads to a nonuniform stress field over a Mg nanoblade, which may explain why it turns into powder upon cyclic hydrogenation. An elastoplastic analysis is then done to predict the deformation and stress fields in a V-coated Mg nanoblade and to show how the morphology evolves over cycles of hydrogenation and dehydrogenation.

ID: 577

Mechanical Characterization of Lithiated Silicon and the Solid Electrolyte Interphase

Siva P.V. Nadimpalli,
E. Buchovecky,
V.A Sethuraman,
V.B.Shenoy,
A.F.Bower,
P. R.Guduru,

Abstract:
We present an experimental investigation to characterize mechanical behavior of lithiated silicon during electrochemical cycling. Stress evolution in thin films of Silicon is measured through the substrate curvature method, while the sample is lithiated and delithiated. The experiments reveal that lithiated silicon undergoes extensive plastic deformation at a flow stress of about 1 GPa; we conclude that plasticity in lithiated Si needs to be taken into account in assessing failure of silicon-based electrode architectures at all length scales. A coupled mechanical-electrochemical model is presented, which captures the relevant experimental features. Further, experiments are carried out to measure the loss of lithium per unit area of Si, which provides a useful guide in assessing the first-cycle capacity loss due to formation of the solid electrolyte interphase (SEI) layer. We show that the results are well described by Tafel kinetics. Additional experiments are presented to characterize stress evolution in the SEI on silicon films, along with measurements of growth rates of the SEI layer under relevant electrochemical conditions.

Missing Abstract

ID: 663

ID: 721

Delineating Local Electromigration for Nanoscale Probing of Lithium Ion Intercalation and Extraction by Electrochemical Strain Microscopy

Jiangyu Li
University of Washington
USA

Abstract:
Lithium ion intercalation and extraction are critically important for high performance Li-ion batteries, and they are highly sensitive to local crystalline morphologies and defects that remains poorly understood. Using electrochemical strain microscopy (ESM) in combination with local transport analysis, we demonstrate that we cannot only probe Li-ion concentration and diffusivity with nanometer resolution, but also map local energy dissipation associated with electromigration of Li-ions. Using these techniques, we uncover drastic difference in ESM response and energy dissipation between micro- and nano-crystalline LiFePO4 under different charging states, which explains superior capacity observed in Li-ion batteries with nanocrystalline LiFePO4 electrode.

IV.10

Multiscale Mechanics of Materials - Multiscale Fracture and Failure of Materials

ID: 095

Elastomer Surfaces with Directionally Dependent Adhesion Strength and Their use in Transfer Printing with Continuous Roll-to-Roll Applications

Huanyu CHENG
Northwestern University

Qingmin Yu

Abstract:
In this paper, we present mechanics and materials aspects of elastomeric stamps that have angled features of relief on their surfaces, designed to enable control of adhesion strength by peeling direction, in a way that can be exploited in schemes for deterministic assembly by transfer printing. Detailed mechanics models capture the essential physics of interface adhesion in this system. Experiments with cylindrical stamps that have this design demonstrate their potential for use in a continuous, roller mode of operation.
.

ID: 116

Multiscale Modeling of Fracture in Composites: A Roadmap Towards Virtual Testing

Javier LLorca
Polytechnic University of Madrid / IMDEA Materials Institute

Carlos Gonzalez

Abstract:
A bottom-up, multiscale modeling approach is presented to carry out high-fidelity virtual mechanical tests of composite materials and structures until fracture. The overall multiscale simulation scheme takes advantage of the fact that composite structures are made up of laminates which in turn are obtained by stacking individual plies with different fiber orientation. This leads to three different entities (ply, laminate and component) whose mechanical behavior is characterized by three different length scales, namely fiber diameter, ply and laminate thickness, respectively. This clear separation of length scales is very useful to carry out multiscale modeling by computing the properties of one entity (e.g. individual plies) at the relevant length scale, homogenizing the results into a constitutive model, and passing this information to the simulations at the next length scale to determine the mechanical behavior of the larger entity (e.g. laminate).

ID: 231

A multiscale computational model for predicting fracture toughness from microstructure

Yan Li
Georgia Institute of Technology
United States

Second Author
Georgia Institute of Technology
United States

Abstract:

Microstructure determines fracture toughness of materials through the activation of different fracture mechanisms. Microstructural design is an important approach for enhancing material behavior such as fracture toughness at the macroscopic scale. We present a cohesive finite element methods (CFEM) based multi-scale framework for analyzing the effect of microstructural heterogeneity, phase morphology, constituent behavior and interfacial bonding strength on fracture toughness. This model enables multiscale delineation of microstructures, explicit tracking of crack propagation process and realistic representation of deformation and fracture at different length scales. The initiation/propagation fracture toughness is extracted by calculating the J-integral. Based on the CFEM results, a semi-empirical model is developed to provide a quantitative relation between the propagation toughness and statistical measures of microstructure, fracture mechanisms, and constituent and interfacial properties. Both the CFEM framework and analytical model are useful tools for designing of new materials with tailored properties.

Introduction

The evaluation of material fracture toughness as functions of microstructure attributes is a fundamental issue in material science. It requires proper characterization of microstructures and quantitative correlation of microstructural attributes with overall material response. Experimental approaches allow systematic studies of microstructure-fracture toughness relations but fail to explore material configurations not yet in existence. Besides, the trial-and-error process is usually associated with high cost and long cycles. To overcome the above shortcomings, a cohesive finite element method (CFEM) based multi-scale framework for analysing the effect of microstructural heterogeneity, phase morphology, constituent behavior and interfacial bonding

strength on the fracture toughness is developed as shown in Fig. 1. This framework allows explicit representation of microstructures and allows explicit representation of microstructures and account of microstructural level of deformation, damage and failure mechanisms, while allowing macroscopic conditions such as controlled loading and structural response to be considered at the same time. This framework provides a means for calibrating model parameters at the microscale through macroscale responses which can be easily measured in experiments. More importantly, it allows macroscopic response measures such as K_{IC} to be evaluated as functions of microstructure by calculating the *J*-integral along an arbitrary contour within the homogenized region.

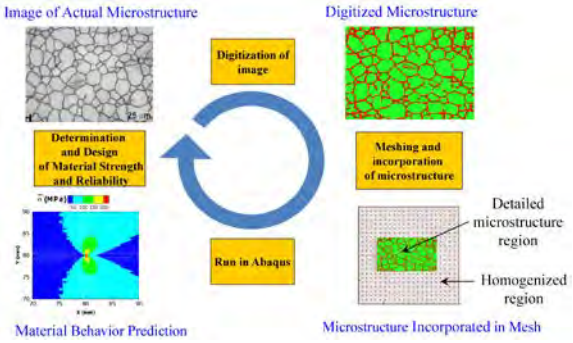

Fig. 1 The multi-scale CFEM framework for material design.

Results and discussion

Calculations carried out concern Al_2O_3/TiB_2 two-phase ceramic composites and focus on the fundamental fracture mechanisms during crack initiation and propagation. Results of CFEM calculations show that both microstructure and constituent properties can significantly influence fracture behavior and combine to determine the overall fracture toughness through the activation of different fracture mechanisms. Interface debonding is the most beneficial fracture mechanism and is primarily promoted by small reinforcement size, rounded particle shapes and appropriately bonded and compliant reinforcement-matrix interfaces. In contrast, particle cracking, which triggers catastrophic material failure, usually occurs in microstructure with large reinforcement particles, lower particle

roundness and over-bonded/stiff interfaces. Important constituent parameters are the fracture toughness of the matrix phase and the toughness of the interface between the matrix and the reinforcement phases.

References

[1] B. Moran and C. F. Shih, "A general treatment of crack tip contour integrals," *Int. J. Fracture.*, vol. 35, no. 4, pp. 295-310, Dec. 1987.

[2] L. B. Freund, *Dynamic fracture mechanics*. Cambridge University Press, 1998.

[3] M. Zhou, G. Ravichandran and A. J. Rosakis, "Dynamically Propagating Shear Bands in Impact-loading Prenotched plates, II - Numerical Simulations", *J. Mech. Physics. Solids*, 44, pp. 1007-1032, 1996

[4] Y. Li and M. Zhou, "Computational Prediction of Fracture Toughness of Ceramic Composites as a Function of Microstructure: I. Numerical Simulation." To be published.

ID: 247

A Multiscale Investigation of Strain and Microstructure in Fatigue Crack Growth

Jay Carroll
Sandia National Laboratories

Wael Abuzai
USA

Abstract:
Fatigue crack growth is currently predicted by the phenomenological Paris relationship. However, crack growth at the grain scale is influenced by many factors such as microstructure, local stress and strain fields, and local crack path. Understanding the interactions between these variables could lead to a better understanding of fatigue crack growth and microstructurally informed fatigue models.In this work, multiscale strain measurements from a high-resolution digital image correlation (DIC) technique were used to study fatigue crack growth in Hastelloy X, a nickel based superalloy. The strain accumulation due to the growing fatigue crack was shown to have inhomogeneities at the macroscale, the grain scale, and the sub-grain scale. These inhomogeneities were spatially aligned with measurements of the grain structure obtained through electron backscatter diffraction (EBSD). A comparison of these measurements with images from both optical and electron microscopy revealed relationships between microstructure, strain localizations, crack path, and crack growth rate.

ID: 286

Multiscale Modeling of Ultra-High-Performance Fiber-Reinforced Concrete Subject to Blast Loading

Brett Ellis
Woodruff School of Mechanical Engineering, Georgia Institute of Technology, Atlanta, GA
United States of America

Min Zhou
Woodruff School of Mechanical Engineering, Georgia Institute of Technology, Atlanta, GA
School of Materials Science and Engineering, Georgia Institute of Technology, Atlanta, GA
United States of America

David L. McDowell
Woodruff School of Mechanical Engineering, Georgia Institute of Technology, Atlanta, GA
School of Materials Science and Engineering, Georgia Institute of Technology, Atlanta, GA
United States of America

Abstract:
Ultra-High-Performance Fiber-Reinforced Concretes (UHPFRCs) are a promising class of granular composites that employ heterogeneity at multiple length scales to withstand dynamic loads. To gain insights into the relevant mechanisms of blast loaded panels, this research introduces a multiscale model consisting of three length scales, as shown in Figure 1. For fibers with surface topology, a 3D finite element model (FEM) of a single fiber with surface topology is embedded in a matrix to account for plastic work of the fiber, granular flow in the matrix, and sliding friction at the fiber-matrix interface. For straight, smooth fibers, values of interfacial shear strength are taken from literature to determine the pullout force versus end slip relations.

The resulting pullout force versus end slip relations are projected onto independently placed fibers at pseudo-random positions within the model at the multiple fiber length scale, which is an adaptation of the Rigid-Body-Spring-Model [1]. This model accounts for fiber embedded length, volume fraction, and inclination angle relative to the displacement vector $\boldsymbol{\delta}$. Four properties – mean of the tensile strength, standard deviation of the tensile strength, mean of the dissipated energy density, and the standard deviation of the dissipated energy density – are calculated from one hundred instantiations.

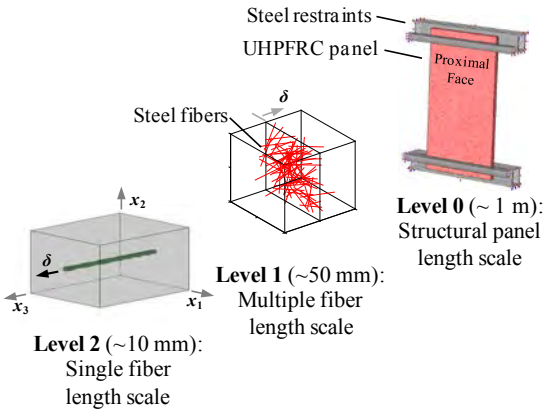

Figure 1. Multiscale model of UHPFRC consisting of three length scales.

The coarsest length scale, i.e. structural panel length scale, consists of a UHPFRC panel (shaded in red in Figure 1) placed between steel restraints

(shaded in gray). The UHPFRC panel consists of bulk elements placed between zero-thickness cohesive elements. Bulk elements utilize pressure-sensitive constitutive laws; cohesive elements utilize a bilinear traction-separation constitutive law incorporating isotropic damage and strain-rate sensitivity. Quasi-static cohesive material properties, namely damage initiation strength and energy dissipation, are assigned from the four properties identified previously at the multiple fiber length scale. At dynamic strain-rates, the quasi-static damage initiation strength is increased by relations given by Zhou et al. [2]. The simulated blast load is applied to the proximal face (cf. Figure 1) via a surface traction in the normal direction. An initial magnitude of p_{max} at 0 ms linearly decays to zero at 15 ms, resulting in an applied impulse of $I = \frac{15\text{ms}}{2} p_{max}$.

Results of the multiscale model are compared to physical experiments that used the same size of structural panel and same material properties: 200-MPa UHPFRC unconfined compressive strength, 2.57-g/cm^3 UHPFRC density, and 2% volume fraction of 14-mm long by 0.185-mm diameter straight, smooth steel fibers, to list a few. Comparisons between the model and the physical experiments are based upon displacements measured during fracture, the critical impulse resulting in complete fracture of the panel, and the fracture patterns shown in Figure 2.

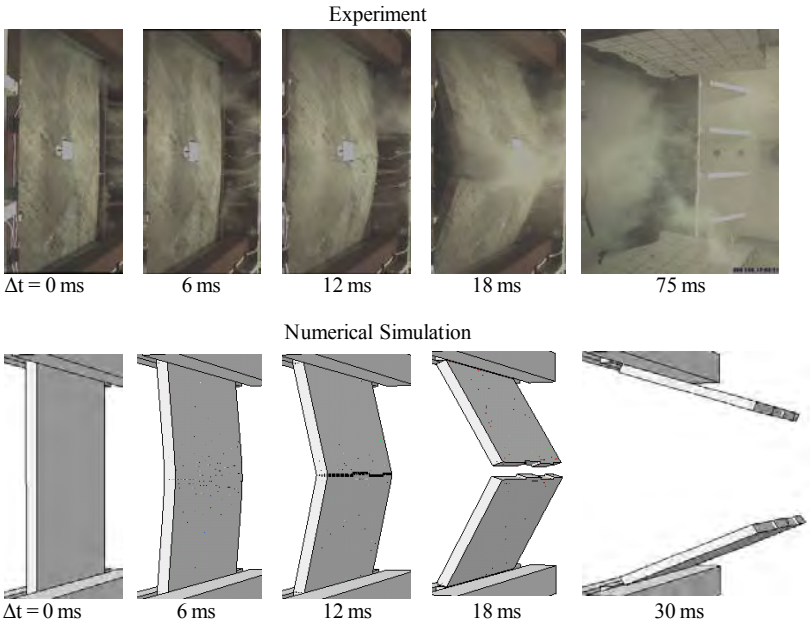

Figure 2. Physical experiment and one instantiation of the multiscale model of a UHPC panel subjected to a 2.05 MPa-ms impulse. The instantiation exhibits distributed cracking at 6 ms before crack coalescence and growth at 12 ms. Both the physical experiments and numerical simulations possess three areas of characteristic fracture – one at the lower restraint, one at the mid-height, and one at the top restraint.

References:

[1] Bolander JE and Saito S, (1997). *Discrete modeling of short-fiber reinforcement in cementitious composites*, Adv Cement Based Matls. 6: 76–86.

[2] Zhou XQ, Kuznetsov VA, Hao H, and Waschl J, (2008). *Numerical prediction of concrete slab response to blast loading*, Int J Impact Eng. 35: 1186–1200.

ID: 290

A Micromechanics Based Damage Model Applied to Asteroid Impacts

Andrew L Tonge
The Johns Hopkins University
United States

K.T. Ramesh
The Johns Hopkins University
United States

Abstract:
One of the major processes that shapes solid bodies in solar systems is impact. These impact events involve the interaction of complex geometries with the variety of physical processes that lead to material failure. Researchers often resort to computational approaches to understand and investigate these large-scale impact events. Traditionally, these computational approaches have used brittle failure models based on heuristic damage evolution laws such as the models by Johnson and Holmquist [1]. One way to improve these damage models is by incorporating the physical mechanisms that are active at the microscale and the microstructural information that these physical mechanisms interrogate. Paliwal and Ramesh developed a micromechanics based damage model, which accounts for the cooperative growth of a distribution of microcracks. This model provides an explicit method to incorporate microstructural information about the flaw distribution. In this work we extend the micromechanics based damage model proposed by Paliwal and Ramesh [2] for use in impact simulations involving geologic materials from the laboratory scale up to asteroid scales.

In this mechanism-based approach, we define the important physical mechanisms that are active in brittle impact events and build up a constitutive model that accounts for each of these mechanisms in a modular fashion. Some of the important physical mechanisms are: cooperative microcracking, damage growth, pressure dependent granular flow of the comminuted material, lattice plasticity, and the material equation of state. These mechanisms are coupled in a finite deformation framework and then implemented as a material model in the Uintah Computational Framework for use in Material Point Method simulations.

Each material point represents a sample volume of a parent material in the same way that each test specimen represents a sample volume from a larger parent material. This volume of material is small compared to the total volume of the simulated problem, but it may also be small compared to the distribution of flaws within the material, which then violates traditional assumptions required for a representative volume element (RVE). Each material point represents a finite sized realization of the subscale distribution; therefore, we expect each material point to be an independent realization of the parent flaw distribution. If the computational resolution is sufficiently fine that some of the larger flaws in the parent distribution can be explicitly incorporated, these flaws are modeled as penny shaped inclusions of fully damaged material. Brittle damage models such as the one described above represent a combination of many physical mechanisms, which together give rise to the complicated failure behavior of brittle

materials. To demonstrate that we are solving the equations in the constitutive model correctly, we verify each portion of the constitutive model separately. First we test the wave propagation and equation of state implementation by simulating plate impact experiments, which are one-dimensional strain. The damage evolution model, the Drucker-Prager type granular flow, and lattice plasticity are verified by looking at the stress and internal variable history of a single material point subjected to a pre-defined deformation history. Although this material model has many parameters, most of the model parameters are related to size independent quantities, which can be measured using standard experimental techniques. We use the quasi-static and dynamic strength of the material to constrain material parameters, which are not constrained by literature. Our primary validation for this material model is through a series of impact experiments that were conducted at the NASA Ames Vertical Gun Range, in which basalt cubes 10 cm on a side were impacted by spheres at velocities ranging from 1 to 4 km/s [4]. The growth of damage was recorded in real time using high speed imaging of the impact event. This validation work is ongoing and presents a thorough test of the material model and its performance in the high to hyper velocity impact regime. Since all of the size and rate effects come from the flaw distribution, we hope to extend this model to asteroid impact events using the flaw distributions proposed by Housen and Holsapple [5] while still maintaining confidence in the physics that was validated at a smaller length scale.

References:

1. Johnson, G. R. and Holmquist, T. J. *An Improved Constitutive Model for Brittle Materials.* High Pressure Science and Technology, 1993. 981-984
2. Paliwal, B. and Ramesh, K.T. *An interacting micro-crack damage model for failure of brittle materials under compression.* Journal of the Mechanics and Physics of Solids. 2008 56:3 896-923
3. Deshpande, Vikram S., Gamble, E. A. Nell, Compton, Brett G., McMeeking, Robert M., Evans, Anthony G., and Zok, Frank W. *A Constitutive Description of the Inelastic Response of Ceramics*. Journal of the American Ceramics Society, 2011. s204-s214.
4. Kimberley, J. and Ramesh, K.T. *Visualization of early stage damage propagation during hypervelocity impacts on brittle materials*, Proceedings of Hypervelocity Impact Symposium 2012.
5. Housen, R. and Holsaple, K. A., *Scale Effects in Strength-Dominated Collisions of Rocky Asteroids.* Icarus. 1999 142:1 21-33.

Missing Abstract

ID: 332

ID: 378

Numerical simulations of a multi-scale damage model using the method of averaging

Arjun Roy[1] Joseph P. Cusumano
Department of Engineering Science and Mechanics
The Pennsylvania State University
University Park, PA

We present a 1-DOF approximation of a previously developed [1] 1-D coupled-field model for damage evolution in a 1-D bar. The non-dimensionalized equations of motion for this system are

$$\ddot{u} + 2\zeta\,\omega_n \dot{u} + {\omega_n}^2\,(1-\phi)\,u = F\cos(\omega t) \tag{1a}$$

$$\dot{\phi} = \eta\,\phi\,\left[\frac{u^2}{2} - \frac{\alpha}{\phi^{1/3}}\right]^+, \tag{1b}$$

where, u is the macroscopic displacement and ϕ is a scalar variable that represents microscale damage and varies between 0 (undamaged) and 1 (completely damaged). F and ω are the forcing amplitude and frequency, respectively, ω_n is the undamaged natural frequency, ζ the damping factor, η and α are two parameters that control the average damage growth rate and the intensity of the damage growth threshold, respectively, and $b^+ = (b + |b|)/2, \forall b \in \mathbb{R}$. We assume that the source of variability observed in failure-time data is the initial unknown damage state and assume that the initial damage (ϕ_0) is uniformly distributed. We thus performed Monte-Carlo life-cycle simulations, for ensembles of initial damage states to obtain failure-time statistics. However, we found that the computational time required for such large scale simulations is enormous and have therefore developed a numerical scheme based on the method of averaging [2] that can reduce the computational time by orders of magnitude.

Since the damage grows at a rate that is much slower than the macroscopic dynamics (i.e. $0 < \eta \ll 1$) we set η to be the smallness parameter in our perturbation calculation. We also assume that this rate is sufficiently small so as to ensure that the macroscopic system always stays close to its unperturbed ($\eta = 0$) steady-state as damage evolves. In other words, we assume that $u(t) = u_{ss}(t) + \mathcal{O}(\eta)$ where $u_{ss}(t)$ is the steady-state of the macroscopic system when $\eta = 0$. For simplicity we focus on the zero-threshold case (i.e. $\alpha = 0$). We calculate $u_{ss}(t)$ and substitute it in Eq. (1b) to obtain

$$\dot{\phi} = \eta\,\phi\,\left[\frac{1}{2}F^2 A(\phi)^2 \cos^2(\omega t + \theta)\right] + \mathcal{O}(\eta^2), \tag{2}$$

where the $FA(\phi)$ and θ are the amplitude and phase, respectively, of $u_{ss}(t)$. The above equation is in the standard form for averaging: integrating the right-hand side over one forcing period and then dividing it by the forcing period yields an averaged ("slow flow") damage evolution law as

$$\dot{\phi} = \frac{1}{4}\eta F^2 \phi A(\phi)^2 + \mathcal{O}(\eta^2). \tag{3}$$

Thus we see that averaging helps us in deriving classical phenomenological power-law damage models from more general first-principle damage evolution models. The solution to Eq. (3) matches that of Eq. (1) very well as shown in Fig. 1(a).

ID: 384

Mechanical Deformation and Failure of Carbon Nanofibers with Different Functional Groups

Jun Lou
Rice University
USA

Jiangnan Zhang
USA

Abstract:
An in situ tensile testing method combining a simple microfabricated device with a quantitative Nanoindenter inside a scanning electron microscope (SEM) chamber was employed to measure individual pristine, fluorinated and amino-functionalized carbon nanofibers (CNFs). The fluorinated CNFs were found to possess higher nominal strength but with similar strain compared to the pristine and amino-functionalized CNFs. The nominal fiber strengths followed Weibull distributions with characteristic strengths between 1.94 and 2.83 GPa. The relatively small Weibull moduli indicating a broad flaw population in fluorinated and amino-functionalized CNFs are attributed to the generation of defects during functionalization. Furthermore, SEM images of fracture surfaces showed that all fibers failed in a cup-cone fracture mode. Interestingly, high resolution transmission electron microscope (HRTEM) image of fractured fluorinated fibers displayed a discrepancy in diameter of the hollow core close to the fracture site. This is thought to be caused by possible introduction of compressive stress on fiber surfaces during fluorination process. These results reveal the important effects of functionalization on mechanical properties of CNFs.

ID: 432

Peeling Adhesive Tape: A Case Study for Understanding the Effective Properties of Heterogenous Materials

Kaushik Bhattacharya
California Institute of Technology
United States

Shuman Xia
Georgia Institute of Technology
United States

Laurent Ponson
Université Pierre et Marie Curie
France

G. Ravichandran
California Institute of Technology
United States

Abstract:
While there is a good understanding of the overall behavior of heterogeneous materials concerning properties that are characterized by a variational principle, much remains unknown concerning those properties that are characterized by evolutionary processes. This talk will discuss the simple process of peeling an adhesive tape from a rigid substrate as a case study to demonstrate the complexities that can arise in this situation. Specifically, we show that that one can dramatically enhance the overall adhesive strength by patterning the elastic modulus of the tape, and induce asymmetry where the force needed to peel the membrane depends not only on the direction but also the sense of the peel. Remarkably, these modifications in peeling strength come from variations in the energy associated with bending of the tape near the peeling front which is negligible compared to the overall energy in the system. This illustrates that in evolutionary processes, perturbations with apparently negligible energy can have an anomalously large macroscopic effect. The talk will conclude with broader lessons for other phenomena including fracture, dislocations, phase boundaries and wetting fronts.

Reference:

[1] S. Xia, L. Ponson, G. Ravichandran and K. Bhattacharya, Toughening and asymmetry in peeling of heterogeneous adhesives, *Phys. Rev. Lett.* **108** 196101, 2012

ID: 476

Damage Sensing in Mechanophore-Linked, Rubber-Toughened Brittle Polymers

Asha-Dee N. Celestine
University of Illinois at Urbana-Champaign
United States

Brett A. Beiermann
University of Illinois at Urbana-Champaign
United States

Scott R. White
University of Illinois at Urbana-Champaign
United States

Abstract:

Damage sensing is a highly desirable functionality in engineering materials. The potential of using mechanophores, stress-sensitive molecules, as material stress sensors has been established by Davis and co-workers through a series of tensile and compressive tests[1]. Spiropyran, SP, is their chosen mechanophore and this molecule undergoes a ring opening reaction (activation) upon the application of mechanical stress. This activation is accompanied by a change in color and fluorescence as the colorless SP is converted to the highly colored merocyanine form. When SP is incorporated into bulk polymers, however, a significant amount of plastic deformation is required before activation is observed [1, 2]. In order to induce this plastic deformation during fracture testing of SP-linked brittle polymers such as poly(methyl methacrylate), PMMA, rubber nanoparticles can be incorporated into the matrix material. These nanoparticles facilitate the increased shear yielding necessary for SP activation during mechanical testing.

Cross-linked SP-PMMA, containing 7.5 wt% rubber nanoparticles was synthesized via a free radical polymerization. Specimens of this material were fabricated for tensile and subsequent Single Edge Notch Tension (SENT) testing. The rubber toughened SP-PMMA specimens were first tensile tested to approximately 35% strain and the activation of the SP in the gage section as a function of strain was monitored via in-situ fluorescence imaging (See Figure 1a). After tensile testing, the specimens were pre-notched and irradiated with 532 nm wavelength light to revert the colored merocyanine to the colorless spiropyran form. Specimens were then fracture tested to failure using the SENT test. The evolution of mechanophore activation was again monitored by fluorescence imaging and inspection of the specimens after testing (See Figure 1b). The fracture planes were also examined using Scanning Electron Microscopy for evidence of shear yielding and rubber particle cavitation. Control specimens in which the mechanophore was absent or tethered in positions in which no mechanochemical activation was expected were also tested and analyzed.

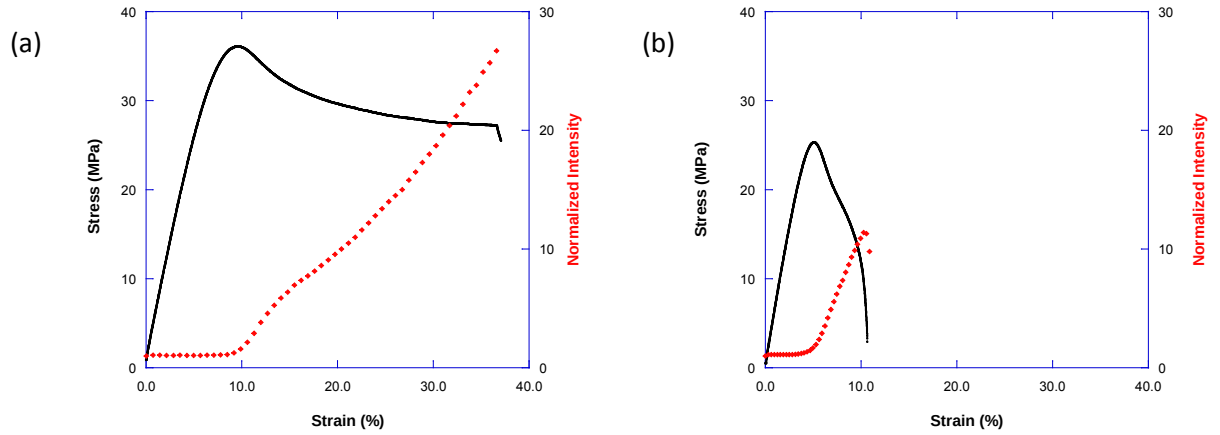

Figure 1: Stress-strain-normalized fluorescence intensity plots for rubber-toughened SP-PMMA specimen (a) Tensile test (b) SENT test

Spiropyran activation in systems in which the SP was placed within the core of the rubber nanoparticles (SP-rubber) was also investigated. SP-rubber nanoparticles were synthesized using a seeded emulsion polymerization process and incorporated into cross-linked PMMA. Specimens similar to those described above were tensile and fracture tested and the onset of activation (i.e. activation strain) of the SP was monitored. The activation strain for SP incorporated in the rubber core of these SP-rubber nanoparticles was then compared to that for SP synthesized in the rubber toughened SP-PMMA polymer.

References

1. Davis, D.A., Hamilton, A., Yang, J., Cremar, L.D., Gough, D.V., Potisek, S.L., Ong, M.T., Braun, P.V., Martínez, T.J., White, S.R., Moore, J.S. and Sottos, N.R. 2009, Force-Induced Activation of Covalent Bonds in Mechanoresponsive Polymeric Materials. *Nature.* **459**, 68-72.
2. Kingsbury, C. M., May, P. A., Davis, D. A., White, S. R., Moore, J. S., and Sottos, N.R. 2011, Shear activation of mechanophore-crosslinked polymers. *Journal of Materials Chemistry*, **21**, 8381-8388.
3. Beiermann, B. A., Davis, D. A., Kramer, S. L. B., Moore, J. S., Sottos, N. R., and White, S. R. 2011, Environmental effects on mechanochemical activation of spiropyran in linear PMMA. *Journal of Materials Chemistry*, **21**, 8443-8447.

ID: 526

Shear Band Prediction in Metallic Glasses Using Finite Element Method

Weidong Li (W. D. Li)
Department of Materials Science and Engineering, The University of Tennessee, USA

Yanfei Gao (Y. F. Gao)
Department of Materials Science and Engineering, The University of Tennessee, USA
Material Science and Technology Division, Oak Ridge National Laboratory, USA

Abstract:
The shear band pattern in bulk metallic glasses was predicted in a couple of mechanical tests using finite element method based on the free volume model and Rudnick-Rice instability theory, respectively. The free volume model defines the plastic flow in the metallic glass as viscoplasticity type, with the free volume being the order parameter controlling the structural change. In the pure shear case, the plastic strain rate is represented as

$$\frac{\partial \gamma^p}{\partial t} = 2f \exp\left(-\frac{\alpha v^*}{v_f}\right)\exp\left(-\frac{\Delta G^m}{k_B T}\right)\sinh\left(\frac{\tau\Omega}{2k_B T}\right) \quad (1)$$

The evolution of the free volume via stress-driven creation and diffusional annihilation controls the homogeneous/heterogeneous deformation of the metallic glass, and the net increase of the free volume is given by

$$\frac{\partial v_f}{\partial t} = v^* f \exp\left(-\frac{\alpha v^*}{v_f}\right)\exp\left(-\frac{\Delta G^m}{k_B T}\right)\left\{\frac{2\alpha k_B T}{v_f C_{eff}}\left(\cosh\left(\frac{\tau\Omega}{2k_B T}\right)-1\right)-\frac{1}{n_D}\right\} \quad (2)$$

Meanings of the parameters can be found elsewhere [1-3]. The plastic flow equation and free volume evolution equation were generalized into small-strian, J2-type multiaxial stress state and implemented in ABAQUS with a user-defined material subroutine.

In the Rudnick-Rice theory, the shear band is considered to be the result of bifurcation of the homogeneous elastic-plastic flow, and the shear band angle in the principal stress space is given by [4,5]

$$\theta_0 = \tan^{-1}\sqrt{\frac{\xi - N_{\min}}{N_{\max} - \xi}} \quad (3)$$

with $\xi = \frac{1}{3}(1+\upsilon)(\mu+\beta) - N(1-\upsilon)$, $N_{\max} = \frac{\sigma_I'}{\bar{\tau}}$, $N = \frac{\sigma_{II}'}{\bar{\tau}}$, $N_{\min} = \frac{\sigma_{III}'}{\bar{\tau}}$ and $\bar{\tau} = \frac{\sigma_{mises}}{\sqrt{3}}$. σ_I', σ_{II}' and σ_{III}' are principal deviatoric stresses, υ is Poisson's ratio, μ is the coefficient of internal friction and β is the dilatancy factor. Accordingly, the shear-band plane will make an angle of $\pm\theta$ with the first principal stress direction and parallel to the second principal stress direction.
Experimentally, the shear band pattern under indentation of the metallic glass can be directly observed through the bonded-interface technique. Observed shear bands on the half-symmetric plane generally consisted of radial and semicircular configurations [6]. Prediction with both the free volume model and the instability theory shows that the conical shear surface (or radial shear band) is the only shear band form in the case of directly indenting a bulk metallic glass. The bonded-interface simulation using the free volume

approach demonstrates that the shear band deviates from a regular conical shape, which is more like a spade. Subsequent loading causes the second shear band formed on the traction-free surface. This somewhat corresponds to semicircular shear bands in bonded-interface indentation experiments and predictions of the instability theory [5, 6]. The deviation of the conical shear band and emergence of the semicircular-like shear band are contributed to the stress relaxation on the bonded interface. Comparative study of the two cases reveals the conical shear band is nature for the metallic glass indentation tests, while the semicircular shear band is resulted from the stress relaxation.

In the case of nanopillar compression test, the free volume modeling was employed to investigate the tapering effect on the deformation behavior of the metallic glass. Due to stress concentration and softening nature of the metallic glass, the shear band is readily initiated at the top edge of the tapered pillar. Further strain increase forces generation and propagation of more shear bands. This leads to signification strain localization at the top portion of the pillar and is quantitatively demonstrated by a dramatic increase in the cross-sectional area at the top surface, which is also supported by TEM observations [3]. This is in sharp contrast to a Mises solid obeying the continuum plasticity, in which the plastic flow initially starts from the pillar top and extend gradually to the entire sample until a relatively homogeneous deformation reaches, without localized strain occurring eventually. In a word, given the significant localized deformation caused by the tapering, the size effect in the metallic glass investigated by compression of the FIB-machined, tapered nanopillar can not be truly reflected.

To investigate if coating can help improve ductility of bulk metallic glasses and how the coating adhesion influences this improvement, different indentations were simulated. Basically, direct indentation on the bulk metallic results in three major pairs of intersecting shear bands in the free volume modeling. By contrast, indenting on the titanium coated metallic glass to the same depth induces formation of multiple shear bands. This should attributes to two mechanisms: shear band reflection at the film/BMG interface as well as abundant shear band branching inside the sample. Both of these two mechanisms are triggered by the geometrical constraint and responsible for the enhanced plasticity in metallic glasses in practice. The results agree with predictions by Rudnick-Rice instability theory. To examine the adhesion effect, two extreme cases are simulated: indentation on the titanium coated metallic glass with perfect adhesion and the same sample with zero adhesion. Consistent with experimental observations, bad adhesion tends to bring about less shear band reflection and branching compared to good adhesion. That is because the delamination easily occurs in the former and once it happens the geometrical constraints imposed by the coating will lose its effect. As a result, only relatively less enhanced plasticity can be obtained in the poorly bonded coating/BMG system.

References

1. Spaepen F. Acta Metall 1977; 25: 407.
2. Gao YF. Modelling Simul Mater Sci Eng 2006; 14: 1329.
3. M.C. Liu, J.C. Huang*, K.W. Chen, et al. *Scripta* Mater 2012; 66: 817.
4. Rudnicki JW, Rice JR. J Mech Phys Solids 1975; 23; 371.
5. Z.N. An, W.D. Li, F.X. Liu, et al. Metallurgical and Materials Transactions A 2012; 43: 2729.
6. Xie S, George EP. Acta Mater 2008; 56: 5202.

ID: 530

Mechanical Behavior of Hierarchical Bio-Inspired Suture Joints

Erica Lin
MIT

Yaning Li

Abstract:
In nature, suture joints of varying degrees of geometric complexities are observed, with some exhibiting fractal-like patterns, or higher orders of hierarchy. The details of the mechanical behavior of different hierarchical suture joints offer insights into why evolution favored certain suture joint designs and also leads to material design principles. Here, bio-inspired prototypes of hierarchical suture joints geometries are fabricated via multi-material 3D printing (Objet Connex500). Tensile tests are performed on the samples allowing quantitative measurements of mechanical properties, including tensile strength, stiffness, and toughness. In addition, the relationship between the failure mechanisms of suture joints and its order of hierarchy is observed. The results show significant differences in mechanical properties and failure mechanisms of different hierarchical suture joints, therefore demonstrating clear advantages of certain degrees of geometric complexities and quantitative ways of designing suture joints to tailor its mechanical properties to different needs.

ID:546

Interface Mechanics of Polymers and Disordered Inorganic Materials: Case of Poly(vinyl) Alcohol and Cement Hydrate

Navid Sakhavand
Department of Civil and Environmental Engineering
Rice University

Rouzbeh Shahsavari (Rouzbeh@rice.edu)
Department of Civil and Environmental Engineering
Rice University

Abstract:

By combining plateletlike ceramic building blocks with organic matrices, nature creates hybrid materials (e.g. bone, teeth and mollusk shells) that have outstanding balance of stiffness, strength and flaw-tolerance. This has inspired fabrication of several human-made polymer-matrix composites with inorganic reinforcing materials such as glass, graphite, SiC, mica, clays and cement [7, 8, 9, 10, 11]. In these hybrid composites, the load transfer between organic and inorganic materials is a complex process that mainly traces back to the cooperative action of several weak chemical bonds (e.g. hydrogen bonds). Earlier studies have either focused on average response of such composites under shear load (e.g. [12, 13]), or have concentrated on the processes of shear transfer only between identical units such as beta-sheets in spider silks [14] where the guest and host sites are aligned in parallel. Despite the importance of the newly emerging hybrid engineered composites, there is currently no fundamental understanding (to our knowledge) on detail mechanisms of interactions at the interface domain of organic-inorganic materials where guest and host sites are arbitrarily located. Here, to address this issue, we focus on polymer-

[7] J. Rexer and E. Anderson, Composites and planar reinforcements (flakes, ribbons)—a review, Polym. Eng. Sci. 19 (1979), pp. 1–11

[8] E. R. Kleinfeld, G. S. Ferguson, Stepwise Formation of Multilayered Nanostructural Films from Macromolecular Precursors, Science (1994), 265, 370-373

[9] Z Tang, N. A. Kotov, S. Magonov, B Ozturk, Nanostructured Artificial Nacre, Nature Materials, (2003), 2, 413–418.

[10] S.C. Mojumdar, L Raki, Characterization and properties of calcium silicate hydrate polymer nanocomposites. Proceedings of The American Ceramic Society 107th Annual Meeting (2005), 1-10.

[11] J.J. Beaudoin, L. Raki, R. Alizadeh, A ^{29}Si MAS NMR study of modified C–S–H nanostructures. Cement and Concrete Composites. (2009), 31:585-90.

[12] N. V. Medhekar, A. Ramasubramaniam, R. S. Ruoff and V. B. Shenoy, Hydrogen Bond Networks in Graphene Oxide Composite Paper: Structure and Mechanical Properties, ACS Nano, (2010), 4 (4), 2300–2306

[13] O. Büyüköztürk, M.J. Buehler, D. Lau, C. Tuakta, Structural solution using molecular dynamics: Fundamentals and a case study of epoxy-silica interface, International Journal of Solids and Structures, (2011), 48, 2131-2140.

[14] S. Keten, Z. Xu, B. Ihle and M. J. Buehler, Nanoconfinement controls stiffness, strength and mechanical toughness of β-sheet crystals in silk, Nature Materials, (2010), 9, 359–367

cement nanocomposites and unravel the complex mechanisms of bonding and shear load transfer in these hybrid materials.

First, by using Molecular Dynamics (MD), potential mean force and time correlation functions, we identify several different hydrogen bonds at the interface of Poly(vinyl) Alcohol (PVA) and Calcium-Silicate-Hydrate (C-S-H), the main product of cement hydration. Next, under computational shear loading, a slip-stick motion between PVA and crystalline silicate chains of tobermorite, a crystalline analog of C-S-H, is observed, which indicate a series of simultaneous dual H-bond formation and breakage of PVA over silicate chains, which is a function of donor and host site conformations. We find the maximum cooperative H-bond strength is achieved with only two mer units of PVA, after which H-bonds strength decreases to an asymptotic level. Next, to predict H-bond strength for different substrate geometries and polymers, we systematically alter the PVA backbone as well as the Silicon tetrahedra chains in toberemorite. The latter is important to study load transfer in realistic C-S-H –PVA nanostructure with disordered features. The results show that the defects decrease the H-bond strength and lead to expanded slip-stick motion due to the removal of potential host and donor sites for H-bonds. These findings have important implications on modifying the cohesion, toughness and strength properties of polymer modified cement-based materials for industrial applications.

ID: 562

The Mechanics of Infrared Photoelastic Inspection of Mono-Crystalline Silicon Photovoltaic Wafers

Harley Johnson
University of Illinois at Urbana-Champaign
USA

Gavin Horn
USA

Abstract:
Large scale solidification processing of crystalline Si PV has become highly cost effective, but residual stress and grown-in defects continue to cause fracture and failure in Si PV wafers and pose significant challenges in the industry. Here we present a promising method for rapid characterization of stress and defects in mono-crystalline Si wafers based on infrared photoelastic (IR-PE) imaging. The method enables high resolution imaging at near infrared wavelengths for full, continuous phase information associated with through-thickness integrated shear stress values. Here we show that wafer scale IR-PE data show a positive and significant correlation with wafer curvature measurements. By mechanically loading a wafer to reduce the curvature and then post-processing the data, the IR-PE measurement is capable of resolving stress and defect distributions that more accurately represent as-grown material quality. We also show that IR-PE imaging more accurately detects crystallographic slip than industry standard photoluminescence (PL) imaging techniques. Together, these observations suggest that IR-PE inspection may enable improved detection of defects that are optically neutral or otherwise undetectable by conventional PL inspection.

ID: 572

Dynamic Failure of Single Crystal Quartz

Leslie E. Lamberson
Drexel University
United States

K.T. Ramesh
Johns Hopkins University
United States

Abstract:

Ceramic materials typically exhibit a larger compressive strength and higher specific strength than metals [1]. For these reasons, ceramics are widely used in armor and shielding applications, and consequently it is important to understand their failure response under dynamic loading conditions. Theoretical models for brittle materials and large-scale computational simulations for these applications all invoke evolving damage to explain the material performance. However, little real-time experimental data is available to provide a physical basis for these models. The difficulty in experimentally characterizing damage evolution in brittle materials under dynamic loading is due to the short times scales and wide range of length scales that must be resolved. This paper presents some of the first real-time in situ characterization of dynamically evolving massive damage in a brittle material under known transient compressive stress histories.

Dynamic uniaxial compression experiments have been conducted on single crystal x-cut α-quartz, loading along the c-axis of the crystal, using a Kolsky (Split-Hopkinson) pressure bar at strain rates of 10^3 s^{-1}. High-speed photography using a Photron SA-5 camera records the failure processes at 175,000 frames per second in the field of view perpendicular to the direction of loading. The resulting images capture the deformation and fracture behavior in the sample. The images are post-processed using a code developed in MATLAB which generates a grayscale histogram of each image based on the reflected light from the growing axial crack surfaces, and are subsequently used to determine the amount of damage in the specimen throughout the loading history.

Damage accumulation and stress as a function of time is shown in Figure 1 for all the dynamic compression experiments. Time is normalized by the peak compressive load, and the compressive stress impulse is normalized by dividing the current stress by the stress reached at the peak. While the various damage rates are not consistent across tests, the overall trend in the results show that in all cases, the region around the peak stress exhibits a significant decrease in the rate of damage accumulation than either the pre- or post-peak values.

The experimentally observed damage plateau near the peak stress could be physically interpreted as a possible rapid reduction in generation of new fracture surfaces, a rapid shutting down of certain cracks, a deceleration in crack growth, or a coalescence of existing cracks in the system. In other words, the plateau of damage accumulation could be the result of a change in the driving failure mechanism of the system. Existing analytical dynamic brittle damage models do not exhibit this plateau [2,3,4,5]. However, these models do not make a grain size distinction, and are derived for isotropic linear elastic-brittle materials; and consequently do not take into account the anisotropy of the single crystal.

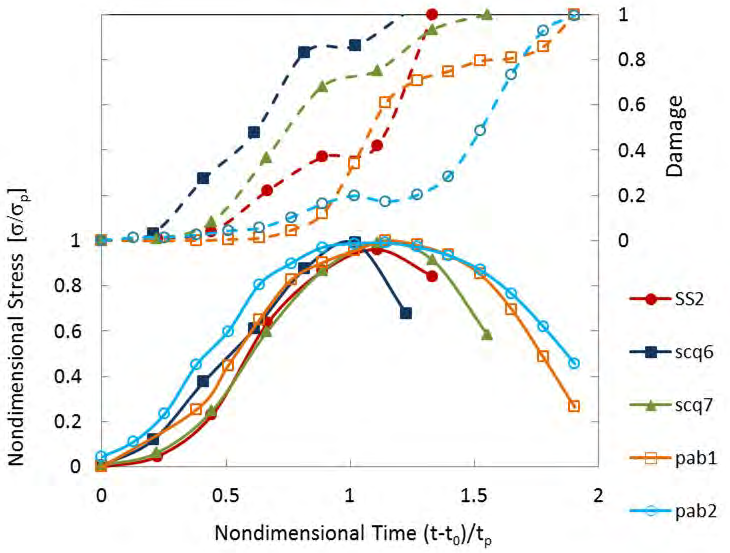

Fig. 1: Normalized stress, time and damage from dynamic compression experiments performed on single crystal x-cut α-quartz.

The quantification of damage during the dynamic compression of single crystals plays a key role in multiscale modeling used to predict the response of more complex materials under various dynamic loading conditions. Insight gained from these high strain-rate experiments on single crystals has the potential to help advance the current understanding of the role of anisotropy, grain size, or more broadly the influence of dominant length and time scales on dynamic fracture mechanisms leading to the catastrophic failure of brittle materials.

REFERENCES

[1] M. Ashby, Engineering Materials and Processes Desk Reference, Butterworth-Heinemann, 2009.
[2] S. Nemat-Nasser, H. Deng, Strain-rate effect on brittle failure in compression, Acta Metallurgica et Materialia 42 (3) (1994) 1013–1024.
[3] G. Ravichandran, G. Subhash, A micromechanical model for high strain rate behavior of ceramics, International Journal of Solids and Structures 32 (17) (1995) 2627–2646.
[4] C. Huang, G. Subhash, S. Vitton, A dynamic damage growth model for uniaxial compressive response of rock aggregates, Mechanics of materials 34 (5) (2002) 267–277.
[5] B. Paliwal, K. Ramesh, J. McCauley, Direct observation of the dynamic compressive failure of a transparent polycrystalline ceramic (AlON), Journal of the American Ceramic Society 89 (7) (2006) 2128–2133.

ID: 592

Integrated Multi-Scale Characterization and Modeling of Ductile Failure in Aluminum Alloys

Somnath Ghosh

Abstract:
Studies on ductile failure in metals and alloys, have shown that morphological variations strongly affect ductility and strain to failure due to void growth and coalescence. Multi-scale modeling provides the necessary framework for selective micro-analysis in a very limited region of a macroscopic computational domain. This paper will discuss three important ingredients of multi-scale modeling of ductile failure in heterogeneous cast aluminum alloys. These include: (i) a multi-scale characterization based preprocessor for multi-scale models; (ii) microstructural analysis module for ductile fracture; and (iii) a homogenization based continuum damage model for ductile materials that can be used in macroscopic analysis modules. For effective micro-mechanical modeling, the Voronoi Cell FEM model will account for particle fragmentation in the microstructure and ductile failure through matrix cracking.

ID: 617

An Adaptive Multiscale Approach to Study the Fracture of Heterogeneous Media

Mirmohammadreza Kabiri

Franck Vernerey

Abstract:
This presentation introduces a concurrent adaptive multiscale methodology in which both macroscopic and microscopic deformation fields strongly interact. The method is based on the balance between numerical and homogenization error; while the first type of error implies that elements should be refined in regions of high deformations, the second implies that elements size may not be smaller than a threshold determined by the size of the representative volume element. In this context, introduce a multiscale method in which RVEs can be embedded in continuum region through appropriate micro-macro boundary coupling conditions. By combining the idea of adaptive refinement with the embedded RVE method, the methodology ensures that appropriate descriptions of the material are used adequately, regardless of the severity of deformations. We show that this method, in conjunction with the extended finite element method, is ideal to study the strong interactions between a crack and the microstructure of heterogeneous media. We are particularly able to capture some important physical quantities such as the onset of crack propagation, the crack path and the energy dissipation during crack growth, all of which are key to quantify the relationship between material microstructure and macroscopic fracture toughness.

ID: 659

Macroscopic versus Microscopic Approaches to Fracture in Ductile Materials

Amine Benzerga
Texas A&M University
USA

Abstract:
The focus of this talk is on materials failing by microscalestrain localization between microscopic defects, e.g., due to void nucleation and growth. In recent years, several macroscopic approaches to the modeling of ductile fracture have been revived. Notable examples include models based on the notion of an intrinsicfracture locus as well as models based on critical stress criteria. The quantitative and qualitative predictive capabilities of such approaches are contrasted with those of micromechanical models. Both approaches are tested against a series of numerical experimentsbased on the voided cell mode. One advantage of using the cell model is that stress state effects as well as microstructure effects on failure are part of an emergent behavior and not posed constitutively. The effect of loading path on the fracture locus is first examined by means of the finite element cell model calculations. The unit cells were subjected to loading along several radial paths, characterized by constant values of stress triaxiality. The strain-to-failure was recorded for each path and the locus relating it to triaxiality was thus uniquely determined. The process was repeated for a set of non-radial loading paths. For these cases, the time-weighted average value of stress triaxiality was used to plot the fracture locus. It was found that the failure locus for nonradial loadings differs substantially from that for radial paths. The peculiar shape of the nonradial failure loci is rationalized on the basis of a model of void growth supplemented with a simple void coalescence criterion. Alternate macroscopic approaches are either incapable to capture the strong path-dependency of the so-defined fracture locusor unable to capture key qualitative trends of the fracture locus.

ID: 671

The Role of Evolving Defect Structure in Dynamic Spall Failure

Justin Wilkerson
Johns Hopkins University
United States

KT Ramesh
Johns Hopkins University
United States

Abstract:
Spall failure is a complex multiscale, multirate process. On the macroscale the process involves a period of shock compression followed by dynamic tension set up by the stress wave interactions. During the shock compression, the material undergoes a myriad of shock stress magnitude and pulse duration dependent microscopic processes that may include dislocation multiplication, nucleation, trapping, pile-up, annihilation, recovery, cell evolution, as well as vacancy generation and clustering. In addition to shock hardening the material, this new shock induced defect structure seeds the material with potential void nucleation sites that may be activated during the proceeding period of dynamic tensile loading. Upon nucleation, the voids undergo dynamic growth to coalescence, constrained by inertia and viscoplastic resistance to deformation. A multiscale predictive model is developed to analyze the role of these time-dependent processes in the experimentally observed spall strength dependence on initial microstructure, preheat temperature, tensile loading rate, and shock stress magnitude.

Effect of tensile strain rate: The figure below is a representative model prediction of the spall strength of pure aluminum as a function of the magnitude of the shock compression wave that passes through the material prior to the dynamic tension. The model prediction is shown for total tensile strain rates ranging from 1e5/s to 1e7/s. Since void growth under dynamic tension is constrained by inertia and viscoplastic resistance to deformation, the rate at which elastic strain can be relaxed through the growth of voids is limited. Thus, higher total tensile strain rates result in the accumulation of more elastic strain and higher maximum tensile stresses as shown in the figure.

Effect of shock hardening: Due to the high shear stresses induced by the shock compression, there is a dramatic increase in dislocation density, which is dependent on the magnitude of the shock stress. This increase results in hardening of the material and a subsequent increase in the spall strength, the effect of which is noticeable only at tensile strain rates less than ~1e5/s and shock stresses less than ~20 GPa. As shown in the figure below, other effects are activated at higher strain rates and shock stresses that overpower this hardening effect.

Effect of shock induced defect structure: Many metals, e.g. aluminum, form dislocation cell walls upon shock compression. These cell walls are assumed to introduce new stress concentration points in the material, which potentially may act as void nucleation sites if the

tensile stresses are high enough. Ultra high tensile strain rates (>1e7/s) result in very high maximum tensile stresses as discussed earlier. In that case, voids are nucleated not only at the initial weak void nucleation sites like grain boundaries and inclusions, but also at these new shock induced void nucleation sites. The complexity arises from the fact that the cell size decreases with increasing shock stress magnitude, thus more nucleation sites. This allows for a faster relaxation of the tensile stresses, and results in a decrease in the spall strength with increasing shock stress as shown in the figure below for the tensile strain rate of 1e7/s.

Effect of temperature: A temperature rise results from both the shock compression and to a much lesser extent the plastic work. For very high shock stress (~50 GPa) the temperature rise is so large that it results in melting upon release. At intermediate shock stresses, the effect of temperature rise is non-trivial. At low strain rates, it results in thermal softening, which decreases the spall strength. However, at the highest tensile strain rates, temperature further constrains the rate at which voids may grow due to temperature dependent dislocation drag and relativistic effects.

Where appropriate, comparisons with experiments will be discussed. Unfortunately, sorting out the particular mechanisms that effect spall strength in different regimes is difficult to accomplish through experimental observations alone; this is, however, the strength of the predictive model.

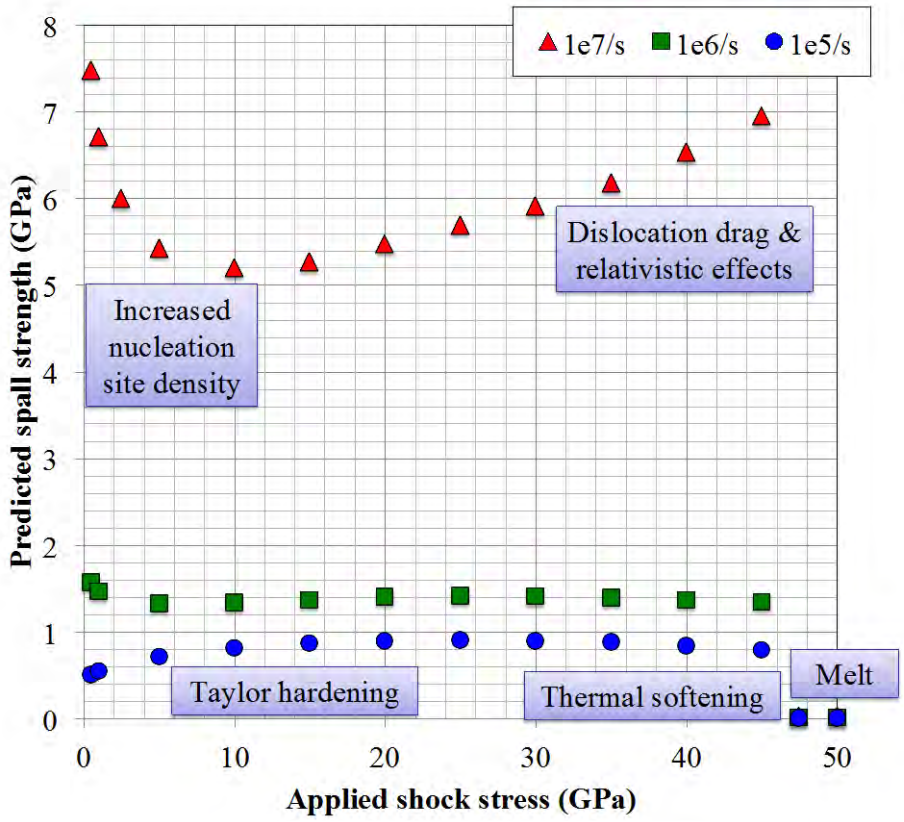

IV.11

Multiscale Mechanics of Materials - Mechanics of Thin Film and Multilayer Structures

ID: 097

Enhanced Adhesion With Pedestal-Shaped Elastomeric Stamps for Transfer Printing

Huanyu CHENG
Northwestern University

Seok Kim

Abstract:
Microscale elastomeric relief structures with 'pedestal' shapes provide enhanced operation in stamps designed for deterministic materials assembly via transfer printing. Experimental measurements of adhesion and finite element analysis both show that for certain geometries, exceptionally large enhancements in adhesion strength (over 15X) can be achieved. Transfer printing of microscale platelets of silicon and ultrathin gallium nitride light emitting diodes onto a silicon substrate without adhesive coatings demonstrates some capabilities in assembly that result from this type of stamp, of interest in diverse applications, including those that involve heterogeneous materials integration.

ID: 146

Mechanics of dynamically tunable electronic eye camera

Jianliang Xiao
University of Colorado

Yonggang Huang

Abstract:
Imaging systems that exploit arrays of photodetectors in curvilinear layouts are attractive due to their ability to match the strongly non-planar image surfaces (i.e. Petzval surfaces) that form with simple lenses, thereby creating new design options. Recent work has yielded significant progress in the realization of such

ID: 263

Path-guided Wrinkling of Nanoscale Metal Films

Rui Huang
University of Texas at Austin

Abstract:
In this study we present a new method for controlling wrinkle patterns in a gold/polystyrene (Au/PS) bilayer system. By locally modifying the mechanical properties of the gold film, we demonstrate high quality wrinkle patterns with various configurations. We directly modify the gold thin film by laser direct writing (LDW) using patterns with feature sizes much smaller than the intrinsic wrinkle wavelength to precisely control the location and shape of wrinkles, which can be lines, curves, dots, and other complex surface structures. The guided wrinkling behavior is attributed to local modification of the elastic modulus of the metal film as a result of LDW. We perform numerical simulations of wrinkling based on a composite film model and compare with experimental measurements. The effects of feature size and laser power are studied both numerically and experimentally. Finally a few potential applications using the path-guided wrinkles are demonstrated.

Missing Abstract

ID: 295

ID: 303

One-Dimensional Nanostructures for Stretchable and Flexible Electronics

Yong Zhu
North Carolina State University

Feng Xu

Abstract:
We present two classes of materials, silicon nanowires (SiNWs) and carbon nanotubes (CNTs) for stretchable/flexible devices. SiNW coils were fabricated on elastomeric substrates by a controlled buckling process. Two buckling modes (the in-plane wavy mode and the three-dimensional coiled mode) were found; a transition between them was achieved by controlling the surface treatment of the elastomeric substrates. The NW coils exhibited very large stretch ability up to the failure strain of the substrate (100%). Such a large stretch ability relies on the effectiveness of the coil shape in mitigating the maximum local strain, with a mechanics that is similar to the motion of a coil spring. In addition to the wavy shape, the coil shape represents an effective architecture in accommodating large tension, compression, bending, and twist. We have fabricated CNT-based stretchable conductors using two approaches: one is the well-known prestrain-then-buckling and the other is a newly-developed interface-medicated buckling. More specifically, in the second approach, the building blocks (e.g., CNTs) are transfer printed onto an unstrained elastomeric substrate. Upon stretching the substrate the building blocks slide on the substrate, but upon releasing the substrate the building blocks buckle (instead of sliding back). The CNT-based conductors exhibit superior stretch ability (100%).

Missing Abstract

ID: 327

ID: 380

Wrinkled Organic Crystals: Determining the Elastic Constants of Highly Ordered Rubrene

Marcos A. Reyes-Martinez
Polymer Science & Engineering,
University of Massachusetts Amherst
United States

Prof. Ashwin Ramasubramaniam
Mechanical & Industrial Engineering,
University of Massachusetts Amherst
United States

Prof. Alejandro L. Briseno
Polymer Science & Engineering,
University of Massachusetts Amherst
United States

Prof. Alfred J. Crosby
Polymer Science & Engineering,
University of Massachusetts Amherst
United States

Abstract:
Organic single crystals (OSCs) hold promise for a new generation of high-performance organic electronic devices. Exceptional charge-transport properties[1] and the advent of large-area patterning techniques[2,3] make OSCs excellent candidates for flexible electronics. However, in order to effectively employ OSCs on mechanically flexible architectures, their mechanical properties need to be understood and characterized. In this presentation, the mechanical properties of rubrene single crystals are investigated.[4] The buckling instability is chosen as a metrology tool for the in-plane elastic constants due to the limited dimensions of as-grown crystals and the associated handling difficulty. Ultra-thin crystals (200nm-1μm) suitable for wrinkling experiments are grown using the physical vapor transport method.[5] Two techniques are introduced to induce one-dimensional wrinkling in crystals laminated to poly(dimethylsiloxane) (PDMS) substrates.[4] The wrinkles generated are periodic and reversible. Our results demonstrate a dependence of wrinkling wavelength on crystallographic direction resembling the well-known anisotropic electrical properties of rubrene. Figure 1a and 1b show optical micrographs portraying one crystal as it wrinkles along the [010] and [001] directions, respectively. Differences in wrinkling wavelengths that are not evident in the optical micrographs were revealed during careful analysis of the wrinkle profiles. According to wrinkling mechanics, the observed discrepancies in wrinkle wavelengths suggest differences in the elastic constants along

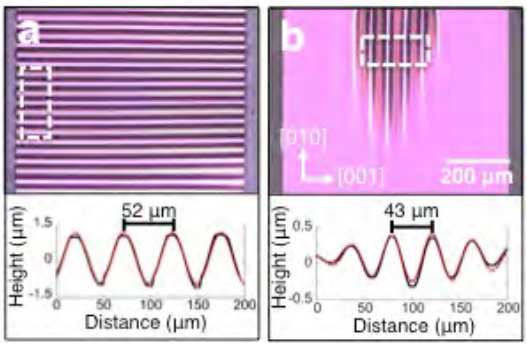

Figure 1. Anisotropic wrinkling in rubrene single crystals.[4] (a) Optical micrograph and height profile of wrinkles propagating along the [010] direction. (b) Optical micrograph and height profile of wrinkles propagating along the [001] direction of the same crystal in (a).

distinct crystallographic directions.[6] To obtain the nine elastic constants corresponding to orthorhombic rubrene, intermolecular interactions were simulated using the empirical Adaptive Intermolecular Reactive Bond Order (AIREBO) potential.[7] The in-plane elastic constants are computed to be $\overline{C}_{22} = 17.77 \pm 1.85$ GPa, $\overline{C}_{33} = 13.01 \pm 2.44$ GPa, and $\overline{C}_{23} = 10.66 \pm 1.43$ GPa.[4] The in-plane elastic constants are also determined experimentally using the measured wrinkle wavelengths of crystals of different thicknesses and the knowledge of the plane-strain modulus of the substrate. The elastic constants of the crystal along the [010] and [001] are found to be $\overline{C}_{22} = 14.89 \pm 0.73$ GPa and $\overline{C}_{33} = 9.89 \pm 0.60$ GPa, respectively.[4] These results show reasonable agreement with the calculated values from atomistic simulations. We demonstrate that due to the in-plane anisotropy of the crystal, the buckling wavelengths will change as a function of load direction as shown in Figure 2a. Figure 2b plots the normalized change in wavelength as $\overline{C}'_{22}(\theta)/\overline{C}_{22} = \left[\lambda(\theta)/\lambda_2\right]^3$. Theoretical predictions do not capture the trend of the experimental data. A peak value for $\overline{C}'_{22}$ is measured at approximately thirty degrees with respect to the axis of preferred crystallization ([010]). Interestingly, thirty degrees correspond to the pitch angle in the crystal structure of orthorhombic rubrene. This observation has significance in developing a thorough understanding of the inter-molecular potential that governs mechanical and electrical properties for rubrene. Our results are the first contribution bringing quantitative details into the correlation between the crystal structure and the mechanical properties of rubrene.

[1] M. E. Gershenson, V. Podzorov, A. F. Morpurgo, Rev. Mod. Phys. **2006**, 78, 973.

[2] A. L. Briseno, S. C. B. Mannsfeld, M. M. Ling, S. Liu, R. J. Tseng, C. Reese, M. E. Roberts, Y. Yang, F. Wudl, and Z. Bao, Nature **2006,** 444, 913.

[3] H. Minemawari, T. Yamada, H. Matsui, J. Tsutsumi, S. Haas, R. Chiba, R. Kumai, T. Hasegawa, Nature **2011**, 475, 364.

[4] M. A. Reyes-Martinez, A. Ramasubramaniam, Alejandro L. Briseno, Alfred J. Crosby, *Adv. Mater*. **2012**, In Press.

[5] R. A. Laudise, Ch. Kloc, P. G. Simpkins, T. Siegrist, J. Cryst. Growth **1998**, 187, 449.

[6] E. Cerda, L. Mahadevan, Phys. Rev. Lett. **2003**, 90, 074302.

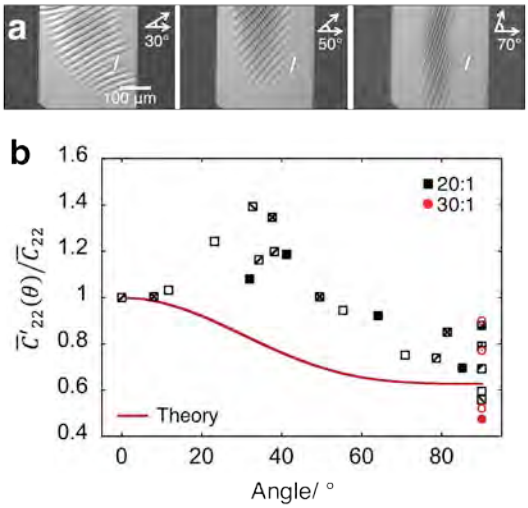

Figure 2. (a) Optical micrographs of a wrinkled crystal at different load angles with respect to [010] direction. (b) Angular dependence of $\overline{C}'_{22}$ normalized by $\overline{C}_{22}$. Marker shape indicates different PDMS preparation. Marker shade/fill pattern indicates different crystal sample.[4]

[7] S. Stuart, A. Tutein, J. A. Harrison, J. Chem. Phys. **2000**, 112, 6472.

ID: 501

Thermo-Mechanical Responses of Small Volume Metals on the Fast Transient Process

George Voyiadjis

ID: 685

EXPERIMENTAL AND NUMERICAL INVESTIGATION OF NONLINEAR STATIC BEHAVIOUR OF A LAMINATED COMPOSITE PLATE SUBJECTED TO UNIFORM PRESSURE LOAD

K. GÜNDOĞAN
Istanbul Technical University, Aeronautics and Astronautics Faculty
Turkey

D. BALKAN, M.SÜER
Istanbul Technical University, Aeronautics and Astronautics Faculty
Turkey

Z. MECİTOĞLU
Istanbul Technical University, Aeronautics and Astronautics Faculty
Turkey

Abstract:

Thin-walled structures, particularly thin plates and shells, are come up in many major of technology, such as mechanical, marine, chemical, civil, aeronautical and astronautical engineering. Such a widespread use of plate and shell structures arises from their fundamental properties. When it is suitably designed, even very thin plates can support large loads and pressures. Thus, they are utilized in structures such as aerospace vehicles in which light weight is essential and composite materials are widely used (Venstel,2001). There are several papers on the large deflection behavior of the laminated composite plates (Chia, 1988).

This paper is also concerned with experimental and numerical investigation of a laminated composite plate subjected to uniform pressure load. If a weighted residual method with multi-term displacement functions is applied to obtain approximate solution to the problem, a tremendous number of integrations should be performed. Therefore, the limited number of approximation functions is used in the approximate solution to reduce the solution efforts and the selection of approximation functions is the crucial to obtain reliable results. The approximate solution methods give the much more accurate results for displacement variations on the plate than the strain or stress variations, since the strains are composed of some derivatives of displacements. The experiments show that the shape of normal displacement depends on the level of large deflection. The deflected mid-surface becomes flatter while the deflection becomes larger. In order to include this deflection behavior, the approximation functions for the displacements are chosen by:

$$u^0 = \sum_{m=1}^{M}\sum_{n=1}^{N} U_{mn}\, 2\sin\left(\frac{2m\pi x}{a}\right)\sin\left(\frac{n\pi y}{b}\right)^2, \qquad v^0 = \sum_{m=1}^{M}\sum_{n=1}^{N} V_{mn}\, 2\sin\left(\frac{m\pi x}{a}\right)^2\sin\left(\frac{2n\pi y}{b}\right)$$

$$w^0 = \sum_{m=1}^{M}\sum_{n=1}^{N} W_{mn}\left(1+\frac{km^2(a-2x)^2(a+am-2mx)^2(a-am+2mx)^2}{a^6}+\cos\left[\frac{m\pi(a-2x)}{a}\right]\right)$$

$$\left(1+\frac{km^2(b-2y)^2(b+bm-2my)^2(b-bm+2my)^2}{b^6}+\cos\left[\frac{n\pi(b-2y)}{b}\right]\right)$$

In this equation k is a parameter which is chosen according to the flatness of the deflected mid-plane. u^0, v^0 and w^0 are the displacement components in the Cartesian axes directions, x, y, and z, respectively. a and b is the plate dimensions. In the approximate solution M and N is taken as unity.

In this study, the equations of motion are derived by the use of the virtual work principle in the frame of the von Kármán large deflection theory of thin plates. It is assumed that the plate is clamped at all edges. One term approximation functions are defined for the in-plane displacements and two terms function is selected for the out-of-plane deflection. The form of out-of-plane displacement is determined by considering the experimental result of the deflection. The approximate displacement functions are substituted into the equations of motion and then the Galerkin Method is used to obtain the nonlinear algebraic governing equations. The equations are solved by the use of MATHEMATICA software. Furthermore, the plate under the uniform pressure is solved using MSC NASTRAN finite element software. The plate is modeled by using 400 shell elements.

In the experimental side of study, a laminated carbon/epoxy plate is produced by the wet-hand layup method and cured in a heated vacuum table, Figure 1. The dimensions of plate are 300 mm x 300 mm. The plate has four layers with a thickness of 0.332 mm. Therefore, the plate thickness is 1.328 mm. In the experimental study, VIC3D digital image correlation device was used to obtain deformation behavior of the plate under various pressure loads. Sand bags are used to apply the pressure loads.

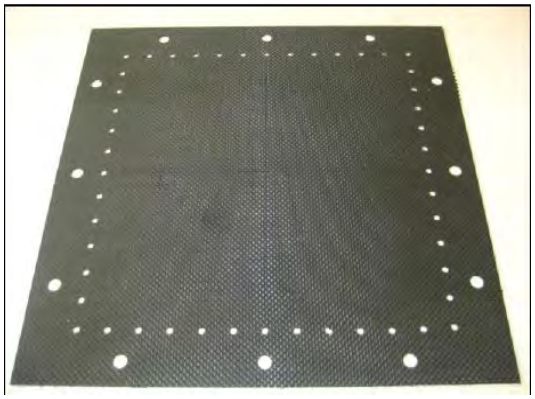

Figure 1. Carbon/epoxy plate.

The mechanical properties of carbon/epoxy are obtained by tensile tests. The material properties are given in Table 1.

Table 1. Material properties of the carbon/epoxy.

E_{11}	GPa	Modulus of Elasticity in the direction of 1	45.5

E_{22}	GPa	Modulus of Elasticity in the direction of 2	45.5
G_{12}	GPa	Shear Modulus	2.70
ν_{12}	-	Poisson Ratio	0.195
ρ	kg/m^3	Material Density	1340

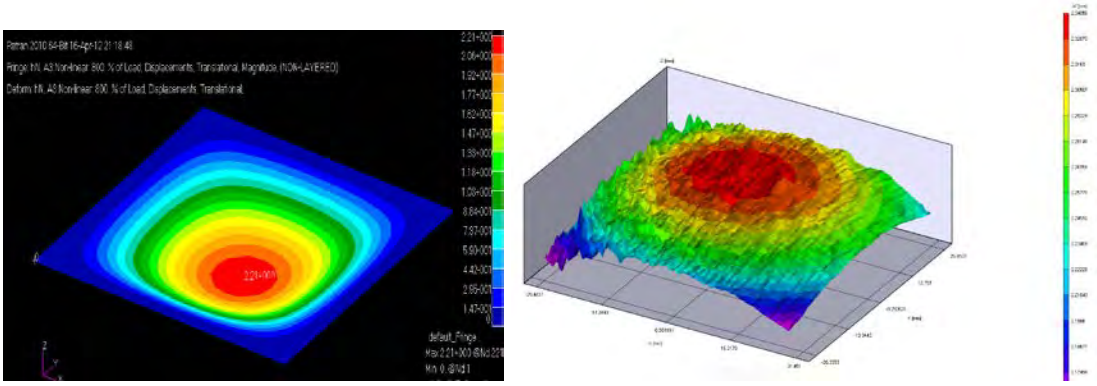

Figure 2. Deflected plates under pressure load.

Finite element (FE), approximate and experimental results are compared for different uniform pressure loads as given in Table 2. A good agreement is found for the maximum deflection of the plate under the magnitude of uniform pressure load.

Table 2. Comparison of approximate, finite element and experimental deflection result.

Pressure (Pa)	FE Results (mm)		Experimantal Results (mm)	Approximate Results (mm)	Differences (%)		
	Nonlinear	Linear			FE-Expt	FE-Aprx	Aprx-Expt
555	0.65	0.74	-	0.69	-	5.67	-
1111	1.08	1.49	1.19	1.12	10.19	3.70	5.88
1667	1.37	2.23	1.49	1.40	8.76	2.19	6.04
2222	1.60	2.97	1.57	1.63	1.88	1.87	3.82
2778	1.79	3.72	1.91	1.82	6.70	1.68	4.71
3333	1.95	4.46	2.01	1.98	3.08	1.54	1.49
3889	2.09	5.20	2.19	2.12	4.78	1.44	3.20
4444	2.21	5.95	2.34	2.25	5.88	1.81	3.85
5000	2.32	6.69	2.44	2.36	5.17	1.72	3.28
5556	2.43	7.43	2.57	2.45	5.76	0.82	4.67

Keywords: Laminated Composite Plate, Geometric Nonlinearity, Galerkin's Method.

References:

Chia, CH-Y., (1988), *Geometrically Nonlinear Behavior of Composite Plates,* Appl. Mech. Rev., Vol. 41, pp. 439–450.

Eduard Venstel, T. K. (2001). *Thin Plates and Shells.* Marcel Dekker Inc. New York.

Vic-3D Digital Image Correlation Software, LIMESS Messtechnik und Software GmbH.

NASTRAN 2010.1 User Manuel, MSC Software Inc.

Missing Abstract

ID: 694

ID: 712

Necking Limit of Polymer-Supported Metal Films under Biaxial Loading

Teng Li

Zheng Jia

Abstract:

Thin metal films deposited on polymer substrates are often used as conductors and interconnects in flexible electronics. Unlike conventional electronic devices, flexible devices are often subject to large deformation (stretches, bending and twists). The mechanical failure of the polymer-supported metal conductors under large deformation poses significant challenge to the functional reliability of flexible electronics. Existing theoretical studies often assume plane strain condition of the deformation of these polymer-supported metal conductors. In reality, however, flexible devices are often subject to large and complicated deformation. For example, the electronic sensitive skins covering the elbow of a robot experience large bi-axial stretches. To decipher the failure mechanisms of polymer-supported metal conductors under arbitrary in-plane loading conditions (i.e., different ratios of tensile strains in two in-plane directions), we determine the critical tensile strain above which necking sets in the metal conductors. We consider two representative material combinations, namely, thin metal conductors on stiff plastic substrates, and thin metal conductors on compliant elastomer substrates. Also emerging from the analysis is the orientation of the necking respect to the tensile loading directions. The results quantitatively correlate the critical necking limit strain as well as the necking orientation with the mechanical properties and the thickness of the metal conductor and the polymer/elastomer substrate. These results offer understandings on the deformability of polymer-supported metal conductors in flexible electronics; therefore shed light on optimizing the material selection and structural design of deformable metal conductors to achieve better mechanical reliability of flexible electronics.

Missing Abstract

ID: 726

Missing Abstract

ID: 779

IV.12

Multiscale Mechanics of Materials - Multiscale Phonon Modeling

ID: 110

Phonon Analysis of Carbon Nanotubes Using Objective Structures Framework

Amin Aghaei
Carnegie Mellon University
United States

Kaushik Dayal
Carnegie Mellon University
United States

Ryan S. Elliott
University of Minnesota
United States

Abstract:
We introduce a method to find the normal modes of vibration of symmetric but non-crystalline nanostructures such as nanotubes. Our method is based on the Objective Structures framework and exploits the symmetries of the structure. In analogy to the standard phonon analysis where the equations are diagonalized by a Fourier transform, we introduce an intermediate transform that enables us to then use the standard Fourier transform. This provides large computational savings by enabling the use of a 2-atom unit cell to describe the nanotube. More importantly, this description in terms of symmetry provides important insights into instabilities in carbon nanotube structure, and in particular analogs to structural phase transformations in crystals.

1. Symmetry-adapted Phonon Analysis:

Phonons, i.e. normal modes, are extremely important to understand the properties of crystals. For instance, phonon analysis provides insight into thermodynamic properties and mechanical stability. In this work, we use the framework of Objective Structures (OS) to extend the notion of phonon analysis to noncrystalline but highly-symmetric nanostructures.

Consider a structure with N unit cells and M atoms within each cell. M is finite but N can be infinity. The position of the atom k inside cell $\mathbf{i} = (i_1, i_2)$ is $\mathbf{x}_{(i_1,i_2),k}$. In a nanotube with axis $\mathbf{e}$ and centered at the origin, atoms of the cell $\mathbf{i}$ are related to the atoms of the unit cell $\mathbf{0}$ by $\mathbf{x}_{(i_1,i_2),k} = \mathbf{Q}_1^{i_1}\mathbf{Q}_2^{i_2}\mathbf{x}_{(0_1 0),k} + i_1\mathbf{c}_1$ where $\mathbf{Q}_1$ and $\mathbf{Q}_2$ are orthogonal matrices with axis of rotation coinciding with $\mathbf{e}$ and $\mathbf{c}_1 \| \mathbf{e}$ and define $\mathbf{Q}_\mathbf{i} = \mathbf{Q}_1^{i_1}\mathbf{Q}_2^{i_2}$. The normal modes of vibration are the solutions of the eigenvalue equation

$$\omega^2 \mathbf{M}\mathbf{u} = \mathbf{H}\mathbf{u} \tag{1}$$

where $\mathbf{H}$ is $3MN \times 3MN$ Hessian matrix with components $\mathbf{H}_{(\mathbf{i},k)(\mathbf{j},l)} = \partial^2\varphi / \partial\mathbf{x}_{(\mathbf{i},k)}\partial\mathbf{x}_{(\mathbf{j},l)}$, φ is the inter-atomic potential energy function depending on the atomic positions, $\mathbf{M}$ is $3MN \times 3MN$ diagonal mass matrix and $\mathbf{u}$ and ω^2 are the eigen-solutions of eqn. (1) (ω is the frequency of the mode corresponding to $\mathbf{u}$). Since N is a large quantity (typically infinity), it is hard (impossible) to brute-force diagonalize the Hessian matrix. In order to diagonalize $\mathbf{H}$ we introduce a linear transformation $\mathbf{u}_{\mathbf{i},k} = \mathbf{Q}_\mathbf{i}\mathbf{v}_{\mathbf{i},k}$. Substituting this transformation into eqn. (1) results in

$$\omega^2 \mathbf{M}\mathbf{v} = \mathbf{D}\mathbf{v} \quad (2)$$

where $\mathbf{D}_{(\mathbf{i},k)(\mathbf{j},l)} = \mathbf{Q}_{\mathbf{i}}^T \mathbf{H}_{(\mathbf{i},k)(\mathbf{j},l)} \mathbf{Q}_{\mathbf{j}}$. Now $\mathbf{D}$ is block-circulant, i.e. $\mathbf{D}_{(\mathbf{i},k)(\mathbf{j},l)} = \mathbf{D}_{(\mathbf{0},k)(\mathbf{j}-\mathbf{i},l)}$, and we can use Fourier transform to diagonalize it. After using Fourier transform eqn. (2) turns into

$$\omega^2 \mathbf{M}\tilde{\mathbf{v}} = \tilde{\mathbf{D}}\tilde{\mathbf{v}} \quad (3)$$

Now $\tilde{\mathbf{D}}$ is block-diagonal with N blocks each of the size $3M \times 3M$. The eigenvalues of each block can be calculated with much less computational effort than the eigenvalues of $\mathbf{H}$. In other words, instead of finding the eigenvalues of a $3MN \times 3MN$ matrix, the eigenvalues of $3M \times 3M$ matrices are calculated N times.

2. Numerical Examples:

To show the power of symmetry-adapted phonon analysis method we plot the dispersion curves of (7,6) carbon nanotube and compare it to the results of the conventional phonon analysis. Figure 1a shows the dispersion curves of (7,6) nanotube. To solve the eigenvalue problem and find the curves the unit cell, which needs to be periodic, should consist of at-least 508 atoms. Therefor for each wave vector the eigenvalues of a 1324×1324 matirx should be found which is computationally expensive. For example on single CPU we spent around 33 minutes to get the full phonon spectra. Furthermore as can been seen from fig. 1a it is hard to distinguish between different modes and the computed information is extremely complex and difficult to analyze.

In contrast the unit cell needs only 2 atoms in order to be able to use our symmetry-adapted method. Fig. 1b shows the phonon spectra of the same nanotube by using our method. We should note that both curves carry the same amount of information. But we spent less than 0.1 seconds on the same CPU to get the full phonon spectra which is around 400 times faster than the conventional method. Moreover the computed information is easier to analyze.

We should note that (7,6) tube is just an example to show the power of our method. For other nanotubes much more atoms may be needed to find a translational cell. Besides for twisted nanotube one may not find a translational cell and therefore conventional phonon analysis cannot be used. But our symmetry-adapted based method is capable of computing the full phonon spectra with only two atoms for all single-walled nanotubes.

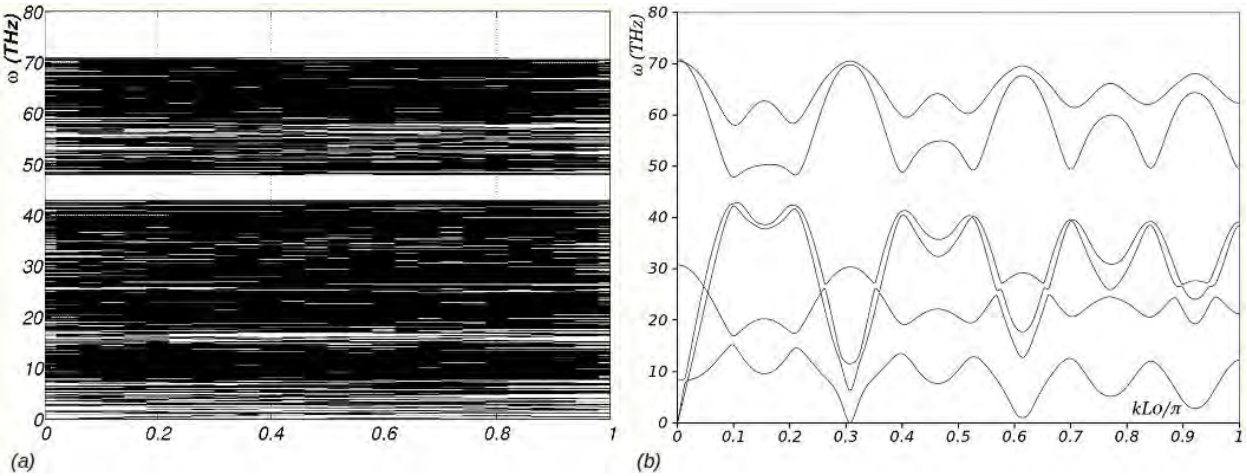

Figure 15. The dispersion curves of (7,6) carbon nanotube. (a) Using conventional phonon analysis (b) Using symmetry-adapted phonon analysis.

ID: 454

Concurrent Atomistic-Continuum Simulation of Phonon Transport in Silicon

Liming Xiong

This work presents a new concurrent atomistic-continuum (CAC) methodology and its applications in simulating phonon transport in silicon. The method combines an atomistic field theory (AFT) and its finite element implementations using rhombohedra-shaped elements to mimic the primitive cell of materials with diamond crystal structures in silicon. Since the atomic information has been naturally built in the governing equations of AFT, with large number of degree of freedom being reduced and the interatomic potentials being the only constitutive rules, the CAC method is shown to be feasible in modeling and simulating both acoustic and optic phonon transport without losing the atomistic features. Complex phenomenon such as phonon wave packets with the well-defined frequency and polarization scattering at the nanoszied pores has been directly observed. We find that the phonon transmission coefficients across the defective Si nanowires are dependent on the size, shape, and the distributions of the nanopores in the defective silicon crystals. All of the CAC simulation results are shown to be comparable with that from full molecular dynamics (MD) simulations. The potential applications of the CAC method and its limitations are also discussed.

ID: 624

Hot Phonon Influence on the Scattering Rates of Carbon Nanotubes for Power Electronics Applications

Pierre Gautreau

Cemal Basaran

Abstract:

Graphene is a one atom thick planar sheet of carbon atoms connected to each other with sp2 bonds. It is often described as an atomic scale chicken wire structure, or honeycomb crystal lattice. Graphene is the building block of many nanostructures. It can be folded into a tube, thus creating carbon nanotubes, or it can also be stacked to form graphite. These structures have attracted a lot of attention over the past few years, due to their potential applications in Mechanical, Structural, and Electrical Engineering. Carbon based nanoelectronics is a strong candidate to replace conventional metal oxide electronic devices. CNTs and graphene do not exhibit failure mechanisms such as thermo-migration and electro-migration as compared to metals. However, the nano-scale of CNTs makes experimentation difficult. Therefore, computational simulations can be used to study and analyze effects and behaviors of CNTs under various Electrical or mechanical loadings. The goal of this analysis is to study the thermal and electrical properties of CNTs using a quantum mechanics formulation integrated in an Ensemble Monte Carlo simulation. In most CNT simulation, phonons and their interaction with other particles, such as electrons or additional phonons, are included. However, phonon interactions and energy distribution are often described as an equilibrium process. In this study, we incorporate hot phonons (out of equilibrium phonons) into the simulation of CNTs, in order to study its influence on the scattering rates of CNTs.

ID: 633

Title: Spatial filters for coupling finite elements and molecular dynamics at finite temperatures.

Abstract: The main motivation of this work is to reduce the computational expenses of Molecular Dynamics (MD) simulations. MD has been successfully used in the modeling of material behavior. However, it is still constrained to small system sizes and to small time scales. Therefore, one often requires concurrent multiscale approaches using MD, in small regions of interest, coupled with a coarse-grained continuum representation such as Finite Elements (FE), thereby reducing the computational costs.

During the last few years, research towards multiscale approaches has been applied to study mechanics problems such as crack propagation/nucleation and crystal plasticity. Different multiscale methods have been developed such as the Quasi Continuum method [1], the Coupled atomistic and discrete dislocation method [2], the Bridging Scale method [3] and the Bridging Domain method [4]. In the case of dynamic simulations, one of the major problem with coupling strategies is the spurious wave reflections occurring across the coupling interface. A large body of work exists to minimize these reflections at low temperatures. But to the best of our knowledge very few approaches [5,6,7] are available at finite temperatures. The objective of this presentation is thus to introduce a method to couple finite elements and molecular dynamics at finite temperatures using spatial filters.

The approach is based on the Generalized Langevin Equation (GLE) [8] applied on an atomic region. The basic idea of using GLE is to separate the total energy into low and high frequency components which is done as follows. The dynamics of atoms in the GLE region are solved according to newton's equation including two additional terms: one frictional and one random force. The frictional term includes a memory kernel convoluted with the atomic velocities in the coupled region. This acts as an energy decomposer thereby distinguishing the low and high frequency components. One can decide a cut off frequency based on the dispersion relations of the material under study and also based on the size of continuum mesh elements. We used a numerical high frequency pass filter as the memory kernel. The filter is applied in space on the atomic velocities to filter the high frequency components [9]. The removed energy is then applied as the thermal boundary conditions to the continuum interface in the overlap-region. Finally, we conclude by presenting some 3D numerical test cases to demonstrate the effectiveness of our strategy ensuring a reflection-less wave transmission across the MD-FE interface and discuss the future directions for the application of this method.

References:

1. R. E. Miller and E. B. Tadmor, "The Quasicontinuum Method: Overview, applications and current directions", *Journal of Computer-Aided Materials Design* 9, no. 3, 2002.

2. W. A. Curtin and R. E. Miller, "Atomistic/continuum coupling in computational materials science", *Modelling and Simulation in Materials Science and Engineering* 11, no. 3, 2003.

3. G. J. Wagner and W. K. Liu, "Coupling of atomistic and continuum simulations using a bridging scale decomposition", *Journal of Computational Physics* 190, no. 1 September 1, 2003.

4. S. P. Xiao and T. Belytschko, "A bridging domain method for coupling continua with molecular dynamics", *Computer Methods in Applied Mechanics and Engineering* 193, no. 17-20 May 7, 2004.

5. G. J. Wagner, R. E. Jones, J. A. Templeton and M. L. Parks, "An atomistic-to-continuum coupling method for heat transfer in solids", *Computer Methods in Applied Mechanics and Engineering*, 2008.

6. Y. Kulkarni, J. Knap and M. Ortiz, "A variational approach to coarse graining of equilibrium and non-equilibrium atomistic description at finite temperature", *Journal of Mechanics and Physics of Solids*,56(4) :1417–1449, 2008.

7. N. Mathew, R. C. Picu and M. Bloomfield, "Concurrent coupling of atomistic and continuum models at finite temperature", *Computer Methods in Applied Mechanics and Engineering*, 2011.

8. S. A. Adelman, "Generalized Langevin equation approach for atom/solid-surface scattering: General formulation for classical scattering off harmonic solids", *The Journal of Chemical Physics* 64, no. 6 (1976): 2375.

9. S. B. Ramisetti, G. Anciaux and J. F. Molinari, "Spatial filters for bridging molecular dynamics with finite elements at finite temperatures" *submitted to Computer Methods in Applied Mechanics and Engineering*.

ID: 718

Continuum-Atomistic Modeling of Phonon Dispersion in Carbon Nanotubes

Michael Leamy
Georgia Institute of Technology
USA

Abstract:
Dispersion calculations are presented for cylindrical carbon nanotubes using a manifold-based continuum-atomistic finite element formulation combined with Bloch analysis. The formulated finite elements allow any (n,m) chiral nanotube, or mixed tubes formed by periodically-repeating heterojunctions, to be examined quickly and accurately using only three input parameters (radius, chiral angle, and unit cell length) and a trivial structured mesh, thus avoiding the tedious geometry generation and energy minimization tasks associated with ab initio and lattice dynamics-based techniques. A critical assessment of the technique is pursued to determine the validity range of the resulting dispersion calculations, and to identify any dispersion anomalies. Two small anomalies in the dispersion curves are documented, which can be easily identified and therefore rectified. They include difficulty in achieving a zero energy point for the acoustic twisting phonon, and a branch veering in nanotubes with nonzero chiral angle. The twisting mode quickly restores its correct group velocity as wave number increases, while the branch veering is associated with a rapid exchange of eigenvectors at the veering point, which also lessens its impact. By taking into account the two noted anomalies, accurate predictions of acoustic and low-frequency optical branches can be achieved out to the midpoint of the first Brillouin zone.

IV.13

Multiscale Mechanics of Materials - Coarse-Grained Atomistic and Concurrent Atom-Cont Methods for Critical Mater Behav

ID: 120

Statistical Mechanical Foundation of the Peridynamic Nonlocal Continuum Theory: Energy and Momentum Conservation Laws

Rich Lehoucq
Sandia National Laboratories

Abstract:
My presentation reviews the derivation the energy and momentum conservation laws of the peridynamicnonlocal continuum theory using the principles of classical statistical mechanics. The peridynamic laws allowthe consideration of discontinuous motion, or deformation, by relying on integral operators. These operators' sumforces and power expenditures separated by a finite distance and so represent nonlocal interaction. The integraloperators replace the differential divergence operators conventionally used, thereby obviating special treatmentat points of discontinuity. The derivation presented employs a general multibody interatomic potential, avoidingthe standard assumption of a pairwise decomposition. The integral operators are also expressed in terms of astress tensor and heat flux vector under the assumption that these fields are differentiable, demonstrating that the classical continuum energy and momentum conservation laws are consequences of the more general peridynamiclaws. An important conclusion is that nonlocal interaction is intrinsic to continuum conservation laws whenderived using the principles of statistical mechanics.

ID: 277

Calculations of Isothermal Elastic Constants Using the Phase-Field Crystal Method

Nirand Pisutha-Arnond
University of Michigan
USA

Victor Chan

Abstract:
The phase-field crystal method is an emerging coarse-grained atomistic model that can be used to predict material properties. In this work, we explore the methods for calculating the isothermal cubic elastic constants and bulk modulus using the phase-field crystal (PFC) method. We identify that the conventional procedure for calculating cubic elastic constants, which is to quasi-statically deform a system with a constant number density (CND), yields elastic constants that are inconsistent with those defined from the standard definition, which is obtained from quasi-statically deforming a system with a constant number of particle (CNP). The results show that the CND and CNP processes yield significantly different values of elastic constants, which indicates that the two processes cannot be used interchangeably. In addition, we use a thermodynamic formulation to obtain relationships between the CNP and CND elastic constants. Furthermore, we show that, while applied previously with the PFC method, a quasi-static deformation process with a constant-volume constraint does not result in the standard bulk modulus. Finally, we propose a procedure that would yield a bulk modulus that is consistent with the standard definition.

ID: 371

The Transferability of Interatomic Potentials and the Knowledgebase of Interatomic Models (openKIM.org)

Ellad Tadmor
University of Minnesota
USA

Daniel Karls
USA

Abstract:
Atomistic and multiscale simulations in materials science play a key role in realistic scientific and industrial applications. These approaches frequently use empirical interatomic models (potentials or force fields) to represent the response of the material. Modern models are fitted to reproduce electronic structure and/or experimental results for a dataset of representative atomic configurations. However, no standardized approach currently exists for quantifying the range of applicability of an interatomic model referred to as its "transferability". This makes it difficult or even impossible to select an appropriate model for a given application. In addition, a lack of standardization in programming interfaces for models and the lack of a systematic infrastructure for archiving them makes it difficult to use interatomic models for new applications and to reproduce published results. This talk will describe a current NSF-CDI funded effort to create an open source online tool that addresses these limitations: the Open Knowledgebase of Interatomic Models (http://openKIM.org). OpenKIM will allow users to compare model predictions with reference data, to generate new predictions by uploading simulation test codes, and to download models conforming to application programming interface (API) standards which are being developed in collaboration with atomistic simulation community. The data accumulating in the openKIM repository is being used to study the transferability of interatomic models.

ID: 399

Efficient Multigrid Methods for Molecular Mechanics Models

Jingrun Chen
University of California, Santa Barbara
United States

Carlos J. Garcia-Cervera
University of California, Santa Barbara
United States

Abstract
Molecular mechanics is a common approach to modeling the behavior of matter, where atoms are treated as the essential degrees of freedom and a potential function is used to describe the interactive effects between atoms. Equilibrium structures can be computed by minimizing the potential energy with respect to the position of the atoms. Extensive applications of molecular mechanics modeling can be found in materials science, chemistry and biology.

Among these, one important application is to extract the mechanical properties of materials under various conditions. The corresponding molecular mechanics model is called lattice statics. It is well-known that the equilibrium configuration is usually a local minimizer of the potential energy. A method for searching local minima is employed, such as nonlinear conjugate-gradient methods and Newton-type methods, to relax and then find the equilibrium configuration. Typically there are only finite neighbor interactions between atoms at the atomistic level. Thus, one relaxation step only has local impact on the atomic configuration. Consider an atomic system with N atoms. If a collective deformation exists in the system, then at least O(N) relaxation steps are required to find the equilibrium configuration. Since one relaxation step costs O(N), the scaling of conventional relaxation strategies is O(N^2).

There are many efforts to reduce the computational cost based on efficient classical numerical techniques, like multigrid method and domain decomposition method. The present work is focused on applying the idea of multigrid method for lattice statics and reducing the computational cost. Brandt [1] highlighted many possible applications of the multigrid method, including lattice statics. Goedecker et al. [2] employed the linear elasticity as the coarse-grid operator in the two-grid method. The efficiency of the method is tested by the silicon crystals with some point defects. A more general approach was proposed by Chen and Ming [3]. They used the one-way multigrid, which can automatically bypass many unphysical local minimizers. The coarse-grid operator was constructed by the Cauchy-Born rule. For homogeneous deformation, such as tension, compression and shear, the optimal cost O(N) was observed. For nanoindentation, however, this approach cost a lot.

The failure of the approach proposed in [3] is that the Cauchy-Born elasticity model is not a good model at coarse levels in nanoindentation when dislocations nucleate and move. To successfully make the multigrid method work in this case, we propose a new coarse-grid model,

the quasi-atomistic model. In the quasi-atomistic description, kinematically, we choose rep-atoms to reduce degree of freedoms and reconstruct loci of other atoms through interpolation. Energetically, we propose the following way to construct the system energy: 1) positions of atoms are obtained by the interpolation of deformations of rep-atoms; 2) site energy of each atom is calculated individually; 3) the system energy is computed by summing up site energies of atoms.

The quasi-atomistic model is used as the coarse-grid operators in multigrid methods. The full approximation scheme (FAS) and the full multigrid (FMG) method are used since they have been proven to work efficiently for nonlinear problems arising from partial differential equations. There are three main features of FAS-FMG method: 1) a hierarchy of shape functions is employed to represent displacement (increment) function at different levels, and then construct the system energy and force, which can replace continuum models used in existing multigrid approaches; 2) the multilevel structure can effectively bypass many local minima, which makes the proposed methodologies robust; 3) these two methods can be applied to not only solids, but also polymers, biological systems in principle. Consider a system of N atoms. From 1), the computational complexity at each level is O(N) and number of levels is O(logN). From 2), only O(1) relaxation steps are required to find the equilibrium configuration. In total, the computational complexity of these two methods is O(NlogN). Above properties are illustrated by different examples.

[1] A. Brandt, *Multigrid methods in lattice field computations*, Nuclear Physics B (Proc. Suppl.) **26** (1992), 137–180.

[2] S. Goedecker, F. Lanc¸on, and T. Deutsch, *Linear scaling relaxation of the atomic positions in nanostructures*, Phys. Rev. B **64** (2001), 161102.

[3] J. Chen and P.B. Ming, *An efficient multigrid method for molecular mechanics modeling in atomic solids*, Commun. Comput. Phys. **10** (2011), 70–89.

ID: 534

Positive-Definiteness of the Blended Force-Based Quasicontinuum Method

Mitchell Luskin
University of Minnesota

Xingjie Li

Abstract:
The development of consistent and stable quasicontinuum models for multi-dimensional crystalline solids remains a challenge. For example, proving stability of the force-based quasicontinuum (QCF) model remains an open problem. In 1D and 2D, we show that by blending atomistic and Cauchy--Born continuum forces (instead of a sharp transition as in the QCF method) one obtains positive-definite blended force-based quasicontinuum models if and only if the width of the blending region scales as O(epsilon^{-1/5}) atomic lattice spacing's (or the blending width is O(epsilon^{4/5}) in the macroscopic scale).We present computational results and analysis.

ID: 537

Reformulation of Energy Equation for Passing Defects and Heat from the Atomistic to the Continuum Region

Youping Chen
University of Florida

Liming Xiong

Abstract:

This work presents a formulation of a field representation of classical atomic-level N-body dynamics and a recast of the governing equations in a form that facilitates the passage of dislocations and heat from the atomistic region to the continuum region. The non-equilibrium statistical mechanics principles as well as mathematic derivations will be introduced. Simple numerical examples will be presented to demonstrate the formulation. The new formulation will enable concurrent atomic and continuum simulation of materials within a single theoretical framework. Application of the formulated field theory in modeling and simulation of dislocation, phase transformation, fracture and failure in crystalline materials will be presented. Potential applications in understanding and predication of thermoelectric materials will be discussed.

ID: 634

Coarse-graining Molecular Dynamics Using an Extended Galerkin Method

Xiantao Li
The Pennsylvania State University
USA

Abstract:
We consider molecular dynamics (MD) model as a microscopic description of mechanical properties of a solid system. It is written as a Hamiltonian system for the position and momentum of the atoms. Many complicated material processes can in principle be understood at the atomic level using MD. However, a realist system often consists of a huge number of atoms, and the computation is too large for numerical simulations.
This talk will present a method to reduce the dimension, i.e., the number of atomic degrees of freedom, associated with the MD model. The method is motivated by traditional Galerkin projection for linear and nonlinear wave equations. Then we generalize this approach by introducing a set of auxiliary variables to extend the approximation to a larger subspace. The latter approach is similar to moment closure methods for kinetic equations. In addition to the numerical methods, we will present some error analysis along with some numerical experiments on the simulation of material defects.

ID: 699

Blending Schemes for Concurrent Coupling of Local and Nonlocal Continuum Models in Multiscale Solid Mechanics

Pablo Seleson

Samir Beneddine

Abstract:
Multiscale modeling in materials science has been recognized in recent years as an important research field critical to achieving feasible and accurate descriptions of the behavior of many complex systems. In this work, we present a novel methodology to derive blending schemes to concurrently couple local and nonlocal continuum models obtained from a single reference framework based upon the peridynamics theory of solid mechanics. Peridynamics is a generalization of classical continuum mechanics based upon differences of the displacement field and not on its derivatives; as a consequence, the theory has been used for the study of material failure. A consistent force-based blended model that couples peridynamics and classical elasticity is presented using nonlocal weights composed of integrals of blending functions. This approach finds particularly useful applications in fracture mechanics where the peridynamics theory can be used to describe regions where fracture is expected, whereas classical elasticity could be efficiently used elsewhere; insights for atomistic-to-continuum coupling are discussed. Numerical experiments demonstrating the accuracy and efficiency of the blended model are presented as well as numerical studies of the error sensitivity on different model and problem parameters. We also generalize this approach to the coupling of peridynamics and higher-order gradient models of any order.

IV.14

Multiscale Mechanics of Materials - Mechanics of Crystalline Nanostructures

ID: 184

Chemical Effects in Nanocrystalline Alloys: Strength and Resistance to Mixing

Pascal Bellon
University of Illinois at Urbana-Champaign
USA

Robert Averback
USA

Abstract:
We will review our recent work on chemical effects in nanocrystalline materials. The first part will focus on the use of solute doping of grain boundaries to stabilize nanocrystalline alloys and to achieve strength that would not be possible by grain refinement only. Model Cu-base alloys will be considered and investigated to illustrate this approach, by combining molecular dynamics simulations and experiments. In the second part, we will focus on the resistance of nanograined and nanolaminate alloys to mixing forced by severe plastic deformation (SPD) in Cu-base alloy systems comprised of immiscible elements. Molecular dynamics simulations reveal the importance of the nature of interfaces, coherent v. incoherent, and the heat of mixing. Orientation relationship is shown to play an important role in designing nanolaminates that are resistant to SPD. Experiments on nanolaminates subjected to high pressure torsion testing will be presented to illustrate the high resistance to mixing in the Cu-Nb system.

ID: 256

Dislocation Emission in Small volumes

William Gerberich
University of Minnesota
USA

Abstract:
For nanocrystalline solids as well as single crystal nanopillars or nanoparticles, dislocation emission becomes extremely important. In silicon, we have been exploring this using in situ TEM and atomistic simulations. It appears there is an emission criteria mediated by both stress concentrations, and dislocation-induced back stresses. Based on contact stresses in single crystalline nanospheres and the activation energy for double-kink nucleation, it is concluded that dislocations are athermally nucleated at very high stresses (~ 5 GPa) in silicon at room temperature. Additionally, the strain at which these nucleate is in reasonable agreement with the atomistic simulations of Izumi and Yip (~ 0.05).

ID: 353

Size-Dependent Nonlinear Elasticity in Pd Nanowhiskers

L. C. Chen

G. Richter

J. P. Sullivan

D. S. Gianola

The deviation of Young's modulus (E) from its bulk value in metal nanowires has been attributed to effects arising from both the miscoordinated surface and the bulk-like core. The former pertains to the increasing influence of surface stiffness arising from the atomic miscoordination, leading to size-dependent variations in stiffness; the latter effect relates to nonlinear elastic behavior of the nanowire core, a result of surface stresses that are balanced by large core stresses in small volumes. To evaluate the surface and core contributions to nanoscale elasticity, we have performed tensile tests on a MEMS-based platform of single-crystalline, nominally defect-free Pd nanowhiskers. Our results reveal not only size-dependence in E in the low-strain limit but also clear deviations from linear elasticity at strains above approximately 1%. By quantifying the nonlinearity in the uniaxial stress-strain relation, we gain further insight on the mechanisms that govern elastic behavior in metal nanostructures.

ID: 416

Simulated Isosurfaces of Inelastic Strain and Dissipation in Nanocrystalline Cu

First Author
Shreevant Tiwari
School of Materials Science and Engineering,
Georgia Institute of Technology, USA

Second Author
Garritt J. Tucker
Sandia National Laboratories,
Albuquerque,NM 87185–1411 USA

Third Author
David L. McDowell
G.W. Woodruff School of Mechanical Engineering,
School of Materials Science and Engineering,
Georgia Institute of Technology, USA

Abstract:
Plasticity of metals in the nanocrystalline (NC) grain size regime involves the activation of both intergranular and intragranular deformation mechanisms. Therefore, predicting the multiaxial yield and flow behavior of NC metals based on classical plasticity theories is presumptuous, since classical theories are based on dislocation glide as dictated by Schmid's law. In NC metals, a variety of non-Schmid effects occur, e.g. frictional sliding of interfaces and interface mediated dislocation nucleation. At higher length scales, these effects can lead to phenomena such as asymmetry in yielding and non-normality of flow, both of which are critical to the design of constitutive theories of plasticity at the nanoscale.

We have performed isothermal molecular dynamics simulations to explicitly compute the yield and flow surfaces for a NC Cu ensemble. As shown in Figure 1, the ensemble is an orthogonal domain, consisting of 100 grains of average grain size 5nm. Biaxial deformation was performed at 10 K by proportionally ramping the normal stress on two pairs of opposite faces of the domain (principal stresses σ_{xx}, σ_{yy}), while fixing $\sigma_{zz} = 0$.

Two different threshold criteria were used to determine the yield point: (a) a threshold on the inelastic strain, obtained by unloading from a loaded state to a stress-free state, and (b), a threshold on dissipation, which was obtained by tracking the activity of a thermostat coupled to the atomic dynamics. To determine a threshold in (a), the inelastic strain tensor was reduced to a scalar effective value ($\bar{\varepsilon}^{\text{in}}$) using the von Mises definition (based on the 2$^{\text{nd}}$ invariant of the deviatoric part of the inelastic strain tensor). In (b), the dissipation was estimated through the activity of a Nose-Hoover thermostat (η) as follows: under plastic deformation, mobile defect structures release strain energy, thereby causing a temperature rise. The thermostat compensates

for the temperature rise by withdrawing microkinetic energy from the system. The compensation rate ($\dot{\eta}$) is therefore a measure of dissipation in the system.

The surfaces obtained through each criterion are shown in Figure 2. Both surfaces exhibit tension-compression asymmetry under uniaxial loading. However, the shapes of these surfaces are perceptibly different, most prominently under biaxial tension. These findings improve our understanding of the effect of hydrostatic stress on both the kinematics and the kinetics of multiaxial plastic deformation, resolving features accessible only through full-resolution simulations. The present work can provide valuable input towards developing a microstructure-sensitive constitutive theory of plasticity in nanocrystalline metals.

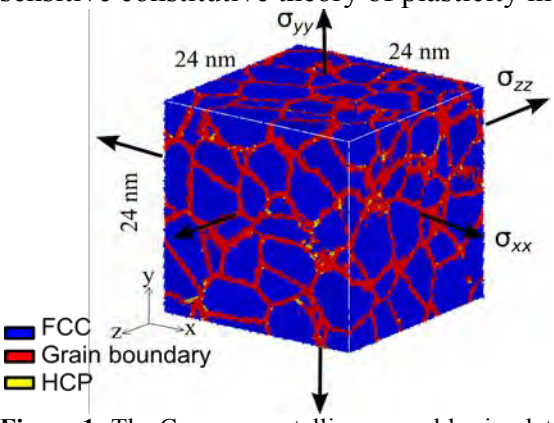

Figure 1: The Cu nanocrystalline ensemble simulated in this work, along with details of the loading scheme.

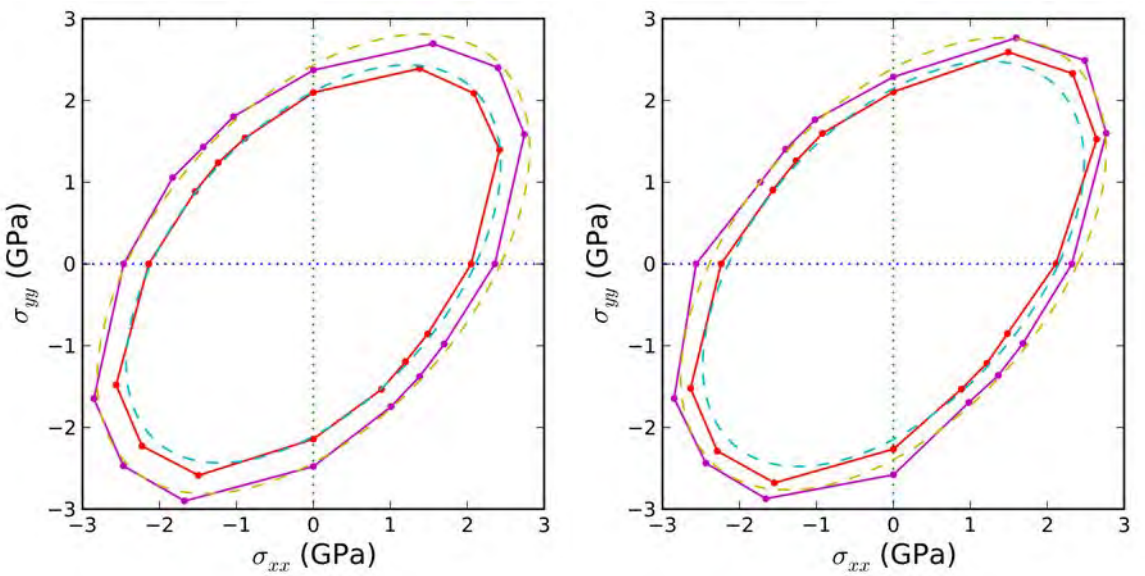

Figure 2: Isosurfaces of (a) constant effective inelastic strain ($\overline{\varepsilon}^{\text{in}}$) and (b), constant dissipation ($\dot{\eta}$). As an aid to the eye, von Mises ellipses have been drawn (dashed curves) to conform to the yield point under pure shear.

ID: 460

Novel Strain-Hardening Mechanisms in Metallic Nanowires

Sankar Narayanan
Georgia Institute of Technology
USA

Abstract:
Recent experiments of metallic nanowires reveal novel deformation mechanisms that contribute to the strain hardening of the nanowires. Our molecular dynamics (MD) simulations provide thorough insights into the atomistic mechanisms operative in the nanoscale regime. Nano-sized stacking fault tetrahedra (SFT) were observed in the sub-20nm face-centered-cubic Au nanowires in an in situ HRTEM study. The MD simulations indicate that the SFTs did not nucleate from vacancy platelets, the mechanism typically operative in the bulk metal, but were instead formed from a series of deformation-induced events in which surface-nucleated partial dislocations interacted to form the SFT in the nanowire bulk. Due to the lock formation, such deformation-induced SFT contributes substantially to the strain hardening of the Au nanowire. In addition, a different mechanism contributing to strain-hardening was found in five-fold twinned Ag-nanowires and is also explored in this work. In this case, the strain hardening arises due to the presence of vertical internal twin boundaries. Our MD simulations reveal the detailed mechanisms of strain hardening by the partial dislocation-twin boundary interactions. Understanding of the aforementioned strain-hardening mechanisms provides valuable knowledge base towards designing ultra-strength materials.

Missing Abstract

ID: 477

ID: 488

Modeling the Atomic Processes of Deformation at Realistic Timescales

Derek Warner
Cornell University
USA

Linh Nguyen

Abstract:
NO ABSTRACT

ID: 496

Understanding Peculiar Deformation Traits in Nanocrystalline Metals

Peter Anderson
The Ohio State University

Lin Li

Abstract:
Nanocrystalline metals display unusual mechanical deformation traits compared to coarse grained counterparts. The macroscopic stress-strain traits include large values of flow strength, elastic-to-plastic transition strain, and hysteric response during unloading/reloading. More recently, x-ray diffraction studies have revealed that nanocrystalline metals have peculiar changes in residual stress following plastic deformation. Metals with conventional grain size show stress redistribution between soft and hard grain families, right at the onset of plastic deformation. But in nanocrystalline metals, the stress redistribution between families can be suppressed and even nonexistent for small (1%) plastic strain. The residual stress in nanocrystalline metals can even decrease following plastic deformation. These unusual traits are studied using the concept of Quantized Crystal Plasticity. Specifically, the plastic strain magnitude in nanograins jumps by large (~1%) values associated with discrete slip events. Each event is associated with unstable propagation of a dislocation loop across a grain, triggered by the depinning of the loop from remnant grain boundary structure. Thus, individual grains must seek out quantized (discrete) plastic states with which to satisfy compatibility and equilibrium. This leads to violent, intergranular stress redistribution during plastic deformation and multigrain plastic instabilities. Finite element simulations with quantized crystal plasticity suggest that the unusual nanocrystalline traits stem from a wide grain to grain distribution in critical stress to activate a slip event and the ability to store large internal stress on a grain-to-grain scale. This creates a wide distribution in flow strength at the grain scale that can supersede normal Schmid factor effects and generate large sensitivity to prior plastic straining. The presentation will conclude with implications for material design and texture development in nanocrystalline metals.

ID: 557

Nonlinear Elastic Behavior of Two-Dimensional Molybdenum Disulfide

Jeffrey Kysar
Columbia University
USA

Changgu Lee
USA

Abstract:

This research explores the nonlinear elastic properties of two-dimensional molybdenum disulfide. We calculate the nonlinear elastic properties of two-dimensional MoS2 with first-principles density functional theory calculations. The nonlinear elastic properties are used to predict the behavior of suspended monolayer MoS2 subjected to a spherical indenter load at finite strains in a multiple length scale finite element analysis model. The model is validated experimentally by loading suspended MoS2 membranes with an atomic force microscope. We find that the Young's modulus and intrinsic strength of monolayer MoS2 is 130 N/m and 16.5 N/m, respectively. The results approach Griffith's predicted intrinsic strength limit of E/9, where E is the modulus. This study reveals the predictive power of first-principles density functional theory, in the derivation of nonlinear elastic properties of two-dimensional MoS2.

ID: 626

Detwinning Mechanisms for Growth Twins in Epitaxial Nanotwinned Cu

Nan Li

Abstract:
Using in situ nanoindentation in a transmission electron microscope (TEM), we have studied the migration mechanisms of Σ3 {112} incoherent twin boundary (ITB) in epitaxial nanotwinned Cu films. ITB migrate via the collective glide of multiple twinning dislocations that form an ITB and the propagation steps or disconnections are with heights of three or multiples of three {111} interplanar distances. The migration may lead to de-twinning process of nanotwins in face-centered cubic metals. The transmission of a glide dislocation across an ITB is shown to form a sessile dislocation in the ITB and locally pin the boundary at the site of the slip transmission.

ID: 651

Plastic Activity in Nanoscratch Molecular Dynamics Simulations of Pure Aluminium

Till Junge
Ecole Polytechnique Fédérale de Lausanne (EPFL),
Doctoral School of Mechanics (EDME),
Computational Solid Mechanics Laboratory (LSMS),
Switzerland

Jean-François Molinari
Ecole Polytechnique Fédérale de Lausanne (EPFL),
School of Engineering (STI),
Materials Science Institute (IMX),
Computational Solid Mechanics Laboratory (LSMS),
Switzerland

Abstract:
Aiming at a better understanding of the atomic origins of friction in crystalline metals, a simple friction case - single-asperity nano-scale scratching of aluminium - is simulated in molecular dynamics (MD). MD and atomistic models in general suffer from strong length- and time-scale limitations and one needs to be very careful to avoid the creation of non-physical phenomena due to too small simulation boxes and too high rates. In order to investigate how the simulation size (substrate thickness and scratching depth) and rate (scratching speed) influence the resulting friction mechanisms, a large parametric study has been performed in which substrate thickness, indentation depth and scratch speed have each been varied for more than an order of magnitude. The general set-up of the simulations can be seen in Figure 1. Both single-crystal and nano-crystalline substrates have been considered. The rigid spherical indenter has a radius of 23 Å, which is about an order of magnitude smaller than a typical atom force microscope probe tip.

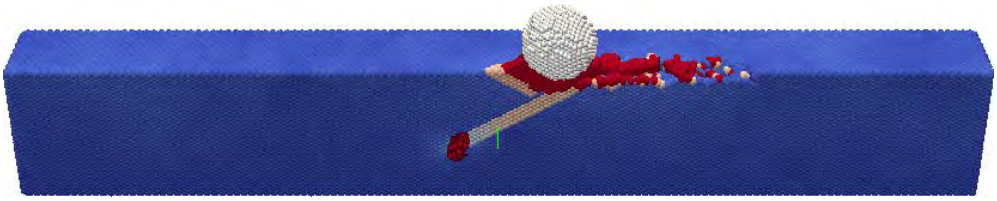

Figure 1: Snapshot during simulation: white atoms belong to the rigid indenter, the red atoms in the centre surround a dislocation loop. Only half of the simulated domain is shown in order to make the plastic deformation in the bulk under the indenter and in the groove behind the indenter visible.

A regression-based method to compute the friction coefficient μ based on measurements extracted from the simulation is presented as well as a statistically motivated criterion to determine whether differences in friction coefficients are statistically significant. Furthermore, a clean way to separate the scratching work into heat production Q and variation of stored plastic energy E_{pl} using molecular dynamics combined with molecular statics is derived. Figure 2 shows a comparison between dislocation activity and the evolution of E_{pl}. The excellent fit between the

evolutions of these two quantities indicates that E_{pl} is indeed a good measure for the energy stored in plastic zones.

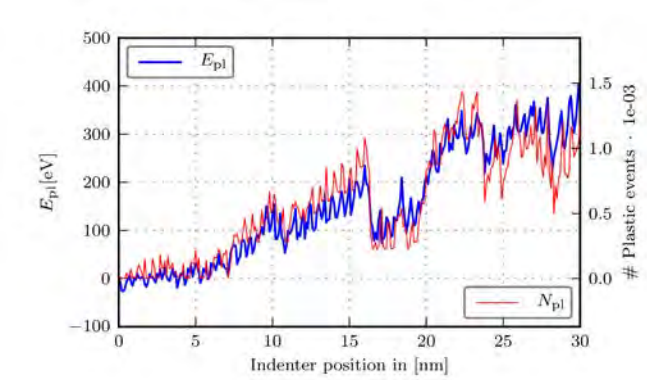

Figure 2: Comparison between plastic energy E_{pl} and plastic count N_{pl}. Both plots share the abscissa. The values of E_{pl} (heavy line) are to be read on the left ordinate, the ones of N_{pl} (light line) on the right ordinate. The good agreement between the two curves suggests that E_{pl} is a good measure for the energy stored in plastic zones.

We demonstrate that in order to understand how the simulation parameters influence the results, it is not sufficient to analyse the sensitivity of μ, because both Q and E_{pl} remain size and rate dependent even in size and rate ranges in which μ appears to have stabilised.

When comparing single-crystal and nano-crystalline substrates, the evolution of E_{pl} reveals fundamentally different friction mechanisms for these two cases. While the single crystal substrates always accumulate plastic energy during scratching, the nano-crystalline substrates actually *release* energy during scratching by relaxing and recrystallising their micro-structure near the surface.

We observe that both Q and E_{pl} are rate dependent over the entire range of scratch speeds considered in this study. However, while the amount of heat Q generated over one scratch increases with increasing scratch speed, E_{pl} shows the opposite trend. Over the range of investigated substrate thicknesses, Q becomes size independent for the larger substrates, but the plastic energy remains size sensitive. This indicates that the plastic zones are not resolved, even for the relatively small scratch case covered in this parametric study.

The research described in this talk is supported by the European Research Council (ERCstg UFO-240332).

ID: 666

First-principle Study of the Size Effects on the Mechanical properties of Multilayer Graphene Nanoribbons

Alireza Tabarraei
University of North Carolina at Charlotte
USA

Abstract:
Quasi-one-dimensional graphene nanoribbons (GNRs), produced by lithographically patterning of two dimensional graphene [1], have recently emerged as a new material. Graphene nanoribbons display a wide variety of band gaps that can be tuned by changing the nanoribbon width and edge crystallographic type. This important feature opens up the opportunity of designing GNR-based nanodevices and circuits. Understanding mechanical properties of graphene nanoribbons (GNRs) is crucial in the reliable engineering design of such nanodevices. Atomistic computational techniques have been used in the past to study size effects on the mechanical properties of monolayer GNRs. However, the results reported by different studies are not consistent. Some researchers report increasing Young's modulus and mechanical strength by reducing GNRs characteristic size [2], while others report an opposite trend [3, 4]. The source of discrepancies between different studies can be attributed to the use of different empirical potentials and methodoligies in the atomistic computations. To address this issue and to minimize the empiricism effects in our simulations, we will employ first-principle-based simulations using density functional theory (DFT) to study size effects on the mechanical properties of multilayer GNRs. The DFT results predict a strong size effect on the modulus of the graphene nanoribbons.

[1] M. Han, B. Ozyilmaz, Y. Zhang, and P. Kim. Energy band-gap engineering of graphene nanoribbons. Physical Review Letters, 98:206805, 2008. [2] C. Reddy, A. Ramasubramaniam, V. Shenoy, and Y. Zhang. Edge elastic properties of defectfree single-layer graphene sheets. Applied Physics Letters, 94:101904, 2008. [3] H. Bua, Y. Chena, M. Zou, H. Yia, K. Bia, and Z. Nia. Atomistic simulations of mechanical properties of graphene nanoribbons. Physics Letters A, 373:3359-3362, 2009. [4] H. Zhao, K. Min, and N. Aluru. Size and chirality dependent elastic properties of graphene nanoribbons under uniaxial tension. Nano Letters, 9:3012-3015, 2009.

ID: 681

Studies in Material Instability under Extreme Loading

T.W. Wright
Johns Hopkins University
USA

Abstract:
Although much is known both experimentally and theoretically about material stability under high pressure, far less is known about the effect of large shear stress superimposed on high pressure. Stress has six independent components, so study of the effects of pressure alone leaves the other five dimensions unexplored. Without some a priori idea of the effect of an arbitrary strain increment it would be a daunting task to explore the full six dimensional stress or strain space for instability boundaries. Knowledge of the crystal structure and requirements regarding theoretical constitutive representations suggests that systematic study of just one additional dimension at a time in stress space could be a valuable guide for exploring material stability under extreme loading conditions. These ideas will be illustrated in the context of a program designed to explore the effect of shear on amorphization in B4C, a ceramic often used for ballistic protection.

Rivlin and Ericksen (1955) presented the first fully general constitutive representation for isotropic elastic materials. Since then work towards achieving general forms for elastic anisotropic representations has been pursued by many authors, see extensive references in Xiao (1997) for a summary of work up till that time. Most of the work has taken a group theoretic approach, and it has been shown that the minimal number of tensor generators is six for a representation of any anisotropic elastic material, Xiao (1996). Xiao also gave many candidate tensor generators for the various crystal classes in his 1996 and 1997 papers. Some sets are minimal, but none appears to lead to linear elasticity in a natural way at small strain. Xiao also has showed how material symmetry requires that a minimal set of generators must lose rank in special circumstances appropriate for the various types of symmetry.

Work on a new approach to linear elasticity began in the 1990s followed by a review of their approach in Cowin and Mehrabadi (1995). The basic idea was to use a slightly modified form of the well-known Voigt 6x6 matrix of elastic moduli to find the eigenvalues and eigentensors that may be used to span the 6-dimensional space of symmetric second order tensors in Euclidean 3-space. Wright (2011) found that the eigenvalues and eigentensors partitioned the 6-space into several subspaces (of one, two, or three dimensions) that are invariant under the group transformations for a material of any symmetry. Therefore, the eigentensors provide an ideal framework for constructing minimal nonlinear constitutve representations for materials of any symmetry.

With the framework provided by linear elasticity and with the many form invariant tensors and the required reductions in rank provided by Xiao, it has been possible to piece together minimal nonlinear representations for most crystal classes, cubic symmetry being one of the classes yet to be properly represented. All completed representations are minimal, fully nonlinear, and provide

the required reductions in rank, but no others. Furthermore, they all reduce smoothly to linear elasticity at small strains.

Given a suitable constitutive representation, it becomes possible to begin theoretical exploration of stability questions involving shear stresses, as well as pressure. It has also been found that if the question of incremental stability is posed with stresses and strains referred to an unstressed reference configuration rather than to the current configuration, then it is easily recognized that stability occurs if the second derivative of energy (internal or free energy) with respect to strain, evaluated at the current strain, is positive definite for small strain increments. The choice of internal energy or Helmholtz free energy would seem to be a question of quasi-static or dynamic conditions. These and other questions and future prospects will be surveyed.

References:

Cowin, S.C. and Mehrabadi, M.M. (1995). Anisotropic symmetries of linear elasticity. Appl. Mech. Rev. **48**, 247-285.

Rivlin, R.S., Ericksen, J.L. (1955). Stress-deformation relations for isotropic materials. J. Rat. Mech. Anal. **4,** 323-425.

Wright, T.W. (2011). Bootstrap elasticity: From linear to nonlinear constitutive representations. J. Elast. DOI 10.1007/s10659-011-9367-9.

Xiao, H. (1996). On minimal representations for constitutive equations of anisotropic elastic materials. J. Elast. **45**, 13-32.

Xiao, H. (1997). On constitutive equations of Cauchy elastic solids: All kinds of crystals and quasicrystals. J. Elast. **48**, 241-283.

ID: 696

Mechanical Behavior of Nanoporous Copper

Antonia Antoniou
Georgia Institute of Technology
USA

Ran Liu
Georgia Institute of Technology
USA

Abstract:
Nanoporous (NP) metal foams are characterized by extremely high surface-to-volume ratios andpossess such desirable properties of metals as high electrical conductivity, catalytic activity, andstrength. These materials have shown great promise in many applications, for example aselectrodes in fuel cells, batteries, supercapacitors and key actuating components in microelectronic-mechanical (MEMS) devices. In this work we examine the mechanical behavior of nanoporous copper and its relation with the internal structure.

ID: 724

Grain Size Effect on Deformation Twinning and Detwinning

Yuntian Zhu
Department of Materials Science and Engineering, North Carolina State University
United States

Xiaozhou Liao
School of Aerospace, Mechanical and Mechatronic Engineering, The University of Sydney
Australia

Xiaolei Wu
State Key Laboratory of Nonlinear Mechanics, Institute of Mechanics, Chinese Academy of Sciences
China

Abstract:
This paper systematically addresses the grain size effect on deformation twinning and detwinning in face-centered cubic (fcc) metals. With decreasing grain size, coarse-grained fcc metals become more difficult to deform by twinning, whereas nanocrystalline (nc) fcc metals first become easier to deform by twinning and then become more difficult, exhibiting an optimum grain size for twinning. The transition in twinning behaviour from coarse-grained to nc fcc metals is caused by the change in deformation mechanisms. An analytical model based on observed deformation physics in nc metals, i.e. grain boundary emission of dislocations, provides an explanation of the observed optimum grain size for twinning in nc fcc metals. The detwinning process is caused by the interaction between dislocations and twin boundaries. Under a certain deformation condition, there exist a grain size range where the twinning process dominates over the detwinning process to produce the highest density of twins.

ID: 733

Grain Boundary Structure and Chemistry: Impact on Nanocrystalline Plasticity

Timothy J. Rupert
University of California Irvine
United States

Amir Khalajhedayati
University of California Irvine
United States

Abstract:
Nanocrystalline metals represent the extreme of grain refinement, exhibiting incredible strength and novel deformation physics. While the majority of research on nanocrystalline mechanical behavior focuses on grain size, we suggest that the atomic-level details of the grain boundaries can also control plasticity. In this talk, the importance of structural and chemical defects at nanocrystalline interfaces will be highlighted using small-scale mechanical testing and molecular dynamics simulations. Efforts to improve strain hardening ability and combat premature failure of nanocrystalline materials through interfacial engineering will be discussed. Finally, potential processing pathways for maximizing strength while improving the ductility and toughness of nanostructured alloys will be identified.

ID: 770

Mechanic Properties of Nanocrystalline Tantalum across the Length and Strain Rate Scales

Qiuming Wei
University of North Carolina at Charlotte

Jonathan Ligda

Abstract:
We have produced nanocrystalline tantalum (Ta, grain size as small as ~40 nm) using severe plastic deformation. The selection of Ta for this study is based on its extraordinary ductility, extremely high melting point (~3300K) and its body centered cubic lattice structure. The nanocrystalline microstructure was obtained via high pressure torsion (HPT) where a pressure of ~5 GPa was applied to the disk of Ta of ~1.2 mm thick and 10 mm diameter. Five turns were imposed to the disk at room temperature. The smallest grain size achievable in this case is ~40 nm as revealed by transmission electron microscopy (TEM), X-ray diffraction and inference from the Hall-Petch relation. Both dynamic (high strain rate) and quasi-static uni-axial compression has been performed on the processed material. The dynamic compression experiments were performed on a desk-top Kolsky bar (DTKB) system, with available strain rate as high as 10,000 /s. The quasi-static compression was based on a location specific mode. The specimens for quasi-static compression were made by focused ion beam (FIB) technique. We have found that under both dynamic and quasi-static compression, a transition of deformation mode from more or less uniform deformation to localized shear banding has taken place in the material as the location of the specimen is moving from close to the center of the HPT disk to the edge of the disk. We have discussed the results based on a recently proposed mechanistic model (Ramesh and Joshi, Physical Review Letters). This is the first observation of such phenomena in nanocrystalline metals produced from a top-down method.

ID: 771

Grain Boundary-Based Plasticity at Small-scale: the Input of in Situ TEM

Marc Legros
CEMES-CNRS

Früric Mompiou

Abstract:
When the mean free path of dislocations is reduced below the micron scale, either by geometrical constraints such as in whiskers, wires and pillars, or by grain boundaries as in small-grain polycrystals, a very large increase of mechanical resistance is observed. Because of their complex and out of equilibrium structures, metallic nanocrystals may deform through dislocations nucleated and absorbed at grain boundaries (GBs)[1], but many other alternate plasticity mechanisms have been foreseen. Shear-migration coupling is one of them and is the focus of many theoretical and experimental studies. At variance from dislocation-based plasticity, the shear produced by a moving GB can result in different values, depending on a parameter called the coupling factor Beta. Recent results obtained by in-situ Transmission Electron Microscopy (TEM) in ultra fine-grained Aluminum, show that many deformation modes are activated, including shear migration coupling. The coupling factor can be measured experimentally using image correlation analysis and therefore confronted to what has been predicted by models such as the one from Cahn and Mishin [2]. Although solid statistical data are still missing, beta appears smaller than what has been predicted. A reason could lie in the atomic-scale mechanisms that guide the migration of GBs. The Cahn and Mishin model assumes collective motion of GB dislocations, while Rae and coworkers insist on the role of steps propagation [3]. High resolution imaging of bicrystals shows that steps decorate GBs and that the motion of imperfect steps could result in the migration of the GB associated with a shear. To take in account these observations we also proposed a geometrical model for the shear migration coupling of grain boundaries [4], based of the shuffling of atoms within extended cells around the GB.

[1] F. Mompiou, D. Caillard, M. Legros, H. Mughrabi, Acta Materialia 60/8 (2012) 3402. [2] J.W. Cahn, Y. Mishin, A. Suzuki, Acta Materialia 54/19 (2006) 4953. [3] C.M.F. Rae, D.A. Smith, Philosophical Magazine 41/4 (1980) 477. [4] F. Mompiou, D. Caillard, M. Legros, Acta Materialia 57/7 (2009) 2198.

IV.15

Multiscale Mechanics of Materials - From Nanopores to Large Structures (Symp. celebrating Prof. Bazant's contributions)

ID: 114

Distributed Damage Creates Flaw Tolerance

Roberto Ballarini
University of Minnesota

Shreevant Tiwari
Georgia Institute of Technology

Abstract:
A qualitative micromechanical fracture mechanics model is presented that shows how a structure that is sensitive to the presence of a single crack or hole can be rendered flaw tolerant by the presence of an interacting distribution of such flaws. The simple model was inspired by and can explain the ductile fracture experienced by the gusset plates recovered from the I-35W Bridge collapse and by the experimentally measured increase in toughness of concrete damaged by fire.

ID: 139

Materials and Mechanics for Stretchable Electronics

Yonggang Huang
Northwestern University
USA

Abstract:
Recent advances in mechanics and materials provide routes to integrated circuits that can offer the electrical properties of conventional, rigid wafer-based technologies but with the ability to be stretched, compressed, twisted, bent, and deformed into arbitrary shapes. Inorganic and organic electronic materials in microstructured and nanostructured forms, intimately integrated with elastomeric substrates, offer particularly attractive characteristics, with realistic pathways to sophisticated embodiments. Here, we review these strategies and describe applications of them in systems ranging from electronic eyeball cameras to deformable light-emitting displays. We conclude with some perspectives on routes to commercialization, new device opportunities, and remaining challenges for research.

ID: 167

Load-Carrying and Energy-Dissipation Capacities of Ultra-High-Performance Concrete Under Transient Loading

Christopher Lammi
Georgia Institute of Technology

Jonathan Buck

Abstract:
The load-carrying and energy-dissipation capacities of ultra-high-performance concrete (UHPC) under dynamic loading are evaluated in relation to mesostructure composition at strain rates on the order of 105 s-1 and pressures of up to 10 GPa. Analyses focus on deformation and failure mechanisms at the mesostructural level during wave propagation through the material. A cohesive finite element framework that allows explicit account of constituent phase's interfaces, and fracture is used. The model resolves essential deformation and failure mechanisms in addition to providing a phenomenological account of the effects of the phase transformation within the quartz sand aggregate. Four modes of energy dissipation are tracked, including pressure-sensitive inelastic deformation, damage through the development of distributed cracks, interfacial friction, and energy released through phase transformation. Simulations are carried out over a range of volume fractions of constituent phases to quantify trends in load-carrying capacity and dissipation. Calculations show that the volume fractions of the constituents have more influence on the energy-dissipation capacity than the load-carrying capacity, that inelastic deformation is the source of over 70% of the energy dissipation, and that the presence of porosity changes the role of fibers in the dissipation process. The results also show that the phase transformation has a significant effect on the load-carrying and energy-dissipation capacities of UHPC for the conditions studied. Although transformation accounts for less than 2% of the total energy dissipation, the phase transformation leads to a two-fold increase in the crack density and yields nearly an 18% increase to the overall energy dissipation. Microstructure-behavior relations are established to facilitate materials design for target-specific applications.

ID: 195

The Buckling Hemisphere – A New Concept for an Energetical Classification of Loss of Stability

Herbert A. Mang
Institute for Mechanics of Materials and Structures, Vienna University of Technology
Austria

Xin Jia
Institute for Mechanics of Materials and Structures, Vienna University of Technology
Austria

Abstract:
Bending in the prebuckling regime may have a great influence on buckling of structures. A hypothesized feature of this influence is the decrease in quality of conversions of originally imperfection-sensitive into imperfection-insensitive structures with increasing percentage bending energy of the total strain energy. Ideally, such conversions are realized by small changes of the original design, taking functional requirements and aesthetic demands into account.

In view of the anticipated significance of bending in the context of buckling, the percentage bending energy of the total strain energy is considered to be a logical criterion for categorization of buckling on the basis of different static initial states of the buckling process. Proof of computability of this relative quantity for arbitrary structures and arbitrary static loading, in the frame of the Finite Element Method (FEM), without previous computation of technologically rather insignificant absolute energy quantities, is of great epistemological as well as practical relevance.

The mathematical tool for this proof is the so-called consistently linearized eigenproblem, introduced first by Helnwein [1]. Its formulation contains the tangent stiffness matrix, used in nonlinear Finite Element Analysis, and its first derivative with respect to a dimensionless load factor. The intellectual foundation of this presentation is the link of structural mechanics with spherical geometry in order to compute the percentage bending energy of the total strain energy. Figure 1 refers to this link. The left part of this figure shows the surface curve $\mathbf{v}_1^*\left(\varphi(\lambda),\theta(\lambda)\right)$ on the upper half of the unit sphere, referred herein as the buckling hemisphere. The eigenvector $\mathbf{v}_1^*(\lambda), \left\|\mathbf{v}_1^*\right\|=1$, is part of the first eigenpair of the consistently linearized eigenproblem. The link of structural mechanics and spherical geometry is established by the functions $\varphi(\lambda)$ and $\theta(\lambda)$, expressing the dependence of the azimuth angle φ and the zenith angle θ of the buckling hemisphere on the load factor λ. $\varphi(\lambda)$ is a measure of the aggregate normalized nonlinearity of the underlying stability problem, and $\theta(\lambda)$ is related to the percentage bending energy of the total strain energy, which is given as $100\cdot\cos^2\theta = 100\cdot U_B/(U_B+U_M)\,[\%]$ where U_M is the membrane energy and U_B is the bending energy.

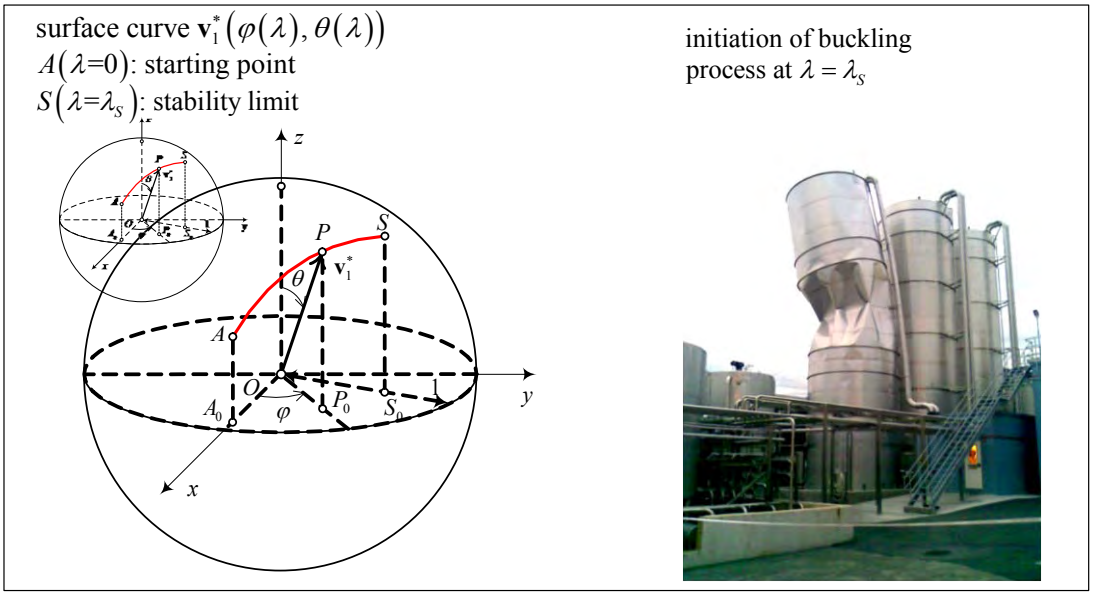

Figure 1 : Illustration of the concept of the buckling hemisphere

After presentation of the mathematical formulation of the consistently linearized eigenproblem and computation of its first three derivatives with respect to the load parameter, which will be needed for distinguishing between different classes of buckling problems, details of linking up structural mechanics with spherical geometry will be explained. The discussion of these different classes begins with the general case, characterized by a variable percentage bending energy in the prebuckling regime. It will be shown that for this case buckling occurs when the percentage bending energy attains a maximum value. Next, it will be demonstrated that a maximum value of the determinant of the tangent stiffness matrix in the prebuckling regime correlates with a minimum percentage bending energy. Thereafter, the special case of a prebuckling stress state characterized by a constant percentage strain energy will be investigated. Emphasis will be laid on the two limiting cases of this special case, i.e., on buckling from a membrane stress state and lateral torsional buckling. Moreover, it will be shown that buckling from a membrane stress state represents a class of buckling problems, independent of the aforementioned limiting case. In the context of buckling from a membrane stress state it will finally be demonstrated that linear prebuckling paths and linear stability problems need not be mutually conditional.

[1] P. Helnwein, “Zur initialen Abschätzbarkeit von Stabilitätsgrenzen auf nichtlinearen Last-Verschiebungspfaden elastischer Strukturen mittels der Methode der Finiten Elemente (Ph. D. thesis) [in German; On ab initio Assessability of Stability Limits on Nonlinear Load-displacement Paths of Elastic Structures by means of the Finite Element Method]”, Vienna University of Technology, Vienna, Austria, 1997.

ID: 480

Nanovoid Nucleation Inside Inelastic Material: Various Scenarios

Valery Levitas
Iowa State University

Abstract:
Thermodynamic and kinetic approaches for nanovi0d nucleation due to fracture, sublimation, and sublimation via the virtual melting inside elastoplastic material under tensile stress are developed for large strains. Various conceptual problems related to irreversible plastic deformation are addressed for a spherical bubble. They include definitions of the thermodynamic driving forces and activation energies, nontraditional concepts of a critical nucleus, path-dependence of its appearance, modes of its growth (sublimation or expansion due to loss of mechanical stability), and the possibility of reverse transformation. The kinetic relationship between sublimation pressure and temperature are obtained. In different tensile pressure ranges, void nucleated via sublimation, fracture, sublimation via virtual melting and evaporation of stable melt. In addition, a mechanochemical approach to the void nucleation and growth in an oxidizing nanoparticle due to the Kirkendall effect is developed. Surprisingly, compressive pressure and reduced promote void nucleation; however, they suppress its growth. Our model describes well experimental results for oxidation of copper nanoparticles of three sizes at three temperatures.

Levitas V.I. Int. J. Plasticity, 2012, Doi:10.1016/j.ijplas.2012.01.006. Levitas V.I. and Altukhova N. Int. J. Plasticity, 2012, Doi:10.1016/j.ijplas.2012.01.005. Levitas V.I. and Attariani H. J. Physical Chemistry C, 2012, 116, 54-62. Levitas V.I. and Altukhova N. Acta Materialia, 2011, 59, 7051-7059. Levitas V.I. and Altukhova N. Physical Review B, 2009, 79, 212101. Levitas V.I. and Altukhova N. Physical Review Letters, 2008, 101, 145703.

ID: 574

Mathematical Homogenization of Particulate Media to Cosserat Continuum using an Asymptotic Approach

Roozbeh Rezakhani
Northwestern University
United States

Gianluca Cusatis
Northwestern University
United States

Abstract:
Concrete, ceramics, fiber and particle reinforced composites, as well as porous media, are materials widely used in industry and engineering. All these materials are heterogeneous at a certain scale and some of their specific macroscopic behaviors during damage can be traced back to their micro structural behavior. In order to obtain realistic results in the numerical simulations of heterogeneous materials, one needs either to perform computationally intensive fine scale simulations or to adopt a multi-scale technique that is able to reduce the computational cost of the analysis while it retains enough accuracy on the quantities of interest. In this paper the mathematical homogenization approach is used to upscale fine-scale discrete models, such as the Lattice Discrete Particle Model (LDPM), that have been successfully formulated to simulate concrete and other quasi-brittle materials at the scale of the major heterogeneities.
The Lattice Discrete Particle Model (LDPM) [1] simulates concrete at the meso-scale considered to be the length scale of coarse particle pieces. Contrarily to continuum-based approaches, in discrete models like LDPM, the displacement and rotation fields are only defined in a finite number of points representing the center of coarse particle particles. The mechanical interaction between adjacent particles is governed by meso-level constitutive equations able to capture tensile fracturing, cohesive and frictional shearing, and non-linear compressive behavior. LDPM has shown superior modeling capabilities under an extremely wide range of loading conditions.
The homogenization theory, originally proposed by Babuska [2] and later developed by many other authors [3], has been used to build multiscale frameworks to model heterogeneous materials at different scales. The basic idea of homogenization is representing each integration point in the macroscopic domain by a representative volume element (RVE). The RVE is a volume of the material in which the related heterogeneity is modeled, while the material is assumed to be homogeneous at the macroscopic scale. Deformation gradient at integration points of the macroscopic domain is the input for the solution of the fine-scale problem formulated at the RVE scale. Then, using an averaging scheme, the macroscopic response derived from RVE is transferred back to the macro-scale. Fig. 1a shows the geometry and particle distribution of a typical 100 mm RVE with 8 mm aggregate size. Periodic boundary conditions are applied on the RVE during the solution procedure. In this work LDPM is first approximated by a micro-polar continuum theory and then a homogenization scheme based on the asymptotic expansion of displacement and rotation fields is developed through the classical mathematical homogenization.

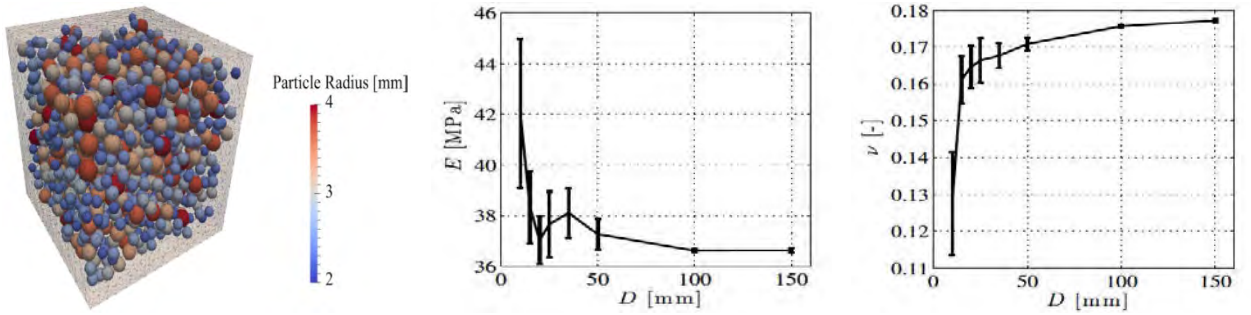

(a) (b) (c)

Fig 1. (a) RVE geometry and particle distribution. (b) Young modulus and (c) Poisson's ratio variation by changing RVE size

Starting from the translational and rotational equations of motion of a single particle and by exploiting scale separation as well as asymptotic expansion of displacement and rotation fields, homogenized multiple scale governing equations are derived. This leads to a Cosserat-type continuum in which macroscopic stress $\boldsymbol{\sigma}$ and moment stress $\boldsymbol{\mu}$ tensors are defined in terms of meso scale quantities as follows:

$$\boldsymbol{\sigma} = \frac{1}{V_0}\sum_{I}\sum_{f=1}^{n_f}\frac{A_f}{2}(\boldsymbol{x}^{IJ} \square \boldsymbol{t}^{IJ}) \qquad \boldsymbol{\mu} = \frac{1}{V_0}\sum_{I}\sum_{f=1}^{n_f}\frac{A_f}{2}(\boldsymbol{x}^{IJ} \square (\boldsymbol{\mu}^{IJ} + \boldsymbol{c}^{I} \times \boldsymbol{t}^{IJ}))$$

Where $\boldsymbol{t}^{IJ}$ and $\boldsymbol{\mu}^{IJ}$ are traction and moment stress vector applying on the center of the contact area (facet) f between two aggregates I and J, respectively; V_0 and A_f are the volume of the RVE and the area of the facet f; n_f is the total number of facets surrounding aggregate I; and $\boldsymbol{x}^{IJ}$ is the vector connecting the center of two particles; $\boldsymbol{c}^{I}$ is the vector connecting center of particle I to the center of the facet f.

Elastic and inelastic simulations have been carried out on the RVE to study the macroscopic homogenized behavior of LDPM. Figs. 1b and 1c show the variation of Young modulus and Poisson's ratio, respectively, as a function of the RVE size. In the figures, mean and standard deviation (error bars) for five different meso-scale realizations are reported. As the size of the RVE is increased, the mean does converge to an asymptotic value and the standard deviation goes to zero as expected. Nonlinear simulations show similar trends. However, the results are distinctly different whether the material experiences strain-hardening as opposed to strain-softening. While in the former case demonstration of convergence with RVE size is straightforward; for the latter case the issues of size-effect and delocalization during damage and fracture need to be addressed in order to prove the validity of the homogenization scheme.

References

[1] G. Cusatis, D. Pelessone, A. Mencarelli. Lattice Discrete Particle Model (LDPM) for failure behavior of concrete. I: Theory. Cement and Concrete Composites 2011; 33:881-890.

[2] I. Babuska, Homogenization and its application. Mathematical and computational problems. Numerical solution of partial differential equations, III. Proc. Third Symp. (SYNSPADE), Univ. Maryland, College Park, MD, 89-116, 1975 (Academic Press, New York, 1976).

[3] J. Fish, W. Chen, R. Li. Generalized mathematical homogenization of atomistic media at finite temperature in three dimensions. Comput. Methods Appl. Mech. Engrg. 2007; 196: 908-922.

ID: 677

Hydrodynamics of Capillary Imbibition under Nanoconfinement

Sinan Keten
Northwestern University

Wylie Stroberg

Abstract:
Understanding fluid flow in nanoconfined geometries is crucial for a broad range of scientific problems relevant to the behavior of porous materials in biology, nanotechnology and the built environment. Due to the dominant importance of surface effects at the nanoscale, long standing assumptions that are valid for macroscopic systems must be revisited when modeling nanoconfined fluids, since boundary conditions and the confined behavior of liquids are challenging to discern from experiments. To address this issue, here we present a novel coarse-grained model that combines parameters calibrated for water with a dissipative particle dynamics thermostat for the purpose of investigating hydrodynamics under confinement at scales exceeding current capabilities with all-atomistic simulations. Conditions pertaining to slip boundary conditions and confinement emerge naturally from particle interactions, with no need for assumptions a priori. The model is used to systematically investigate the imbibition dynamics of water into cylindrical nanopores of different diameters. Interestingly, we find that the dynamic contact angle depends on the size of the nanopore in a way that cannot be explained through a relationship between contact line velocity and dynamic contact angle, suggesting non-local effects of the flow field may be important. Additionally, a size-dependent characteristic timescale for imbibition is found, which could be useful for the interpretation of experiments and design of novel nanofluidic devices. Our modeling approach lays the foundation for broader investigations on the dynamics of fluids in nanoporous materials in conjunction with experimental efforts.

ID: 683

On the Relative Density of Nanoporous Metals

Ran Liu
Georgia Institute of Technology
USA

Antonia Antoniou
Georgia Institute of Technology
USA

Abstract:
Relative density controls different material properties in porous media from mechanical response to conductivity. In this work we examine experimentally the relative density of nanoporous metal foams and its relation to sample shrinkage and alloy composition. We also examine the effects of strut geometry on the relative density and provide a comparison with dimensional analysis predictions. These observations can serve to distinguish between differences of bulk metal foams and nanoporous metal foams.

ID: 746

Phase-Field Models for Dynamic Crack Propagation in Ductile Material

Michael J. Borden
The University of Texas at Austin
United States

Thomas J.R. Hughes
The University of Texas at Austin
United States

Chad M. Landis
The University of Texas at Austin
United States

Abstract:
The phase-field approach to predicting fracture supplements the usual linear momentum equation with an additional scalar valued phase-field equation. In this approach, discontinuities are not introduced into the geometry or displacement field. Instead, the fracture surface is approximated by a phase-field, which smoothes the boundary of the crack over a small region (see Figure 1). A major advantage of using a phase-field is that the evolution of fracture surfaces follows from the solution of a coupled system of partial differential equations. Implementation does not require additional ad hoc rules to determine crack initiation, propagation direction, or bifurcation.

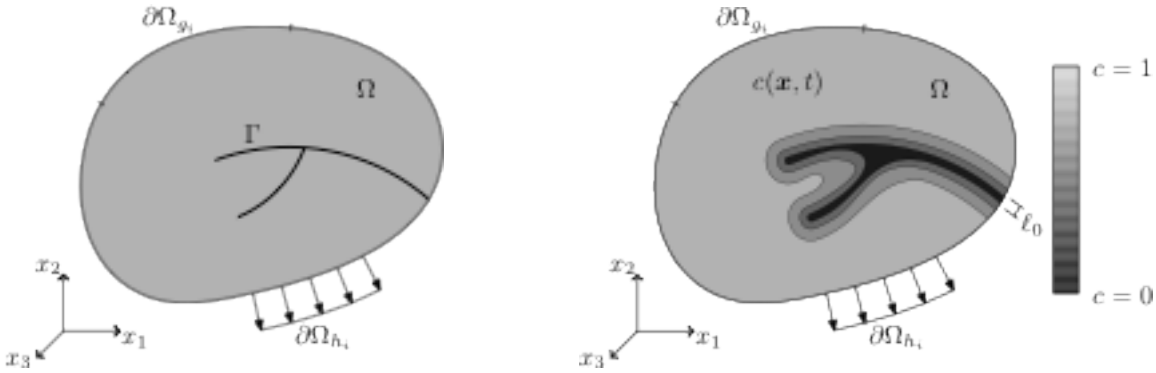

Figure 16. The sketch on the left shows a schematic representation of a solid body Ω with internal discontinuity Γ. The sketch on the right shows an approximation of the discontinuity by the phase-field $c(x,t)$. The model parameter ℓ_0 controls the width of the approximation.

In this presentation, we will extend the phase-field model for dynamic brittle fracture described in [1] to dynamic fracture of ductile materials. We will discuss our work to develop constitutive theories for phase-field models of ductile fracture. For example, we will present a formulation that is based on the multiplicative decomposition of the deformation gradient $\mathbf{F} = \mathbf{F}^e\mathbf{F}^p$ where $\mathbf{F}^e$

and $\mathbf{F}^p$ are the elastic and plastic parts of the deformation gradient respectively. For this formulation, the elastic strain energy is represented as

$$W = c^2 W^+(\mathbf{F}^e) + W^-(\mathbf{F}^e) \tag{1}$$

where W^+ is a tensile energy, W^- a compressive energy and $c \in [0,1]$ is the phase-field parameter. When $c = 1$ the material is at full strength and when $c = 0$ the crack is fully formed. The surface energy associated with cracks is approximated by the volume integral

$$\int_\Omega G_c \left(\frac{(1-c)^2}{4l_0} + l_0 |\nabla c|^2 \right) d\Omega \tag{2}$$

where G_c is the surface energy density and l_0 is a length scale parameter. Letting P_{iJ} be the components of the first Piola-Kirchhoff stress tensor (which are dependent on c), the strong form of the coupled problem is stated as

$$\begin{cases} P_{iJ,J} + B_i = \rho_0 \ddot{u}_i & \text{(linear momentum)} \\ \left(\dfrac{4cl_0 W^+}{G_c} + 1 \right) c - 4l_0 |\nabla c|^2 = 1 & \text{(phase-field).} \end{cases} \tag{3}$$

We will show that the solution to (3) fully determines the behavior of ductile fracture in Ω for this model.

To conclude this presentation, we will show the results of a number of numerical benchmark experiments for crack propagation in ductile material. These results will show that the phase-field model can capture complex ductile fracture behavior in both two and three dimensions.

References:

[1] M.J. Borden, C.V. Verhoosel, M.A. Scott, T.J.R. Hughes, C.M. Landis, "A phase-field description of dynamic brittle fracture," Comp. Meth. in Appl. Mech. Engng. **217-220,** 77-95 (2012).

ID: 751

Active gels

Zhigang Suo
Harvard University
USA

Abstract:
Long and flexible polymers can be covalently crosslinked to form a three-dimensional network. The network can imbibe a solvent and swell, forming a gel. Gels have many uses, including personal care, drug delivery, tissue engineering, microfluidic regulation, and oilfield management. Mixtures of macromolecular networks and mobile molecules also constitute most tissues of plants and animals. The amount of swelling can be large and reversible. The gels are active in that the amount of swelling can be regulated by environmental stimuli, such as force, electric field, pH, salinity, and light. This talk describes a theory that combines the mechanics of large deformation and the chemistry of molecular mixtures. The theory is illustrated with examples of swelling-induced large deformation, contact, and bifurcation. The theory is further illustrated with recent experiments.

ID: 831

MODEL VALIDATION AND UNCERTAINTY QUANTIFICATION IN ENGINEERING SCIENCE

John Oden
The University of Texas at Austin
USA

Abstract:
Engineering Science makes use of models of physical phenomenon, conceived through a combination of observations of physical events and inductive reasoning represented in theories. Thus, the core value of Engineering Science hinges on the predictability of these models. This presentation examines the broad subject of model validation, model selection, and predictability for classes of problems with general Bayesian frameworks. The use of multiscale models in this process is also discussed.

IV.16

Multiscale Mechanics of Materials - Non-Local and Strain Gradient Elasticity, Plasticity, and Damage

ID: 316

Wave Propagation in Heterogeneous Media with Local and Non-Local Material Behavior

Hüseyin Gökmen Aksoy
İstanbul Kemerburgaz University, Department of Mechanical Engineering
Turkey

Abstract:
Wave propagation in heterogeneous solids has been an interest of researchers due to industrial applications. In order to model the effect of discrete phases in microstructure on macroscopic material behavior, multiscale methods or homogenization techniques are used. Some of the heterogeneous materials can exhibit power law scaling in the material behavior, which can be characterized by the fractal dimension of the microstructure such as colloidal aggregates [1]. Fractional calculus has been used for modeling such material behavior [2-4].

In this study, wave propagation in fractal media is investigated via fractional calculus [5] by using finite element method. Local fractional derivative proposed by Tarasov [6] and Riesz potential based on modified Riemann-Liouville derivative [7] is used for modeling local and non-local material behavior respectively. It is assumed that stress strain relation is linear assuming that strains are small. 1D suddenly loaded bar and 2D suddenly loaded plate from its center are studied under plain strain conditions.

Numerical Results:

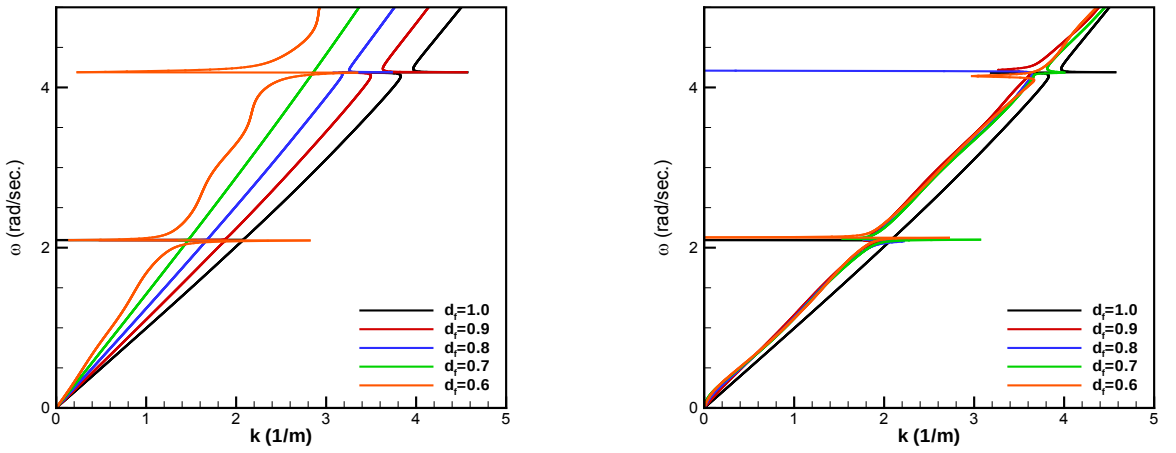

(a) local fractional derivative (b) non-local fractional derivative

Figure 1. Dispersion curves for local and non-local materials with different fractal dimensions d_f obtained from 1D suddenly loaded bar.

Numerical results show that wave propagation with local and non-local derivatives does not possess dispersive characteristics as seen in Figure 1. Phase velocity is constant over wide range of frequencies. In case of computations with local derivatives, phase velocity monotonically increases with the decrease of fractal dimension which is not seen in computations with non-local derivatives. Attenuation is observed in both cases and it is higher in computations with the local derivatives compared to computations with non-local derivatives. In addition attenuation coefficient increases with the increase in fractal dimension in computations with local derivatives whereas it decreases in computations with non-local derivatives. Peak stress decreases with decrease of fractal dimension in computations both with local and non-local derivatives.

Suddenly loaded plate from its center is also studied. Computations shows that stress waves propagates faster as the fractal dimension decreases both with local and non-local fractional derivatives similar to the 1D case. Apart from that, peak stress decreases with the decrease of fractal dimension in both cases. On the other hand, as wave proceed in plate amplitude of the stress waves increases and becomes higher than the homogeneous material in both cases.

Conclusion:

Results presented in this study are based on hypothetical material. It is seen that local and non-local fractional derivatives poses non-dispersive characteristics with attenuation. Local fractional derivatives are proposed as alternatives of non-local fractional derivatives. In this study, it is shown that results obtained with local fractional derivatives and non-local fractional derivatives are not identical for dynamic problems.

References:

[1] Wyss, H. M., Tervoort, E. V. and Gauckler, L. J., 2005, “Mechanics and microstructures of concentrated particle gels,” Journal of American Ceramic Society, Vol. 88, pp. 2337-2348.

[2] Demmie, P. N. and Ostoja-Starzewski, M., 2011, “Waves in fractal media,” Journal of Elasticity, Vol. 104, pp. 187-204.

[3] Cornetti, P., Carpinteri, A., Sapora, A., Di Paola, M. and Zingales, M., 2009, “An explicit mechanical interpretation of Eringen non-local elasticity by means of fractional calculus,” XIX Congress AIMETA, 14-17 September, Ancona-Italy.

[4] Rosikhin, Y. A. and Shitikova, M. V., 1997, “Applications of fractional calculus to dynamic problems of linear and nonlinear hereditary mechanics of solids,” Applied Mechanics Review, Vol. 50, pp. 15-67.

[5] Samko, S. G., Kilbas, A. A. and Marichev, O. I., 1993, "Fractional integrals and derivative: theory and applications". Gordon & Breach Sci. Publishers.

[6] Tarasov, V. E., 2009, "Fractional dynamics: applications of fractional calculus to dynamics of particles, fields and media". Springer.

[7] Jumarie, G., 2009, “Table of some basic fractional calculus formulae derived from a modified Riemann-Liouville derivative for non-differentiable functions,” Applied Mathematics Letters, Vol. 22, pp. 378-385.

ID: 427

Damage Smoothing Effects in BCJ Metals with Damage Delocalization

K. Enakoutsa[1], F. Ahad[1], K. Solanki[2], Y. Tjiptowidjojo[1] and D. J. Bammann[1]

[1] *CAVS, Mississippi State University, 200 Research Boulevard, Mississippi State, MS 39762*

[2] *SEMTE, Arizona State University, Tempe, AZ 85287*

Abstract

It has been long time established that the addition of a characteristic length scale to softening constitutive models *via* delocalization of the softening parameter yields numerical results that are independent of the size of the finite element. For instance, the work of Tvergaard and Needleman (1995) in the context of ductile fracture of materials has shown that the delocalization of the damage (softening parameter) in the Gurson (1977)'s model did eliminate the pathological mesh size dependence in finite element computations. Recently, Enakoutsa et al. (2007) have confirmed these findings. Despite this success, the damage delocalization method did not yield satisfactory results with respect to its ability to predict real-world experimental results, Enakoutsa et al. (2007). Indeed, the load-displacement curves generated by the delocalized Gurson model for various pre-cracked axisymmetric specimens loaded in tension remain quasi-stationary for too long period of time and suddenly drops, contrary to the experiments. According to Enakoutsa et al. (2007), this undesirable feature is due to unlimited smoothing of the damage distribution in the ligament ahead of the crack tip of the specimen. These authors provide a theoretical explanation of the excessive smoothing of damage shortcoming based on such as crude assumptions as unboundness of the body considered and homogeneity of the mechanical fields. Namely, they showed that the nonlocal evolution equation for the damage is qualitatively similar to some diffusion equation which results in an excessive smoothing of the damage. Following this theoretical analysis, they proposed a simple remedy to deal with the excessive smoothing of the damage. It consists of adopting the nonlocal concept for the logarithm of the damage instead of the

damage itself; this has the avantage to eliminate the analogy between the nonlocal evolution equation and a diffusion equation.

The objective of the present paper is to follow up the study of the applicability of the delocalization method in the context of high rate damage of metals. The model considered will be that proposed by Bammann-Chiesa-Johnson (denoted BCJ model for shortness), Bammann and Johnson (1984), Bammann et al. (1995), but with a modified, delocalized evolution equation for the damage (nonlocal variable) the introduction of which incorporates a diffusive effect in the constitutive model; this prevents the nonlocal damage variable to spuriously localize into vanishing bands in problems involving localization. However, the diffusive effect unavoidably leads to an unwanted excessive smoothing of the damage. Just like in Enakoutsa et al. (2007), we provide a theoretical explanation of this shortcoming, following which a simple remedy is suggested to deal with it. Future works involve the numerical implementation of the new version of the delocalized model in order to assess its ability to reproduce real-world problems.

References

Bammann, D.J., Chiesa, M.L., and Johnson, G.C., 1995. "A State Variable Model for Temperature and Strain Rate Dependent Metals," eds. A.M. Rajendran and R.C. Batra, *Constitutive Laws: Experiments and Numerical Implementation.*

Bammann, J.D. and Johnson, G.C., 1984. "Developement of a Strain Rate Sensitivity Plasticity Model," in *Engineering Mechanics in Civil Engineering*, eds. Boresi A.P. and Chong, K.P., p.154.

Enakoutsa K., Leblond J.B. and Perrin G., 2007. "Numerical Implementation and Assessment of a Phenomenological Nonlocal Model of Ductile Rupture," *Comput. Meth. Appl. Mech. Engng.*, **196**, 1946-1957.

Gurson A.L. 1977. "Continuum Theory of Ductile Rupture by Void Nucleation and Growth: Part I - Yield Criteria and Flow Rules for Porous Ductile Media," *ASME J. Engng. Materials Technol.*, **99**, 2-15.

Tvergaard V. and Needleman A., 1995. "Effects of Nonlocal Damage in Porous Plastic Solids," *Int. J. Solids and Structures*, **32**, 1063-1077.

ID: 661

Interfacial Effects on Size-Dependent Mechanical Behavior of Micro and Nanostructured Metals through Gradient Plasticity Theory

Rashid K. Abu Al-Rub
Zachry Department of Civil Engineering, Texas A&M University
USA

Mahmood Ettehad
Zachry Department of Civil Engineering, Texas A&M University
USA

Abstract:
There are numerous experimental results that indicate a size-dependent mechanical behavior of materials at the micron or submicron length scales, in the sense that "smaller is stronger". Unlike classical continuum mechanics which fail to interpret the size effect in micro/nano structured materials, mechanism-based theory of strain gradient plasticity based on a multi-scale framework linking the microscale notion of statistically stored and geometrically necessary dislocations (GNDs) to the mesoscale notion of plastic strain and strain gradient has been noticed to remove the shortcoming of this area. In this paper, first, a thermodynamic based higher-order gradient plasticity model that enforces nonstandard boundary conditions that relate the micro-tractions to the interfacial energy at the interfaces is presented. Next the application of the proposed gradient plasticity model on the overall mechanical behavior is shown by incorporating different forms of the interface yield conditions, identified as soft, intermediate, and stiff interfaces.

1. Higher-Order Gradient Plasticity Model
The principle of virtual power, which is the assertion that given any sub-volume Γ with surface $\partial\Gamma$ and interfaces $\partial\Gamma^{int}$, the virtual power expended on Γ by materials or bodies exterior to Γ be equal to the virtual power expended within Γ and at $\partial\Gamma^{int}$, can be expressed as:

$$\int_{\Gamma}\left(\sigma_{ij}\delta\dot{\varepsilon}^{e}_{ij}+R\delta\dot{p}+Q_{k}\delta\dot{p}_{,k}\right)dV+\int_{\partial\Gamma^{int}}M_{I}\delta\dot{p}^{I}dS=\int_{\partial\Gamma}\left(T_{i}\delta\dot{u}_{i}+m\delta\dot{p}\right)dS \qquad (1)$$

where $\boldsymbol{\sigma}$ is the Cauchy stress tensor, $\boldsymbol{\varepsilon}^{e}$ is the elastic strain tensor, R is the drag-stress associated with local isotropic hardening and is the conjugate to the effective (equivalent) plastic strain p, $\mathbf{Q}$ is a higher-order force vector associated with nonlocal isotropic hardening and is conjugate to the gradient of the effective plastic strain $p_{,k}$, $\mathbf{T}$ is the macroscopic surface traction vector, $\dot{\mathbf{u}}$ is the velocity vector, m is a higher-order moment stress that is prescribed at the external surface boundary $\partial\Gamma$ with an outward unit normal vector $\mathbf{n}$, and the moment tractions M_I represent the work conjugates to the effective plastic strains p^I at the interfaces.

From Eq. (1) one can derive the *macroscopic stress equilibrium equation*, *macrotraction boundary condition*, *microforce balance governing the plastic flow*, and *microtraction condition*. By introducing the Helmholtz free energy ($\Psi=\Psi^{Bulk}+\Psi^{int}$) and dissipation function ($\Pi=\Pi^{Bulk}+\Pi^{int}$) for both bulk and interface, one can derive the energetic (E) and dissipative (D) parts of thermodynamic conjugated forces $\boldsymbol{\sigma}=\boldsymbol{\sigma}^{E}$, $R=R^{E}+R^{D}$, $\mathbf{Q}=\mathbf{Q}^{E}+\mathbf{Q}^{D}$, and

$M_I = M_I^E + M_I^D$ through applying nonlocal Clausius-Duhem inequality [see Abu Al-Rub and Ettehad (2011) for details]. Here the special form of these two functions is assumed which finally yields the following microforce balances:

$$f^{Bulk} = \left\| \tfrac{3}{2}\tau_{ij} \right\| - \sigma_Y - hp + 2h\ell^2\nabla^2 p = 0, \qquad f^{int} = 2h\ell^2\nabla p^I.\mathbf{n} + \gamma + \beta p^I = 0 \tag{2}$$

It is obvious that the Eq. (2) incorporates two-different forms of nonlocal yield conditions for the material's bulk and interface. Here σ_Y and γ are the yield strength, h and β are the plastic hardening rate for bulk and interface, respectively, while ℓ is the material bulk length scale.

2. Application to a Thin film on an Elastic Substrate

Fig. 1 shows the effect of interface properties on the normalized shear stress versus normalized shear strain response of a thin film bonded to a substrate for different film thicknesses. Here the interface strength and hardening are controlled by two dimensionless variables $\delta_1 = \gamma / h\ell\gamma_Y$ and $\delta_2 = \beta / 2h\ell$, respectively, where γ_Y is the shear yield strain.

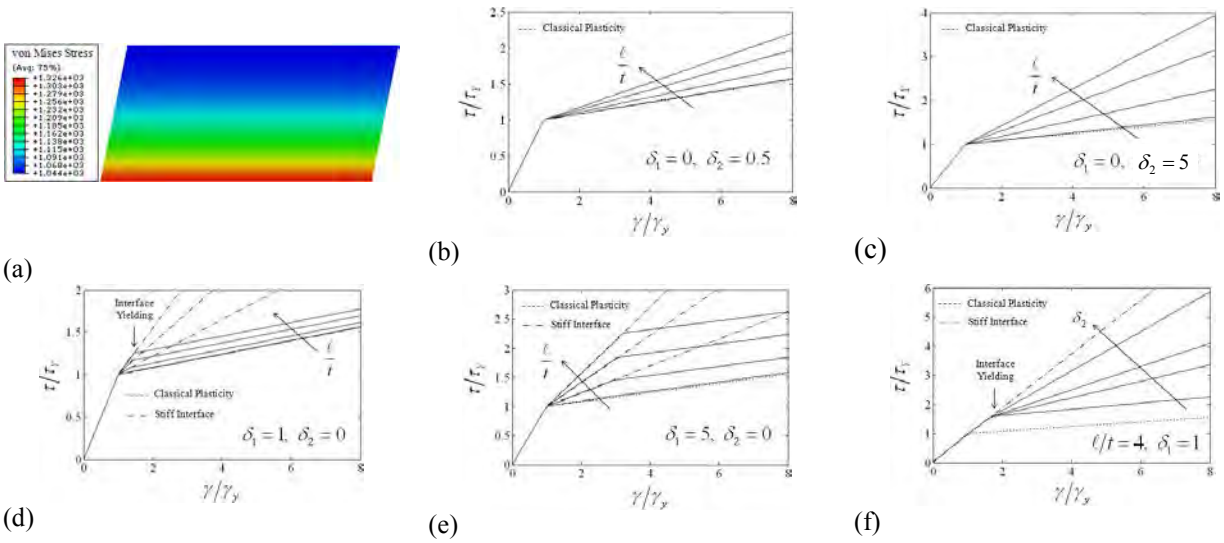

Fig.1. (a) contour of normalized shear stress for stiff interface, normalized shear stress versus shear strain for (b) and (d) soft, (c) and (e) intermediate for different $\ell/t = 0.5, 1, 1.5, 2$.

The formation of a boundary layer is obvious from Fig. 1(a), which cannot be captured by classical plasticity theory. Also one can see that the interface hardening can control the material plastic hardening rate while the interface yield strength controls the behavior up to the macroscopic stress where the interface yields. The combination effects are shown in Fig. 1(f).

Reference

Abu Al-Rub, R.K., Ettehad, M., 2011, Modeling interparticle size effect on deformation behavior of metal matrix composites by a gradient enhanced plasticity model, ASME Journal of Engineering Materials and Technology, 133, 015104.

ID: 736

Nonlocality Induced Phenomena in Wave Propagation

Jiaoyan Li
The George Washington University
United States

James D. Lee
The George Washington University
United States

Abstract:

When dealing with micro- or nano- structures, Molecular Dynamics (MD) simulation provides a feasible option which can capture the physical phenomena at micro- or nano- scale. At nanoscale, the material system can be viewed as a collection of atoms whose motions are governed by

$$m^i \frac{d^2\mathbf{r}^i}{dt^2} = \mathbf{f}^i + \boldsymbol{\varphi}^i \tag{1}$$

where $\boldsymbol{\varphi}^i$ is the force due to external field and/or thermostat; $\mathbf{f}^i$ is the interatomic force which can be obtained from the derivation of a scalar-valued function called interatomic potential

$$\mathbf{f}^i = -\frac{\partial V}{\partial \mathbf{r}^i} \tag{2}$$

Generally, the interatomic potential can be expressed as follows

$$V = \frac{1}{2!}\sum_{i,j=1}^{N} V^{ij}(\mathbf{r}^i,\mathbf{r}^j) + \frac{1}{3!}\sum_{i,j,k=1}^{N} V^{ijk}(\mathbf{r}^i,\mathbf{r}^j,\mathbf{r}^k) + \frac{1}{4!}\sum_{i,j,k,l=1}^{N} V^{ijkl}(\mathbf{r}^i,\mathbf{r}^j,\mathbf{r}^k,\mathbf{r}^l) + \cdots \tag{3}$$

A typical one in the class of pair potential, the Coulomb-Buckingham potential can be expressed by

$$V^{ij} = \frac{q^i q^j}{r^{ij}} + A^{ij} e^{-\frac{r^{ij}}{B^{ij}}} - C^{ij}\left(r^{ij}\right)^{-6} + D^{ij}\left(r^{ij}\right)^{-12} \tag{4}$$

The first term on the right hand side is Coulomb potential and all the other three terms are Buckingham potential. They are all characterized by ranges of interaction, a long range and a short range. For any atom, the long range and short range interatomic force acting on it can be

calculated through the summation of all the interatomic forces contributed by all the other atoms within the long range and short range, respectively. This means nonlocality has been unintentionally introduced into MD simulation. The interatomic potential is the only "constitutive equation" needed, which renders almost all material properties accessible and involves the interaction between all atoms.

On the other hand, Eringen's nonlocal continuum theory allows one to account for the effect of small length scale, which becomes significant when dealing with micro- or nano- structures. In the nonlocal model, the state of the body at a material point is a function of all the independent constitutive variables of all the points in the neighborhood. To be specific, when the stress-strain relation is concerned, nonlocality means the stress at a generic point $\mathbf{x}$ is a function of the strains at all points $\mathbf{x}'$ around the point $\mathbf{x}$, i.e.,

$$t_{ij}(\mathbf{x}) = \int_{\Omega(\mathbf{x}')} A_{ijmn}(\mathbf{x},\mathbf{x}')e_{mn}(\mathbf{x}')d\Omega(\mathbf{x}') \tag{5}$$

For isotropic material, eq.(5) is simplified to

$$t_{ij}(\mathbf{x}) = H(\mathbf{x})(\lambda\delta_{ij}\delta_{mn} + 2\mu\delta_{im}\delta_{jn})\int_{\Omega(\mathbf{x}')} f(\mathbf{r})e_{mn}(\mathbf{x}')d\Omega(\mathbf{x}') \tag{6}$$

where $f(r)$ is the weight function,

$$f(\mathbf{r}) = \begin{cases} 1-6r^2+8r^3-3r^4, & \text{if } r \le 1 \\ 0, & \text{if } r > 1 \end{cases} \tag{7}$$

and $H(\mathbf{x}) = 1\Big/\int_{\Omega(\mathbf{x}')} f(\mathbf{r})d\Omega(\mathbf{x}')$, $\mathbf{r} \equiv |\mathbf{x}-\mathbf{x}'|/R$.

Noted that R is the radius of nonlocality. When R approaches zero, the weight function becomes the delta function, and the nonlocal theory reduces to the local theory.

The nonlocal theory is in accordance with atomic theory of lattice dynamics and experimental observations on phonon dispersion. In this paper, the nonlocality induced phenomena are investigated by using both MD simulation and Eringen's nonlocal continuum theory. The results show that the dispersion phenomena in wave propagation problem, induced by the nonlocality, becomes more and more significant when the radius of influence increases. Our results also show that the total energy, includes kinetic energy and potential energy, is conserved when the system is free from external disturbance. This can be taken as a verification.

ID: 743

Return Mapping Algorithm for Micromorphic Plasticity

Zhen Zhang
The George Washington University
USA

James D. Lee
The George Washington University
United States

Abstract:
A strain-based return mapping algorithm for Micromorphic plasticity is formulated in this work. In microcontinuum field theories, a material body is envisioned as a continuous collection of deformable particles; each has a finite size and possesses inner structure. This significant and unique property raises the difficulty in the study of Micromorphic plasticity. A large set of internal variables has to be added to the list of dependent constitutive variables. Also, one needs to supply a set of governing equations for the newly added internal variables. Lee and Chen (2003) introduced a set of internal variables $\mathbf{W} = \{\boldsymbol{\alpha}^P, \boldsymbol{\beta}^P, \boldsymbol{\gamma}^P, \mathbf{R}\}$, where $\boldsymbol{\alpha}^P, \boldsymbol{\beta}^P, \boldsymbol{\gamma}^P$ are the plastic strains corresponding to the generalized Lagrangian strains (or called Eringen tensors) $\boldsymbol{\alpha}, \boldsymbol{\beta}, \boldsymbol{\gamma}$, respectively; $\mathbf{R}$, named as the hardening parameters, is a generalized vector of internal variables other than $\boldsymbol{\alpha}^P, \boldsymbol{\beta}^P, \boldsymbol{\gamma}^P$.

In return mapping algorithm for Micromorphic plasticity, first the three Eringen tensors are decomposed into elastic and plastic parts. To simplify the formula, a generalized column vector $\mathbf{E}$ including all elements in Eringen tensors is introduced.

$$\mathbf{E} = \begin{pmatrix} \boldsymbol{\alpha} \\ \boldsymbol{\beta} \\ \boldsymbol{\gamma} \end{pmatrix} = \begin{pmatrix} \alpha_{11} \\ \vdots \\ \beta_{11} \\ \vdots \\ \gamma_{111} \\ \vdots \end{pmatrix}, \qquad \mathbf{E}^p = \begin{pmatrix} \boldsymbol{\alpha}^p \\ \boldsymbol{\beta}^p \\ \boldsymbol{\gamma}^p \end{pmatrix}, \qquad \mathbf{E}^e = \begin{pmatrix} \boldsymbol{\alpha} - \boldsymbol{\alpha}^p \\ \boldsymbol{\beta} - \boldsymbol{\beta}^p \\ \boldsymbol{\gamma} - \boldsymbol{\gamma}^p \end{pmatrix}$$

In this work, we further assume a linear relationship between the elastic Eringen vector $\mathbf{E}^e$ and the corresponding generalized Lagrangian stress.

Stress-based yield criterion is a widely used criterion in continuum theory of plasticity. However, this approach becomes much more complicated, if not impossible, for Micromorphic plasticity because it involves much more internal variables. Instead of using stress-based yield criterion, a

strain-based yield criterion is proposed here. The yield function is written as $f=f\left(\mathbf{E}^e,\mathbf{R}\right)$. In general, the evolution equations for the internal variables can be expressed as

$$\dot{\mathbf{E}}^p=\gamma g\left(\mathbf{E}^e,\mathbf{R}\right) \quad , \quad \dot{\mathbf{R}}^p=\gamma h\left(\mathbf{E}^e,\mathbf{R}\right)$$

where g and h are prescribed constitutive functions that define the direction of the plastic flow and type of hardening; γ is a nonnegative function and obeys the Kuhn–Tucker conditions $f\le 0, \quad \gamma\ge 0, \quad \gamma f=0$.

We now further formulate the return mapping algorithm for Micromorphic plasticity with a generalized J_2 flow theory. Let the strain-based yield function be

$$f\left(\mathbf{E}^e,\mathbf{R}\right)=f\left(\mathbf{E}^e,\mathbf{\Phi},\phi\right)=\left|\boldsymbol{\xi}\right|-\left(E_Y+cH\phi\right)$$

The flow rule and hardening law follow the equations below:

$$\dot{\mathbf{E}}^p=\gamma\frac{\boldsymbol{\xi}}{\left|\boldsymbol{\xi}\right|} \quad , \quad \dot{\mathbf{\Phi}}=\gamma C_1\left(1-c\right)H\frac{\boldsymbol{\xi}}{\left|\boldsymbol{\xi}\right|} \quad , \quad \dot{\phi}=\gamma C_2 \quad , \quad \boldsymbol{\xi}\equiv\mathbf{E}^e-\mathbf{\Phi}$$

where E_Y is a critical strain value; H,C_1,C_2 are material constants; c is a constant in the range $0\le c\le 1$. There are two extreme cases: $c=1$ and $c=0$ imply isotropic and kinematic hardenings, respectively.

At time $t=t_n$, assume that the total strain, the plastic strain, and all the other internal variables are known. Then using the return mapping algorithm with $\Delta\gamma=\gamma_{n+1}\Delta t$, the exact solution can be obtained in the following procedures:

$$\tilde{\boldsymbol{\xi}}_{n+1}=\mathbf{E}_{n+1}-\mathbf{E}_n^p-\mathbf{\Phi}_n \quad , \quad \tilde{f}_{n+1}=\left|\tilde{\boldsymbol{\xi}}_{n+1}\right|-\left(E_Y+cH\ \phi_n\right)$$

$$\mathbf{E}_{n+1}^p=\mathbf{E}_n^p+\Delta\gamma\frac{\tilde{\boldsymbol{\xi}}_{n+1}}{\left|\tilde{\boldsymbol{\xi}}_{n+1}\right|} \quad , \quad \mathbf{\Phi}_{n+1}=\mathbf{\Phi}_n+\Delta\gamma C_1\left(1-c\right)H\frac{\tilde{\boldsymbol{\xi}}_{n+1}}{\left|\tilde{\boldsymbol{\xi}}_{n+1}\right|} \quad , \quad \phi_{n+1}=\phi_n+\Delta\gamma C_2$$

The exact closed-form solution for $\Delta\gamma$ is (1) $\Delta\gamma=0$ if $\tilde{f}_{n+1}\le 0$, or (2) if $\tilde{f}_{n+1}>0$, then

$$\Delta\gamma=\frac{\tilde{f}_{n+1}}{1+C_1H-\left(C_1+C_2\right)cH}$$

No restrictive assumptions about the smallness of strains or material isotropy are made in the development of this general theory.

Track V

Fluids, Thermal and Energy

V.1

Fluids, Thermal and Energy - Thermal Transport in Graphene and Carbon Nanomaterials

ID: 108

Hot phonon effect in Graphene Nanoribbon

Yanbiao Chu
Electronic Packaging Laboratory, University at Buffalo
University at Buffalo

Cemal Basaran
Electronic Packaging Laboratory, University at Buffalo
University at Buffalo

Abstract:
Nowadays, the current density in circuit increases dramatically as the size of electronic devices scales down to nano-scale. Thermomigration and electromigration under the high current density will limit the using of traditional materials in nanoelectronics. Since the single layer of graphene was produced[1], recent studies recommend graphene nanoribbon (GNR) as a replacement[2, 3].

The ultimate use of GNRs will require understanding of their electrical and thermal properties. Similar to the case of carbon nanotubes [4, 5], experimental studies indicate that high currents induce a significant overpopulation of nonequilibrium optical phonons (hot phonons) in GNR[6, 7]. These phonon modes may in turn impede transport and enhance scattering with electrons as a result of strong electron-phonon interactions [8]. However, the phonon properties and their interaction with other elementary excitations are not well understood, particularly at large electric field and high temperatures. Determination of the relaxation rate and decay path ways of hot phonons is of critical interest to both the fundamental understanding and future development of GNR devices. To get a more accurate picture, the hot phonon effect will be studied by Ensemble Monte Carlo (EMC) simulations.

References

1. Novoselov, K.S., et al., *Electric Field Effect in Atomically Thin Carbon Films.* Science, 2004. **306**(5696): p. 666-669.
2. Murali, R., et al., *Breakdown current density of graphene nanoribbons.* Applied Physics Letters, 2009. **94**(24): p. 243114-3.
3. Murali, R., et al., *Resistivity of Graphene Nanoribbon Interconnects.* Electron Device Letters, IEEE, 2009. **30**(6): p. 611-613.
4. Bushmaker, A.W., et al., *Direct Observation of Mode Selective Electron−Phonon Coupling in Suspended Carbon Nanotubes.* Nano Letters, 2007. **7**(12): p. 3618-3622.
5. Steiner, M., et al., *Phonon populations and electrical power dissipation in carbon nanotube transistors.* Nat Nano, 2009. **4**(5): p. 320-324.
6. Chae, D.-H., et al., *Hot Phonons in an Electrically Biased Graphene Constriction.* Nano Letters, 2009. **10**(2): p. 466-471.
7. Hale, P.J., et al., *Hot phonon decay in supported and suspended exfoliated graphene.* Physical Review B, 2011. **83**(12): p. 121404.
8. Meric, I., et al., *Current saturation in zero-bandgap, top-gated graphene field-effect transistors.* Nat Nano, 2008. **3**(11): p. 654-659.

Missing Abstract

ID: 252

ID:519

Thermal Conductivity Enhancement of Paraffins by Increasing the Alignment of Molecules Through Adding CNT/Graphene

Hasan Babaei
Auburn University
United States

Pawel Keblinski
Rensselaer Polytechnic Institute
United States

Jay M. Khodadadi
Auburn University
United States

Abstract:
By utilizing molecular dynamics (MD) simulations, we investigate the relationship between the crystalline structure of paraffins (n-octadecane as specific material) and its thermal conductivity and the thermal conductivity enhancement achieved by increasing the alignment of paraffin molecules in a particular direction by introducing cylindrical carbon nanotubes (CNT) and planar grapheme sheets into the paraffin. We observed that the thermal conductivity of a perfect crystalline structure in the direction of molecular axis is nearly one order of magnitude greater than the thermal conductivity value for the regular paraffin solid. Our results indicate that introducing CNT and graphene into paraffin leads to a considerable enhancement in thermal conductivity along the direction parallel to the CNT's symmetry axis or graphene plane. This happens due to the fact that these nanofillers increase the alignment of molecules along a particular direction. An alignment parameter was defined to quantitatively study the relationship between the thermal conductivity and the alignment of molecules along a particular direction. The calculations show that, generally, the thermal conductivity increases with the alignment parameter.
We considered four different systems including a regular solid pure octadecane, a perfect crystal of solid octadecane and enhanced crystals by CNT and graphene sheet additives. For all cases except the perfect crystal case, we started from liquid phases and we conducted crystallization and re-melting cycles to obtain the solid phases. Snapshots of the solid phase of all cases are shown in Fig. 1. The direct method for the determination of thermal conductivity was utilized in combination with the Non-equilibrium Molecular Dynamics (NEMD) simulation method. It should be noted that for thermal conductivity calculations, to study the size effect we replicated the systems and the thermal conductivities were obtained by extrapolating the values to infinity size. To investigate the thermal conductivity-alignment relationship, we evaluate the molecular alignment parameter, s, defined as follows

$$s = \left| \frac{\left\langle \cos^2 \theta \right\rangle - 1/3}{2/3} \right| \quad (1)$$

where θ is the angle between the end-to-end vector of individual molecules and the desired axis and $\langle\ \rangle$ indicates the average over all molecules.

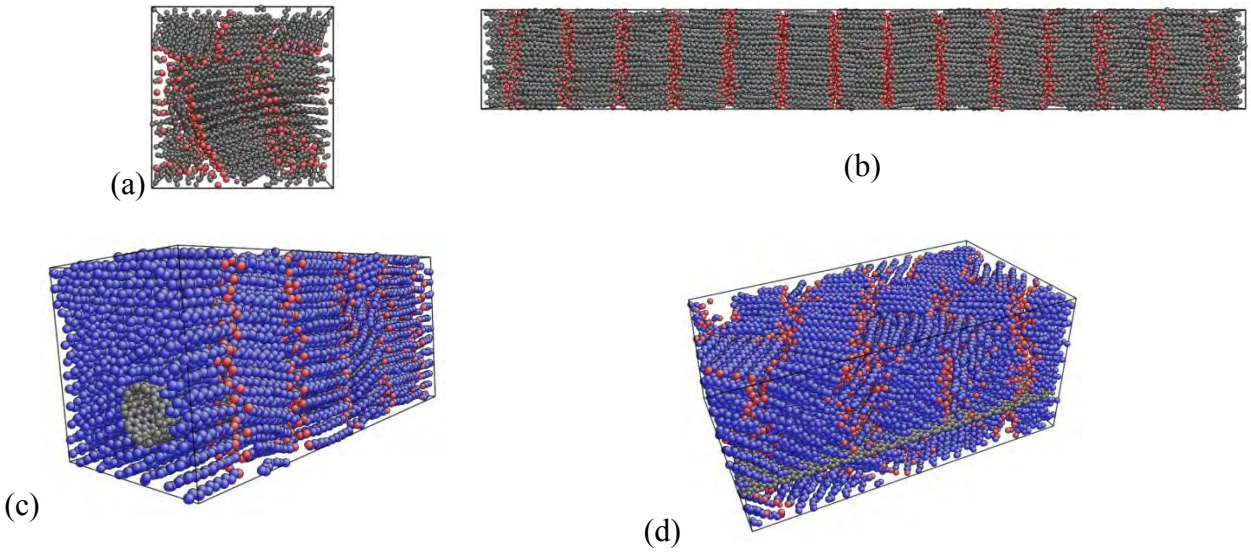

Figure 1 Snapshots of solid regular octadecane (a), perfect crystal octadecane (b), octadecane-CNT composite (c) and octadecane-graphene composite (d).

The thermal conductivity values for liquid and solid phases of all cases and the corresponding alignment parameter values are given in table 1. The predicted thermal conductivity values exhibit a strong dependency of thermal conductivity along a particular direction on the alignment parameter in that direction. The solid CNT-octadecane mixture exhibits an enhancement of 66% when compared to the pure solid. The enhancement for the liquid CNT-octadecane suspension is 48%. Also, for the graphene-octadecane mixture, the enhancement of the solid phase (87%) is higher than the liquid phase (52%). The fact that the solid mixture accommodates greater enhancement is due to significant ordering brought about by directed crystallization.

Table 1. Summary table for thermal conductivity values and alignment parameters for all cases.

Case	Phase	Temperature (K)	*k* (W/m K)	Alignment parameter
Pure	**Liquid**	300	0.164	0.02
Pure	**Solid**	270	0.30	0.15
Pure	**Perfect crystal – along molecules**	270	1.126	0.987
Pure	**Perfect crystal perpendicular**	270	0.347	n/a
CNT-mixture	**Liquid**	300	0.243	0.11
CNT-mixture	**Solid**	270	0.499	0.908
Graphene-mixture	**Liquid**	320	0.249	0.20
Graphene-mixture	**Solid**	270	0.560	0.28

V.2

Fluids, Thermal and Energy - Modeling and Characterization of Solid State Conduction and Thermophysical Properties

ID: 124

Multiscale Modeling of Heat Transfer in Cementitious Materials

Mohammad Javad Abdolhosseini Qomi
Massachusetts Institute of Technology

Franz-Josef Ulm
Not specified

Abstract:
This work addresses the physics of heat transfer in cementitious materials through via multi-scale modeling approach. At the nano-scale, the heat transfers through the inhomogeneous multi-phase texture of cement paste. Depending on the phase, the heat transfer has different mechanisms. By using Green-Kubo method in equilibrium molecular dynamics, these mechanisms are studied in both crystalline and glassy phases. The heat transfer in Calcium-Silicate-Hydrate phase is mostly described as local vibrations with short mean free paths in the order of interatomic bonds. The heat transfer in crystalline phases includes formation of phonon with long life-times and large mean free pathes. Therefore, the thermal conductivity of solid matrix of paste is described as a function of morphology of each individual combining phase. By applying the basic ideas of scale separability and micromechanics of heat transfer in porous media, the upper and lower bounds for thermal conductivity of cement paste at micron-scale are derived consequently. The concrete at the engineering scale is mixture of aggregates and cement paste. Having identified the thermal conductivity of cement paste, the effect of chemical modification of cement paste on thermal conductivity of the concrete is studied afterward. To summarize, this work provide a bottom-up multi-scale framework for identification of the effect of nano-engineering cementicious materials on macroscopic heat transfer metrics.

ID: 483

Strain Effects on Raman based Thermal Conductivity Measurements

Thomas Beechem
Sandia National Laboratories

Luke Yates

Abstract:
The performance and reliability of modern microsystems is increasingly defined not by the manner in which materials are capable of transporting charge but by the efficiency in which thermal energy can traverse the system. For example, high-performance electronics in applications ranging from data centers to electric vehicles, solid-state lighting, and even many microelectromechanical systems (MEMS) devices are known to be adversely compromised by thermal effects. As a result, experimental techniques must be available that can accurately assess the thermal environment. Interrogating the thermal environment, meanwhile, necessitates that devices be examined not only as to their level of self-heating but also that the thermal properties of the materials making up these devices be quantified as well. Raman spectroscopy is capable of meeting each of these challenges due to the technique ability to perform noncontact thermal measurements with a resolution of ~1 □‹C in a manner that is unobtrusive to device operation. The technique also provides a spatial resolution that is on par with the structures themselves (~1 *f*Êm), coupled with the ability to sample in a material-specific fashion. For these reasons, Raman thermometry is often utilized to examine self-heating in operating devices and has recently been extended to measure the thermal conductivities of materials ranging from graphene and carbon nanotubes to transparent oxides.

A popular Raman based thermal conductivity measurement implements the incident laser to not only serve as the probing □gthermometer but to heat the sample as well. Thus, by successively heating the sample to higher temperature excursions via increasing laser power, temperature is measured as a function of absorbed heat thereby allowing for the deduction of thermal conductivity. In a typical arrangement, the analyte is an extremely thin material affixed at either end. As the laser heats the material, these fixed ends arrest expansion thereby inducing compressive strain. Strain, in turn, alters most Raman temperature measurements and will therefore influence the resulting thermal conductivity deduction. In response, we quantify the degree by which strain can influence Raman based thermal conductivity measurements by analyzing the response of a variety of materials including both silicon and graphene.

ID: 576

The Effect of Copper Oxide Nanoparticles on the Effective Thermal Conductivity of Solid Eicosane-Based Phase Change Materials

Mahdi Nabil
Auburn University
United States

Jay M. Khodadadi
Auburn University
United States

Abstract:
Copper oxide (CuO) nanoparticles, stabilized by sodium oleate acid (SOA), were used to enhance the thermal conductivity of eicosane ($C_{20}H_{42}$). Eicosane ($C_{20}H_{42}$) that possesses a melting point of approximately 37°C at the atmospheric pressure was the selected base phase change material (PCM). It was shown that the CuO nanoparticles were nearly spherical-shaped and most of them had a diameter within the range of 5 to 15 nm. Nano-structure enhanced phase change materials (NePCM) samples with five different mass fractions (0, 1, 2, 5 and 10 wt%) of nanoparticles were prepared by dispersing the desired amounts of CuO nanoparticles into a 99% pure eicosane (Sigma-Aldrich, St. Louis, MO) in liquid phase followed by rigorous stirring on a hot-plate magnetic stirrer (SP131325Q, Thermo Fisher, Dubuque, IA) at 80°C for 30 minutes. No significant precipitation was visually found at the bottom of the containers, even for the most concentrated 10 wt% sample.

Upon preparation of the liquid samples, appropriate amount of colloids were immediately poured into custom-fabricated molds and a batch of the samples were placed inside a vacuum oven (Fischer Scientific, Isotemp® Vacuum Oven Model 281A) for at least 20 hours. The oven was operated at -40 kPa gage at a set temperature of 65 °C in order to degas the samples. The aluminum molds were machined disks with a diameter of one inch and height of 0.375 inches. Before pouring the colloid samples, detachable aluminum molds (diameter of 1 inch) was pressed into the machined aluminum molds using a custom-designed molding handle. Upon removing the samples from the oven, phase transition of the liquid samples was realized by subjecting them to one of three procedures that follows. One batch was allowed to solidify at the ambient temperature of the laboratory. The second batch was prepared by placing the metallic tray that supported the molds in the oven directly in contact with an ice-water bath. The third one was left in the oven to solidify there under no vacuum (ambient pressure) and high initial temperature of oven which was turned off. Thus, three distinct batches were obtained that differed only in their phase transition route. Upon completion of solidification (at least 5, 30, and

240 minutes for the ice-water bath, ambient temperature and oven solidification methods, respectively), the samples were easily removed from the aluminum sheet. For each particle concentration, a pair of samples was available for testing.

Thermal conductivity measurements of these samples were performed using the transient plane source (TPS) technique. The data were obtained by utilizing a Hot Disk Thermal Constants Analyzer (TPS 500, Hot Disk AB, Gothenburg, SWEDEN) based on the TPS technique. This instrument offers rapid means of measuring the thermal conductivity with the measurement time being as short as 2.5 s. With the aid of a controllable temperature bath, measurements were conducted at various temperatures between 10 and 35°C for the solid samples. At each temperature, three different runs were performed and the standard deviation of data was less than 1.4%. Measured thermal conductivity data of the composites were found to be nearly independent of the measurement temperature for a given loading of CuO nanoparticles regardless of the solidification scheme. Irrespective of the solidification method, as the melting temperature was approached, thermal conductivity data of the solid disks rose sharply for the three sets of experiments. The composites prepared using the ice-water bath solidification scheme consistently exhibited the lowest values of thermal conductivity, while the samples which solidified in the oven showed the highest values. The measured thermal conductivity values for the most concentrated samples (10 wt%) of all three different methods of solidification are shown in the Figure below.

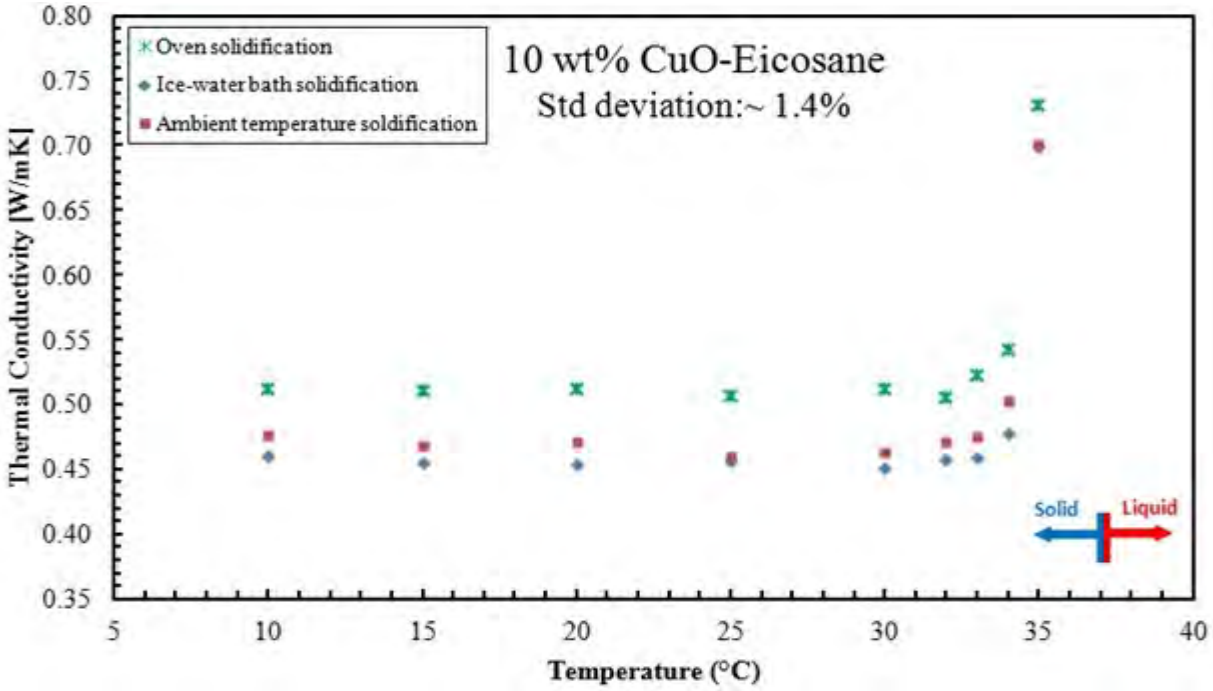
Oven solidification
Ice-water bath solidification
Ambient temperature soldification
10 wt% CuO-Eicosane
Std deviation:~ 1.4%
Solid
Liquid
Thermal Conductivity [W/mK]
Temperature (°C)
0.80
0.75
0.70
0.65
0.60
0.55
0.50
0.45
0.40
0.35
5
10
15
20
25
30
35
40

ID: 621

Phonon Transport Analysis at Graphene-Metal Interface

Liang Chen
G.W. Woodruff School of Mechanical Engineering
Georgia Institute of Technology
United States

Zhen Huang
International Business Machine
United States

Satish Kumar
G.W. Woodruff School of Mechanical Engineering
Georgia Institute of Technology
United States

Abstract:
Graphene, a prominent nano-material for future electronics, has exceptional electronic, thermal and mechanical properties. Phonon transport at graphene nano-contacts in its electronic devices is critical for the efficient thermal management of graphene based nano-electronics. Thermal transport at graphene-metal contact becomes particularly important in short channel field effect transistors [1] and graphene-Cu hybrid-interconnects [2] where the metal contact can turn into a crucial heat removal pathway. Therefore, a good understanding of phonon transport at the graphene-metal interface is essential for the development of graphene based nano-electronics.

In this study, we consider a single layer graphene sandwiched between two (1 1 1) surfaces of Cu to explore interface thermal interactions (Fig. 1). Density functional theory (DFT) calculations and atomistic Green's function (AGF) approach [3, 4] have been considered to simulate interface phonon conductance. A supercell of graphene residing on Cu substrate is used in VASP package for DFT simulations. The harmonic matrices used in the AGF calculations were constructed using the force constants obtained from the DFT calculations [5]. The distance between graphene and Cu substrate is first optimized and then the force constants are calculated by displacing atoms. Phonon dispersion relations and density of states (DOS) are obtained using lattice dynamics calculations. The calculated results of phonon dispersions and DOS are shown in Fig. (2). A distinct phonon spectra mismatch is observed between Cu and graphene. The phonon modes in Cu are below 8 THz while phonons in graphene are dominated by modes above 8 THz.

The force constants calculated from the DFT simulations and the developed AGF based model will facilitate the estimation of the phonon transmission coefficients and interfacial thermal conductance across the Cu/graphene/Cu interface. The phonon transmission function will show the coupling between phonons of different frequencies in Cu/graphene/Cu system. In addition, the effects of interaction strength on the thermal conductance can be studied by varying the equilibrium distances between graphene and Cu.

References

[1] Liao, A. D., Wu, J. Z., Wang, X. R., Tahy, K., Jena, D., Dai, H. J., and Pop, E., 2011, "Thermally Limited Current Carrying Ability of Graphene Nanoribbons," Phys Rev Lett, 106(25), p. 256801.

[2] Yu, T. H., Liang, C. W., Kim, C., Song, E. S., and Yu, B., 2011, "Three-Dimensional Stacked Multilayer Graphene Interconnects," IEEE Electr Device L, 32(8), pp. 1110-1112.

[3] Huang, Z., Fisher, T. S., and Murthy, J. Y., 2010, "Simulation of phonon transmission through graphene and graphene nanoribbons with a Green's function method," J Appl Phys, 108(9), p. 094319.

[4] Zhang, W., Fisher, T. S., and Mingo, N., 2007, "Simulation of interfacial phonon transport in Si-Ge heterostructures using an atomistic Green's function method," J Heat Trans-T Asme, 129(4), pp. 483-491.

[5] Hafner, J., 2008, "Ab-initio simulations of materials using VASP: Density-functional theory and beyond," J. Comput. Chem., 29(13), pp. 2044-2078.

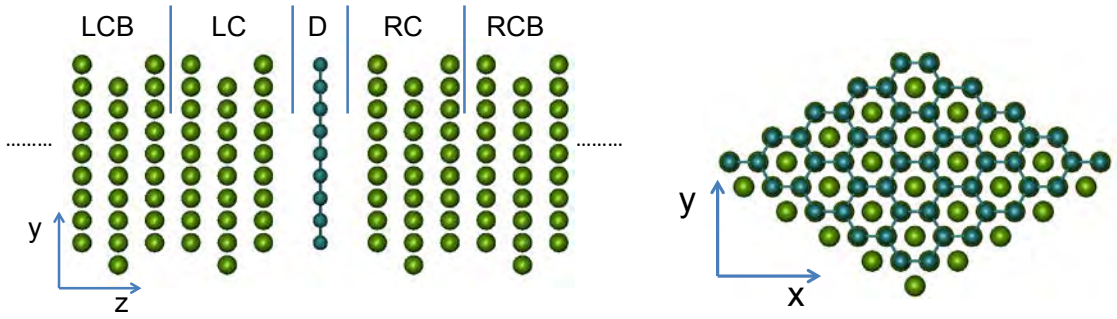

Figure 1. Schematic diagram of the single layer graphene sandwiched between two Cu (1 1 1) layers. (a) y-z plane; and (b) x-y plane.

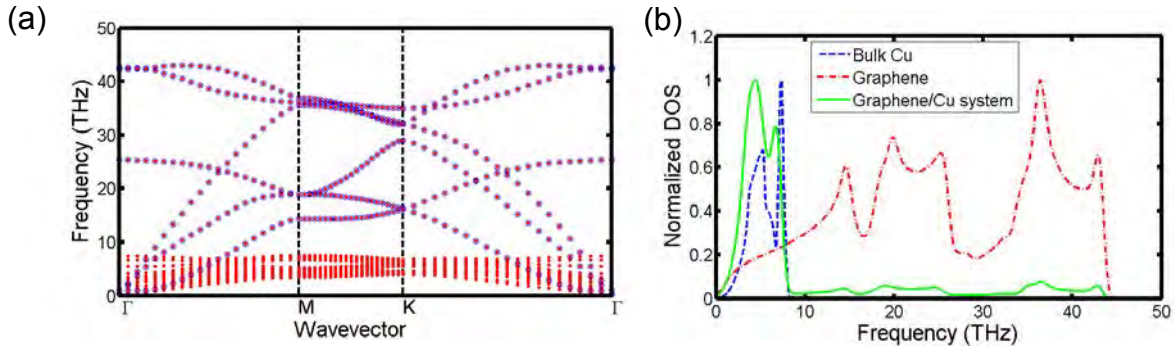

Figure 2. (a) Phonon dispersion relation of graphene sandwiched between two Cu layers. The blue circles show the modes in graphene, and the red dots show the modes in Cu; (b) Phonon density of states in bulk Cu, graphene, and graphene/Cu system.

ID: 731

Temperature at Nanoscale: A Wave-Diffusion Duality

Xianqiao Wang
The George Washington University

James Lee

Abstract:
NO ABSTRACT

V.3

Fluids, Thermal and Energy - Fluid Mechanics in Biological Systems

ID: 462

Water Nano-Hydrodynamics: The Interplay between Interfacial Viscosity, Slip and Chemistry

Hsiang-Chih Chiu
School of Physics
Georgia Institute of Technology
United States

Deborah Ortiz
School of Chemistry and Biochemistry
Georgia Institute of Technology
United States

Suenne Kim
School of Physics
Georgia Institute of Technology
United States

Elisa Riedo
School of Physics
Georgia Institute of Technology
United States

Abstract:

The understanding and the ability to manipulate fluid flows in nano-confined geometries are important for several research fields such as polymer science, biology and geophysics. In this work, we present experiments demonstrating that the boundary viscosity of water strongly depends on the wettability of the confining surfaces using an Atomic Force Microscope. The observed dependence can be fully understood by considering the slippage of water at the stationary solid surface. The boundary viscosity of confined water as a function of the gap size for five surfaces with different wettability is fitted with a modified form of the Newtonian definition of viscosity, which takes the fluid slip into consideration. This simple relationship can explain our data and allows us to extract a “slip parameter” for each studied surface. The obtained slip parameter is found to increase with the static contact angle of the surface, bringing further evidence to the relationship between viscosity and slip.

V.4

Fluids, Thermal and Energy - Energy Utilization in Buildings and Building Mechanical Systems

ID: 125

Modeling Energy Transfer at the Scale of Cities

Mohammad Javad Abdolhosseini Qomi
Massachusettes Institute of T echnology

Jameson Toole
Not specified

Abstract:
Space heating and cooling is a significant source of energy consumption in cities. At this scale, consumption is a function of a city population, density, demand, climate, and the thermal characteristics of individual buildings. More specifically, a structures R-value, heat capacity, infiltration rate, and emissivity are crucial for determining energy loss. By application of the principle of energy conservation, the thermal behavior of each building describes the way a building receives and transfers energy with surrounding buildings and the atmosphere. This leads to an interlocked multi-million degree of freedom problem which is computationally intractable to solve even when assuming a-priori knowledge of each house thermal parameters. This problem can be resolved by analogy to atomistic simulation methodologies. We present an inter-building energy consumption function (analogous to inter-atomic potentials) that describes the energy loss of a building as a function of its own thermal characteristic as well as interactions with surround structures. The undetermined nature of thermal properties leads to a statistical form for the energy consumption of a building. Having access to the topology of cities through public census and parcel data, we predict the heating and air-conditioning energy consumption of a city utilizing a coupled statistical-mechanical approach. Within a margin of uncertainty, this model predicts the impact of applying refurbishing and insulation techniques and policies on the energy consumption at the scale of cities.

ID: 542

Numerical Investigation of Solidification and Melting Under the Presence of Voids in Thermal Energy Storage Composites

Mahmoud Moeini Sedeh and Jay M. Khodadadi
Auburn University
United States

Abstract:
Impregnation of phase change materials (PCM) into high thermally-conductive porous structures occurs during the infiltration process to produce thermal energy storage (TES) composites with high effective thermal conductivity. Depending on the PCM properties and structure of the pores, the infiltration process can lead to formation of voids in the form of stable air pockets or bubbles inside the TES composites (figure 1). In TES composites, not only any portion of the void affects the energy storage capacity, but also it influences the thermal and phase change behavior during the subsequent charge/discharge cycles due to different thermal properties of air pockets in comparison with the infiltrated PCM or porous structure. Therefore, it is essential to investigate the effect of voids on phase change behavior (i.e. solidification and melting) of latent heat TES composites.
In complementing the recent work by the investigators devoted to modeling of the infiltration of PCM into graphite foams and prediction of voids, numerical investigations of solidification and melting of PCM infiltrated into a graphite pore were conducted in the presence of a void. Using the Volume-of-Fluid (VOF) method, multiphase flow and thermal simulations were performed to investigate the effect of the void on the solidification and melting processes. Due to the size of the pores in porous structure, surface tension plays a significant role compared to gravity, pressure gradient and thermally-induced driving forces.
Starting from results of previous work, the final state of the infiltration process (figure 1c) with two phases of liquid PCM and air (as the *infiltration void*) was considered as the initial state of solidification. The enthalpy-porosity method was used in combination with the VOF method to simulate the freezing and melting of the PCM in presence of the void. Thermal boundary conditions were set based on the PCM properties. During the solidification, liquid PCM starts freezing next to the walls of the pore and as a result three physical phases of solid, liquid and gas were present (figures 2a and 2b). Finally, the whole liquid PCM available inside the pore solidified (figure 2c) and led to formation of an additional void known as the *shrinkage void* caused by the difference in densities of liquid and solid PCM (figure 3).
Then, thermal boundary conditions were set for simulation of the melting process. The initial two phases at the start of melting are the solid PCM and air. During melting, flow currents due to natural convection and possible sinking of the remaining solid PCM due to its higher density compared to the liquid PCM might occur when the gravitational and interfacial forces are of the same order of magnitude (figure 4).
For verification, the infiltration process of wetting liquids was found to be in agreement with the experimental measurements. Furthermore, the obtained volume of shrinkage void was 1.4 percent (by area) for this case (figure 3c), that in comparison with the theoretical volume change of PCM due to density change (corresponding to 1.3 %) was in good agreement.

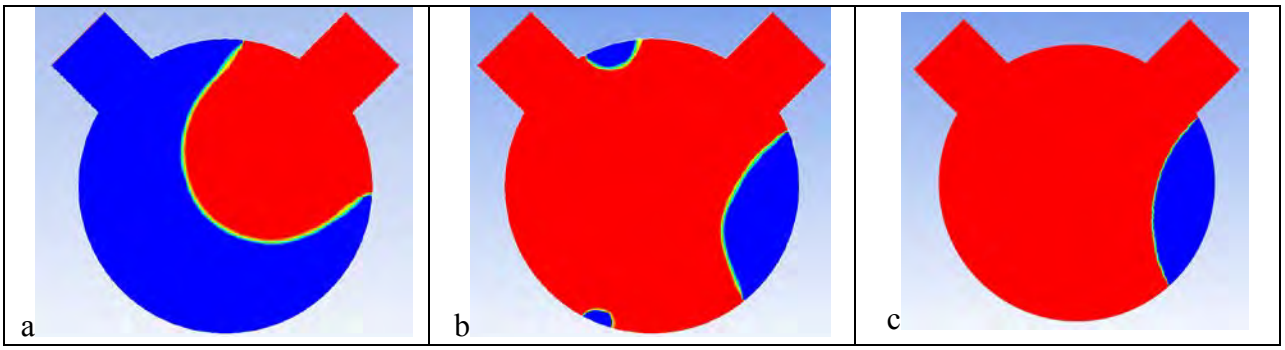

Figure 1 Contours of volume fraction during the infiltration of the pore and formation of stable 'infiltration' void (in blue color, 9.8 %) for wall contact angle of 90°

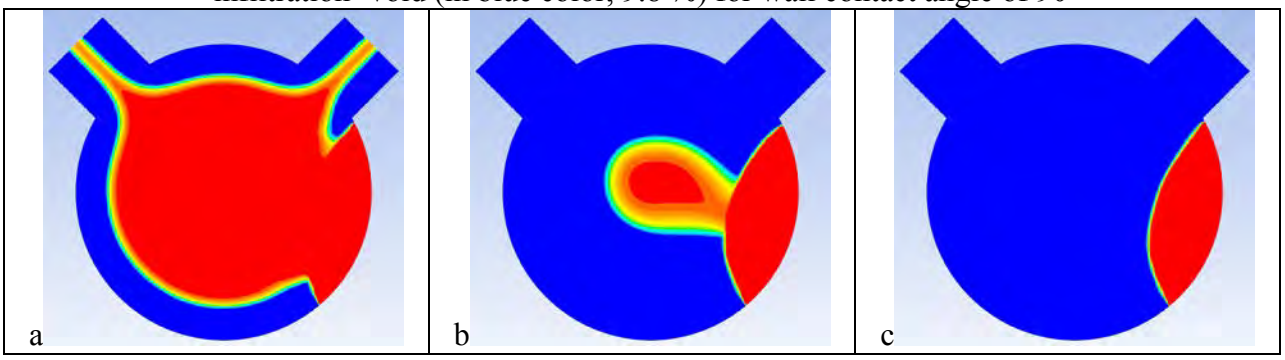

Figure 2 Contours of liquid fraction during the solidification of liquid (PCM) within the pore during the charge/discharge (freezing/thaw) cycles and total void of 11.1%

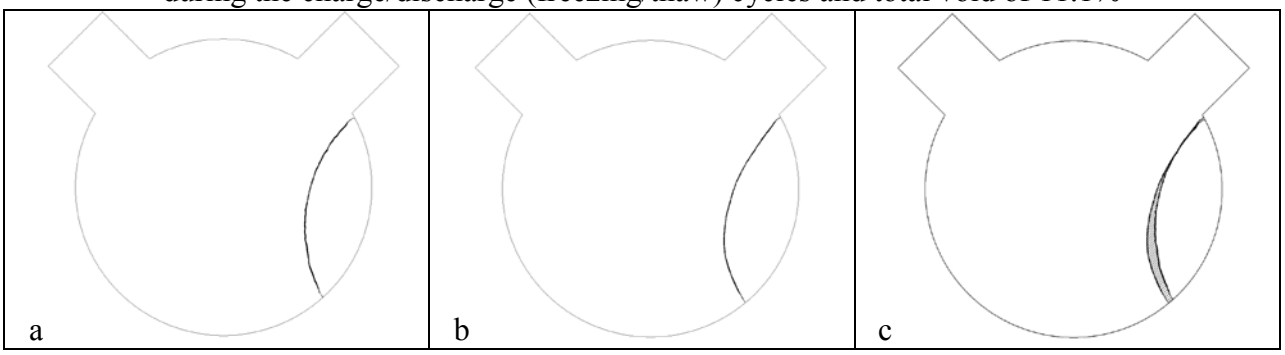

Figure 3 Final interface positions and formation of void (a) after infiltration, (b) after solidification and (c) shrinkage void due to solidification (shaded area, 1.3%)

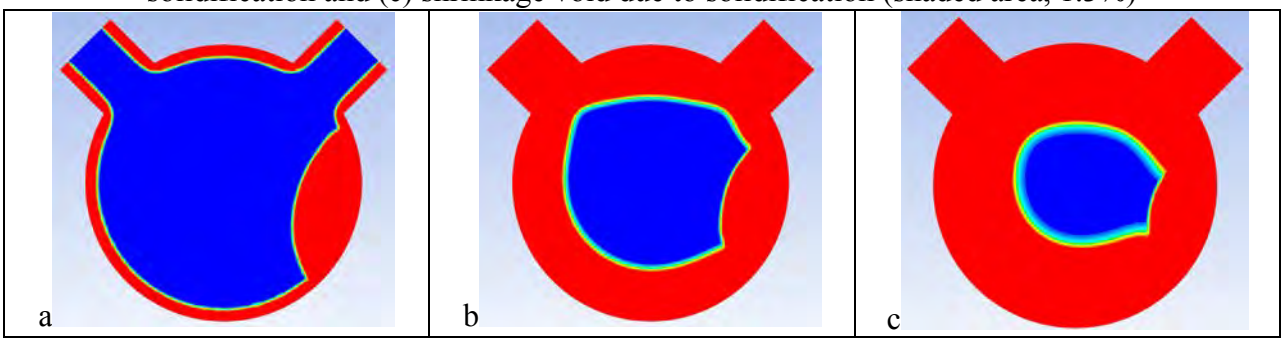

Figure 4 Melting of frozen PCM after solidification process within the pore during the charge/discharge (freezing/thaw) cycles of TES composites utilization

ID: 805

Effect of the Thermophysical Properties of Nanoparticles on Solidification of Colloid Suspensions

Yousef M. F. El Hasadi
Mechanical Engineering Department, Auburn University
USA

J. M. Khodadadi
Mechanical Engineering Department, Auburn University
USA

Abstract:
Nanoparticle-enhanced phase change materials (NePCM) were proposed recently as alternatives to traditional phase change materials due to their enhanced thermophysical properties. In this study, the effect of using nanoparticles with different properties, on the morphology of the solid-liquid interface and the evolving concentration field during solidification was investigated numerically. The numerical method that has been used was based on the one-fluid-mixture model. The model takes into account the thermal as well as the solutal convection effects. A model square cavity was used in the simulation. Three different NePCM suspensions were used for the current study, and those are the copper (Cu)-water, alumina oxide (Al_2O_3)-water, and copper oxide (CuO)-water suspensions. The suspensions with the nanoparticle diameters of 5nm and 2nmwere solidified from the bottom of the cavity. The temperature difference between the hot (top) and cold (bottom) sides was 5 degrees centigrade and the loading of the nanoparticles that have been used in the simulation was 10% by mass. The results obtained from the model were compared with those existing in the literature, and the comparison was fair. The solid-liquid interface for the case of NePCM with 5 nm particle size was planar throughout the solidification process for the three suspensions used in the study as shown in Figure 1. However, for the case of the NePCM with particle size of 2 nm, the solid-liquid interface evolved from planar stable shape to an unstable dendritic structure, as the solidification process proceeds with time as it is illustrated in Figure 2. This was attributed to the constitutional supercooling effect. The shape and the distribution of the dendrites are different depending on the nanoparticle type that was usedas shown in Figure 3. The thermo-solutal convection cells are clearly seen for the case of aluminum oxide (Al_2O_3) NePCM. This can be attributed to the lower density if it is compared to that of copper (Cu), and copper oxide (CuO) nanoparticles. It was also found that the concentration of the copper (Cu) nanoparticles on the liquid side of the interface was higher if it is compared with other two nanoparticles used in the study.

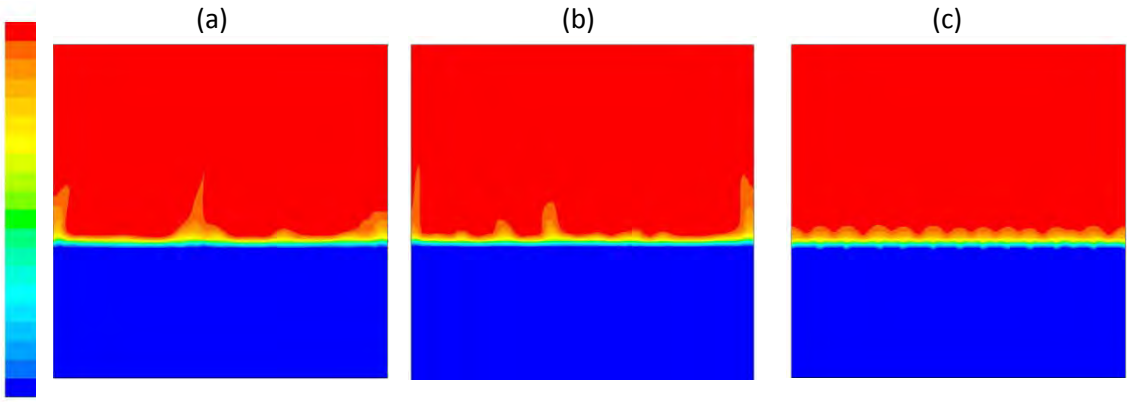

Figure 1 Liquid fraction field after 1000s, and particle size of 5nm for (a) CuO-water suspension, (b) Al_2O_3-water suspension and (c) Cu-water suspension..

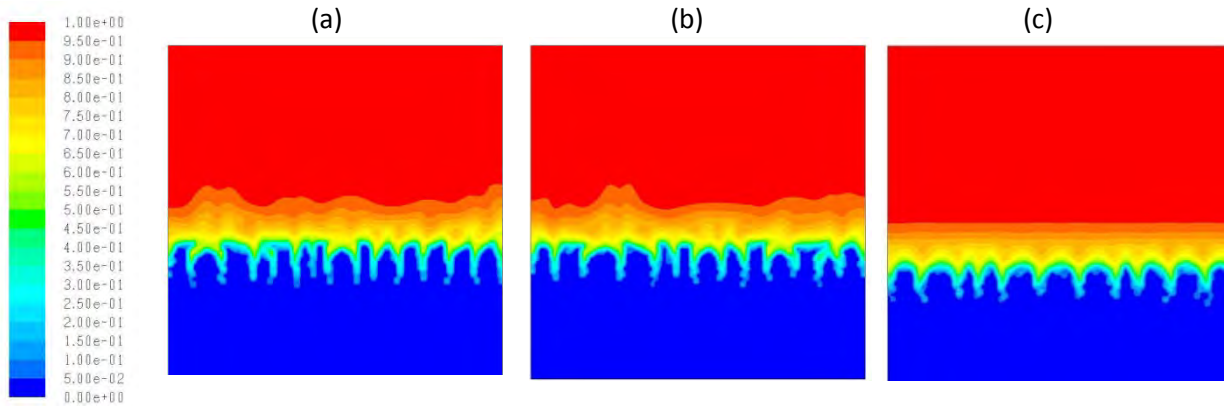

Figure 2 Liquid fraction field after 1000s, and particle size of 2nm for (a) CuO-water suspension, (b) Al_2O_3- watersuspension and (c) Cu-water suspension.

(a) (b) (c)

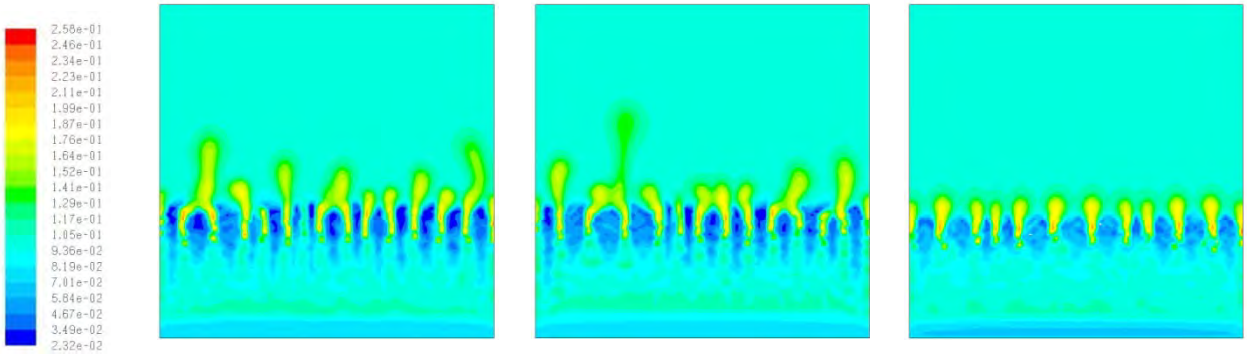

Figure 3 Concentration field after 1000s, and particle size of 2nm for (a) CuO-water suspension, (b) Al_2O_3–suspension and (c) Cu-water suspension.

ID: 570

Optimization of Microencapsulated Phase Change Materials in Gypsum Wall Boards

Matthew Perrella
Auburn University
United States

J. M. Khodadadi
Auburn University
United States

Mahmoud Moeini Sedeh
Auburn University
United States

Abstract:

Phase change materials (PCM) have been utilized extensively for thermal energy storage and insulation due to their high latent heat and variable melting temperatures. Currently, the most promising work being conducted with PCM involves the encapsulation of the phase change materials with a polymer or resin coating, which helps to protect the PCM from the surrounding environment and also increases the exposed surface area. Micro-encapsulated phase change materials (MEPCM) offer a distinct advantage over larger PCM capsules because they can be mixed or dispersed into almost any medium with little concern of physical damage or reactivity. For this reason, they have gained popularity as an additive to common building materials to increase their thermal storage capacity and reduce energy consumption during daily cooling and heating cycles.

In this experiment, commercial microencapsulated paraffin wax was used to enhance the thermal storage capacity of gypsum tiles. Four (4) tiles of different compositions were made to serve as analogues for common sheetrock or drywall building material. The first tile was pure gypsum plaster with no PCM enhancement. The second tile contained 10% PCM by total weight evenly dispersed throughout the plaster matrix. The third contained 20% PCM by total weight also evenly dispersed. The fourth tile consisted of two layers. The first layer was pure gypsum plaster, and the second contained 10% PCM by total weight. Both layers were of uniform thickness and together made a single tile of the same thickness as the other samples. A small control volume with an internal heating source was used to simulate hot, outdoor conditions, while the conditioned lab space simulated a conditioned space. Each tile was fitted onto one side of the control volume and subjected to a temperature gradient of approximately 22 to 37˚C. The double-layered tile was tested twice with each side facing the heat source and the conditioned space. Surface and ambient temperature measurements were taken as each sample was allowed

to warm steadily until reaching a steady state. The temperature measurements from each sample were then compared to see what effect the PCM enhancement had on the gypsum tiles' thermal performance (Figure 1).

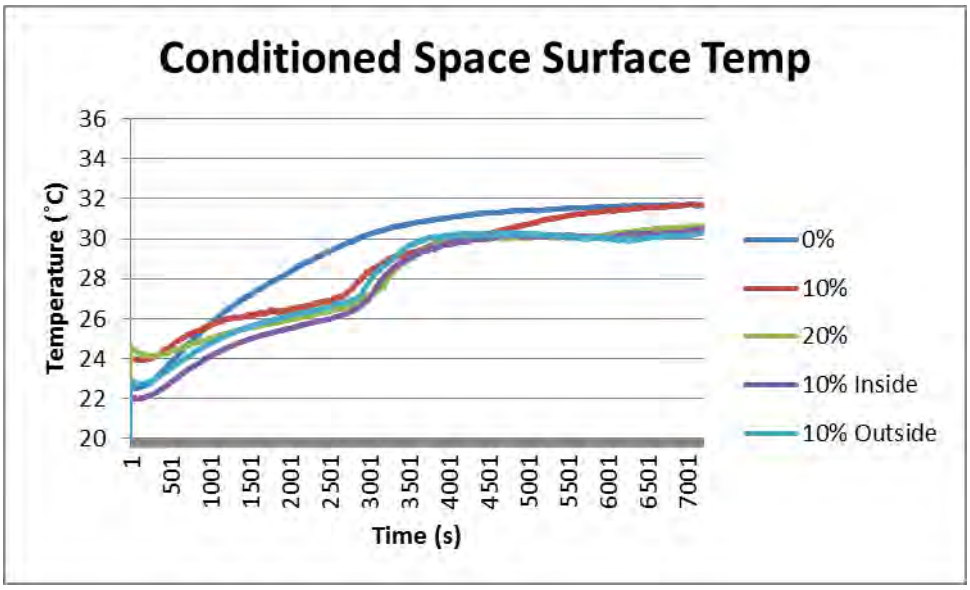

Figure 17: Conditioned Space Surface Temp

When assessing the performance of a MEPCM-enhanced wallboard, two characteristics are of particular importance, namely the *decrement factor* and the *time lag*. The *decrement factor* is the ratio of the maximum surface temperature adjacent to the conditioned space of the non-enhanced wallboard to the enhanced wallboard. The *time lag* is the difference in time between when the enhanced and non-enhanced wallboards reach their maximum conditioned surface temperature. A high decrement factor and time lag indicates that the PCM was successful in absorbing enough thermal energy to reduce the total heat infiltration into the conditioned space. The analysis of experimental results showed that for each MEPCM-enhanced configuration, the addition of MEPCM was effective at delaying the plaster tile from attaining its maximum surface temperature, but did not greatly reduce the maximum surface temperature. This is likely due to the fact that wallboards were only exposed to a maximum air temperature to simulate hot weather conditions, but they were not subjected to a complete daytime/nighttime heating and cooling cycle. Experimental data also indicated that a plateau in surface temperature occurs at the melting point of the PCM. This further indicates that the MEPCM incorporated in the wall board is absorbing thermal energy as it is passing through the gypsum plaster. These results indicate that MEPCM holds significant promise as an energy saving implement in passive heating/cooling applications. With further investigation, it would be possible to determine the exact amount of heat that can be absorbed by a particular configuration and further specialize PCM-enhanced wallboard for energy saving applications.

Track VI

Mechanics of Structures

VI.1

Mechanics of Structures - Dynamics of Thin, Flexible Members

ID: 123

VIBRATION OF THIN WALLED BUCKLED BOX BEAM WITH A CRACK

PATANELLA, Alejandro J. (UID GEMA Aeronautical Department, School of Engineering, Universidad Nacional de La Plata, Argentina)

ACTIS, Marcos D. (UID GEMA Aeronautical Department, School of Engineering, Universidad Nacional de La Plata, Argentina)

Abstract:

The purpose of this research is to analyze the influence of a crack on a thin walled buckled box beam structure in its vibration characteristics using analytical models and a specified method of analysis. Results from these methods and models are compared with experimental set ups. The differences in the determination of natural frequencies of a healthy structure and the same structure but with the presence of the crack are shown and quantified. This phenomenon is studied with buckling conditions with a completely developed diagonal tension field on the lateral skin of the box beam. The methodology and models for determining the natural frequencies in a lightweight structure which is working on a non-linear (buckling) regime with the presence of a crack can be extended to other configurations.

Thin Walled Box Beam

A structural configuration similar to the one used by *Actis et al [1]* was chosen *(see Figure 1)*. Only the effect of a crack in the station closer to the fix points is considered for the purpose of this research, but the same procedure can be extended to any station. The crack produces an increment in the local flexibility of that station. The case under analysis corresponds to the one with a perpendicular crack to the diagonal tension field in station closer to the fixed end.

The model proposed by *Patanella (ref [3])* is used. The rigidity of a plate buckled under a fully developed diagonal tension field is reduced in 30% with the presence of a 40 mm crack.

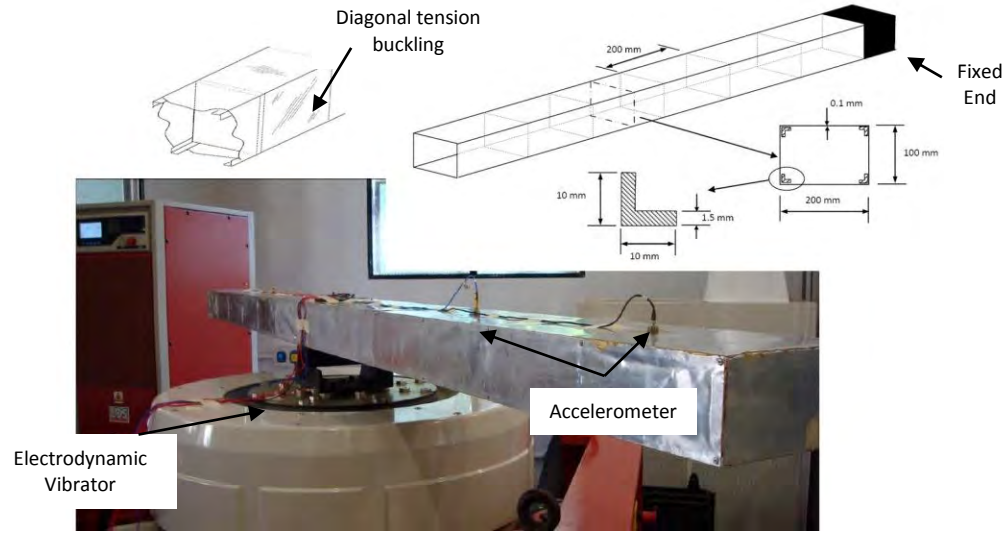

Figure 1.- Geometrical and experimental setup

Experimental determination of the box beam natural frequency

A dynamic study based in the stationary dynamic state (sine swept) is chosen due to the complexity of the structure. The thin walled box beam has several individual components that can hide the real response of the whole structure using a transient state technique (impulse test).

The box beam is placed in an electrodynamic vibrator *LDS model V875-440-LPT750-SPA40K*. Two accelerometers *Endevco ISOTRON 2256A-100* are placed on the top face of the beam (see *Figure 1*) and a sine swept of *1 octave/minute* with a *2 g* peak acceleration is done up to *1000 Hz*. The geometry of the beam was reflected by symmetry to minimize the influence of a lack in the rigidity at the fixed point. In that case, the box beam is doubled in length to balance mass and to avoid any rotation at the fixed point. (see *Figure 1*).

Results comparison and Conclusions

Experimental results are compared against analytical ones. In the case of the box beam without a crack they are compared with the ones obtained using the model proposed by *Actis (ref [2])*. In the case of the box beam with a crack they are compared using the model proposed by *Patanella (ref [3])*. The results of those comparisons show a difference not bigger than 12% (see Table 1). The results obtained through several tests shows a good correlation between the analytical models and the ones obtained experimentally. This shows that the proposed models can be used in such structural configuration, widely used in light aluminum construction, under a nonlinear state (buckled).

Table 1.- Results comparisons

	Beam without a crack			Beam with a 40 mm crack near fixed end		
Order	Frequency Model (Hz)	Frequency Experimental (Hz)	Difference %	Frequency Model (Hz)	Frequency Experimental (Hz)	Difference %
1	52.5	46.8	10.9%	52.37	45.9	12.4%
2	253.6	249.7	1.5%	247.5	226.5	8.5%

This research shows how a crack affects the dynamic characteristics of a thin walled buckled semimonocoque structure. An analytical model is proposed to introduce the damage in the lateral skin of the box beam nearest to the fixed edge. The model is used when the top and bottom plates are buckled under compression and the lateral one under a fully developed diagonal tension field. The model proposed was experimentally validated at first stage obtaining differences not bigger than 4% under simpler structural configurations, then, it is extrapolated to a complex structure.

After complex theoretical analysis a practical and simple methodology was found and its application both validated to a specific problem.

References

[1] M. Actis, A. Patanella, “Flexión en una viga cajón semimonocasco debido a la presencia del pandeo”, 1er Congreso Argentino de Ingeniería Aeronáutica (CAIA – 2008), La Plata, 2008

[2] Actis, Marcos D., “Estudio de la Variación de Propiedades Mecánicas de Estructuras de Paredes Delgadas ante la Presencia de Inestabilidades Elasto-Plásticas”, Tesis de Doctorado, UNLP, 2007.

[3] Patanella, Alejandro J. , “Variación de Propiedades Dinámicas de Estructuras de Paredes Delgadas ante la Presencia de Daño”, Tesis de Doctorado, UNLP, 2010.

ID: 720

Wave-Based Stability Analysis of Slender Frames

Michael Leamy
Georgia Institute of Technology
USA

Abstract:
This work reports a wave-based analysis approach for predicting static buckling instabilities in slender columns and frames. It builds upon recent work on the wave-based vibration analysis of frame-like structures modeled by Timoshenko beams. To predict buckling, axial preload modeling is included in the equations of motion and the wave-based analysis approach is reformulated accordingly. This reformulation includes development of reflection and transmission matrices for a general, four-member angled joint. An eigenvalue problem (EVP) is then solved for example systems by setting the frequency of the wave solutions arbitrarily close to zero while seeking the axial preload which zeroes the EVP determinant. Numerical conditioning of the EVP problem is discussed as an essential step for ensuring successful application of the method. Notably, the method allows exact solutions to parameterized systems to be computed quickly and easily without the need for special discretization or mesh generation. This is exploited, for example, to find the optimal cross-brace location for a slender H-frame by varying a single parameter in the EVP determinant, avoiding the need to regenerate geometry and/or discretization (e.g., mesh topology). For a conservatively-loaded column, and for example portal and H-frames, results from the introduced approach show excellent agreement with known solutions.

VI.2

Mechanics of Structures - Nonlinear Dynamics of Multifunctional Composite Structures

ID: 83

Modelling of a Multifunctional Composite Structure with Electrical Energy Storage Capability

First Author
H Sreedhara
National Aerospace Laboratories

Second Author
Dineshkumar Harursampath

Abstract:

The present work targets a specific category of multifunctional composites, wherein electrical energy storage functionality is integrated into the load bearing structure. Apart from kinetic energy in a dynamic application, such materials exhibit/store more than one type of energy, such as elastic, electrical, chemical, thermal etc. The formulation begins with the derivation of a free energy density functional, which depends on several independent applied fields,which are coupled to the material behavior through a set of multi-field constitutive relations. The total Helmholtz free energy density along with the physical constraints, introduced through Lagrange multipliers, constitutes the Lagrangian. The resulting functional reaches a minimum at equilibrium. Numerical solution to this 3-D multi-science problem is computationally demanding. Hence, the small parameters natural to the geometry and physics are identified from the problem definition and asymptotically correct solutions are derived, by employing the Variational Asymptotic Method (VAM) for a plate-shaped battery. The dimensionally reduced multi-field constitutive law, thus derived, exhibits the fully coupled electro-chemical and thermo-mechanical responses to the various combinations and directions of applied field types. The solution for a generic 3-D plate-battery problem is obtained through 1-D linear through-the-thickness and 2-D nonlinear reference plane analyses in the framework of VAM.

ID: 175

An Experimental Method to Validate a Gradient-damage Model for Viscoplastic Plates under Shock Waves

An Danh Nguyen
Institute of General Mechanics, RWTH-Aachen,
Templergraben 64
Germany

Marcus Stoffel
Institute of General Mechanics, RWTH-Aachen,
Templergraben 64
Germany

Dieter Weichert
Institute of General Mechanics, RWTH-Aachen,
Templergraben 64
Germany

Abstract:
This work aims to establish both a numerical and experimental methodology to validate a gradient-damage model [1,2,3,4] for shock-wave loaded plates [5]. For a finite element computation, the model is formulated by introducing a gradient-enhanced free energy. This enhancement gives rise to an introduction of gradient parameters *c(l)* in terms of a substructure related intrinsic length-scale and a relationship between non-local and local damage variable. To identify the physical damage length scale *l*, micro-bend and micro-tensile tests are performed. Using the proposed gradient-enhanced free energy, the method of Stölken and Evans (1998) [6,7,8] is adopted to determine the length scale *l* by using the micro-bend tests (Fig. 1).

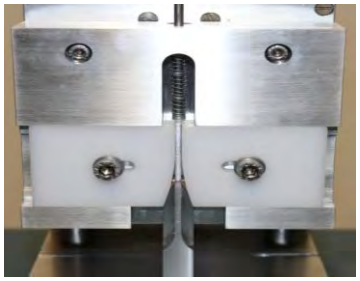

Fig. 1: Micro-bend test

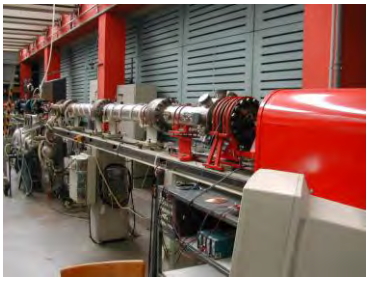

Fig. 2: Small shock tube [5]

Fig. 3: Big shock tube [5]

The gradient damage parameter *c(l)* is then identified by solving the inverse problem in finite element simulations in comparison with the global displacement-force curves obtained from shock-tube tests on small copper plate specimens (Fig.2). Here a copper plate with 138 mm diameter is subjected to shock waves in a small shock tube leading to viscoplastic deformations

of the plate specimen. After all material parameters have been identified, shock-tube tests on larger plate specimens of 553 mm diameter (Fig. 3) are set up to validate the entire finite element model. The performance of the proposed approach is illustrated through numerical and experimental results.

References

[1] A.D. Nguyen, M. Stoffel, D. Weichert, A gradient-enhanced damage approach for visco-plastic thin-shell structures subjected to shock waves, Comp. Meth. App. Mech. Eng. 217-212: 236-246, 2012.
[2] Y. Basar, D. Weichert, Nonlinear continuum mechanics of solids, fundamental mathematical and physical concepts, Springer, 2000.
[3] B.J. Dimitrijevic, K. Hackl, A method for gradient enhancement of continuum damage models, Tech. Mech. 28(1): 43-52, 2008.
[4] J. Velde, U. Kowalsky, T. Zümendorf, D. Dinkler, 3D-FE-analysis of CT-specimens including visco-plastic material behaviour and nonlocal damage, Comp. Mat. Sci. 46: 532-357, 2009.
[5] M. Stoffel, An experimental method for validating mechanical models, Mechanik Berichte Nr. 5, RWTH-Aachen, 2007.
[6] Stöken J.S., Evans A.G. (1998). A microbend test method for measuring the plasticity length scale. Acta mater., 46: 5109-5115.
[7] M. Kuroda, Lecture-2: Experimental study of the size effects, Plasticity and beyond: Microstructures, crystal plasticity and phase transformations, Udine, June 27-July 1, 2011.
[8] Hayashi I., Sato M., Kuroda M. (2011). Strain hardening in bent copper foils. J. Mech. Phys. Sol., 59 (9): 1731–1751.

Missing Abstract

ID: 207

ID: 269

Dynamic Response of Composite Structures Subjected to Low Velocity Impact

Fedor Antonov
Research Institute of Mechanics Lomonosov Moscow State University
Russia

Marina Ryazantseva
Research Institute of Mechanics Lomonosov Moscow State University
Russia

Abstract:
It is known that structural elements of modern aerospace engineering constructions are designed and produced using composite materials. The most applicable modules of such structures are thin layered shells made of composite materials. In the course of regular maintenance, calibration and repair, such structures may be conducted to different low-velocity impact events. That is why the problem of stress and damage (residual strength) analysis of multilayered composites occurres in the real spectrum of operational and accidental impacts. The complex approach to the investigation of dynamic behavior of multilayered composite structures is developed suggesting a direct computer modeling in conjunction with the verification experiments and development of new dynamic models of layered structures.

1. Determination of damage and residual strength of a layered composite elastic plate under low-velocity impact event.

The residual strength calculation at low velocity impact event consists of two stages. At the first stage the degradation of strength and stiffness properties of material is determined and the size of the delamination area is calculated. At the second stage the parameters of the damaged material failure criterion are determined and the static strength of the structure subjected to low-velocity impact is estimated. The evaluation of residual strength is carried out by comparing the ultimate strength of the damaged and undamaged samples under compression. The verification of calculation methods, failure initiation criteria and damage evolution law is performed by comparing the numerical results with experimental data.

For the damage calculation under impact and subsequent residual strength determination, the finite-element models reproducing the natural conditions of impact and static tests were created. The developed computational finite-element model reproduces the test conditions of the impact effect on the wing skin samples in accordance with Boeing 7260 standard. The impact energy varied from 50 to 140 J. The sample was loaded with 25.4 mm diameter rigid hemispherical impactor. The calculation of impact damage of 6.4 mm wing skin samples made of Cycom 977-2 material was performed. The plates (150x100 mm) were fixed between two undeformable clamps with contact interaction given between the clamps and the plate. The size of an open window in the clamps was 127x76 mm. The linear orthotropic material model was assumed for the plate. To model the elastic deformation before the damage initiation the classical laminate theory was used. The damage and failure initiation process was induced by Hashin failure criterion. Damage evolution was calculated using linear elastic stiffness degradation law.

The computational model of real static test setup of the damaged plate accounting the impact-induced damage was developed to determine the residual stress of the shell. Effective elastic properties of damaged material were given taking into account previously induced impact damage. In addition, the initial delamination area was set, which evolution was determined during the calculation. The loading was carried out prior to the sample failure. As a result of the calculation, the displacement curves were obtained, on the basis of which the ultimate compressive stress was determined.

The calculation results showed that the application of 50 J energy impact results in 60% static strength reduction. At higher impact energies the decrease in the compressive strength is even more significant. Calculated values of ultimate compressive stresses, depending on the impact energy, are shown in table below.

Impact energy, J	0	50	100	140
Ultimate stress, MPa	750	250	190	140

Verification of the method was performed by comparing calculation results with real data on impact and static tests. The dependence of contact force and kinetic energy on time is shown in figure below for numerical and full-scale tests at 50 J energy. As it is seen form the figures, there is good qualitative and quantitative coincidence between the calculated and experimental results.

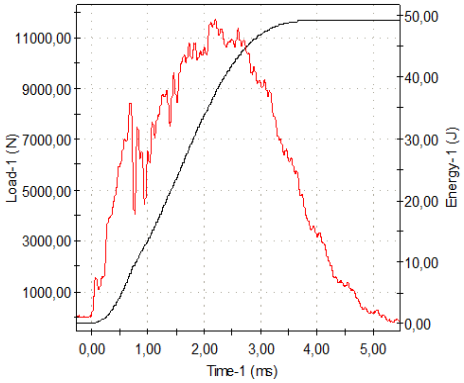

Calculation

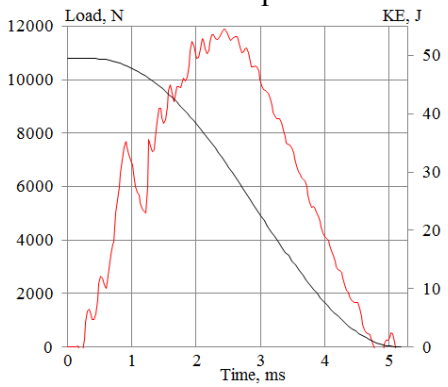

Experiment

2. High-frequency vibration theory of elastic sandwich plates.

The dynamic behavior of elastic sandwich plates of symmetric structure on thickness (skin-core composite) is proposed to study on the basis of the high-frequency vibrations equations obtained by the authors earlier. Each layer is made of homogeneous isotropic material, the contact between the layers is ideal. The main idea assumed as a basis of a derivation of this refined dynamic theory is to take into consideration the interaction of low-frequency modes of vibration with three first high-frequency modes. Appropriate 2D dynamic equations and boundary conditions were obtained with the help of combination of variational-asymptotic method worked out by V. Berdichevsky and averaging method for 3D action functional. This model allows to describe such effects as transverse shear and transverse compression asymptotically correctly on long waves and qualitative correctly on sufficiently short waves.

ID: 310

Synergistic damage mechanics modeling of progressive damage failure in multifunctional composite materials

Chandra Veer Singh
University of Toronto
Canada

Abstract:
Presently, composite structures are designed against strength failure. The criteria used are often empirical and overly conservative. A series of World-Wide Failure Exercises (WWFEs) have been conducted to compare and analyze different failure criteria [1-2]; however initiation and progression of sub-critical events and their effect on the mechanical response has not been adequately addressed. Furthermore, many applications involve design functions such as structural deflections, vibrations, etc., where critical performance is determined by material stiffness. Design of these structures with strength criteria alone is inaccurate as subcritical damage in form of ply cracking and interfacial debonding occurs well before ultimate failure. Here we present a siffness based progressive failure modeling approach for multifunctional composite materials. The approach taken here to address this problem is to retain the framework of *Continuum Damage Mechanics* (CDM) but enrich its capabilities by combining it with micromechanics. We have called this approach synergistic damage mechanics (SDM). This talk will first briefly describe the SDM methodology and then apply it to selected examples of multidirectional composite laminates. The proposed methodology is being implemented in commercial FEA package ABAQUS via user subroutine to enable practical usage.

Retaining the CDM framework and considering a representative volume element (RVE) of the damaged material, the damage mode tensor is defined by

$$D_{ij}^{(\alpha)} = \frac{1}{V}\sum_{k_\alpha}\left(d_{ij}\right)_{k_\alpha} \tag{1}$$

where N denotes the number of damage entities, such as microcracks, of the given damage mode in the given RVE, $k_\alpha = 1,2,...,N$ and V is the volume of the RVE. For the particular case of multiple matrix cracking, the damage mode representing intralaminar cracks in an off-axis ply of orientation θ, can be derived as

$$D_{ij}^{(\alpha)} = \frac{\kappa t_c^2}{st\sin\theta} n_i n_j \tag{2}$$

where $n_i = \left(\sin\theta,\quad \cos\theta,\quad 0\right)$. When progressive damage takes place, it reduces the stiffness properties of the whole composite laminate, which is given by [3]

$$\mathbf{C_{pq}} = \mathbf{C_{pq}^0} + \sum_{\alpha}\mathbf{C_{pq}^{(\alpha)}} \tag{3}$$

where $\mathbf{C}_{\mathbf{pq}}^{\mathbf{0}}$ is the stiffness matrix for pristine (undamaged) material and $\sum_{\alpha} \mathbf{C}_{\mathbf{pq}}^{(\alpha)}$ represents the stiffness changes brought about by all the damage modes. The evolution of damage can be predicted using a fracture mechanics based energy method [4]. Accordingly, the damage progression from State 1 with N parallel off-axis cracks to State 2 where the cracks have multiplied to $2N$, occurs when the work required in going from State 1 to State 2 exceeds the critical energy release rate, i.e., if

$$W_{2N\to N} \geq N.G_c.\frac{1}{\sin\theta}t_c \qquad (4)$$

where G_c is the critical (threshold) value of energy required for ply crack formation within the given laminate. Combining damage progression and stiffness degradation data, the whole stress-strain response of the damaged composite structure is finally obtained. For illustration purpose, the predictions for stiffness reduction (longitudinal Young's modulus), and damage progression (evolution of crack density) using the SDM approach for a quasi-isotropic laminate with cracks in 90,+45 and -45 orientations, are shown in Figure 1.

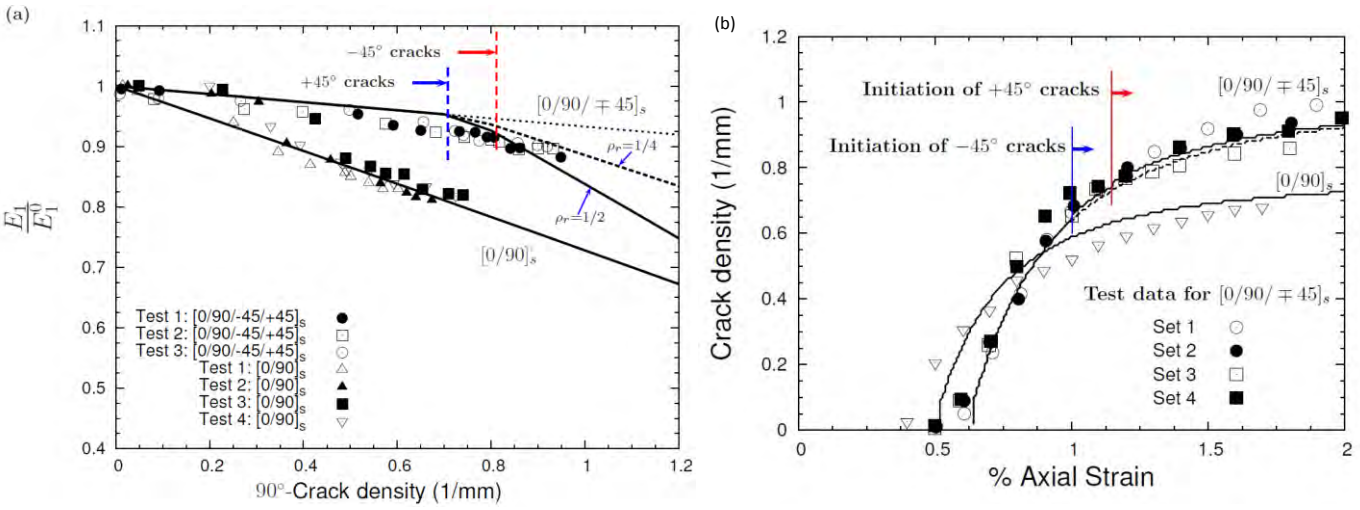

Figure 1: SDM predictions and comparisons with experimental data for quasi-isotropic composite laminate: (a) Stiffness degradation, and (b) ply-crack density evolution.

References

[1] Hinton, M.J. and P.D. Soden, Predicting failure in composite laminates: The background to the exercise. Composites Science and Technology, 1998. 58(7): p. 1001-1010.

[2] Hinton, M.J., A.S. Kaddour, and P.D. Soden, Evaluation of failure prediction in composite laminates: Background to 'part c' of the exercise. Composites Science and Technology, 2004. 64(3-4): p. 321-327.

[3] Singh, C.V. and R. Talreja, A synergistic damage mechanics approach for composite laminates with matrix cracks in multiple orientations. Mechanics of Materials, 2009. 41(8): p. 954-968.

[4] Singh, C.V. and R. Talreja, Evolution of ply cracks in multidirectional composite laminates. International Journal of Solids and Structures, 2010. 47(10): p. 1338-1349.

ID: 345

Nonlinear analysis of pretwisted anisotropic strips in the presence of interlaminar and intralaminar cracks

P. J. Guruprasad
Department of Aerospace Engineering
Indian Institute of Technology Bombay, Powai, Mumbai
India

Chandra Veer Singh
Department of Materials Science and Engineering
University of Toronto
Canada

Dineshkumar Harursampath
Department of Aerospace Engineering
Indian Institute of Science, Bangalore
India

Abstract:
An asymptotically exact cross-sectional model coupled with geometrically nonlinear one-dimensional (1D) theory is developed for a thin composite strip in the presence of damages. Two types of damages are considered: interlaminar cracks and intralaminar cracks. This analytical model is based on the dimensional reduction of laminated shell theory to nonlinear 1D theory using the variational asymptotic method. The cross-sectional nonlinearity, which is induced due to geometry and material distribution, also accounts for damage parameters: crack size and crack density. The model developed is used to investigate the effect of damage on the trapeze effect. The effect of stiffness degradation due to the damages on the end-twist of the strip is analyzed and the results are compared with the experimental studies available in the literature. Finally, formulation to extend the model for nonlinear dynamic analysis is discussed.

Rotor blades are consistently subjected to high magnitudes of tensile loads. In hingeless and bearingless rotor blades majority of the tensile load is carried by the flexbeams. In such a loading scenario, the flexbeams, made of laminates, often develop damage in the form of multiple matrix cracking, delamination, among others. Multiple matrix cracking, also known as `intralaminar cracking', is usually the first form of damage observed in experiments on composite laminates. Although it does not cause laminate failure as such, it can cause substantial degradation in the stiffness properties of the component, and also provide pathways for other forms of damage, such as delamination. Delamination between two layers of the laminate, can however be quite detrimental and may directly cause component failure. It is thus very important to develop analysis procedures to account for these damage modes. In particular their effect on the trapeze effect is of importance as this will affect the extension-twist coupling in flexbeam like thin composite strips used in rotor blades. Only a few studies have analyzed the effect of

delamination on the behavior of the rotor blades. The present effort aims to carefully investigate this problem.

The approach presented here will extend the variational asymptotic based analyses. First we will describe the analytical modeling of ply cracking and delamination. This will be followed by thin composite strip modeling to investigate the trapeze effect. The effect of inter- and intralaminar cracking on stiffness properties and extension-twist coupling will then be analyzed for a specific case of antisymmetric laminated strips.

Preliminary result from the analysis of thin composite strips in the presence of matrix cracks of different densities is shown in Fig. 1.

Fig. 1: Effect of matrix cracking on the end-twist. The X-axis shows the variation in the applied end force (F) and the Y-axis represents the end-twist for thin composite strips with different crack densities (ρ).

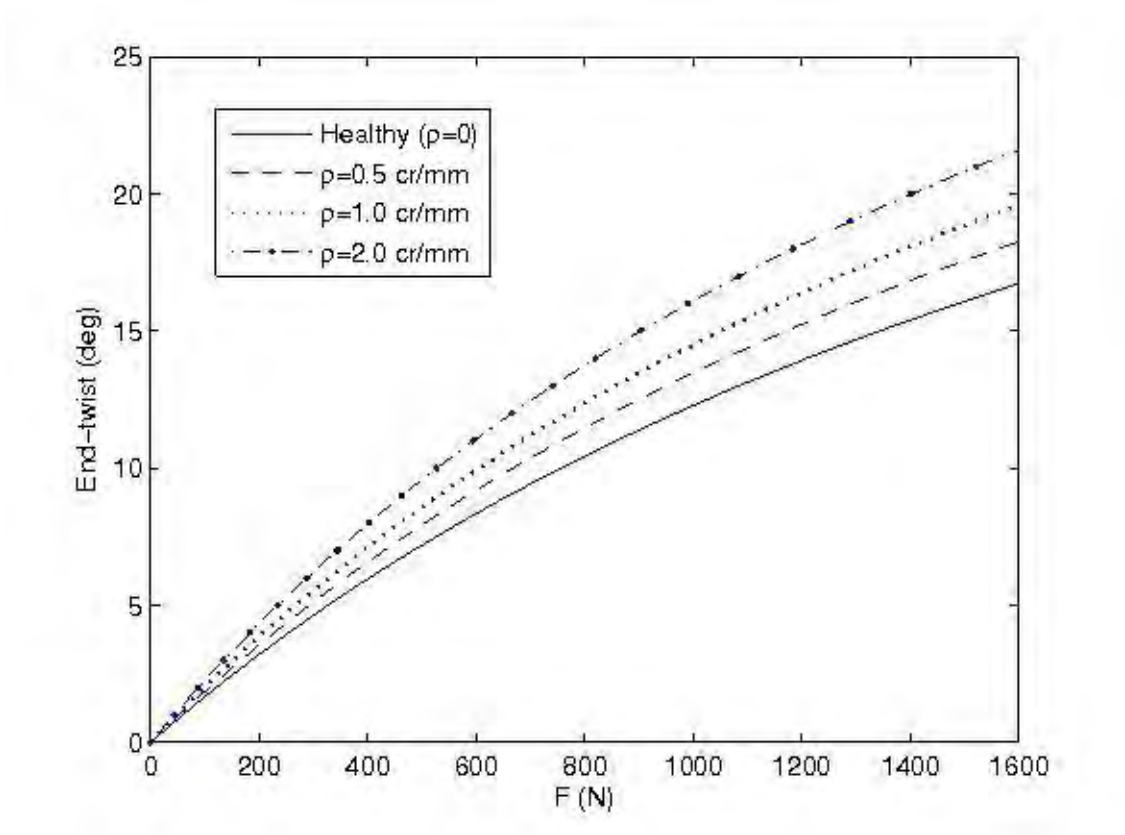

Fig. 1 shows the effect of matrix cracking on the end-twist for different crack densities. It is observed that with increase in crack density for the same applied end force the end-twist of the strip is higher. A similar analysis was carried out to investigate the effect of delamination also in the composite strip. Results are compared with the available experimental data. The formulation developed is then extended for nonlinear dynamic analysis.

ID:390

Effect of Delamination on Dynamic analysis of Piezoelectric Fiber Reinforced Composite Beams

Venkatesh
Indian Institute of Science, Bangalore

PS Prasah
[1]Indian Institute of Science, Bangalore

Dineshkumar Harursampath
[1]Indian Institute of Science, Bangalore

Abstract

Delamination is one of the commonly observed failure mechanisms unique in laminated composites. Delamination is caused by high interlaminar normal and/or shear stresses near free edges as well as interiors during manufacturing of the structure or during service conditions. The presence of delamination in laminated composites causes a significant reduction in mechanical properties like stiffness, strength affecting the global deformation behaviour of beams. The appearance of cracks and delamination in composite rotorcraft ex beams, which affects flapwise and lagwise performance of a helicopter, may lead to catastrophic results. Hence, there is strong need and requirement for online damage detection and health monitoring. This calls for the development of novel modeling techniques and sensors for providing damage detection. Piezoelectric Fiber Reinforced Composites (PFRCs) are relatively new multifunctional smart materials finding applications in sensing, actuation, energy harvesting and structural health monitoring apart from displaying the typical merits of conventional composites. The present work is aimed at studying the effect of delamination on the electromechanical dynamic characteristics of the PFRCs.

Variational Asymptotic Method (VAM) is used as a mathematical tool to decompose the original 3-D problem in to two simpler problems: 2-D nonlinear cross sectional analysis to determine closed-form expressions for the nonlinear stiffness and piezoelectric coupling terms as functions of delamination length and location and a non-linear one-dimensional (1D) problem along the length of the beam. The nonlinear effects that arise due to the geometry of the structure in the presence of delamination are automatically captured using VAM and are reflected in the dimensionally reduced beam cross section stiffness terms. Further simplifications are achieved by modelling the delaminated structure through a sub-laminate approach by appropriately applying global and interface boundary conditions in addition to

the natural and essential boundary conditions resulting from minimization of strain energy. The laminated strip is made up of antisymmetric lay-up with symmetric mid-surface free edge delamination is considered in the formulation and the effect of delamination length on the degradation of linear and nonlinear stiffness are studied.

The geometrically nonlinear one dimensional (1D) analysis is then carried out accounting for large deflections and rotations. Geometrically exact intrinsic beam theory derived using variational principle developed by Hodges is adopted for the analysis. A nonlinear mixed finite element formulation following the procedure adopted by Shang and Hodges is employed for the structural analysis, where the nonlinear constitutive law for the delaminated beam derived using VAM serves as the input. The present analysis considers both 1D nonlinearity arising due to large average deflections or rotations of each cross-section and cross sectional nonlinearities due to nonclassical effects like trapeze effect and predicts the effect of delamination on the static and dynamic analysis of beams in terms of deflection profiles. The effect of cross sectional nonlinearities in presence of delamination on the dynamic global behaviour is studied. A free vibration analysis is carried out to predict the effect of delamination on the natural frequencies and the mode shapes. The reduction in natural frequencies found to be predominant because of the change in the mechanical properties due to delamination. The natural frequencies are more affected by delamination length and location when compared to the mode shapes. Finally, the effects of delamination size and location on the electric filed generated in the Piezo- electric layers are investigated.

ID: 439

Multiscale Thermopiezoelectric Analysis of Laminated Plates with Integrated Piezoelectric Fiber Composites

Senthil Vel
University of Maine
USA

Alden Cook

Abstract:
We present a methodology for the comprehensive multiscale analysis of laminated plates with integrated piezoelectric fiber composite actuators. A detailed framework based on the asymptotic expansion homogenization method is developed to couple the microscale and macroscale field variables. The microscale fluctuations in temperature, mechanical displacement and electric potential are related to the macroscale temperature change, deformation and electric fields through 43 distinct characteristic functions. The local thermal, mechanical and charge equilibrium equations yield a system of partial differential equations for the characteristic functions that are solved using standard finite element techniques. The homogenized thermoelectroelastic properties of a representative material element are computed using the characteristic functions and the constituent material properties. The Eshelby-Stroh formalism is used to analytically solve the three-dimensional macroscopic equilibrium equations for thick and thin laminated piezoelectric plates with arbitrary boundary conditions at the edges. Interscale transfer operators emerging from the asymptotic expansion homogenization method relate the macroscale fields to the microscale heat flux, stress and electric displacement in the individual fibers and matrix. The present multiscale analysis procedure is demonstrated by considering model problems consisting of graphite/epoxy laminates with extension and shear mode piezoceramic fiber actuators.

ID: 497

Effect of Nanoclay Addition on the Fatigue Behavior of Composites.

Suong Hoa
Concordia University

Kabir Ahmed

Abstract:
The effect of nanoclay addition into epoxy on the damping and fatigue behavior of glass/epoxy laminates are presented. Nanoclay was dispersed in epoxy resin by solvent free high speed mixing method using a high speed homogenizer. The modified resin was used to manufacture S-glass/epoxy composite laminate by hand lay-up and autoclave curing. The dynamic properties of the samples were tested using DMA 983. A maximum of 16.8% improvement in the flexural storage modulus was achieved for adding up to 2 wt.% nanoclay in unidirectional laminate, while a maximum improvement in the loss modulus was 22.5% in quasi-isotropic laminate for same amount of clay loading. ForTo see the damping effect of nanoclay at higher frequency and amplitude, log decrement test was carried out where a maximum of 57% increase in damping ratio was observed. It was also interesting to investigate the significance of property development including damping improvement on fatigue life as vibration represents flexural fatigue load acting on the structure. A fixed amplitude flexural fatigue test method was designed using MTS machine. 66% and 133% improvement in flexural fatigue life at respectively 1 and 2 wt.% nanoclay incorporation was achieved in case of cross-ply laminate. To validate these results, log decrement test was done and fatigue damage indexes were calculated after different fatigue cycles. Both of them agree quite well with flexural fatigue test results.

ID: 668

Prediction of Delamination Initiation and Propagation in Laminated Composites under Fatigue Loading using Variational Approach

Maqsood Ameen
Indian Institute of Science

Sathiskumar Ponnusami

Abstract:
An asymptotically exact methodology is presented for predicting delamination initiation in laminated composite beams under fatigue loading. The model employs a cohesive zone interface element degradation law, which combines phenomenological SN-curves for damage initiation with a fracture and damage mechanics approach for crack propagation. The energy functional of the model is computed by taking into account the strain energies of each lamina and the cohesive zone. Variational Asymptotic Method (VAM) is used to minimize the energy functional, thereby reducing the cross-section yielding a damage based one-dimensional constitutive law. The beam constitutive law is then combined with geometrically exact non-linear one-dimensional theory in order to predict the stresses. This damage mechanics based model is used for fracture studies including damage initiation followed by subsequent propagation under Mode I fatigue loading.

ID: 670

Closed-Form Asymptotic Sectional Analysis of Thick Rectangular CFRP Laminated Beams

Atul Kumar
Indian Institute of Science, Bangalore

Dineshkumar Harursampath

Abstract:
Composite materials have relatively stiff and strong fibers reinforcing a soft matrix. The low transverse shear and transverse normal moduli therefore call for a method that can accurately capture the inter-laminar and other three-dimensional stresses. Asymptotically correct analytical solution to the three dimensional elasticity problem of generally orthotropic laminated composite thick rectangular cross-section beams is formulated using the Variational Asymptotic Method (VAM). The VAM reduces the three dimensional geometrically nonlinear elasticity analysis for beam-like structures into a linear two-dimensional analysis governing the cross-sectional elastic constants feeding into a nonlinear one-dimensional beam analysis. The resulting byproducts, namely the three dimensional stress recovery relations are accurate over the interior cross-sections. Asymptotically correct warping functions are derived utilizing the computationally efficient method VAM by using the advantage of small parameters such as strain and the slenderness. The closed-form recovery relations are used along with the results of the one dimensional beam analysis to obtain asymptotic approximations to the required 3-D elasticity solutions.

ID: 709

Smart composite and morphing analysis using VAM

Krishan Kumar
Indian Institute if Science, Bangalore

Dineshkumar Harursampath

Abstract:
Smart composite structural and morphing analysis are attempted here using Variational Asymptotic Method (VAM). Piezoelectric Fiber Reinforced Composites (PFRCs) are the chosen smart structural materials in the current work for incorporation onto the laminate to simultaneously perform the dual functions of structural load-bearing and actuation of flexure, torsion and/or extension. Using VAM, the original 3-D problem is mathematically split into a 1-D through-the-thickness analysis and a non-linear 2-D mid-surface analysis, accounting for transverse shear deformation. Through-the-thickness analysis is done for the laminate to get the stiffnesses matrices. These results are used for non-linear 2-D analysis of the laminate structure. The work thus includes the analysis of a PFRC-based shell structure having a pre-defined initial configuration followed by the desired change in the profile to get the final shape. Different combinations of active and passive laminae along with their orientation and different voltage inputs required for active laminae are studied to get the shape control in active laminate.

VI.3

Mechanics of Structures - Multiphysical, Multiscale Modeling of Thin Structural Members

ID: 113

Laminated Beams with Initial Curvature: A Variational Asymptotic Approach

Anurag Rajagopal
Georgia Institute of Technology
United States

Dewey H. Hodges
Georgia Institute of Technology
United States

Abstract:

The introduction of composite materials has revolutionized the field of structural engineering, most notably due to their high strength-to-weight ratio and their directional tailorability. Modeling of structures with one dimension significantly larger than the other two as beams results in a much simpler mathematical formulation and helps save computational costs. With the advent of composites and structural members with initial twist/curvature, particularly in the field of aerospace engineering, using beam theories based on traditional approaches/ideas will not yield accurate results. Modeling of slender structural members with initial curvature is thus of paramount importance. The VAM provides a rigorous framework to model such structures without *ad hoc* assumptions regarding their deformation. The deformation is expressed in terms of an unknown set of warping functions, which is extracted using an asymptotic analysis on the variational problem using the system's inherent small parameters. The computer program VABS (Variational Asymptotic Beam Section) is constructed on the principles of the VAM.

With the onset of the 21st century, due to the efforts of the second author and his co-workers, VABS was established as an analysis tool of good standing in the circles of both academia and industry. Recent updates and developments to VABS are discussed in detail in Refs. [1] and [2]. Though novel ideas are not lacking in several beam theories in the current literature, the ability and generality of a VAM framework has maintained the superiority of VABS, subsequently making it popular analysis tool for helicopter blades and wind turbines. Since then several efforts have contributed to the validation and verification of VABS results, and this work is one such.

In this work, we propose a beam theory to analyze the in-plane deformation of an initially curved laminated strip-beam. The validity of this theory is limited to laminates whose in and out-of-plane deformations are decoupled (e.g. symmetric layup configurations). This work serves as a good validation tool for VABS and also provides analytical expressions for the stiffness matrix and stress-strain recovery, a rarity for composite structures, and consequently the authors believe that this can serve as a verification tool for researchers working on slender, initially curved structural members made of composite material.

A beam theory must address the three aspects: a cross-sectional analysis leading to a stiffness matrix which is input into the 1D analysis, the 1D analysis itself, and the formula or procedure to recover stress, strain and 3D displacement. This work can be chiefly divided into three parts. The first part comprises of a theoretical development which addresses the first and

third aspects described above. Geometrically exact expressions of the strain are developed and used to pose a variational problem, whose unknowns are a set of warping functions. An asymptotic method perturbs the above system of equations in terms of small parameters, which are identified by beam geometry assumptions, to systematically solve the system while tracking its order of accuracy. The zeroth-order warping is used to develop a classical theory, and the subsequently perturbed first-order warping is used to obtain a Generalized Timoshenko model. For both the cases, for the stiffness matrix and recovery are presented as closed-form analytical expressions.

In the second part, the rigor in dimensional reduction from 3D elasticity will be demonstrated using the results from the corresponding plate theory. Since the VAM performs the dimensional reduction with no *ad hoc* assumptions, for a given structural member, a plate (2D) and the corresponding beam (1D) theory will be consistent with not only the starting point which is 3D elasticity, but amongst themselves as well. The last part comprises of a validation of the current theory using results from VABS for a particular layup configuration. An excellent agreement is observed between the results obtained either way, thus completing a successful verification. A sample result for the stiffness and stress recovery is presented below.

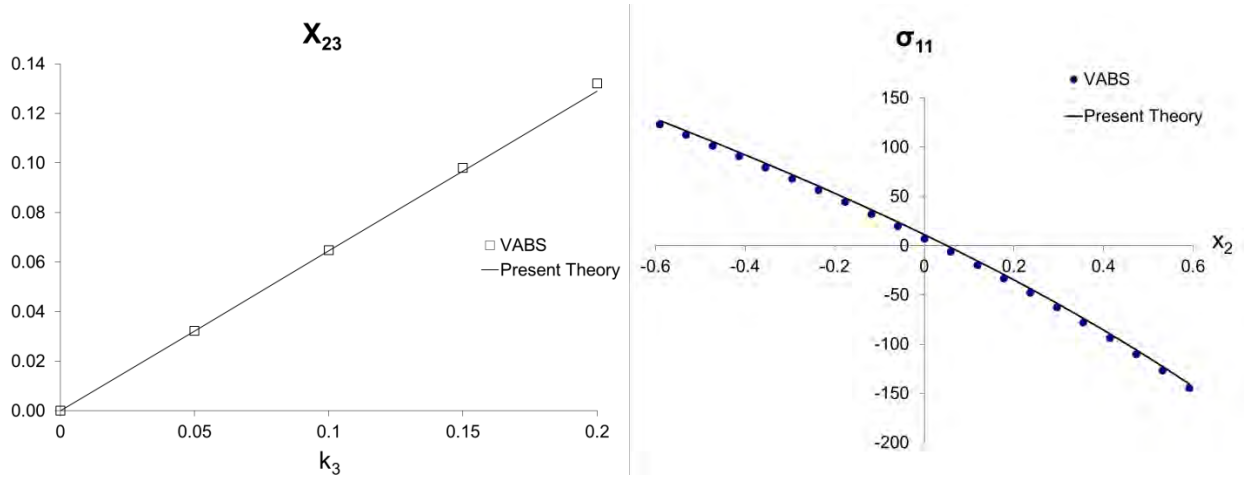

(a) (b)

Fig 1: Sample results for cross-sectional stiffness (bending-shear coupling, non-dimensional) and stress (psi) recovery for a 1.182 in.×0.0579 in. graphite-epoxy strip with layup $[45°/0°]_{3s}$. The latter is at the mid-section of the beam for a constant loading of a unit bending moment with k_3=0.2 in.$^{-1}$.

References

[1]. Rajagopal A, Hodges DH, Yu W. Asymptotic beam theory for planar deformation of initially curved isotropic strips. Thin-Wall Struct (2012); 50:106–15.

[2]. Yu W, Hodges DH, Ho JC. Variational asymptotic beam sectional analysis - An updated version. Int J of Eng Sci (2012); http://dx.doi.org/10.1016/j.ijengsci.2012.03.006

ID: 210

Mechanics of Representative Structural Element

Wenbin Yu
Utah State University
Logan, Utah 84322-4130

Abstract:
The concept of representative structural element (RSE) is generalized from the well-known concept of representative volume element (RVE) in micromechanics. RSE is defined as the smallest building block of the structure which the analyst wants to use to find the effective properties for the macroscopic structural analysis. RSE must be representative, but we do not formally specify representativeness. Instead, we rely on the analyst's expert opinion to determine what will be the representative building block of the structure. This liberal definition is intended for maximizing analyst's freedom in choosing RSE. It can be justified from the view point of material characterization using experiments. When experimentalists want to find properties of a material, they cut representative pieces of the material according to their own judgment and do the testing to get the properties and associated statistics. As we are not doing physical experiments, RSE should be interpreted as the smallest mathematical building block.

RSE is conceptually different from RVE, even if the macroscopic structural analysis uses 3D continuum elements. For example, for a structure made of binary composites of two alternating layers (Figure 1), RSE will be a straight line with two segments denoting the corresponding phases. In a thought experiment, we can repeat this straight line in plane to build the binary composite, and then repeat the binary composite out of plane to build the entire structure. For a structure made of unidirectional fiber reinforced composites, the RSE will be 2D, and for a structure made of particle reinforced composites, the RSE will be 3D. Clearly, RSE uses the lowest dimension (thus highest efficiency) possible to describe the heterogeneity, while the dimension of RVE is determined by heterogeneity and by what type of properties are required for the macroscopic structural analysis. For example if 3D properties are needed for a unidirectional fiber reinforced composites, a 3D RVE is required instead.

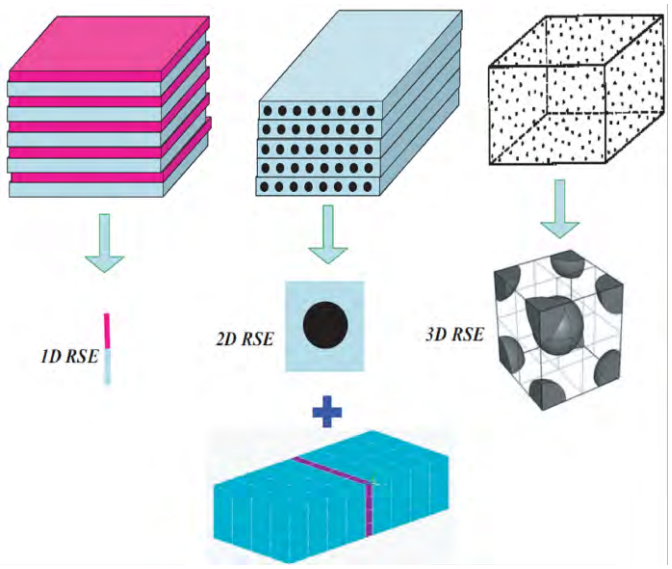

Figure 1. RSE for 3D structures

Unlike RVE, RSE directly applies to dimensionally reducible structures. For example, if the macroscopic structural analysis uses beam elements (Figure 2), RSE for a composite beam with uniform cross-section is the 2D cross-sectional domain. This inspires a new perspective toward structural mechanics. If we consider the beam reference line as 1D continuum, every material point of this continuum has a 2D cross-section as its microstructure. In other words, structural mechanics can be effectively viewed as a specific application of micromechanics. If the beam is also heterogeneous in the spanwise direction, we need a 3D RSE to describe the microstructure of the 1D continuum, the behavior of which is governed by the 1D macroscopic beam analyses.

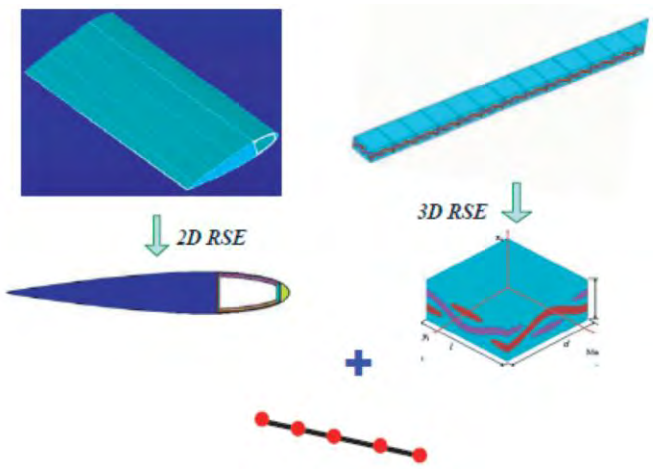

Figure 2. RSE for beam-like structures

To fully realize the conceptual advantages of RSE, the mechanics governing RSE should satisfy the following challenging requirements:

- To use the lowest possible dimensions, the dimensions of the effective properties predicted by RSE analysis should not be directly related with RSE dimensions. For example, for a 3D structure made of binary composites, although the RSE is 1D, we must compute the 3D effective properties, in terms of a 6 by 6 stiffness matrix, as required by the 3D macroscopic structural analysis.

- To directly connect with the macroscopic structural analysis, RSE analysis should predict effective properties corresponding to the constitutive relations of the macroscopic structural analysis. For example, for 1D beam analysis using the Euler-Bernoulli beam model, we need the effective properties in terms of a 4 by 4 matrix containing stiffness terms related with extension, torsion, bending in two directions, and their couplings.

- To treat structural modeling as a specific application of micromechanics, thus unify structural mechanics with micromechanics, RSE analysis should reproduce the structural models. For example, the RSE analysis for composite beams with uniform cross-sections should be the same as the well-established cross-sectional analysis.

These requirements can be met if the mechanics of RSE is formulated based on fundamental mechanics principles without invoking any apriori assumptions that are not inherent to the concept itself, the details of which will be given in the presentation.

ID: 297

Localization (s-cones) in thin shells under indentation

Alice Nasto
Massachusetts Institute of Technology
United States

Amin Adjari
Northeastern University
United States

Arnaud Lazarus
Massachusetts Institute of Technology
United States

Ashkan Vaziri
Northeastern University
United States

Pedro Reis
Massachusetts Institute of Technology
United States

Abstract:

We perform a hybrid experimental and numerical investigation of the localization of deformation in indented thin spherical elastic shells (Figure 1A). Past the initial linear response, an inverted cap develops as a Pogorelov circular ridge[1]. For further indentation, this ridge looses axisymmetry and sharp points of localized curvature form (Figure 2B). We refer to these localized objects[2] as *s-cones* (for shell-cones), in contrast with their developable cousins in plates (d-cones) [3].

[1] Pogorelov. *Amer Mathematical Society*, **72**, (1988).
[2] Vaziri and Mahadevan. *PNAS*, **105**, 7913 (2008).
[3] Cerda and Mahadevan. *Phys. Rev. Lett.* **80** 2358-2361 (1998).

A.

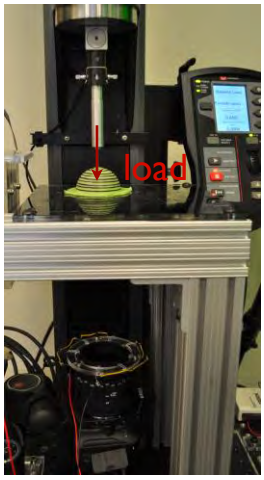

B.

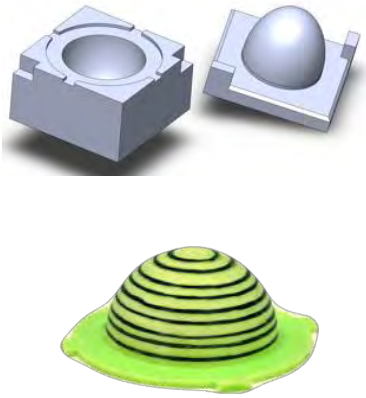

Figure 2: Experimental Setup. (A) An Instron materials testing machine indents the shell and captures the indentation load. A camera captures images from below. (B). A digitally fabricated mold is used to cast shells with an elastomeric polymer.

We quantify the effect of systematically varying the indenter's radius of curvature (from point to plate load as shown in Figure 2A) on the formation and evolution of s-cones. In our precision desktop-scale experiments we use digitally designed and rapid prototyped elastomeric shells (Figure 1B) and rigid indenters of various shape (Figure 2A). The mechanical response is measured through load-displacement compression tests and the deformation process is further characterized through digital imaging (Figure 1A).

The experimental results are contrasted against nonlinear Finite Element simulations (Figure 2B). Merging these two complementary approaches allows us to gain further physical insight towards rationalizing this geometrically nonlinear process.

Figure 3: Experimental setup. (A) A hemispherical shell is indented with indenters of various radii of curvature. The indenter shapes range from $R_1/R_2 = 0$ (point load) to $R_1/R_2 = \infty$(plate load). (B) Experimental and simulation results for a hemispherical shell under point indentation. When the inverted cap ridge loses is axisymmetry, three *s-cones* form. Upon further indentation, one of the *s-cones* splits to form a fourth.

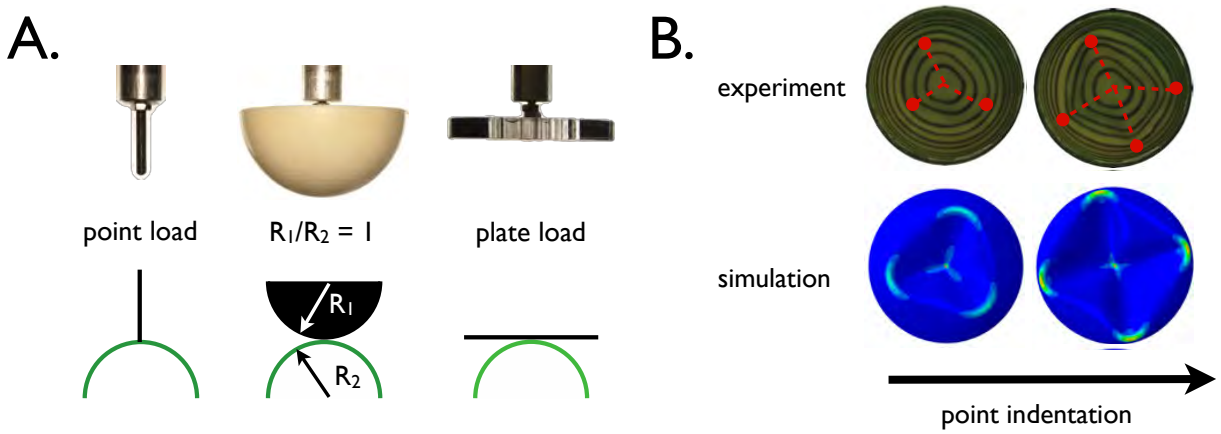

References:

ID: 401

Homogenization and Dimensional Reduction Modeling of Composite Dimensional Reducible Structures

Chang-Yong Lee
Department of Mechanical Engineering,
Pukyong National University
Republic of Korea

Wenbin Yu
Department of Mechanical and Aerospace Engineering,
Utah State University
United States

Abstract
Along with the rapidly increasing popularity of composite materials and structures in various engineering applications, research on accurate and general modeling of structures made of them has remained as a very active field in the last several decades. Moreover a wide understanding and elaborate fabrication techniques of them are even possible to manufacture new multifunctional composite materials and structures based on optimized microstructures to achieve the ever-increasing performance requirements, including high-strength and low-weight, superior noise and energy absorption, and high-temperature resistance. Two famous examples of employing a multifunctional concept into aerospace structures are illustrated in Fig. 1.

Fig. 1 Two multifunctional structure examples: (a) Grid stiffened spar for a rotor blade [1] and (b) Corrugated-core sandwich structure for thermal protection systems [2].

Unlike the well-established finite element analysis (FEA) and the homogenization-based two-step approaches suggested in the literature, this abstract proposes a new efficient and high-fidelity method to construct effective beam/plate models [3,4] for these materials/structures through simultaneous homogenization and dimensional reduction under the variational asymptotic method (VAM) [5,6]. The 3D heterogeneous structure considered as a periodic assembly of many unit cells (UCs) is first formulated in an intrinsic form suitable for geometrically nonlinear beam/plate analyses. Then, considering both smallness of the geometric parameter (ε) and heterogeneity (η), we use VAM to rigorously decouple the original 3D elastic problem into a nonlinear 1D beam/2D plate analysis on the macroscopic level and a linear 3D/2D UC micromechanical analysis with 1D/2D periodicity on the microscopic level. Especially, the UC one is implemented in two computer code VABS/VAPAS using the finite

element technique for numerically obtaining the effective stiffness/mass matrices for global 1D beam/2D plate analyses, such as classical and refined beam/plate analyses, and recovering the local displacement, strain, and stress fields based on the macroscopic behavior, respectively. Fig. 2 shows a flowchart for the overall process based on homogenization and dimensional reduction.

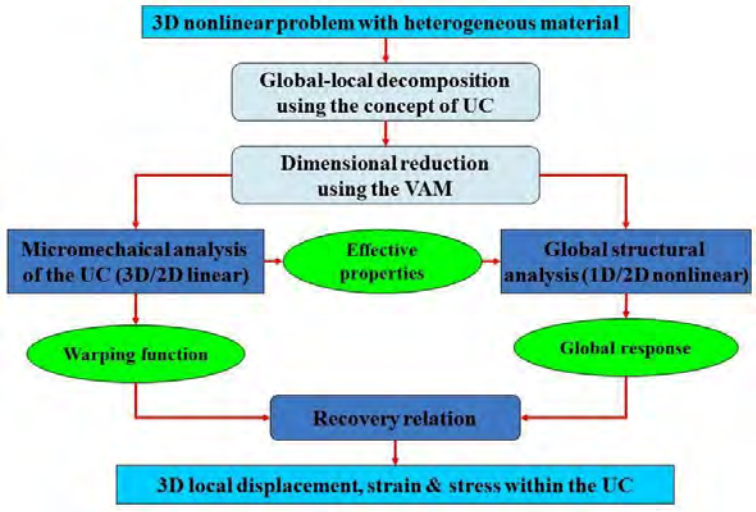

Fig. 2 Overview of efficient high-fidelity modeling approach

Finally, implementation of VABS and VAPAS can be used as an alternative of the 3D FEA for efficient yet accurate analysis of multifunctional composite materials and structures with complex microstructures. The full procedures and several examples for validation may be found in detail in Refs. 3 and 4.

References

[1] Nampy, N. S. and Smith, E. C., 2009, “An Innovative Structural Design Concept for Heavy-Lift Rotor Blades,” Presented at the *Technical Specialist's Meeting on Rotorcraft Structures and Survivability*, Williamsburg, VA, Oct 27~29.

[2] Bey, K. and Butcher, K., 2008, "Thermal-Structural Analysis of Structurally-Integrated Thermal Protection Systems," in *Fundamental Aeronautics Program Annual Meeting*, Atlanta, GA.

[3] Lee C.-Y. and Yu, W., 2011, "Variational Asymptotic Modeling of Composite Beams with Spanwise Heterogeneity," *Computers and Structures*, Vol. 89, pp.1503~1511.

[4] Lee, C.-Y. and Yu, W., 2011, "Homogenization and Dimensional Reduction of Composite Plates with In-Plane Heterogeneity," *International Journal of Solids and Structures*, Vol. 48, No. 10, pp.1474~1484.

[5] Berdichevsky, V., 1979, "Variational-Asymptotic Method of Constructing a Theory of Shells," *PMM*, Vol. 43, No. 4, pp. 664~68

[6] Yu, W., 2002, "Variational Asymptotic Modeling of Composite Dimensionally Reducible Structures," Ph.D. thesis, Georgia Institute of Technology

VI.4

Mechanics of Structures - Structural NDE and Structural Health Monitoring

ID: 84

Nonlinear ultrasonic methods to monitor microstructural evolution in metals

Katie Matlack
Georgia Institute of Technology

Abstract:
The capabilities of using nonlinear ultrasonics (NLU) to monitor microstructural evolution in metallic materials are discussed. This nondestructive evaluation method has the ability to detect damage in materials prior to macroscopic damage. Microstructural changes such as dislocation and precipitate formation cause the generation of a second harmonic wave as a tone burst propagates through the material, and this is tracked by measuring the amplitudes of the received primary and second harmonic waves. The associated experimental parameter – the acoustic nonlinearity parameter – generally increases with increasing plastic damage. However, other factors can cause an increase in the acoustic nonlinearity parameter, such as varying surface conditions of a material. Experimental results are presented that decouple material nonlinearity from contact nonlinearity by measuring the acoustic nonlinearity parameter over increasing levels of surface roughness. These results can be used to extract material nonlinearity information to accurately measure remaining structural life of a material.

ID: 172

Saliency-Informed Anomaly Detection via Pattern Interrogation of Propagating Wavefields

Stefano Gonella
University of Minnesota
United States

Harvis D. Haupt
University of Minnesota
United States

Abstract:

This work is concerned with the development of a model-agnostic adaptive strategy for multiresolution diagnostics based on the concepts of spatial saliency and data sparsity. The idea originates within the context of laser-based structural health monitoring, which leverages the ability of scanning interferometers to acquire two-dimensional acoustic wavefields and resolve spatial variations with a remarkable level of detail.
Laser-based diagnostic techniques have pros and cons. On one hand, their applicability is limited to sensing scenarios where optical access to the structure surface is possible; moreover, they require that the structure is two-dimensional, or that some inference of its internal state can be made from its surface behavior. On the other hand, the spatial measurement diversity inherently provides a superior detection capability when compared to traditional echo-pulse or pitch-catch methods, based on the radar paradigm, which rely on sparse measurements and require some *a priori* knowledge of the structural and material properties of the medium.
The concepts of adaptivity and visual saliency are here combined to introduce a parallel strategy for data acquisition and anomaly detection that fully exploits the measurement diversity of 2D wavefields. The idea is to incrementally reconstruct a wavefield through a response-driven adaptive sequence of self-refining scans performed over nested regions. This enables the acquisition of high spatial resolution measurements limited to the most interesting regions of the structure, thus avoiding the burden of exhaustive sampling of the whole domain and promoting efficiency. The algorithms that drive the adaptivity pinpoint the location(s) of highest likelihood of structural anomaly from the detection and classification of salient features in the wavefield. A region is here labeled salient when its behavior does not belong to a common subspace of a certain feature space, i.e. when its signature is markedly different from the typical one observed in the surrounding medium.
The approach is illustrated in a simulated environment using the benchmark problem of flexural waves in a thin plate. This allows testing the flexibility of the method in a variety of anomaly configurations, in the presence of multiple defects and scattering-generated interference clutter. A first look at the challenges associated with under-sampled wavefields is explored to pave the way for future work on actual experimental data sets.

ID: 206

Calibration of dynamic models based on experimental measurements in a rotating environment

Maria Chierichetti
Worcester Polytechnic Institute
United States

Massimo Ruzzene
Georgia Institute of Technology
United States

Abstract:
Reliable stress and strain predictions in rotating systems, such as rotor- and wind-turbine blades, are essential to accurately estimate their remaining life and to schedule appropriate maintenance processes. From a usage monitoring perspective, this leads to limited predictive capability in terms of fatigue, which ultimately results in overly conservative designs[1].

Numerical inaccuracies are mostly due to structural degradation, unmodeled dynamics and errors in the representation of the applied loads, and could be improved by the identification of corrections to the model based on experimental measurements. The integration of experimental measurements into a numerical algorithm allows a continuous and accurate tracking of the dynamic strain and stress fields without requiring detailed initial models. This combined numerical and experimental approach is ideally suited to monitoring the response of periodic systems such as wind-turbines and helicopters, in which strong interactions between the unsteady aerodynamic loads and the dynamic behavior of the system make numerical predictions particularly challenging.

The proposed approach, called Confluence Algorithm, updates either the external loads or the dynamic properties of the model to improve the accuracy of the full-field dynamic response by iteratively applying linearized corrections to a non-linear model based on experimental measurements at few locations. From these limited measured data it is possible to accurately extract information on the complete behavior of the system, Figure 4. Numerical and experimental analyses show in fact that the reconstruction of the response field is possible and accurate. This paper aims to present a review of the confluence algorithm and of its findings.

A procedure for the update of external loads, called Load Confluence Algorithm[2-5], has been developed in which externally applied loads are iteratively corrected so that the prediction of the dynamic response match experimental measurements. This approach considers measured strains as inputs to a strain mapping procedure that employs a modal basis estimated through a numerical model of the system. A linearized modal representation is developed in terms of Fourier coefficients, providing a simple algebraic relationship between the externally applied loads and the measured strains or displacements.

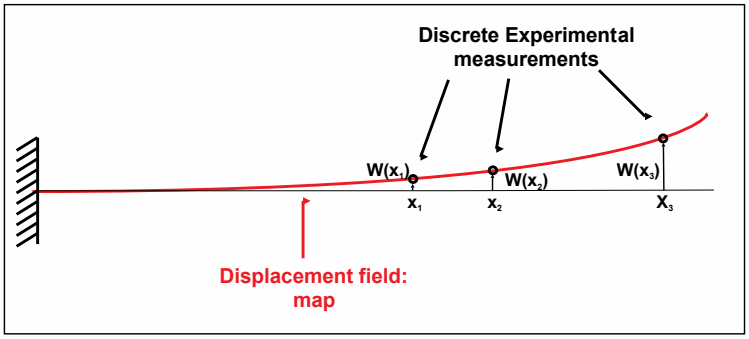

Figure 4. Concept

A procedure for the updating of the mass and stiffness parameters, called Property Confluence Algorithm[6], is based on an iterative procedure that computes new estimates of the physical parameters based on the current measurement of the dynamic response. This approach differs from traditional model updating techniques because it is not based on vibration tests, but on the continuous tracking of the dynamic response at a limited number of locations.

These analyses demonstrate that the integration of the Confluence Algorithm into non-linear models improves the accuracy of the numerical prediction of the dynamic response of systems characterized by a periodic behavior, even in presence of non-linearities. The algorithm enables the use of simplified models that are corrected through experimental data to achieve accurate tracking of the system.

1. Vaughan, R., Chang, J., and Rogers, M., Obtaining Usage Credits from Monitoring of Helicopter Dynamic Components without Impacting Safe Life Reliability, American Helicopter Society International 63th Annual Forum Proceedings, Virginia Beach, VA, May 1-3, 2007.
2. Chierichetti, M., McColl, C., Palmer, D., Ruzzene, M., and Bauchau, O., Combined Analytical and Experimental Approaches to Rotor Components Stress Predictions, The 1st Joint International Conference on Multibody System Dynamics, May 25-27, 2010.
3. Chierichetti, M., McColl, C., Palmer, D., Ruzzene, M., and Bauchau, O., Combined analytical and experimental approaches to rotor components stress predictions, Proceedings of the Institution of Mechanical Engineers - Part K, Journal of Multibody Dynamics, Vol. 225, 2011, pp. 322-330.
4. Chierichetti, M., Ruzzene, M., Bauchau, O., McColl, C., and Palmer, D., Prediction of UH-60 blade loads: an insight on Confluence Algorithm to correct internally generated airloads, Proceedings of the American Helicopter Society International 67th Annual Forum, Virginia Beach, VA, May 3-5, 2011.
5. Chierichetti, M. and Ruzzene, M., Dynamic displacement field reconstruction through a limited set of point measurements: application to plates, Journal of Sound and Vibrations, vol. 331(21), 2012, pp. 4713-4728.
6. Chierichetti, M. and Ruzzene, M., Model updating in structural dynamics through a confluence algorithm, in Proceedings of the 53rd AIAA/ASME/ASCE/AHS/ASC Structures, Structural Dynamics, Honolulu, April 23-26, 2012.

ID: 282

Multiscale finite element analysis of wave scattering from sub-wavelength defects

Filippo Casadei
Georgia Institute of Technology – Department of Aerospace Engineering
United States

Massimo Ruzzene
Georgia Institute of Technology – Department of Aerospace and Mechanical Engineering
United States

Abstract:
Among different approaches used for the monitoring of structural integrity, guided waves (GW) have shown great potentials for their capability to scan relatively wide portions of a structure and for being sensitive to a variety of damage types [1,2]. The development of effective GW-based inspection techniques that not only detect damage but also provide some quantitative measure of its severity, relies on numerical simulations which investigate the interaction between propagating waves and defects of different type, orientation and size. Specifically, numerical simulations of wave propagation play a key role for the development of novel damage detection algorithms and are useful to support the interpretation of experimental measurements. Typically, the length scale characterizing localized imperfections or periodic microstructures is small compared to the global size of the structural component, and often smaller than the shortest wavelength deformation. Hence, the size of the spatial discretization is dictated by the size of the microstructure, which may result in high memory and CPU requirements. A concise yet meaningful understanding of these phenomena is often obtained by means of scattering diagrams illustrating the directivity of the wavefield scattered by defects. Such simulations are computationally intensive, not only due to the scale difference between the global and local features, but also because scattering information requires several parametric studies for damage of different size and orientation. Consequently, significant effort related to model preparation and re-meshing is often required.

This research proposes a geometric multiscale finite element method (GMsFEM) for the efficient analysis of wave scattering from small defects in plates. The proposed GMsFEM combines the idea of multi-node elements to the concept of numerical shape functions. Such elements, denoted as multiscale elements (MSEs), explicitly model the geometry of heterogeneities at sub-elemental length scales, and automatically satisfy compatibility of the solution across the boundaries of adjacent elements. As shown in Fig 1.a this allows modeling small defects without requiring extensive mesh refinements that inevitably increase the size of the numerical model and generated unwanted mesh distortion.

In this work, the GMsFEM is applied to study the scattering patterns of three-dimensional (3D) defects. A three-dimensional discretization is used to represent the propagation of all the fundamental anti-symmetric (A0), shear-horizontal (SH0), and symmetric (S0) Lamb wave modes that are not satisfactory approximated by means of two-dimensional plane-stress or plane-strain models. Furthermore a 3D model allows to represent part-depth defects and to investigate mode conversions occurring when either S0, or A0 incident waves are considered. The present study focuses on the analysis of part-depth elliptic defects in order to highlight the effects of different damage parameters on the scattering coefficients. Such information is essential for the development of reliable detection algorithms based on adaptive imaging techniques [3].

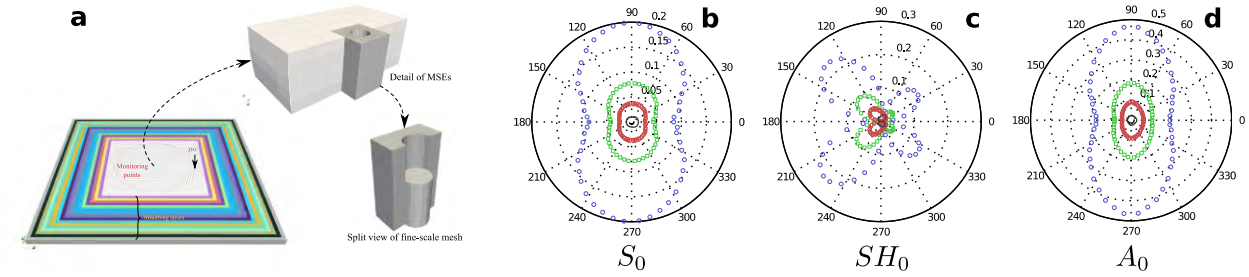

Figure 5. Numerical model of the 3D plate with multiscale elements (a). Scattering coefficients computed for incident S0 waves as a function of the defect's radius to wavelength ratio: 5.6% (blue-o-markers), 3.4% (green-□-markers), 2.2% (red-✷-markers), and 1.1% (gray-•-markers)

The adopted three-dimensional finite element model is illustrated in Fig.1.a. The proposed multiscale method allows using a relatively coarse numerical grid capable of capturing the global wave motion in the homogeneous portion of the domain, while the presence of defects is modeled by means of a limited number of 3D multiscale elements. Both incident S0 and A0 waves are independently considered in this study.

A summary of the scattering diagrams for different values of the defects' major axis Ra and fixed depth are illustrated in Fig. 1.b-d. The defect's radii are expressed in terms of the incident wavelength (λS0 = 26.8 mm) to provide insights on the effects of the excitation frequency on directivity. As expected, the magnitude of the scattering plots reduces as the wavelength increases with respect to the characteristic length of the defect. This implies that a higher excitation frequency is required to maintain the same sensitivity to smaller defects. Results also indicate that the shape of the scattering plots is slightly affected by the size to wavelength ratio. Such change is also partially related to the different eccentricity of the ellipse since, in this study, its minor axis Rb = 0.1 mm is held constant while Ra changes. Additional results for varying defects' depth and orientation with respect to the direction of incoming waves are also computed. Analyses are finally repeated considering incident A0 waves.

References:

[1] Aarnes, J., Krogstad, S., and Lie, K., "A hierarchical multiscale method for two-phase flow based upon mixed finite elements and nonuniform coarse grids," Multiscale Modeling and Simulation, vol. 5, no. 2, p. 337, 2006.

[2] Alleyne, D. and Cawley, P., "The interaction of lamb waves with defects," Ultrasonics, Ferroelectrics and Frequency Control, IEEE Transactions on, vol. 39, no. 3, pp. 381-397, 1992.

[3] Michaels, J., Hall, J., and Michaels, T., "Adaptive imaging of damage from changes in guided wave signals recorded from spatially distributed arrays," in Proceedings of SPIE, vol. 7295, pp. 729515-1, 2009.

ID: 357

Wave Propagation and Creep Behavior of Smart GFRP Sandwich Composites

Anaïs Farrugia
Ecole des Mines d'Albi-Carmaux, Albi CT Cédex
France

Valeria La Saponara
Department of Mechanical and Aerospace Engineering, University of California, Davis
United States

Wahyu Lestari
Department of Aerospace Engineering, Embry-Riddle Aeronautical University, Prescott, AZ
United States

Abstract:

Fiber-reinforced polymer sandwich composites have higher damage tolerance with respect to monolithic composites, especially under bending, impact and compressive loading. This makes them attractive for a variety of applications (e.g. aerospace, civil, transportation, ship and wind turbine engineering). Ultrasonic waves transmitted from off-the-shelf surface-mounted or embedded piezoelectric wafers have been used to monitor the structural health of these materials, in particular to investigate impact damage [1-2] and debonding problems [3].

The current research project has two main goals: to investigate 1) the creep behavior of sandwich composites with embedded piezoelectric wafers, and 2) the behavior of ultrasonic waves in such sandwich composites, under the given creep and high temperature conditions.

Specimens were prepared with polyurethane foam core (type FR-3704 by General Plastics) and glass-fiber reinforced polymers (GFRP) facesheets (predominantly unidirectional glass weave, type 7715 by Applied Vehicle Technology, infiltrated by Proset LV117 epoxy mixed with Proset 237 hardener). The specimens were manufactured with conventional Vacuum Assisted Resin Transfer Molding. Moreover, the GFRP facesheets had three different layups, $[0]_8$, or $[90]_8$, or $[\pm45]_4$, to better investigate fiber-driven (in the $[0]_8$ specimens) and matrix-driven ($[90]_8$ and $[\pm45]_4$) damage. Two lead zirconate titanate (PZT) piezoelectric wafers (type SM411, Steiner and Martins, Inc.) were embedded in the middle of one sandwich facesheet, ~76 mm apart from each other, in a ~178 mm long beam. The specimens were positioned on a custom-made three-point bending fixture located in an oven, at a temperature of 80 deg. C, under constant loading (creep bending). The PZTs were in the part of the beam in tension, and were offset with respect to the displacement gauge tip. Each test lasted ~60 hours, after which a steady-state

creep deflection was achieved. The displacement gauge was an analog dial test indicator, which monitored the displacement of the center of the facesheet under tension. The measurement of the dial test indicator (one per sandwich beam) was recorded by a webcam during the tests. Typically, two specimens were tested simultaneously, in a sequence dictated by a random number generator to minimize potential confounding effects.

Results for goal 1) have been published in [4-5]. Results for goal 2) are still work in progress.

The ultrasonic wave consisted of a sinewave pulse modulated by a Hamming window, which has been shown to produce Lamb waves with low dispersion at low ultrasonic frequencies, e.g. [6]. The input signal was amplified twenty times, and launched at center frequencies ranging from 20 kHz to 70 kHz, where the amplifier's nonlinearity was deemed acceptable.

The waveform analysis includes the use of a signal processing technique based on Gabor wavelet transforms applied to denoised acquired waveforms. Wavelet transforms have been used for frequency-time resolution of noisy, non-stationary signals; Gabor wavelet transforms have shown the ability to detect structural damage, e.g. [7]. The technique adopted for the current work was originally introduced in [8-9], to assess global damage progression in static and fatigue tests. In [9], the area of a contour of the Gabor wavelet transform was quantified and plotted versus the fatigue life of the specimens. The area may be correlated with the so-called *characteristic damage state* that is typical of monolithic and woven cross-ply composites, and can give an overall picture of the global damage state of the specimen. The hypothesis on this physical interpretation of this signal processing technique is being validated with the use of the edge replication technique and static loading/unloading static tests.

A similar signal processing procedure is being applied to the waveforms from the smart sandwich composites under creep. Potential confounding effects include the manufacturing variability of the specimens, the use of two dial test indicators, and temperature fluctuations across the fixture. Upon completing this investigation, we will be able to better understand how smart sandwich composites behave under creep conditions, and how Lamb waves change due to creep bending. This will aid, in the long term, their condition-based maintenance.

References:

[1] Diamanti, K., Soutis, C., Hodkinson, J. M., "Non-destructive inspection of sandwich and repaired composite laminated structures", 2005, *Composites Science and Technology*, 65, pp. 2059-2067.

[2] Osmont, D., Devillers, D., Taillade, F., "Health Monitoring of Sandwich Plates Based on the Analysis of the Interaction of Lamb Waves with Damages", 2001, *Proceedings of SPIE*, 4327, pp. 290-301.

[3] Mustapha, S., Ye, L., Wang, Dong, Lu, Y., "Assessment of debonding in sandwich CF/EP composite beams using A_o Lamb wave at low frequency", 2011, *Composite Structures*, 93, pp. 483-491.

[4] Farrugia, A., Winkelmann, C., La Saponara, V., Kim, J.-S., Muliana, A., "Creep Responses of Smart Sandwich Composites at Multiple Length Scales: Experiments and Modeling", 2011, *ASME Journal*

of Engineering Materials and Technology, 133, pp. 011008-1 to -6.

[5] Kim, J. S., Arronche, L., Farrugia, A., Muliana, A., La Saponara, V., "Multi-scale modeling of time-dependent response of smart sandwich constructions", 2011, *Composite Structures*, 93, pp. 2196-2207.

[6] Guo, N., Cawley, P., "The interaction of Lamb waves with delaminations in composite laminates", 1993, *Journal of the Acoustical Society of America*, 94, pp. 2240-2246.

[7] Quek, S.-T., Wang, Q., Zhang, L., Ong, K. H., "Practical Issues in the Detection of Damage in Beams Using Wavelets", 2001, *Smart Materials and Structures*, 10, pp. 1009-1017.

[8] La Saponara, V., Horsley, D. A., Lestari, W., "Structural Health Monitoring of Glass/Epoxy Composite Plates Using PZT and PMN-PT Transducers", 2011, *ASME Journal of Engineering Materials and Technology*, 133, pp. 011011-1 to -8.

[9] Tang, H.-Y., Winkelmann, C., Lestari, W., La Saponara, V., "Composite structural health monitoring through use of embedded PZT sensors", 2011, *Journal of Intelligent Material Systems and Structures*, 22, pp. 739-755.

ID: 409

Experimental Evaluation of Uniaxial Compression on Shear and Mode-Converted Ultrasonic Scattering

Christopher Kube
University of Nebraska-Lincoln
USA

Joseph Turner
USA

Abstract:
Recent theoretical developments in ultrasonic materials characterization demonstrated the influence of applied loads on elastic wave scattering in polycrystalline materials. These developments were the first to consider second-order elastic moduli in the scope of ultrasonic stress evaluation. Experimental confirmation was also recently demonstrated for longitudinal wave scattering (L-L) from 1018 steel under uniaxial compression. This presentation builds on those results while also observing the influence on other propagation modes in a sample of rail steel under uniaxial compression. The propagation modes examined include shear (T-T) and mode-converted longitudinal to shear (L-T). Grain size parameters extracted from the mode-converted scattering will be presented for the first time. Application of these measurements may lead to a new method for stress and microstructural evaluation in polycrystalline materials.
[Research supported by the Federal Railroad Administration]

ID: 417

Theoretical Model of Mode-Converted Diffuse Ultrasonic Backscatter for Materials Characterization

Ping Hu

Diffuse ultrasonic backscatter describes how elastic waves are scattered at interfaces in heterogeneous materials. Theoretical models have previously been developed to model the diffuse backscatter for longitudinal (L-L) and shear (T-T) wave scattering within polycrystalline materials. Following a similar formalism, a mode-conversion scattering model is presented here to describe how longitudinal waves are scattered and converted to shear waves (L-T) at material grain boundaries. Using a pitch-catch transducer configuration, the model was used to fit the response and an average grain size was extracted and found to be in agreement with results from the L-L model. This presentation outlines the theoretical framework and compares the observed grain size results with those obtained from optical micrographs. Mode-converted backscatter removes the influence of the front-wall reflection and may lead to improvements in microstructural characterization and material property evaluation. [Research supported by FRA].

ID: 440

Dependence of the Fatigue Life of Laminated Beams on the Fiber Orientation Angle

Erdem Akay

Abstract:
Current study is intended to investigate the fatigue life of fiber reinforced polymeric composites with different fiber orientations using embedded Fiber Bragg Grating (FBG) sensors. The study includes both experimental and numerical aspects. In the experimental side, Resin Transfer Molding (RTM) method is used for producing specimens with different fiber orientations. The specimens are made of glass fibers and epoxy resin. Tensile fatigue tests are performed on the specimens using a universal testing machine. During the experiments, real-time strain data is acquired through FBG sensors. The relation between the fiber orientations and the strain response of the composite structure under the fatigue loading is studied. Experimentally obtained data is used to develop a model for the prediction of the remaining life of the laminated beams with different fiber orientation angles. A model based on the strain energy is developed to predict the remaining useful life of the each specimen type using the strain energy methods.

ID: 521

Detection of Aerospace Chemical Penetrants in Glass Fiber Reinforced Composites

Bryan R Loyola

Sandia National Laboratories/CA*

United States

Kenneth J Loh

Department of Civil and Environmental Engineering, University of California, Davis

United States

Timothy M. Briggs

Sandia National Laboratories/CA*

United States

Jack L. Skinner

Department of General Engineering, Montana Technical University

United States

Valeria La Saponara

Department of Mechanical and Aerospace Engineering, University of California, Davis

United States

* Sandia National Laboratories is a multi-program laboratory managed and operated by Sandia Corporation, a wholly owned subsidiary of Lockheed Martin Corporation, for the U.S. Department of Energy's National Nuclear Security Administration under contract DE-AC04-94AL85000.

Abstract:

Recent work in structural health monitoring (SHM) has focused on detecting damage by monitoring changes in electrical conductivity of conductive epoxies and films that are embedded or applied to structures. This conductivity in otherwise non-conductive polymers is accomplished by the incorporation of carbon nanotubes (CNTs). This approach has demonstrated the ability to detect cracks [1], strain [2], impact damage [3], and changes in pH [4]. However, this work has focused on monitoring methods that use 2-pt probe resistance measurements, which only allow for the detection of damage between the electrodes. These measurements do not provide any spatial information regarding the damage. This spatial information can be collected by using a technique called electrical impedance tomography (EIT), which can measure the spatially distributed conductivity across an area that is bounded by electrodes. By performing EIT on these embedded or applied nanocomposites materials, the presence, location, and size of damage can be determined. In this study, a spray-deposited multi-walled carbon nanotube (MWCNT)- poly(vinylidene fluoride) (PVDF) thin film is embedded within a glass fiber-reinforced polymer (GFRP) composite for detection of the penetration of aircraft anti-icing fluid and hydraulic fluid. Preliminary data suggests that the MWCNT-PVDF film is deteriorated by direct exposure to both of these chemicals typical of aircraft operations. This dissolution of the conductive MWCNT network facilitates the sensitivity of the films to the presence of these chemicals.

The GFRP specimens were manufactured with a $[0/+45/90/-45]_s$ stacking sequence (for a total of 8 layers) of glass fiber unidirectional mats with the MWCNT-PVDF films spray-deposited on the outer surfaces. Prior to infusion of epoxy, the MWCNT-PVDF film was manufactured by mixing a latex solution of the PVDF particles with a stable suspension of MWNTs that were polymer wrapped with poly(sodium 4-styrenesulfonate) (PSS). N-methylpyrrolidone (NMP) was added as a coalescing agent for the PVDF particles. A square sensing area of 78×78 mm^2 was spray-deposited on each specimen, and eight electrodes were placed on each side of the sensing area in a way to allow exposure after epoxy infusion. The specimens were then infused with a two-part epoxy using Vacuum Assisted Resin Transfer Molding, and fully cured. The final specimens were cut to 100×100 mm^2. Polypropylene centrifuge tubes with their bottoms removed were mounted to the surface of each specimen using silicone adhesive. These centrifuge tubes were filled with either anti-icing fluid or hydraulic fluid, which were doped with dansylamide as a fluorescent marker.

EIT measurements were taken of each specimen prior to the introduction of the chemical penetrants. These measurements entail injecting a current between two electrodes and measuring the corresponding differential voltage at the remaining electrodes. This is done several times for different current electrode pairs for a complete EIT measurement. After the introduction of the chemical penetrants, EIT measurements were taken every other day, for a period of two months. The spatial conductivity reconstructions were performed in a differential manner in reference to the initial EIT measurements to determine the change in the conductivity distributions over time. The reconstruction algorithm is based on a linear method developed by Adler and Guardo [5] allowing for a reconstruction on the order of seconds, which is significantly better than iterative solvers.

The approach taken in this study allowed for the detection of chemical penetrants as well as determining the severity and the location of the penetration. This was accomplished by performing EIT measurements on a conductive MWCNT-PVDF film that embedded within the outer boundary of GFRP composites. This is the first time where EIT is used for chemical penetrant detection, and results will be presented in the near future.

References:

[1] E. T. Thostenson, T.-W. Chou, "Real-time in situ sensing of damage evolution in advanced fiber composites using carbon nanotube networks," *Nanotechnology,* vol. 19, no. 21, pp. 215713, 2008.

[2] B. R. Loyola, V. La Saponara, K. J. Loh, "In Situ Strain Monitoring of Fiber-Reinforced Polymers using Embedded Piezoresistive Nanocomposites," *Journal of Material Science,* vol. 45, no. 24, pp. 6786-6798, 2010.

[3] S. Yesil, C. Winkelmann, G. Bayram, V. La Saponara, "Surfactant-modified multiscale composites for improved tensile fatigue and impact damage sensing," *Materials Science and Engineering: A,* vol. 527, no. 27-28, pp. 7340-7352, 2010.

[4] K. J. Loh, J. Kim, J. P. Lynch, N. W. S. Kam, N. A. Kotov, "Multifunctional layer-by-layer carbon nanotube polyelectrolyte thin films for strain and corrosion sensing," *Smart Materials and Structures,* vol. 16, no. 2, pp. 429-438, 2007.

[5] A. Adler, R. Guardo, "Electrical impedance tomography: regularized imaging and contrast detection," *IEEE Transactions on Medical Imaging,* vol. 15, no. 2, pp. 170-179, 1996.

ID: 607

Inverse Scattering Analysis of Elastic Half Space by Means of the Fast Volume Integral Equation Method

Terumi Touhei
Tokyo University of Science
Japan

Takuya Hinago
Tokyo University of Science
Japan

Abstract:
A method for an inverse scattering analysis is developed in this article by means of the fast volume integral equation method (Touhei, 2011). The property of the volume integral equation, which is the direct of representation of the relationship between the wave field and the fluctuation of the wave field, is used for the formulation. Figure 1 shows the concept of the inverse scattering analysis. Scattered waves observed at the grid points set at the free surface are used to reconstruct fluctuations of the medium. The reconstruction of the fluctuation is carried out at the reference grid points that are set at inside the elastic half space.

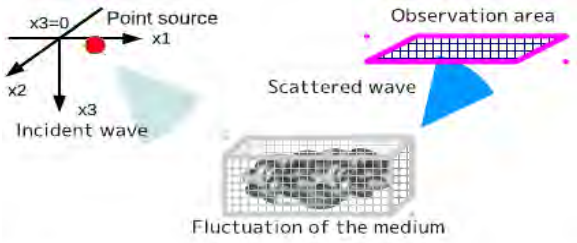

Figure 1: Concept of the analyzed model

The equation for the inverse scattering analysis derived from the volume integral equation becomes

$$u_i = A_{ij} q_j \tag{1}$$

where u_i is the scattered waves at the free surface and q_j is the state vector for expressing on the fluctuation of the medium as follows:

$$(q_j) = (\tilde{\lambda}, \tilde{\mu}, \tilde{\rho}) \tag{2}$$

where λ, μ and ρ are fluctuation of the Lamé constants and the mass density, respectively. In addition, A is the operator constituented by the fast generalized Fourier transform (Touhei, 2011). Note that the subscript index for u_i is the components of the vector. It is well known that the equation for the inverse scattering analysis shows ill-posed properties. Therefore, Tikhonov regularization method is introduce into Eq. (1) to resolve the problem, which becomes as

$$A^*_{ji}u_j = (\alpha\delta_{ik} + A^*_{ji}A_{jk})q_k \qquad (3)$$

where A^* is the adjoint operator for A and α is the regularization parameter. Figure 2 shows the target model of the inverse scattering analysis. The fluctuation of the wave field is expressed by a cube whose one side length is 3 km, that is embeded at the depth of 5 km from the free surface. The fluctuation is expressed by the deviation of the Lamé constants from the background properties of the wave field. To reconstruct the fluctuation, scattered waves are obtained from the fast volume integral equation method. The amplitude and excitation frequency of the point source are 10^7 kN and 1.0 Hz, respectively, and the direction of the force is vertical. Figure 3 shows the scattered waves at the free surface used for the inverse scattering analysis. In order to solve Eq. (3), Bi-CGSTAB method is used. Figure 4 shows the convergence properties of Eq. (3), for the case that the regularization parameter α=10^{-6}. According to Fig. 5. the rapid decrease of relative error can be observed with respect to the iteration number. Figure 5 shows the results of the reconstruction of the fluctuation of the medium, which is shown in the dimensionless form as the ratio of the fluctuation and the background Lamé constants. It is found from Fig. 6, the reconstruction of the fluctuation of the wave field is almost successful.

References

Touhei, T. (2011) A fast volume integral equation method for elastic wave propagation in a half space, International Journal of Solids and Structures 48, 3149-3208

Colton, D. and Kress, R (1998) Inverse Acoustic and Electromagnetic Scattering Theory, Springer-Verlag, Belrin, Heidelberg

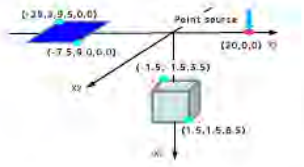

Figure 2: Target model

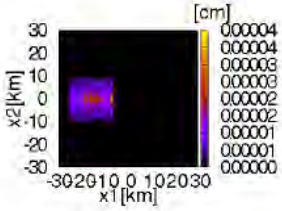

Figure 3: Observed data

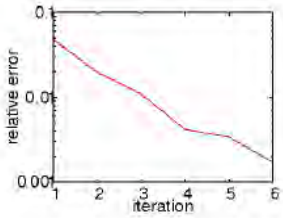

Figure 4: Convergence of the solusion by the Bi-CGSTAB method

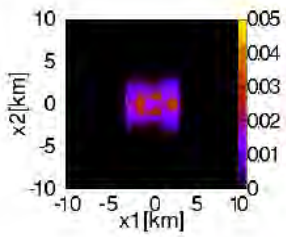

Figure 5: Reconstructured fluctuation in the form of $\widetilde{\mu}/\mu$

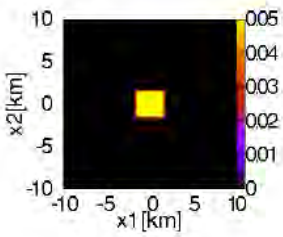

Figure 6: Target model fluctuation in the form of $\widetilde{\mu}/\mu$

Missing Abstract

ID: 646

VI.5

Mechanics of Structures - Computational Modeling of Damage and Fracture in Solids

ID: 118

Interface Affected Cascading In Nuclear Materials and Its Correlation with Bond Strength

Vikas Tomar
Perdue University

You sung Han

Abstract:
Recent results indicate that nanostructured materials may revolutionize the development of radiation damage resistant materials for Gen IV reactors, [1]. One promising candidate is Silicon carbide (SiC). SiC is an important material for several nuclear applications (e.g. high temperature structural material, fuel cladding, and waste form for storage of inert gases, insulation blocks, insulating blankets/weaves, tiles and columns) from the point of view of Gen IV reactors. Factors affecting use of SiC in nuclear applications include dimensional stability under irradiation, effect of grain boundaries, effect of grain size and orientation, and effect of multiple length scales and multiple time scales that come into play when the material properties get influenced by imposed radiations. A common denominatior to these issues is the correlation of radiation damage with bond strength. In this work a quantum mechanical analysis of such factors with a view of cascading effects is presented. Analyses show that a significant electronic and phononic correlation effect exists which leads to a direct dependence of nuclear radiation damage on mechanical strength.

ID: 154

Surface Energy Effects on Evolution of a Nanovoid in a Plastic Material

Jinxing Liu,
King Abdullah University of Science and Technology
Saudi Arabia

Tamer El-Sayed
King Abdullah University of Science and Technology
Saudi Arabia

Abstract:
Surface effects, represented in terms of surface tension/energy, are important on the nanometer scale. Its physical picture is the lower coordination of surface atoms. Due to the Laplace-Young equation, surface energy effects become more and more important with decreasing the material characteristic length. When it comes to the void evolution in plastic materials, surface energy effects become comparable to the yield flow when the void radius deduces to few or few tens of nanometers. Within the framework of static finite deformations, this study provides a theoretical analysis of the evolution of a nanovoid in a plastic material by considering surface effects.

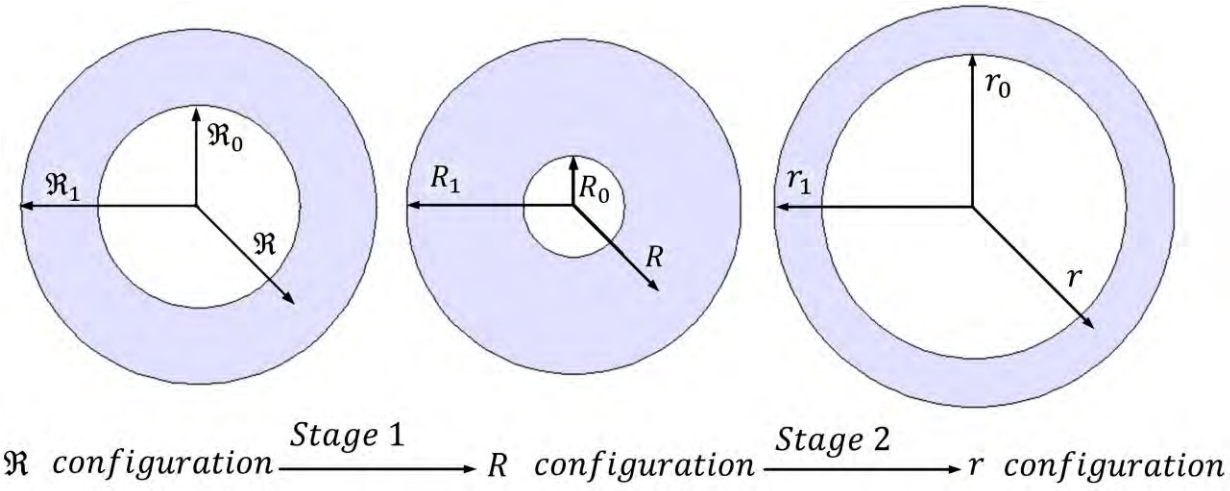

Fig. 1 A spherical void in a finite sphere with A_0 and A_1 the inner and outer radii in the fictitious stress-free configuration A, and, R_0 and R_1 are the radii in the initial configuration R, while r_0 and r_1 are the radii in the external load-driven deformed configuration r.

Based on the previous studies, this investigation accounts for the following additional factors: (1) The initial configuration is obtained by applying the surface actions onto a fictitious stress-free configuration. Therefore, it becomes a prestressed problem. (2) The response under compressive hydrostatic stress is discussed as well as the tensile case. The surface effect tends to hinder the void expansion, but facilitate the shrinkage.

The analytical equilibrium equation under the external hydrostatic pressure is accomplished by a two-stage strategy, as shown in Fig. 1: The first stage evolves under the drive of surface energy from a fictitious stress-free configuration to the initial configuration, and the second proceeds from the initial prestressed configuration to the final configuration under the actions of both surface energy and external loadings.

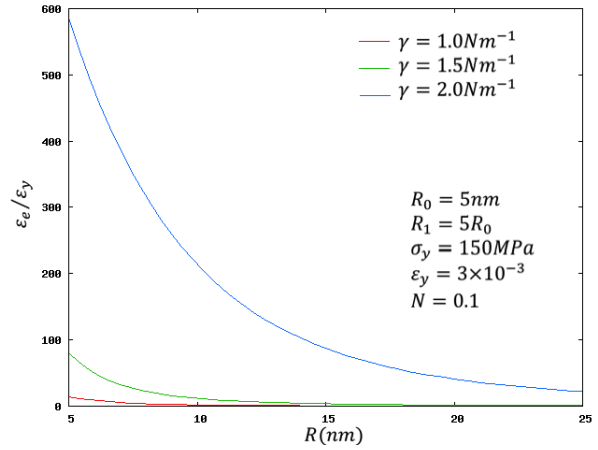

Fig. 2 Distribution of the dimensionless Mises effective strain, $\varepsilon_e/\varepsilon_y$, in relation to the radius-direction position, R, under different surface energies, γ.

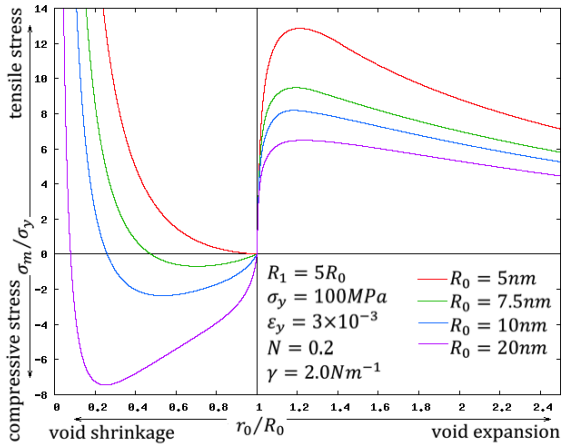

Fig. 3 Loading-deformation curves during shrinkage/expansion of voids with different radii.

This illustrative solution provides a reasonable physical background for the following phenomena: (1) when the void size is under some critical value, finite plastic flow arises in the process from the fictitious stress-free configuration to the initial configuration, and will dramatically influence the subsequent responses (Fig. 2); (2) the evolution of nanovoids is strongly related to their sizes (Fig. 3); (3) the tension-compression asymmetry becomes easy to understand when surface tension is included (Fig. 3); (4) void shrinkage instability is predicted (Fig. 3).

ID: 165

Peridynamic Simulation of Dynamic Hardness and Penetration of Concrete Mesostructures

Christopher Lammi
Georgia Institute of Technology

Tracy Vogler

Abstract:
Numerical simulation of concrete mesostructures during impact is performed using peridynamics, a non-local framework that accounts for finite-range force interactions between material points and therefore is well-suited for capturing distributed fracture. Contact and interaction of the impactor with heterogeneities are explicitly modeled in addition to plastic deformation and fracture. Results of dynamic hardness experiments on ultra-high performance concrete, with loading rates on the order of 1-10 MN/s, are used to calibrate the mesoscale peridynamic material models. The stress fields and damage within the material are characterized. Calculations with systematic variations of mesostructure configurations reveal trends in dissipation and penetration behavior. Optimal material configurations for penetration resistance at different length scales are established. The results will be used for design of penetration-resistant materials.

ID: 260

A Mixed FE Formulation for the Alleviation of Mesh Dependence in Finite-Deformation Inelasticity

Alejandro Mota
Sandia National Laboratorie
USA

James Foulk
USA

Abstract:
A mixed three-field finite element formulation is proposed as a method for the alleviation of mesh dependency in finite-deformation inelastic problems subjected to bifurcation.
The additional fields in the formulation are the internal variables that cause bifurcation and the corresponding conjugate thermodynamic forces. The formulation leads to expressions for the additional fields that are akin to nonlocal averages that extend to a domain defined by the interpolation functions selected for these fields. The size of the nonlocal domain controls the length scale of the problem. The formulation provides effective regularization, entirely by-passes the introduction of new and independent mechanical variables into the problem, discretizes naturally, computes averages with regular interpolation functions, and does not require changes to constitutive relationships.

The performance of the formulation is demonstrated by several examples where it is shown that it is effective in alleviating mesh dependence.

ID: 323

Modeling Fracture within the Optimal Transportation Meshfree (OTM) method

B. Li
Graduate Aeronautical Laboratories, California Institute of Technology, Pasadena, CA 91125 U.S.A.

A.Pandolfi
Dipartimento di Ingegneria Strutturale, Politecnico di Milano 20133 Milano Italy

M. Ortiz
Graduate Aeronautical Laboratories, California Institute of Technology, Pasadena, CA 91125 U.S.A.

Abstract:
We evaluate the performance of an innovative approach to dynamic fragmentation in applications involving high rate deformations and strain localization in ductile materials. The approach combines the Optimal Transportation Meshfree (OTM) method of Li et al. [1], developed for the analysis of the dynamics of general solid and fluid flows, with the energy-based eigenerosion method to track the propagation of cracks [2, 3].
The OTM method is an incremental Lagrangian meshfree scheme that combines: i) The Optimal Transportation approach to time discretization of the action which leads to geometrically-exact updates of the local volumes and mass densities, and exact conservation properties including symplecticity, linear and angular momentum; ii) material-point sampling (cf., e. g., [4]) in order to track the local state of material points, carry out complex constitutive updates and perform spatial integrals; iii) local Maximum-entropy (max-ent) meshfree interpolation [2] from a nodal-point set which offers the advantage of being meshfree and entirely defined, essentially explicitly, by the current nodal-set positions, thus effectively sidestepping the need for continuous remeshing in simulations of materials undergoing extreme conditions. In addition, local max-ent interpolation satisfies a Kronecker-delta property at the boundary, which greatly facilitates the enforcement of essential boundary conditions, and has good accuracy convergence and monotonicity conditions. Because of interpolatory nature, OTM is free from the tensile numerical instabilities that plague particle methods.
Many of the applications where Lagrangian meshfree schemes, such as the OTM method, are attractive involve material failure and fracture. In this paper we assess the performance of a recently proposed approach to fracture, termed eigenfracture [5], within a meshfree framework. When combined with the material-point scheme, eigenfracture may be implemented as material-point failure, i.e., the material-points can be either intact or be completely failed and have no load bearing capacity. To this end, the energy functional depends on two fields: the displacement field and an eigendeformation field that describes such cracks as may be present in the body. In addition, in the eigenfracture scheme the fracture energy is set to be proportional to the volume of the ϵ-neighborhood of the support of the eigendeformation field, suitably scaled by $1/\epsilon$. The optimal crack set is obtained by minimizing the resulting energy functional with respect to both

the displacement and the eigendeformation fields, subject to irreversibility constraints. The eigenfracture scheme is known to properly converge to Griffith fracture in the limit of vanishingly small mesh sizes [5]. In particular, the local-neighborhood averaging of the energy which underlies the calculation of the effective energy-release rate has the effect of eliminating spurious mesh-dependencies.
The evaluation takes the form of a conventional validation analysis, supported by the experimental results on spherical shell caps undergoing explosive loading, as documented in [6]. The simulations have been conducted in concurrent computing setting. The complex outcomes of the experimental tests are captured by the numerical simulations, in terms of extension of the fully damaged area, crack pattern, velocity of flying cap and fragment size distribution.

References

[1] B. Li, F. Habbal, and M. Ortiz. Optimal transportation meshfree approximations schemes for fluid and plastic flows. International Journal for Numerical Methods in Engineering, 83(12):1541-1579, 2010.
[2] A. Pandolfi and M. Ortiz. An eigenerosion approach to brittle fracture. International Journal for Numerical Methods in Engineering, Accepted, 2012.
[3] A. Pandolfi, B. Li, and M. Ortiz. Modeling fracture within local max-ent meshfree approximation schemes. International Journal for Numerical Methods in Engineering, In Preparation, 2012.
[4] D. Sulsky, Z. Chen, and H. L. Schreyer. A particle method for history-dependent materials. Computer Methods in Applied Mechanics and Engineering, 118:179-196, 1994.
[5] B. Schmidt, F. Fraternali, and M. Ortiz. Eigenfracture: an eigendeformation approach to variational fracture. SIAM Journal on Multiscale Modeling and Simulation, 7:1237-1266, 2009.
[6] G. H. Campbell, G. C. Archbold, O. A. Hurricane, and P. L. Miller. Fragmentation in biaxial tension. Journal of Applied Physics, 101:033540, 2007.

ID: 375

Crystalline Plasticity as a Source of Hot Spots in Energetic Molecular Polycrystals

D. Barrett Hardin
Georgia Institute of Technology
USA

Min Zhou
Georgia Institute of Technology
USA

Abstract:
A fully dynamic, 3D Lagrangian finite element framework accounting for anisotropic elasticity, crystalline plasticity, polycrystalline material structure, plasticity-induced heat generation, and thermal diffusion is developed to analyze the contribution of plastic slip to hot spot formation in energetic HMX during impact loading. The material of interest has polycrystalline microstructures with grain sizes in the range of 300 The simulations focus on the thermomechanical response under planar impact with impact velocities between 100 800 m/s . Calculations are carried out to quantify the sizes and temperatures of hot spots as functions of grain size and loading rate. The quantification provides insight into the microstructure-performance relationships which determine the thermal stability and mechanical integrity of energetic materials under dynamic loading.

ID: 464

An Inverse Analysis for Determining Cohesive Zone Model Parameter Values For Simulating Crack Growth in a Ductile Material

Xin Chen
Department of Mechanical Engineering, University of South Carolina
United States

Xiaomin Deng[4]
Department of Mechanical Engineering, University of South Carolina,
United States

Michael A. Sutton
Department of Mechanical Engineering, University of South Carolina,
United States

Pablo Zavattieri[5]
GM Research and Development Center,
United States

Abstract:
An inverse analysis using a modified Levenberg-Marquardt method is carried out to identify cohesive zone model parameter values for use in 3D finite element simulations of stable tearing crack growth events in Arcan specimens under Mode I and mixed-mode I/II loading conditions. The specimens are made of 2024-T3 aluminum alloy. The triangular cohesive law is employed in the simulations. A set of cohesive parameter values is determined in the inverse analysis by minimizing the difference between simulation predictions of key points on the load-crack extension curve with experimental measurements. Using the identified cohesive parameter values, the predicted CTOD variation with crack extension is compared with experimental measurements, which provide a validation of the cohesive parameter values and of the finite element simulation predictions.

Figure 1 shows a comparison of the predicted and measured load vs. crack extension curve for the Mode I loading experiment. Two predictions are included. One prediction uses cohesive parameter values identified from the inverse analysis, and the other uses cohesive parameter values obtained manually by trial and error. The two sets of cohesive parameter values are not the same, but they lead to basically the same predictions. This non-unique issue needs further investigation.

[4] Corresponding author; Email: deng@engr.sc.edu (X. Deng).
[5] Currently at Purdue University, West Lafayette, IN, USA.

Figure 2 shows a comparison of predicted and measured CTOD variation (at 1.0 mm behind the crack tip) with crack extension. Averages of the two sets of predicted CTOD values for crack extensions beyond 10.0 mm are similar and match with measured CTOD value from experiment.

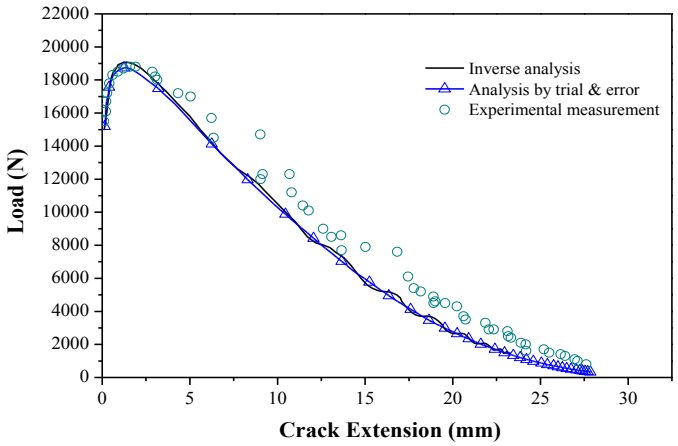

Fig. 1 Comparison of predicted and measured load vs. crack extension curves.

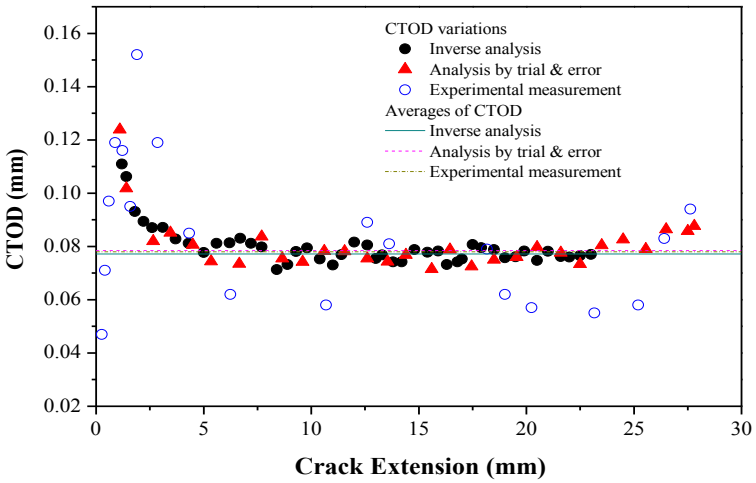

Fig. 2 Comparison of predicted and measured CTOD variation with crack extension.

Acknowledgements:
The authors gratefully acknowledge the financial support provided by AFOSR (Grant # FA9550-09-0543; program manger Dr. David S. Stargel) and by the GM R&D Center.

ID: 468

3D VCCT with Locally Structured Re-meshing for Evaluating Mixed-Mode Stress Intensity Factors in Crack Growth Simulations along Curved Crack Paths

Xiaomin Deng[6]
Department of Mechanical Engineering, University of South Carolina
United States

Xiaodan Ke
Correlated Solutions
United States

Michael A. Sutton
Department of Mechanical Engineering, University of South Carolina,
United States

Eileen E. Miller
Department of Mechanical Engineering, University of South Carolina,
United States

Hubert W. Schreier
Correlated Solutions
United States

Abstract:
Finite element simulation techniques have been developed to evaluate three-dimensional mixed-mode stress intensity factors (SIFs) in crack growth simulations along curved crack paths. These have been achieved using the three-dimensional virtual crack closure technique (3D VCCT) with a locally structured re-meshing approach, in which the local region immediately surrounding a moving crack front is automatically re-meshed with a structured mesh pattern to facilitate the 3D VCCT and maintain its accuracy. The prediction of the crack growth direction is achieved using the maximum circumferential stress criterion. Numerical SIF verification examples and experimental validations of crack path predictions are performed. Numerical verification examples show that the locally structured re-meshing approach for 3D VCCT can accurately determine mixed-mode SIF values even with relatively coarse meshes. Experimental validation studies for 3 curvilinear crack growth cases demonstrate that the predicted curvilinear crack paths compare well with experimentally measured crack paths.

Figure 1 shows the deformed shape of an automatically generated mesh for a plate containing a central hole and an offset crack. The crack originates from the left edge of the plate and runs into

[6] Corresponding author; Email: deng@engr.sc.edu (X. Deng).

the hole under displacement loading along the top and bottom edges of the plate. The mesh is composed of 10-node tetrahedral elements. The overall mesh is unstructured. A locally structured mesh is automatically generated around the moving crack front.

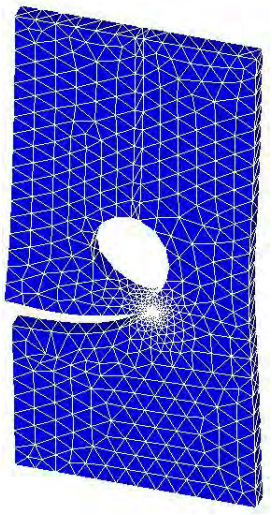

Fig. 1: Deformed shape of a mesh for a plate containing a central hole and an offset crack.

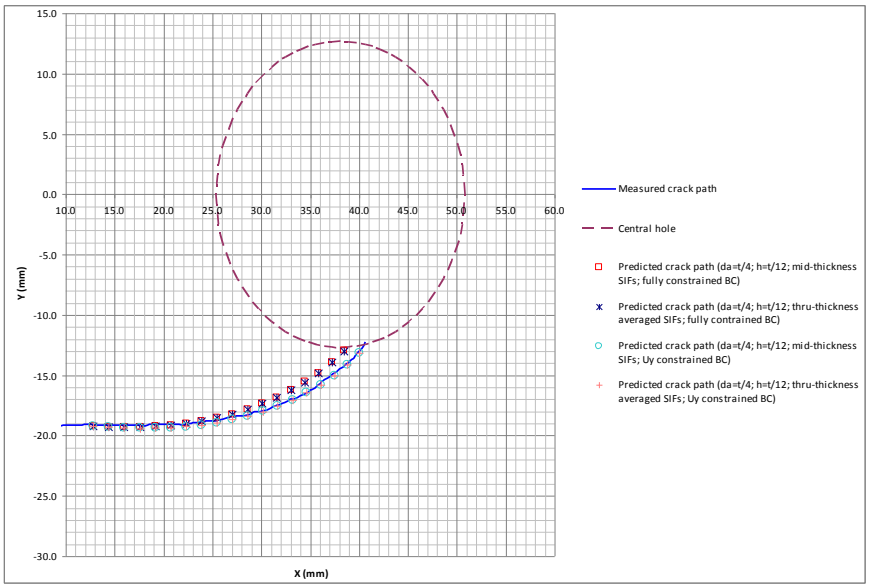

Fig. 2: Comparison of simulation predicted and experimentally measured crack paths.

For the experimental case shown in Fig. 1, two ways of approximating the applied displacement BCs along the top and bottom edges are considered: (1) all 3 displacement components are constrained and (2) only the displacement component in the loading direction is constrained. Also, two ways of predicting the crack paths are considered: (1) using mid-thickness SIF values and (2) using thickness-averaged SIF values. As such, there are 4 predictions. Figure 2 shows a comparison of the predicted and measured crack paths.

Acknowledgements:
The authors gratefully acknowledge the financial support provided by an AFRL SBIR project (Contract#: FA8650-10-C-3001). They would also like to express their gratitude to AFRL engineers Mr. Robert Reuter and Mr. Jim Harter for their support and helpful discussions.

ID: 493

Fatigue Stage I/II Transition at a Microstructural Scale

Gustavo Castelluccio
Georgia Institute of Technology
USA

David McDowell
Georgia Institute of Technology
USA

Abstract:
Fatigue crack formation and early growth can be significantly influenced by microstructuctural features such as grain size and morphological and crystallographic texture. In spite of its significance in industry applications in the high cycle fatigue regime, the prediction of the influence of microstructure on early stages of crack formation and growth in engineering alloys remains underdeveloped. This work considers finite element simulations that explicitly render the microstructure of selected FCC metallic systems and a fatigue methodology that estimates transgranular fatigue growth for microstructurally small cracks. By extending the crack on a grain-by-grain basis, we study the orientation of the crack in an attempt to describe the fatigue StageI/StageII transition. Crack growth is considered with an analytically embedded damage model that redistributes stress and strain as the cracks extend. The methodology is implemented using a crystal plasticity algorithm in Abaqus and calibrated to study the effect of microstructure on early fatigue life of a powder processed Ni-base RR1000 superalloy at elevated temperature under constant amplitude loading.

ID: 510

New Tensors for Anisotropic Damage in Continuum Damage Mechanics

George Voyiadjis
Louisiana State University

Mohammed Yousef

Abstract:
NO ABSTRACT

ID: 518

On the Numerical Integration of the Modified Gurson Model for Shear-dominated Ductile Failure Simulation: Hypo- and Hyper-elastic Formulations at Finite Strains

Qiushi Chen and Jakob T. Ostien
Sandia National Laboratories,
United States

Abstract:
The Gurson damage model has been broadly applied in simulating ductile failure of metals, which is traditionally associated with the nucleation, growth, and coalescence of micro-voids, eventually leading to rupture. Recent advances in the Gurson model have afforded it the ability to account for low stress triaxiality by introducing the third-stress-invariant into the void evolution law. As the complexity of the model increases, so does its numerical integration, especially in the large deformation region. In this work, various aspects of numerical integration are considered. In particular, we will discuss in detail the implicit stress integration algorithms within the finite deformation regime using both hypo- and hyper-elastic formulations. With regard to consistent tangent computation, unlike the conventional methods where tangents are derived analytically or approximated by a finite difference method, we will show a new way of exactly computing the consistent tangents by forward automatic differentiation. Benchmark material point simulations will be carried out to verify the modified model and its implementation. Numerical implementation issues will be presented and finite element simulations of a 3D cylindrical specimen under uniaxial tension are then analyzed.

Shear-modified Gurson model

A recent modification to the Gurson model was proposed in [1] to address the issue of void growth under low stress triaxiality. The modified void growth function is given as

$$\dot{f} = (1-f)\dot{\varepsilon}^p_{kk} + k_w \frac{f\,\omega(\sigma_e, J_3)}{\sigma_e} s_{ij}\dot{\varepsilon}^p_{ij}$$

where $\dot{\varepsilon}^p_{ij}$ is the plastic strain rate, k_w is a material constant. $\omega(\sigma_e, J_3)$ is a function of the equivalent stress and the third stress invariant, and affords the model the ability to predict void growth under pure shear state.

Numerical integrations: hypo- and hyper- elastic formulations at finite strains

In the hypo-elastic formulation, the modified Gurson model is integrated using a corotational stress update algorithm. We have retained, as a basic assumption, the additive decomposition of the strain rate tensor into an elastic and a plastic part. A key feature of this corotational algorithm is the uncoupling of material and geometrical nonlinearities. It is based on an *incrementally objective* elastic predictor, followed by a return mapping preformed on a rotated configuration, such that the return mapping is formally identical to that of the equivalent constitutive model in the small deformation region. Because of this uncoupling, the hypoelastic formulation is very

versatile and can be applied independent of material-specific details of the constitutive model. As far as accuracy is concerned, as will be shown in the numerical examples, the hypo-elastic formulation is very close to the hyperelastic counterpart.

For hyper-elastic formulation, the modified Gurson model is formulated within the framework of geometrically exact finite multiplicative elastoplasticity, where the deformation gradient is multiplicatively decomposed into an elastic and a plastic part. The elastic response is derived from the Helmholtz free energy function, which is assumed to be an isotropic function of the spatial elastic logarithmic Hencky strain tensors. For integration, exponential map stress integrators are applied. The advantage of this hyper-elastic formulation is that it is founded upon thermodynamic basis, and the choice of logarithmic strain measure yields convenient stress integration algorithm.

While fully-implicit integration algorithms are more stable and allow for larger time increments to be used compared to explicit algorithms, they also requires the iterative solution of a nonlinear system of equations, for which the algorithmic or consistent tangent moduli have to be computed. In this work, we adopted a novel, exact numerical method employing Forward Automatic Differentiation (FAD) to obtain the consistent tangent. The exact computed tangent yields quadratic convergence rates.

Numerical examples

The numerical implementations of the modified Gurson model using both hypo- and hyperelastic formulations are verified through representative examples. Results of a simple shear tests are shown in Figure 1. The modified Gurson model has also been applied to simulate 3D cylindrical specimens under uniaxial tension.

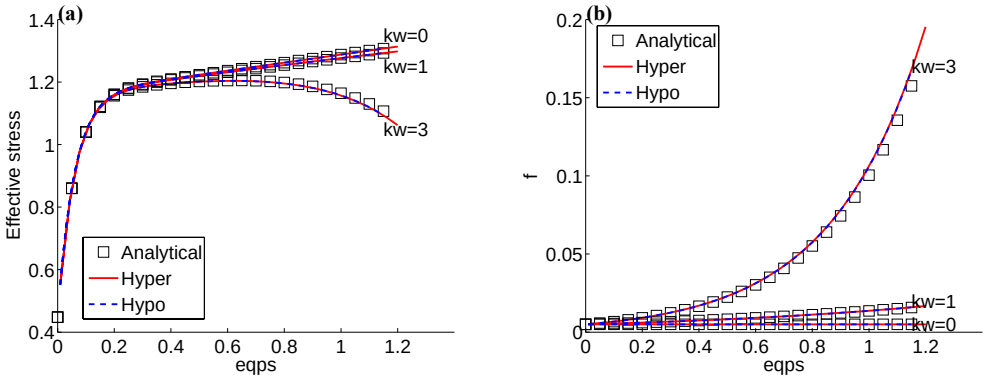

Figure1. (a) Stress-strain response for simple shear tests. (b) Void growth. (kw=0 recovers the original Gurson model)

Acknowledgements

Sandia is a Multiprogram Laboratory Operated by Sandia Corporation, a Lockheed Martin Company, for the United States Department of Energy Under Contract DE-ACO4-94AL85000.

References

[1] Nahshon, K., Hutchinson, J.W. Modification of the Gurson model for shear failure. European Journal of Mechanics, 27:1-17, 2008.

ID: 547

Mesoscale model for the inelastic behavior and fracture of cellulose nanocrystals

F. Dri, P.D. Zavattieri, A. Martini, R. Moon

Purdue University, West Lafayette, IN 47906

Abstract: We present an atomistically-informed mesoscale model to study the fundamental mechanical behavior of the Cellulose Nanocrystals (CNC). The proposed model explicitly accounts for the structural behavior of individual cellulose chains and their interaction through short- and long-range forces. Preliminary molecular dynamic studies based on thought-experiments provided the necessary information to describe the individual chains using a conventional finite element framework. Special care is taken for the non-covalent interaction such as hydrogen bonds and van der Waals forces using local and non-local approaches. In this talk, we describe the model and a methodology to quantify and characterize the forces involved in the deformation of CNCs under various loading conditions.

Introduction

Nature has created efficient strategies to make materials with hierarchical internal structure that often exhibit exceptional mechanical properties. One such example is found in cellulose. These natural materials achieve a high order of functionality and mechanical properties through a well designed hierarchical structure with an exceptional control from the atomic level all the way to the macroscopic level.

For engineering purposes, cellulose-based materials have been used for thousands of years essentially for their great qualities in many fields. However, nature has used cellulose for very specific and highly specialized purposes (e.g. structural support in plants, trees, etc.) based on its particular mechanical properties.

The aim of this work is to present a multiscale framework to develop the appropriate models that can be used to describe and predict the cellulose mechanical behavior using state-of-the-art tools to connect atomistic-based models (QM, MM and MD) to experiments (X-Ray diffraction, Nanoidentation) using continuum-based modeling techniques (FEM, continuous theories).

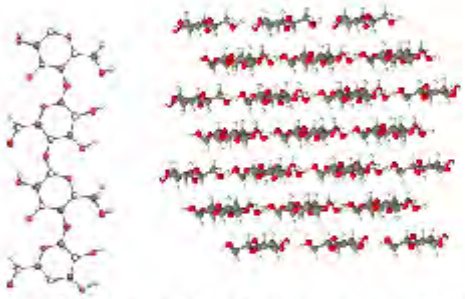

Figure 1: [left] Single chain representation made using β(1→4) linked D-glucose units. [Right] Front view of a CNC crystal made using cellulose chain in a I-β configuration.

Numerical methods

Atomistic simulations: Atomic-scale modeling has been used in this work to predict structural, energetic, and mechanical characteristics of cellulose as well as provide a fundamental understanding of the atomic-scale origins of these characteristics. Both, cellulose chains and CNC crystals, were constructed using β(1→4) linked D-glucose units.Several thought experiments were conducted such as uniform-stretching tensile test, uniform-curvature bending and fixed-axis torsion. Key parameters were extracted from these simulations to provide the necessary information that defines the continuum based model.

Finite element method: Three continuum elements were developed to characterize the main physical features of the system. A modified 3D beam element with 6 d.o.f. per node was used to simulate the elastic behavior of each of the single chains that conform a crystal. This element uses regular Euler-Bernouli type shape functions with a special treatment for the material properties and section characteristics. An interface element was developed to simulate the internal forces product of hydrogen bonding. The definition of the element is coupled with the formulation utilized to model single chains allowing direct transfer of forces and moments between both elements. Finally, an interface element was developed to treat the forces product of van der Waals interactions from a local point of view.

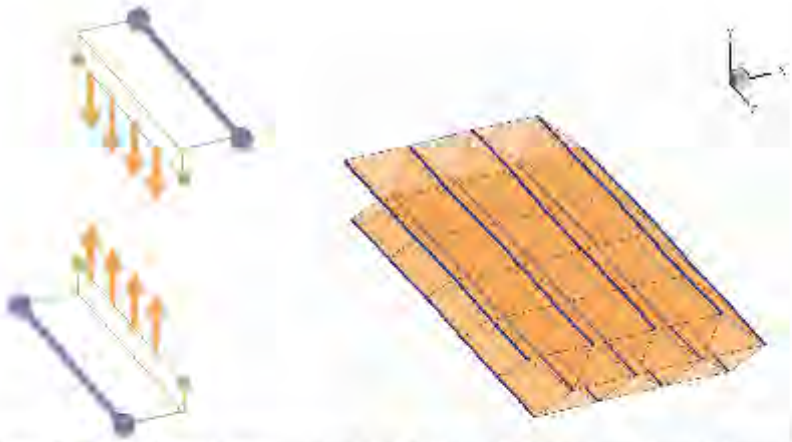

Figure 2: [Left] Schematic representation of the hydrogen bond interaction (orange) between to adjacent beam elements (purple). [Right] Finite element model of a single CNC crystal, beam elements in purple, interface elements in orange.

ID: 550

Application of Cohesive Zone Models for Biomineralized and Biomimetic Materials

Pablo Zavattieri
Purdue University

Isaias Gallana

Abstract:

Biomineralized materials have the ability to employ high volume fraction of modest and brittle materials and still exhibit surprising mechanical performance. Decoding the structure-function relationship of these materials is a challenging task that requires knowledge about the actual loading and environmental conditions of the material in their natural habitat, as well as a complete characterization of their constituents and hierarchical ultrastructure through the use of modern tools such as in-situ electron microscopy, small-scale mechanical testing capabilities, prototyping, and advanced numerical models. In turn, this provides the necessary tools for the design and fabrication of biomimetic materials with remarkable properties. In this talk, I will review some of our research activities covering the numerical aspects of fracture and damage in naturally occurring and biomimetic materials, including biomineralized materials found in the shell of abalones, teeth of chitons and hyper-mineralized exosqueleton of mantis shrimps. In our approach, we adopt a finite element methodology that uses a cohesive approach to brittle and quasi-brittle fracture in the mineral.

ID: 568

Modeling failure in 304-L laser welds through 3-D void structures and strong thermo-mechanical coupling

James W. Foulk III[1], John M. Emery[2], Michael G. Veilleux[1], Glen A. Hansen[2], Jakob T. Ostien[1], Alejandro Mota[1], WaiChing Sun[1], Jonathan D. Madison[2], Brad L. Boyce[2]

[1]Sandia National Laboratories, 7011 East Ave., Livermore, CA 94550
[2]Sandia National Laboratories, 5800 Eubank Blvd., Albuquerque, NM 87185

Abstract for the 49th meeting of the SES at Georgia Tech, October 10-12, 2012

The failure of Nd:YAG laser welds in 304-L stainless steel have been investigated through the direct incorporation of void structure at the specimen level. Micro-computed tomography (μCT) is employed to characterize the porosity and develop statistical representations of the size, shape, and spacing of the voids. Ellipsoidal voids with major axes on the order of 150 μm are located within a weld ligament of only 500 μm. Because the 304-L load-bearing ligaments have limited thermal conductivity and generate substantial plastic work through continued hardening, an explicit 3-D representation and a fully coupled thermo-mechanical finite deformation scheme are needed to simulate the onset of necking and subsequent (and rapid) unloading of the specimen. Large deformations prior and throughout the necking process necessitate mesh adaptivity. Through explicit incorporation of the void structures and strong coupling, simulations naturally yield the rapid unloading that delineates weld failure.

Sandia National Laboratories is a multi-program laboratory managed and operated by Sandia Corporation, a wholly owned subsidiary of Lockheed Martin Corporation, for the U.S. Department of Energy's National Nuclear Security Administration under contract DE-AC04-94AL85000.

ID: 583

A Hybrid Structure Evaluation and Fatigue Damage Assessment Toolkit for Hybrid Materials and Structures

Eugene Fang
Global Engineering and Materials, Inc.
United States

Michael Stuebner
Global Engineering and Materials, Inc.
United States

Phillip Liu
Global Engineering and Materials, Inc.
United States

Henry Sklyut
Alcoa Technical Center
United States

Markus Heinimann
Alcoa Technical Center
United States

Abstract:

A Hybrid Structure Evaluation and Fatigue Damage Assessment (HYSEFDA) toolkit for Abaqus has been developed to perform fatigue damage and life prediction of hybrid materials/structures of arbitrary configurations. A mesh independent discrete multi-mode damage insertion, propagation, and interaction solution module has been developed and implemented within Abaqus via its user-defined subroutines. The resulting HYSEFDA toolkit can perform the co-simulation of metal ply cracking and its associated delamination evolution at the composite and metal ply interface under fatigue loading. The most attractive feature of the HYSEFDA toolkit is that it can accurately capture the thin layered structural response via a user-defined solid element, characterize multiple initial delaminations and ply cracks that are independent of an existing finite element mesh and track their moving fronts without remeshing. To determine the strain energy release rates (SERRs) at a moving delamination crack front that is not in conformation to the existing finite element mesh, both a user-defined interface and a user-defined element for a discrete spring have been developed and coupled with a virtual crack closure technique (VCCT). Driven by the high accuracy requirement in determination of SERRs for its subsequent fatigue crack growth prediction, a locally smoothed VCCT has been implemented to improve the accuracy in extraction of SERR at an arbitrary delamination front.

This delamination model is further extended to simulate multiple arbitrarily shaped delamination cracks located either at the same or different composite and metal interfaces. Such a complicated problem will pose a great challenge using a conventional remeshing or an adaptive mesh approach. As shown in Fig. 1, a virtual front and an FE front are used to track the evolution of a delamination zone. The FE front is defined to pass a set of FE nodes that divide the debonded zone and the bonded zone; it always conforms to the FE mesh, so it is zigzagged in most cases. The virtual delamination front is considered as being more "physical" or "actual"; it can be curves of any shapes, and there is no restriction that it has to pass any specific node or element. The growth direction and its growth step size are determined from the normality condition and a Paris fatigue law under a given increment number of cycles ΔN. To demonstrate the capability and versatility of the developed

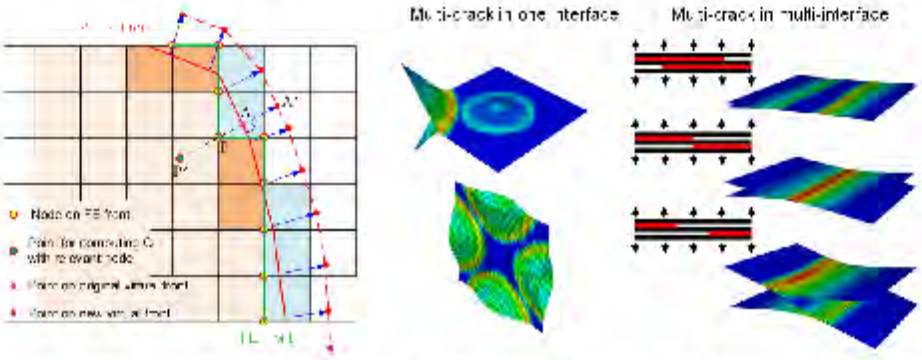

Figure 1. Geometric Tracking Module in HYSEFDA for Propagation of Arbitrary Delamination Crack Front

delamination tracking module, several demonstration examples are shown in Fig. 1 with delamination zones either at one interface or different composite and metal ply interfaces.

In parallel with the mesh independent delamination characterization and tracking of multiple delamination fronts under fatigue loading, we have also developed a mesh independent curvilinear crack growth characterization module for simulation of metal ply cracking based on a phantom-paired element. A user-defined element via an Abaqus interface, UEL, is shown in Figure 2. The element is similar to the C3D8 solid element except that it has doubled degrees of freedoms (DoFs) at each node. When a crack cuts the element, the relevant phantom DoFs are automatically activated and the original connectivity is regrouped into a pair of separated elements.

A virtual extension strategy has been implemented to extract the energy release rate where its conversion to the corresponding stress intensity factor can be achieved under a given plane stress or plane strain condition. Penalty springs are inserted at the physical crack for detecting the closing forces and the energy release rate is extracted via VCCT. A virtual extension approach

has been implemented in HYSEFDA to remove the root rotation lock. By using the virtual extension coupled with the application of penalty springs along the virtual extended crack surface, a correct kinematic description of the crack opening in the vicinity of its tip can be captured.

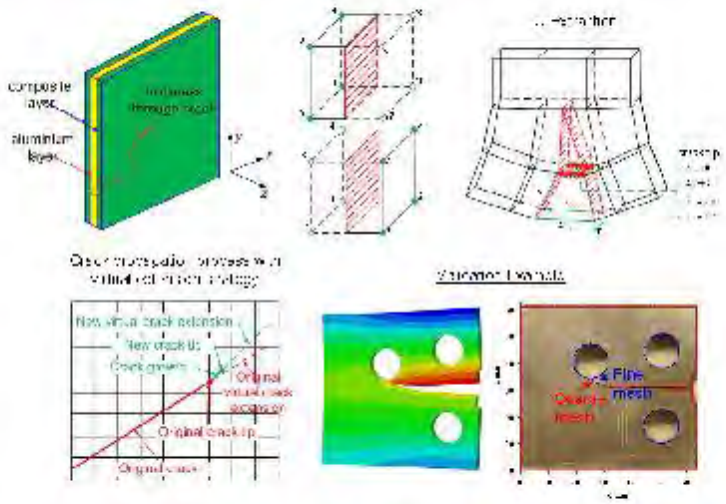

Figure 2. A Mesh-Independent Solution Module for Metal Layer Cracking

A fundamental problem shown in Fig. 3 is designed to test our coupling strategy that works for a pair of cracks in the FML. This example is generated based on Alcoa's bond-preg example. An initial through-the-thickness crack is introduced in all layers to activate the crack propagation in the metal ply and its associated delamination at the interface between the composite and the metal ply. Assuming the symmetric nature of the system after the damage, Alcoa's problem can be further simplified by modeling and simulating only half of the system that involves one (1) metallic layer crack and one (1) delamination crack.

We use the same in-plane dimension and material properties as those used by Alcoa for their bond-preg problem. An initial residual stress field is introduced by performing a thermal-mechanical analysis with a temperature drop of 98 ^{o}C. The initial metal ply crack is assumed to have a length of 0.4 in and the initial delamination zone is assumed to have its band shape of width 0.05 in. Despite the simplification of Alcoa's bond-preg system via GEM's 1-pair of cracks model, the predicted shape of the delamination zone has a good agreement with the result from the ASPAN model.

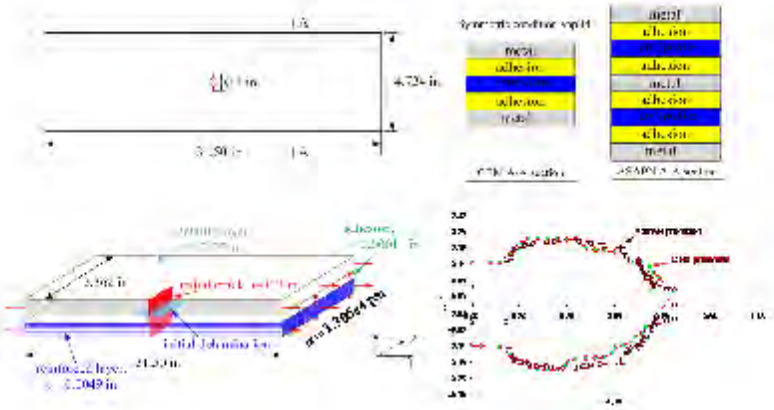

Figure 3. A 2/1 FML with a Horizontal Crack in a Metal Ply

ID: 584

A Mesh-Independent Crack Growth Simulation in 3D Structures Using XFA2D/XFA3D

Michael Stuebner
Global Engineering and Materials, Inc.
United States

Philip Liu
Global Engineering and Materials, Inc.
United States

Eugene Fang
Global Engineering and Materials, Inc.
United States

Jim Lua
Global Engineering and Materials, Inc.
United States

David Chopp
Northwestern University
United States

Abstract:
Aggressive performance and weight optimization are driving the aerospace industry towards the use of an advanced numerical simulation tool coupled with a reduced number of structural tests for design certification and durability assessment. A crack growth pattern in a large scale welded or bolted metallic structure is complex because of the presence of 3D stress field, local stress concentration, material heterogeneity, structure discontinuity, and applied load mixity. To alleviate the computational burden associated with the insertion and propagation of arbitrary cracks in a large scale structure, an extended finite element (X-FEM) based toolkit for Abaqus, XFA, has been developed for both the static failure and life prediction of a solid structure. A nodal enriched displacement field coupled with a level set description is developed and implemented in Abaqus implicit solver via its user-defined subroutines. The mesh independent curvilinear crack growth is captured through a new variant of an explicit crack representation with a front tracking algorithm within a structured finite difference domain.

To reduce the computational burden for characterization of a 3D crack along with its growth, a 2D crack modeling approach has still found to be very attractive for a quick life assessment of a flawed component. Despite a possible curvilinear crack growth path, the numerical challenge associated with a non-planar crack growth does not exist. While a 2D model can be treated as a special case of the 3D model, it is still a time consuming process to solve a 2D crack growth using its associated 3D model.

The 2D X-FEM toolkit for Abaqus (XFA2D) has been developed by integrating the key solution modules with the Abaqus user-defined subroutines. The formulation of XFA2D and its capability is illustrated in Fig. 1 and 2, respectively. For a give initial crack, a level set initiation module is performed to compute both the crack line and crack tip level set functions. The crack morphology is included by enrichment with a priori knowledge of the analytical solution for the displacement field around a crack tip in an infinite domain. Additional unknowns corresponding to enrichment terms are added to the global stiffness matrix. Based on the user-defined number of tip enrichment layers and the sign of level set (LSET) values associated with all the nodes of an element, either the tip (yellow colored nodes) or jump (blue colored nodes) enrichment can be identified as shown in Fig. 2. The tip enrichment is based on the asymptotic solution (B_α) while the jump enrichment is formed using the Heaviside step function (H). For an element cut by the crack segment either fully or partially, a slicing technique has been implemented in XFA2D for the subdomain integration to account for the presence of the displacement discontinuity. After solving the X-FEM equations, a post-analysis module is used to extract the SIFs (K_I, K_{II}) based on the crack opening displacement (U_I, U_{II}) at a sampling point with distance r from the tip. Since Abaqus/Viewer cannot display the results associated with the user-defined elements, a visualization shown in Fig. 2 has been implemented in XFA2D using element triangulation. The applicability and accuracy of the current XFA2D have been demonstrated in Fig. 2 via the solution to a multiple cracks problem, a modified compact tension specimen with both the sink and missing hole configurations, and a curvilinear fatigue crack growth from a welding toe.

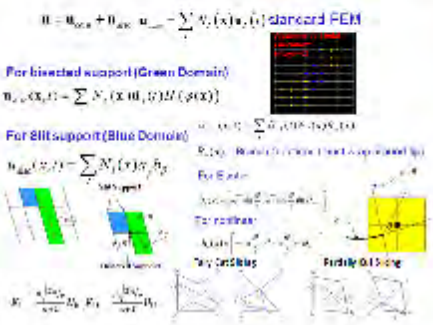

Figure 1. Summary of XFA2D methodology

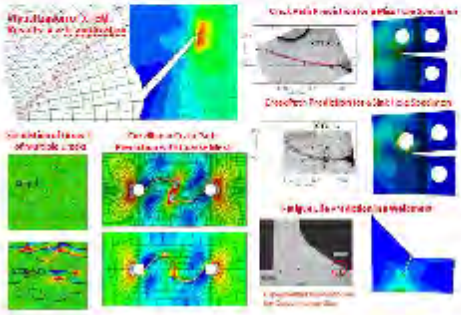

Figure 2. Capability Illustration of XFA2D

In addition to the XFA2D toolkit, a three-dimensional extended finite element method (XFA3D) has been also developed to capture the nonplanar crack growth in the presence of the structural complexity, initial stress distribution, arbitrary initial crack geometry, and mixed mode loading condition. The XFA3D coupled with an explicit crack front tracking for Abaqus is used to perform curvilinear crack growth predictions for metallic structures. An explicit representation, where the crack is tracked by a collection of triangular elements, provides the crack tip location effectively. Given a triangulated surface associated with a propagating crack, the level set values

can be computed at an arbitrary finite element nodal point for the subsequent determination of the crack growth driving force at the new crack front via the X-FEM solver. The main features of the XFA3D include: 1) model preparation and arbitrary insertion of initial cracks that are independent of the base model via Abaqus/CAE; 2) extraction of stress intensity factors on static or growing crack fronts in metallic structures via the crack tip opening displacement (CTOD) and life predictions; and 4) post-processing of the cracked region using Abaqus/Viewer. The capability demonstration for 3D crack growth under monotonic and fatigue loading is shown in Fig. 3.

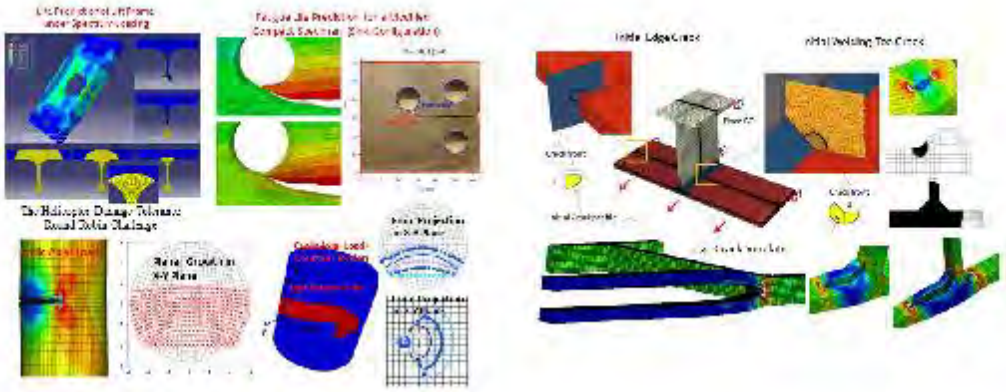

Figure 3. Capability demonstration of XFA3D in metallic structures without and with welding

ID: 585

Ductile Fracture and Crack Path Prediction of Thin-Walled Aluminum Structures under Dynamic Loading

Eugene Fang
Global Engineering and Materials, Inc.
United States

Phillip Liu
Global Engineering and Materials, Inc.
United States

Tingting Zhang
Global Engineering and Materials, Inc.
United States

Ling Liu
Utah State University
United States

Jack Chessa
University of Texas at Al Paso
United States

Ted Belytschko
Northwestern University
United States

Abstract:
Various structural failure modes contribute to the loss of integrity of large scale aluminum structures subject to blast loading; these being dependent on material selection and structural configuration. Modeling the structure's response encompasses material constitutive equations, fracture and damage mechanics, nonlinear dynamics simulation codes and structural finite element analyses. To perform dynamic crack path and load-deflection prediction with key capabilities in characterization of the effects of strain rate, stress triaxiality, and nonlinear fracture induced energy dissipation, a software toolkit for Abaqus' explicit solver (XSHELL) has been developed for welded metallic structures subjected to impulsive loading. The mesh independent crack description and fracture energy dissipation is achieved in XSHELL through the implementation of two overlay elements with an embedded cohesive interaction along an arbitrary crack segment without in conformation to the existing finite element mesh. An advanced ductile fracture model coupled with a nonlocal failure theory is implemented to capture the nonlinear fracture initiation in aluminum alloys. An advanced cohesive and a crack growth direction law are used to drive the subsequent crack propagation and its associated energy dissipation.

Neither element reconstruction (change of element connectivity) nor mass allocation (re-distribution of mass) can be achieved using the built-in Abaqus modules, so they have to be implemented in XSHELL via the user-defined subroutines. Three different types of user-defined shells (Belytschko-Tsay, Hughes-Liu, and Triangular) are developed within their phantom paired framework which consists of two internal elements (namely, the real and phantom elements). The UEL performs the following functions for the kinematic description of the element:

- Determination of cracking status based on plastic strain, stress and other criteria.
- Re-assignment of element connectivity based on the updated cracking status.
- Re-assignment of nodal mass based on the rearranged element connectivity and updated cracking status.
- Kinematic calculation of strain, stress and nodal forces based on the input nodal velocities and positions, as well as the updated element connectivity and nodal mass.

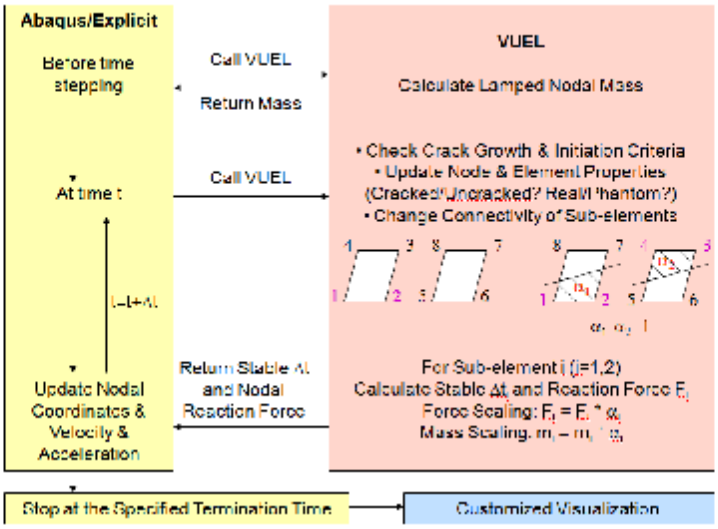

Figure 1. Logic diagram of the VUEL developed for XSHELL

Compared with element reconstruction, mass allocation is conceptually more straightforward but technically more difficult in an Abaqus implementation. The difficulty is mainly driven by Abaqus' architecture, where element mass can only be defined once at the beginning of the simulation and it cannot be changed during subsequent solution steps. To circumvent this difficulty of not being able to change the mass, an alternative approach based on a force scaling is adopted within the VUEL as shown in Figure 1.

Since the plasticity zone at advancing crack tips is relatively large for ductile materials, the associated energy dissipation is non-negligible and should be included during the crack growth simulation. From numerical perspectives, the incorporation of such a nonlinear fracture process zone can also enhance computational stability and improve robustness by suppressing spurious mesh-dependent pathological behavior. For these reasons, we implemented a cohesive crack model in XSHELL by introducing a set of cohesive forces along newly injected strong discontinuity surfaces until the crack opening is fully developed, i.e. cohesive traction has vanished. The benefits of introducing the cohesive zone model includes the alleviation of the mesh-dependent pathological behavior by providing a bounded solution at the crack tip and the elimination of the excessive accumulation of elastic energy for the acceleration of the crack growth.

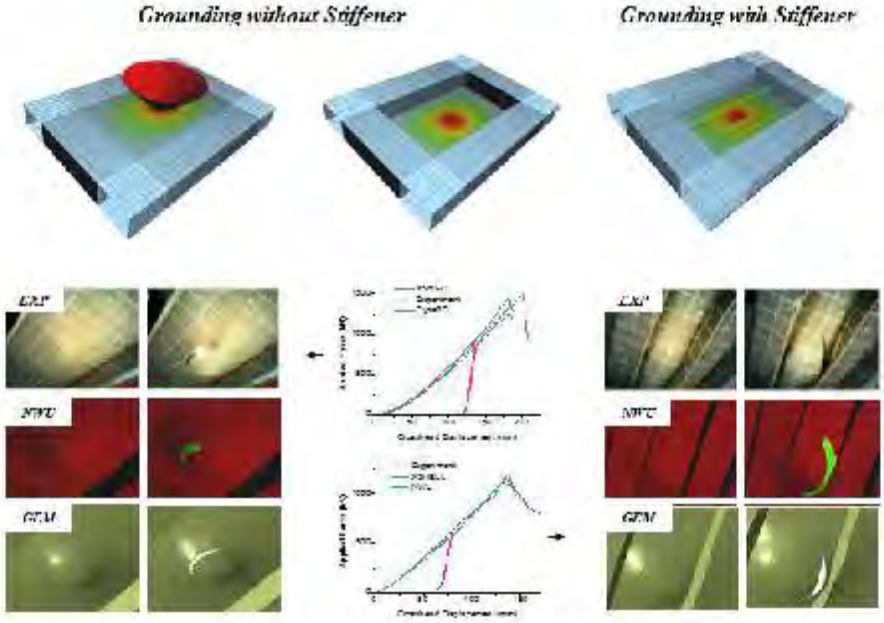

Figure 2. Comparison of GEM's XSHELL prediction of unstiffened and stiffened panels along with its comparison with the corresponding experimental data and NWU simulation results.

To examine XSHELL's capability of modeling the mesh-independent crack growth in a shell structure, the indentation tests conducted by Alsos and Amdahl [1] and Alsos et al. [2] are revisited here for both unstiffened and stiffened steel panels. An Abaqus model based on the coarse mesh is developed as shown in Fig. 2 where the number of nodes and elements is 10092,

and 9276, respectively. Fig. 2 displays the computational model associated with the coarse mesh along with its fringe plot for the vertical displacement. A comparison of the predicted deformation is shown in Fig. 2 at two instants, before the crack initiation and after the final fracture pattern is formed; the three graphs in each case show respectively: 1) the experimental data reported by Alsos et al. [2], 2) the simulation results using NWU's DYNA3D, and 3) the simulation results using our XSHELL toolkit. As shown in Fig. 2, the predicted fracture pattern and load deflection curve agree well with both the test data and NWU's simulation results. The example also demonstrates that the ignorance of the contact force during the force scaling for mass calculation will have a small impact on the response and failure prediction.

References

[1] Alsos H. S. and Amdahl J (2009) On the resistance to penetration of stiffened plates, Part I – Experiments. *Int. J. Impact Engineering*, 36, pp. 799-807.

[2] Alsos H. S., Amdahl J, and Hopperstad O. S. (2009) On the resistance to penetration of stiffened plates, Part II – Numerical analysis. *Int. J. Impact Engineering*, 36, pp. 875-887.

ID: 591

Electromigration Analysis of Solder Joints under AC Load: a Mean Time to Failure Model

Wei Yao
University of Buffalo

Cemal Basaran

Abstract:
In this study, alternating current (AC) electromigration (EM) degradation simulations were carried out for Sn95.5%Ag4.0%Cu0.5 (SAC405- by weight) solder joints. Mass transport analysis was conducted with viscoplastic material properties for quantifying damage mechanism in solder joints. Square, sine and triangle current wave forms AC were used as input signals. DC and pulsed DC (PDC) electromigration analysis were conducted for comparison purposes. The maximum current density ranged from 2.2 10?^6 A/?cm?^2 to 5.0?10?^6 A/?cm?^2, frequency ranged from 0.05 Hz to 5 Hz, with ambient temperature varying from 350 to 450. Since the room temperature is nearly two thirds of SAC solder joints melting point on absolute temperature scale (494.15), viscoplastic material model is essential. Entropy based damage evolution model was used to investigate mean time to failure (MTF) behavior of solder joints subjected to AC stressing. It was observed that MTF was inversely proportional to ambient temperature T1.1 in Celsius, and also inversely proportional to current density j0.27 in A/cm2. Higher frequency will lead to a shorter lifetime with in the frequency range we studied, and a relationship is proposed as MTF? f^(-0.41). Lifetime of a solder joint subjected to AC is longer compared with DC and PDC loading conditions. By introducing frequency, ambient temperature and current density dependency terms, a modified MTTF equation was proposed for solder joints subjected to AC current stressing.

ID: 682

Application of Conjugate-Directions Meshes to Crack Propagation Analysis

Julian Rimoli
Georgia Institute of Technology
USA

Juan Rojas

Abstract:
The classical cohesive theory of fracture finds its origins in the pioneering works by Dugdale, Barenblatt and Rice. In their work, fracture is regarded as a progressive phenomenon in which separation takes place across a cohesive zone ahead of the crack tip and is resisted by cohesive tractions. One of the main approaches proposed to implement the cohesive theory of fracture in finite element analysis consists on the insertion of cohesive finite elements along the edges or faces of the 2D or 3D mesh correspondingly. This approach has been widely adopted due to the fact that it can be easily implemented in standard finite element codes. However, a number of issues that affect the accuracy of the models appear when dealing with cohesive finite elements. Among them, two are a consequence of absolutely mesh dependent effects: (i) the anisotropy induced by the mesh adopted to represent the analysis domain, and (ii) the mesh induced toughness due to the inability of the discrete mesh to reproduce an infinite number of directions at any given point. These issues have been recently addressed by Rimoli et al. by means of a new type of mesh, termed conjugate-directions mesh. However, their formulation is purely geometrical and mechanics was not consider in their analysis. In this work, we adopt conjugate-direction meshes as well as other commonly adopted meshes to solve crack propagation problems in order to asses their effectiveness in capturing correct crack patterns.

ID: 697

An Improved Creep and Shrinkage Model for Modern Concrete

Mija Hubler
Northwestern University
USA

Roman Wendner

Abstract:
The most prominent phenomena in the time dependent-behavior take place on the micro- and nano-scales and yet they matter most for the macro-scale, since they must be captured on a structural level by a prediction formula required to design or evaluate the world largest structures. The mechanisms occurring on the micro- and nano-scales that must be considered include diffusion, capillary stresses, disjoining pressures and the stresses in the solid skeleton of hydrated cement balancing these pressures. The B3 model, which became a standard recommendation of RILEM in 1995, was developed at Northwestern University in the early 1990s by Baweja to describe the compliance and shrinkage functions of concrete in general and to predict them from the composition and environmental parameters, using optimal empirical data fitting aided by understanding some underlying theoretical trends and the relevant mechanisms. Recent deflection data collected from many large-span bridges around the world confirm that model B3 still has the theoretically most correct form and gives the most realistic shapes of the creep and shrinkage curves. However, these deflection data also show that the multi-decade form of the creep curves (or compliance function) requires updating, by which the terminal asymptotic slope of the creep curves in semi-logarithmic plots is significantly increased by the rescaling of the flow term and the aging viscoelastic term in the compliance function. The improved model B3.1 is statistically based on a combination of a new world-wide Northwestern laboratory creep and shrinkage database, which greatly expands the previous RILEM database, and the aggregate of collected data on excessive deflections of large-span prestressed concrete segmental bridges, which are structures particularly sensitive to multi-decade creep. The ranges of the input composition and environmental parameters are expanded to include newer cements that contain admixtures and reach higher strengths.

ID: 716

Algebraic Multigrid for Fracture Problems Modeled with Extended Finite Elements

Badri Hiriyur
Columbia University and Weidlinger Associates

Abstract:
Algebraic Multigrid (AMG) is typically highly efficient for solving linear systems arising from discretizing elliptic partial differential equations using the finite element method. However AMG does not work very well when directly applied to fracture mechanics problems modeled with extended finite element methods (XFEM). The value of XFEM for modeling fracture mechanics problems lies in its ability to address discontinuities by directly incorporating them into the shape functions. These shape functions span seamlessly across the elements containing the discontinuities, so that the mesh itself need not conform to them. However, this result in graph patterns of the tangent stiffness matrix that contains strong couplings that cross crack discontinuities causing algebraic multigrid to break down. Moreover the different number of degrees of freedom in XFEM for regular mesh nodes and enriched nodes poses a difficulty for AMG. In this work, we present a brief overview of three different approaches that have been developed by the authors to overcome the limitations posed by XFEM towards algebraic multigrid. The first approach involves taking the Schur complement of the XFEM linear system (in which the enriched degrees of freedom were condensed out) to develop a Hybrid-AMG method in which crack-conforming aggregates were formed. The second approach involves Domain Decomposition techniques such that AMG is tasked with solving only on the "healthy" subdomains that do not contain any discontinuities while the "cracked" domains are tackled by a direct solver. A Schwarz method is developed to combine the resulting solutions from the different domains. A third approach involves transforming the original XFEM linear system into a modified system that is amenable to a direct application of AMG. It is shown that if only Heaviside-enrichments are present, a simple transformation based on the phantom-node approach is readily available and which decouples the linear system along the discontinuities and retains only the regular degrees of freedom in the AMG mesh hierarchies. The first two approaches have been tested on two dimensional fracture problems and the last approach has been extended to three dimensional crack problems. User XFEM elements have been developed to work with the finite element program FEAP and its parallel version ParFEAP. The proposed AMG solution algorithms are implemented using the ML and MueLu packages within the Trilinos framework developed by Sandia National Laboratories. User solution routines are developed withing FEAP and ParFEAP to work with the Trilinos framework such that the resulting methods can be scaled up to solve large problems on parallel computing clusters with distributed memory architectures. Various numerical examples are presented to verify the accuracy of the resulting solutions and the convergence properties of the AMG algorithm. The parallel scalability performance of the implementation will be discussed.

ID: 780

Dynamic Failure of Composite Panels Subjected to Underwater Impulsive Loads

Horacio D. Espinosa
Northwestern University
United States

Xiaoding Wei
Northwestern University
United States

Abstract:
Designing lightweight high-performance materials that can sustain high-pressure impulsive loading is of great interest for marine applications. In this study, a finite element fluid-structure interaction model is developed to understand the deformation and failure mechanisms of both monolithic and sandwich composite panels. A modified Hashin failure model with strain-rate effect was developed and implemented to simulate fiber (E-glass fiber) and matrix (vinylester resin) damage and degradation in individual unidirectional composite laminas. The delamination between laminas was modeled by a strain-rate sensitive cohesive law. In sandwich panels, core compaction (H250 PVC foam) was modeled by a crushable foam plasticity model with volumetric hardening and strain-rate sensitivity. These models predicted deformation histories, fiber/matrix damage patterns, and inter-lamina delamination, in both monolithic and sandwich composite panels, which were compared with experimental observations. We demonstrate that the delamination process is strongly rate dependent and that the rate dependent composite-damage model accurately captures the spatial distribution and magnitude of damage. The model also reveals that the foam plays an important role in improving panel performance by mitigating the transmitted impulse on the back-sheet while maintaining overall bending stiffness.

ID: 781

Multiscale Modeling of Crack Growth in Peridynamics

Stewart Silling
Sandia National Laboratories

James Cox

Abstract:
Peridynamics is a mathematical theory of solid mechanics that allows discontinuities such as cracks. The theory treats deformations containing growing cracks on the same basis as continuous deformations. The field equations of peridynamics are integro- differential equations containing a natural length scale. Because the underlying theory contains a length scale, a multiscale method can be obtained by varying this length scale within a region. One way to accomplish this variation is by defining a succession of coarsening levels. Each higher level has a larger length scale. Level 0 has the finest resolution, appropriate for modeling the relevant details in the vicinity of growing defect. Lower levels provide coarse-grained material properties to higher levels. The higher level deformation fields act as boundary conditions on the lower levels. This talk will review the peridynamic model and describe the multiscale approach with applications to static and dynamic fracture, including comparison with known crack solutions.

ID: 782

Large Scale Simulations of the Impact Response of Ceramic Plates using s Sharp and Smeared Crack Descriptions of Fracture

Raul Radovitzky

Abstract:
NO ABSTRACT

ID:794

Multiscale Crystal Plasticity Modeling of Microtwinning Induced Deformation in γ–γ' Nickel based Superalloys

Somnath Ghosh
Department of Civil and Mechanical Engineering
Johns Hopkins University
USA

ABSTRACT:

The aim of this work is to develop a physically motivated multi-scale approach for simulating the response of Nickel-based superalloys. At the lower scale, a dislocation density based crystal plasticity model is developed to simulate the response of microstructures designed with various shapes and volume fractions of γ' precipitates. A new model for simulation of anti-phase boundary shearing of the precipitates with matrix dislocations is developed. The lower scale model is homogenized as a function of various micro-structural parameters and the homogenized model is used hierarchically at the next level of crystal plasticity model. In addition, a new criterion for initiation of microtwin and a constitutive model for twin strain accumulation are also developed. This new formulation along with the homogenized crystal plasticity model is used to simulate the polycrystalline response as well as the tension-compression asymmetry as observed in single crystal experiments of these nickel based superalloys.

VI.6

Mechanics of Structures - Acoustic Metamaterials

ID: 248

Topological and Spectral features of Wave motion in Nonlinear Chains

R. Ganesh
University of Minnesota, Minneapolis
United States

Stefano Gonella
University of Minnesota, Minneapolis
United States

Abstract:

The use of nonlinear phononic crystals in applications such as acoustic filters, waveguides, etc., are largely motivated by the inherent flexibility in modulation of the propagation and attenuation zones. Furthermore, phenomena such as solitons, discrete breathers, etc., are features unique to nonlinear wave propagation. These features are well established for continuous systems – long wavelength regime for discrete systems. However, the modulation of cutoff frequencies for the propagation and attenuation zone occur in the short wavelength regime, and the features of wave propagation in this region are seldom studied. Hence, wave motion in periodic chains with weakly cubic nonlinearities is investigated with the objective of providing a comprehensive account of the distinctive topological and spectral features of one-dimensional nonlinear wave propagation.

Full-scale transient analysis is carried out to generate dispersion curves, which are verified with unit-cell based perturbation methods. The topological/spatiotemporal features of wave propagation in the Brillouin zone are monitored for different magnitudes of nonlinearity. Distortion of the wave packet is observed, however the maximum amplitude of the wave packet is preserved. This is in contrast to linear chains, where the amplitude is found to significantly reduce with dispersion. The topological features exhibit a solitary-wave like behavior; observed in continuous systems modeled by the Korteweg-de Vries (KdV) or the Boussinesq equations.
The spectral content of the distorted wave packet is analyzed with a Short Term/Space Fourier Transform (STFT in space). Even for small magnitudes of nonlinearity, localization of the frequency content is observed.

The localization of spectral and topological features are not reflected in the dispersion curve. Dispersion curves establish the wavenumber-frequency relation for a mono-frequency signal. Typically, multi-banded signals are used in experiments and simulations, which lead to dispersion associated distortion of the spatio-spectral features. Hence, the entire spectrum of these banded signals are studied. It is observed that for high wavenumbers (low wavelength), the spectral blob of a regular banded signal consists of two different contributions – one corresponding to the linear chain and another which propagates without dispersion. The non-dispersive feature is seen to separate from the linear dispersive feature with increasing magnitude of nonlinearity. Even though multiple blobs are observed, majority of spectral content is contained in the non-dispersive feature – asserting the preservation of spectral and topological

content. Furthermore, the non-dispersive feature is not found to be continuous i.e., they do not form a single curve for multiple frequency excitations. The slope of the non-dispersive blob seems to be dependent on the dominant frequency/wavelength of the input signal.
In order to determine the slope of the nonlinear-nondispersive blob, the velocity of propagation is evaluated. The knowledge of group and phase velocity from the dispersion relation provides the relation between the topological and spectral features. For linear systems, the group velocity of a wave packet is associated with the velocity of the centroid of the wave packet. Hence, the displacement centroid of the wave packet is monitored in the simulation. Apart from the displacement centroid, the energy centroid and the maximum displacement are also monitored. The velocities obtained from the simulation are compared with the group velocity derived from the perturbation relation. The linear group velocity is also used as a benchmark to delineate the linear and nonlinear features. It is found that the displacement centroid of the wave packet travels at the group velocity of the nonlinear system, which is in accordance with observations for linear systems. However, the energy centroid lags the displacement centroid, and is observed to travel at the group velocity of the corresponding linear system. The maximum amplitude is also found to have similar features as the energy centroid. The velocity of maximum amplitude of wave propagation can be easily estimated from experiments; providing an useful method for inverse reconstruction of nonlinear properties of the system.

The analysis is extended to chains with quadratic nonlinearities. The evolution of the wave packet is significantly different from that of the cubic chain. Similar comparisons are carried out for the quadratic nonlinearity.

Using the relations from quadratic and cubic nonlinearities, any weakly nonlinear system can be analyzed using the above mentioned descriptors by using a Taylor series expansion for the nonlinear function.

ID: 284

Shunted piezoelectric arrays for the design of tunable waveguides

Filippo Casadei
Georgia Institute of Technology – Department of Aerospace Engineering
United States

Tommaso Delpero
ETH Zurich - Center of Structure Technology
Switzerland

Andrea Bergamini
Swiss federal laboratories for Materials science and technologies (EMPA)
Switzerland

Paolo Ermanni
ETH Zurich - Center of Structure Technology
Switzerland

Massimo Ruzzene
Georgia Institute of Technology – Department of Aerospace and Mechanical Engineering
United States

Abstract:
Phononic crystals and acoustic metamaterials have attracted significant interest for their unique dynamic behavior [1,2]. Their interesting properties rely on the ability to tailor the propagation of acoustic waves through the generation of acoustic bandgaps, i.e. frequency ranges of strong wave attenuation. One of the outstanding challenges in phononic crystals and acoustic metamaterials development is the ability to tune their performance without requiring structural modifications. While most of the proposed metamaterial configurations operate at fixed frequency ranges, recent investigations have considered the use of large deformations [3], or electro/magneto mechanical couplings [4] as viable solutions to achieve tunable bandgaps and equivalent mechanical properties.

This research reports on a new tunable waveguide configuration, whereby Bragg scattering bandgaps are combined with piezoelectric resonators to confine and control the propagation of elastic waves in a phononic crystal plate. As shown in Fig 1.a, the waveguide consists of a periodic array of cylindrical stubs bonded to the plate surface. The stubs produce a large frequency bandgap that confines the propagation to the waveguide. A second array of piezoelectric resonators is added to the vertical portion of the waveguide for wave transmission control. The resonating characteristics of the shunted piezos lead to strong wave attenuation at the tuning frequency, and provide the waveguide with resonating mechanical properties which lead to negative group velocities. From this perspective, the waveguide can be considered as an

example of a tunable acoustic metamaterial, with equivalent properties defined by the electro-mechanical resonators.

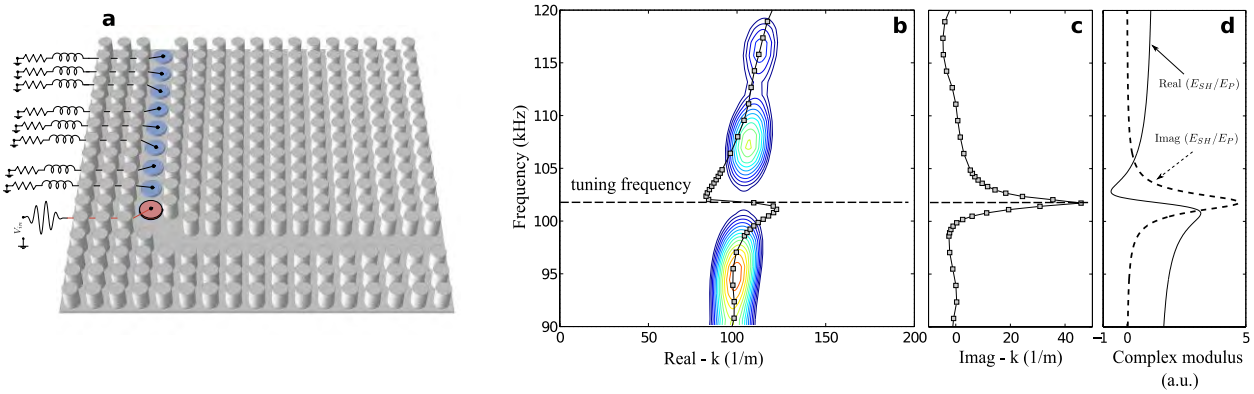

Fig.6: Tunable waveguide with electrical resonating units (a), and experimental evidence of the tunable resonant-type bandgap (b,c,d).

The wave propagation properties of the structure are characterized through two-dimensional wavefield measurements, recorded by a scanning laser vibrometer (Polytec PSV-400). The measured data are analyzed through spatial and temporal Fourier transforms to eliminate disturbances from boundary reflections and to obtain direct estimates of real and imaginary parts of the wavenumber. Shunting of the piezos through the electrical networks produces a resonant, complex modulus (see Fig 1.d), which in turn generates a frequency region of strong attenuation centered at the tuning frequency. Contours of the frequency/wavenumber representation of the response, shown in Fig. 1.b, indicate that the resulting medium features a bandgap centered at the tuning frequency. The measured data also allow the experimental evaluation of real and imaginary part of the wavenumber, also known as attenuation and propagation constant. The real component of the wavenumber, overlapped as a solid line with square markers to the contour plots in Fig. 1.b, reveals the back-bending of the dispersion curve typical of internally resonating metamaterials. In this range of frequencies, elastic waves travel with a negative group velocity, antiparallel to the phase velocity. Also, the imaginary part, shown in Figs. 1.c, exhibits a sharp peak of attenuation in a small range of frequencies centered at the resonance of the electrical circuit (tuning frequency).

The resulting attenuation properties of the waveguide are responsible for the onset of the tunable bandgap, and can be correlated to the frequency variation of the effective modulus of the resonating units as shown in Fig. 1.d. Furthermore, the back-bending characteristics of the dispersion curves and the associated negative group velocity confirm the interpretation of the proposed waveguide as a tunable, internally resonating metamaterial.

References:

[1] M. Sigalas and E. Economou, “Band structure of elastic waves in two dimensional systems,” Solid state communications 86, 141-143 (1993).
[2] Z. Liu, X. Zhang, Y. Mao, Y. Zhu, Z. Yang, C. Chan, and P. Sheng, “Locally resonant sonic materials,” Science 289, 1734 (2000).
[3] K. Bertoldi and M. Boyce, “Mechanically triggered transformations of phononic band gaps in periodic elastomeric structures,” Physical Review B 77, 052105 (2008).
[4] L.Airoldi and M. Ruzzene, “Design of tunable acoustic metamaterials through periodic arrays of resonant shunted piezos,” New Journal of Physics 13, 113010 (2011).

ID: 623

Micro-structured Topologically Interlocked Materials as Acoustic Metamaterials

Srinivas Varanasi
School of Mechanical Engineering,
Purdue University
USA

Thomas Siegmund

Abstract:
Topologically Interlocked Materials (TIMs) are materials assembled from multitudes of unit elements in the shape of Platonic solids. We hypothesize that TIMs possess acoustical characteristics superior to conventional solids, and that micro-structured TIMs will have superior acoustical characteristics compared to TIMs with homogeneous unit elements. Unit elements with characteristically different microstructures, namely, layered and chiral, were considered. Topologically interlocked assemblies of such unit elements will be investigated with regard to the sound transmission and absorption capabilities. A numerical model of a 3D TIM tile acoustically loaded in a Standing Wave Impedance Tube setup is considered. The effect of microstructural factors (volume fraction, chirality, modulus contrast) influencing the acoustical response of the TIM tile will be studied through parametric variation. Experimental investigations using the standard Impedance Tube setup are considered to verify numerical predictions of sound transmission.

ID: 719

Nonlinear Phononic Metamaterials for Wave Management and Control

Michael Leamy
Georgia Institute of Technology
USA

Kevin Manktelow
Georgia Institute of Technology
USA

Abstract:
We analyze wave propagation in continuous and discrete nonlinear metamaterials using a Bloch wave-based perturbation analysis. The intent is to uncover amplitude-dependent band gaps and wave directionality. The analysis leads to an open set of difference equations which are solved for first-order corrections to the dispersion band structure. Geometrically complex structures are analyzed using system matrices that result from a finite-element discretization. Using the developed approach, we investigate the influence of material and geometric nonlinearities on dispersion, and explore how this can be exploited to conceive tunable wave devices. Multilayer nonlinear metamaterials are simple systems which exhibit amplitude-dependent band gaps. Higher-dimensional systems with more complex geometry and nonlinearities are also investigated using topology optimization. The nonlinear interaction of two waves and its effect on the dispersion structure is further considered as an option for wave propagation management and control.

VI.7

Mechanics of Structures - Vibration and Noise Control

ID: 479

Wave Propagation in Phononic Crystals Tunable by Post-buckling Finite Deformation

Pai Wang
Harvard University

Jongmin Shim

Abstract:
We present the analysis of wave propagation in mechanically tunable phononic crystals with large deformation and pattern transformation. Both geometry and material nonlinearities are investigated. The post-buckling behaviors of various porous patterns are studied. The dispersion relations of deformed phononic crystals are calculated using Bloch-wave analysis. Numerical simulations are performed on the periodic continuum microstructures. Frequency band-gaps are obtained and compared among different deformation configurations, volume fractions, and material properties, demonstrating the characteristics of phononic crystals with adjustable band-gap and refractive index. Potential applications include acoustic / elastic wave filters in noise-cancelling devices, wave guides, acoustic imaging equipment and vibration isolators.

Track VII

Infrastructure and Infrastructure Materials

VII.1

Infrastructure and Infrastructure Materials - Mechanics of Substructure Materials

ID: 752

Micromechanical Modeling of Quasi-Brittle Materials

Yifei Ma
Georgia Institute of Technology
United States

Haiying Huang
Georgia Institute of Technology
United States

Abstract:
The discrete element method (DEM) has become an indispensable research tool to study the behaviors of quasi-brittle materials such as rocks and concrete. Though the method is originally formulated and is ideally suited to model the behaviors of dry granular media, DEM has found wide range of applications for cohesive frictional materials. DEM has unique advantages over continuum mechanics based numerical methods in that the failure mechanisms emerge as a generic consequence of particle sliding and separation at the microscale.

The most critical issue in applying DEM to solve any boundary value problem is the identification of the microscale parameters for the contact model. Unlike the constitutive parameters in continuum models, which could be measured directly from laboratory experiments, the microscale parameters in DEM, bond strength parameters in particular, are generally obtained through a calibration process by conducting numerical tests such as uniaxial/triaxial compression and tension tests and matching the numerically measured material parameters with those obtained from laboratory experiments. An outstanding issue in modeling quasi-brittle materials with DEM is the issue of low strength ratio. Given a linear contact model that consists of normal and shear springs with tensile and shear bond strengths and residual friction obeying coulomb's law, the numerically obtained macroscale failure envelope is fairly linear. While the internal friction angle inferred from the failure envelope is comparable to the realistic values of rocks or concrete, the largest compressive over tensile strength ratio is only around 3 – 4, much lower than typical values of rocks ~10 - 20. In other words, the highly nonlinear strength envelope at the low confining stresses is not reproduced numerically. In the literature, the strength ratio has been shown to increase by using techniques such as particle clumping. That is to cluster the particles in the assembly and do not allow particle rotation inside the cluster. The approach however has a disadvantage since the degree of freedom is decreased due to clustering.

In this work, we investigate the effect of a micromechanical model of the linear contact model type, but with limited moment contribution to the contact stress. By allowing the second moment of area to be independent of the contact area and therefore reducing the moment contribution to the contact stress, we show that realistic strength ratios can be obtained. Such a contact model is in essence similar to the particles clumping model in that the length scale associated with rotation is larger than the particle size. But the model has the advantage of retaining the degree of

freedom from initial discretization. The effect of the moment contribution on the failure modes in triaxial compression and tension tests as well as sphere indentation tests is illustrated. Scaling laws relating the microscale parameters to the macroscale strength parameters are also presented.

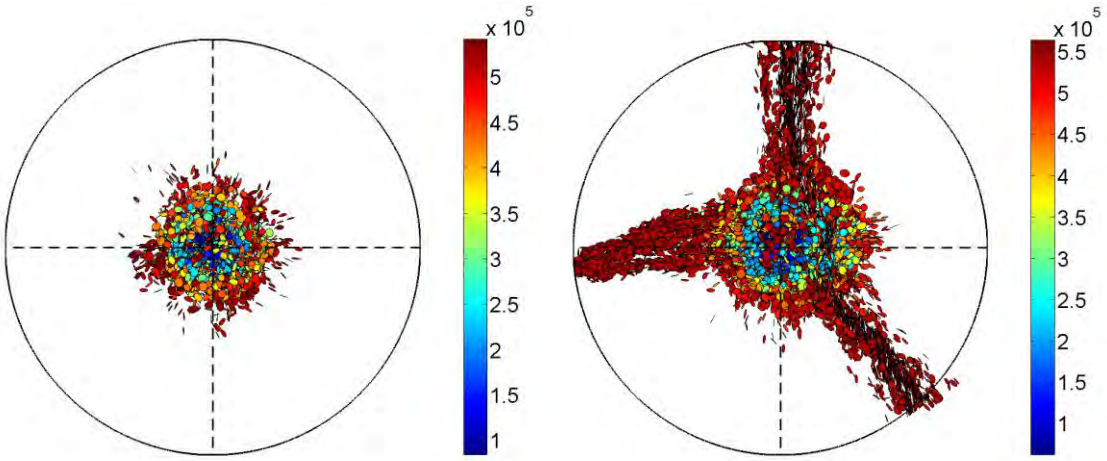

(a) (b)

Figure 1. Accumulation of the microcracks from sphere indentation in a cylindrical sample: (a) a ductile model of failure with the moment contribution factor β = 0.5; (b) ductile mode of failure leading to development of three radial cracks with β = 0.1. The ratio between the uniaxial compressive and tensile strength and consequently the brittleness of the particle assembly increase as the moment contribution factor β decreases. The color bars indicate the number of calculation cycles.

ID: 792

Grain Size Distribution Effects on the Mechanical Response of a 2D Granular Material

T. M. Evans[1], H. Mojarrad[2], and A.A. Tayebali[3]

[1] Associate Professor, School of Civil and Construction Engineering, Oregon State University, Corvallis, OR 97331, matt.evans@oregonstate.edu.
[2] Geotechnical Engineering Project Manager, Geotech Engineering and Testing, 800 Victoria Drive Houston, TX 77022.
[3] Associate Professor, Department of Civil, Construction, and Environmental Engineering, North Carolina State University, Raleigh, NC 27695.

ABSTRACT

Discrete element method (DEM) simulations are often performed on assemblies of particles whose sizes vary over a relatively narrow range. The reasons for this are practical: (i) it greatly reduces the number of particles necessary; and (ii) it simplifies analysis of the results. Nonetheless, with the exception of some uniformly graded sands and gravels, these near-uniform assemblies are not generally representative of natural soils. It is well-established, however, that grain size distribution (GSD) has a significant effect on the mechanical and hydraulic behavior of granular materials. Mechanical behavior is investigated in this manuscript. In the current work, two dimensional granular assemblies of varying GSD are subjected to biaxial compression to establish resilient elastic properties and failure properties. Macroscale observations indicate that coarser gradations have higher shear resistance, greater volume increase with shearing, and higher resilient moduli. It was also observed that increasing the bulk stress will result in increased resilient modulus values. Microscale parameters are used to provide insight to macroscale results.

ID: 796

Mechanical Response of Microbial Induced Cemented Sands under Varying Stress Paths: Physical and Numerical Experiments

K. Feng[1], B. M. Montoya[2], and T. M. Evans[3]

[1]Graduate Student Researcher, Department of Civil, Construction, and Environmental Engineering, North Carolina State University, Raleigh, NC 27695
[2]Assistant Professor, Department of Civil, Construction, and Environmental Engineering, North Carolina State University, Raleigh, NC 27695, bmmorten@ncsu.edu
[3]Associate Professor, School of Civil and Construction Engineering, Oregon State University, Corvallis, OR 97331.

ABSTRACT

Subgrade soils for temporary and permanent roadways often require improvement to meet the demands of traffic loading. The strength and stiffness of incompetent soil can be improved using microbial induced cementation. This sustainable treatment method harnesses natural biological processes to catalyze chemical reactions which induce cementation, bonding soil grains together. Microbial induced cementation significantly increases the strength and stiffness of loose sand, as shown experimentally using conventional triaxial compression tests. Discrete element method (DEM) simulations are used to model the stress-strain behavior observed from the microbial induced cemented sands and to evaluate the micromechanics of the cemented sands during shearing. The loading of roadway subgrade soils is a complex combination of multiple sequential stress paths acting on a given soil element. As the stress path changes, stress transmission and deformation within the soil element also changes. The stress-strain behavior and the structure degradation of the microbial induced cemented sands is presented as a function of the stress path.

ID: 806

49th Annual Meeting of the Society of Engineering Science,
Symposium on "Infrastructure and Infrastructure Materials", Georgia Tech, October 10-12, 2012

Discrete versus Continuum Modeling Of Ballast Particle Crushing

Chloé ARSON[1]
1. School of Civil and Environmental Engineering, Georgia Institute of Technology, USA

Background. Millions of dollars are spent every year to ensure the maintenance and rehabilitation of rail tracks (Indraratna et al., 1998). Cyclic loads from heavy hauling trains degrade and foul the ballast, which induces track settlements and densification (Thakur et al., 2010). Particle crushing can change the frequency of the rail track (Kuo & Huang, 2009), therefore understanding ballast dynamic behavior is a priority to ensure rail transportation safety.

Limitations of Current Finite Element Approaches. Finite Element ballast models were coupled to half-space Boundary Element models, in order to account for the presence of inclusions (including tunnels) in the ground mass (Galvin et al., 2010). Other models include spring ties between blocks of elements (Kuo & Huang, 2009). Such continuum-based approaches proved to be efficient methods to predict rail track frequency modes. However, the granular nature of ballast needs to be accounted for when modeling the mechanical behavior of railroad ballast subjected to cyclic loading, especially when compressive strength and failure threshold are expected to play an important role (Ishikawa et al., 2011).

Advantages of the Discrete Element Method. Ballast is an assembly of crushable particles of various sizes and shapes. Dynamic loads promote particle rearrangement, resulting in permanent deformation. This mechanism is enhanced by the occurrence of particle crushing (Lobo-Guerrero & Vallejo, 2006). Discrete Element Methods (DEM) were used to model the influence of crushing on the macroscopic compressive strength of ballast material. A Representative Elementary Volume (REV) typically contains several thousands of particles (or "balls"), within "walls" representing boundary conditions (Potyondy & Cundall, 2004). For instance, the University of Illinois Aggregate Image Analyzer (UIAIA) was coupled to a DEM software to account for the size and shape distributions of real ballast particles. A parameter was first introduced to represent the effect of particle angularity in the contact models (Tutumluer et al., 2006). The approach was then extended to ballast containing fouling agents stemming from particle abrasion (Huang & Tutumluer, 2011). Image analysis is useful to get realistic geometric descriptions of particle assemblies at a given time step or loading cycle. But the method does not model the degradation process over time. Recent DEM frameworks allowed modeling abrasion as bond breakages within a cluster of bonded particles. However the yield stress predicted with clusters of spherical particles turned to be less than that for the real ballast (Lim & McDowell, 2005). Balls were replaced by rigid assemblies of spherical particles (called "clumps"), in order to better mimic the geometry of real ballast particles (Lu & McDowell, 2007 & 2010, Thakur et al., 2010, Stahl & Konietzky, 2011). The method proved to reproduce well ballast degradation observed in cyclic triaxial tests, where asperity fracture dominates.

Limitations of the Current Discrete Element Models. Lim and McDowell (2007) showed that the size effect on ballast particle strength (i.e. on clump strength) follows Weibull law only for high coordination numbers: clumps should contain at least 500 spheres. Bond

breakages associated to ballast degradation tend to reduce the coordination number. Therefore, the initial coordination number in the intact clumps needs to be large enough to ensure a minimal coordination number at highly degraded stages. As a result, DEM-based models cannot predict highly damaged macroscopic properties, unless a large number of spheres are modeled (typically, thousands of spheres per clump).

An Alternative Phenomenological Approach. In order to simulate ballast degradation not only at the REV scale, but also at the rail track scale, reduced computational costs are desirable. It is proposed to model ballast as a mixture of solid constituents subject to phase changes. Ballast particles are gathered into "geometrical families" characterized by particle shapes and sizes. Each family defines a solid species, and degradation is considered as a phase change. The main advantage of the phenomenological approach is that scale effects are governed by particle size instead of particle connectivity. The typical sizes of the "intact" and "degraded" particles being considered as inputs, the heterogeneity scales are known *a priori*, which enables the definition of a REV. This is a considerable asset for future couplings with thermo-hydro-mechanical ballast weathering processes, in which several observation scales have to be introduced to model all the damaged evolution functions at stakes (Lacy et al., 1999).

Keywords: infrastructure sustainability, ballast, cyclic loading, particle crushing, modeling

References

1. P. Galvin, A. Romero, J. Dominguez, 2010. Fully three-dimensional analysis of high-speed train–track–soil-structure dynamic interaction. *Journal of Sound and Vibration*, 329:5147-5163
2. H. Huang, E. Tutumluer, 2011. Discrete Element Modeling for fouled railroad ballast, *Construction and Building Materials*, 25:3306–3312
3. B. Indraratna, D. Ionescu, H.D. Christie, 1998. Shear behavior of railway ballast based on large-scale triaxial tests. *ASCE J Geotechn Geoenviron Eng*, 124(5):439-449
4. T. Ishikawa, E. Sekine, S. Miura, 2011. Cyclic deformation of granular material subjected to moving-wheel loads. *Can. Geotech. J.*, 48: 691–703
5. C.M. Kuo, C.H. Huang, 2009. Two Approaches of Finite-Element Modeling of Ballasted Railway Track. *ASCE J Geotechn Geoenviron Eng*, 135(3):455-458
6. T.E. Lacy, D.L. McDowell, R. Talreja, 1999. Gradient Concepts for the Evolution of Damage. *Mechanics of Materials*, 31:831-860
7. W.L. Lim, G.R. McDowell, 2005. Discrete element modelling of railway ballast. *Granular Matter*, 7: 19–29
8. W. L. Lim, G. R. McDowell, 2007. The importance of coordination number in using agglomerates to simulate crushable particles in the discrete element method. *Géotechnique*, 57(8):701-705
9. M. Lu, G. R. McDowell, 2007. The importance of modelling ballast particle shape in the discrete element method, *Granular Matter*, 9:69–80
10. M. Lu, G. R. McDowell, 2010. Discrete element modelling of railway ballast under monotonic and cyclic triaxial loading. *Géotechnique*, 60(6):459-467
11. S. Lobo-Guerrero, L.E. Vallejo, 2006. Discrete element method analysis of railtrack ballast degradation during cyclic loading. *Granular Matter*, 8: 195–204
12. D.O. Potyondy, P.A. Cundall, 2004. A bonded-particle model for rock. *International Journal of Rock Mechanics & Mining Sciences*, 41:1329–1364
13. M. Stahl, H. Konietzky, 2011. Discrete element simulation of ballast and gravel under special consideration of grain-shape, grain-size and relative density, *Granular Matter*, 13:417–428
14. P.K. Thakur, J.S. Vinod, B. Indraratna, 2010. Effect of particle breakage on cyclic densification of ballast: a DEM approach. *IOP Conf. Series: Materials Science and Engineering* 10, n.012229 (7 pages)
15. E. Tutumluer, H. Huang, Y.M.A., J. Ghaboussi, 2006. "Imaging Based Discrete Element Modeling of Granular Assemblies", in: *Multiscale and Functionally Graded Materials*, edited by G. H. Paulino, M.-J. Pindera, R. H. Dodds, Jr., F. A. Rochinha, E. V. Dave, and L. Chen, pp. 544-549

VII.2

Infrastructure and Infrastructure Materials - Sustainable Substructure Materials and Systems

ID: 459

Experimental Study on Reusable Adhesive Layers in Layered Beams

Mohit Kumar Singh
Indian Institute of Technology Bombay, Mumbai, India

Rameshchandra Shimpi

Abstract:
NO ABSTRACT

ID: 602

Performance of wicking fabric to mitigate frost boils in Alaskan pavements

Xiong Zhang

ID: 612

Geocell-reinforced RAP Pavements A New and Sustainable Solution

Jie Han
The University of Kansas
USA

Abstract:
During the re-construction of existing asphalt pavements, deteriorated asphalt pavements are often removed to generate waste materials. It is a common practice that these waste materials need to be transported out of the site and then new materials are hauled in for the construction. This construction practice generates a significant amount of CO2; therefore, it is not sustainable. For the sustainable use of these materials, they have been increasingly recycled as aggregates for the re-construction of roadways. Due to the existence of asphalt in the recycled asphalt pavement (RAP) material, its mechanical properties (mainly strength and stiffness) decrease. They may also have long-term durability problems, such as the breakage and creep, especially under repeated traffic loading. Geocell has been proposed to improve the mechanical properties and long-term durability of RAP because it can provide confinement to RAP. Test results showed this confinement effect increased the strength (or higher resistance) and stiffness (or stiffer response) and reduced the creep of RAP. This presentation will discuss the recent research work at the University of Kansas on the use of geocell to stabilize RAP bases in roadway construction, summarizes the main research findings, and show the field construction of a geocell-reinforced RAP pavement.

ID: 791

Elevated Temperature Effects on Geosynthetic Interface Shear Behavior

Tanay Karademir
Maltepe University
Turkey

David Frost
Georgia Institute of Technology
United States

Abstract:
The use of *polymer-based* construction materials (i.e. geosynthetics) strongly influences geotechnical practice and the interaction between these man-made geo-materials and soil plays a critical role in governing the integrity as well as the stability of numerous important sustainable substructure systems (i.e. critical infrastructures) and the demand for installation of such composite soil–synthetic material systems is continuously increasing. The placement of these dis-similar materials adjacent to one another creates interfaces which can lead to relatively weak shear strengths and relative movement is likely to occur as a result of discontinuities at the interface which can make it the weakest point of the overall substructure system in terms of frictional shear strength properties compared to that of neighboring materials such as the inherent frictional strength of the soil mass itself. Therefore, the mobilized frictional shear resistance at the interfaces frequently controls the overall design and stability of the infrastructural systems consisting of more than one material. Such composite installations are frequently preferred in diverse construction activities such as landfills, tunnels, dams and foundations. Examples may include flat or inclined surfaces and interfaces composed of particulates (soil) and fabrics/continua (geotextiles/geomembranes) in landfill, reservoir and canal applications. The overall stability of such a composite system and the integrity of the geosynthetics are dependent on the shear strength mobilized at the interface between the various materials. One issue which has not been extensively studied to date is how changes in temperature effect interface behavior between different geosynthetic components as well as between soil and geosynthetics, and most importantly, the temperature dependency of the interface friction is generally not taken into consideration during design. However the long term performance, strength and deformation characteristics (i.e. mechanical and durability properties) of most geosynthetics (i.e. geotextiles, geomembranes) in the geotechnical applications are influenced by the change in ambient temperature such as seasonal temperature variations. As such, the functional engineering properties of the geosynthetic interfaces should remain within acceptable limits during the required service life as is a critical factor governing the integrity as well as the stability of the sustainable substructures. Further, interface shear behavior at different ambient temperature conditions is not a single attribute, but a collection of performance attributes of the counterface components which require a suite of tests to assess the engineering strength properties of the components both independently and collectively as the properties and behavior of *polymeric* geosynthetics are sensitive to temperature changes. Limited understanding exists as to the effect of these temperature variations on the engineering behavior of these composite systems. In

response to these issues noted above, an extensive research study was performed to investigate temperature effects on interface shear behavior between: (a) needle punched non-woven (NPNW) polypropylene geotextiles and either smooth polyvinylchloride (PVC) or smooth/textured high-density polyethylene (HDPE) geomembranes; or (b) sands (rounded or angular) and smooth PVC or HDPE geomembranes. The physical laboratory testing program consisted of a series of direct interface shear tests between combinations of these aforementioned geo-materials under different load conditions and at various temperatures. A unique temperature controlled chamber (TCC) was designed and developed to be utilized to simulate the field conditions at higher temperatures and to replicate and evaluate triggered shear displacement-failure mechanisms under elevated temperature conditions. Complementary geotextile single filament tensile tests at different temperatures using a dynamic thermo-mechanical analyzer (DMA) were performed to evaluate the fabric global matrix properties and micro-scale characteristics of the geotextile such as filament strength and how it interacts with the geomembrane macro-topography. Additionally, geomembrane surface hardness and geomembrane surface roughness tests provided insight into the role of temperature in the observed behavior differences of the individual materials as well as into the influence of temperature on collective interface shear behavior between fabric-continuum as well as particulate-continuum interfaces with the goal of understanding the fundamental mechanisms responsible for the observed behavior differences.

VII.3

Infrastructure and Infrastructure Materials - Mechanics of Pavement Materials

ID: 627

A Phase Field Method for Computing Residual Thermal Stress

Yue Hou
Via Department of Civil and Environmental Engineering, Virginia Polytechnic and State University
USA

Pengtao Yue
Department of Mathematics, Virginia Polytechnic and State University,
USA

Linbing Wang
Via Department of Civil and Environmental Engineering, Virginia Polytechnic and State University
USA

Abstract:
The residual thermal stress in asphalt binder has always been a very serious problem in the pavement industry. In this paper, we present the calculation of the residual thermal stress of asphalt by using a phase field approach based on the asphalt chemistry. The asphalt composition is simplified to three compositions based on the standard Marcusson model. Furthermore, considering a binary system, only resin and oil are calculated as the different phases in the Phase field method. The phase separation is modeled by the conserved Cahn-Hilliard dynamics, which is coupled with the thermal loading module in the commercial software COMSOL. Only one-way coupling is considered in our simulation, which means the phase separation will affect the thermal stress through the elastic modulus and the thermal expansion coefficient that are both phase dependent. In the Finite Element calculations, a self-adaptive mesh is employed in order to capture the moving interface. Our simulation results indicate that during a fast cooling down process, the phase separation has a significant effect on the residual thermal stress and results in a non-uniform stress distribution in the whole system. Besides, near microstructure boundaries, a high stress occurs, which is in accordance with the previous results in literature.

ID: 637

Multiscale Modeling of Tension Failures in Cement Concrete

Wenjuan Sun
Virginia Polytechnic Institute and State University
United States

Dong Wang
Virginia Polytechnic Institute and State University
United States

Linbing Wang
Virginia Polytechnic Institute and State University
United States

Abstract:
Cement concrete is inherently a type of heterogeous composite materials with multiscale phases (Nguyen et al., 2012). The microstructure of cement concrete could be discretized into four scales, from C-S-H solid phase at level 0 (10^{-9}-10^{-10} m), low density and high density C-S-H phases at level I (10^{-6}-10^{-9} m, microscale), C-S-H matrix and CH crystals at level II (10^{-6}-10^{-3} m), up to cement paste and sand at level III (>10^{-3} m, i.e., macroscale), as tabulated in Table 1. At the macroscale, cement concrete can be considered as continuous materials consisting of cement paste, aggregates, sand, and interfacial transition zone. At the microscale, cement paste is considered as a mixture of calcium silicate hydrate (C-S-H) solid, calcium hydroxide (CH) crystals and gel pores. Due to the complexity nature of cement-based materials, it is essential to investigate the fundamental mechanisms of mechanical failures in cement paste and cement-based materials.

Table 1 Cement concrete structures at different scales (Ulm et al., 2004).

Scales	Compositions	Features
Level 0 10^{-9}~10^{-10} m	○ C-S-H solid ○ Gel porosity	○ low-density (LD) C-S-H: 37% gel porosity ○ high-density (HD) C-S-H: 24% gel porosity
Level I 10^{-6}~10^{-9} m	○ C-S-H matrix ○ two types of C-S-H	○ ultimate building blocks of C-S-H
Level II 10^{-4}~10^{-6} m	○ C-S-H matrix ○ clinker phases ○ CH crystals ○ macroporosity	○ inclusions embedded in porous C-S-H matrix
Level III ≥10^{-3} m	○ cement paste ○ sand ○ interfacial transition zone (ITZ)	○ porous cement matrix & sand particle inclusions ○ ITZ between inclusions and matrix

This paper proposes a mutiscale modeling method to simulate the mechanical failures in cement concrete using both molecular dynamics (MD) method and finite element method (FEM). At the macroscale, FEM is conducted in ABAQUS over the entire cement concrete to locate stress concentration areas, where cracks are most likely to happen, and mechanical failure of cement concrete is represented by cracks in the cohesive zone using user-defined element (UDE). At the atomic scale, the molecular structure of cement concrete is established using first-principle-based ReaxFF force field method based on the molecular structure of ettringite (Liu et al, 2012), and the mechanical behavior of hardening cement concrete is studied using a MD model in LAMMPS over stress concentration areas. The MD simulation is to identify the initiation and propagation of cracks. The size and location of the regions, where MD simulation is performed, are adapted according to the development of cracks. By bridging the MD model and the FEM model using the cohesive zone, the nodes of UDE are constrained to the MD simulation results, including displacements and internal forces. The internal element nodes of UDE correspond to the atomic structures. The equations of motion for the internal nodal fields are derived from the atomistic model. The nodal fields represent the average properties of the underlying atoms, and the equations of motion are constructed to describe the mean behavior. Numerical simulations of mode I and mode II failures in cement concrete are performed for cement concrete using this multiscale modeling method.

References

Liu, L. C., Jaramillo-Botero, A., Goddard, III, W., and Sun, H. Development of a ReaxFF Reactive Force Filed for Ettringite and Study of its Mechnical Failure Modes from reactive Dynamics Simualtions. The Journal of Physical Chemistry A, **116** (2012), 3918-3925.

Nguyen, V. P., Stroeven, M., and Sluys, L. J. Multiscale failure modeling of concrete: Micromechanical modeling, discontinuous homogenization and parallel computations. Compute Methods in Applied Mechanics and Engineering, **201-204** (2012), 139-156.

Ulm, F.-J., Constantinides, G. and Heukamp, F. H. Is concrete a poromechanics material? - A multiscale investigation of poroelastic properties. Materials and Structures, **37** (2004) 43-58.

ID: 638

Integrated Monitoring System for both Pavement and Traffic

Wenjing Xue
Virginia Tech
USA

Linbing Wang

Abstract:
With the grown support of information technology, many monitoring systems have been used for pavement health or traffic monitoring. A significant advantage is expected if traffic and pavement monitoring systems can be integrated together. An integrated wireless transportation (both pavement and traffic monitoring) monitoring system was installed on Virginia Route 114. This sensing network includes strain, stress, temperature, and moisture sensors, and can monitor both the pavement and the traffic. The embedded sensors can help to investigate the pavement performance, monitor the health condition and ensure the ride safety. At the same time, the collected pavement responses can be used to back calculate certain useful information, such as speed, wandering and axle load, of the passing vehicles for traffic statistic purpose, and serve as a high-speed Weigh-in-Motion system. The back calculation algorithm is verified by many experiments and improved via integrated comparison.

ID: 650

Molecular Dynamics Simulation of Atomic Friction Mechanism at the Tire-Pavement Interface

Xinfei Wang
Virginia Tech
USA

Abstract:
This paper presents a molecular dynamics simulation of pavement friction based on the surface structure of tire and aggregate at atomic scale, in which both surfaces are theoretically modeled as an interface with molecular structure. The crystal structure of different minerals in limestone aggregate is provided through mineralogical analysis, which indicates that natural limestone is composed majorly of calcium and magnesium carbonate. It treats the limestone as three different types, pure calcite, pure dolomite and combination of calcite and dolomite with the ratio of 8:2. The 3D interface surface layer is 100nm×20nm;20nm. The cap tread part of tire as one of the bearing surfaces in friction is commonly the compound material that contains various rubbers and fillers. This paper compares two widely used tire rubber, natural rubber and styrene-butadiene rubber (SBR), and for simplification the effects due to fillers are not considered. Two different shapes of rubber surface have been employed, that is half sphere with 15nm diameter and cub with 15nm;15nm;15nm dimension. Subsequently, the atomic friction mechanism has been studied under various conditions with molecular dynamics simulation, in which the interaction among the atoms are given by the function of empirical chemical potentials. The smooth sliding process has been investigated at different velocities and normal loads to analyze the friction force, friction coefficient and local deformation in the contact. The pile up phenomenon also has been studied to evaluate the influence of adhesion. The study shows that the atomic friction majorly derives from the adhesion and deformation in the interaction between the surfaces. The friction behavior heavily relies on the velocities, loads, and chemical properties of surfaces.

ID: 652

Mix Design of Low Noise Micro-Surfacing Mix

Liping Cao

Abstract:

Micro-surfacing technology, which was developed and widely applied in asphalt pavement in recent years, is one of the effective and low-cost methods for preventive maintenance. It can improve the pavement in waterproof, anti-slip, wear-resisting and rut filling. Nevertheless, it has clearly greater interior and outside noise than common asphalt pavement. In order to decrease the noise of micro-surfacing, this research uses an orthogonal design method to optimize mix design. In this research, three key sieve sizes were selected as influence factors as they will affect the texture depth of micro-surfacing. Nine micro-surfacing mixtures were designed by the orthogonal design method. The exposure rate index obtained by the digital image processing technology and texture depth of micro-surfacing specimens were measured and used as evaluation indices. Based experimental data, an optimum mixture design with the lowest noise will be obtained.

ID: 660

Discrete Element Modeling of Compression Test to Determine the Film Thickness of Asphalt Mixture

Ying Li
Northwestern University

Dong Wang

Abstract:
NO ABSTRACT

ID: 676

Piezoelectric Energy Harvesting from the Public Right-of-Way

First Author
Haocheng Xiong
United States

Second Author
Dong Wang
United States

Third Author
Cristian Druta
United States

Fourth Author
Linbing Wang
United State

Abstract:

The last decade has seen a growing focus in the research community of energy harvesting systems. While the grown of concern of the robustness of the roadways have significantly and the sensing technology, the limit of power source has become an impediment force of the research of sensing technology. Energy harvesting is proved as a promoting solution. It also provides a new source of clean and renewable energy that can help reduce negative environmental impacts while contributing to improve roadway mobility. Piezoelectric energy harvesting is known as a stable technology converting kinetic energy into electricity. The dimension of the harvesting systems mostly depends on its application.

The energy harvesters which have received most attention are built with PZT (Lead Zirconate Titanate) rods packaged with rigid materials like engineering plastic, concrete and etc. Kinetic energy is converted into electric energy by D-33 mode, in which the harvester transforms its vertical deformation into a vertical electric potential. The overall objective of this work is to design an energy harvesting system which can be used on public highways without affecting the robustness of the existing pavement. A circuit storing the harvested electric energy is also designed and optimized according to the characteristic of the harvester's components. This study is motivated by the need of a new source of clean and renewable energy that can help reduce negative environmental impacts. The power generation performance of the harvesting systems is evaluated using a Model Mobile Load Simulator (MMLS). The performance is measured in terms of capacitor charging time and voltage output spectrum. To further understand the power generation performance of the harvesting system on public highways, field tests are conducted in real pavement on different public highways. The tests are also performed on the Smart Road of Virginia Tech Transportation Institute with controlled traffic and on a weigh station near Roanoke City with real traffic. The presentation will outline the discoveries of this project.

ID: 693

Determination of Optimal Air Void Content for the Permeability and Stability of Drainage Layer

Yinning Zhang
Virginia Polytechnic Institute and State University
United States

Xinfei Wang
Virginia Polytechnic Institute and State University
United States

Linbing Wang
Virginia Polytechnic Institute and State University
United States

Abstract:
Moisture in pavement structure is a major cause of structure and material distresses. Water can always find its way into the pavement structure such as infiltration from the joints and cracks at the surface, vapor movement and rising water table. There is no way to completely prevent moisture from entering into the pavement but it is possible to effectively remove the water out before any distress is caused. The drainage layer has been widely adopted by many states to remove water out of the pavement structure effectively. With a high air void content typically ranging from 20% to 30%, the drainage layer incorporated into base or subbase course also works as a component of pavement structure and a loading bearing layer. However, with such high air void content the stability of the drainage layer becomes a big concern. It is necessary to investigate the structural contribution of the drainage layer and to confirm its satisfaction of structural stability requirement.

Specimens of typical open-graded asphalt stabilized aggregates adopted by Virginia with 20% to 30% air void content were compacted to investigate the resilient modulus and permeability of the drainage layer. The resilient modulus of the drainage layer determined from laboratory testing is then put into FEM simulation to predict the structural contribution of the drainage layer at different air void contents. The stability of the drainage layer with different air void content is investigated in terms of rutting and shear stress. An optimal air void content achieving both good permeability and adequate stability of the drainage layer is recommended.

VII.4

Infrastructure and Infrastructure Materials - Protection of Substructures against Dynamic Loading

ID: 422

Dynamic Response of Hybrid Metal-Composite Sandwich Structures Subjected to Underwater Impulsive Loading

Siddharth Avachat
Georgia Institute of Technology
USA

Min Zhou
Georgia Institute of Technology
USA

Abstract:
The dynamic response of hybrid metal-composite sandwich structures subjected to underwater impulsive loads is analyzed. The analysis focuses on the effect of varying structural attributes on load-carrying capacity, deflection, energy dissipation and damage in sandwich structures. The three structural designs studied are unmodified metallic sandwich structures, metallic sandwich structures with a carbon-fiber composite affixed to the front-face (impulse-receiving face), and metallic sandwich structures with a PVC foam and carbon-fiber composite affixed to the front-face. Underwater impulsive loads are generated using a novel experimental setup involving diagnostics for in-plane and out-of-plane strain measurement. The experiments are supported by fully dynamic numerical calculations which account for fluid-structure interactions and damage and failure mechanisms in the materials. For the same applied impulse, the unmodified sandwich structures experience significant dynamic plasticity, core-crushing and rupture while the hybrid structures do not experience rupture. The results suggest that hybrid metal-composite sandwich structures have superior blast-resistance than metallic sandwich structures with only relatively small increases in overall mass.

ID: 789

Dynamic Soil-Structure Interaction Macroelements for Pile Supported Waterfront Structures: Optimizing Soil Remediation Strategies Against Liquefaction

Dominic Assimaki
Associate Professor, Georgia Institute of Technology
USA

Varun Varun
Geomechanics Engineer, Itasca Consulting Group, Inc
United States

Abstract:
Simulation of the seismic response of pile-supported wharfs is a complex problem that involves realistic representation of phenomena such as large ground displacements, liquefaction, nonlinear response of piles, deck elements and their connections, and coupling of the transverse, longitudinal, and torsional response of the wharf to the response of super-structures such as cranes. Fully coupled non-linear 3D finite element (FE) analyses should be employed for the transient analysis of this system, which are, however, associated with enormous computational effort. This further prohibits their implementation for performance-based design engineering applications, which require realization of large numbers of seismic hazard scenarios. Addressing this drawback, we here present a simplified mechanical model for soil-structure interaction analyses of piles in liquefiable soils, which captures the behavior of saturated granular media for soil-structure interaction analyses at reduced simulation time, and allows its implementation in risk analyses of port systems.

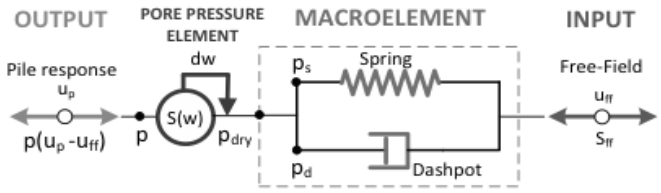

Figure. Schematic representation of the macroelement components, comprising spring, dashpot and pore pressure element

The nonlinear macroelement is formulated as a nonlinear Winkler-type model, and accounts for the primary soil resistance mechanisms including drag, and the interface nonlinearities. A coupled model is used for radiation damping to capture the reduction in damping force with increasing material and interface non-linearity.
Plane-strain FE simulations are conducted for a pile in radially homogeneous soil to identify the critical parameters governing the response. Dimensional analyses are next conducted, and the importance of hydraulic conductivity and loading rate of dynamic loading in saturated soils is emphasized. Next, the macroelement parameters are calibrated as a function of the soil properties

and the effective stress. A semi-empirical approach is used to generate pore pressure histories and detect the onset of liquefaction in absence of the structure. The macroelement is then implemented in a simplified 3D FE structural model of the wharf, coupled to a free-field site-response numerical model, and the estimated response of structural members is benchmarked by comparison with fully coupled 3D FE analyses and centrifuge experiments.

References:

1. Varun V. and Assimaki D. (2012). A Generalized Hysteresis Model for Biaxial Response of Pile Foundations in Cohesionless Soils, *Soil Dynamics and Earthquake Engineering*, 32(1), 56-70
2. Varun V. and Assimaki D. (2012). A Nonlinear Dynamic Macroelement for Soil-Structure Interaction Analyses of Pile-Supported Waterfront Structures, *International Journal for Analytical and Numerical Methods in Geomechanics* (in press)
3. Varun V., Assimaki D. and Shafieezadeh A. (2012). Soil-Pile-Structure Interaction Simulations in Liquefiable Soils via Dynamic Macroelements: Formulation and Validation, invited paper, *Soil Dynamics and Earthquake Engineering, Jose Rœsset Special Issue* (in press)

Track VIII

Materials Design

VIII.1

Materials Design - Hierarchical Design of Materials

ID: 204

Intricate Mechanics of Hierarchical Honeycombs

Babak Haghpanah Jahromi

Abtract:
Hierarchy plays an important role in the mechanical response of many natural materials and structures [1]. A novel hierarchical family of cellular honeycomb geometries has been recently defined by the systematic introduction of successively smaller hexagons wherever three walls meet [2]. The in plane stiffness of such hierarchical honeycomb with the one and two orders of hierarchy is 2 and 3.5 times the stiffness of regular honeycomb structure of same density, respectively [2]. In this work, the plastic collapse strength of hierarchical honeycombs under different states of loading (e.g. uniaxial, biaxial and shear loading) was estimated through upper- and lower- bound plastic limit analyses. The upper bound plastic collapse load was obtained by comparing several possible plastic deformation mechanisms of the unit cell of the hierarchical structure. It was shown that hierarchical honeycombs can exhibit a 70% increase in plastic collapse load per unit mass compared to regular hexagonal honeycomb. Keywords: Structural hierarchy, honeycombs, cellular structures, plastic analysis References [1] R. Lakes, “Materials with Structural Hierarchy", Nature, 361 (1993) pp. 511-515. [2] A. Ajdari, B. H. Jahromi, J. Papadopoulos, H. Nayeb-Hashemi, A. Vaziri, Hierarchical Honeycombs with Tailorable Properties, Int. J. Solids and Structures, 49 (2012) pp. 1413-1419.

ID: 287

Design of Ultra-High-Performance Fiber-Reinforced Concrete to Withstand Blast Loading

Brett Ellis
Woodruff School of Mechanical Engineering, Georgia Institute of Technology, Atlanta, GA
United States of America

David L. McDowell
Woodruff School of Mechanical Engineering, Georgia Institute of Technology, Atlanta, GA
School of Materials Science and Engineering, Georgia Institute of Technology, Atlanta, GA
United States of America

Min Zhou
Woodruff School of Mechanical Engineering, Georgia Institute of Technology, Atlanta, GA
School of Materials Science and Engineering, Georgia Institute of Technology, Atlanta, GA
United States of America

Abstract:
Although well suited to dynamic loading conditions, Ultra-High-Performance Fiber-Reinforced Concretes (UHPFRCs) have been slow to transition from laboratory testing to structural applications, partly due to a trial-and-error materials development process that is lengthy and expensive. To address these problems, this research applies the Inductive Design Exploration Method (IDEM) [1] to determine UHPFRC material designs that when used in panels will withstand blast loading.

It is assumed that the multiscale model shown in Figure 1 represents a UHPFRC panel subject to blast loading [2]. At the finest length scale, the model at the single fiber length scale accounts for the fiber's length, cross-sectional area, and surface topology to determine the energy dissipated due to granular flow of the matrix, friction between the fiber and the matrix, and the plastic work of the fiber. The resulting pullout force versus end slip relations are projected onto each fiber at the multiple fiber length scale. This intermediate length scale accounts for the overall fiber volume fraction as well each fiber's embedded length and inclination angle to the displacement vector δ. From the multiple fiber length scale, a Gaussian distribution of the tensile strength and energy dissipated due to separation is projected onto cohesive elements at the structural panel length scale. At this coarsest length scale, linear elastic steel restraints provide boundary conditions to the UHPFRC panel. The blast load

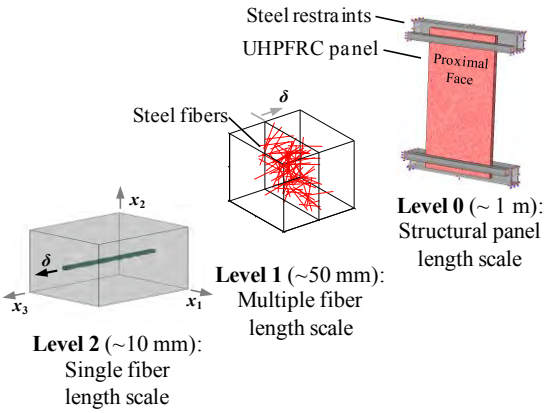

Figure 1. Multiscale model of UHPFRC panels subjected to blast loading.

is simulated by applying a surface traction to the proximal face in the normal direction that starts at a magnitude of p_{max} at 0 ms and linearly decays to zero at 15 ms. The goal of this research is to determine UHPFRC materials designs such that a panel constructed of these materials can withstand a reflected impulse I of 1.5 MPa-ms, where $I = \frac{15\,\text{ms}}{2} p_{max}$.

Although the goal of multiscale modeling is to be as accurate as possible, each individual model contains errors due to at least three uncertainties: natural, model parameter, and model structure. Furthermore, errors are introduced due to the linking of models, which propagates uncertainty from one length scale to another. In this work, three types of robustness are employed to mitigate the effects of uncertainty and propagated uncertainty. Type I robustness seeks to achieve the desired performance while minimizing variation due to noise factors. Type II and III robustness minimizes variation in performance due to variation in control factors and uncertainties in the models, respectively. Note that Type III robustness is critical to designing materials through computational approaches.

IDEM determines robust solutions through a systematic, three-step method that determines feasible values of input variables for a given performance requirement. Across a given level of hierarchy, IDEM discretizes input variables, projects the discretized set of input variables to a range in the output space, and determines which sets of discrete input values satisfy the output space performance requirements. For example, the structural panel length scale relates the two input variables – tensile strength, t, and dissipated energy density, E_{dis} – to the single output variable – panel survival. In the first step, the tensile strength and dissipated energy density are discretized. Then each combination of tensile strength and dissipated energy density is projected with uncertainty through the structural panel model to determine the range of results. Finally, if all of the possible solutions survive the blast load, the tensile strength and energy dissipation density are determined to be a feasible set of inputs. For multiscale problems, the feasible input space is then used as the performance requirement for the next scale problem. In this manner, robust solutions of multilevel problems can be determined.

Results of IDEM indicate the required fiber volume fractions, types of fiber (i.e., twisted fiber or straight, smooth fiber), and matrix compressive strengths required for the panel to withstand a 1.5 MPa-ms impulse. Through this method, material designers can determine feasible ranges of material parameters applicable to specific problems in a manner not possible via conventional trial-and-error materials design methods.

References:

[1] Choi,H-J. (2005). A Robust Design Method for Model and Propagated Uncertainty. Ph.D. Thesis, Georgia Institute of Technology, Atlanta, GA.

[2] Ellis BD, Zhou M, and McDowell DL. (2012). *Multiscale modeling of Ultra-High-Performance Fiber-Reinforced Concrete subject to blast loading*. Society of Engineering Sciences 49th Annual Technical Meeting (SES 2012). ID 286, Oct 2012, Atlanta, GA.

Missing Abstract

ID: 349

ID: 540

Hierarchical Modeling and Design of Composite Materials with Negative Stiffness Inclusions

Timothy Klatt
University of Texas at Austin
United States

Jordan Matthews
University of Texas at Austin
United States

Dr. Michael R. Haberman
University of Texas at Austin
United States

Dr. Carolyn Conner Seepersad
University of Texas at Austin
United States

Abstract:
Motivation: Recent research in the field of composite materials has shown that it is theoretically possible to produce composite materials whose macroscopic mechanical stiffness and loss properties surpass those of conventional composites when small portions (1-2% by volume) of constrained negative stiffness (CNS) domains are embedded into a continuous host material [2-5]. These studies suggest that it is possible to produce stiff absorptive materials, which are of significant importance in the areas of vibration and acoustics. It is therefore of interest to investigate the means to produce negative stiffness inclusions that are designed for specific applications. Achieving negative stiffness behavior by design, however, is a nontrivial task. Indeed, the ability to demonstrate negative stiffness behaviors has been limited to materials undergoing phase change or to large-scale structural elements [1, 5]. One emerging area of study in the fields of electromagnetics and acoustics, known as metamaterials, provides a possible route to the production of negative stiffness inclusions. The research presented here explores the possibility of using negative stiffness mechanisms as material inclusions to enable sound and vibration absorption over a broadband range of frequencies while minimally altering the stiffness of the absorptive material.

Approach: The work presented here exploits the unique non-monotonic force-displacement nature of bistable systems to produce highly absorptive composite materials. Such bistable systems are exemplified by an axially compressed beam, which, under transverse loading, initially exhibits positive stiffness until it buckles and consequently "snaps-through" to its second stability position. During this transition, the beam exhibits negative stiffness. Taking inspiration

from a buckled beam, the inclusion design presented here mimics such a system on four of the six cubic faces to induce negative stiffness in two orthogonal directions under specific thermo-mechanical fabrication conditions. The microscale inclusions presented in this paper are unique in that they employ a thermal expansion mismatch to induce negative stiffness behavior.

The design of the composite material containing CNS inclusions consists of three distinct scales of interest: the micro-, meso-, and macroscales. The microscale is defined by descriptive length scale of the structure within the inclusions. It is ultimately the microstructure that leads to mesoscopic negative stiffness behavior and significant increases in absorptive capacity on the macroscopic scale. The geometry and constituent material properties are defined at this scale and finite element (FE) based representative volume element (RVE) homogenization leads to the determination of the effective mesoscopic stiffness of the metamaterial inclusions, $\mathbf{C}_{\text{eff}}$. Under certain microstructural material combinations, geometric configurations, and thermo-mechanical fabrication conditions, components of $\mathbf{C}_{\text{eff}}$ may possess negative values.

Modeling at the mesoscale considers the effective mesoscale metamaterial inclusion stiffnesses (including anisotropy) as well as their geometry, orientation, and volume fraction in a homogeneous matrix material of known properties. This homogenization is achieved using well-established effective medium theories. The mesoscale modeling results in the determination of the effective behavior of a composite material containing negative stiffness metamaterial inclusions. These properties can then be employed in conventional macroscopic models, such as layered plate models to analyze structures that contain materials with negative stiffness inclusions.

To illustrate the utility of this approach, a case study was performed using the macroscale values computed using the multi-scale design approach described above as the coating properties in a composite beam stiffness and loss model, based on well-established composite beam theory [6]. This case study investigates the ability of microstructural changes to influence the damped vibration response of a composite beam.

The large number of interdependent design variables at each level of this modeling approach makes it difficult to find combinations that demonstrate advantageous negative stiffness behaviors. A Bayesian classifier technique is therefore used in conjunction with an exploratory search to identify and map regions of the design space with desirable characteristics at each hierarchical level [7]. Those satisfactory regions of the design space can then be intersected across levels to identify satisfactory system-level designs. Bayesian classifiers have the benefit of being able to classify arbitrarily shaped regions, which occur especially when designing nonlinear systems.

Results/Findings: The results from an exploratory search of the mesoscale design space reinforces the need for understanding the interrelationship between negative stiffness behavior, inclusion geometry, and thermal loading is a key part of the design process, because beam elements with excessive thickness or insufficient loading from thermal expansion do not buckle. The exploratory search of the design space facilitated finding design variable values that yielded highly desirable macro-scale stiffness and loss performance. Initial results indicate that coatings with negative stiffness inclusions yield a two order of magnitude increase in composite beam damping when compared with positive stiffness inclusions of equal magnitude.

Closure: These results suggest that viscoelastic materials containing even very low volume fractions of structured negative stiffness inclusions display drastic increases in energy absorption, while the change in overall stiffness can be tuned based on the ratio of the inclusion to matrix stiffness. Our proposed design is advantageous for tuning and optimizing macroscale response. The inclusion design can easily be adjusted to offer high damping in one direction and low in another simply by removing one or more of the buckled beam elements. Additionally, we demonstrate that the inclusion geometry can be optimized to produce, for instance, an optimal amount of negative stiffness, and therefore, macroscale damping.

References:

[1] Kashdan, L.B., Seepersad, C.C., Haberman, M.R. and Wilson, P.S., 2012, "Design, Fabrication, and Evaluation of Negative Stiffness Elements Using SLS," *Rapid Prototyping Journal*, Vol. 18, No. 3, pp. 194-200.

[2] Lakes, R.S., 2001, "Extreme damping in compliant composites with a negative stiffness phase," *Philosophical Magazine Letters*, Vol. 81, No. 2, pp. 95-100.

[3] Lakes, R.S., 2001, "Extreme damping in composite materials with a negative stiffness phase," *Physical Review Letters*, Vol. 86, No. 13, pp. 2897-2900.

[4] Lakes, R.S. and Drugan, W.J., 2002, "Dramatically stiffer elastic composite materials due to a negative stiffness phase?" *Journal of the Mechanics and Physics of Solids*, Vol. 50, pp. 979-1009.

[5] Lakes, R.S., Lee, T., Bersie, A. and Wang, Y.C., 2001, "Extreme damping in composite materials with negative stiffness inclusions," *Nature*, Vol. 410, pp. 565-567.

[6] Ross, D., Ungar, E.E. and Kerwin, E.M., 1959, "Damping of plate flexural vibrations by means of viscoelastic laminae," *Structural Damping*, pp. 49-87.

[7] Shahan, D. and C.C. Seepersad, 2012, "Bayesian Network Classifiers for Set-Based Collaborative Design," *Journal of Mechanical Design*, Vol. 134, No. 7, pp. 071001-14.

Missing Abstract

ID: 548

Missing Abstract

ID: 580

ID: 625

Bioinspired Dense Tensegrity

Biological structures (spinal column, shark tesserae, armadillo armor) combine strength and toughness with flexibility. These assemblies of hard unit elements joint by tendons are in essence tensegrity structures. Typically, manmade tensegrity structures are not dense. It is hypothesized that dense tensegrity structures can be constructed based on Topologically Interlocked Materials (TIMs) embedded into a net of woven fibers. Sample materials were constructed by 3D printing of unit elements and weaving with a range of different fibers. The resulting two-dimensional solids were subjected to transverse loading. Recorded force-deflection data exhibit a non-linear hardening response typical of tensegrity. Subsequent failure was found to occur step-wise with partial load recovery, indicating an instantaneous self healing mechanism. Analytical mechanics and finite element models are employed to elucidate the details of deformation and failure characteristics as these emerge from the interaction of unit element elasticity, weave pattern and weave elasticity, contact, and control of prestress.

ID: 673

Multiscale Heterogeneous Materials Modeling with Surfacelets

Yan Wang
Georgia Institute of Technology
United States

Wei Huang
Georgia Institute of Technology
United States

David W. Rosen
Georgia Institute of Technology
United States

Abstract:
Product innovation heavily depends on the availability of new materials. It can be envisioned that multiscale computer-aided design (CAD) tools are needed in the future to allow for construction (specification), analysis (verification), and modification (optimization) in product-materials design. Engineers can not only perform the traditional geometry construction and structural analysis in such a multiscale CAD environment, but also customize the material properties for some local region of the design by simply zooming into the specific section to specify material compositions or crystalline configurations. The traditional boundary-representation based parametric modeling approaches become inefficient in constructing complex geometries at nano- and meso-scales. They do not support seamless zoom-in and zoom-out operations that are important for interactive design. As illustrated in Fig.1, with the zoom operations, the same region of interest can be modeled as either internal continuous distribution or boundary singularity, depending on the particular length scale of the model. Such information and role exchange between different representations should be supported in multiscale CAD tools.

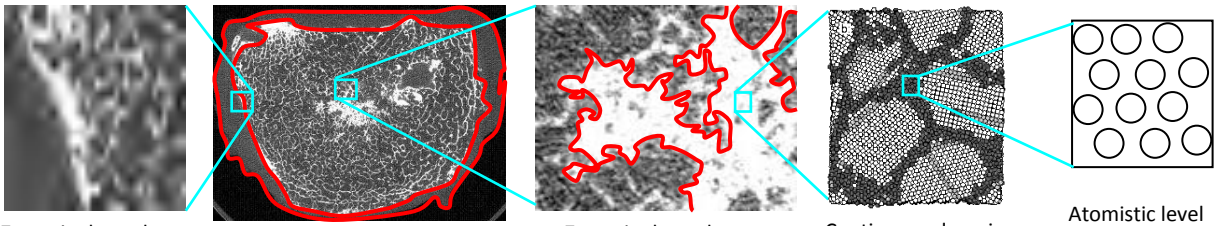

Fig. 1: Information and role exchange between models of internal continuous distribution and boundary singularity during the zooming process

Recently, a dual-Rep approach [1] was proposed to represent geometry and material property distribution for multiscale heterogeneous materials modeling. It represents both internal distributions

and boundaries of materials in a unified implicit form. The approach is based on a novel basis function, called *surfacelet*. A surfacelet is regarded as a hybrid of implicit surface model and wavelet. Surfacelets can represent various three-dimensional boundary singularities efficiently, e.g. planar, cylindrical, ellipsoidal, and other shapes, where the surfaces are defined implicitly with shape parameters specified according to the geometries. The additional transformation parameters are used to specify positions and orientations of the surfaces. The scales of the basis functions are controlled in a way similar to wavelets.

The dual-Rep approach uses a combination of wavelets and surfacelets. Wavelet bases are applied to represent the internal continuous distributions in material domains, whereas surfacelet bases are for domain boundaries. The type of surfacelets is selected based on the particular shape of the boundaries in specific problems. The shape parameters are chosen to maximize the representation efficiency for the boundaries. The wavelet component of the surfacelet can be the same as the wavelet for internal distribution. The dual-Rep provides a convenient framework for materials modeling, while the singularity information is concisely captured.

The new approach of representation can be applied to model material and property distributions at different scales. When zoom-in and zoom-out operations are used, the approximations between wavelets and surfacelets can be done by minimizing least-square errors. Linear constraints can also be applied for enforcement of values at selected grid points. The unified form of the bases shows the potential in supporting multiscale design.

From the microscopic images of materials, the boundaries of grains or phases can be detected automatically from surfacelet transforms. Such transforms can capture the knowledge of materials and achieve data compression without losing important singularity information. Numerical methods for the surfacelet transform and its inverse are developed. The forward transform enables model reconstruction from microscopic images via a surface integral operation followed by a one-dimensional wavelet transform. The inverse transform reconstruct the images by solving under-constrained problems. Example models of polycrystalline and composite materials are demonstrated.

References

[1] Wang, Y. and Rosen, D. (2010) Multiscale heterogeneous modeling with surfacelets. Computer-Aided Design & Applications, **7**(5): 759-776

Missing Abstract

ID: 741

VIII.2

Materials Design - Inverse Methods in Materials Design

ID: 301

Localization Relationships for Elastic Deformation of Cubic Polycrystalline Aggregates

Yuksel C. Yabansu
Department of Mechanical Engineering, Drexel University, Philadelphia, PA, USA

Dipen Patel
Department of Mechanical Engineering, Drexel University, Philadelphia, PA, USA

Surya R. Kalidindi*
Department of Mechanical Engineering, Drexel University, Philadelphia, PA, USA
Department of Materials Engineering, Drexel University, Philadelphia, PA, USA
*corresponding author

Joshua B. Shaffer
Materials Resources LLC, Dayton, OH, USA

1. Introduction

There is a critical need for multi-scale simulation tools that employ physics-based material models, which allow us to accurately capture the important details of the inherently anisotropic constitutive behavior exhibited by most polycrystalline structural metals. Beyond the elemental compositions and phase volume fractions, two of the most important features of the microstructure are the crystallographic texture (distribution of lattice orientations in each of the constituent phases) and the morphological texture (details of the spatial placement of individual crystals of different orientations and phases in the microstructure including grain size and shape distributions). These microstructural details play a dominant role in controlling the anisotropy of the mechanical properties exhibited by the metal.

It is generally acknowledged that for the foreseeable future most multiscale modeling will be accomplished in practice by information passing between stand-alone codes (i.e. hierarchical modeling) that address details at disparate length scales. The main drawback of current hierarchical modeling approaches is that they usually employ various simplifying assumptions, and therefore trade accuracy for computational speed. On the other hand, the scale-bridging relationships used in hierarchical modeling are computationally better suited for capturing quantitatively the specific influence of any selected microstructure parameter on the macroscale material response of interest. This information is central to the materials design efforts [1-2]. In most hierarchical modeling approaches to date, the focus has been in communicating the effective properties to the higher length scales, i.e., on homogenization. Consequently, there is often very little information passed in the opposite direction, i.e., localization. As an example, localization might involve the spatial distribution of the response field of interest (e.g. stress or strain rate fields) at the microscale for an imposed loading condition at the macroscale.

2. Materials Knowledge Systems (MKS)

The fidelity of the homogenization and localization relationships used in hierarchical multiscale modeling can be significantly improved by employing better description of the material structure at the

lower length scale (referred to as the microstructure in this paper). This is the central idea behind the recently formulated scale-bridging framework called Microstructure Knowledge Systems (MKS) [3-8]. Building on the statistical continuum theories developed by Kroner [9-10], MKS establishes high fidelity microstructure-property-processing relationships that are amenable for bi-directional exchange of information between the constituent hierarchical length scales. The MKS approach dramatically improves the accuracy of the localization expressions by calibrating the convolution kernels in these expressions to results from previously validated physics-based models. In recent work [7], the MKS approach was demonstrated to successfully capture the tails of the microscale stress and strain distributions in composite systems with relatively high contrast, using the higher-order terms in the localization relationships. It was also demonstrated that the MKS approach can be applied to problems involving non-linear material behaviour such as spinodal decomposition [3] and rigid-plastic deformation [8].

Let $\langle \mathbf{p} \rangle$ denote the macroscale imposed variable (e.g. local stress, strain or strain rate tensors) that needs to be spatially distributed in the microstructure as $\mathbf{p_s}$ for each spatial cell indexed by **s**. In the MKS framework, the localization relationship is expressed as [2]

$$\mathbf{p}_{\mathrm{s}} = \left(\sum_{\mathrm{h}=1}^{\mathrm{H}} \sum_{\mathbf{t} \in \mathbf{S}} \boldsymbol{\alpha}_{\mathrm{t}}^{\mathrm{h}} \, \mathrm{m}_{\mathbf{s}+\mathbf{t}}^{\mathrm{h}} + \sum_{\mathrm{h}=1}^{\mathrm{H}} \sum_{\mathrm{h}'=1}^{\mathrm{H}} \sum_{\mathbf{t} \in \mathbf{S}}^{\mathrm{S}} \sum_{\mathbf{t}' \in \mathbf{S}}^{\mathrm{S}} \boldsymbol{\alpha}_{\mathbf{t}\mathbf{t}'}^{\mathrm{h}\mathrm{h}'} \, \mathrm{m}_{\mathbf{s}+\mathbf{t}}^{\mathrm{h}} \mathrm{m}_{\mathbf{s}+\mathbf{t}+\mathbf{t}'}^{\mathrm{h}'} + \cdots \right) \langle \mathbf{p} \rangle \tag{1}$$

where $\mathrm{m}_{\mathbf{s}}^{\mathrm{h}}$ is the microstructure function which represents the volume fraction of local state h at spatial cell, s. H represents the total number of local states and S the total number of spatial cells in the microstructure.

3. Generalized Spherical Harmonics

In this study, MKS is explored for elastic deformations in cubic polycrystals. The focus is to extend the MKS framework to include a continuous local state space, i.e. the orientation space. In order to address this task in a computationally efficient manner, Generalized Spherical Harmonics (GSH) are used to represent functions in the orientation space. Using orthogonal properties of the GSH, the terms in the MKS formulation can be expressed as

$$\sum_{\mathrm{h}=1}^{\mathrm{H}} \sum_{\mathbf{t} \in \mathbf{S}} \boldsymbol{\alpha}_{\mathrm{t}}^{\mathrm{h}} \, \mathrm{m}_{\mathbf{s}+\mathbf{t}}^{\mathrm{h}} = \sum_{t \ell \mu \nu} \boldsymbol{A}_{\mathrm{t}\ell}^{\mu\nu} \boldsymbol{F}_{(\mathrm{s}+\mathrm{t})\ell}^{\mu\nu *} \tag{2}$$

where $\boldsymbol{A}_{\mathrm{t}\ell}^{\mu\nu}$ are the Fourier coefficients of $\boldsymbol{\alpha}_{\mathrm{t}}\ (g)$ and $\boldsymbol{F}_{\mathrm{s}\ell}^{\mu\nu}$ are the Fourier coefficients of $\mathrm{f}_{\mathbf{s}}\ (g)$, * denotes a complex conjugate, and indices ℓ, μ, ν enumerate the generalized spherical harmonics.

4. Conclusions

The MKS framework has been extended to create microstructure-property-processing linkages for polycrystalline structures by using compact GSH functions for orientations space. This representation produced major computational advantages over primitive binning of the orientation space.

References

1. Choi, H.J., D.L. McDowell, J.K. Allen, and F. Mistree, *An inductive design exploration method for hierarchical systems design under uncertainty.* Engineering Optimization, 2008. **40**(4): p. 287-307.

2. Fullwood, D.T., S.R. Niezgoda, B.L. Adams, and S.R. Kalidindi, *Microstructure sensitive design for performance optimization.* Progress in Materials Science, 2010. **55**(6): p. 477-562.
3. Fast, T., S.R. Niezgoda, and S.R. Kalidindi, *A new framework for computationally efficient structure-structure evolution linkages to facilitate high-fidelity scale bridging in multi-scale materials models.* Acta Materialia, 2011. **59**(2): p. 699-707.
4. Kalidindi, S.R., S.R. Niezgoda, G. Landi, S. Vachhani, and A. Fast, *A novel framework for building materials knowledge systems.* Computers Materials & Continua, 2009. **17**(2): p. 103-126.
5. Landi, G. and S.R. Kalidindi, *Thermo-elastic localization relationships for multi-phase composites.* Computers, Materials & Continua, 2010. **16**: p. 273-293.
6. Landi, G., S.R. Niezgoda, and S.R. Kalidindi, *Multi-scale modeling of elastic response of three-dimensional voxel-based microstructure datasets using novel DFT-based knowledge systems.* Acta Materialia, 2009. **58**(7): p. 2716-2725.
7. Fast, T. and S.R. Kalidindi, *Formulation and Calibration of Higher-Order Elastic Localization Relationships Using the MKS Approach* Acta Materialia, 2011. **59** p. 4595-4605.
8. Kalidindi, S.R., S.R. Niezgoda, G. Landi, S. Vachhani, and T. Fast, *A Novel Framework for Building Materials Knowledge Systems.* Computers Materials & Continua, 2010. **17**(2): p. 103-125.
9. Kroner, E., *Statistical Modelling*, in *Modelling Small Deformations of Polycrystals*, J. Gittus and J. Zarka, Editors. 1986, Elsevier Science Publishers: London. p. 229-291.
10. Kroner, E., *Bounds for effective elastic moduli of disordered materials.* Journal of the Mechanics and Physics of Solids, 1977. **25**(2): p. 137-155.

ID: 387

Taylor-type crystal plasticity model in the spectral representation for low-symmetry metals

Marko Knezevic, Rodney J. McCabe, and Bogdan Mihaila

Materials Science and Technology Division, Los Alamos National Laboratory,
Los Alamos, NM 87545, USA

We present a single crystal dislocation densities based constitutive law for multiple slip and twinning modes implemented within a Taylor-type homogenization scheme for simulating mechanical response and texture evolution of orthorhombic and hexagonal metals. Crystallographic slip, deformation twinning, and slip inside twinned regions are considered as contributing mechanisms for the plastic strain in the model. The model is calibrated to predict the anisotropic mechanical response and texture evolution as a function of strain, strain rate and temperature in wrought uranium and zirconium. This approach is a key stepping stone towards developing a framework for fast retrieval of crystal plasticity solutions in the spectral representation for low-symmetry metals and formulating an inverse design of deformation processing operations to achieve desired textures in low-symmetry polycrystas. Details of this approach are described and validated through a few example case studies.

ID: 516

Microstructure Informatics to Collate and Visualize High-Dimensional Materials Datasets

Tony Fast
University of California Santa Barbara
USA

Surya Kalidindi
Drexel University
USA

Abstract:
Materials specialists have triumphed over engineering challenges associated with interrogating rich three-dimensional spatial features of materials. Improvements in data generation and the subsequent deluge of large datasets segue to a new host of problems associated with their analysis. This work highlights advances in collating and, moreover, visualizing high-dimensional materials datasets. Recent work has shown the ability of n-point statistics of high-dimensional data to provide a natural ordering of the data when placed in a low-dimensional embedding (e.g. Principal Orthogonal Decomposition). Building off this work, new microstructure segmentation tools are developed that improve this ordering and provide improved microstructure taxonomy. Materials datasets embedded in a low-dimensional space present some fresh visualization methods (i.e. Dendograms, Parallel Coordinate Plots) that can be extended to an array of problem sets. These protocols will be extended to natural materials, Ni-based superalloys, and a spatiotemporal grain coarsening model to illustrate the materials insensitivity. Two ancillary visualization tools will included: (1) interactive visualization of 4-D datasets and (2) tablet-based interaction with 3-D material volumes.

ID: 755

Optimization of Thermal and Electrical Conductivity of Porous YSZ-Ni Composites via Inverse Modeling

S. Ali Tabei
Georgia Institute of Technology

Majid Baniassadi

Abstract:
Yittria-Stabilized Zirconia (YSZ)-Ni composite is widely used as the anode in solid oxide fuel cells (SOFCs). Due to operation requirements, possession of high electrical and thermal conductivity is vital for all the SOFC components, including the anode. In this work different digital realizations of three dimensional (3D) porous YSZ-Ni microstructures are generated by altering the parameters affecting the grain growth. The digital microstructures are obtained by Monte Carlo simulations based on two-point statistical correlation functions. An inverse modeling approach was applied in order to optimize the thermal and electrical conductivity of the porous composites. The thermal and electrical properties of each digital microstructure were simulated by finite elements method (FEM) to yield the optimal microstructure with the highest possible thermal and electrical conductivity.

ID: 759

Informatics for Inverse Design of Materials

KRISHNA RAJAN
Iowa State University
USA

Abstract:
In this presentation we show how informatics methods help to explore and analyze data and infer materials properties and structure-property relationships when models are ill-defined. Using informatics, we have been able to discover new compounds with targeted functionalities, the chemical design rules governing the stability of these compounds as well new structure-property relationships. The presentation explores the use of statistical learning methods to develop inverse design approach to materials design.

ID: 760

Inverse Design of Morphologies for Enhanced Performance in Organic Photovoltaics

Baskar ganapathy Subramanian
Iowa State University

Oloa Wodo

Abstract:
Organic solar cells (OSC) have the potential for widespread usage due to their low cost-per-watt and mechanical flexibility. Their wide spread use, however, is bottlenecked primarily by their low solar efficiencies. Experimental evidence suggests that a key property determining the solar efficiency of such devices is the final morphological distribution of the electron-donar and electron-acceptor constituents. By carefully designing the morphology of the device, one could potentially significantly enhance their performance. This is an area of intense experimental effort that is mostly trial-and-error based, and serves as a fertile area for introducing mechanics and computational thinking. Standard approaches for computationally linking morphology with performance involve interrogating the morphology using extremely compute intensive frameworks. These include implementations of the excitonic-drift-diffusion model as well as Monte Carlo based strategies. Incorporating these strategies into an inverse design problem becomes computationally intractable. We showcase a two stage approach to this problem. In the first stage, we develop a purely mechanistic based description of the performance of the device by characterizing performance using carefully chosen morphology descriptors. This mechanics based surrogate model that links morphology with photovoltaic performance is built using (a) concepts from graph theory, (b) and the underlying equivalence between a two phase morphology and an undirected, weighted graph. We subsequently wrap this simple and fast model with a massively parallel genetic algorithm that enables the inverse design of morphologies that maximize certain performance criterion. We illustrate the differences in optimized morphologies resulting from 2D and 3D assumptions.

ID: 773

Inverse Materials Design in Wrought Magnesium Alloys to Increase Crash Worthiness

Dongsheng Li
Pacific Northwest National Lab

Curt Lavender

Abstract:
To improve crashworthiness of wrought magnesium, it is critical to enhance strength and ductility of wrought magnesium in order to match the crashworthiness of traditional aluminum alloys, such as Al6061. Our research work demonstrated that it is achievable by high strain thermomechanical processing. This processing introduced fine grain structure and distributed precipitation morphology, which contributed high strength and large ductility. Microstructure of Magnesium alloys AZ31 and ZK60 were characterized by metallurgical microscope, scanning electronic microscope and transmission electronic microscope. Texture was characterized by X-ray diffractometer equipped with pole figure goniometer. Mechanical properties of these magnesium alloys were measured by uniaxial tension and compression tests. To study the energy absorption properties, crash tests of hollow tubes were performed, as shown in Fig. 1(a). Similar mechanical properties and energy absorption of Al6061 are also measured for comparison. Integrated with these experimental results, we developed crashworthiness model using finite element method with failure prediction. Sample geometry optimization was used to guide sample design in crashworthiness test. Simulated results and experimental results demonstrated that it is achievable for magnesium alloy to reach higher specific absorption energy (SAE) than Al6061. From simulation results in Fig 1(b), SAE of AZ31 is 27.8% lower than Al6061; while SAE of ZK60 is 21.6% higher than Al6061. The relationship between the SAE and grain size is also investigated. With the decrease of grain size, the simulation results of SAE increase further. To guide the processing design to achieve this advance, we developed statistical representative microstructure based finite element method to stochastically predict the failure and energy absorption of magnesium alloys with different microstructure. The microstructure descriptors we focused on are correlation functions implicitly based on a set of features including grain size, size distribution, texture and precipitation. Statistical stable microstructure was reconstructed from the statistical descriptors using a novel developed optimization method: adaptive multiple super fast simulated annealing. The efficiency in reconstruction was increased by orders, compared with other stochastic reconstruction processing. The synthetic microstructure is statistically stable with high resolution and enough components to represent the local and global structure. Simulated behavior from this synthetic microstructure is stable and accurate, comparing with simulation using microstructure information obtained by discrete chemical

imaging modality. Simultaneously, we also applied crystal plasticity finite element method to predict the microstructure evolution during thermomechanical processing after large strain. Combining this with microstructure reconstruction and crashworthiness model, we developed the capability.

ID: 775

Advantages and Challenges Facing Informatic Approaches to Materials Discovery

Kim F. Ferris
Pacific Northwest National Laboratory

Abstract:
Informatic approaches can accelerate the process of materials discovery, but face challenges in data support for predictive model development. Some properties such as density and band gap can be characterized as early-stage as their estimation methods and measurements converge at earlier development stages. These situations are often have more supporting data available, and are amenable to direct property value estimation. Other properties such as electron mobilities tend to mature slowly, can change significantly as synthetic methods and processing conditions improve, but still require reliable methods to project eventual performance. Herein, we exemplify the design of CZT-like II-VI semiconductors and its materials chemistries based upon Z_{eff} and electron mobility considerations. Balancing screening and optimization approaches provide design guidance for future materials composition searches.

Discussion:

Selection of an appropriate *set of physical properties* to serve as a performance target is the first order of business for sorting through potential chemical compositions for a semiconducting material, followed by determining the sufficiency of appropriate data support for predictive model development [7,8]. A set of properties for a candidate radiation detection material would include high density for a measure of absorption cross-section [9], a sufficient band gap E_g for carrier generation and minimal dark current background, and electron mobility for efficient carrier collection [10]. To be able to provide a measure of merit, a reference semiconducting material was chosen; cadmium zinc telluride (CZT) whose physical properties are density=5.8 g/cm^3, Z_{eff}(CZT)=49.1, E_g=1.5-2.2 eV, and μ~1000 cm^2/V*s.

In the current example, we use Z_{eff} as a surrogate for the physical density, which can be directly estimated for low energy photons as $Z_{eff}=\Sigma\ w_i*Z_i^4$ where w_i is the weight fraction of the i-th component, and Z_i as its atomic number. Band gap values may be found by one of several methods providing consistency across the chemical composition space is maintained; direct measurement, electronic structure calculation, structure-property relationship, or Moss-type estimation. However, electron mobilities present several challenges typical in materials development. These values tend to change significantly as fabrication and processing methods improve, direct computation by electronic structure methods requires detailed information of the atomic coordinates, limited numbers of reliable values are available to construct structure-property relationships, and experimental quantities are extremely sensitive to the measurement technique. We have addressed these challenges to property values through a coarse-graining approach to property estimation; an initial 1-D charge transport model (Figure 1), followed by

[7] K.F. Ferris et al., Proc. SPIE Optics and Photonics (2009) 8507-44.
[8] K.F. Ferris and D.M. Jones, 2010 Proc. Inst. Nucl. Mat. Mgmt (INMM), Baltimore, MD.
[9] P.A. Rodnyi Physical Processes in Inorganic Scintillators, Boca Raton: CRC Press (1997), p.13-15.
[10] A. Owens and A. Peacock, Nucl. Instr. and Meth. A531 (2004) 18–37.

subsequent estimation of its theoretical upper limit, electronic structure calculation, and experimental measurement.

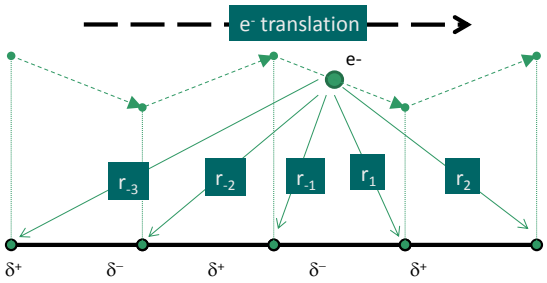

$$E_{interaction} \approx \sum_{sites} E_{electrostatic} + \sum_{sites} E_{polarizability}$$

± X dimension until 1% convergence in $E_{interaction}$

Figure 1 -One-dimensional charge mobility model based upon topology of site-to-site atomic charges. Estimated charges derived from electronegativity equalization using Martynov-Batsanov electro-negativities and provides categorical guidance relative to reference material.

To provide design guidance whether a particular series of materials chemistries is compatible with a needed physical property value, property values are estimated for each trial candidate composition, and a normalized figure of merit (FM) is generated. For Z_{eff}, the CZT value of 49.1 with a 90% window was used: $FM(Z_{eff}) = (Z_{eff}(candidate)/49.1)$ for compositions with $Z_{eff} \geq 0.9*49.1$, $FM(Z_{eff})=0$ for $Z_{eff} \leq 0.9*49.1$. For $FM(\mu)$, $(\Delta_{charge}(candidate)/\Delta_{charge}(CZT))*(dist_{A-B}(CZT)/dist_{A-B}(candidate))$, where $dist_{A-B}$=sum of atomic radii for A and B. The composite FM provides combines the individual property maps per composition over the property requirement specification: $FM(composite)=FM(Z_{eff})*FM(\mu)$ for each of the individual entries. With the ideal 'CZT' materials FM=1, the composite property map shows the heavier materials chemistries compatible with the design requirements; the individual mappings illustrate the property trends within the candidate materials series.

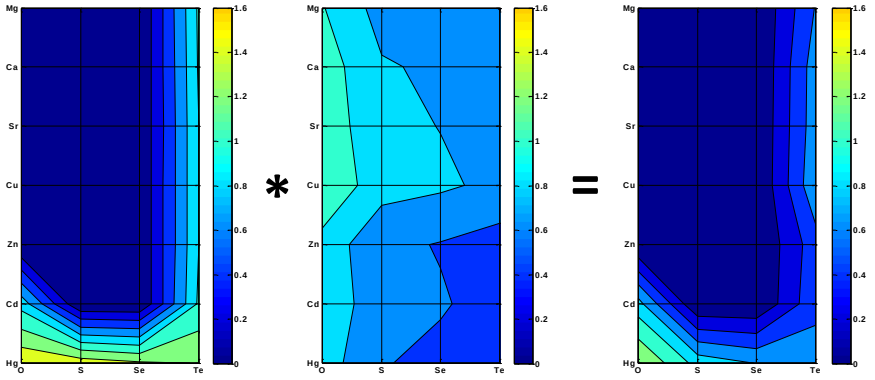

Figure 2 – Composite property mapping for Z_{eff} and charge mobility for candidate main group II-VI semiconductor compositions (II=Mg,Ca,Sr, Cu,Zn,Cd, Hg; VI=O,S,Se,Te). Color coding for figures of merit ranges from blue (< CZT reference) to yellow (>CZT), mid-point (~CZT) is green.

The author gratefully acknowledges financial support from U.S. Department of Homeland Security under Contract No. HSHQDC-08-X-00872 under competitively awarded contract/IAA HSHQDC-08-X-00872. This support does not constitute an express or implied endorsement on the part of the Government.

ID: 797

Design Rules for Rare-earth Replacement Magnetic Materials: MnBi and MnSb Families

Soo Kyung Kim, Kim F Ferris, Dongsheng Li and Moe A. Khaleel
Pacific Northwest National Laboratory
Fundamental and Computational Material Science Directorate
USA

Hamid Garmestani
Georgia Institute of Technology
School of Material Science and Engineering
USA

Abstract:
MnBi has gained much attention as a replacement rare earth magnetic material due to its strong magnetization and coercive powers, but also from its ability to retain its magnetization at elevated temperatures while related compositions suffer large diminishment. To investigate the origin of this temperature dependence, we have performed a series of first principles electronic structure calculation on the thermo magnetic properties of MnBi and MnSb within the local density approximation and plane wave basis using the ABINIT program system[1]. Experimental studies on MnBi indicate that it is a strong ferromagnetic compound with a 2.0 T coercive force and 4.6 MGOe energy product at 400K for the NiAs hexagonal phase [2, 3]. While the magnetic anisotropies of MnBi and MnSb are similar in terms of spin-alignment, the difference in the transition temperatures for spin alignment is large. To discern potential structural roles, three crystal forms common to the MnX series were investigated for compositions, MnBi and MnSb, the room temperature hexagonal NiAs structure with 2 formula units, an elevated temperature orthorhombic MnP structure with 2 formula units, and tetragonal zincblende structure (ZB) with 1 formula unit. The total magnetization and local magnetic moment in easy direction (c-axis) of these two compounds have been calculated as a function of temperature. All three forms have been observed for MnAs by earlier investigators [4]. Finite temperature effects on the electronic structure were examined by cold smearing and Fermi-Dirac population methods.

Figure 1 shows the computed total magnetization per one Mn atom and one Bi (or Sb) atom as a function of increasing electronic temperature from 31.57 K to 315.77 K, for the three structural forms of MnBi and MnSb. Although the differences for total magnetization of the ZB forms at various electronic temperatures was very small, we can clearly see the different thermomagnetic behavior between MnBi and MnSb compound in NiAs structural phases. The total magnetization of MnBi remains effectively constant over the temperature range while the magnetization for MnSb decreased with as a negative concave-shaped first derivative function. In the orthorhombic MnP-type structure, the total magnetization of MnBi saturates to an approximate 2μB with only a small decrease for MnSb, and shows little temperature dependence. Figure 2 shows a linear increasement of total magnetization following the cell expansion. Thermal expansion effects on the MnBi unit cell have been taken consideration using the experimental non-linear thermal expansion coefficient in a separate investigation. According to Willis and Roberts [5, 6], the *a*

and *c* lattice constants for MnBi increase almost linearly until 613K. At 613K, discontinuous structural transformations occur and the c axis contracts 3% and the *a* axis expands 1%, suggesting that the magnetic change which takes place in MnBi near 613K is caused by decomposition of the material and is not a Curie point phenomenon. Starting from the optimized hexagonal NiAs-type geometry of MnBi, cell lattice parameters are expanded corresponding to the experimental data. The sharp drop occurring at 613K reflects the structural changes due to the cell transformation reported in the Willis results. As shown in our results, the MnBi compound maintains its thermomagnetic response compared with MnSb which has similar crystallographic and electronic properties. This result is clearly structurally dependent, observed in hexagonal NiAs-type structure with differences observed for the other structural forms. Considering our calculations were done in aligned spin moment with one-direction, these results suggest that the thermomagnetic property of MnBi would be distinguished from MnSb even with easy-axis aligned magnetic spin moment where spin reorientation does not occur. As MnBi has a positive temperature coefficient for coercivity, these results indicate that the crystal structure will be a design constraint for applications where magnetic power needs to be maintained at elevated temperatures.

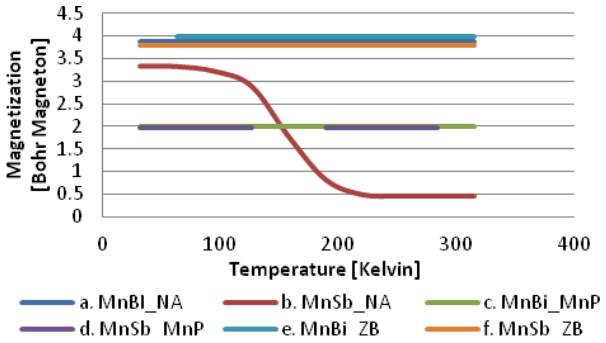

Figure 1

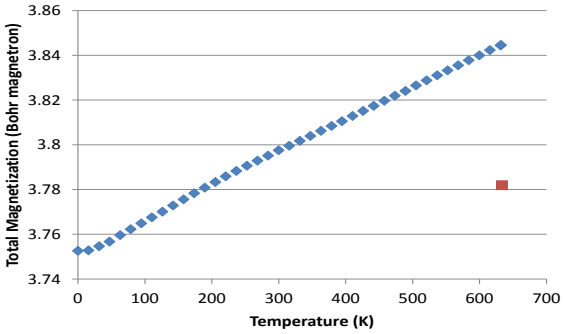

Figure 2

KFF gratefully acknowledges financial support from U.S. Department of Homeland Security under Contract No. HSHQDC-08-X-00872 under competitively awarded contract/IAA HSHQDC-08-X-00872. This support does not constitute an express or implied endorsement on the part of the Government.

References:

1. Payne, M.C., et al., *Iterative Minimization Techniques for Abinitio Total-Energy Calculations - Molecular-Dynamics and Conjugate Gradients.* Reviews of Modern Physics, 1992. **64**(4): 1045-1097.
2. Ravindran, P., et al., *Magnetic, optical, and magneto-optical properties of MnX (X=As, Sb, or Bi) from full-potential calculations.* Physical Review, 1999. B**59**(24): 15680-15693.
3. Yang, J.B., et al., *Crystal structure, magnetic properties and electronic structure of the MnBi intermetallic compound.* Journal of Physics-Condensed Matter, 2002. **14**(25): 6509-6519.
4. Suzuki, T. and H. Ido, *Relation between Structural and Magnetic-Properties of Compound* $MnAs_{1-X}P_x$ *(*$0 \leq X \leq 0.275$*).* Journal of the Physical Society of Japan, 1982. **51**(10): 3149-3156.
5. Roberts, B.W., *Neutron Diffraction Study of the Structures and Magnetic Properties of Manganese Bismuthide.* Physical Review, 1956. **104**(3): 607-616.
6. Willis, B.T.M. and H.P. Rooksby, *Magnetic Transitions and Structural Changes in Hexagonal Manganese Compounds.* Proceedings of the Physical Society of London Section 1954. B**67**(412): 290-296.

ID: 829

Physics-Based Prior Knowledge for Regularized Inversion of Image Data to Determine Structural Information

Jeff Simmons

Materials and Manufacturing Directorate, Air Force Research Laboratory

USA

Stephen Bricker

Wright State University/Southwestern Ohio Council for Higher Education

USA

Craig Przybyla

Materials and Manufacturing Directorate, Air Force Research Laboratory

USA

Michael Jackson

Blue Quartz Software

USA

Charles Bouman

Charles Bouman, Electrical and Computer Engineering, Purdue University

USA

Abstract:

In an informal way, microstructural information is inferred from images obtained from materials with microscopy. That is, it is assumed that “what you see is what you get.” But, the image obtained from a microscope is the forward evolution of some probing beam and, to infer the structure requires the inverse of this evolution. Due to noise and other effects, this inverse problem is generally ill-posed and, to select among the many mathematically correct inversions generally requires some knowledge of the material to be incorporated as a regularization. Often, this is in the form of a mathematical “reasonableness” type of smoothing, but to incorporate physics into the regularization has many benefits. This presentation addresses the general problem of interpreting microscope data as a Bayesian regularized inverse problem and focuses on the physical phenomena used for the regularization.

VIII.3

Materials Design - Processing-Microstructure-Performance Relations

ID: 372

Modeling the Effects of Shot-Peened Residual Stresses on Microstructure-Sensitive Fatigue of Ni-Base Superalloy Components

William D. Musinski
Georgia Institute of Technology, Atlanta, GA
United States

David L. McDowell
Georgia Institute of Technology, Atlanta, GA
United States

Abstract:
The simulation and design of advanced materials for fatigue resistance requires an understanding of the response of their hierarchical microstructure attributes to imposed load, temperature, and environment over time. For Ni-base superalloy components used in aircraft jet turbine engines, different competing mechanisms are present depending on applied load, temperature, and environment. For example, there is a transition from surface- to subsurface-dominated failure mechanisms with decreasing stress amplitude (from low cycle to high cycle fatigue). In the transitional fatigue regime, the life-limiting fatigue crack initiation site tends to be located at inclusions near the surface. Compressive surface residual stresses are often introduced in Ni-base superalloy components to help retard fatigue crack initiation and early growth at near surface inclusions and shift the fatigue crack initiation sites from surface to sub-surface locations, thereby increasing fatigue life. However, the ability to computationally predict the amount of improvement in fatigue life response and scatter due to induced compressive residual stresses are non-existent within the literature. Furthermore, these computational models also need to be able to account for residual stress relaxation due to thermal and loading exposure. Hence, this work aims to develop a framework to assess (1) the effect that microstructure has on residual stress and fatigue variability and (2) the effect that loading has on residual stress relaxation in polycrystalline Ni-base superalloy components.

In this study, residual stresses are introduced within statistical samples of polycrystalline microstructures by inducing a distribution of quasi-thermal eigenstrain as a function of depth from the specimen surface. Two different material models are used, a J2 plasticity and a crystal plasticity model. First, the J2 plasticity model with combined isotropic and kinematic hardening is used to determine the necessary distribution of thermal expansion coefficients as a function of depth from the surface to induce the target residual stress profile within the microstructure. This distribution of thermal expansion coefficients is then used within a crystal plasticity framework, via the decomposition of the deformation gradient into elastic, plastic, and “quasi-thermal” portions, to model the effects of residual stresses and microstructure heterogeneity on fatigue crack driving force and fatigue variability. Figure 1 shows an example of the polycrystalline

microstructure used in the crystal plasticity simulations to represent a smooth specimen and the resulting scatter of residual stress as a function of depth (x-distance) from the surface. As shown in this figure, the quasi-thermal expansion method is able to capture the mean experimental X-ray diffraction (XRD) residual stress behavior as a function of depth from the surface. With this residual stress applied, the microstructure can then be cyclically loaded in the y-direction to study (1) residual stress relaxation due to initial and subsequent fatigue loading and (2) scatter in fatigue life in the presence of residual stress among multiple realizations. This method is repeated for multiple random instantiations to determine the variability in fatigue response among multiple realizations.

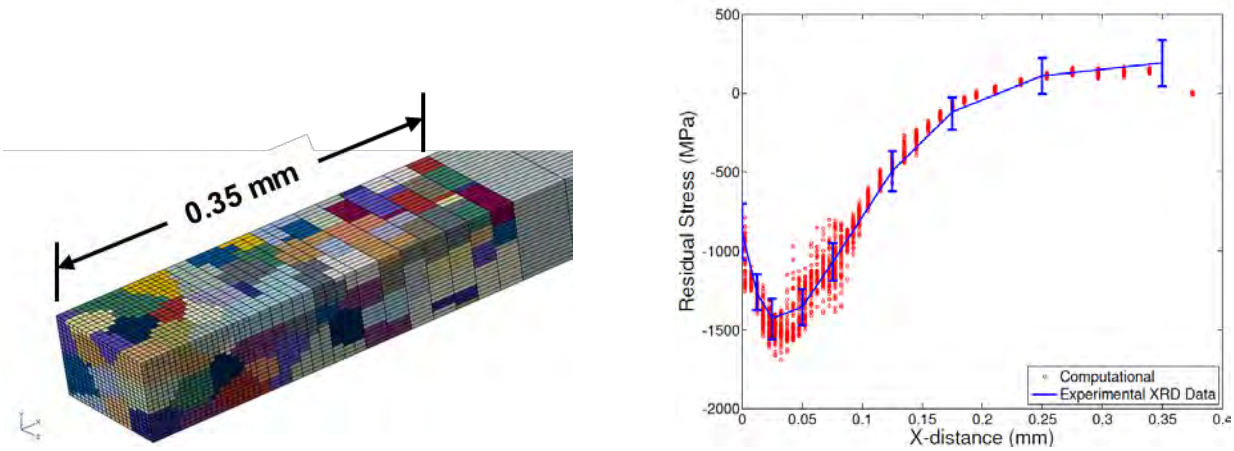

Fig. 1: Example polycrystalline microstructure used for crystal plasticity simulations and the resulting scatter of residual stress as a function of depth. Crystal plasticity is used up to a depth of 0.35mm while J2 plasticity is used for elements deeper than 0.35mm. The cross section of the polycrystalline microstructure is 0.102mm x 0.102mm square.

Using the method of residual stress application described above in conjunction with deterministic microstructurally small crack growth laws, the effect of the applied residual stress on the fatigue response of smooth specimens are demonstrated. In addition, the effect that residual stresses have on near surface inclusions and pores is also displayed in this work. The benefit of this approach is that it can be used to query multiple microstructure variations for a given residual stress application and it can suggest an optimal residual stress profile for a given loading condition. The methods used in this study can contribute to integrated computational materials engineering (ICME) by assessing the potential for optimizing processing-microstructure parameters in surface and heat treatments to support the design of materials for enhanced fatigue resistance.

ID: 414

Computing Overall Thermo-Mechanical Properties of Materials Characterized by Micro-CT

Andrew Gillman
University of Notre Dame
USA

Karel Matou

Abstract:
Accurately characterizing and modeling polydisperse particulate media such as energetic materials, concrete, geomaterials, and other granular materials is essential to improving design and developing new material formulations. The focus of this work is to compute bounds on thermo-mechanical properties using detailed microstructural information obtained from micro-computer tomography (micro-CT). We aim to develop microstructure-statistics-property relations in order to predict macroscopic behavior and its link to microstructure.Material characterization begins by acquiring a detailed three-dimensional image set using a micro-CT system. Individual particles are then identified, and similar particles are grouped into geometric modes in order to analyze the effects of these modes on macroscopic properties. Using n-point probability function tostastically describe the microstructure and considering variational principles that are formulated using these statistical descriptors, bounds on thermo-mechanical properties are computed. Using the described methods, bounds on the macroscopic properties of polydisperse packs will be presented.

ID: 420

Heating in Microstructures of Granular HMX during Impact Loading

Seokpum Kim
Georgia Institute of Technology
USA

Ananda Barua
Georgia Institute of Technology
USA

Abstract:

The thermomechanical response of granular HMX during impact loading is analyzed. The study focuses on the effect of microstructural attributes on the hot spot density and temperature rises. The HMX microstructures studied have mono-modal and bimodal grain size distributions with the mean sizes of the smaller and larger grains as 120 and 360 respectively. This analysis uses a Lagrangian cohesive finite element method (CFEM) framework which allows the effects of large deformation, thermomechanical coupling, failure in the forms of microcracks, and frictional heating to be tracked and analyzed. The results suggest that increasing the mean grain sizes leads to decreases in the hot spot density and increases in peak temperature rises. The evolution of hot spots is quantified as a function of loading intensity, deformation and microstructural attributes. The microstructure-response relations obtained can be used to assess the performance of granular HMX.

ID: 708

Shape Memory Alloys Synthesis Utilizing Laser-based Digital Direct Processing

Reginald Hamilton
Pennsylvania State University

Joseph Giordano

Abstract:
Shape memory alloys (SMAs) undergo a solid-solid phase transformation referred to as the martensitic phase transformation (MT). Deformation can be recovered via unloading and/or recovery via heating. For the past two decades, researchers have studied Laser-based powder processing is a novel fabrication technique for SMAs that offers two primary advantages. Fully dense, near net-shaped SMA constructs can be designed with complex geometries which better engage the embedded SMAs. Furthermore, the surface of compositionally graded SMAs can be tailored in order to enhance binding with dissimilar components. The proposed research investigates the processing-structure-property relationships for SMAs synthesized using laser-based powder processing. We systematically study the effects of processing parameters on the compositonal and the atomic structureal homogeneity utilizin in-situ electron microscopy, as well as ion microscopy, and ion microscopy. Furthermore, we characterize the transformation morphology during deformation using variable magnification in-situ digital image correlation.

Track IX

Student Program

IX.2

Undergraduate Student Symposium

ID: 788

Effects of Interfacial Morphology on Polymer Electrolyte Fuel Cell Performance

Arvind Kalidindi
Drexel University
USA

Reyhan Taspinar
USA

Abstract:
Polymer electrolyte fuel cells (PEFCs) are promising renewable energy candidates with environmentally friendly products (water, electricity, and heat) and the potential for high energy efficiency. Liquid water generation in PEFCs is necessary to achieve high ionic conductivity in the perfluorosulfonic acid membrane, but also creates flooding problems in the electrode and catalyst layer by inhibiting the flow of reactants and thereby limiting cell performance. Furthermore, the inherent roughness of the catalyst layer and electrode leaves void spaces for water pooling at their interface that can hold up to 18% of the full-cell water content. In this work, a two-phase performance model of the cathode of a PEFC is developed with an electrode|catalyst interfacial region directly measured from a commercial fuel cell using optical profilometry. The effect of the imperfect contact along this interface on the spatial distribution of key parameters is studied to better understand water management in PEMFCs.

ID: 807

Mechanics of Deformation and Fracture of Soft Fiber Reinforced Composites

Brian Ramirez
California Institute of Technology
USA

Michael Rauls

Abstract:
The demand for lightweight materials which can undergo large amounts of deformation and remain in the elastic region in deployable space structures and tissue engineering, have led to an increase usage of soft fiber reinforced composites. This provides the motivation for understanding the mechanical behavior of such composites. In the present work, tensile experiments were conducted on carbon fiber/polydimethylsiloxane (CF-PDMS) composites to study their deformation and fracture response. Digital image correlation (DIC) technique was used to measure the full field displacements around notches and cracks in the composite. The experiments together with micromechanical models are used to understand the mechanics of load transfer and failure mechanisms of soft matrix composites. The mechanics insights gained from this study can be used to design and analyze new generation of soft fiber reinforced composites for emerging novel applications.

ID:808

FerroFluid Heat Exchanger Pump

Author
Caleb Piercy

The efficiency of any heat exchanger is defined by (what you get out/what you put in) so that the less energy required by the heat exchanger, the more efficiently it operates. Increasingly, as we are becoming ever more aware of our carbon footprint, engineers are pushing existing technologies to squeeze as much efficiency as possible out of every device we plug into our grid. Many of these devices use heat exchangers and so a significant portion of energy used in the world is applied to pumping fluid through closed systems. With the rise of nanotechnology, a fairly inexpensive and more efficient alternative is possible through the use of Ferrofluids.

Various research has been conducted concerning the magnetic susceptibility of Ferrofluids, which has concluded that while a static magnetic field can deform the surface of a container of Ferrofluid, much more useful is the fact that an alternating magnetic field can actually be used to "spin up" Ferrofluids as a result of the gyromagnetic nature of the nanosized magnetic particles in the fluid suspension. If this solution was applied to heat exchangers it would significantly reduce the power consumption of the heat exchanger, because the moving parts of a typical fluid pump can be replaced by electrical coils powered by alternating current.

It is my goal to design such a heat exchanger that can take advantage of the closed system by incorporating the right combination of electrical coils. Such a system needs to be tested under the influence of variable frequencies and coil designs. The Ferrofluid itself is readily available, though at about $168 per liter and the research I referred to can be presented at your request. Thank you for reviewing my abstract for the undergraduate symposium.

ID: 815

Growth Time Performance Dependence of Vertically Aligned Carbon Nanotube Supercapacitors Grown on Aluminum Substrates

Radu Reit

Justin Nguyen

Abstract:
Vertically aligned carbon nanotubes (VACNTs) present a uniform pore size as compared to activated carbon or nonaligned carbon nanotubes, increasing the available surface area for electric double layer formation. In this study, we fabricate VACNTs grown directly on thin aluminum foils using only conductive support layers in a scalable, low-pressure chemical vapor deposition (LPCVD) process. These highly flexible and conductive electrodes were optimized by utilizing combinations of diffusion barrier layers and catalyst support layers to alter the electrode porosity and available surface area. Specific capacitances for five growth times (5, 10, 15, 20 and 25 minutes) were measured to be 30 to 79 F g-1 and compare favorably to similar studies. Power densities for all supercapacitor sheets exceeded 3 MW kg-1 and consistently exceeded other VACNT supercapacitor studies. Our study demonstrates the benefits and applicability of fabricating VACNTs on metal substrates using scalable techniques for flexible and conductive supercapacitors.

ID: 819

Automated Procedure for Functionalization of Non Magnetic Micro Particles

Stefan Stephenson-Moe
Georgia Tech
USA

Abstract:
Micro particles, or small spheres between the sizes of 0.1 microns to about 100 microns, have become an area of much research in the area of biotechnology. These small beads are currently used in some drugs already such as the Gardasil vaccine for HPV. They promise to be of use in the future being of current use in many different areas of research such as cancer and infection research. A common problem for researchers studying micro particles is functionalization. Functionalization is the process of attaching different compounds, such as proteins or antibodies, and attaching them to the surface of the micro particle. The chemical procedures for attaching many of these compounds is well understood, however most of these processes are done by hand. This is time consuming as it requires a technician to essentially nurse the particles throughout the procedure, which although a simple task can tie up the technician for hours adding chemicals, centrifuging, pipetting, incubating, etc... This research project attempted to solve this problem by designing a device that only requires the user to add the required chemicals and run an Arduino program, the rest being done automatically. The device created is a small bench top device currently capable of functional BSA (Bovine Serum Albumin) onto polystyrene beads. Currently the only other automated procedures for functionalizing micro particles involves the use of robots that cost around $100,000 and these robots are only capable of functionalizing magnetic particles. This device offers a cheaper alternative, having cost around $900 to build and is capable of functionalizing both magnetic and non magnetic particles.

ID: 820

Side Specific Responses of Shear Stress on AV Calcification

Anita Rajamani
Georgia Institute of Technology
USA

Swetha Rathan

Abstract:
Aortic valve (AV) calcification leads to stenosis which is the most common heart valve disease. However the mechanism of this disease is not fully understood. Due to the location of AV it experiences dynamic mechanical environment such as shear stress, tension, and pressure that regulate the AV biology and when these stimuli are altered, it could lead to alterations in AV mechano-biology. Variation in shear stress has been known to initiate AV pathophysiology. To understand the effects of the magnitude of the shear stress and its side specificity, we exposed fibrosa and ventricularis sides of porcine AV to different shear stress patterns (oscillatory and steady) using an ex vivo cone and plate viscometer for 72 hours. An osteogenic media was used to accelerate the calcification process. Quantitative and qualitative tests were done on the samples after the experiments. Arsenazo assay was used to quantitatively determine the amount of calcium and Von Kossa stains were performed to visualize the extent of mineralization. Results show that significant calcification occurred on the fibrosa side of the AV tissue, caused by low magnitude oscillatory shear stress. Changes in shear stress frequency had no effects on calcification. Thus our results indicate that low oscillatory shear stress can potentially trigger calcification on the fibrosa side of porcine AVs as previously observed in calcified human AVs.

ID: 822

Cyber-enabled Modeling of Adhesion-Based Deformation in Low-Dimensional Nanostructures

Emmanuel Ochoa
University of Texas at El Paso - Purdue University (SURF program)

Fernando Dri

Abstract:
Understanding, quantifying and predicting the long-range adhesion forces at the nanoscale is essential for tuning the electrical and mechanical properties of low-dimensional nanostructures. The first step towards a multiscale theoretical/numerical framework to analyze this complex problem is through cyber-enabled advanced simulation tools for education and research purposes. In this talk we present a molecular dynamics analysis of the interaction between 1- and 2D nanostructures to extract key information to feed continuum-based coarse-grained models. As a case study, we present the analysis of nanometer-thick nano-membranes covering partially or completely a nanotube lying on a substrate. The long-range non-bonded interaction between the nano-membrane and the substrate impose a compressive load to the nanotube, inducing substantial transverse deformation that lead to significant changes in their electrical properties. Our simulations show good agreement with AFM based experiments. Additionally, this computational tool (which has been developed for NanoHUB.org) is accessible for all researchers and educators.

ID: 823

Influencing Encapsulated Stem Cell Factor Secretion through Hypoxic Conditioning

Mohamad Ali Najia

Jenna Wilson

Abstract:
Embryonic stem cells (ESCs) have the unique ability to differentiate into cell types of all germ lineages. However, there are several challenges in using ESCs for regenerative medicine and stem cell bio-manufacturing applications, namely scalable cell production and dynamic regulation of cell fate. A recent paradigm shift has emerged suggesting that the beneficial effects of stem cells may not be restricted to cell restoration alone, but also due to their transient paracrine actions. Constructs to engineer paracrine delivery can enhance therapeutic efficacy. First, microencapsulation of ESCs in alginate can be exploited to modulate cell phenotype and secretory profile via the ratio of guluronic and mannuronic acid content, as well as allow for high density culture in bioreactors. Second, preconditioning of ESCs under low oxygen tension (3% O2) has promoted expression of several growth factors and mimics in vivo embryogenesis conditions. Therefore, the ability to exploit and regulate paracrine actions can prove essential for novel therapies and scalable stem cell bioprocessing.

ID: 825

Water Hammer Suppression using Voided PDMS Liners

Chandana Edirisinghe

Abstract:
Unsuppressed pressure waves formed by rapid valve closure in piping systems cause irritating noise and costly pipe damage to building and home owners. The current research is focused on understanding the behaviour and applicability of microsphere voided polydimethylsiloxane liners in passive pressure arrestor devices as a replacement for piston or bladder devices which can fail after prolonged use. Physical testing with prototype microsphere voided liners proved promising, displaying the ability to damp peak pressures to acceptable levels. However, further work is required to increase overall damping in these PDMS liners to match that of current piston devices. A numerical model of the PDMS arrestor was developed in Simulink to investigate how the nonlinear material properties of PDMS and buckling microspheres affect the overall damping ability of the PDMS liner. This knowledge will allow the creation of more reliable arrestors than those currently available, reducing costs and discomfort for building owners.

ID: 827

Solar, Thermal, and Mechanical Energy transfer using Piezoelectric Nanowire and its Application

Yean Lee
Georgia Tech Mechanical Engineering

Abstract:
Light carries energy as described by the equation, E=hxf where h is Plank's constant and f is the frequency of the electromagnetic wave. Hence, scientists were able to induce electricity on metal antennas using photoelectric effect as demonstrated by microwave power transmission (MPT) and produce photoluminescence from semiconductors by exciting electrons to conduction band. The idea of transferring light energy to electrons can be applied piezoelectric nanowires. Piezoelectric materials vibrate when applied with voltage as a result of dipole created by asymmetrical crystal lattice between ions. The effect is reversible; hence, one can harvest energy from mechanical stress. And by combining piezoelectric nanowire with thermal and solar cell into a single entity, one can minimize the size of the hybrid cell while increasing its output power. In this study we examine energy conversion and harvesting energy from multiple sources simultaneously.

ID: 828

Mechanics of Sickle Cell Disease: A Purely Physical Cause of Endothelial Cell Dysfunction

Robert Mannino
Georgia Institute of Technology
USA

Abstract:
Sickle cell disease (SCD) is a genetic disorder characterized by deformed and stiff erythrocytes and endothelial dysfunction, for reasons that remain unclear. As previous research has shown that endothelial cells biologically respond to mechanical forces, we hypothesize that the direct mechanical interactions between the physically-altered sickle erythrocytes and endothelial cells are a separate and additional l cause of endothelial dysfunction in SCD. To test our novel hypothesis, we used our novel end othelialized microfluidic system developed by our laboratory to emulate the geometric and flow conditions of the microvasculature. . By simply flowing chemically-stiffened erythrocytes versus normal control erythrocytes into our system, we found that that flowing stiffened erythrocytes significantly increased the expression of VCAM-1, a known marker for endothelial dysfunction, as compared to the control condition using normal erythrocytes. Our data suggests that mechanical interactions alone between sickle erythrocytes and endothelium are sufficient to cause endothelial dysfunction in SCD.

Notes:

Notes:

GEORGIA TECH HOTEL MAP